Summary of Low-Speed Airfoil Data

Michael S. Selig, Christopher A. Lyon, Philippe Giguère,
Cameron P. Ninham and James J. Guglielmo

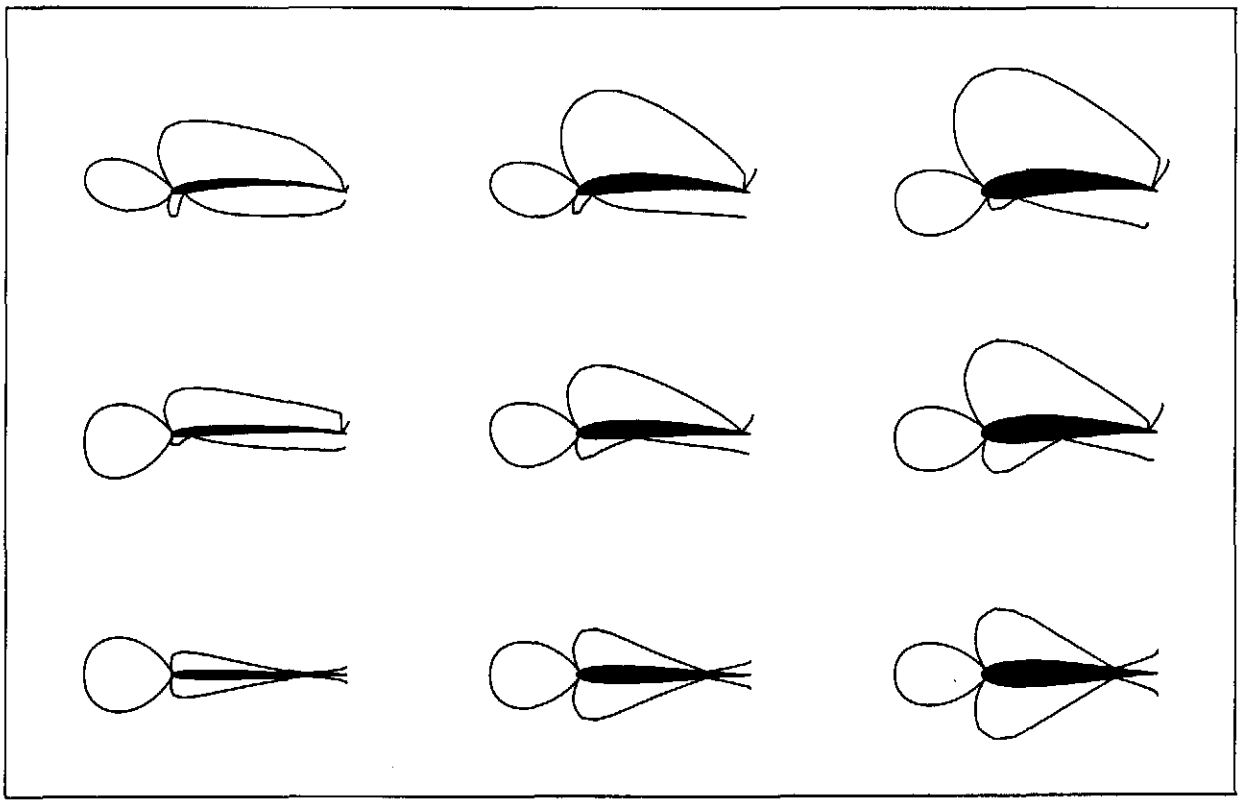

Volume 2

Summary of Low-Speed Airfoil Data

Volume 2

About the Authors

DR. MICHAEL S. SELIG, an accomplished applied aerodynamicist and airfoil designer, is an Assistant Professor of Aeronautical and Astronautical Engineering at the University of Illinois at Urbana-Champaign. He received his B.S. (1984) from the University of Illinois, his M.S.E. (1988) from Princeton University and his Ph.D. (1992) from the Pennsylvania State University. His current research areas include low-speed aerodynamics, airfoil design, wind energy and flight simulation. He teaches courses in applied aerodynamics and aircraft design. He has been active in R/C soaring for over 20 years.

CHRISTOPHER A. LYON received his B.S. in Aerospace Engineering from the University of Notre Dame in the spring of 1995. He joined the UIUC LSATs team upon his arrival at UIUC in the fall of 1995 and is currently working toward his M.S. degree. Besides his thesis research regarding lift hysteresis, he is also interested in boundary-layer tripping techniques and the optimization of flying wings. He has been involved in R/C aircraft for the past 12 years with the previous eight being focused on scale aerobatics. He also designs R/C aircraft ranging from biplanes to flying wings.

PHILIPPE GIGUÈRE is currently working toward a Ph.D. degree with research in horizontal-axis wind turbine blade design and optimization. Other research interests include airfoil performance enhancement and design, wind-tunnel boundary corrections, design of unmanned aerial vehicles, and Gurney flaps. His previous studies were conducted at McGill University and Université Laval located in Quebec, Canada. He has been involved with the UIUC LSATs since his arrival on campus in September 1994. His experience with R/C model airplanes comes from his participation in the Society of Automotive Engineer's Aero-Design competition from 1991–1994. He flies full-scale gliders.

CAMERON P. NINHAM is a graduate student (M.S. degree candidate in Aeronautical Engineering) at the University of Illinois. Originally from South Africa, he obtained both his Bachelors and Honors Degree in Computer Science, majoring in Computer Science and Applied Mathematics. He was previously employed as a computer programmer at a company that develops computer software and provides various computer related services. He started his studies at the University of Illinois in January 1995, and he hopes to finish his degree by December 1996 or early 1997. His passions in life, other than his family, include R/C gliders/modeling, soaring, hang gliding.

JAMES J. GUGLIELMO, the co-founder and first coordinator of the UIUC Low-Speed Airfoil Tests, received his Bachelor of Science degree in Aeronautical and Astronautical Engineering from the University of Illinois at Urbana-Champaign in May 1992. Remaining at the University of Illinois for graduate studies, his research has included such topics as conceptual aircraft design and experimental supersonic and subsonic wind-tunnel testing. Mr. Guglielmo will receive his Master of Science degree in experimental low Reynolds number airfoil aerodynamics from the University of Illinois in May 1996, and is currently working in the Phantom Works Division of McDonnell Douglas Aerospace, Huntington Beach, CA.

Michael S. Selig
Christopher A. Lyon
Philippe Giguère
Cameron P. Ninham
James J. Guglielmo

Department of Aeronautical and Astronautical Engineering
University of Illinois at Urbana-Champaign

Summary of Low-Speed Airfoil Data

Volume 2

SoarTech Publications
Virginia Beach, Virginia

SoarTech Publications
1504 N. Horseshoe Circle
Virginia Beach, Virginia 23451, USA

The cover illustration shows the variation in the inviscid pressure coefficient distribution around a series of airfoils with varying thickness and camber. In each case the angle of attack is 0 deg. The airfoils in the first, second and third columns have a maximum thickness of 5%, 10% and 15%, respectively, while airfoils in the bottom, middle and top rows have a maximum camber of 0% (symmetric), 3% and 6%, respectively. For each airfoil, the lobe at the leading edge is positive pressure, and thereafter, they alternate between negative (suction) and positive pressure. The airfoils were designed by Ashok Gopalarathnam using PROFOIL, and the input files can be found at http://www.uiuc.edu/ph/www/m-selig.

First Printing, April 1996

Library of Congress Cataloging in Publication Data

Selig, Michael Scott
Summary of Low-Speed Airfoil Data, Volume 2 / by Michael Selig,
Christopher A. Lyon, Philippe Giguère, Cameron P. Ninham and James J. Guglielmo.

Includes bibliographical references.
1. Aerofoils (Airfoils). 2. Aerodynamics. 3. Airplanes—Models.
I. Model Aviation. II. Title
ISBN 0-9646747-2-6

Contents

Preface

Summary of Low-Speed Airfoil Data, Volume 2 is the second book in the series that documents the ongoing work of the University of Illinois at Urbana-Champaign Low-Speed Airfoil Tests (UIUC LSATs) program. As described in the first volume, most of the airfoils are intended primarily for model aircraft, although much of the results of this work will have wider application.

Much to our surprise (and to others), this effort continues largely through the generous support of model-aviation enthusiasts. Without their contributions as listed in the Acknowledgments section, this work would not be possible or nearly as rewarding.

Since the writing of the previous volume, Jim Guglielmo, the first UIUC LSATs coordinator and co-founder, has taken a position as an Engineer/Scientist at McDonnell Douglas Aerospace, Huntington, CA. Chris Lyon (M.S. candidate and a graduate of Notre Dame) arrived in August 1995 to become the new coordinator. The remainder of the test team includes the continuing members: Philippe Giguère (Ph.D.), Cameron Ninham (M.S.), Andy Broeren (Ph.D.) and Ashok Gopalarathnam (Ph.D.). This group, together with the help of Christopher J. Fisichella (Ph.D.) and Farooq Saeed (Ph.D.), took the data for this volume over the period from mid-September to mid-October 1995.

This Book and Its Organization

For the most part, the current volume follows the format of the first. Chapter 1 illustrates the airfoils tested by category. Chapter 2 provides an update to the discussion of the wind-tunnel test facility and the experimental procedures given in *Volume 1*. In the first volume, a limited amount of computational results were presented. Given the importance of computational aerodynamics and the large role it plays in the current work, it seems timely to present a more detailed discussion of the methods used as well as their limitations and strengths. Chapter 3 is devoted to this topic. Chapter 4 includes a discussion of the airfoils tested, and the associated performance plots are presented in Chapter 5. As in *Volume 1*, the tabulated airfoil coordinates and performance data (available on diskette) are given in Appendices A and B. Appendix C contains the UIUC Low-Speed Airfoil Tests Manifesto that outlines the scope and purpose of this work. Finally, the Errata contains corrections to *Volume 1*.

Acknowledgments

The airfoil testing effort would not have been possible without the support of many people. *To each of them we are indebted.* In particular, for monetary contributions that were used for equipment and graduate student support, we are especially grateful to the following organizations, clubs, businesses, individuals and t-shirt patrons. Shown in parentheses for each category is that category's fraction of the total support received. Each donor will be listed in two volumes of this book. Thus, those mentioned in the last volume are listed here as well as new donors to be mentioned in the next volume.

- *Organizations (11%):* Academy of Model Aeronautics (with special appreciation to Bob Underwood and Jerry Rouillard), ISF-International R/C Soaring Forum (with special appreciation to Rolf Grisberger), National Association of Rocketry (Mark Bundick), and National Free Flight Society (with special appreciation to Bob Waterman).

- *Businesses (22%):* Airtronics, Inc. (Bob & Tim Renaud), B^2 Streamlines (Bill & Bunny Kulhman), Dan Parsons Products (Dan Parson), Design and Manufacturing, Ltd. (Jack Spitz and Ernest Trent, Jr.), F3F Newsletter (Preben Norholm), Gulf R/C (John Rimmer), Ingersoll-Rand (Dr. T. Sean Travares), Kennedy Composites (Barry Kennedy), Landing Products (Fred Burgdorf), Microsoft Corp (Steven Seim), Muncie Pawn Brokers (Bill Greene), Northeast Sailplane Products (Carolyn & Sal DeFrancesco), Planeador RC News-Spain (Peter Atkinson), Quiet Flight International (Dave Jones), R/C Soaring Digest (Jerry & Judy Slates), Slegers International, Inc. (Ed Slegers), SoarTech Publications (H.A. Stokely), Top Flite (Don Anderson), Traplet Publications (Dave Jones), and Websoft, Inc. (Robert Webester).

- *Model Clubs (7%):* B.A.R.C.S., Baltimore Area Soaring Society, Champaign County Radio Control Club, Clent Soaring Association (England), Downeast Soaring Club*, Fairlop Silent Flyers (England), Florida Soaring Society, FMSG Alling/Obb. (Germany), Greek Aeromodelling Federation (Greece), Ivinghoe Soaring Association (England), Lincoln Area Soaring Society, Miniature Aircraft Association of Westchester County, North American Scale Soaring Association (NASSA), Northeast Drone Society, Paducah Aero Modelers, Pasadena Soaring Society, Peninsula Channel Commanders, Portland Area Sailplane Society, Inc., Round Valley Radio Control Club, S.E.F.L.I., S.O.A.R., S.W.I.F.T., San Gabriel Valley Radio Control League, Santa Clarita Soaring Assoc., Sheffield Soc. of Aeromodellers (England), Sundancers R/C Model Club, Tidewater Model Soaring Society, Tri County Aero Club, Tri-Cities Radio Control Modelers Club, Tyler Modelers Club, Victorian Association of Radio Model Soaring (Australia), W.A. Radio Soarers Club, Inc. (Australia), and White Sheet Radio Flying Club.

- *Individuals (54%):* Anonymous, Dennis Adamisin*, G. Richard Adams, Arnold Angelici, M.D., Thomas Anthony*; Garry Armstrong*, Thomas Atwood, Bruce Baker*, Gary S. Baldwin, Charles Baltzer, Mark Barbee* & Charlene Olsen, Matt Barbian*, Richard Bartkowski, Plenny J. Bates, M.D., David Batey, Jr., Hans Walter Bender, Robert Bender*, Bernard Biales, Byron Blakeslee, Eric Blanke, Bill Bogart*, Charles Botzko, Chris Bovais, Arthur J. Boysen*, Ronald Bozzonetti, Andy P. Broeren*, Phillip Burnside, Wil Byers*, Myron & Felissa Cagan*, Kenny Carpenter*, Edward Carter, W.B. Cavanaugh*, Robert Champine*, Paul Clark, Don Coburn, Joseph Conrad, John L. Cranmer, Jr., Michael J. Cresanta, Michael D. Denton*, Alfred J. DeRenzis*, Michael W. Derr*, Armand DeWeese, Dan J. Dobbins, John Donelson, John Drab*, Doug Drullenger*, Chas Dunster*, Hilmar Durden*, Frits Donker Duyvis*, Robert Dyer, Dr. Don Edberg, Stefan Eder*, R.J. Edmonds, Waldron Ehrlich*, Nanette & William Entriken, Lars Ericsson*, Stephen J. Fauble*, George L. Fiocca*, Bill Forrey, Norman D. Frank, William S. Friedlander*, Roland Friestad, David Garwood, Laurent Gasser, Bill I. Gaston*, Robert C. Glover, II, Greg Goldstein, Ed Granger*, Martin Gregorie*, Thomas Gressman*, Rolf Grisberger, Charles Griswold, Brian R. Gyles, Henry Hain, James B. Halbert*, David L. Hall*, Bob Harold, George Harper*, George B. Herider*, Richard Hognes*, Chuck Hollinger, Takashi Hoshizaki, C.D. Houge, III*, Dale C. House, Nelson Itterly, John S. Jensen*, Vince Johnkoski*, Darrell Johnson*, Kerry Jones, Chris Kaiser*, John Kallend*, Daniel Kong*, Bill & Bunny Kuhlman (in memory of Bill's father), Michael Lachowski, James Ladwig, Walter Larew, Benjamin Lawless, Donald Leath, Laurent Lebrun*, A.G. Lennon, Dr. Robert Livin*, Robert Lockwood, Jr.*, Chuck Lohre, Eric Loos*, Marco Lorenzomi, Keith C. Love*, Eugene F. Lovejoy*, Warren Lucas*, Steven Lucke, Bob Mabli*, Andrew Macdonald, G.M. Magarian, Fred Mallet, Stefano Martini*, Burt Marx, Joseph Mastropaolo, Robert Matheson*, Kevin McKiou*, Merlin Meisner, Eric Meyers, Edward Mitchell*, Luther Mitchell*, Owen Morris, Gilbert Morris*, Jeff Morris*, Allen Morse, Tim Mountain, Mark Nankivil*, John D. Newell, MD*, Robert Nielsen, Greg Nilsen, Steve Nue*, Ted Off, Alan Oliver, Paul Ortman, Jean G. Pailet, Bob Peirson*, Paul J. Penna*, D.N. Penton, John Perry*, Carol Pesch, James I. Pilkington, Dr. John Ponsford*, Ralph Prey, Horst Rabiger, Gordon J. Rae*, Blaine Beron-Rawdon, David Register, Francis Reynolds, Jerry Robertson, H.J. Rogers*, Stefano Rossi, Dr. Stan Sadorf, David Schenken, Prof. Allan K. Scidmore, Marty I. Selig, Martha I. Selig (in memory of John G. Selig), Prof. Michael S. Selig, Glenn Sembroski*, Robert L. Simon, Authur Slagle, Charles Smith*, John W. Smith*, Michael J. Smith*, Howard F. Sosbee, Glen Spackman*, Robert Stanford*, David Steere, Peter Steinmeyer, Helmut Stettmaier, Larry Storie, Tim Stover*, Joe Stute*, Al Sugar, R.T. Sunderland*, Jim Tangler, Jose M. Tellez*, Willard L. Teommey, D'Anne Thompson*, G.J. Tonnelli, Jorgen Tonnesen, Dr. T. Sean Travares, Craig Uridil*, John Vennerholm*, Rick Waitulionis, Sean

Walbank*, Jess Walls*, Garth Warner, Rod Watkins*, Ralph M. Weaver*, I. Jay Welch*, W. D. Williams*, Oliver C. Wilson*, Vern Winston, Graham Woods*, Joe Wurts, Scott Youmans* and Frank Zaic.
(* denotes T-Shirt Patron as well)

- *T-Shirt Patrons (6%):* Anonymous, Dan Abel, David Acker, Les Akers, Helene Anderson, James T. Armstrong, III, Peter Averill, Kendra Baier, Robert Barrows, Douglas Barry, David Beardsley, Mari K. Bebeau, R.P. Beloff, Dan Bernauer, Carl Bice, Ben Bierman, S.C.M. Blake, Woody Blanchard, William Boisvert, Jeanna Bonello, Doug Boyd, Gene Boyko, Delmar Brengman, Joyce C. Broeren, Richard Broeren, Sue Broeren, Gary Brokaw, Doug Buchanan, Lois Budill, Chip Bullen, Richard Bums, Roy Bunnell, Gilbert Bureau, John Burke, George Burns, Steve Cameron, Jim Carlton, Juan Chi, Dale D. Christensen, Michael Christiansen, Gary Claiborne, Ben Clerx, Dave Corven, Bruce Cronkhite, Thomas Cunningham, Brenden Cyze, David Darling, David Diesen, Ray DiNoble, Brian Dirman, Lawrence Drennan, Peter Dudley, F.G. Durand, Merrill Farmer, David H. Fletcher, Joel S. Freeman, John Fulton, R. Marc Gellart, Browne Goodwin, Ashok Gopalarathnam, Chris Gregg, Kenneth Griffin, W. Grundler, Jim Guglielmo, Keith J. Hanz, Don Harris, Pat Hart, Roger Hebner, Bob Harman, George M. Hilliard, MD., Gary Hyde, Denis Jenkins, Gordon Jennings, Kelly Johnson, Gordon Jones, Douglas Joyce, Stephen J. Kaye, Barry Kennedy, Bruce Kimball, Leon Kincaid, Bruce Kirstein, Ron Konicke, Bill Kubiak, Bill & Bunny Kuhlman, Barry Kurath, Rick Lacy, Michael R. Laible, Dwayne Lane, Stephen Lee, Sam Lee, Todd Lee, Brian Levy, Phillip Lontz, Carl Luft, Bill Malvey, Skip Miller, William Miller, Myles Moran, Bob Morford, Mark Morimoto, Thomas W. Moritz, Roger Morrell, Chris Munson, Nick Neve, Cameron Ninham, Jerome B. O'Mara, Harold Ochs, Ray Olsen, Richard Orobitg, Steve Pasierb, Don Pesznecker, Pete Peterson, Daryl Pfaff, William L. Potter, Mike Prager, Todd Presley, John Raley, Michael D. Reed, Gary Rexroad, Waid Reynolds, David Rice, Sensei John M. Roe, John J. Salvatini, Toshiro Saruwatari, Erkko Saviaro, Don C. Scharf, Herm Schmidt, Charles Schmitz, John Schmoll, John Schultz, Dr. Alan Schwerin, Jason Seal, Paul Sherman, David Sieger, Jerry Slates, Ed Slegers, Frank Smith, Andy Smith, Scott Smith, Karl M. Sorensen, Sandee Stedwell, Bob Steele, Robert Stewart, Larry Storie, Glenn Strickland, Mike Stump Family, Stephen Syrotiak, Manny Tau, Jim Thomas, Keith Thomson, Gene Trevino, Paul Trist, Jr., Aaron Valdes, Gregory Vasgerosian, Jean Vendette, John Vennerholm, Buzz Waltz, Roy W. Wampler, Randall Warner, Charlie Waugh, Dennis Weatherly, B.J. Weisman, Dr. John B. West, Dan Westergren, Prof. Frank Wicks, Frank Williams, Michael Wilson, Alan Wirth, David Wood, Wayne Yamamoto, John Yee, Gerald Zeigenfuse and Michael Ziaskas.

The meticulous building efforts of the following individuals are greatly appreciated.

- *Wind-Tunnel Model Builders:* Roger Adams (DU 86-084/18), Mark Allen (M06-13-128, S822, S823), Michael Bame (E374), Ronald Bozzonetti (NACA 2414), Delmar Brengman (SD7037), Bob Champine (RG15), Henry Cole (Davis 3R), Les DeWitt (LD-79), Ralph Cooney (MA409), David Glaze and Mark Lazor (E423), Gordon Jones (S7055), Doug Imes (NACA 2415), Mike Lachowski (S7012), Mark Levoe (S4083), Charlie Richardson (S1223 RTL), Jerry Robertson (CR-001, RG15 flap installation, S7075), Leo T. Spychalla (M6-65%, M6-85%), Jim Thomas (S4083, S7075), D'Anne Thompson (SD7037), Jim Thurmond (S8025), Tinel Technologies/Yvan Tinel (S1223), Jorgen Tonnesen (MH32) and Oliver Wilson (S5010).

Those individuals who have helped to promote the airfoil test effort or offered technical assistance include:

- *Other Supporters:* Hermann Andresen, Robert Alexander, Bruce Baker, Serge Barth, Jim Boxmeyer (Boxmeyer Composites), Leonard Burz, Erik Dahl Christiansen, Peter Compton, Dr. Don Edberg, Wally Foote, William S. Friedlander, Greg Goldstein, Paul Grassel, Dale House, John Jensen, John Kallend, Michael Laible, Mark Morimoto, Alan Mayhew, Mike McMahon, James Neal, Nick Neve, Mike O'Donnell, Dermot O'Flynn, Paul Penna, John Raley, David Register, Gary Rexroad, John Rimmer (Gulf R/C), Dr. Alan Schwerin, Jörgen Skogh, Charles Smith, Paul Trist, Jr., John West, Richard Williamson and Scott Winans.

In this volume, flap data on four R/C soaring airfoils is presented. This data would not have been taken were it not for the efforts of Jack Spitz and Ernest Trent, Jr. (Design and Manufacturing, Ltd.) who produced the flap endplate brackets used to secure the flaps.

Finally, the remaining acknowledgments updated from *Volume 2* still apply. Several others (some already acknowledged) deserve special mention. It is with a deep sense of gratitude that we thank Herk Stokely (SoarTech Publications) for his diligent and ongoing efforts related to distributing *Airfoils at Low Speeds* and now this book. Also, we have been very fortunate to have received a large donation from an anonymous individual to support the purchase of a new computer and additional equipment that has helped to improve and expand the scope of the program. We have benefited greatly from the earlier work of Dr. John Donovan and the late David Fraser, as well as the many other individuals who contributed to the Princeton Tests. The efforts of Cody Robertson in designing the 1994 UIUC LSATs t-shirt is sincerely appreciated. Special thanks are also extended to Karen Evans for her assistance in designing the UIUC LSATs logo. We are also appreciative of Gilbert Morris for organizing the construction of the

free flight wind-tunnel models and for providing background information used in the discussion of the F1B airfoils. Also, Lisa Selig's efforts and encouragements are greatly appreciated.

Of those at the University of Illinois, we wish to thank Mike Kerho (now at McDonnell Douglas) and Stan Berkovich for their help with the data acquisition software. With respect to digitizing the wind-tunnel models, we thank Prof. Michael Philpott for the use of his coordinate measuring machine and also Stephen Craggs for initial setup support. Andy Broeren especially wishes to acknowledge his research advisor, Prof. Michael Bragg, for his patience and support thoughout the course of this project. We are indebted to Carol Winkler for her efforts in maintaining the mailing lists and processing the donations.

It should be mentioned that some of the work reported here has benefited from other research activities, such as research sponsored by the Univerisity of Illinois and also research in wind energy supported by the DOE National Renewable Energy Laboratory. Finally, we must apologize to those whom we have inadvertently omitted.

Airfoil Data Distribution

All of the airfoil coordinates and performance data presented in this book (see Chapter 5) are available on IBM and Macintosh compatible diskettes through SoarTech Publications. SoarTech will be returning a portion of the proceeds from all disk and book sales to help support the continuation of these airfoil wind tunnel tests. For more information, write to

SoarTech Publications
c/o Herk Stokely
1504 N. Horseshoe Circle
Virginia Beach, VA 23451
e-mail: herkstok@aol.com

The data is also available on the Internet from the host **opus.aae.uiuc.edu** using anonymous FTP. See the file `/pub/lsat/AIRFOIL.DATA` for directions on which files to copy. The data can also be obtained from the world wide web at http://www.uiuc.edu/ph/www/m-selig.

The airfoil performance data is copyrighted, and restrictions are placed on its use. The data may be freely copied and used in any way, e.g., for personal use, in magazine articles or with a commercial product. If the data is used in a magazine article or book, the author must reference this book and state where it can be obtained. If the data is used in a commercial product, there must be no extra charges for providing it—other than the cost of reproduction and distribution. All products that make use of this data must conspicuously state that it was produced under the UIUC Low-Speed Airfoil Tests program, and no restrictions can be placed on the recipient with respect to their use of the source data. Furthermore, they must be allowed to copy the original data and freely distribute it as well. It is in this sense that all access to this data is *free*. More details can be found in the general public license that accompanies the data distribution files. A copy of the license, the copyright notice and the UIUC Low-Speed Airfoil Tests Manifesto must be included with each distribution of the data.

If you find the airfoil performance data useful, **please send a donation** to support our work. If you have already made a donation, we hope that you will consider renewing your commitment. Your tax deductible donations (see Appendix C) can be mailed to

Prof. Michael Selig
Dept. of Aeronautical and Astronautical Eng.
University of Illinois at Urbana-Champaign
306 Talbot Laboratory, 104 S. Wright St.
Urbana, IL 61801-2935
e-mail: m-selig@uiuc.edu
http://www.uiuc.edu/ph/www/m-selig

List of Figures

List of Tables

List of Symbols

c	airfoil chord
C_l	airfoil lift coefficient
C_L	aircraft lift coefficient
$C_{l_{max}}$	maximum lift coefficient
C_d	airfoil drag coefficient
C_D	aircraft drag coefficient
$C_{m,c/4}$	airfoil pitching moment about the quarter-chord point
d	drag per unit span
h	trip height or Gurney flap height
L/D	aircraft lift-to-drag ratio
n	parameter used for transition predition in XFOIL
N_{crit}	same as n
$\mathcal{R}$	reduced Reynolds number, $Re\sqrt{C_L}$
Re	Reynolds number based on airfoil chord
u_e	boundary-layer edge velocity
u_{inv}	inviscid velocity on airfoil surface
V	inviscid or viscous local velocity on airfoil surface
α	angle of attack
Δ	an increment
δ^*	boundary-layer displacement thickness
θ	boundary-layer momentum thickness
ρ	fluid density

Chapter 1

The Airfoils Tested

In this volume, the wind-tunnel test results of over 30 airfoils (shown in Fig. 1.1) are presented. Although a wide selection of airfoils were tested, considerable attention was focused in three particular areas. First, in R/C soaring competition, the use of camber-changing flaps in competition has become essential. Unfortunately, until now, there has been little flap data available, and consequently it has been difficult to identify the favorable characteristics of airfoils designed for use with flaps. Thus, several airfoils were tested with flaps. These results, combined with flight-test reports, have helped to identify some of the desirable qualities of flapped airfoils for R/C soaring. Second, a new approach to making optimal use of boundary-layer trips on low Reynolds number airfoils was initiated. More work in this area is planned, but the preliminary results are encouraging. Third, interest in the potential use of Gurney flaps, which are small downward-deflected

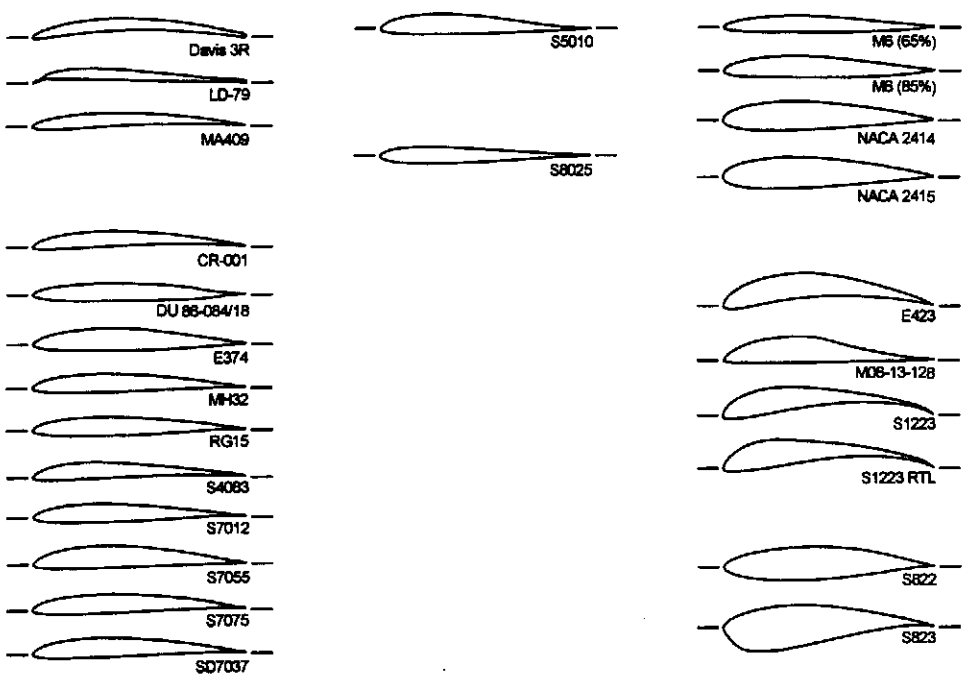

Fig. 1.1 The collection of airfoils tested during Test Series 2 of the UIUC Low-Speed Airfoil Tests (September–October 1995)

tabs at the airfoil trailing edge, has lead to tests on five airfoils equipped with this type of flap.

Aside from the aforementioned areas of special interest, work has continued in several of the categories first given in *Volume 1*, namely, airfoils for free flight models (F1B), R/C sailplanes, R/C hand launch, flying wings, sport models, heavy-lift cargo models and small wind turbines.

Chapter 2

Wind-Tunnel Facility and Measurement Techniques

All experiments were performed in the UIUC Department of Aeronautical and Astronautical Engineering Subsonic Aerodynamics Research Laboratory. Detailed descriptions of the low-speed wind tunnel, lift and drag measurement techniques, data acquisition equipment and data reduction procedures are presented thoroughly in Refs. 1 and 2. The remainder of this chapter deals with the validation of the data and details related to the arrangement of the flaps on the models.

2.1 Lift and Drag Data Validation

As part of the ongoing validation of the data from one test series to the next, the E374 (B) has been selected as the "calibration" model since it was tested both at Princeton and during Test Series 1. As compared with the previous UIUC test data,[2] the current results co-plotted in Fig. 2.1 show good agreement over the majority of the test range. A slight difference in drag, however, is observed at low angles of attack for most of the Reynolds numbers. Also, some differences exist for Re of 60,000.

The discrepancy is associated with variations in the spanwise drag, which is particularly large at low angles of attack for the E374 (B) model. Ideally, there should be no variation in the spanwise drag since airfoil flows are "two-dimensional." The flow, however, is markedly three-dimensional, especially at low Reynolds numbers. Data taken previously[3,4] with the current setup is shown in Fig. 2.2 to illustrate the spanwise drag variation measured in the wake of the E374 (B) at a Reynolds number of 200,000. Below an angle of attack of 0.3 deg, significant spanwise variations are present with amplitudes deviating approximately 20% from the mean. Between an angle of attack of 0.3 and 5.9 deg, the amplitude of the variations decreases dramatically to 5–10% from the mean value. At and above an angle of attack of 7.8 deg, the spanwise drag appears skewed, which may be caused by corner vortices developing in the juncture between the model and endplates at the high-lift conditions.

When wake surveys are used to obtain drag data, the surveys must be taken at discrete locations. The reported drag, therefore, depends on the location of

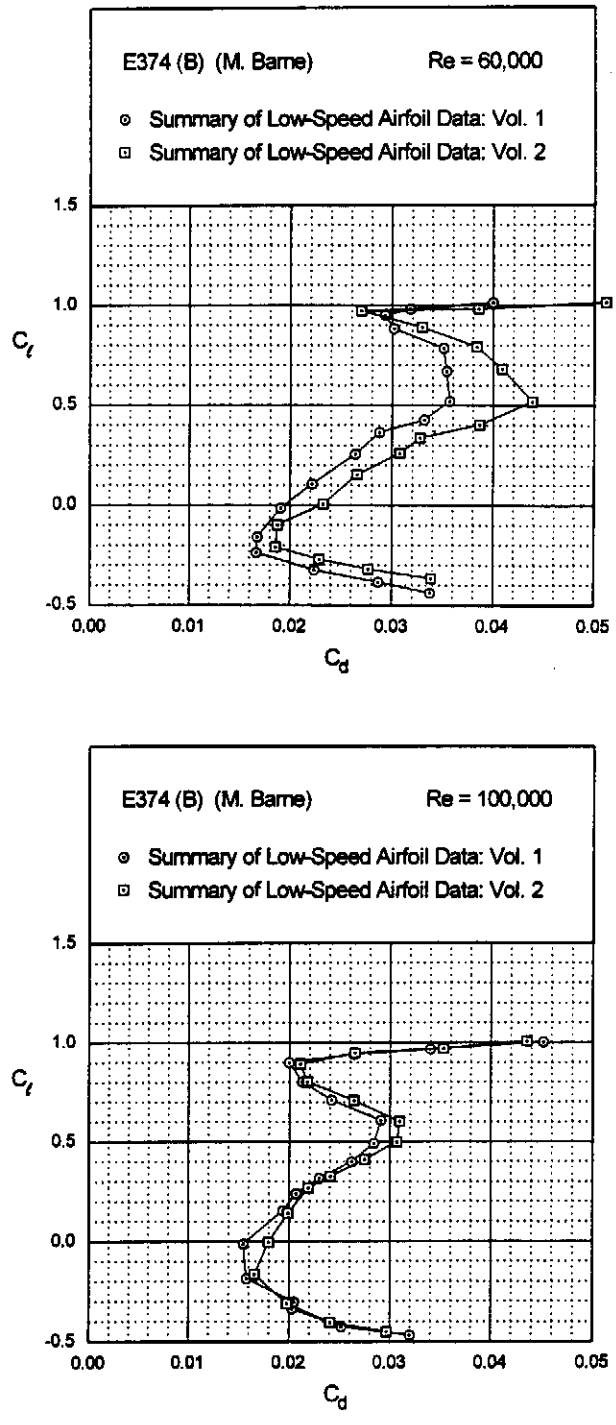

Fig. 2.1 Comparison of drag data for the E374 airfoil with data from Test Series 1 for $Re = 60,000$, 100,000, 200,000 and 300,000.

(figure continues)

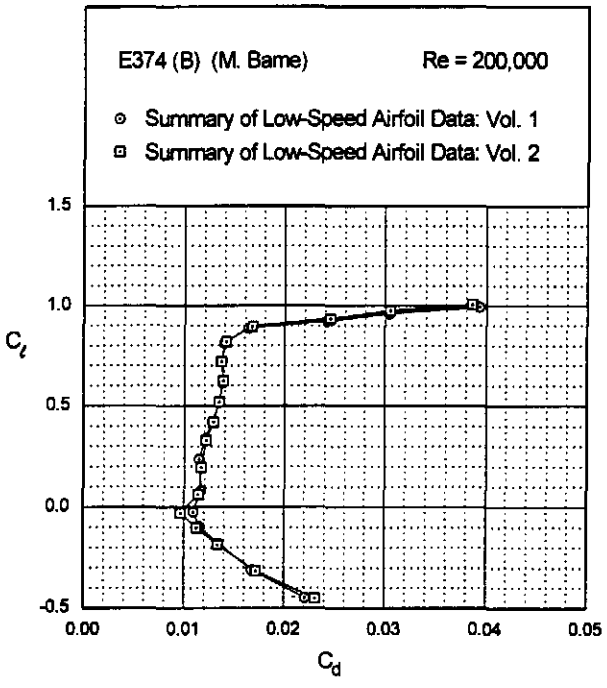

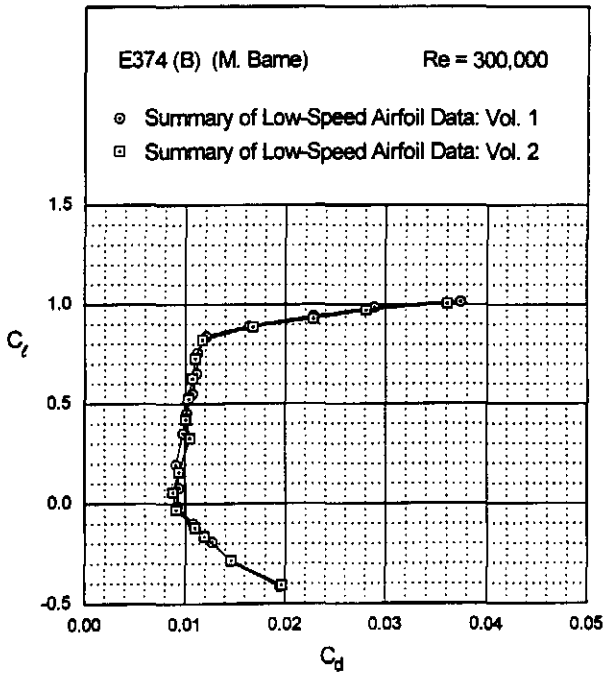

Fig. 2.1 Continued.

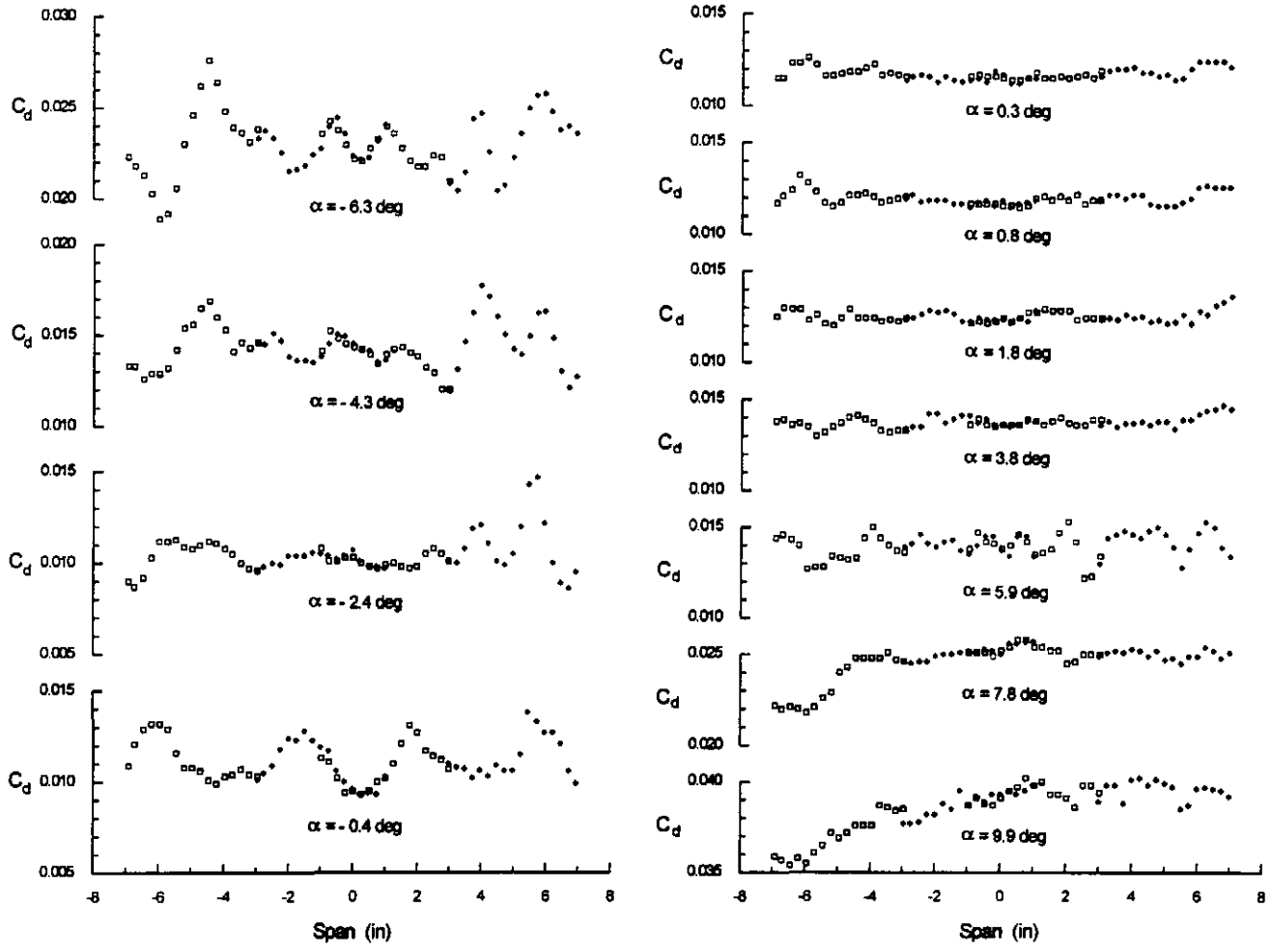

Fig. 2.2 Spanwise drag variation measured in the wake of the E374 (B) for $Re = 200,000$.

the survey, or if multiple surveys are taken, their number and locations. Owing to the intrinsic three-dimensional nature of the nominally two-dimensional flow, there exist opportunities for differences in measurements from one test series to the next. The spanwise variations may change slightly (the cause for the variations is not known), and the location of the wake surveys may differ from one test series to the next. Thus, the differences in the drag data for the E374 (B) are expected, especially near 0 deg angle of attack where the spanwise variations are large.

Lift data for the E374 (B) is given in Fig. 5.16 and shows excellent agreement with the previous test results.[2] Lift measurements were also repeated for the S1223 (see Fig. 5.77), and the results are likewise in agreement with past measurements.

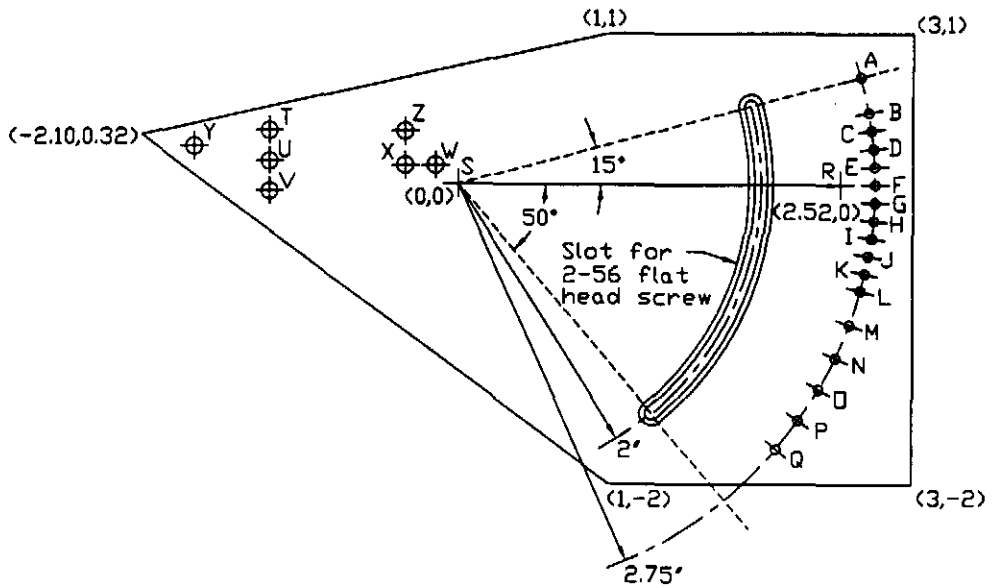

Fig. 2.3 Flap brackets used on the ends of the flapped wind-tunnel models (units are in inches).

2.2 Wind Tunnel Models

Four models tested during the current series were outfitted with a 21% chord flap with a tape hinge along the lower surface of the model. Gap seal (Airtronics Inc. #AIRGAPH100) was used above the hinge line along the top of the model. The tape hinge was quite thin (0.0025 in), and the gap seal was 0.005 in thick. The gap seal had a width of 1 in, and the front edge was located at the 73% station. As to be discussed in Chapter 4 (see S7012 discussion), the gap seal was thick enough to affect transition much like that of a boundary-layer trip. For a given setting, the flap was held in place by 0.090 in thick brackets (see Fig. 2.3) mounted flush on the ends of the model. For reference, point R in the figure is the trailing edge (for a 21% chord flap), and S is the hinge point. Points T–Z are mounting holes, two of which were used for any given model. Index holes in the brackets were drilled to allow for flap settings of −15, −10, −7.5, −5, −2.5, 0, 2.5, 5, 7.5, 10, 12.5, 15, 20, 25, 30, 35 and 40 deg. Only the 0, 5 and 10 deg settings were used during the current test series.

Chapter 3

Computational Methods and Validation

With the broadening scope of the UIUC LSATs, which now also includes airfoils for R/C powered aircraft as well as airfoils for small wind turbines, there is a need for airfoil data beyond the current test capability, which is limited to Reynolds numbers less than 500,000. A change in the present experimental setup to allow for testing at higher Reynolds numbers would require major and costly modifications. A more convenient way to achieve the same goal is to rely on computational airfoil analysis and design codes.[5–9] With recent improvements in this field, it is now possible to obtain fairly accurate aerodynamic characteristics of airfoils in a straight forward manner. Already in the first volume of *Summary of Low-Speed Airfoil Data*, some computational results obtained with XFOIL[9] were presented for the S8052, an airfoil designed for Quickie 500 pylon racers. Furthermore, the pitching-moment data presented to date has been obtained using computational tools. In addition, computational airfoil analysis tools are currently used to provide velocity distributions in the *Summary of Low-Speed Airfoil Data* book series.

Of course, differences between experimental and computational data do exist, especially in the stall region and at fairly low Reynolds numbers. Consequently, some care must be taken when interpreting airfoil data obtained from numerical tools. Nonetheless, computational results should become increasingly important in the future volumes of *Summary of Low-Speed Airfoil Data*, and accordingly the objective of the present chapter is to provide some insight into the computational tools used, in particular, XFOIL. In this chapter, a general description of XFOIL will be provided. Then a discussion of the velocity distributions will be given followed by several comparisons between experimental and computational results at low Reynolds number. Finally, it should be mentioned that the Eppler code[5,6] is also used extensively, but no discussion of that code is given here.

3.1 General Description of XFOIL

The computer program XFOIL is an interactive/user-friendly design and analysis package for isolated subsonic airfoils. Other programs, such as the Eppler code,[5,6] have similar capabilities, while others, such as PROFOIL,[10,11] are solely

used for design purposes. For the time being, only the analysis mode of XFOIL will be described. Brief discussions of PROFOIL and the Eppler code were previously given in the Notes section of *Summary of Low-Speed Airfoil Data, Volume 1.*

XFOIL uses a linear-vorticity stream-function panel method coupled with a viscous integral formulation that allows for the analysis of airfoils with free or fixed transition, separation bubbles, blunt trailing-edges, and limited trailing-edge separation all over a range of Reynolds numbers and Mach numbers. XFOIL provides lift, drag and pitching-moment data, pressure and velocity distributions, and boundary-layer characteristics such as the displacement and momentum thickness developments along the airfoil surface. Transition can be fixed or predicted by a built-in transition criterion partly based on the e^n method of predicting transition.

3.2 Velocity Distributions

The goals for this volume of *Summary of Low-Speed Airfoil Data* are twofold. First and foremost, as the title implies, this book serves as a convenient source for low-Reynolds number airfoil data. Acting as a supplement to this data, the second goal is to educate the reader regarding fundamental problems associated with low-Reynolds number aerodynamics and the computational tools used to predict them. To fulfill this second goal, a change has been made in the contents of the current volume by replacing each airfoil inviscid velocity distribution with its viscous one calculated using XFOIL. In doing so, the reader will hopefully attain a better understanding of effects of viscosity on airfoil performance.

As a result of the very complicated nature of viscous aerodynamics, interpreting viscous velocity distributions can be a difficult task. Because of this, the information that follows is only a small part of a much larger picture. It will suffice, however, in explaining the fundamental effects of viscosity.

Figure 3.1 shows a comparison between the E374 viscous ($Re = 100,000$) and inviscid velocity distributions for a C_l of 0.5. As would be expected, the presence of viscosity has resulted in a small but discernible change over a large percentage of the distribution. This change is a consequence of the growing boundary layer along the airfoil surface. To be more accurate, it is a result of changing surface pressures associated with boundary-layer streamline deflections. Aerodynamicists find it convenient to define a new airfoil geometry that matches these deflected streamlines. The resulting change in airfoil geometry at a given location is known as the displacement thickness, and it is directly attainable from the local boundary-layer velocity profile. Simply put, differences between the two distributions are a result of displacement thickness effects.

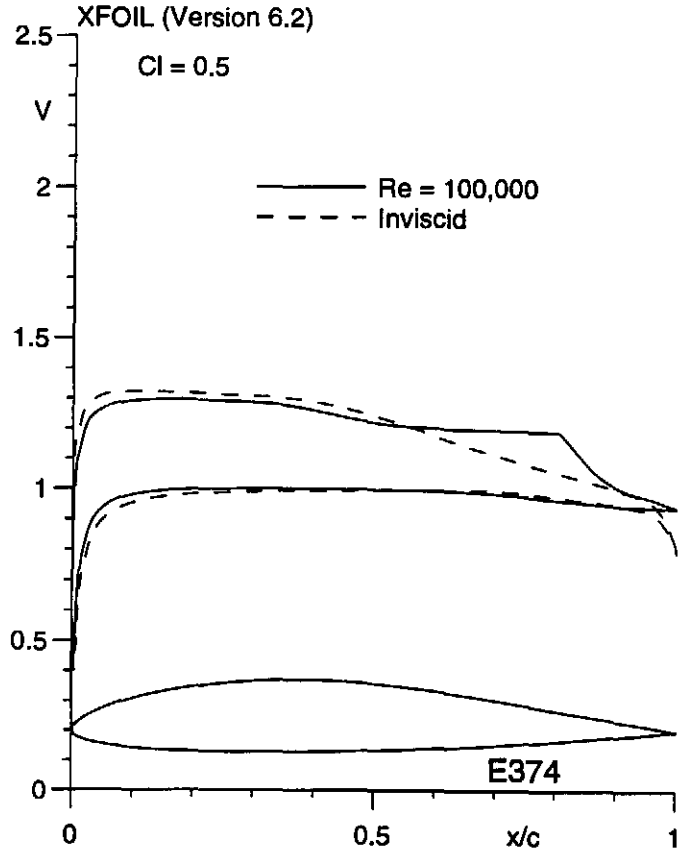

Fig. 3.1 Comparison of viscous and inviscid distributions for E374 at $C_l = 0.5$.

When flow separates from an airfoil, large changes occur in its velocity distributions—changes that can not be attributed solely to the effects of displacement thickness. Instead, more complicated theories must be used, which are beyond the scope of this discussion. It is a simple matter, however, to identify the presence of separated regions and make rough estimates concerning whether drag increases will be negligible or significant.

A separated region can be identified by unexpected areas of constant pressure. (On a velocity distribution, constant pressure is seen as constant velocity.) Upon inspection of Fig. 3.1 and using the previous criterion, it becomes obvious that a separated region exists just aft of 50% chord. Now that a separated region has been identified, the question should be posed: "Is this a region of laminar or turbulent separation?" Again, using simple inspection, the answer is easy. If the viscous velocity distribution appears to re-converge to the inviscid case, this is a signal that the flow has reattached. Therefore, the separated region has been confined to a limited distance along the airfoil surface—a result that can only occur when separation is laminar. (This assumes a "normal" airfoil geometry.) The flow reattachment is prompted by the onset of transition identifiable by

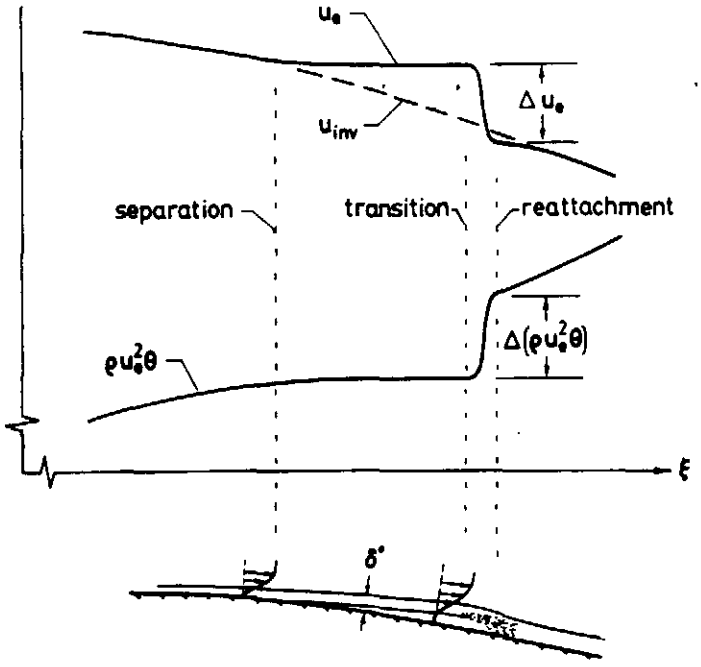

Fig. 3.2 Velocity and boundary-layer characteristics through a laminar separation bubble (taken from Drela[12]).

a rapid decrease in velocity just before reattachment. An exploded view of a laminar separation bubble effect on the velocity distribution is given in Fig. 3.2.

Recognizing turbulent separation is even simpler. Because turbulent separation is unable to reattach under normal circumstances, it is unable to form a separation bubble. Therefore, the separated region persists from the point of separation to the airfoil trailing edge creating an extensive region of constant pressure (velocity).

To estimate the increase in drag due to a laminar separation bubble, a fairly simple relationship between bubble location, bubble size, displacement thickness, and drag needs to be understood. It can be shown that[12]

$$\Delta d = \Delta \rho u_e^2 \theta = \rho u_e \delta^* \Delta u_e$$

This equation allows for the following conclusions to be made: 1) If a separated region occurs at a high velocity (u_e), the associated change in drag will be high; 2) If the displacement thickness (δ^*) is large, drag will be high; 3) If the drop in velocity (Δu_e) associated with reattachment is large, drag will again be high. Whether a bubble occurs at high velocity or has a large decrease in velocity associated with flow reattachment is easy to determine from the velocity distributions. The displacement thickness, however, poses a problem as a result of this limited explanation. It is reasonably safe to assume, however, that displacement thickness increases in size as flow approaches the trailing edge.

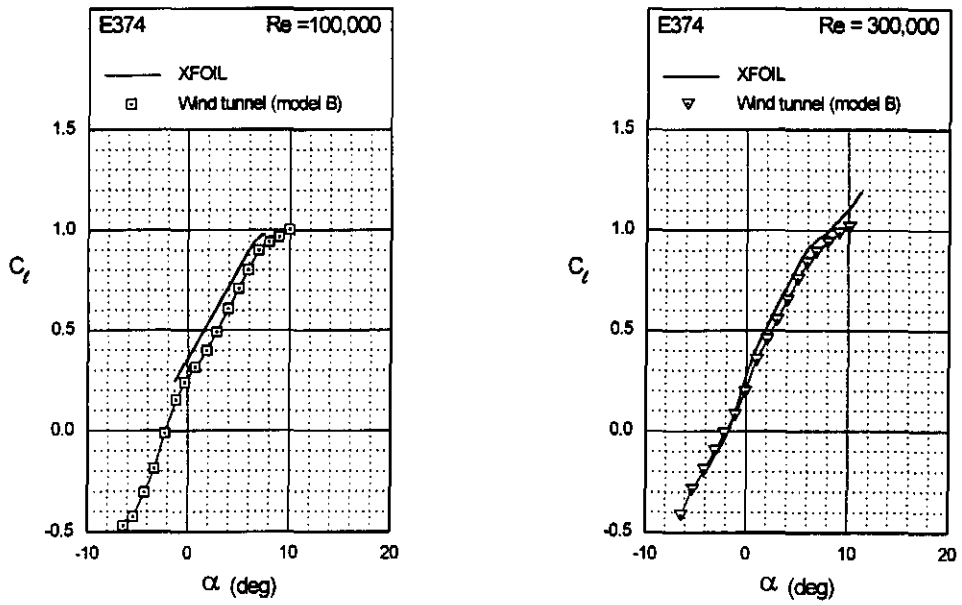

Fig. 3.3 Comparison between the computational and experimental lift curves for the E374, SD7037 and SD7003 for $Re = 100,000$ and 300,000.

(figure continues)

Armed with the information presented in this chapter, interpreting the viscous velocity distributions shown in Chapter 5 should be more straight forward. Also, with the ability to correlate unexpected changes in polars with changes in airfoil pressure distributions, the reader will hopefully gain some insight into the complicated nature of airfoil aerodynamics.

3.3 Computational vs. Experimental Results

In this section, the computational and experimental results will be compared for the E374, SD7037 and SD7003 airfoils, which as a group represent a range of performance owing to varying degrees of laminar separation. As seen from the drag polars and viscous velocity distributions of these airfoils shown in Chapter 5, the E374 generates relatively large separation bubbles while the SD7037 and the SD7003 are less affected by this phenomenon at the Reynolds numbers tested. Lift and drag data were obtained from XFOIL for Reynolds numbers of 100,000 and 300,000. Unless indicated, the computational results were obtained using $n = 9$, where n is the parameter used in the transition criterion. The airfoils were modeled with 200 panels. The experimental results presented in this section are for the E374 (B), SD7037 (C) and SD7003 models listed later in Table 4.1.

As shown in Fig. 3.3, the predicted lift from XFOIL shows fairly good agreement with the experimental data. This is especially true for the results at a

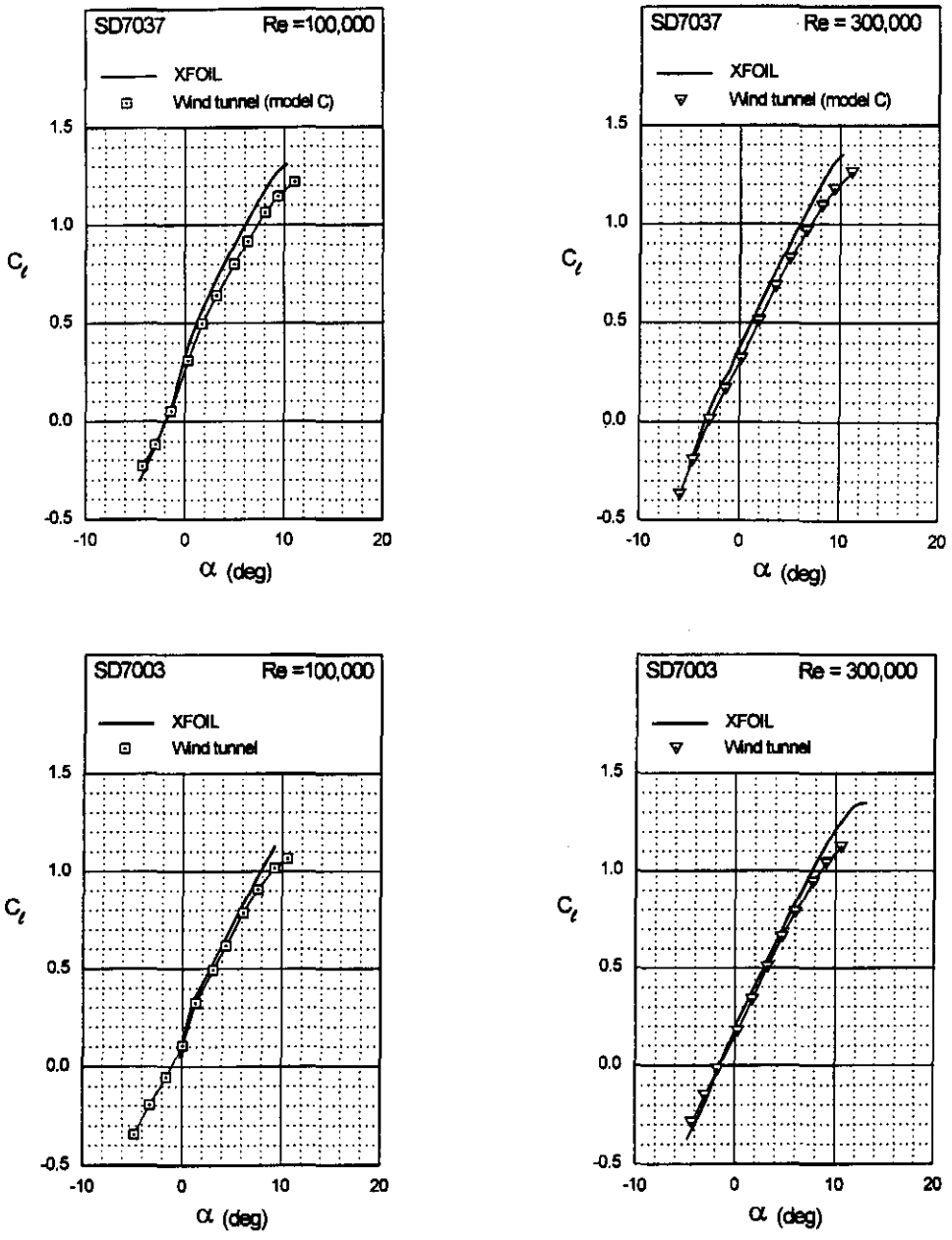

Fig. 3.3 Continued.

Reynolds number of 300,000 where separation bubble effects are not as predominant as in the case of a Reynolds number of 100,000. XFOIL, however, overpredicted the maximum lift coefficient in all cases considered. It is important to note that part of the differences between the computational and experimental results may be attributed to the inaccuracies of the wind-tunnel models as well as the inaccuracies in the wind-tunnel data as described previously.[2] The average difference between the nominal coordinates and the actual model coordinates is

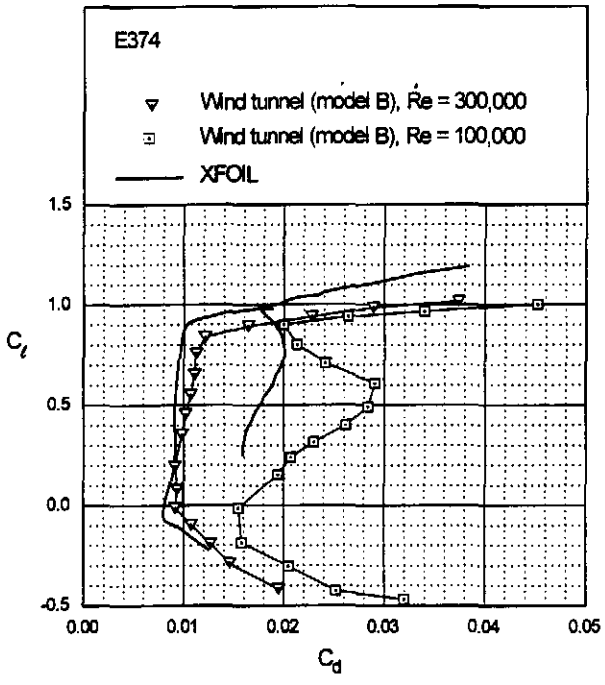

Fig. 3.4 Comparison between the computational and experimental drag polars for the E374, SD7037 and SD7003 for $Re = 100,000$ and 300,000.

(figure continues)

0.008 in for the E374(B), 0.0141 in for the SD7037(C), and 0.0065 in for the SD7003. These differences, however, are probably not a contributing factor to the general bias toward increased lift in the computations. Moreover, the error estimates[2] in the wind-tunnel test results cannot fully account for the discrepancies observed. Note that in regions where the predicted lift curve is incomplete (as in the case of the E374 at a Reynolds number of 100,000) the solution did not converge.

The computational and experimental drag polars are shown in Fig. 3.4. As shown, the differences in the drag data are much greater when compared to the differences in the lift data, especially at a Reynolds number of 100,000. The discrepancies in the drag results can be largely attributed to the difficulty in modeling the complex flow phenomena that occur at low Reynolds numbers. At a Reynolds number of 300,000, XFOIL captures the correct trend in the drag polar and yields fair agreement with wind-tunnel data. For a Reynolds number of 100,000, the larger laminar separation bubbles are a challenge for the drag prediction method of XFOIL. It also appears that XFOIL has more difficulty in predicting the drag of airfoils with large laminar separation bubbles since the drag predictions were better for the SD7003 than the E374, which suffers from larger bubbles. This last statement is also supported by the computational results for the E374 and SD7003 airfoils at a Reynolds number of 100,000. For

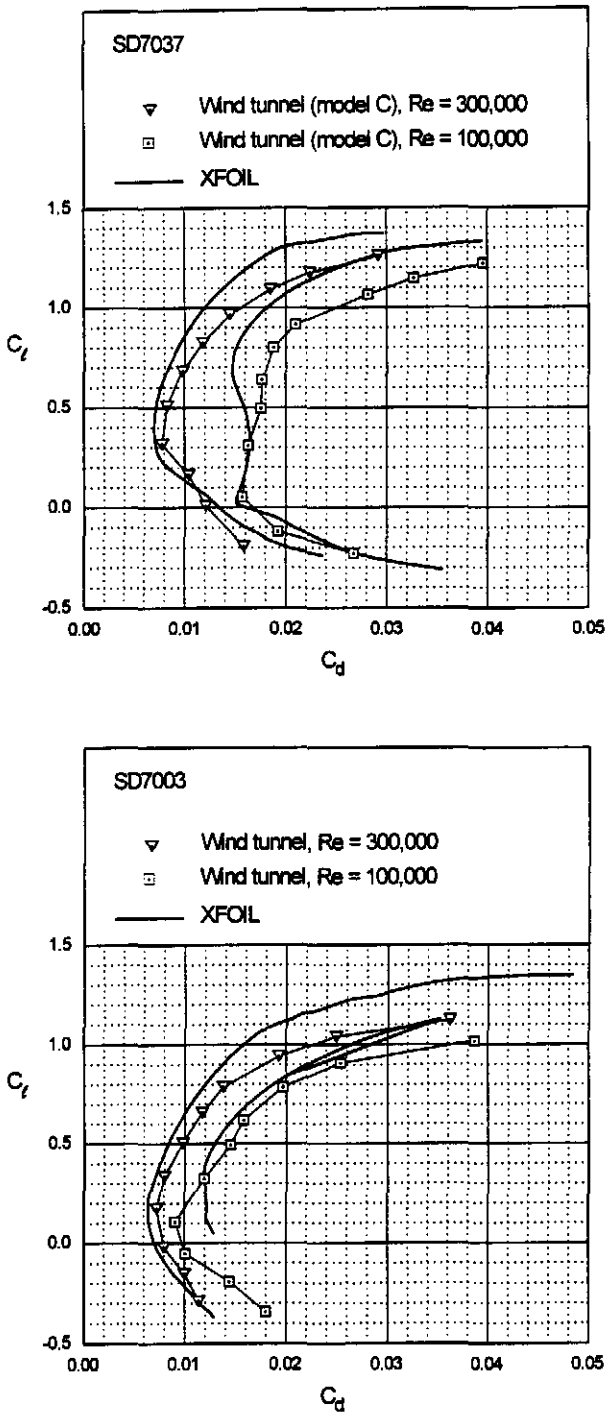

Fig. 3.4 Continued.

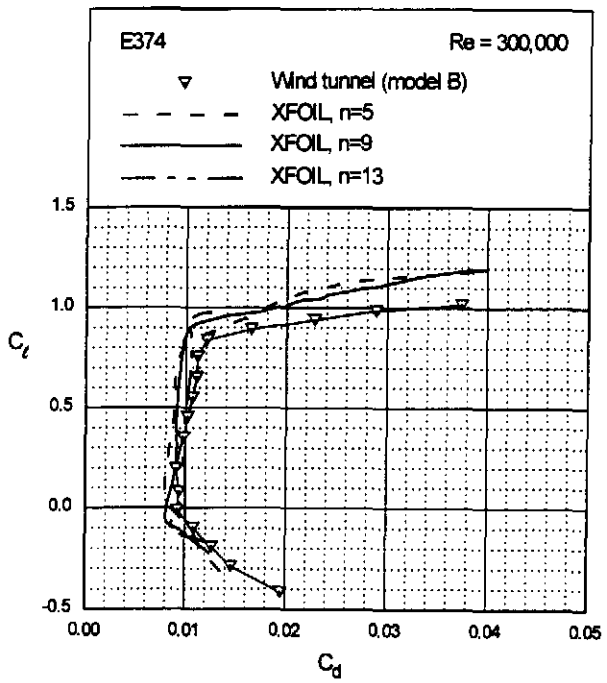

Fig. 3.5 Drag polars obtained from XFOIL with different values of n for the E374 for $Re = 300,000$.

this Reynolds number, XFOIL gives reasonable predictions for the SD7003 while it underestimates the bubble effects on the E374.

As mentioned previously, all the computational results shown so far have been determined using $n = 9$. To show the effect of a change in n, Fig. 3.5 presents the polar for the E374 airfoil at $Re = 300,000$ for $n = 5$, 9 and 13. The predictions for $n = 13$ provided the best agreement with the experimental results for most of the lift range, but the upper limit of the low drag range was over-predicted. A low value for n in the computations, say, $n = 5$, would simulate a wind tunnel with relatively high turbulence in which transition to turbulent flow (with or without laminar separation) would be triggered earlier along the airfoil chord. A high value of n (≥ 9) simulates the opposite effect—lower turbulence and later transition. It is possible to adjust the value for n until predictions best match the experiment. This approach was taken by Evangelista, et al.[13,14] in which they showed that values of n between 13 and 15 predicted the drag well for airfoils with moderate laminar separation bubble formation; whereas, values between 7 and 11 worked well when transition occurred without laminar separation. This rule of thumb seems to be appropriate since, as mentioned above, the best agreement with the experimental data for the E374 was obtained with $n = 13$, and the E374 is known to have moderate laminar separation bubbles much like the E387 studied by Evangelista, et al.

In light of this discussion, it is clear that XFOIL can be used as an effective tool during the design process. The trends predicted are in agreement with the experiments. The code, however, is no substitute for wind-tunnel testing. Nevertheless, as shown in this section, the predictions of XFOIL improve with increasing Reynolds number, and as a result XFOIL can be used to predict performance for Reynolds numbers beyond our existing test capabilities.

Chapter 4

Summary of Airfoil Data

In this chapter, the airfoil performance characteristics are discussed. To aid in the navigation of the data, the airfoils are grouped and discussed by category, e.g., airfoils for free flight models, airfoils for thermal soaring, and so on. The categories in order of discussion are listed in Table 4.1 along with the associated airfoils. Also, for reference, Table 4.1 lists the thickness, camber and pitching moment for the true airfoils, as well as the wind-tunnel model construction method, model accuracy and model builder.

Within each category, the discussion is organized according to how the airfoils relate to each other in terms of performance. Tables are included that list each airfoil in the category. For each airfoil, the table then lists the general configuration tested, e.g., clean, tripped, flapped, etc., and the first figure and page number corresponding to the given configuration. The details of the configuration are shown on the profile plot. Occasionally embedded within the discussion of the airfoils are sections on more general but related topics. These special sections are typeset between centered horizontal rules.

Following the discussion of the airfoils by category in this chapter, all of the figures (airfoil profile and performance plots) are included separately in Chapter 5. The figures are organized alphabetically by airfoil name for quick indexing.

Some general comments apply to the data and discussion.

- As shown in Table 4.1, some of the airfoils listed were previously tested at Princeton[1] or earlier in the UIUC LSATs program.[2] In most cases, these tests were done to ascertain the airfoil performance with boundary trips, flaps, or some other modification from the baseline airfoil previously tested. The baseline data can be found in an earlier reference.
- In *Airfoils at Low Speeds*,[1] the designation "-PT" (for Princeton Tests) was used after the names of the actual airfoils (as tested) to distinguish them from the true airfoils (as designed). In this book, no special designation is applied to the airfoil name to make this distinction between the actual and true airfoil.
- It is important to note that the discussion of each airfoil is based on the actual contour shape of the model. If the average difference between the actual and true airfoil coordinates is large (greater than approximately 0.010 in.

Table 4.1: Airfoils Sorted by Category

Airfoils for:	Airfoil	Thickness (%)	Camber (%)	$C_{m,c/4}$
Free Flight Models	Davis 3R	5.87	5.91	−0.170
	LD-79	5.25	4.11	−0.090
Sailplanes	CR-001	7.32	4.06	−0.120
	DU 86-084/18	8.46	1.12	−0.026
	E374 (B)†	10.91	2.24	−0.056
	MH32	8.71	2.39	−0.058
	RG15 (C)	8.92	1.76	−0.058
	S4083 (A)‡	8.00	3.47	−0.099
	S4083 (B)‡	8.00	3.47	−0.099
	S7012 (B)	8.75	2.02	−0.068
	S7075 (A)‡	9.00	3.05	−0.094
	S7075 (B)‡	9.00	3.05	−0.094
	SD7037 (B)†	9.20	3.02	−0.085
	SD7037 (C)	9.20	3.02	−0.085
Flying Wings	S5010	9.83	2.21	−0.007
Tail Sections	S8025‡	8.00	.49	−0.003
Sport Planes	M6 (65%)	8.20	1.59	−0.027
	M6 (85%)	9.84	2.08	−0.069
	NACA 2414	14.00	2.00	−0.059
	NACA 2415	14.00	2.00	−0.059
Heavy Lift	E423	12.34	9.92	−0.246
Cargo Planes	S1223 RTL	13.36	8.48	−0.248
Small Wind Turbines	S822†	16.00	1.89	−0.070
	S823†	21.00	2.49	−0.150
Airfoils with	M06-13-128 (B)†	12.81	5.16	0.004
Gurney Flaps	MA409†	6.69	3.33	−0.115
	S1223†	11.93	8.67	−0.300
	S7055†	10.50	3.55	−0.068
	SD7037 (C)	9.20	3.02	−0.085

† Wind-tunnel models previously tested (see Refs. 1 and/or 2).
‡ New airfoils designed and built for the current test series.

depending on the model), then the interpretation of the true airfoil performance from the wind-tunnel test data might be difficult. The accuracy of the lower surface is not as critical as that of the leading and trailing edges and the upper surface. The useful lift range is most affected by differences at the trailing edge, while inaccuracies along the upper surface contour influence pressure (bubble) drag. If the top or bottom surface error of the actual airfoil is uniformly thicker or thinner than the true, then the wind-tunnel indicative of

Table 4.1: continued

Airfoil	Surface Finish	Avg. Difference (in)	Builder
Davis 3R	tissue over balsa	0.0023*	Cole
LD-79	silk over balsa	-	DeWitt
CR-001	smooth	0.0048*	Robertson
DU 86-084/18	smooth	0.0183	Adams
E374 (B)	smooth	0.0083	Bame
MH32	smooth	0.0117	Tonnesen
RG15 (C)	obechi/monokote	0.0101	Champine/Robertson
S4083 (A)	smooth	0.0033	Levoe
S4083 (B)	smooth	0.0170	Thomas
S7012 (B)	smooth	0.0066	Lachowski
S7075 (A)	smooth	0.0053	Robertson
S7075 (B)	smooth	0.0128¶	Thomas
SD7037 (B)	smooth	0.0081	Thompson
SD7037 (C)	smooth	0.0141	Brengman
S5010	smooth	0.0251	Wilson
S8025‡	smooth	0.0046	Thurmond
M6 (65%)	smooth	0.0117	Spychalla
M6 (85%)	smooth	0.0199	Spychalla
NACA 2414	monokote	0.0044	Bozzonetti
NACA 2415	smooth	0.0138	Imes
E423	monokote	0.0189	Glaze/Lazor
S1223 RTL	smooth	0.0059	Levoe
S822	smooth	0.0054	Allen
S823	smooth	0.0073	Allen
M06-13-128 (B)	smooth	0.0112	Allen
MA409	smooth	0.0195	Cooney
S1223	molded, smooth	0.0100	Tinel
S7055	smooth	0.0160	Jones
SD7037 (C)	smooth	0.0141	Brengman

* Smoothed model coordinates were taken as true coordinates.
¶ Does not reflect true model accuracy. See airfoil discussion.

test results will be more the true airfoil than if the error were nonuniform (wavy) along the chord. A wavy error in the airfoil contour will produce a wavy velocity distribution (relative to the true airfoil), which may significantly alter the transition behavior relative to the true airfoil.

- The suffixes "(A)", "(B)", etc. on the airfoil names refer to multiple models of the particular airfoil. If only one version previously existed and another

one was built for the current tests, the models are designated here as versions "(A)", "(B)", etc.

- Coordinates for the airfoils are tabulated in Appendix A. The performance characteristics are tabulated in Appendix B and ordered according to the airfoil name and figure. This data is available in various forms as mentioned in the Airfoil Data Distribution section.
- For some airfoils, the wind-tunnel model coordinates were mathematically smoothed (using the computer program AFSMO[15]) and taken as the true airfoil since no "as designed" true airfoil coordinates were available. In such cases, the smoothed wind-tunnel model coordinates were then compared with the actual model coordinates as measured. These airfoils are identified in Table 4.1 by the notation "*" in the column for accuracy. As the comparison plots reveal (see Chapter 5), the differences between the smoothed and actual coordinates are nominally 0.003 in, which in some sense is a measure of the surface waviness.
- The nominal Reynolds numbers are listed in the figures while the actual Reynolds numbers are listed in the tabulated data in Appendix B.
- If a model was tested with a boundary-layer trip or modified in some other way (e.g., plain flap, Gurney flap), the configuration of the model is listed in the data summary table and drawn on the related figures.
- The airfoil moment coefficients listed in Table 4.1 were determined computationally using either the Eppler code,[5] ISES[7,8] or XFOIL.[9] The values given are for the airfoils without flaps and are representative of the value over the low drag range.
- In Table 4.1, in the column for surface finish, "smooth" indicates that the model finish was produced by smooth fiberglass over foam (via vacuum bag technique). Monokote listed in the table is a smooth mylar covering.
- Although the airfoils are categorized by application, the airfoils, of course, can have a wider application. For example, some airfoils might fit equally well into two groups or more.
- For airfoils that were previously tested in the program, the discussion is sometimes brief, in which case a more thorough discussion of the airfoil can be found in the appropriate reference(s) indicated in Table 4.1.
- Velocity distributions for the true airfoils as predicted by XFOIL[9] are included with the airfoil polars, lift plots, etc. For each case, the velocity distributions correspond to the clean airfoil (i.e., no boundary-layer trips or roughness) without flaps at a Reynolds number of 200,000 with $n = 9$. Throughout, solid lines is used to denote the viscous XFOIL velocity distri-

Table 4.2: Various Trip Geometries Used During Test Series 2

Trip Name	Airfoil	Trip Geometry		Also See
		Top View	Height	Fig.
Plain	Davis 3R	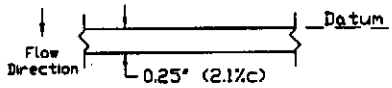	0.018 in 0.15%c	5.6
Plain	S7075	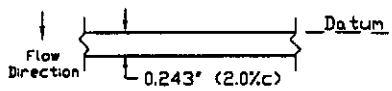	0.020 in 0.17%c	5.111
Plain	S822	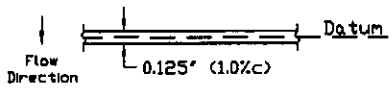	0.0225 in 0.19%c	5.66
Zig-Zag Type C	S822 S823	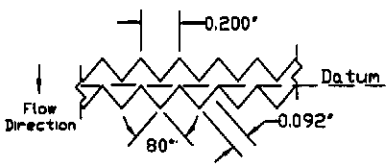	0.0225 in 0.19%c	5.66 5.72
Zig-Zag Type D	S7075	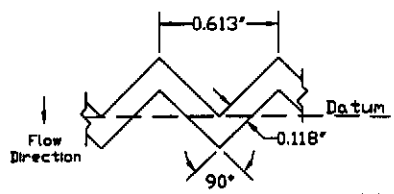	0.030 in 0.25%c and 0.047 in 0.39%c	5.111

butions, while the dotted lines are used for the inviscid velocity distributions predicted by the Eppler code.[5] With experience (see Chapter 3), much can be gleaned from this information to help interpret the airfoil polars and lift curves.

- For the lift plots, increasing and decreasing angles of attack are denoted by solid-triangle and open-circle symbols, respectively.
- For the LD-79 model listed in Table 4.1, no value is given for the model accuracy. For this airfoil, only the actual model coordinates are plotted in Chapter 5 and subsequently listed in Appendix A. The true model coordinates were not available and smoothing the actual model coordinates would have been difficult.
- Finally, Table 4.2 includes drawings for the various trips used on the models mentioned in this volume. The locations of the trips are drawn together with the airfoil geometry in Chapter 5.

4.1 Airfoils for Free Flight Models

Table 4.3: Summary of Airfoil Data for Free Flight Models

Airfoil	Configuration	Figures Begin
Davis 3R	Tripped	Fig. 5.5, p. 54
LD-79	Clean; 0 deg flap	Fig. 5.21, p. 70

Davis 3R & LD-79 These airfoils have been used on free-flight rubber-powered F1B (Wakefield) models named after Lord Wakefield who initiated the Wakefield Trophy in 1928. F1B is the oldest of the international free flight events. Models typically have wing areas of 275 in^2 and weigh 190 grams in addition to 40 grams for the rubber motor, which results in an operating Reynolds number range of 25k–80k.

Henry Cole, a Hall of Fame member of the NFFS (National Free Flight Society) and aeronautical engineer, developed a series of model airfoils in the 1940's using the Davis formula which (in an interesting story[16]) was used to create the Davis airfoil employed on the B24 bomber. For Wakefield models, airfoil No. 3 has been his favorite, and it was used on his HC17 TILTWING, Model of the Year, described in the NFFS 1992 Symposium Report.[17] The Davis 3R, now his favorite, is the same except that the top surface has been rotated (whence the "R" designation) about the leading edge to produce a 1.3% chord thick trailing edge; whereas, the No. 3 has a sharp trailing edge. The airfoil is also reported as having good performance with a sharp *leading edge*.

The airfoil makes use of Pfenninger strips, or multiple boundary-layer turbulators, which were made out of 4 layers of masking tape (making them 0.018 in thick) and placed at 28.1%, 42.4%, 54.4%, 65.4% and 76.3% chord as depicted in Fig. 5.6 (also see Table 4.2). The performance is shown in Fig. 5.7. The airfoil has particularly encouraging high-lift performance at the lower *Re*'s representative of F1B conditions. No other airfoil in the current series developed lift-to-drag ratios as high as this airfoil for *Re*'s of 40k, 60k and 100k.

The sharp leading-edge/blunt trailing-edge LD-79 airfoil designed by Les DeWitt was used on his quite successful ICONOCLAST Model of the Year, which won many contests during the mid to late 70's.[18] It was the product of extensive flight tests on 30 wings with different airfoils and various turbulator combinations.

The LD-79 airfoil was only tested with the flap in the 0 deg position, which is used at the start of the near vertical climb. Gradually (over the first 10 sec of a 40 sec motor run), the flap droops to a 10 deg position, which was not tested during this series. Although the airfoil was not tested with the flap deflected for better comparison with the Davis 3R, it is interesting to note that the overall level of the drag is quite comparable to the Davis 3R. Thus, it can be speculated that

with the flap deflected, the performance might prove comparable to the round leading-edge Davis 3R. This airfoil challenges the conventional wisdom that the all good airfoils have round leading edges and sharp trailing edges. Finally, the airfoil shown in Fig. 5.22 is for the actual model since the comparison program could not properly deal with the sharp leading edge.

4.2 Airfoils for Sailplanes

Table 4.4: Summary of Airfoil Data for Sailplanes

Airfoil	Configuration	Figures Begin
CR-001	Clean	Fig. 5.1, p. 50
DU 86-084/18	Clean	Fig. 5.9, p. 58
E374 (B)	Clean	Fig. 5.13, p. 62
MH32	Clean	Fig. 5.41, p. 90
RG15 (C)	Clean (obechi case); 0 deg flap	Fig. 5.53, p. 102
	Clean (smooth case); 0, 5, 10 deg flaps	Fig. 5.57, p. 107
S4083 (A)	Clean	Fig. 5.82, p. 134
S4083 (B)	Clean	Fig. 5.86, p. 138
S7012 (B)	Clean; 0, 5, 10 deg flaps	Fig. 5.94, p. 146
S7075 (A)	Tripped; 0 deg flap	Fig. 5.110, p. 164
	Tripped; 0 deg flap	Fig. 5.114, p. 169
	Tripped; 0, 5, 10 deg flaps	Fig. 5.118, p. 176
S7075 (B)	Tripped; 0 deg flap	Fig. 5.124, p. 184
SD7037 (B)	Clean; 0, 5, 10 deg flaps	Fig. 5.132, p. 192
SD7037 (C)	Clean	Fig. 5.142, p. 204

The R/C sailplane airfoils discussed in this section cover a wide range, from hand launch to thermal soaring to F3B.

CR-001 & S4083 The Cody Robertson CR-001 and the new S4083 were designed for R/C hand-launch competition. Since pilots (in the U.S.) are allowed to change gliders during a hand-launch contest, a suite of wings should be used: a low-speed wing for low winds conditions, a moderate-speed wing for moderate winds, and a high-speed wing for high winds. As the data will show, the S4083 should prove best for use in windy conditions, while the CR-001 is better suited for lighter winds.

R/C hand-launch gliders typically operate at a reduced Reynolds number ($\mathcal{R}= Re\sqrt{C_l}$) of near 80,000. Thus, for $C_l = 1$, the aircraft operates at Re of

80k, and for $C_l = 0.4$ the Re is approximately 125k. A discussion of the reduced Reynolds number is given in Ref. 2.

For thermal speeds corresponding to high-lift conditions ($C_l = 1$, $Re = 80$k), the CR-001 has a clear advantage over the S4083; whereas, at cruise speeds ($C_l = 0.4$, Re =125k), the S4083 has an advantage. As a result, the S4083 should penetrate upwind faster and sink less in the process. For the cruise condition, the S4083 is also an improvement over two other popular R/C hand-launch airfoils—SD7037 and E387. As with the CR-001, the SD7037 and E387 are better than the S4083 for thermalling.

SD7037 The SD7037 along with the RG15, S7012, S7075 airfoils—all applicable to R/C sailplanes—were each tested with flaps. Flaps (driven through the use of a computer radio) have become standard equipment in nearly all classes of R/C soaring competitions. More recently, camber-changing flaps have also been used on 60 in span R/C hand-launch gliders that typically weigh under 15 oz. Thus, the need for accurate data for airfoils with flaps has been great.

Optimum Flap Settings for R/C Sailplanes A particular question in R/C soaring that needs to be addressed deals with determining the optimum flap/camber settings for given speeds in several different flight modes, namely, launch, speed, cruise, thermal, and landing. The problem viewed in this general scope has not been fully addressed in the past for two reasons. First, flap data on low Reynolds number airfoils was rare and for popular R/C soaring airfoils nonexistent (with the exception of the E214[1]). Second, the mixing features in computer radios were often limited to linear coupling. For instance, the coupling between the elevator (speed control) and camber was a specified constant (a percentage), e.g., 2 deg of elevator gave 1 deg of flaps/camber and 4 deg of elevator gave 2 deg of flaps/camber. Recent advances in computer radios have now made it possible to specify nonlinear mixing functions to optimize, for example, the elevator-to-camber mixing.

The problem of determining the best elevator-to-camber mixing could be approached as follows. A series of lift coefficients in, say, 0.05 increments from cruise to thermal could be selected. For each given lift coefficient, the optimum flap setting could be determined graphically from the wind-tunnel test data. The corresponding pitching moment data could then be used to determine the required elevator angle for trimmed flight. A plot of flap setting vs. elevator angle for trim could then be created and programmed into the computer radio. Then as the elevator angle is changed (through the joystick), the optimum flap angle is set automatically for the lowest drag condition. A more detailed discussion of this topic goes beyond the scope of this book.

The SD7037 is widely used on R/C sailplanes with flaps for camber changing, launch and landing. To measure the effects of flaps, the SD7037 (B), which was tested during Test Series 1, was retrofitted with a 21% chord flap described in Chapter 2. Figures 5.132–5.141 show the effects of flap settings at 0, 5 and 10 deg. The results show an improvement in thermal performance ($C_l \geq 1.0$) for a 5 deg flap deflection, but there is no additional advantage for the 10 deg case. The data on the SD7037 will be used somewhat as a basis for comparison in the discussion of the other three flapped airfoils. (It should be noted that the plot of the actual profile is for the original model without the flap.)

Two characteristic trends can be observed in the data. These features are also seen in the data on the other airfoils to follow. First, the stall angle of attack decreases slightly with an increase in the flap deflection. The reduction in angle of attack can be understood by considering the airfoil 0.5–1.0 deg below the stall angle with no flap deflection. As the flap is then deflected the flow will eventually separate for the lower angle of attack, thereby causing an earlier stall with flap deflection.

Second, at low Reynolds numbers as the flap angle is increased, the loss in lift at the low angles of attack occurs over a wider range. For instance, at *Re* of 60k with 0 deg flap, there is a loss in lift up to an angle of attack near 2 deg; whereas, for the 5 deg flap case, the loss in lift extends to 4 deg angle of attack. This feature can be explained as follows. Consider the *Re* of 60k case only. With no flap deflection, the loss in lift at low angles of attack is attributable to a large bubble that produces a large boundary-layer thickness, which thereby effectively de-cambers the airfoil. The large bubble is primarily caused by transition relatively far aft on the airfoil. When the flap is deflected, the pressure gradients on the airfoil cause transition to happen far aft on the airfoil for higher angles of attack relative to the 0 deg flap case. Thus, the late transition/large bubble again produces a de-cambering effect and the associated loss in lift, but this time over a wider range in angle of attack.

RG15 The RG15 (C) model was first tested with a varnished obechi sheeting and then with Top Flite MonoKote mylar covering to examine the effects of wood-grain roughness on performance. The results in Figs. 5.53–5.56 show that for $C_l < 0.5$–0.6 the varnished obechi sheeting enhances the performance as compared with smooth mylar covering. In particular, in the range $0 < C_l < 0.2$, the drag reduction at the higher *Re*'s (200k and 300k) is as great as 8% in some areas.

As the angle of attack increases toward stall, the rough case shows at the lower *Re*'s (60k and 100k) a greater loss in lift than for the smooth case. The greater loss in C_l for the rough case could be caused by a de-cambering effect resulting from a more rapid growth in the boundary-layer thickness. If this hypothesis were true, the thicker boundary layer would logically be assumed to be caused by the rough wood-grain surface. A thicker boundary layer, however, is associated with

higher drag for a given angle of attack—a fact that is not observed in the data. To better understand the effects of "distributed roughness," such as that due to wood-grain roughness, work in this promising area should continue.

The effect of flaps for the smooth RG15 are shown in Figs. 5.57–5.64. A discussion of these results is included with the S7012 airfoil discussion to follow.

S7012 The S7012 (B) model is a refurbished version of the S7012 tested previously. An average improvement of 0.001 in was achieved in the process during which the model was also equipped with a flap. For the 0 deg flap case, the results compare well with the previous tests, except at the lower lift coefficients where the drag of the flapped model is higher. A similar trend is seen with the smooth RG15 (C) model as compared with the RG15 (B) tested during the last series. It should be noted, however, that the RG15 (B) and (C) versions were two distinct models that differed more than the previous S7012 and the current modified version. It may be that the mylar gap seal on the upper surface promotes transition too early at the lower lift coefficients in which case a thinner gap seal would be preferred.

For the 0 deg case, the results from the RG15 (C) and S7012 (B) are consistent with the conclusions stated in *Summary of Low Speed Airfoil Data, Volume 1* and will not be restated here in any great detail. Briefly, the S7012 is better than the RG15 at low C_l's for speed and high C_l's for duration. The improvements in speed noted in *Volume 1* are, however, now smaller since the airfoils are both equally influenced by the gap-seal trip at 73% chord.

For flap deflections of 5 and 10 deg, the S7012 has lower drag than the RG15 over most of the C_l-range greater than 0.9. The lower drag is particularly noticeable at the higher Re's. Thus, the S7012 may have an advantage in relatively high-speed turns such as those experienced in the F3B distance and speed tasks.

S7075 The S7075 is a new airfoil designed to take advantage of a boundary-layer trip from the outset; that is, the trip was considered during the airfoil design process. A detailed discussion of the design philosophy will be delayed for a later book because the problem is still a "work in progress." Nevertheless, the objectives of the current work will be briefly stated.

In the past, boundary-layer trips on low Reynolds number R/C sailplane airfoils have typically been used as an afterthought in an attempt to fix or "repair" an otherwise poorly performing airfoil. In such cases, the performance almost invariably improves over a narrow range of the drag polar, but overall the performance is often degraded relative to the the best performing clean airfoils. The improved performance over what has been a narrow range has spurred the current interest in trying to design an airfoil with a trip that functions effectively over the entire operating range. Such an airfoil with an optimized trip could perhaps prove superior to the best current clean airfoils now used as benchmarks for comparison, such as the SD7037.

The S7075 was designed for R/C thermal soaring, and the trip location was set at 68% chord. The idea behind placing the trip so far aft can be explained as follows. When no trip is used, the bubble ramp on the upper surface is tailored so that the bubble starts far aft at low angles of attack and moves forward toward the leading edge until the airfoil stalls. Thus, the entire upper surface serves as a bubble ramp to promote transition. In the current philosophy, the bubble ramp and the trip assume more or less an equal role in promoting transition. At low angles of attack, the trip placed far aft on the airfoil acts to promote transition; whereas, for higher angles of attack the bubble ramp causes transition. Thus, the bubble ramp can be better tailored to operate over a narrower range while the trip promotes transition over the remainder of the operating range. These ideas were integrated into the S7075 during the design process.

Although the trip location at 68% is thought to be near the optimum based on predictions, the height and type of trip were determined experimentally. The existing guidelines for determining the best trip size and type are often misleading. Thus, a simple parametric study was done to set the trip type and height. Figures 5.112, 5.114 and 5.116 for the S7075 (B) show the performance with a 0.020 in high plain 2D trip and a 0.030 in and 0.047 in high zig-zag trip (type D), respectively. The 0.030 in high zig-zag trip was the most effective.

The 0 deg flap case with the 0.030 in high zig-zag trip can be compared with the SD7037 (B) results (Fig. 5.134). The tripped S7075 is an improvement over the SD7037 for reduced Reynolds numbers $\mathcal{R}$ of near 100k, which is a typical value for R/C sailplanes. These results are quite encouraging in light of past results[1,2] that showed improved performance over only a narrow range. When camber-changing flaps are deployed, however, the results are not as promising. The thermal performance is not as good as that of the SD7037 (B). Thus, the airfoil in its current configuration is not recommended. An effort to develop a more efficient trip is currently underway. Specifically, distributed roughness such as that produced by obechi wood grain (see RG15 discussion) holds promise.

The performance of the S7075 (B) is not as good as the more accurate A version. Referring to the model accuracy plot (Fig. 5.125), the airfoil is too thick on the forward upper surface and thinner toward the flap. This shape produces a stronger adverse pressure gradient than designed and consequently a larger bubble drag. Owing to a slightly reflexed flap (corresponding to the neutral 0 deg setting), the overall accuracy of the model is better than the indicated 0.0128 in. The effect of the reflexed flap can be seen in the zero lift angle of attack as compared with that of the A version.

DU 86-084/18 This airfoil, discussed in more detail in Ref. 19, was designed to take advantage of zig-zag boundary-layer trips at 67% chord on the upper surface and 78% on the lower surface. The airfoil was tested without trips owing to time constraints. Nevertheless, the drag at the lower *Re*'s (60k and 100k) is comparable to many other airfoils. At the higher *Re*'s (200k and 300k), however,

the steep pressure recovery results in a relatively large bubble and high drag. The relatively narrow lift range is expected since the airfoil is intended to be used with flaps.

MH32 The specific design requirements for the Martin Hepperle MH32 are not known to the authors. Based on the airfoil thickness and lift range seen in the polars, however, it clearly has application to R/C sailplanes.

4.3 Airfoils for Flying Wings

Table 4.5: Summary of Airfoil Data for Flying Wings

Airfoil	Configuration	Figures Begin
S5010	Clean	Fig. 5.90, p. 142

S5010 This airfoil, together with the thinner S5020, was designed for flying wings where a near zero pitching moment is usually desirable. The pitching moment requirement does constrain the airfoil performance. For instance, as compared with the S7012, which has a similar lift range, the drag of the S5010 is almost everywhere slightly higher.

4.4 Airfoils for Tail Sections

Table 4.6: Summary of Airfoil Data for Tail Sections

Airfoil	Configuration	Figures Begin
S8025	Clean	Fig. 5.128, p. 188

S8025 The 8% thick S8025 is a slightly cambered airfoil designed for horizontal tails, in particular, full-flying stabilators. The airfoil, however, also has application to conventional elevator-type tails. When used on a down-loaded horizontal tail, the airfoil should be place upside down with respect to its orientation as shown in the figures.

Cambered airfoils for use on horizontal tails are desirable for two reasons. First, past work on symmetrical airfoils has shown that a deadband often appears in the lift curve near zero degrees. This nonlinearity can lead to undesirable longitudinal handling characteristics. Interestingly, cambered airfoils do not appear to have a similar, intrinsic deadband region. Second, symmetrical airfoils produce symmetrical lift characteristics that are not required because, for the most part, a download on the tail is required for normal trimmed flight. Thus, the tail airfoil should be designed around the non-zero tail download condition.

From the lift characteristics, the nonlinearity about 0 deg is significantly reduced as compared with the symmetrical SD8020 airfoil.[2] The S8025 also features lower drag over most of the operating range experienced by horizontal tails.

4.5 Airfoils for Sport Planes

Table 4.7: Summary of Airfoil Data for Sport Planes

Airfoil	Configuration	Figures Begin
M6 (65%)	Clean	Fig. 5.29, p. 78
M6 (85%)	Clean	Fig. 5.33, p. 82
NACA2414	Clean	Fig. 5.45, p. 94
NACA2415	Clean	Fig. 5.49, p. 98

NACA 2414 & NACA 2415 The NACA 2414 airfoil geometry, having a high thickness and non-cusped trailing edge, is typical of airfoils used on powered, sport aircraft. The polar shows broad regions of constant drag that suggests trade-offs being made between skin friction drag and bubble drag. At low angles of attack, the low drag associated with laminar flow is offset by high-bubble drag. The opposite is true at high angles of attack as the drag increase resulting from more extensive turbulent flow is offset by a decrease in bubble drag. These two phases interact in such a way to keep drag constant over a broad range of angles of attack. While the higher drag at low lift coefficients associated with this type of trade-off is unattractive for racing aircraft, it serves to favorably moderate the performance of sport aircraft.

For the sport flier, a soft stall is particularly important, and this is where the NACA 2414 performance suffers the most. At all four Reynolds numbers the airfoil has a very abrupt loss in lift accompanied with a slight amount of hysteresis. While there is some decrease in the lift curve slope when approaching stall which may serve as a warning to the pilot, the break is quite sharp and the loss in lift is significant. These two qualities, along with the hysteresis, make this airfoil particularly undesirable for pilots unable to recognize the signs leading up to stall and unfamiliar with the steps needed to recover.

The NACA 2415 has become increasingly popular on $1/4$-scale pylon racers. Due to the high speeds of these aircraft, data was not obtained at cruise Reynolds numbers. However, our data does extend into the landing phase of these aircraft. As would be expected, the thicker NACA 2415 has higher drag at all lift coefficients when compared with the NACA 2414. Contributing to this higher drag are larger regions of laminar separation, which can be seen by comparing velocity distributions for these two airfoils. The undesirable stall type and hysteresis has changed little from the NACA 2414.

M6 (65%) & M6 (85%) Typical of thinner sections, the M6 (65%) demonstrates a narrow drag bucket with low minimum drag. The low drag for *Re*'s of 60k and 100k is indicative of low bubble drag as can be deduced from the velocity distributions. While $C_{l_{max}}$ is low, resulting in increased landing speeds, the gentle stall should provide sufficient warning to the pilot on final approach. (This assumes that the aircraft wing area has been designed for cruise.) Unexpectedly, at *Re*'s of 60k and 100k, a deadband is present around 0 deg angle of attack. This type of behavior is usually only seen on symmetrical airfoils at low *Re*'s. At higher *Re*'s the deadband is not present. If this deadband proves to be a problem, carefully placed trips should succeed in alleviating the phenomenon. On scale applications such as the R-2, trips are unacceptable. However, because most scale aircraft are quite large (i.e., higher Reynolds numbers), they can be left off with no noticeable change in lift performance. Due to a combination of features (low drag at low C_l, narrow drag bucket, and low $C_{l_{max}}$), the M6 (65%) is well suited for aircraft that must fly straight and fast.

Associated with its higher thickness, the M6 (85%) has a wider drag bucket than the 65% version. However, as with everything else in aerodynamics, there is no "free lunch," and this wider drag bucket comes at the price of higher minimum drag. When comparing lift characteristics, the 85% version is seen to have a higher $C_{l_{max}}$ (a typical effect produced by thickening a section) and more warning of impending stall. When stall does occur, however, the loss in lift is much larger. While either of these airfoils might have individual applications, considering them as a pair to be blended across a wing prone to tip stalling should prove interesting. As an example, consider the thinner 65% section used as the root airfoil and the 85% section used at the tip. The higher $C_{l_{max}}$ of the 85% section could possibly keep flow attached over the ailerons, helping to maintain control in critical situations, while the low drag of the 65% section will help keep drag to a minimum.

4.6 Airfoils for Heavy-Lift Cargo Planes

Table 4.8: Summary of Airfoil Data for Heavy-Lift Cargo Planes

Airfoil	Configuration	Figures Begin
E423	Clean	Fig. 5.17, p. 66
S1223 RTL	Clean	Fig. 5.79, p. 130

S1223 RTL This modified version of the S1223 was designed by Richard T. LaSalle. The airfoil was designed using his optimization method in which XFOIL was used for analysis during the iterations. Based on XFOIL predictions, the airfoil achieves a $C_{l_{max}}$ of near 2.47 for *Re* of 250k. Wind-tunnel test results, however, indicate a $C_{l_{max}}$ of near 2.05—slightly less than the baseline S1223,

which has a $C_{l_{max}}$ of near 2.1.

If indeed the airfoil could achieve a $C_{l_{max}}$ of nearly 2.5 in free air, it would be challenging to measure such a result in the wind tunnel as it is currently configured. High-lift airfoils can produce sidewall boundary-layer separation, which in turn can cause premature separation on the airfoil and produce a lower $C_{l_{max}}$ than that which would be otherwise measured in free air. To prevent the sidewall boundary-layer separation, suction can be used on the walls, but this is not done in the current setup.

For 0 deg angle of attack, XFOIL predicts $C_l = 1.16$ for the S1223 and 1.20 for the S1223 RTL; and for 5 deg angle of attack, $C_l = 1.76$ for the S1223 and 1.70 for the S1223 RTL. Since the predicted trends are consistent with the experimental results, the S1223 RTL was at least expected to achieve a higher $C_{l_{max}}$ than the S1223, but this was not the case.

E423 This Eppler airfoil found in Ref. 6 is one in a series of airfoils that are used to demonstrate the Eppler airfoil design method. This example, in particular, was designed for high lift and based on predictions operates well down to Re of 500k. In fact, as the wind-tunnel results indicate, the operating range extends to Re of 200k below which massive separation occurs before the design $C_{l_{max}}$. For Re of 200k, the $C_{l_{max}}$ is nearly 2.0; and for Re of 300k, the $C_{l_{max}}$ is slightly less. The higher lift at the lower Re probably comes about because of the effect of the laminar separation bubble on the upper surface; the bubble effectively adds camber to the airfoil through a displacement thickness effect. Although this airfoil does not reach a $C_{l_{max}}$ of 2.1 like the S1223, it is likely to be easier to build owing to the reduced amount of aft camber and greater thickness in the trailing-edge region.

4.7 Airfoils for Small Wind Turbines

Table 4.9: Summary of Airfoil Data for Small Wind Turbines

Airfoil	Configuration	Figures Begin
S822	Tripped	Fig. 5.65, p. 118
	Clean and tripped	Fig. 5.69, p. 122
S823	Tripped	Fig. 5.71, p. 124

S822 & S823 These NREL (National Renewable Energy Laboratory) airfoils,[20] designed for small horizontal-axis wind turbines and tested in the previous test series, were tested this time with fixed transition. The idea was to simulate the effect of insect debris and other roughness elements that accumulate on wind turbine blades. As opposed to the wings of an airplane, wind-turbine blades are not frequently cleaned, and therefore wind-turbine airfoils often operate under dirty-

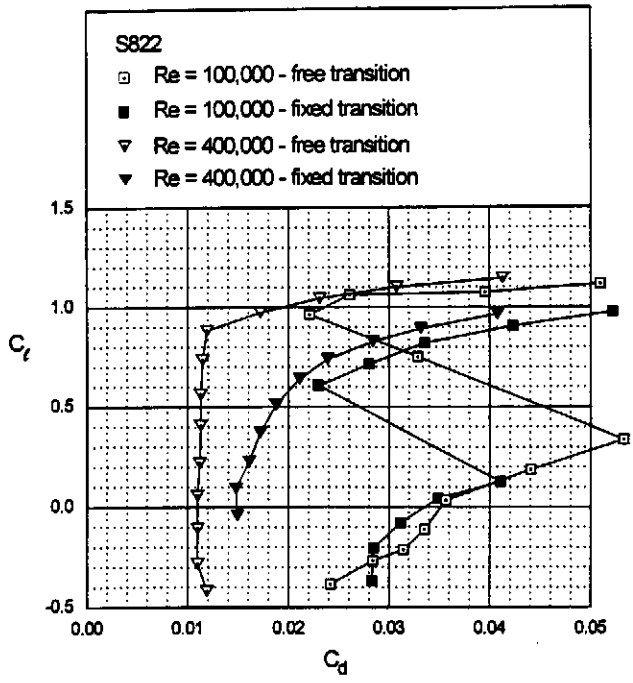

Fig. 4.1 Drag polars for the S822 airfoil with free and fixed transition for $Re = 100,000$ and 400,000.

blade conditions. Insect debris causes early transition that reduces the airfoil performance and, thus, the energy capture. Consequently, a reduced roughness sensitivity is desired for airfoils designed for wind-turbine applications, such as the Advanced NREL Airfoil Families.[20] As to be discussed, the meaning of the descriptor "reduced roughness sensitivity" must be qualified.

To force transition, a zig-zag trip (type C) was positioned at 2% chord on the upper surface and at 5% chord and 10% chord on the lower surface for the S822 and S823 airfoils, respectively. The thickness of the trip was set at 0.022 in and was kept constant for all Reynolds numbers. A plain trip of the same thickness was also used instead of the zig-zag trip on the S822 for a single lift run at a Reynolds number of 100,000. As expected, the zig-zag trip had more of an effect than the plain trip. It is important to note that there is no ideal way to simulate leading-edge bug roughness (short of actually impacting bugs on the leading edge). Furthermore, it has been shown that transition does not occur immediately at the trip location. Instead, forced transition takes place slowly over a considerable distance along the airfoil.[21] Nevertheless, the method used here to cause transition and other methods that employ grit roughness are a convenient and suitable means of simulating bug-roughness effects on airfoil performance.

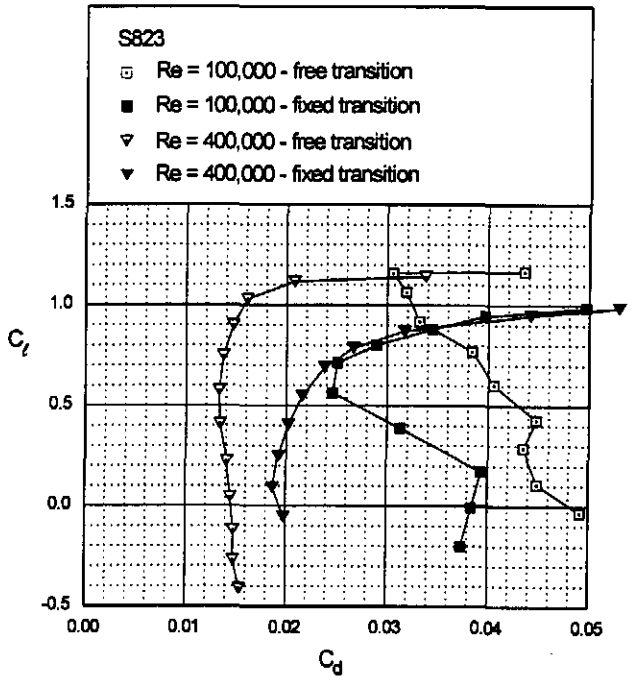

Fig. 4.2 Drag polars for the S823 airfoil with free and fixed transition for $Re = 100,000$ and 400,000.

As seen from Figs. 4.1 and 4.2, forcing early transition causes a considerable change in the aerodynamic characteristics of the S822 and S823 airfoils. At *Re* of 100k, the use of a zig-zag trip actually lowered the drag for most of the lift range but the maximum lift-to-drag ratio was reduced. The maximum lift-to-drag ratios of both airfoils also decreased for all the other Reynolds numbers considered owing to the significant increase in drag caused by the addition of the trip.

The decrease in lift-to-drag ratio and the variation in maximum lift coefficient with Reynolds number for the S822 and S823 airfoils are summarized in Tables 4.10 and 4.11, respectively. Interestingly enough, in the results for clean conditions, the maximum lift-to-drag ratios of both airfoils with fixed transition remain relatively constant with increasing Reynolds number. Note that it was not possible during the current tests to obtain data at *Re* of 500k because of problems with the speed controller of the wind tunnel.

As previously mentioned, the meaning of the term "reduced roughness sensitivity" as applied to the S822 and S823 must be qualified. Based on the results for the lift-to-drag ratio, one could say that the S822 and S823 airfoils are rather sensitive to roughness. Nevertheless, the reason for which the S822 and S823 airfoils are said to be insensitive to roughness is because the maximum lift coefficient of the airfoils with or without roughness is nearly constant over the design

Table 4.10: S822 Maximum Lift-to-Drag Ratio and Lift Coefficient

	Maximum Lift-to-Drag Ratio			Maximum Lift Coefficient		
Re	Free	Fixed	% Decrease	Free	Fixed	% Decrease
100,000	43.6	26.3	39.7	1.15	1.14	0.9
200,000	58.2	27.4	52.9	1.17	1.15	1.7
300,000	63.5	30.6	51.8	1.21	1.17	3.3
400,000	74.3	30.9	58.4	1.18		

Table 4.11: S823 Maximum Lift-to-Drag Ratio and Lift Coefficient

	Maximum Lift-to-Drag Ratio			Maximum Lift Coefficient		
Re	Free	Fixed	% Decrease	Free	Fixed	% Decrease
100,000	33.4	28.4	15.0	1.17	1.15	1.7
200,000	48.2	26.7	44.6	1.17	1.14	2.6
300,000	56.2	27.8	50.5	1.16	1.12	3.4
400,000	63.9	29.5	53.8	1.15	1.08	6.1

Reynolds number range. This consistency in maximum lift coefficient is important for stall-regulated wind turbines for which the peak power is determined by the airfoil $C_{l_{max}}$. Therefore, the S822 and S823 airfoils are good candidates for small stall-regulated wind turbines. The relatively high thickness of these airfoils (root airfoil, S823-21% and tip airfoil, S822-16%) also provides structural advantages.

As a last comment, it is important to note that airfoils traditionally used on aircraft have been widely used in the design of wind turbines. These airfoils are typically even more sensitive to roughness effects.

4.8 Airfoils with Gurney Flaps

In total, Gurney flaps were tested on five airfoils taken from the following categories: free flight/F1C (MA409), thermal duration sailplanes (S7055 and SD7037) and high-lift cargo planes (M06-13-128 and S1223). Some background information about this simple, yet intriguing device is provided in the Extended Notes to the Text section.[n1]

The main goal of the present tests with Gurney flaps was to investigate the possible benefits of this device when applied to airfoils for free flight models and sailplanes. A priori, it would seem that a Gurney flap is less likely to positively

Table 4.12: Summary of Data for Airfoils with Gurney Flaps

Airfoil	Configuration	Figures Begin
M06-13-128 (B)	0.4% Gurney flap	Fig. 5.25, p. 74
MA409	0.4% Gurney flap	Fig. 5.37, p. 86
S1223	Clean	Fig. 5.75, p. 128
	0.4% Gurney flap	Fig. 5.75, p. 128
S7055	1.0% Gurney flap	Fig. 5.104, p. 158
	0.4% Gurney flap	Fig. 5.104, p. 158
SD7037 (C)	0.4% Gurney flap	Fig. 5.143, p. 204

influence the performance of airfoils for free flight and sailplane applications due to the relatively small thickness of the airfoils from these categories. This last statement is based on a finding stipulating that the potential benefits of Gurney flaps in terms of drag reduction (for a given lift condition) may be limited to airfoils with large trailing-edge closure angle (thick airfoils) and/or operating at high lift coefficients.[22] Some results from the Princeton tests,[1] however, show that the addition of a 0.6% Gurney flap to the S2091 airfoil (10.1% thick) can enhance the performance of this airfoil. If one takes the time to plot the lift-to-drag ratio and the endurance parameter ($C_l^{3/2}/C_d$) against C_l, one finds that the 0.6% flap increased the performance of the S2091 airfoil for moderate to high lift coefficients. This increase in airfoil efficiency and endurance parameter translates into better glide and thermalling performance but worse performance for tasks performed at high speeds.

MA409 The results for this free flight airfoil equipped with a small 0.4% flap for Reynolds numbers of 60,000 and 300,000 are summarized in Fig. 4.3. The results for the baseline airfoils are also shown to facilitate comparison. Overall, the baseline airfoil has better drag characteristics than with the Gurney flap. Comparable performance is observed for Re of 300k between lift coefficients of 0.3 to 0.7. Practically, however, this has little value since free flight models operate at high Reynolds numbers only during the climb phase of the flight, which is performed at a lift coefficient near zero. Results were also obtained for Re of 100k and 200k but as for the results presented in Fig. 4.3, the performance of the MA409 with the Gurney flap does not surpass the performance of the baseline airfoil.

The relative thickness of the MA409 (6.7%) is probably too small for a Gurney flap to be effective. Local separation on the upper surface at the trailing-edge is less likely to happen on such thin airfoils. Consequently, it appears that for free flight applications, the effectiveness of Gurney flaps is challenged by the small thickness of the airfoils usually employed in this category despite the low Reynolds numbers associated with the glide portion of the flight which provides

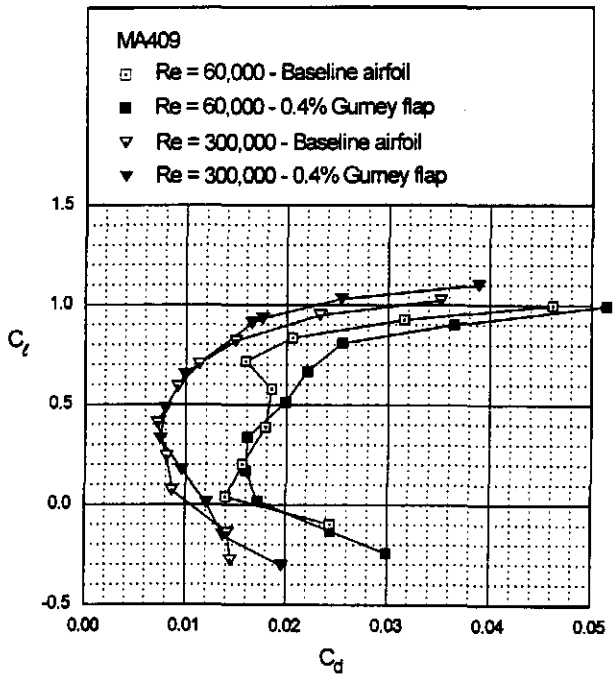

Fig. 4.3 Drag polars for the MA409 with and without a 0.4% Gurney flap for for $Re = 60,000$ and 300,000.

thick boundary-layers. The airfoil thickness is then the predominant effect as compared to Reynolds number effects.

Perhaps better use of Gurney flaps for free flight applications could be to combined a small Gurney flap with a thicker airfoil. This way, the Gurney flap would be more effective and at the same time some structural gains could be made in terms of reducing airplane weight. Of course, the value of this suggestion would need to be verified in the wind tunnel or in test flights. Moreover, the Gurney flap could be retracted during the climb portion of the flight and then somehow deflected for the gliding part. In this case, the trade-off becomes one between construction simplicity and possible gains during the gliding portion of the flight.

Finally, as a matter of interest, the lift curves demonstrate that the addition of the Gurney flap did not change the stall characteristics of the MA409. A gentle stall can still be observed. Note that this previous observation is not specific to the MA409 but to most airfoils equipped with Gurney flaps.

S7055 & SD7037 The results for these thermal duration airfoils equipped with a small 0.4% flap for *Re* of 60k and 300k are summarized in Figs. 4.4 and 4.5. Here again, the results for the baseline airfoils are shown. The trends are similar for both airfoils. The drag reduction found at low lift coefficients and at *Re* of 60k

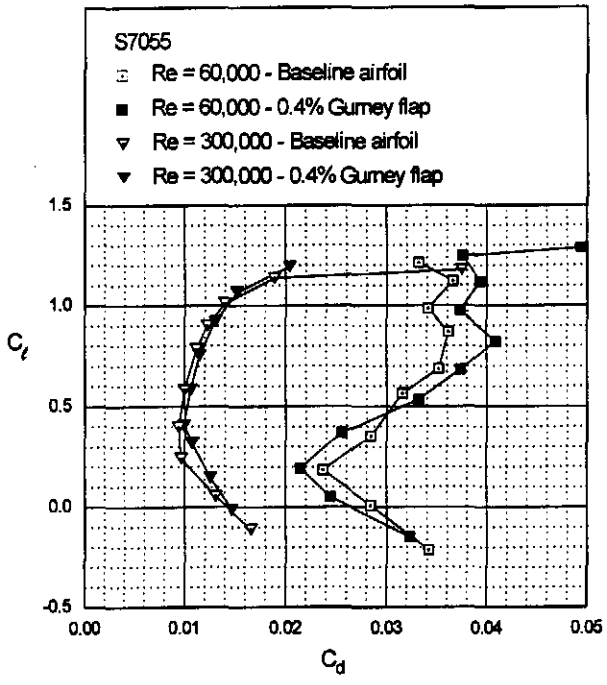

Fig. 4.4 Drag polars for the S7055 with and without a 0.4% Gurney flap for for $Re = 60,000$ and 300,000.

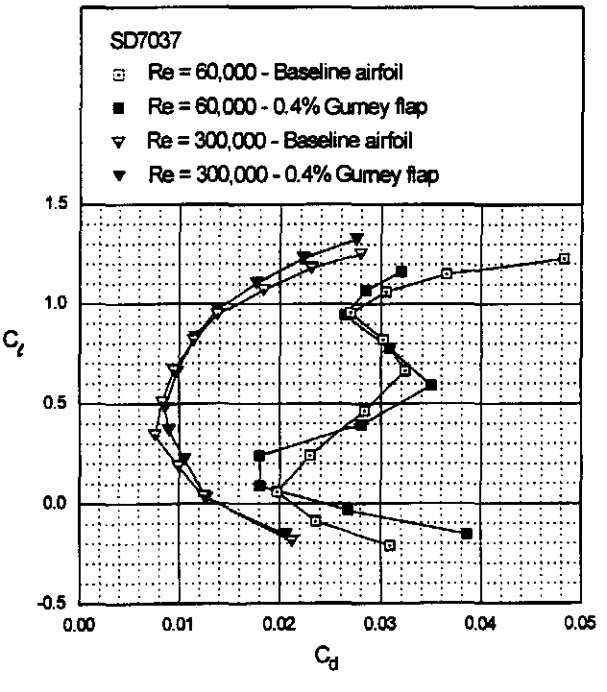

Fig. 4.5 Drag polars for the SD7037 with and without a 0.4% Gurney flap for for $Re = 60,000$ and 300,000.

is of little importance since flight at such Reynolds number is performed at high lift coefficients (slow flight). The SD7037, however, shows additional reduction in drag at lift coefficients above 0.8 for both Reynolds numbers considered. One could have expected that the addition of the Gurney flap would yield better results for the S7055 than the one obtained owing to its larger thickness and trailing-edge closure angle. The results for the S7055 with a 1% flap showed an increase in lift greater than for the smaller flap, but the drag penalty was greater.

One of the main reasons to have tested these two thermal duration airfoils was to see if the S7055 (flat-bottom airfoil) equipped with a Gurney flap could reach the performance of the SD7037, one of the favorite airfoils in the R/C soaring category. A similar study,[23] which has been conducted with airfoils used for long-endurance unmanned aerial vehicles, has shown that a 0.5% Gurney flap enhanced the performance of a flat-bottom airfoil to the level of an airfoil with a more complex geometry that originally had better performance. Based on the results shown in Figs. 4.6 and 4.7, one can easily see that the S7055 airfoil equipped with the small flap has more drag for a given lift coefficient than the SD7037 with or without a Gurney flap. Nevertheless, the performance for these two airfoils with and without Gurney flaps was computed for a reduced Reynolds number $\mathcal{R}$ of 120,000, which is typical for F3B ships with wing loadings near 12 oz/ft^2 (an approach first used in the comparison of the S7012, RG15 and the SD7003 in the first volume of *Summary of Low-Speed Airfoil Data*). Figures 4.6 and 4.7 present the two key performance parameters plotted against the sailplane lift coefficient. One can see that, the performance of the S7055 is for the most part below the performance of the SD7037. It is interesting to note that at moderate lift coefficients the SD7037 with the 0.4% Gurney flap yields performance similar to the baseline SD7037 and also yields the maximum value for the endurance parameter. The addition of a small Gurney flap to these two airfoils did not provide, however, evidence of important gains in performance. The results obtained at Princeton for the S2091 airfoil with a 0.6% Gurney flap are more promising.

M06-13-128 The Miley airfoil, M06-13-128, was tested with a 1% flap to see if this device could reduce the size of the laminar separation bubble on the upper surface, thereby providing a drag reduction over most of the lift range. It is known, that a Gurney flap effectively allows for some of the pressure to be recovered along the recirculation region right behind the flap (for the case of an attached recirculation region behind the flap), which in turn reduces the pressure drag associated with local trailing-edge separation. The results obtained, however, show that the large separation is still present. The addition of the Gurney flap shifted the polar upwards and provided lower drag for lift coefficients between 0.2 and 0.65. It would thus seems that even though a Gurney flap is known to affect the overall pressure distribution of an airfoil,[22,23] the 1% flap had a limited effect on the strong laminar separation bubble.

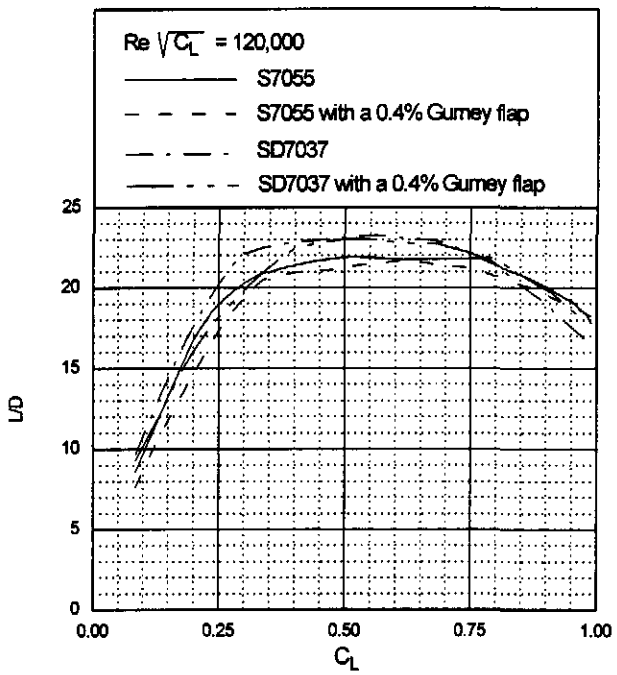

Fig. 4.6 L/D for sailplanes based on the S7055 and SD7037 with and without a 0.4% Gurney flap for $\mathcal{R} = 120{,}000$.

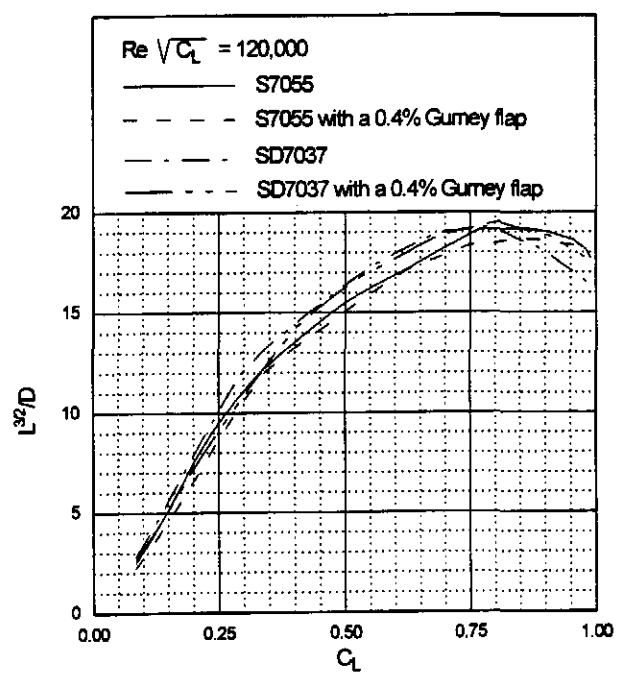

Fig. 4.7 Endurance parameter for sailplanes based on the S7055 and SD7037 with and without a 0.4% Gurney flap for $\mathcal{R} = 120{,}000$.

Table 4.13: Maximum Lift Coefficient of Airfoils with Gurney Flaps

Airfoil	*Re*	No flap	0.4% c	% Increase	1.0% c	% Increase
M06-13-128	200,000	1.47			1.60	8.8
MA409	200,000	1.07	1.15	7.5		
S1223	200,000	2.11	2.19	3.8	2.20	4.3
S7055	300,000	1.19	1.28	7.6	1.33	11.8
SD7037	300,000	1.26	1.35	7.1		

S1223 A single lift run was performed with the S1223 equipped with a 0.4% Gurney flap to provide a means for comparison with the results obtained for the 1% flap during the previous test phase. Interestingly enough, the 0.4% Gurney flap provided an increase in lift similar to the 1% flap (C_l of 2.18 instead of 2.20). The increase in lift owing to the addition of a Gurney flap is clearly non-linear with flap size. The smaller flaps yield a greater percentage increase than the longer flaps. This observation, which is elaborated elsewhere,[23] supports the previous statement made that in most cases, optimum Gurney flap heights are less than 1%.

Finally, Table 4.13 summarizes the increase in maximum lift coefficients for all the airfoils tested with Gurney flaps. From these results, it appears that the addition of a 0.4% flap to most airfoils should yields a 7–8% increase in lift, except for airfoils like the S1223, which are already highly aft loaded. Also, in the case of the S7055 airfoil, an increase in Gurney flap size from 0.4% to 1.0% (150% increase) provided only a 55% increase in lift increment, which again shows the non-linear increase in lift with increasing flap size.

To conclude, it appears that the use of a Gurney flap may require some trade-offs. In the case of high-lift applications, however, the addition of a Gurney flap is definitely an attractive one. For free flight models and R/C sailplanes, the trade-offs are between thermalling/glide and penetration/launch performance. As discussed previously, a retractable Gurney flap could be a solution to the loss in penetration/launch performance. In this case, the trade-off becomes one between construction simplicity and possible performance gains. Finally, although the application of Gurney flaps to the current group of airfoils does not show an overall gain in performance, the collective body of information on Gurney flaps still indicates that Gurney flaps are advantageous in some applications. Further studies on the use of Gurney flap are encouraged to better define their strengths and limitations.

Chapter 5

Airfoil Profiles and Performance Plots

In this chapter, the airfoil profiles and performance plots are presented. For quick reference, the airfoil names are listed in the margins. Also presented is a table that lists all the data sets and associated figures and page numbers. In the table, a '†' indicates that the corresponding lift data is not plotted to save space, but it is included with the data distribution disk. As a matter of record, the wind-tunnel run numbers are included in the table, and these also appear with the polar data in Appendix B and in the data distribution files for cross reference. Finally, the "Avg Difference" listed in the comparison plots of the true and actual coordinates is the average error of the model, which had a 12 in chord.

Model (Builder) Designer	Configuration	Velocity & Profile		Drag Data				Lift Data			
		Fig.	p.	Fig.	p.	*Re*	Run	Fig.	p.	*Re*	Run
CR-001 (J. Robertson) C. Robertson	Clean	5.1 5.2	50	5.3	51	60,000 100,000 200,000 300,000	658 660 662 664	5.4	52 53	60,000 100,000 200,000 300,000	657 659 661 663
Davis 3R (H. Cole)	Multiple u.s.t.'s	5.5 5.6	54	5.7	55	40,000 60,000 100,000 200,000 300,000	752 754 756 872 874	5.8	▮ 56 57	40,000 60,000 100,000 200,000 300,000	751 753 755 871 873
DU 86-084/18 (R. Adams) Delft University	Clean	5.9 5.10	58	5.11	59	60,000 100,000 200,000 300,000	790 792 794 796	5.12	60 61	60,000 100,000 200,000 300,000	789 791 793 795
E374 (B) (M. Bame) Eppler	Clean	5.13 5.14	62	5.15	63	60,000 100,000 200,000 300,000	616 618 620 622	5.16	64 65	60,000 100,000 200,000 300,000	615 617 619 621
E423 (D. Glaze/ M. Lazor) Eppler	Clean	5.17 5.18	66	5.19	67	60,000 100,000 200,000 300,000	844 846 848 850/851	5.20	68 69	60,000 100,000 200,000 300,000	843 845 847 849
LD-79 (L. DeWitt) L. DeWitt	Clean 0 deg flap	5.21 5.22	70	5.23	71	60,000 100,000 150,000 200,000	945 947 951 949	5.24	72 73	60,000 100,000 150,000 200,000	944 946 950 948

M06-13-128 (B) (M. Allen) Miley	Gurney flap h/c = 1.0%	5.25 5.26	74	5.27	75	300,000	918	5.28	76	200,000 300,000	914 917
M6 (65%) (L. Spychalla)	Clean	5.29 5.30	78	5.31	79	60,000 100,000 200,000 300,000	758 760 762 764	5.32	80 81	60,000 100,000 200,000 300,000	757 759 761 763
M6 (85%) (L. Spychalla)	Clean	5.33 5.34	82	5.35	83	60,000 100,000 200,000 300,000	666 715 723 725	5.36	84 85	60,000 100,000 200,000 300,000	665 714 722 724
MA409 (R. Cooney) Achterberg	Gurney flap h/c = 0.4%	5.37 5.38	86	5.39	87	60,000 100,000 200,000 300,000	921 923 925 927	5.40	88 89	60,000 100,000 200,000 300,000	920 922 924 926
MH32 (J. Tonnesen) Hepperle	Clean	5.41 5.42	90	5.43	91	60,000 100,000 200,000 300,000	632 634 636 638	5.44	92 93	60,000 100,000 200,000 300,000	631 633 635 637
NACA 2414 (R. Bozzonetti) NACA	Clean	5.45 5.46	94	5.47	95	60,000 100,000 200,000 300,000	774 776 778 780	5.48	96 97	60,000 100,000 200,000 300,000	773 775 777 779
NACA 2415 (D. Imes) NACA	Clean	5.49 5.50	98	5.51	99	60,000 100,000 200,000 300,000	782 784 786 788	5.52	100 101	60,000 100,000 200,000 300,000	781 783 785 787

RG15 (C) (B. Champine/ J. Robertson) Grisberger	Clean (Obechi) 0 deg flap	5.53 5.54	102	5.55	103	60,000 100,000 200,000 300,000	884 886 888 890	5.56	104 105 	60,000 100,000 200,000 300,000	883 885 887 889
	Clean 0 deg flap			5.57	107	60,000 100,000 200,000 300,000	929 931 933 935	5.58	108 109 	60,000 100,000 200,000 300,000	928 930 932 934
	Clean 5 deg flap	5.59	110	5.60	111	60,000 100,000 200,000 300,000	954 956 958/959 961	5.61	112 113 	60,000 100,000 200,000 300,000	952 955 957 960
	Clean 10 deg flap	5.62	114	5.63	115	60,000 100,000 200,000 300,000	965 967 969 963	5.64	116 117 	60,000 100,000 200,000 300,000	964 966 968 962
S822 (M. Allen) Somers	u.s.t./l.s.t. (see fig)	5.65 5.66	118	5.67	119	100,000 200,000 300,000 400,000	827 829 831 854	5.68	120 121 	100,000 200,000 300,000 400,000	826 828 830 853
	Clean							5.69	122	100,000	728
	u.s.t./l.s.t. (see fig)							5.70	122	100,000	731
S823 (M. Allen) Somers	u.s.t./l.s.t. (see fig)	5.71 5.72	124	5.73	125	100,000 200,000 300,000 400,000	730 834 836 733	5.74	126 127 	100,000 200,000 300,000 400,000	729 833 835 734

S1223 (Y. Tinel) Selig	Clean	5.75	128						▮	150,000	697
		5.76						5.77	129	200,000	698
	Gurney flap h/c = 0.4%							5.78	129	200,000	912
S1223 RTL (C. Richardson) R. LaSalle	Clean	5.79	130					5.81	131	100,000	970
		5.80								150,000	971
									132	200,000	972
										250,000	973
									133	300,000	974
S4083 (A) (M. Levoe) Selig	Clean	5.82	134	5.84	135	60,000	648	5.85	136	60,000	647
		5.83				100,000	650/651			100,000	649
						200,000	653		137	200,000	652
						300,000	656			300,000	655
S4083 (B) (J. Thomas) Selig	Clean	5.86	138	5.88	139	60,000	640	5.89	140	60,000	639
		5.87				100,000	642			100,000	641
						200,000	644		141	200,000	643
						300,000	646			300,000	645
S5010 (O. Wilson) Selig	Clean	5.90	142	5.92	143	60,000	766	5.93	144	60,000	765
		5.91				100,000	768			100,000	767
						200,000	770		145	200,000	769
						300,000	772			300,000	771
S7012 (B) (M. Lachowski) Selig	Clean 0 deg flap	5.94	146	5.96	147	60,000	825	5.97	148	60,000	824
		5.95				100,000	838			100,000	837
						200,000	840		149	200,000	839
						300,000	842			300,000	841
	Clean 5 deg flap	5.98	150	5.99	151	60,000	856	5.100	152	60,000	855
						100,000	858			100,000	857
						200,000	860		153	200,000	859
(continues)						300,000	862			300,000	861

S7012 (B) (continued)	Clean 10 deg flap	5.101	154	5.102	155	60,000 100,000 200,000 300,000	864 866 868 870	5.103	156 157	60,000 100,000 200,000 300,000	863 865 867 869
S7055 (G. Jones) Selig	Gurney flap h/c = 1.0%	5.104 5.105	158	5.106	159	100,000 300,000	909 911	5.107	160	100,000 300,000	908 910
	Gurney flap h/c = 0.4%			5.108	161	60,000 100,000 200,000 300,000	892 894/895 897 899	5.109	162 163	60,000 100,000 200,000 300,000	891 893 896 898
S7075 (A) (J. Robertston) Selig	u.s.t. 0 deg flap (see fig)	5.110 5.111	164	5.112	165	100,000 200,000 300,000	700 702/703 705	5.113	166 167	100,000 200,000 300,000	699 701 704
	u.s.t. 0 deg flap (see fig)			5.114	169	60,000 100,000 200,000 300,000	707 709 711 713	5.115	170 171	60,000 100,000 200,000 300,000	706 708 710 712
	u.s.t. 0 deg flap (see fig)			5.116	173	100,000 200,000 300,000	717 719 721	5.117	174 175	100,000 200,000 300,000	716 718 720
	u.s.t. 5 deg flap (see fig)	5.118	176	5.119	177	60,000 100,000 200,000 300,000	736 738/976 740 742	5.120	178 179	60,000 100,000 200,000 300,000	735 737 739 741
	u.s.t. 10 deg flap (see fig)	5.121	180	5.122	181	60,000 100,000 200,000 300,000	744 746 748 750	5.123	182 183	60,000 100,000 200,000 300,000	743 745 747 749

S7075 (B) (J. Thomas) Selig	u.s.t. 0 deg flap (see fig)	5.124 5.125	184	5.126	185	60,000 100,000 200,000 300,000	937 939 941 943	5.127	186 187	60,000 100,000 200,000 300,000	936 938 940 942
S8025 (J. Thurmond) Selig	Clean	5.128 5.129	188	5.130	189	60,000 100,000 200,000 300,000	876 878 880 882	5.131	190 191	60,000 100,000 200,000 300,000	875 877 879 881
SD7037 (B) (D. Thompson) Selig	Clean 0 deg flap	5.132 5.133	192	5.134	193	60,000 100,000 200,000 300,000	977 800 802 804/975	5.135	194 195	60,000 100,000 200,000 300,000	797 799 801 803
	Clean 5 deg flap	5.136	196	5.137	197	60,000 100,000 200,000 300,000	806 808 810 812/813	5.138	198 199	60,000 100,000 200,000 300,000	805 807 809 811
	Clean 10 deg flap	5.139	200	5.140	201	60,000 100,000 200,000 300,000	815 817 819/820 822/823	5.141	202 203	60,000 100,000 200,000 300,000	814 816 818 821
SD7037 (C) (D. Brengman) Selig	Clean	5.142 5.143	204	5.144	205	60,000 100,000 200,000 300,000	624 626 628 630	5.145	206 207	60,000 100,000 200,000 300,000	623 625 627 629
	Gurney flap h/c = 0.4%			5.146	209	60,000 100,000 200,000 300,000	901 903 905 907	5.147	210 211	60,000 100,000 200,000 300,000	900 902 904 906

CR-001

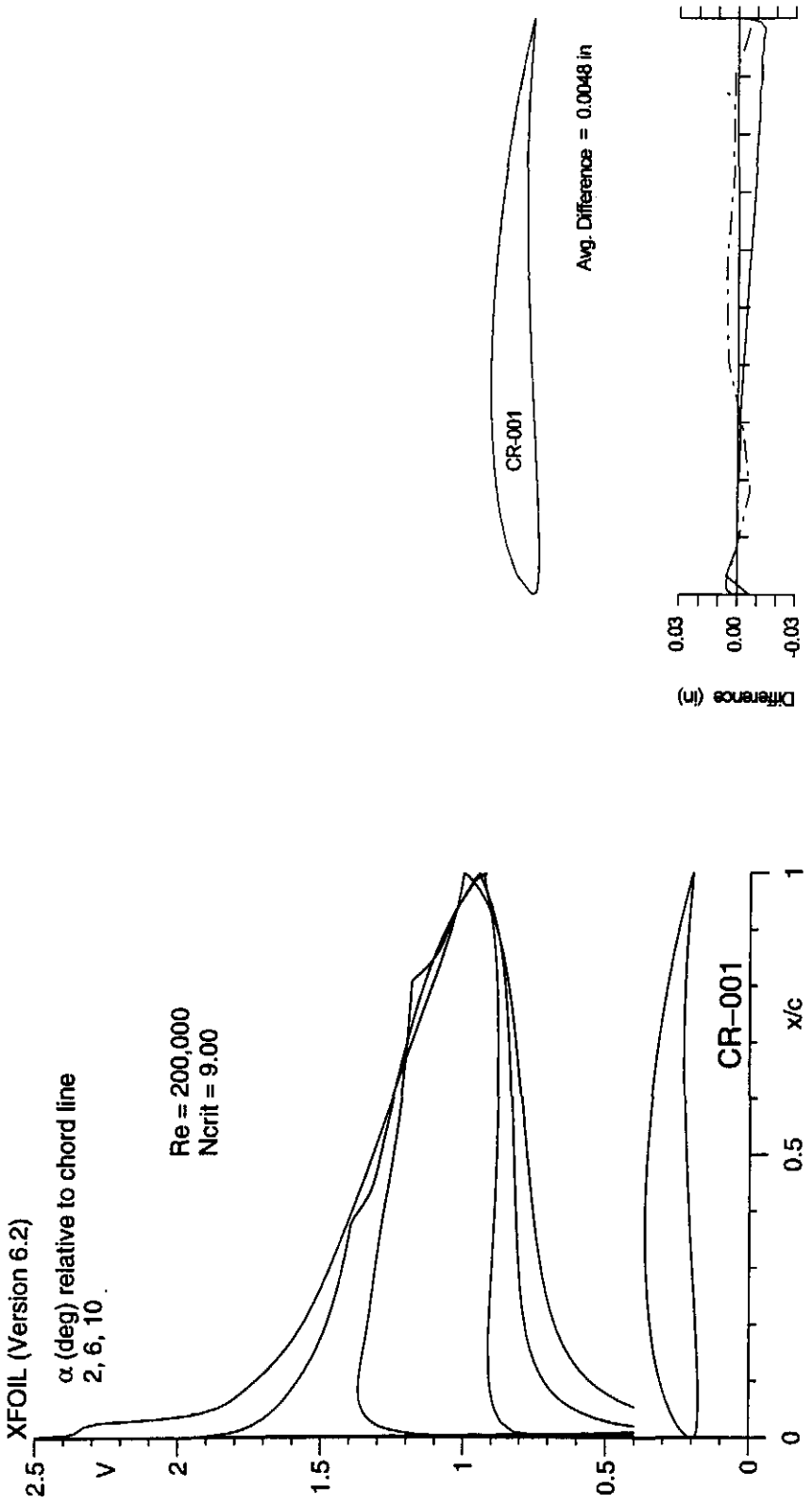
XFOIL (Version 6.2)
α (deg) relative to chord line
2, 6, 10
Re = 200,000
Ncrit = 9.00
V
2.5
2
1.5
1
0.5
0
0
0.5
1
x/c
CR-001
CR-001
Avg. Difference = 0.0048 in
0.03
0.00
-0.03
Difference (in)

CR-001

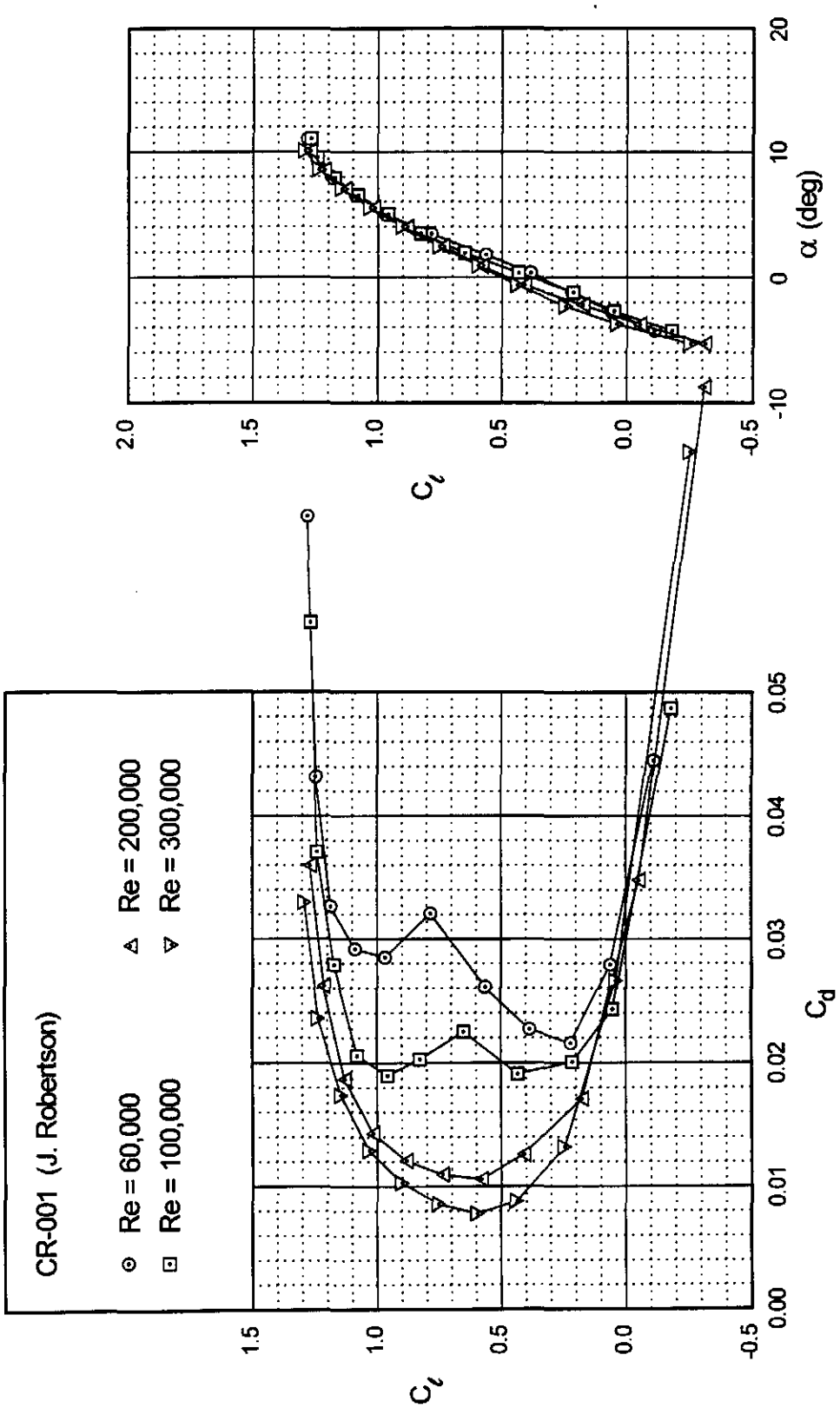
CR-001 (J. Robertson)
Re = 60,000
Re = 100,000
Re = 200,000
Re = 300,000
C_l
C_d
α (deg)
2.0
1.5
1.0
0.5
0.0
-0.5
-10
0
10
20
0.00
0.01
0.02
0.03
0.04
0.05

Fig. 5.4

CR-001

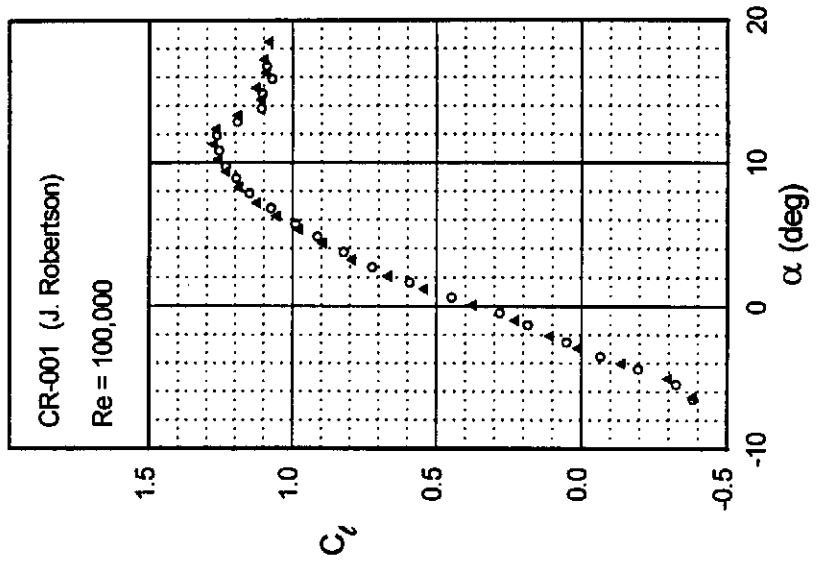
CR-001 (J. Robertson)
Re = 100,000
1.5
1.0
0.5
0.0
-0.5
C_l
-10
0
10
20
α (deg)

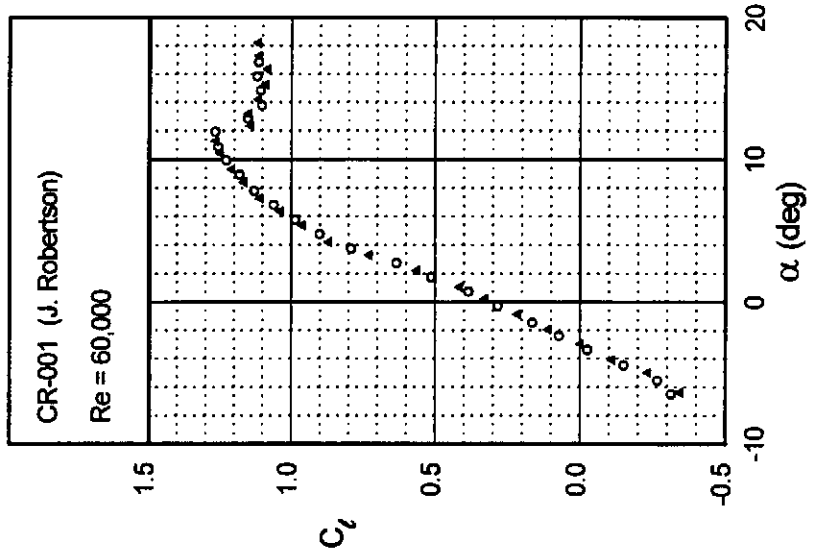
CR-001 (J. Robertson)
Re = 60,000
1.5
1.0
0.5
0.0
-0.5
C_l
-10
0
10
20
α (deg)

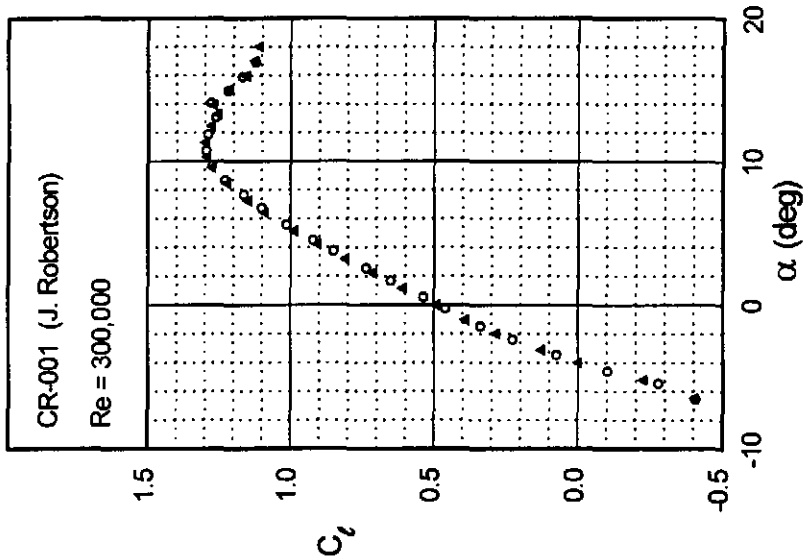
CR-001 (J. Robertson)
Re = 300,000
1.5
1.0
0.5
0.0
-0.5
C_l
-10
0
10
20
α (deg)

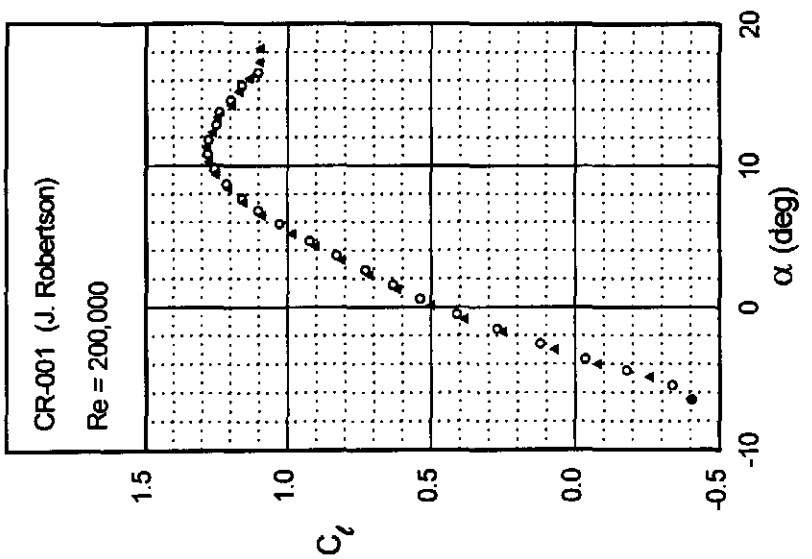
CR-001 (J. Robertson)
Re = 200,000
1.5
1.0
0.5
0.0
-0.5
C_l
-10
0
10
20
α (deg)

Davis 3R

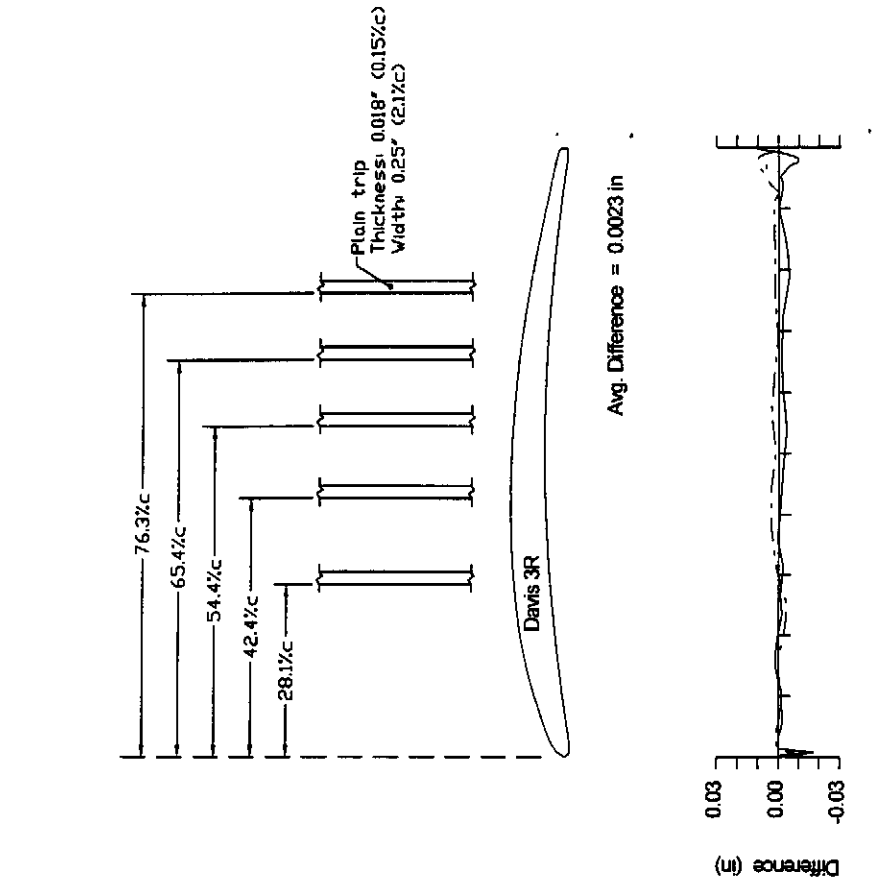
Plain trip
Thickness: 0.018" (0.15%c)
Width: 0.25" (2.1%c)
76.3%c
65.4%c
54.4%c
42.4%c
28.1%c
Davis 3R
Avg. Difference = 0.0023 in
0.03
0.00
-0.03
Difference (in)

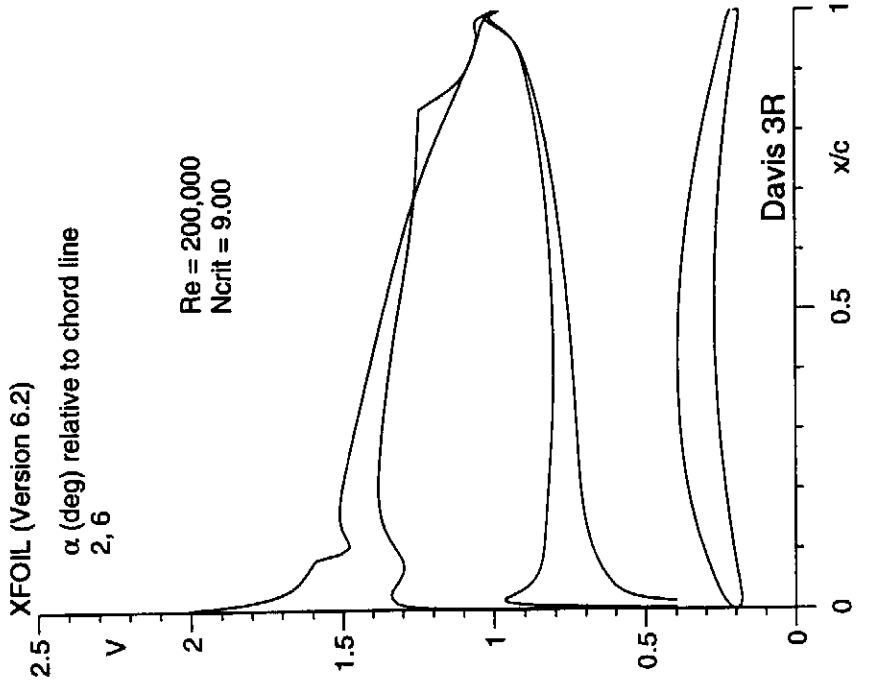
XFOIL (Version 6.2)
α (deg) relative to chord line
2, 6
Re = 200,000
Ncrit = 9.00
Davis 3R
V
2.5
2
1.5
1
0.5
0
0
0.5
1
x/c

Davis 3R

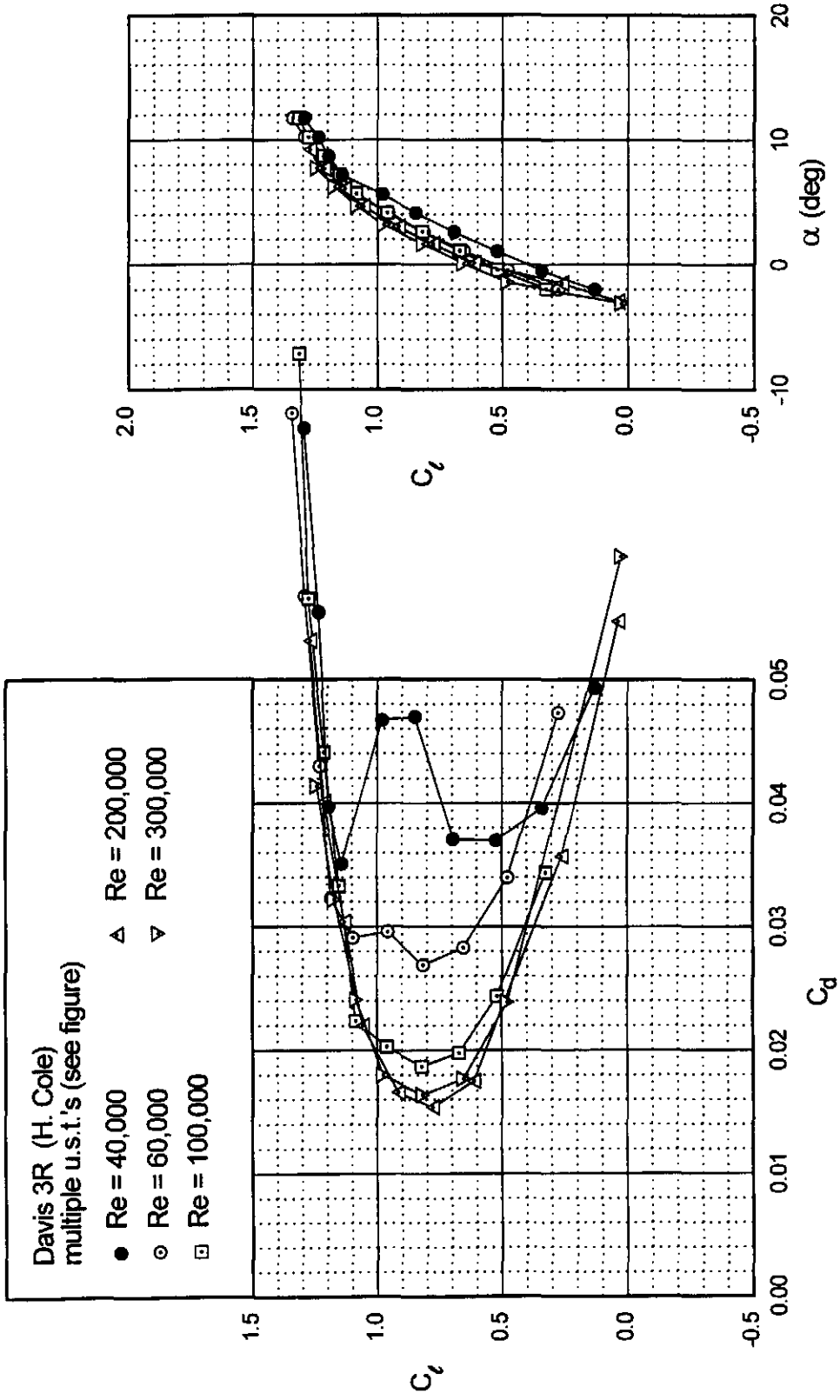
Davis 3R (H. Cole)
multiple u.s.t.'s (see figure)
Re = 40,000
Re = 60,000
Re = 100,000
Re = 200,000
Re = 300,000
C_l
C_d
α (deg)

Fig. 5.8

Davis 3R

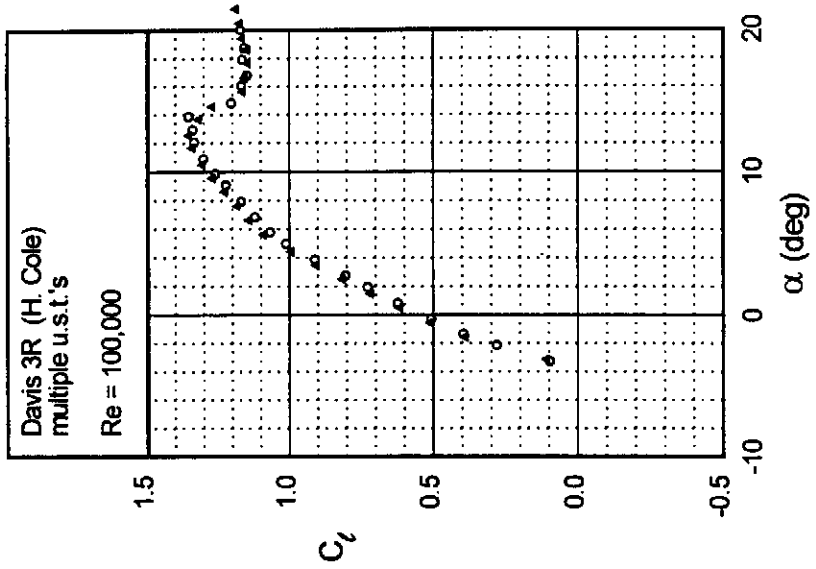

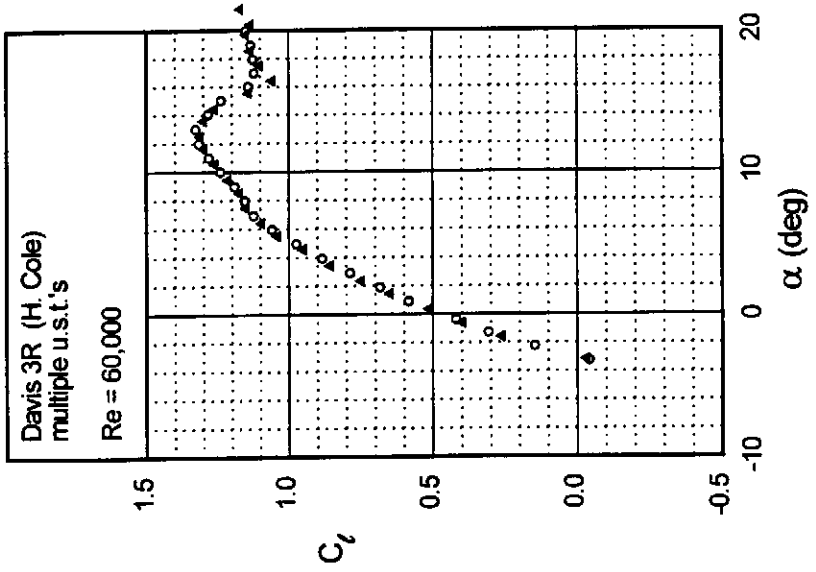

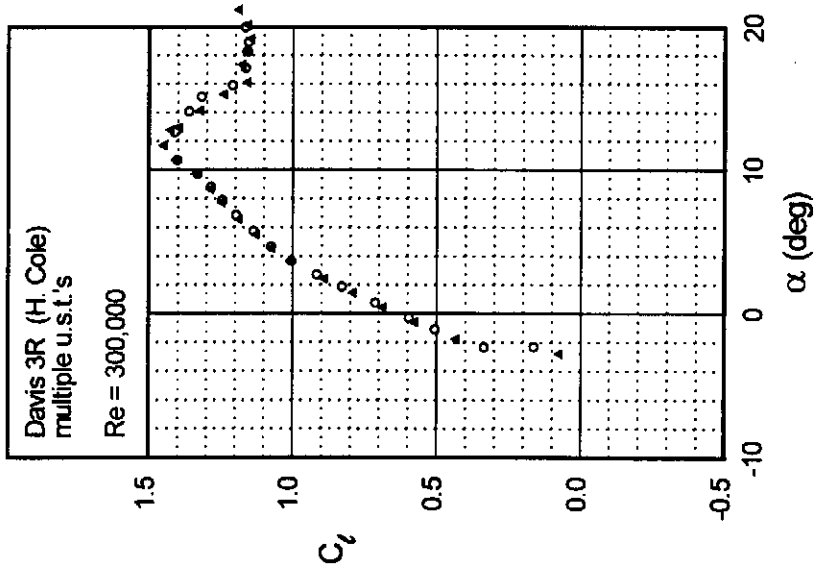
Davis 3R (H. Cole)
multiple u.s.t.'s
Re = 300,000
1.5
1.0
0.5
0.0
-0.5
C_l
-10
0
10
20
α (deg)

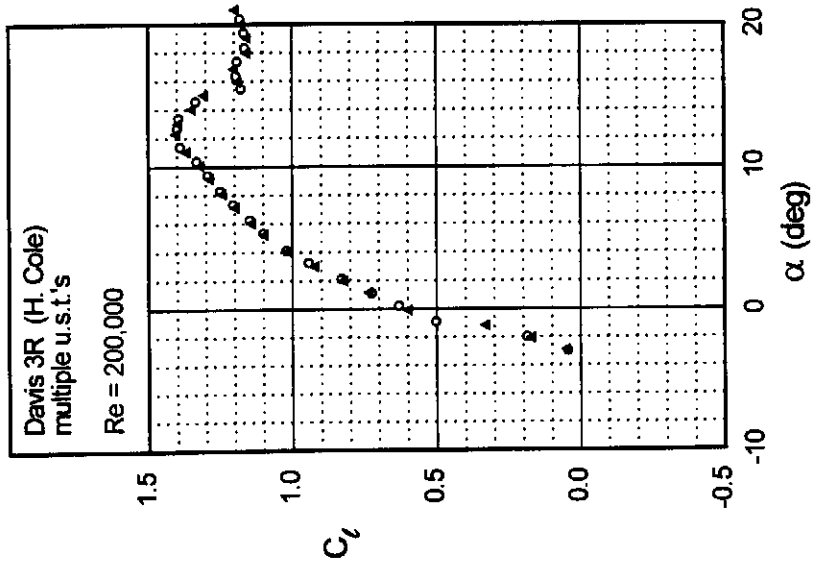
Davis 3R (H. Cole)
multiple u.s.t.'s
Re = 200,000
1.5
1.0
0.5
0.0
-0.5
C_l
-10
0
10
20
α (deg)

DU 86-084/18

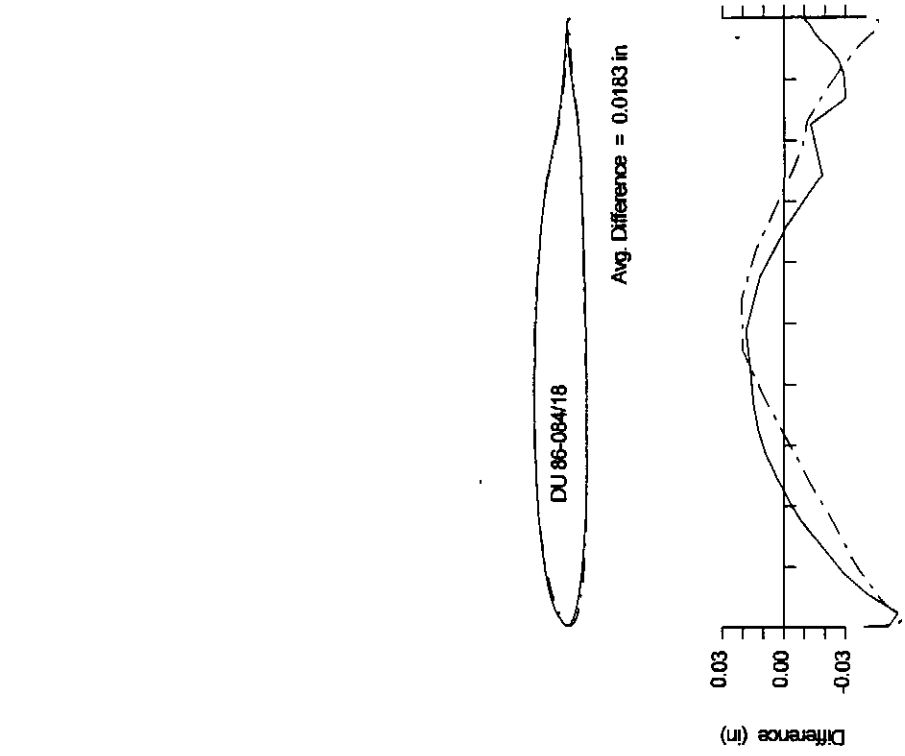
DU 86-084/18
Avg. Difference = 0.0183 in
0.03
0.00
-0.03
Difference (in)

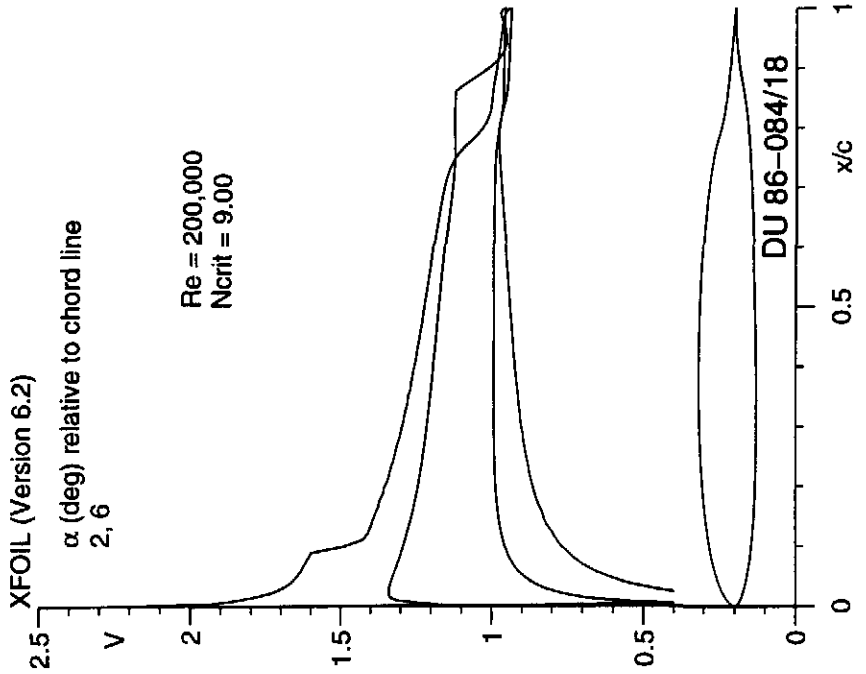
XFOIL (Version 6.2)
α (deg) relative to chord line
2, 6
Re = 200,000
Ncrit = 9.00
V
2.5
2
1.5
1
0.5
0
0.5
1
x/c
DU 86-084/18

DU 86-084/18

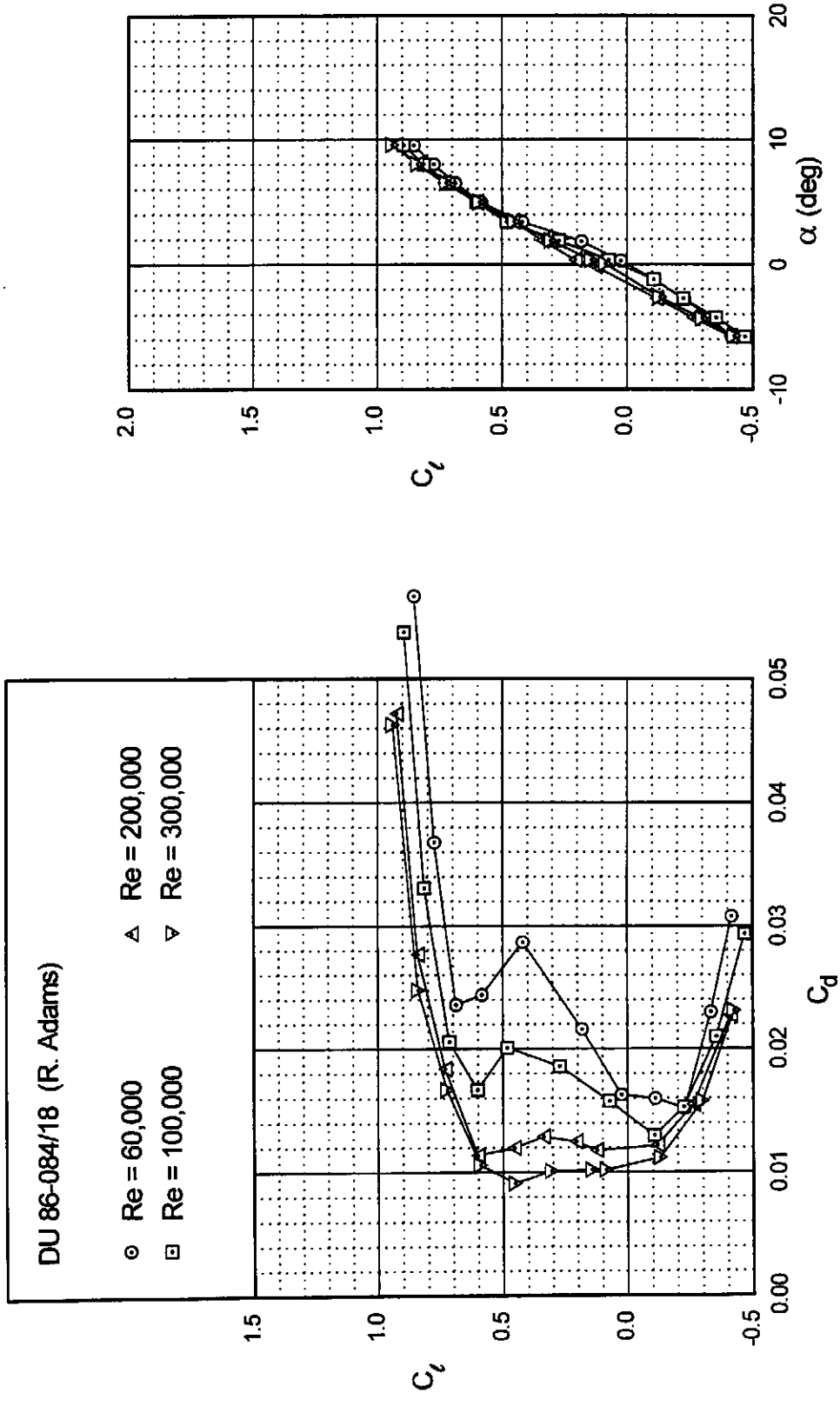
2.0
1.5
1.0
0.5
0.0
-0.5
C_l
20
10
0
-10
α (deg)
DU 86-084/18 (R. Adams)
Re = 60,000
Re = 100,000
Re = 200,000
Re = 300,000
1.5
1.0
0.5
0.0
-0.5
C_l
0.05
0.04
0.03
0.02
0.01
0.00
C_d

DU 86-084/18

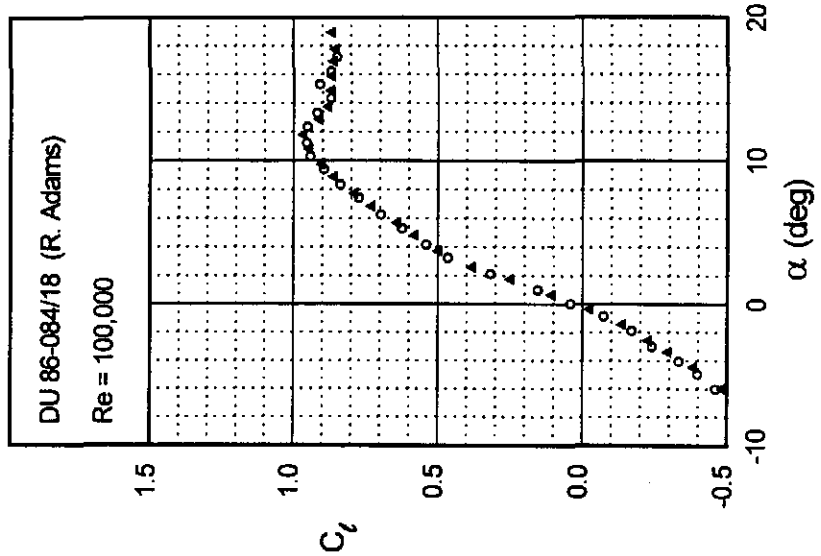
DU 86-084/18 (R. Adams)
Re = 100,000
1.5
1.0
0.5
0.0
-0.5
C_l
-10
0
10
20
α (deg)

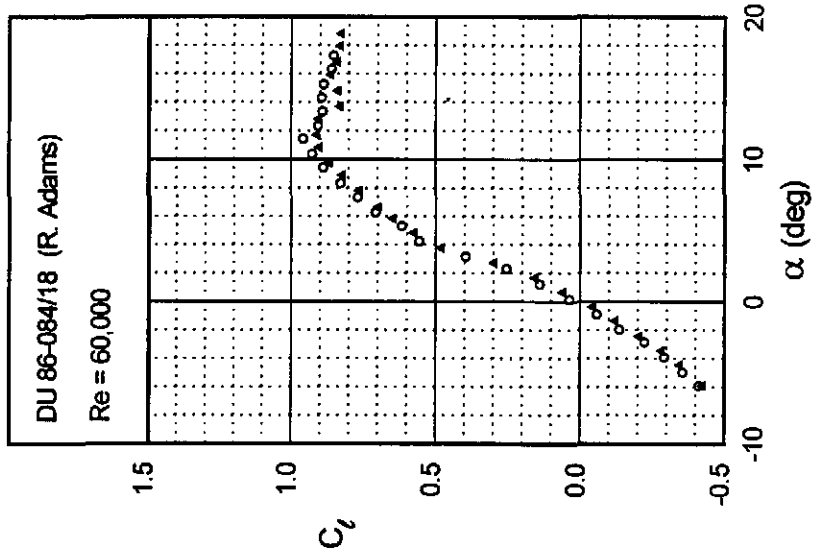
DU 86-084/18 (R. Adams)
Re = 60,000
1.5
1.0
0.5
0.0
-0.5
C_l
-10
0
10
20
α (deg)

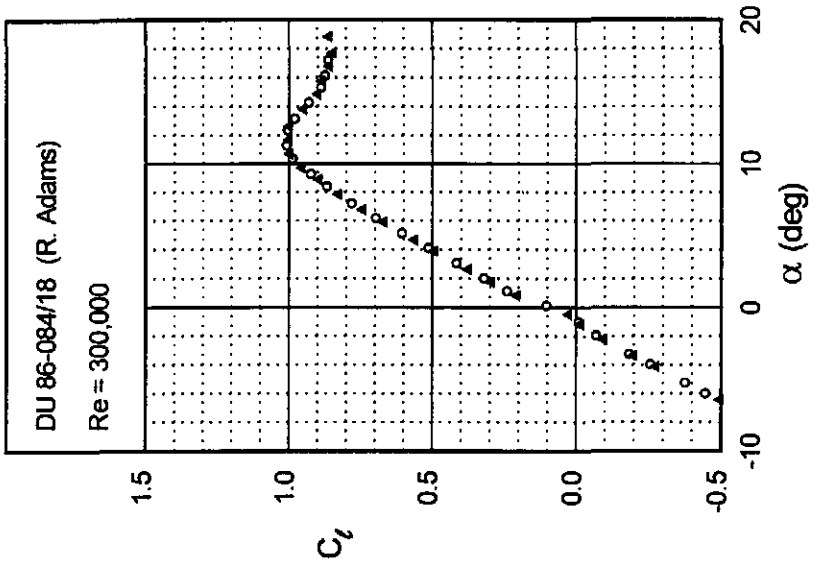
DU 86-084/18 (R. Adams)
Re = 300,000
1.5
1.0
0.5
0.0
-0.5
C_l
-10
0
10
20
α (deg)

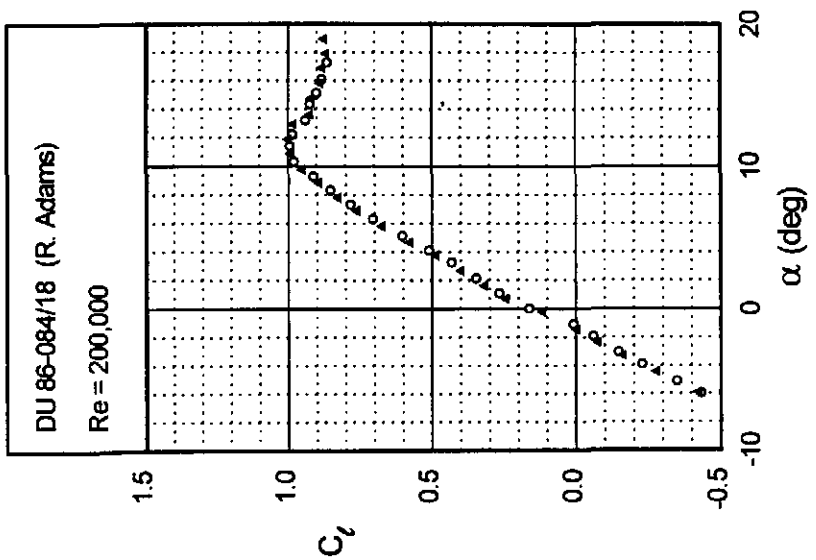
DU 86-084/18 (R. Adams)
Re = 200,000
1.5
1.0
0.5
0.0
-0.5
C_l
-10
0
10
20
α (deg)

E374 (B)

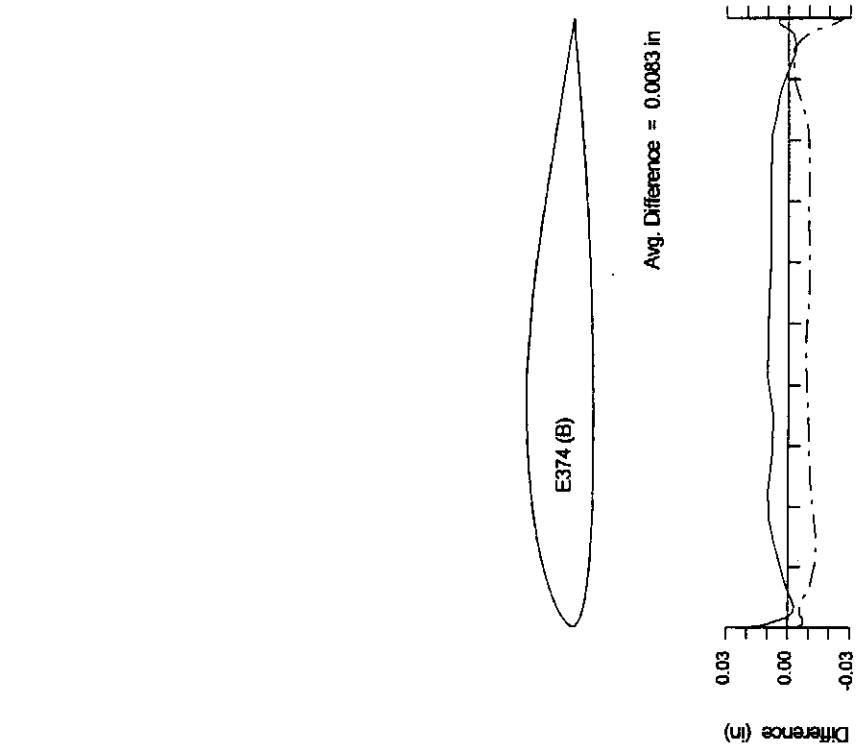
E374 (B)
Avg. Difference = 0.0083 in
0.03
0.00
-0.03
Difference (in)
Page 2

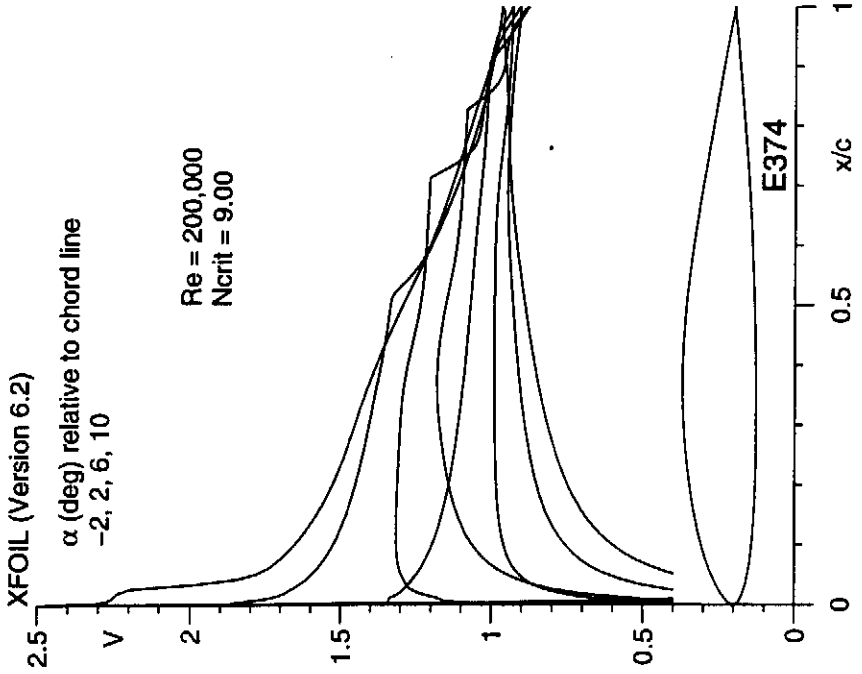
XFOIL (Version 6.2)
α (deg) relative to chord line
-2, 2, 6, 10
Re = 200,000
Ncrit = 9.00
E374
2.5
2
1.5
1
0.5
0
V
0
0.5
1
x/c

E374 (B)

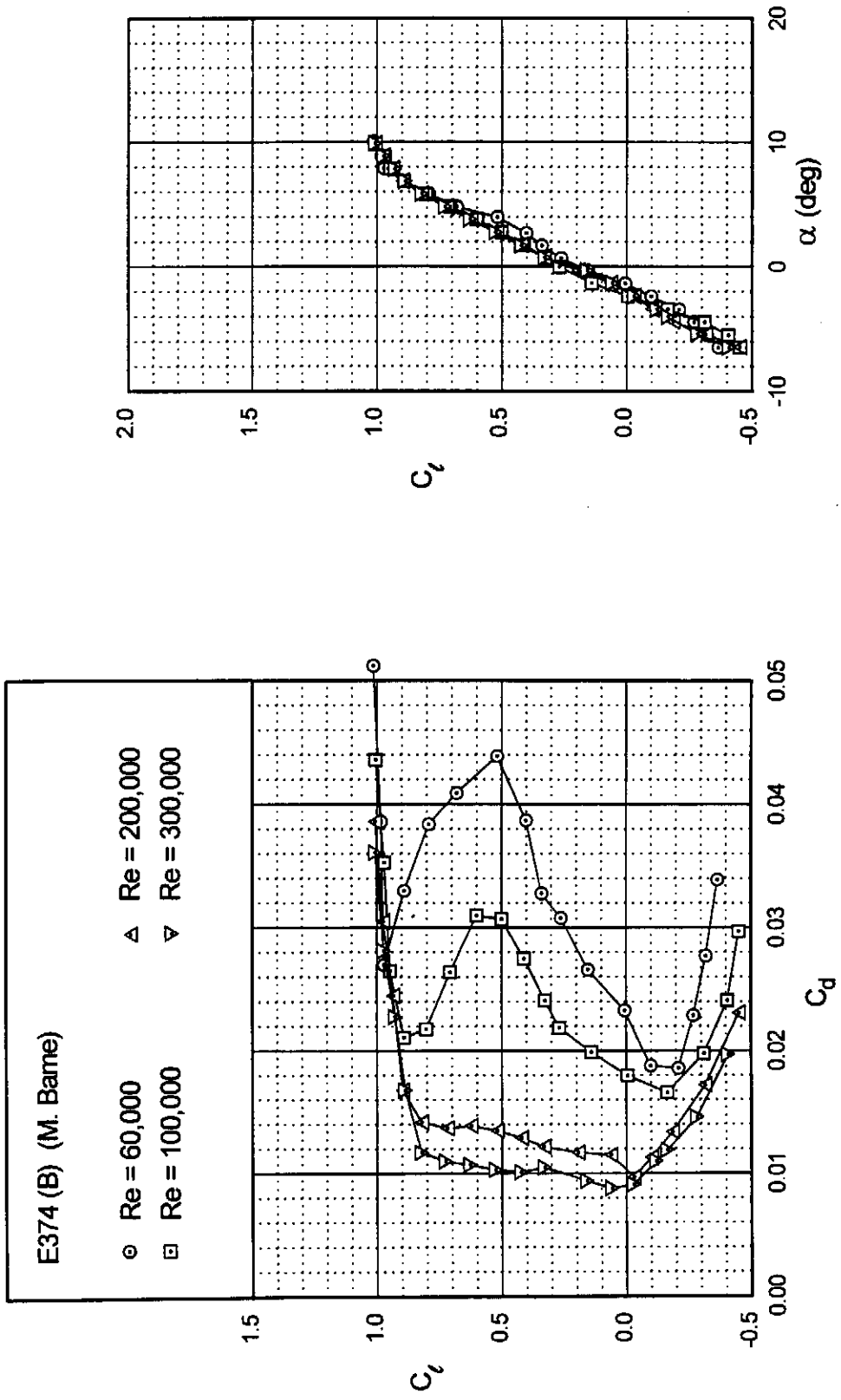
E374 (B) (M. Bame)
Re = 60,000
Re = 100,000
Re = 200,000
Re = 300,000
C_l
C_d
α (deg)
2.0
1.5
1.0
0.5
0.0
-0.5
20
10
0
-10
0.05
0.04
0.03
0.02
0.01
0.00

E374 (B)

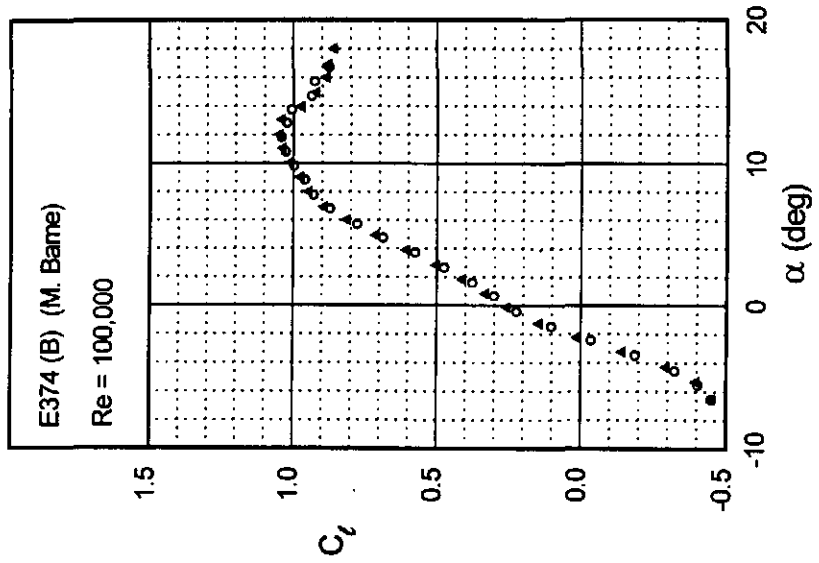
E374 (B) (M. Bame)
Re = 100,000
1.5
1.0
0.5
0.0
-0.5
C_l
-10
0
10
20
α (deg)

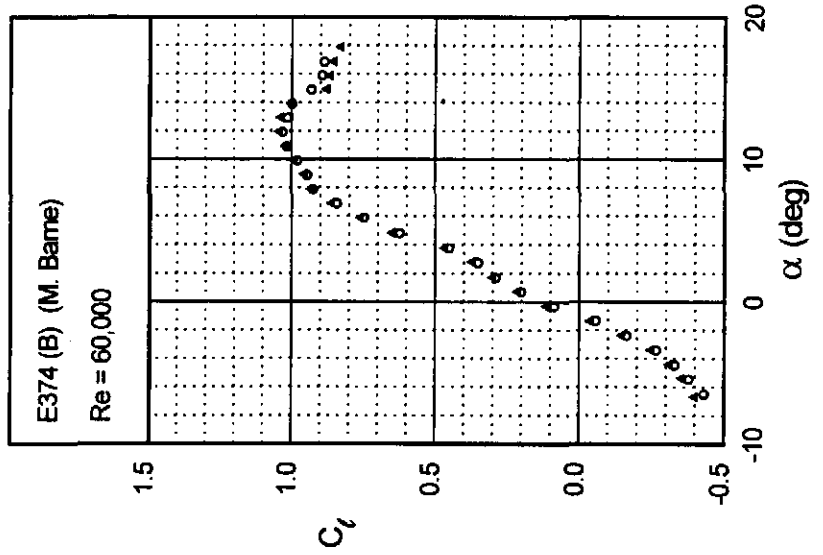
E374 (B) (M. Bame)
Re = 60,000
1.5
1.0
0.5
0.0
-0.5
C_l
-10
0
10
20
α (deg)

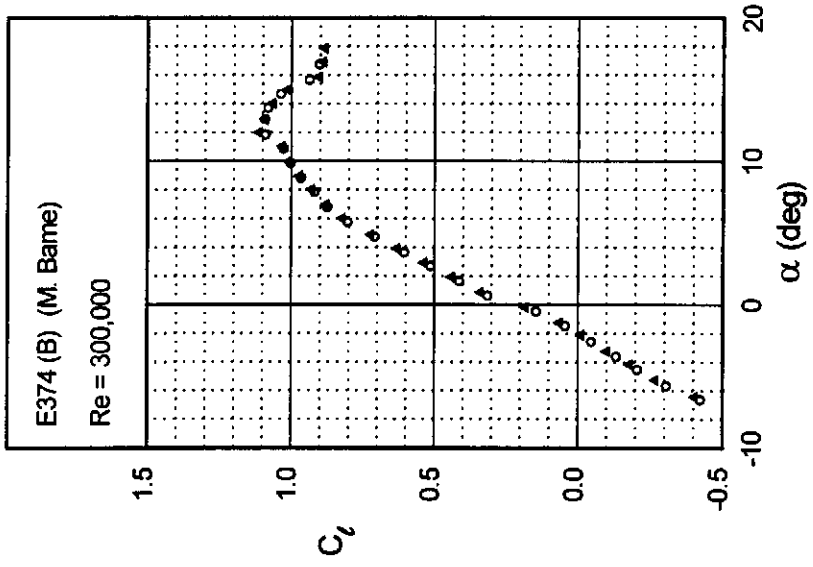
E374 (B) (M. Bame)
Re = 300,000
1.5
1.0
0.5
0.0
-0.5
C_l
-10
0
10
20
α (deg)

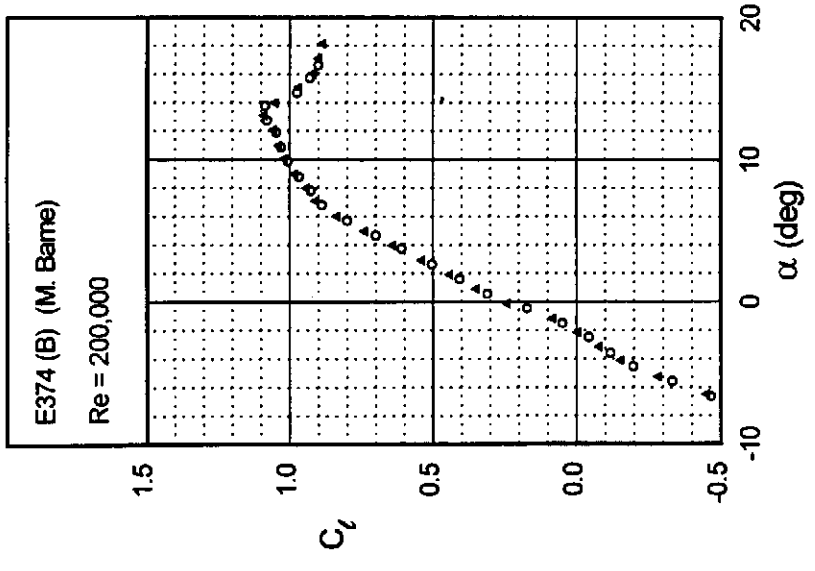
E374 (B) (M. Bame)
Re = 200,000
1.5
1.0
0.5
0.0
-0.5
C_l
-10
0
10
20
α (deg)

E423

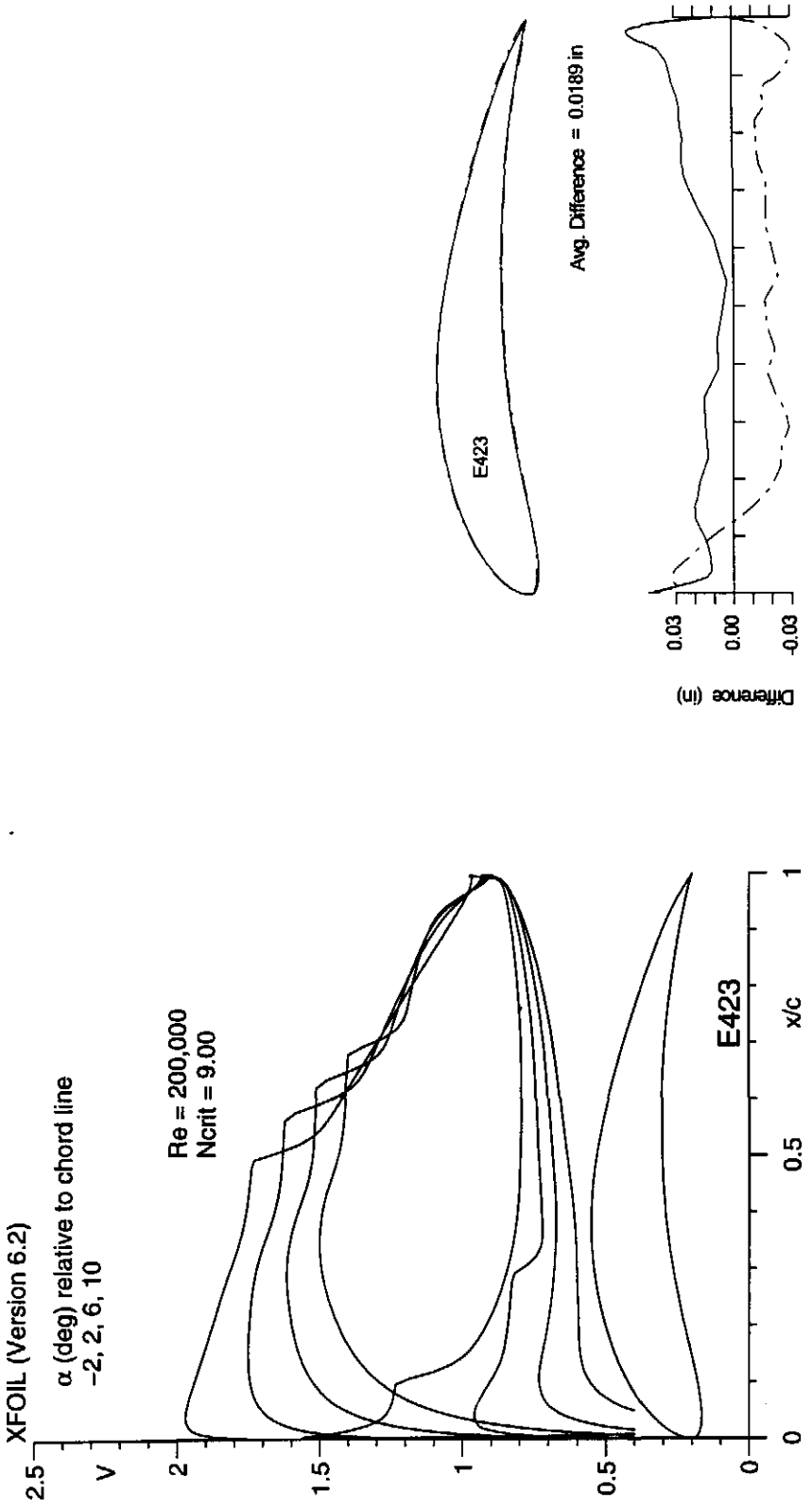
E423
Avg. Difference = 0.0189 in
0.03
0.00
-0.03
Difference (in)
XFOIL (Version 6.2)
α (deg) relative to chord line
-2, 2, 6, 10
Re = 200,000
Ncrit = 9.00
V
2.5
2
1.5
1
0.5
0
E423
0
0.5
1
x/c

E423

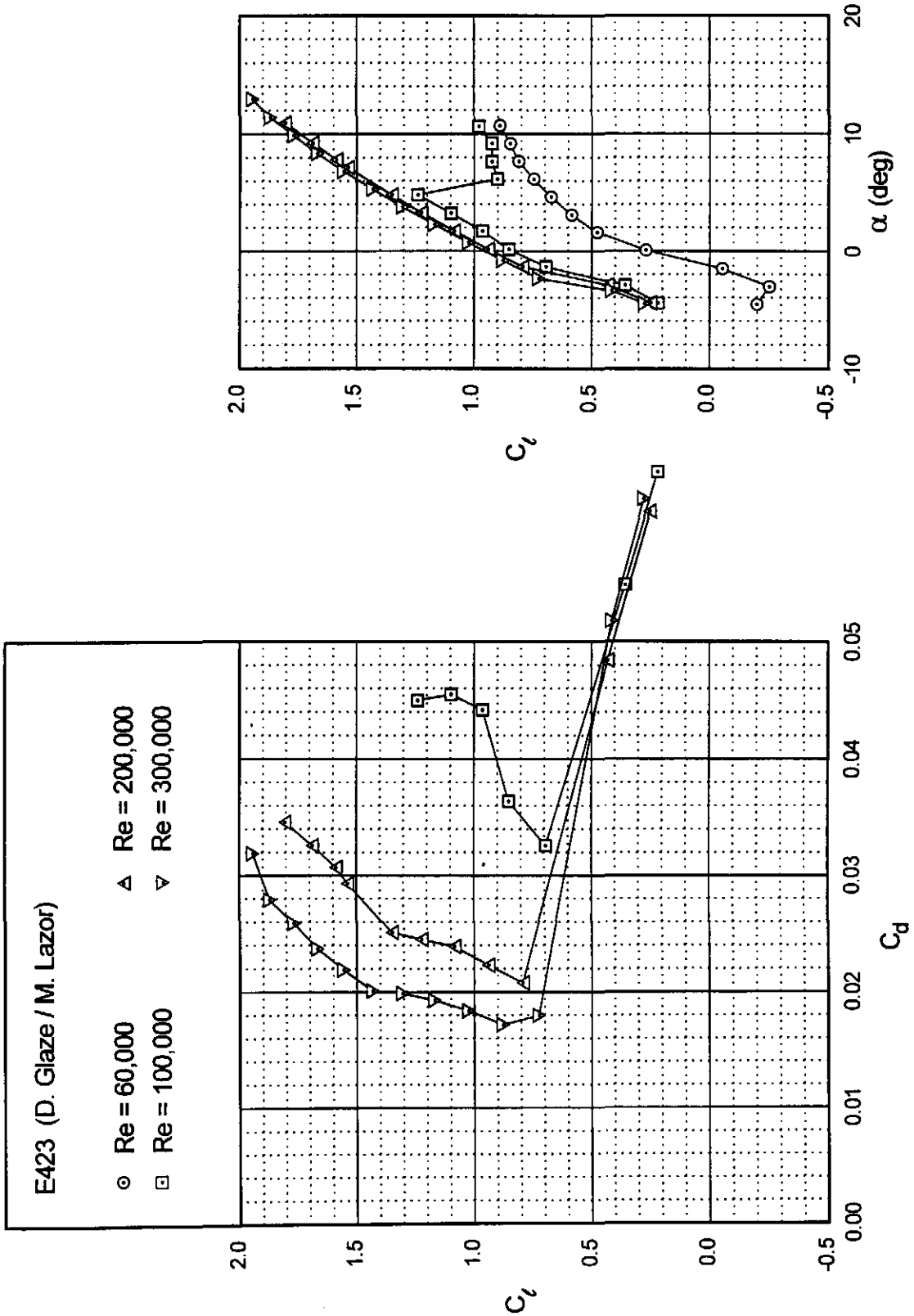
E423 (D. Glaze / M. Lazor)
Re = 60,000
Re = 100,000
Re = 200,000
Re = 300,000
C_l
C_d
α (deg)
2.0
1.5
1.0
0.5
0.0
-0.5
0.00
0.01
0.02
0.03
0.04
0.05
-10
0
10
20

E423

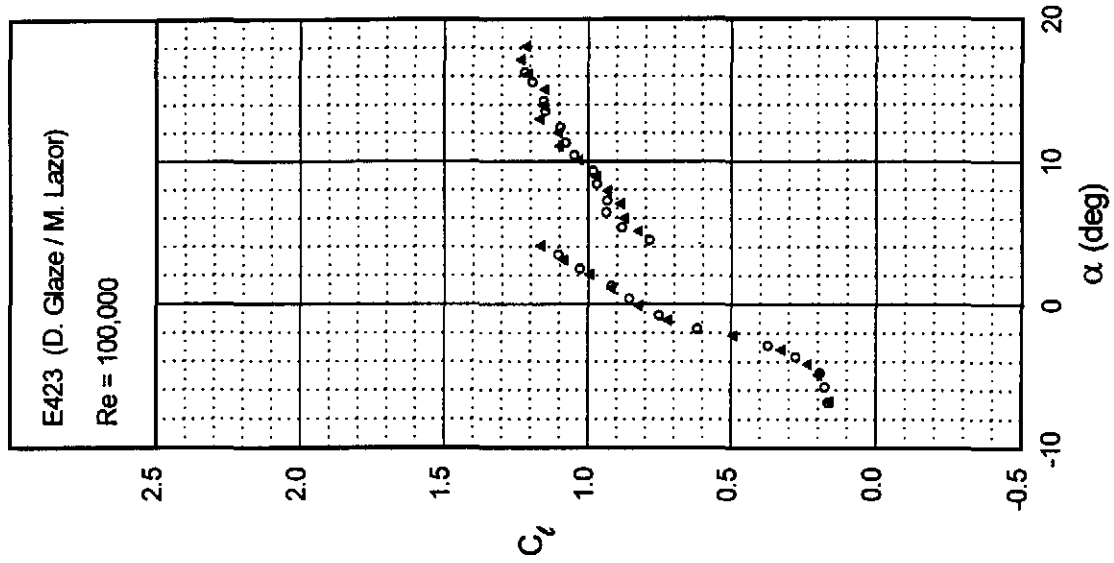
E423 (D. Glaze / M. Lazor)
Re = 100,000
2.5
2.0
1.5
1.0
0.5
0.0
-0.5
C_l
-10
0
10
20
α (deg)

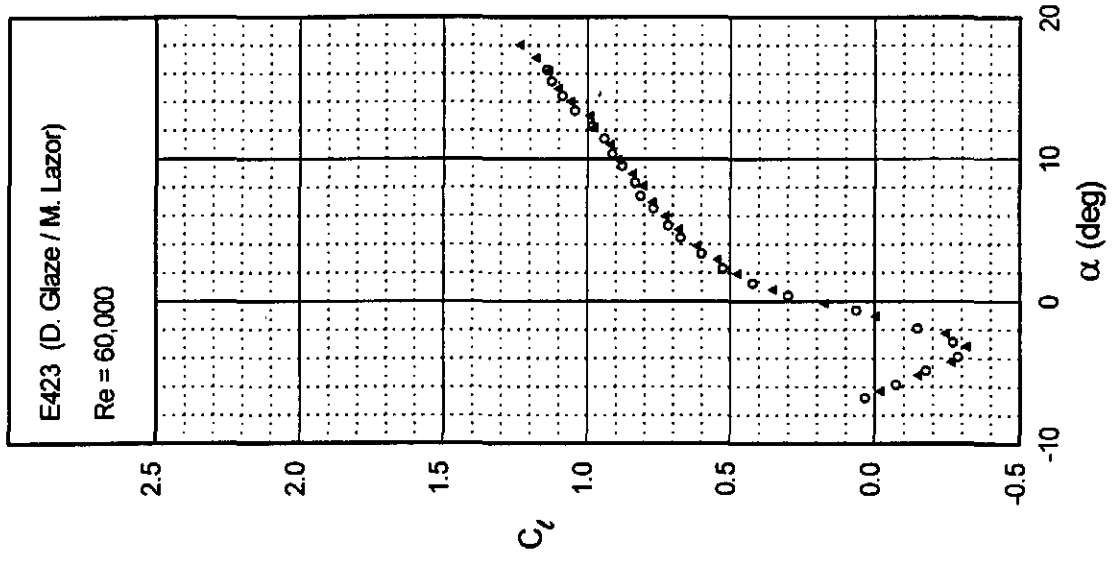
E423 (D. Glaze / M. Lazor)
Re = 60,000
2.5
2.0
1.5
1.0
0.5
0.0
-0.5
C_l
-10
0
10
20
α (deg)

E423

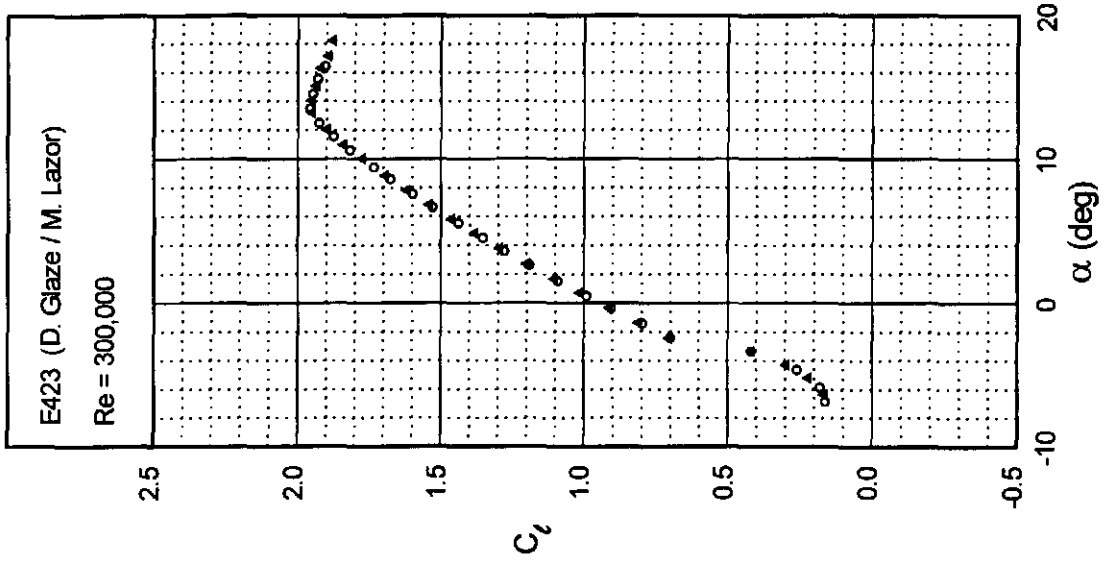
E423 (D. Glaze / M. Lazor)
Re = 300,000
2.5
2.0
1.5
1.0
0.5
0.0
-0.5
C_l
-10
0
10
20
α (deg)

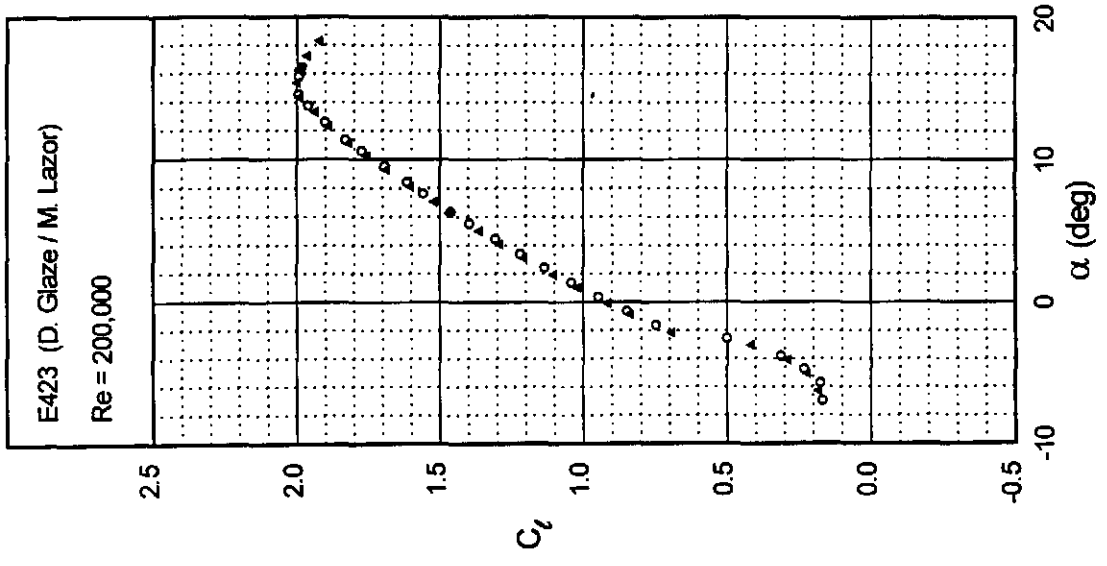
E423 (D. Glaze / M. Lazor)
Re = 200,000
2.5
2.0
1.5
1.0
0.5
0.0
-0.5
C_l
-10
0
10
20
α (deg)

LD-79

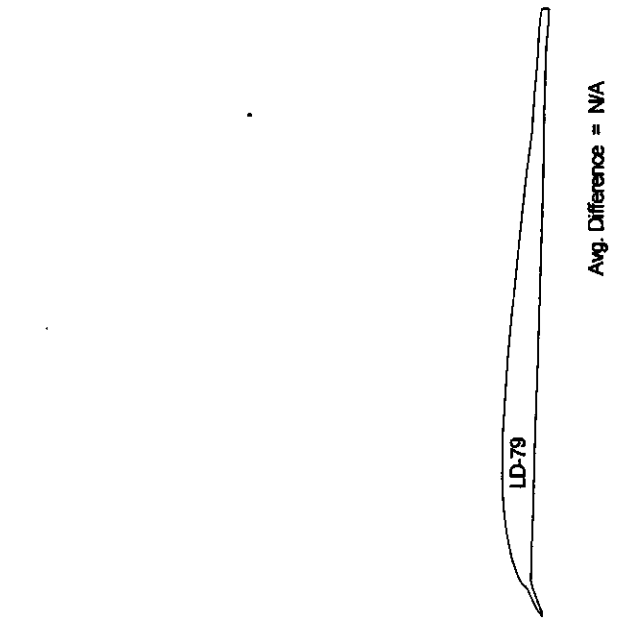
LD-79
Avg. Difference = N/A

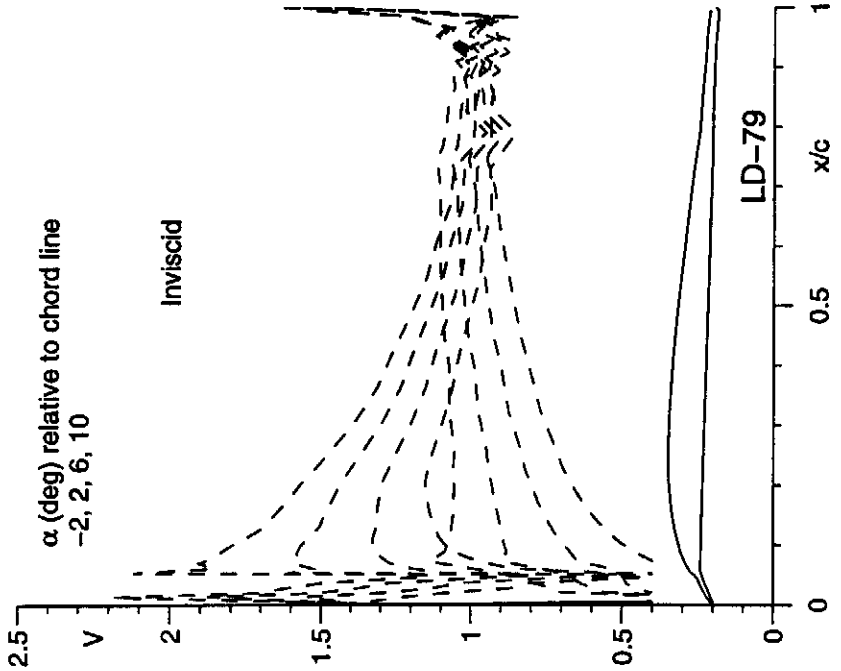
α (deg) relative to chord line
−2, 2, 6, 10
Inviscid
LD−79
V
x/c
2.5
2
1.5
1
0.5
0
0
0.5
1

LD-79

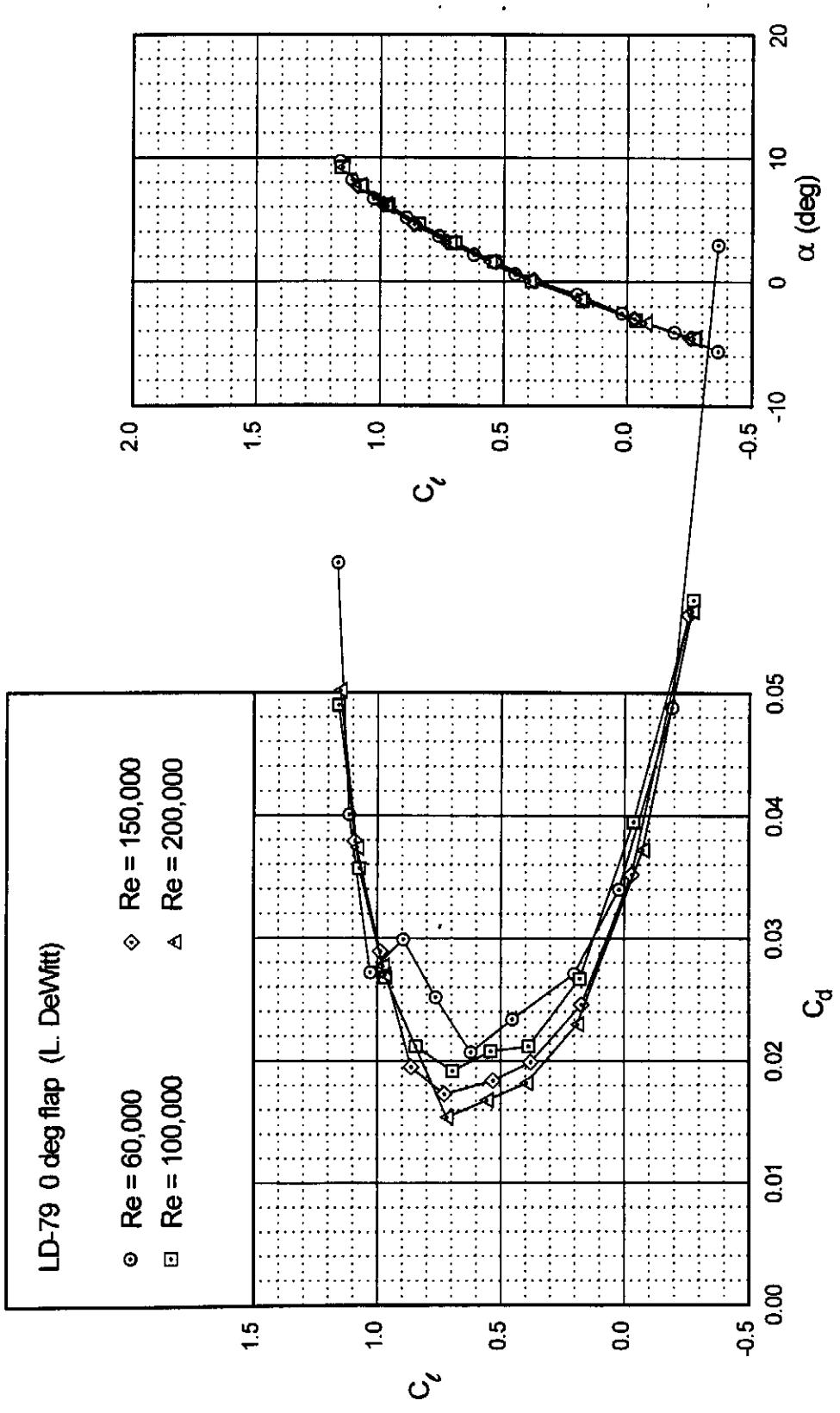
LD-79 0 deg flap (L. DeWitt)
Re = 60,000
Re = 100,000
Re = 150,000
Re = 200,000
C_l
C_d
α (deg)
2.0
1.5
1.0
0.5
0.0
-0.5
-10
0
10
20
0.00
0.01
0.02
0.03
0.04
0.05

Fig. 5.24

LD-79

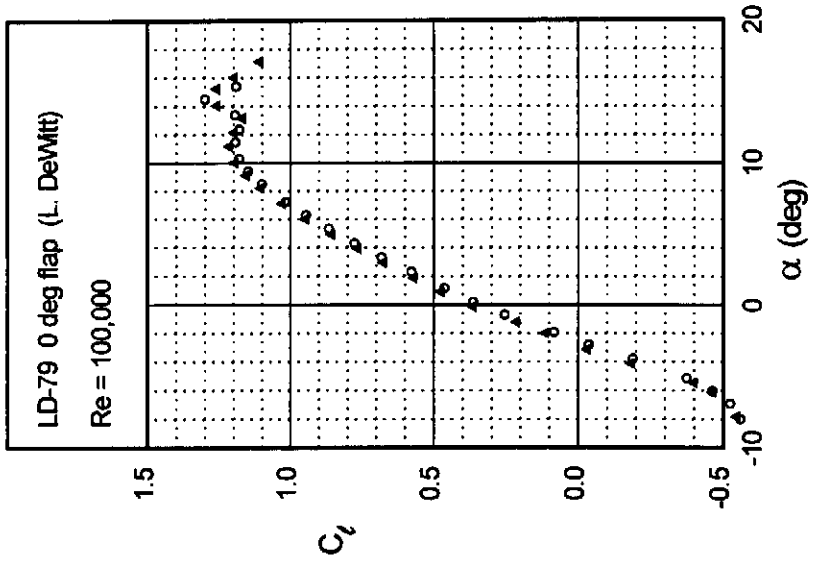
LD-79 0 deg flap (L. DeWitt)
Re = 100,000
1.5
1.0
0.5
0.0
-0.5
C_l
-10
0
10
20
α (deg)

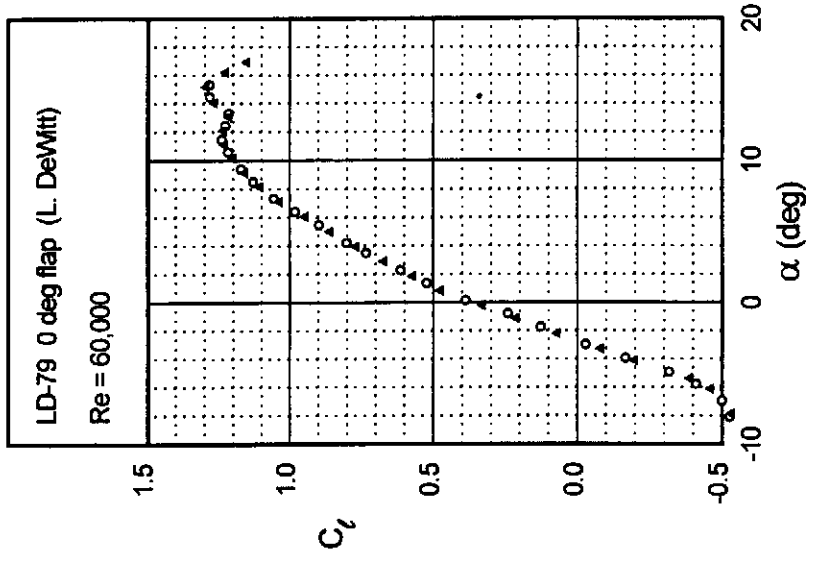
LD-79 0 deg flap (L. DeWitt)
Re = 60,000
1.5
1.0
0.5
0.0
-0.5
C_l
-10
0
10
20
α (deg)

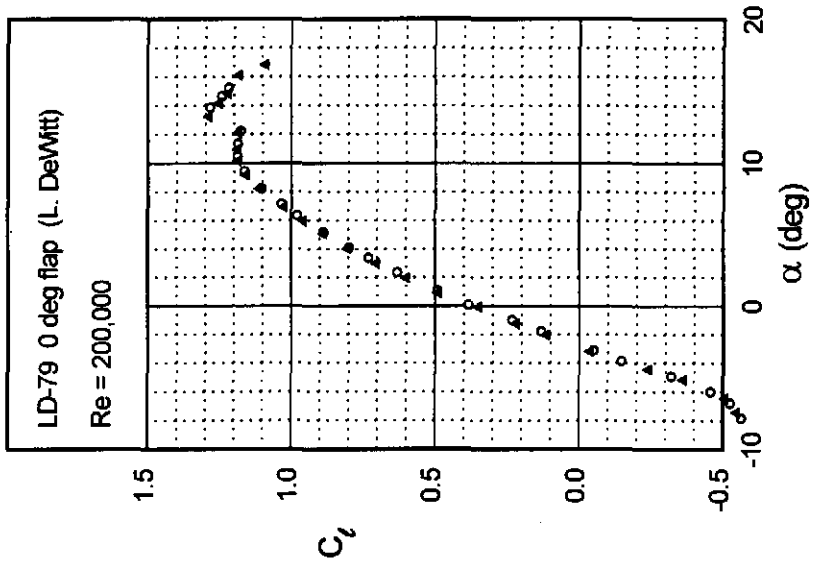
LD-79 0 deg flap (L. DeWitt)
Re = 200,000
1.5
1.0
0.5
0.0
-0.5
C_l
-10
0
10
20
α (deg)

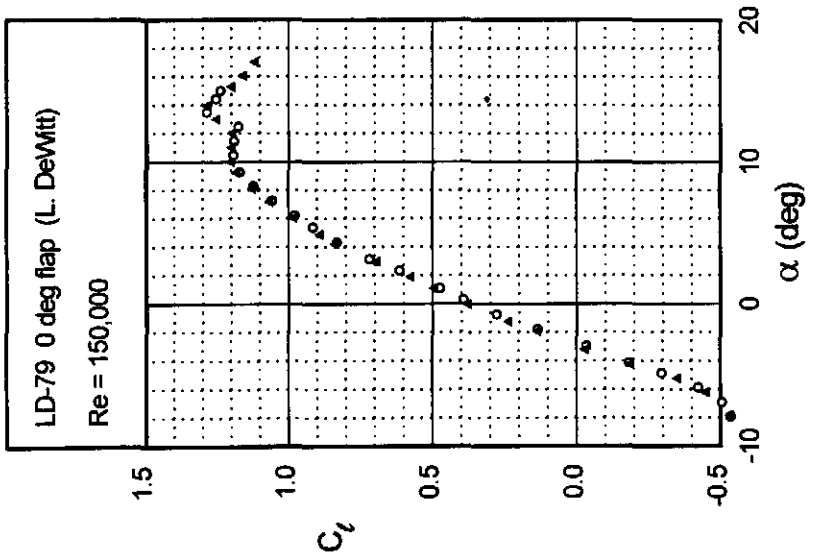
LD-79 0 deg flap (L. DeWitt)
Re = 150,000
1.5
1.0
0.5
0.0
-0.5
C_l
-10
0
10
20
α (deg)

M06-13-128 (B)

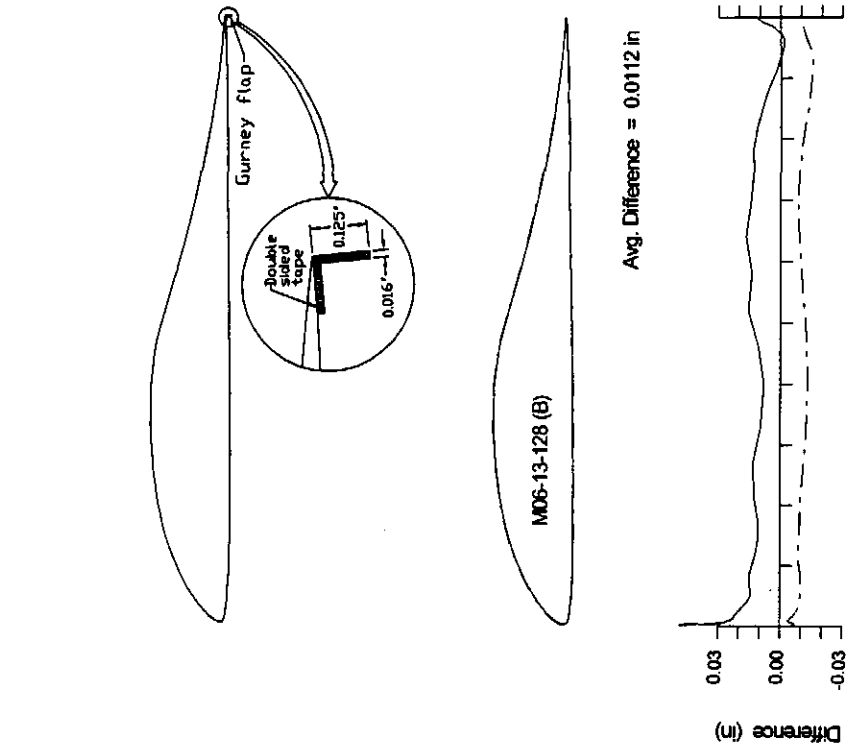
Gurney flap
Double sided tape
0.125"
0.016"
M06-13-128 (B)
Avg. Difference = 0.0112 in
0.03
0.00
-0.03
Difference (in)

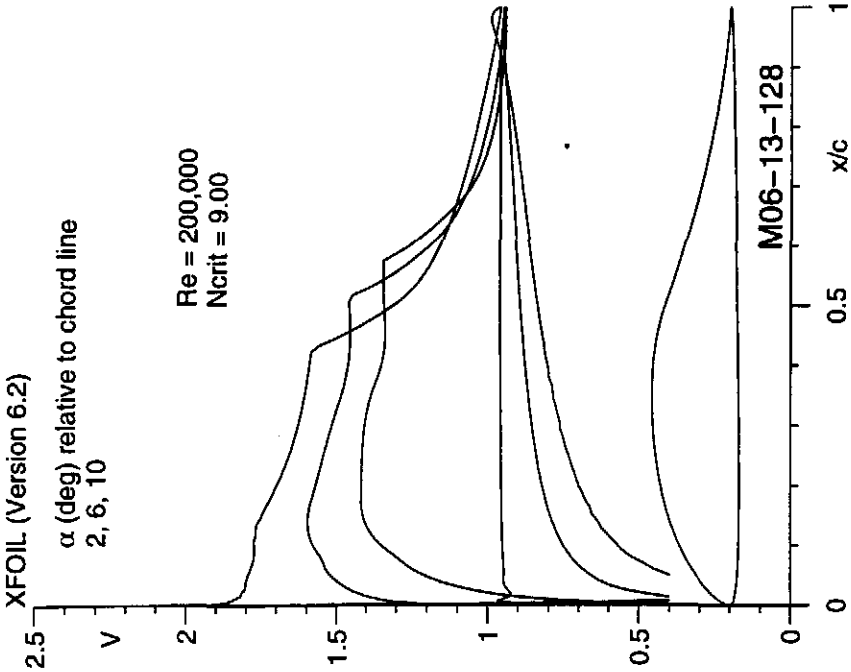
XFOIL (Version 6.2)
α (deg) relative to chord line
2, 6, 10
Re = 200,000
Ncrit = 9.00
M06-13-128
V
x/c
2.5
2
1.5
1
0.5
0
0.5
1

M06-13-128 (B)

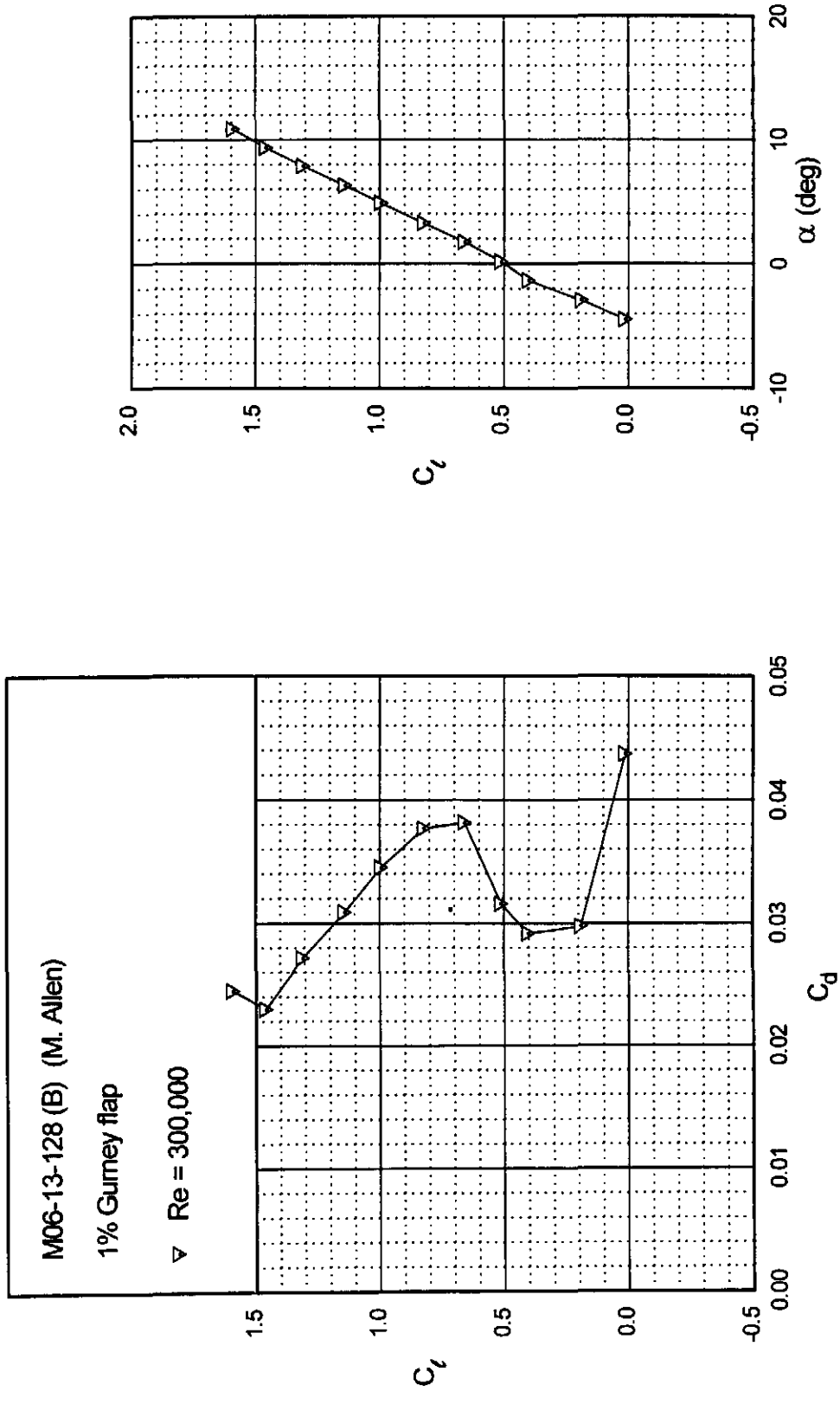
M06-13-128 (B) (M. Allen)
1% Gurney flap
Re = 300,000
C_l
C_d
α (deg)
2.0
1.5
1.0
0.5
0.0
-0.5
20
10
0
-10
0.05
0.04
0.03
0.02
0.01
0.00

M06-13-128 (B)

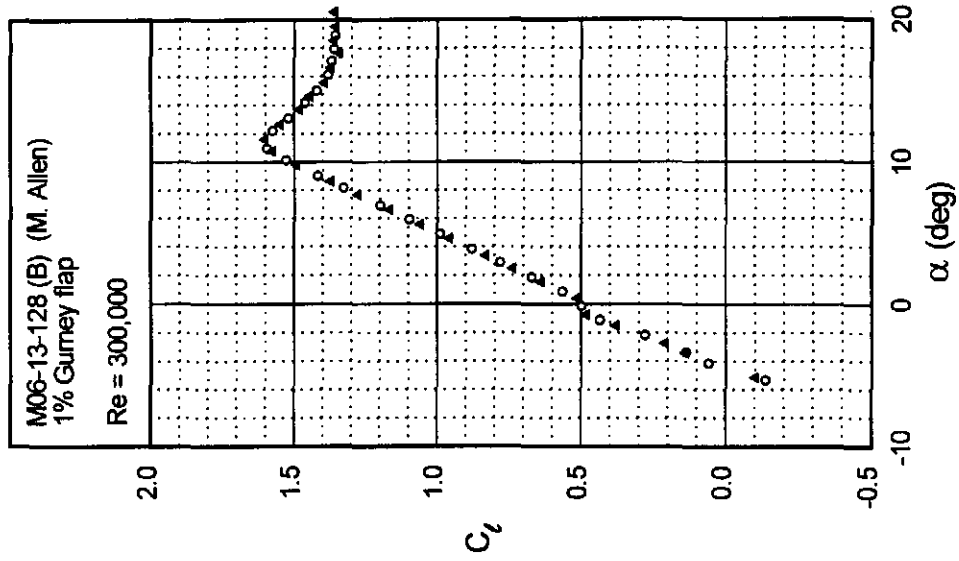
M06-13-128 (B) (M. Allen)
1% Gurney flap
Re = 300,000
2.0
1.5
1.0
0.5
0.0
-0.5
C_l
-10
0
10
20
α (deg)

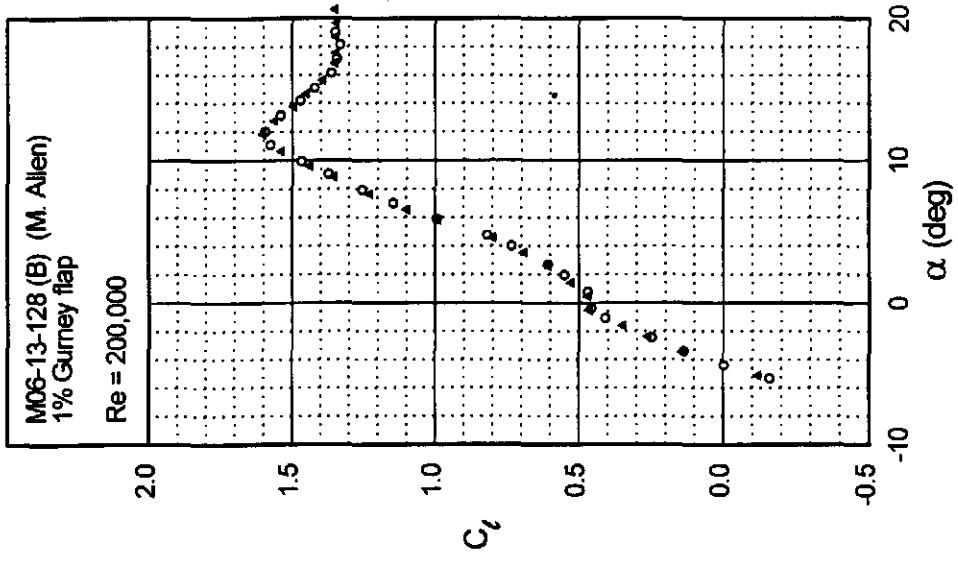
M06-13-128 (B) (M. Allen)
1% Gurney flap
Re = 200,000
2.0
1.5
1.0
0.5
0.0
-0.5
C_l
-10
0
10
20
α (deg)

M6 (65%)

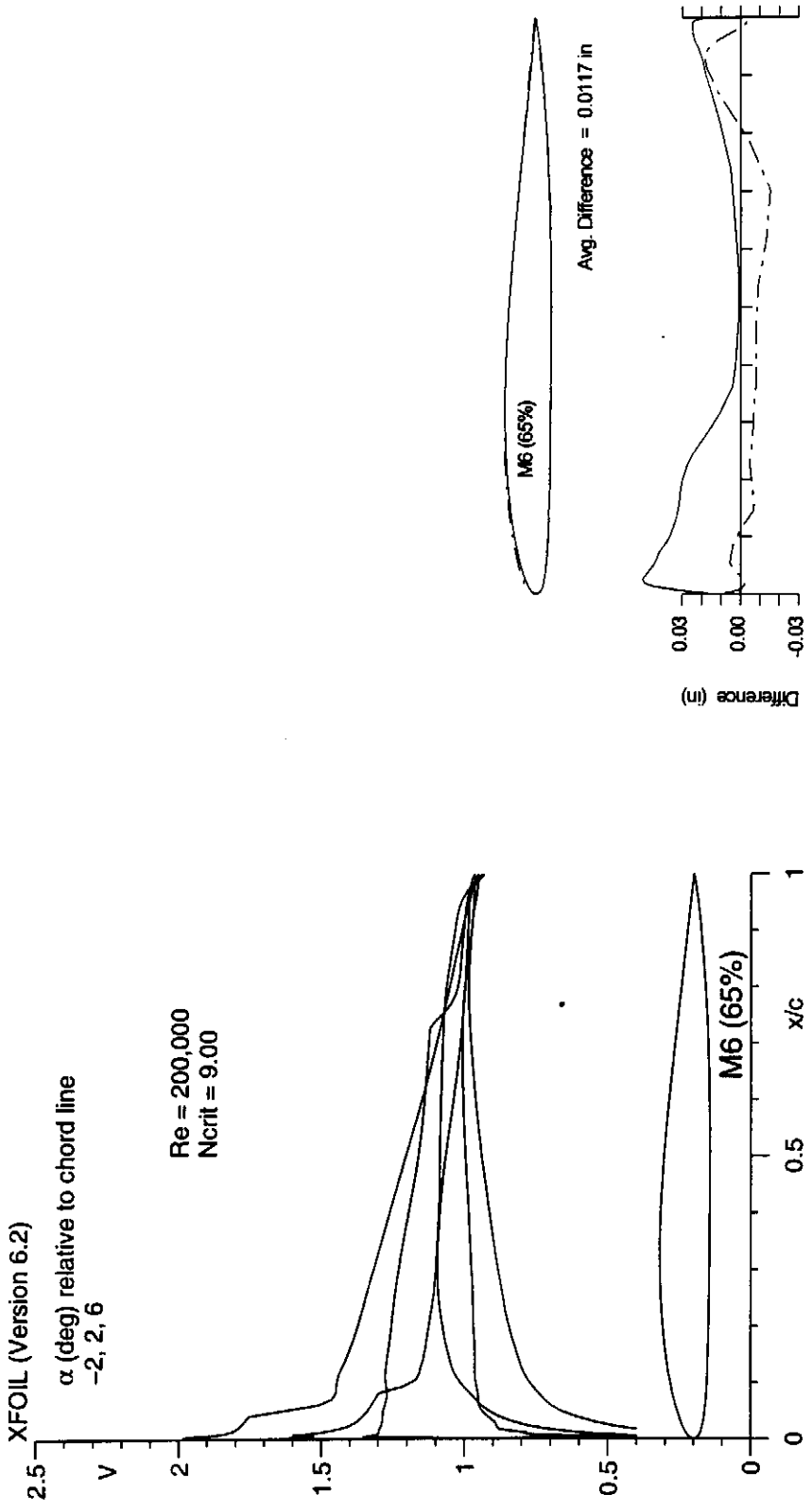
XFOIL (Version 6.2)
α (deg) relative to chord line
-2, 2, 6
Re = 200,000
Ncrit = 9.00
V
2.5
2
1.5
1
0.5
0
0
0.5
1
x/c
M6 (65%)
M6 (65%)
Avg. Difference = 0.0117 in
0.03
0.00
-0.03
Difference (in)

M6 (65%)

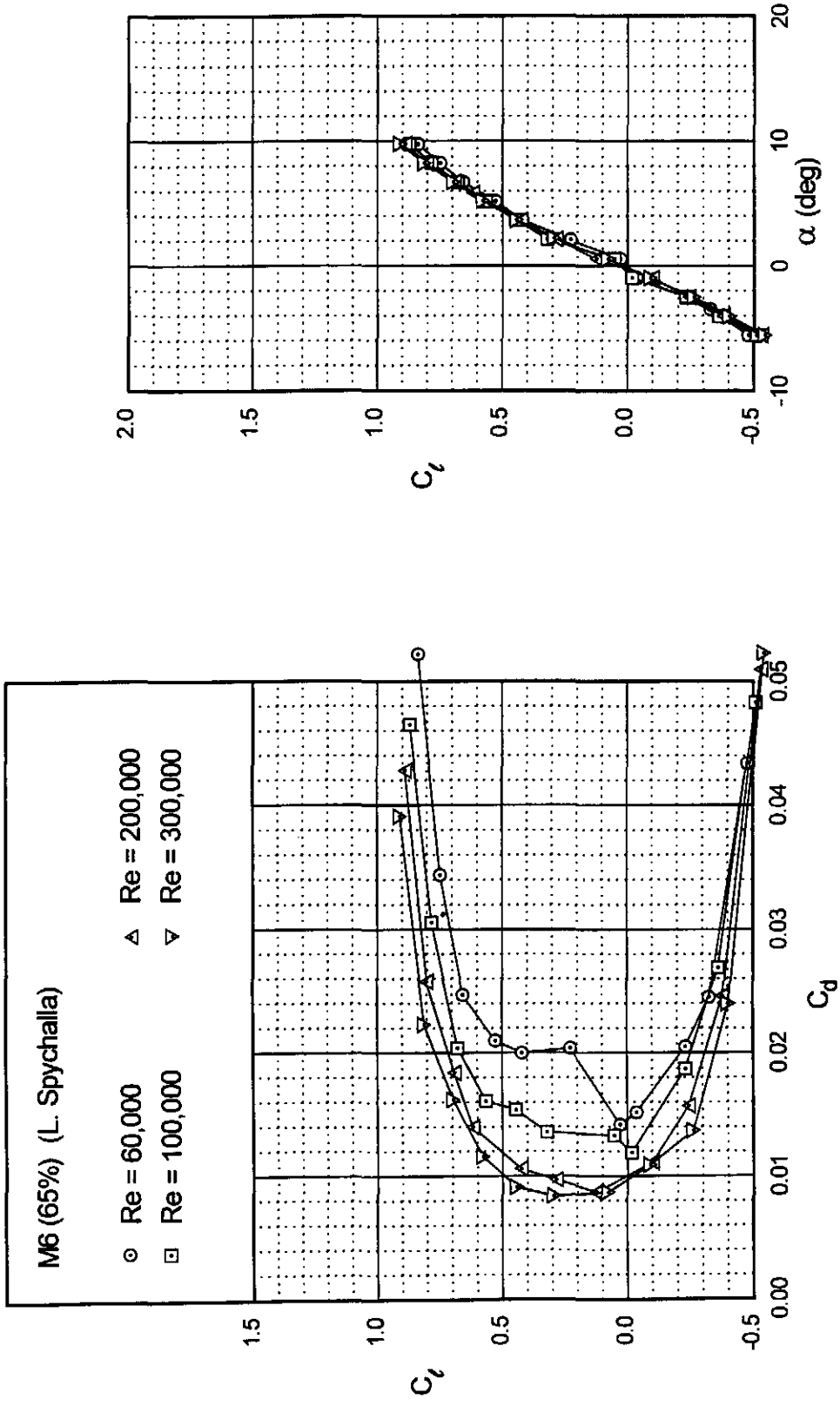
M6 (65%) (L. Spychalla)
Re = 60,000
Re = 100,000
Re = 200,000
Re = 300,000
C_l
C_d
α (deg)

M6 (65%)

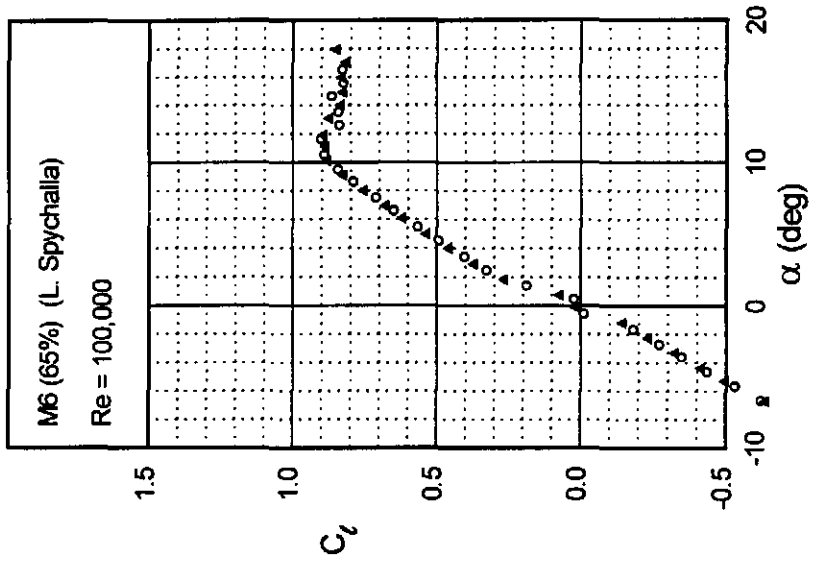
M6 (65%) (L. Spychalla)
Re = 100,000
1.5
1.0
0.5
0.0
-0.5
C_l
-10
0
10
20
α (deg)

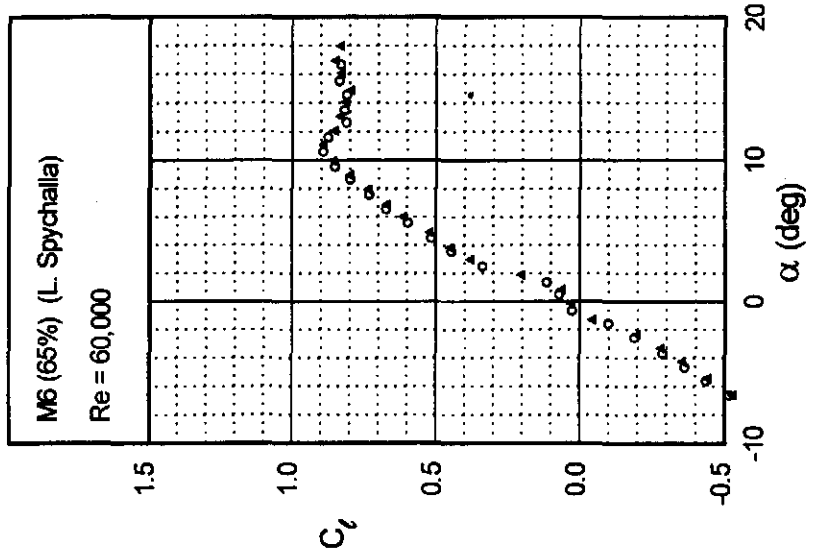
M6 (65%) (L. Spychalla)
Re = 60,000
1.5
1.0
0.5
0.0
-0.5
C_l
-10
0
10
20
α (deg)

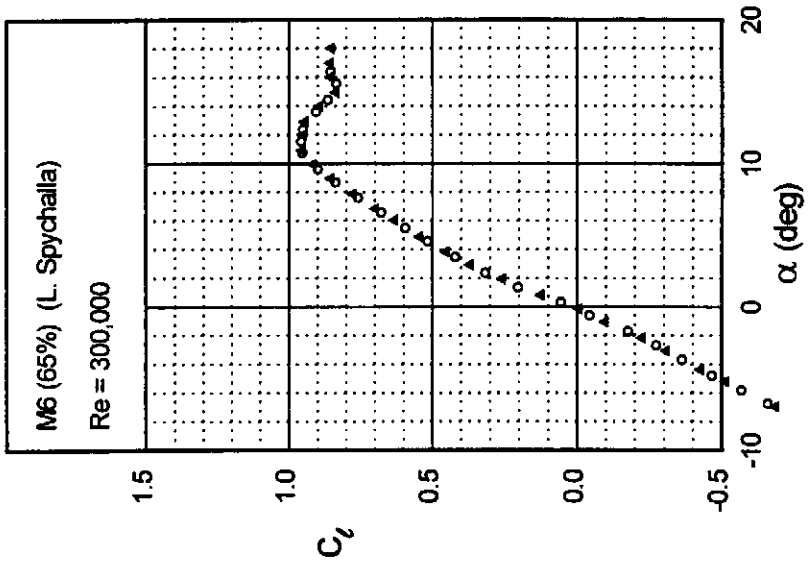
M6 (65%) (L. Spychalla)
Re = 300,000
1.5
1.0
0.5
0.0
-0.5
C_l
-10
0
10
20
α (deg)

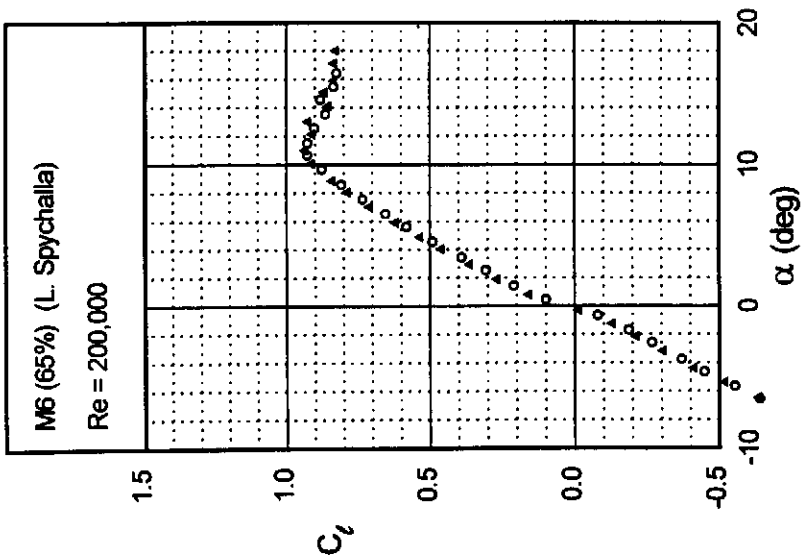
M6 (65%) (L. Spychalla)
Re = 200,000
1.5
1.0
0.5
0.0
-0.5
C_l
-10
0
10
20
α (deg)

M6 (85%)

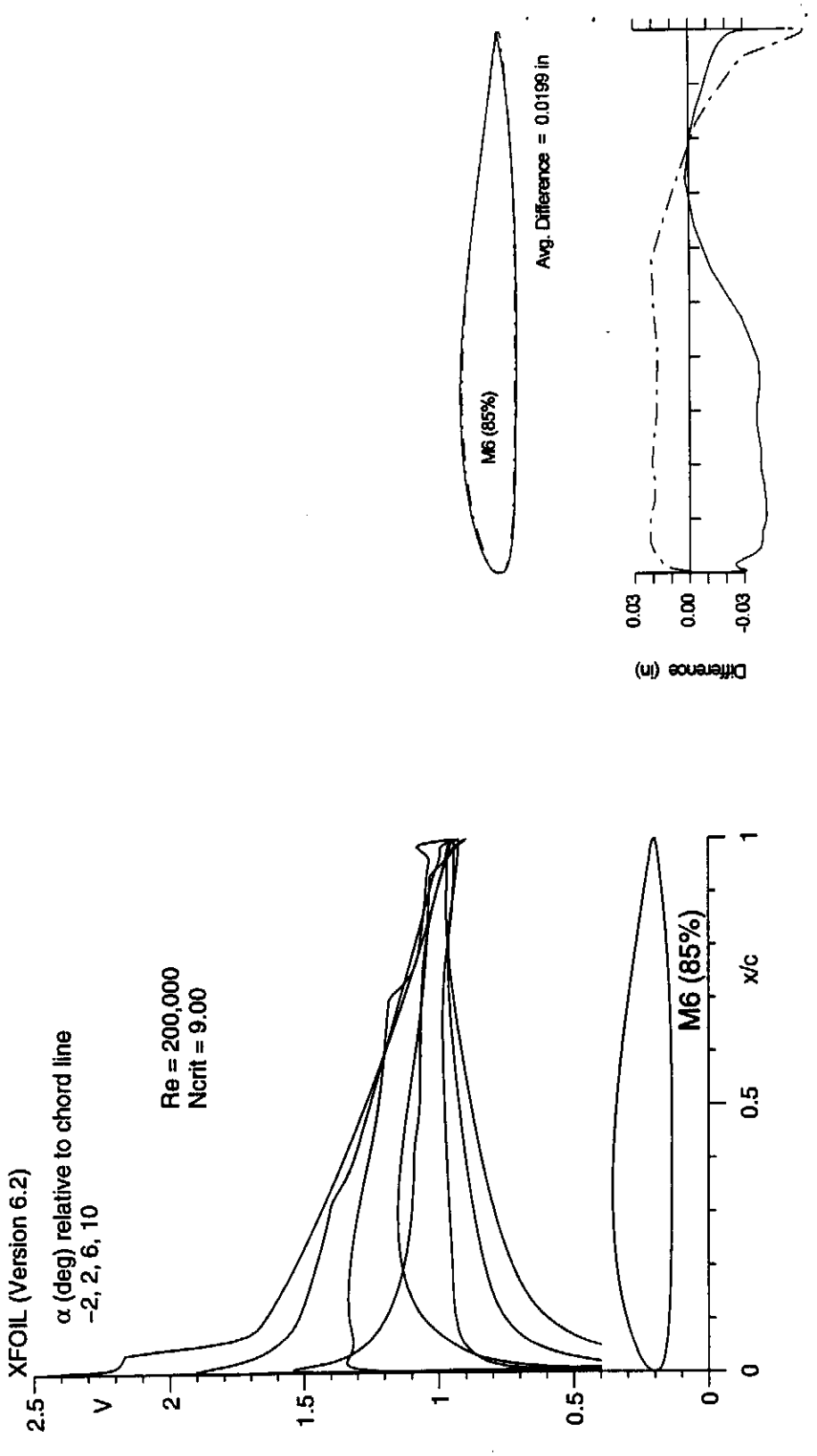
XFOIL (Version 6.2)
α (deg) relative to chord line
-2, 2, 6, 10
Re = 200,000
Ncrit = 9.00
V
2.5
2
1.5
1
0.5
0
0.5
1
x/c
M6 (85%)
Avg. Difference = 0.0199 in
M6 (85%)
0.03
0.00
-0.03
Difference (in)

M6 (85%)

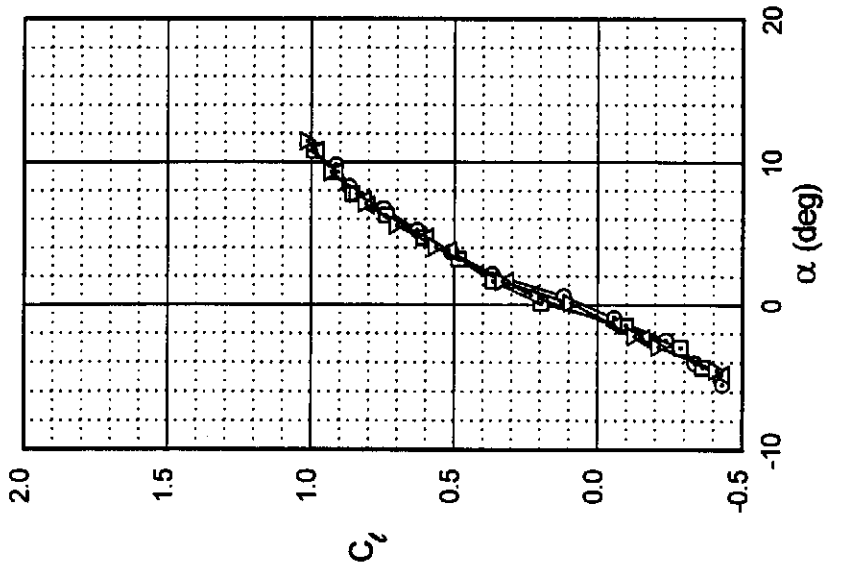
2.0
1.5
1.0
0.5
0.0
-0.5
C_l
20
10
0
-10
α (deg)

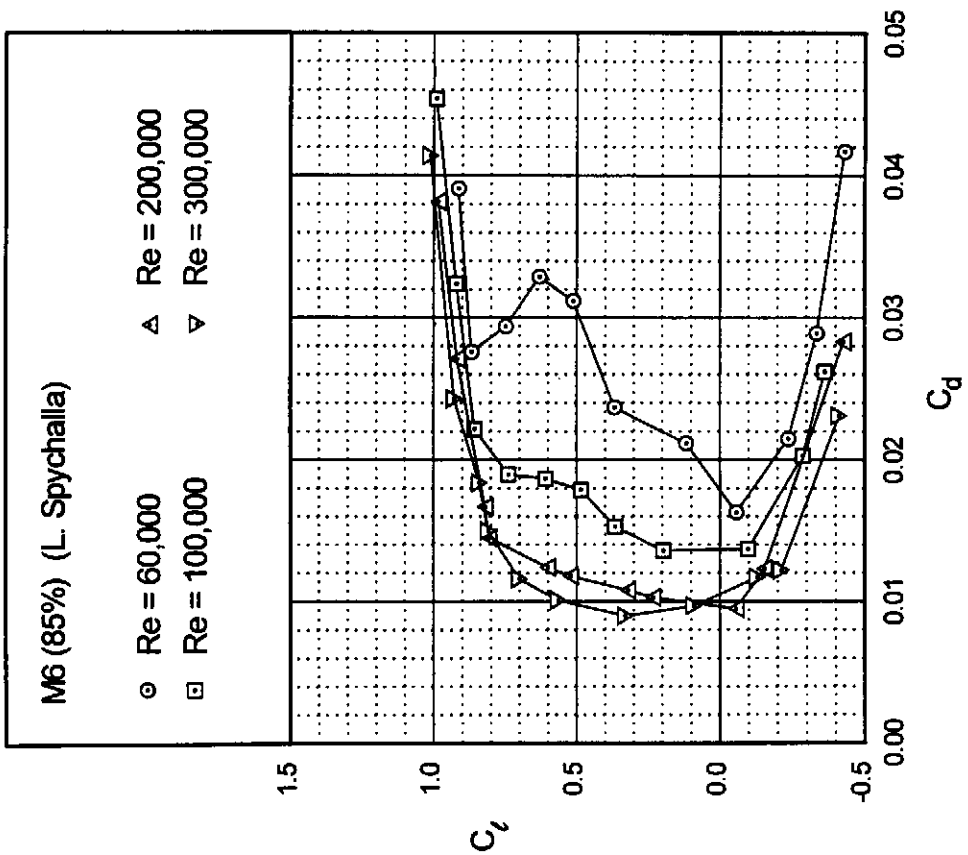
M6 (85%) (L. Spychalla)
Re = 60,000
Re = 100,000
Re = 200,000
Re = 300,000
1.5
1.0
0.5
0.0
-0.5
C_l
0.05
0.04
0.03
0.02
0.01
0.00
C_d

M6 (85%)

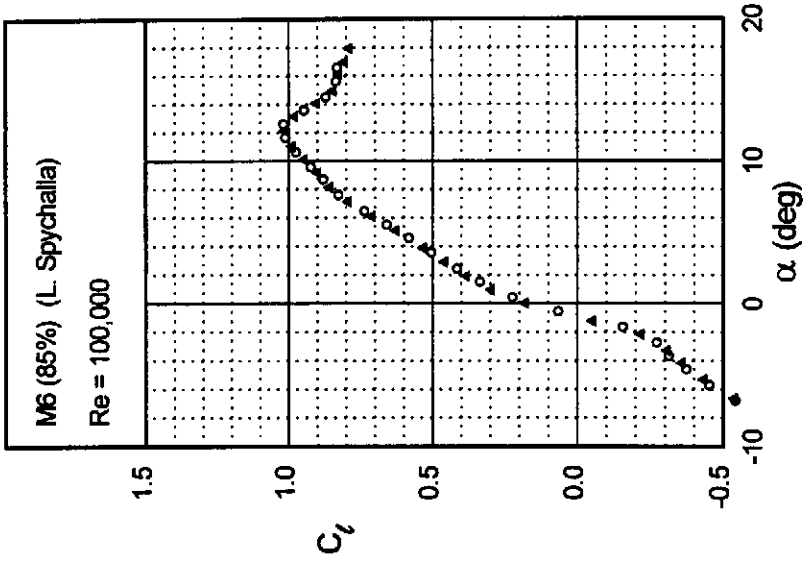
M6 (85%) (L. Spychalla)
Re = 100,000
1.5
1.0
0.5
0.0
-0.5
C_l
-10
0
10
20
α (deg)

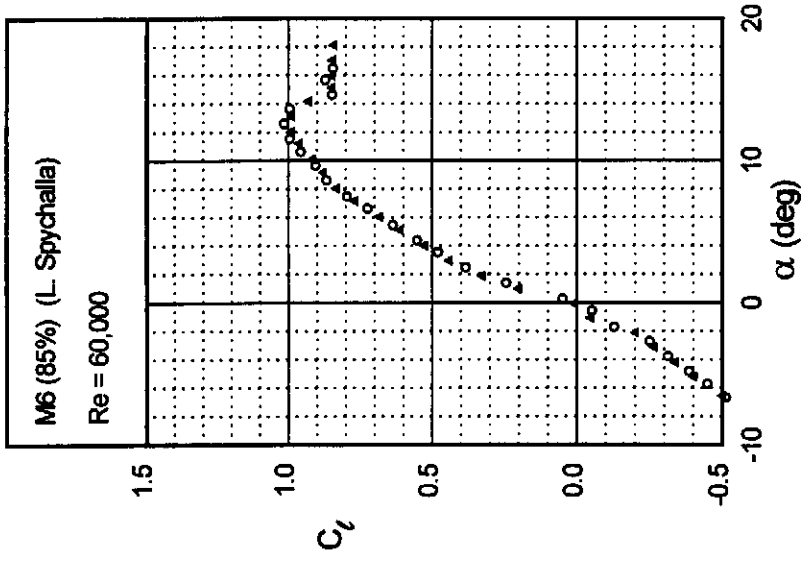
M6 (85%) (L. Spychalla)
Re = 60,000
1.5
1.0
0.5
0.0
-0.5
C_l
-10
0
10
20
α (deg)

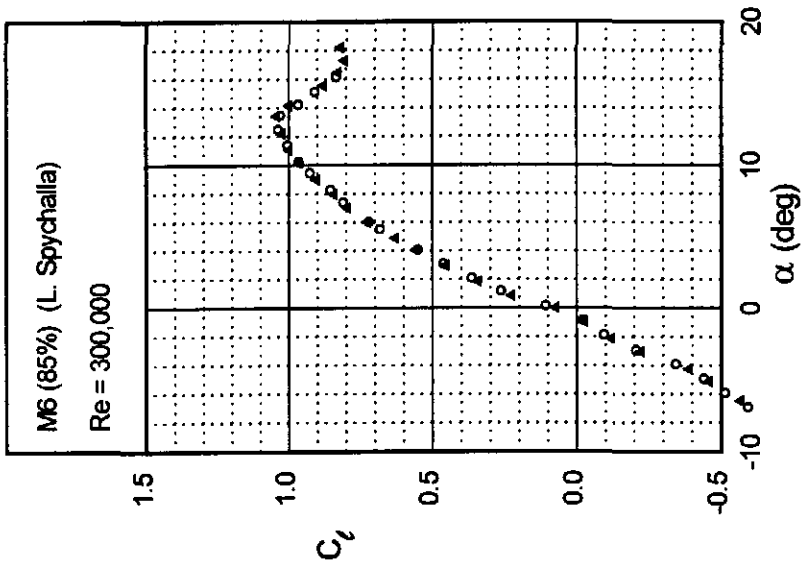
M6 (85%) (L. Spychalla)
Re = 300,000
1.5
1.0
0.5
0.0
-0.5
C_l
-10
0
10
20
α (deg)

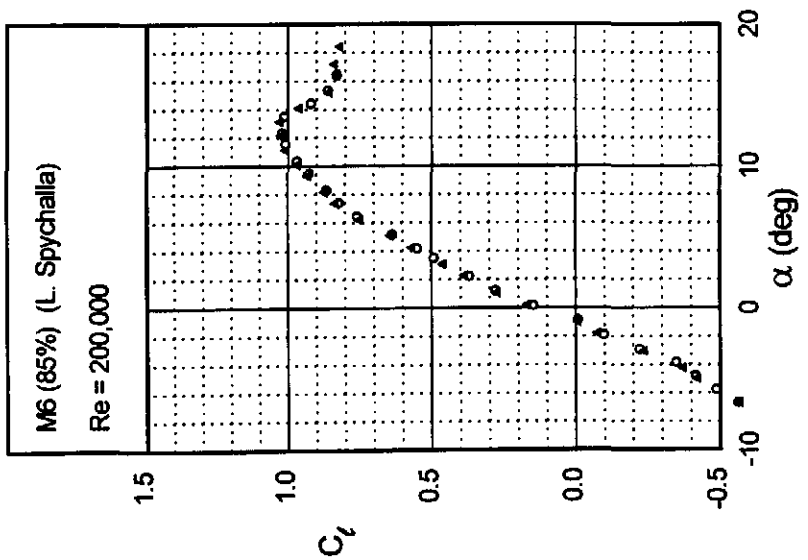
M6 (85%) (L. Spychalla)
Re = 200,000
1.5
1.0
0.5
0.0
-0.5
C_l
-10
0
10
20
α (deg)

MA409

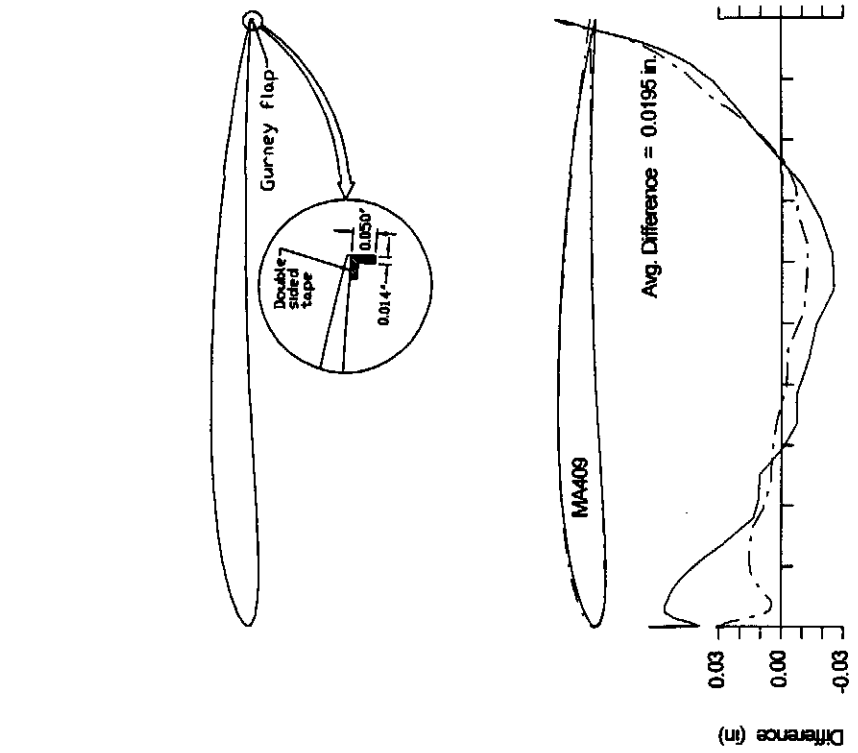
Gurney flap
0.050"
0.014"
Double sided tape
MA409
Avg. Difference = 0.0195 in.
0.03
0.00
-0.03
Difference (in)

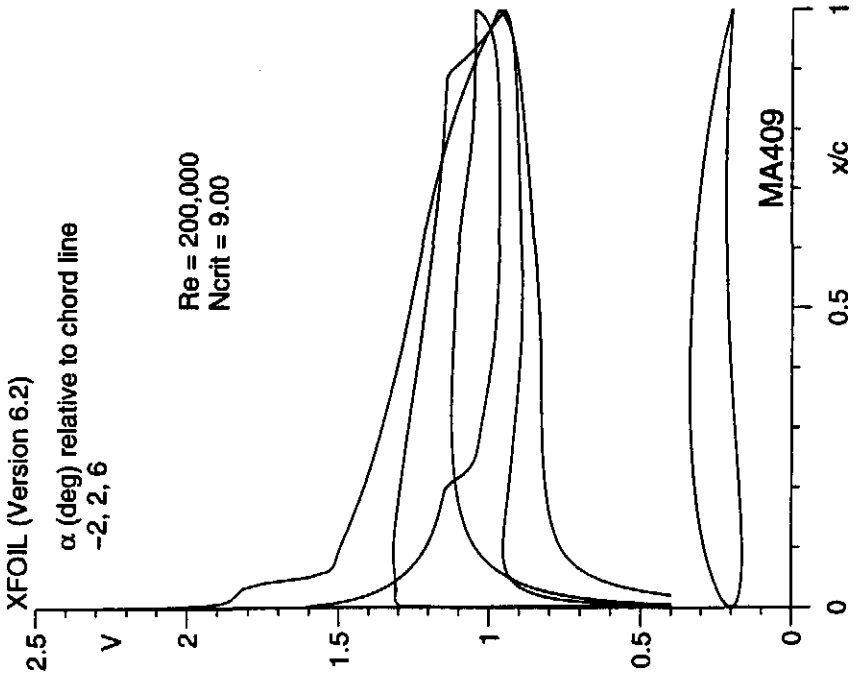
XFOIL (Version 6.2)
α (deg) relative to chord line
-2, 2, 6
Re = 200,000
Ncrit = 9.00
MA409
V
x/c
2.5
2
1.5
1
0.5
0
0.5
1

MA409

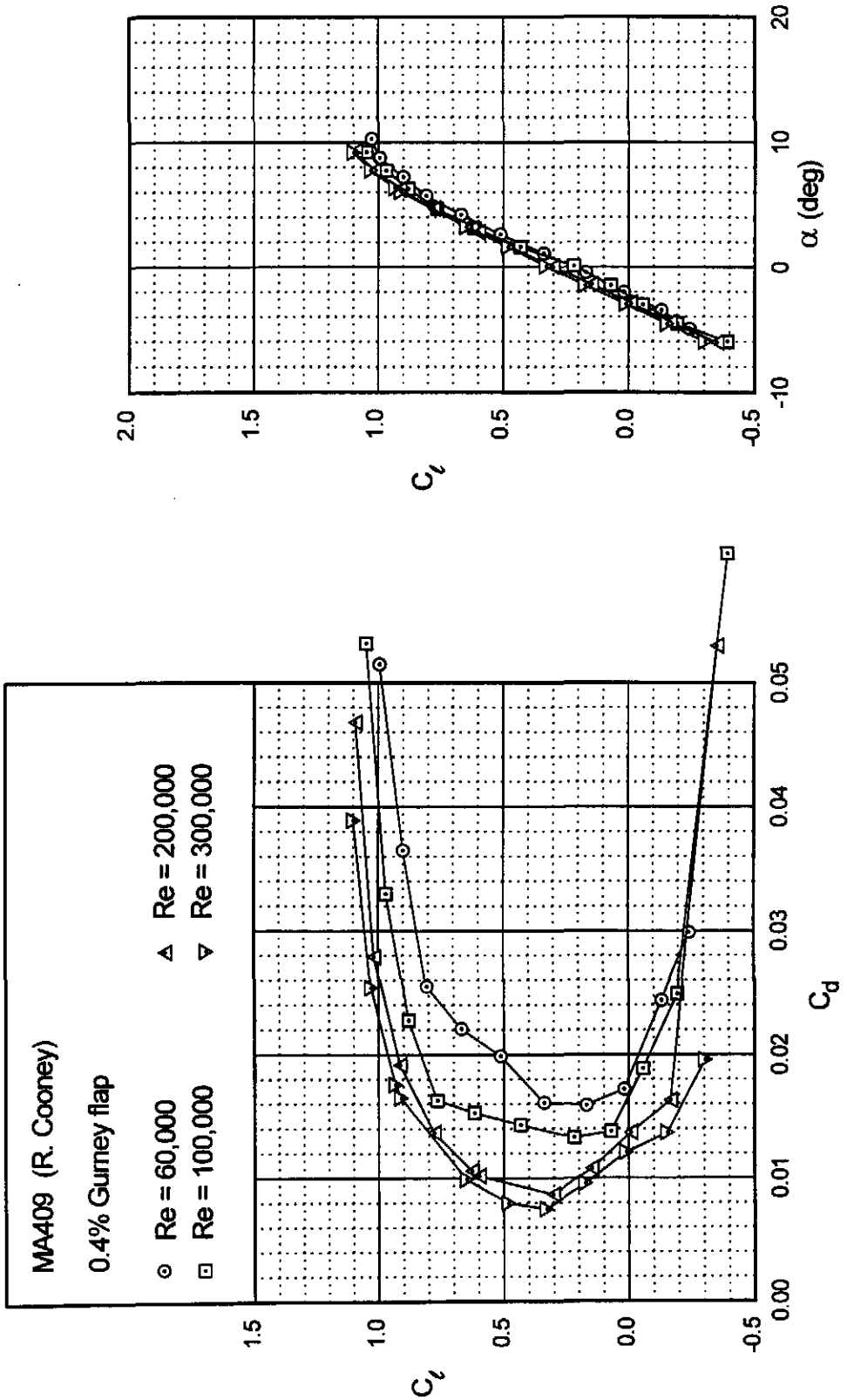
MA409 (R. Cooney)
0.4% Gurney flap
Re = 60,000
Re = 100,000
Re = 200,000
Re = 300,000
C_l
C_d
α (deg)

MA409

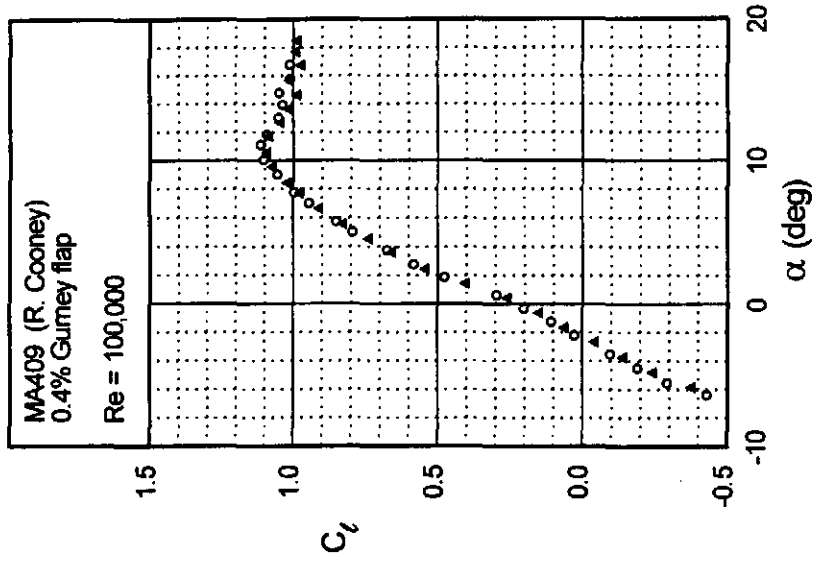
MA409 (R. Cooney)
0.4% Gurney flap
Re = 100,000
1.5
1.0
0.5
0.0
-0.5
C_l
-10
0
10
20
α (deg)

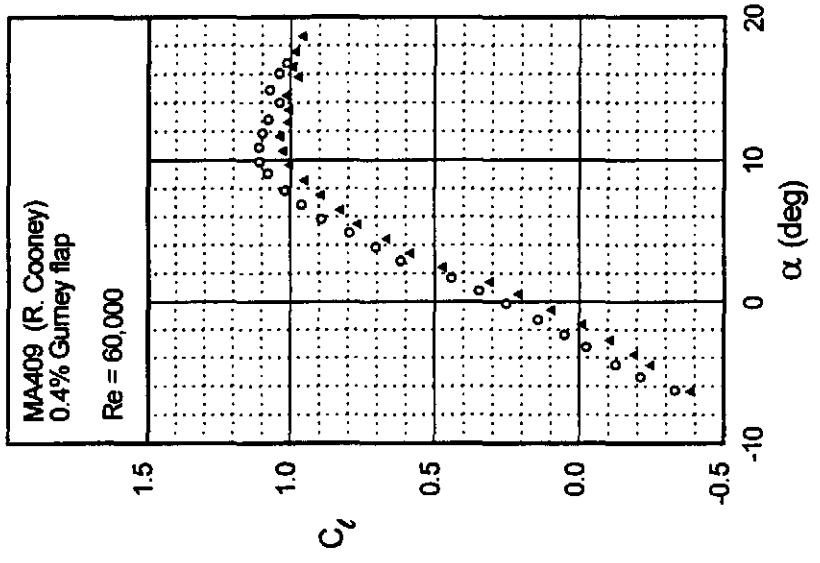
MA409 (R. Cooney)
0.4% Gurney flap
Re = 60,000
1.5
1.0
0.5
0.0
-0.5
C_l
-10
0
10
20
α (deg)

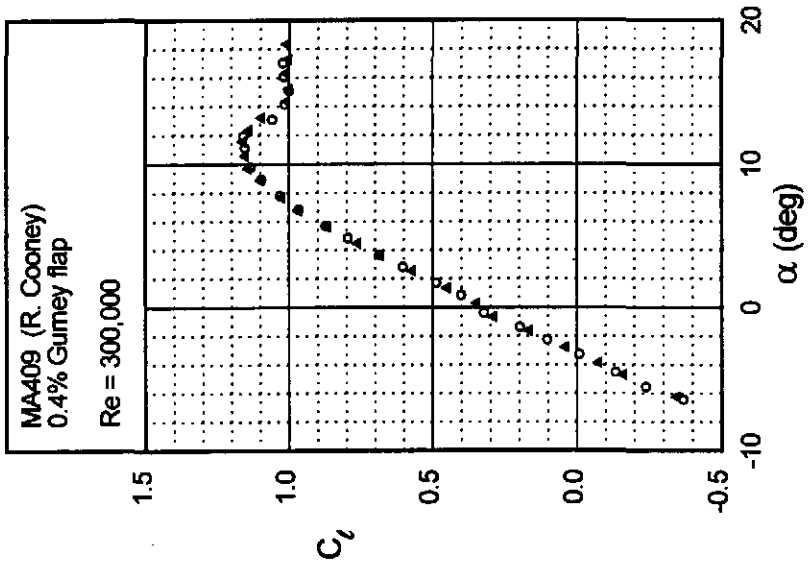
MA409 (R. Cooney)
0.4% Gurney flap
Re = 300,000
1.5
1.0
0.5
0.0
-0.5
C_l
-10
0
10
20
α (deg)

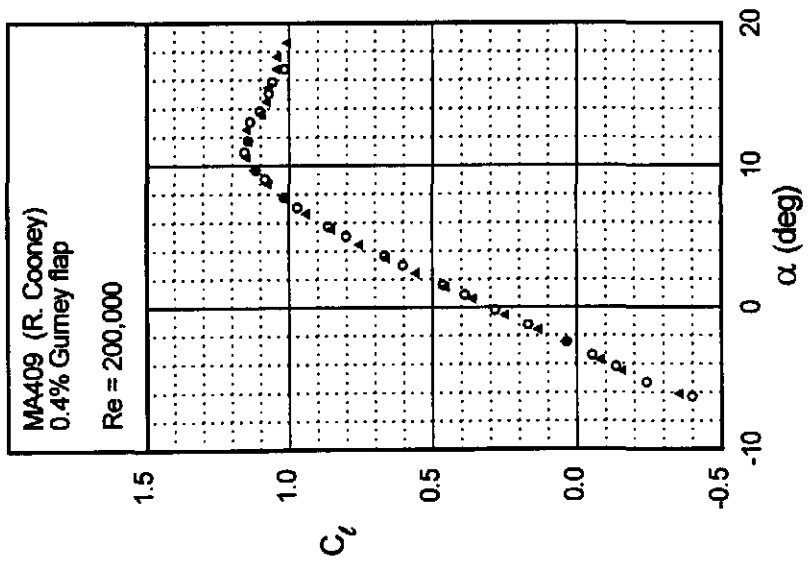
MA409 (R. Cooney)
0.4% Gurney flap
Re = 200,000
1.5
1.0
0.5
0.0
-0.5
C_l
-10
0
10
20
α (deg)

MH32

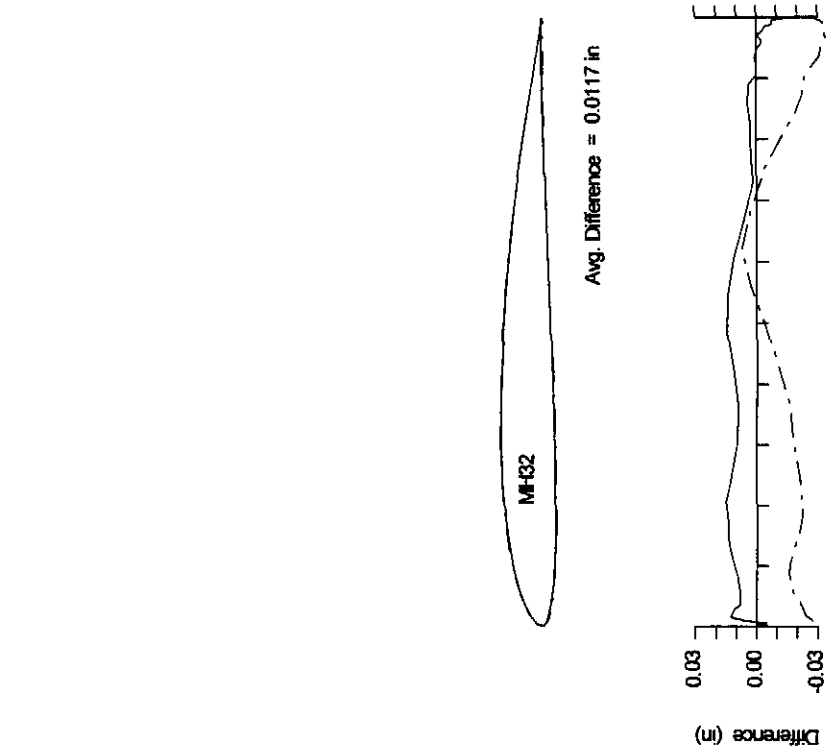
MH32
Avg. Difference = 0.0117 in
0.03
0.00
-0.03
Difference (in)

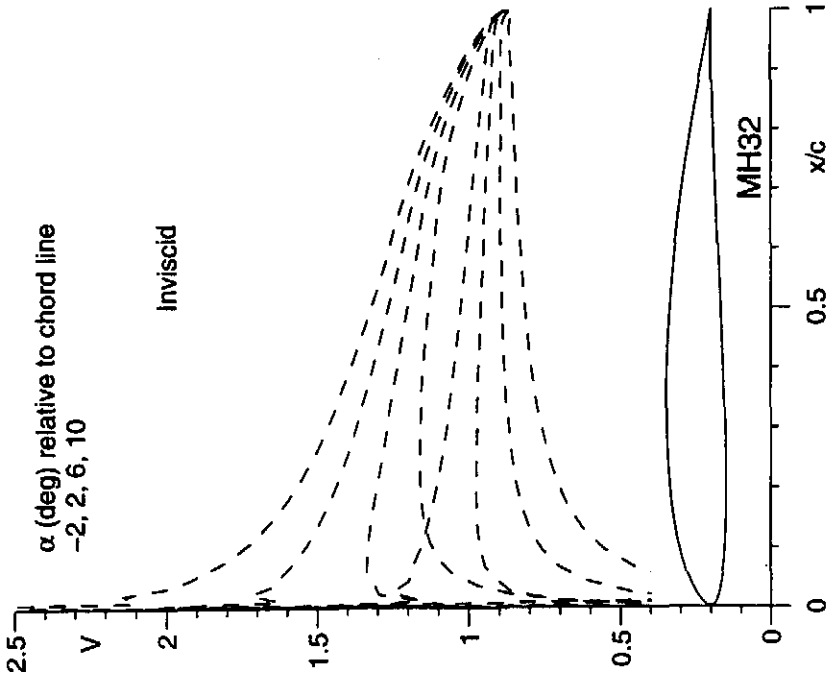
α (deg) relative to chord line
-2, 2, 6, 10
Inviscid
V
2.5
2
1.5
1
0.5
0
MH32
0
0.5
1
x/c

MH32

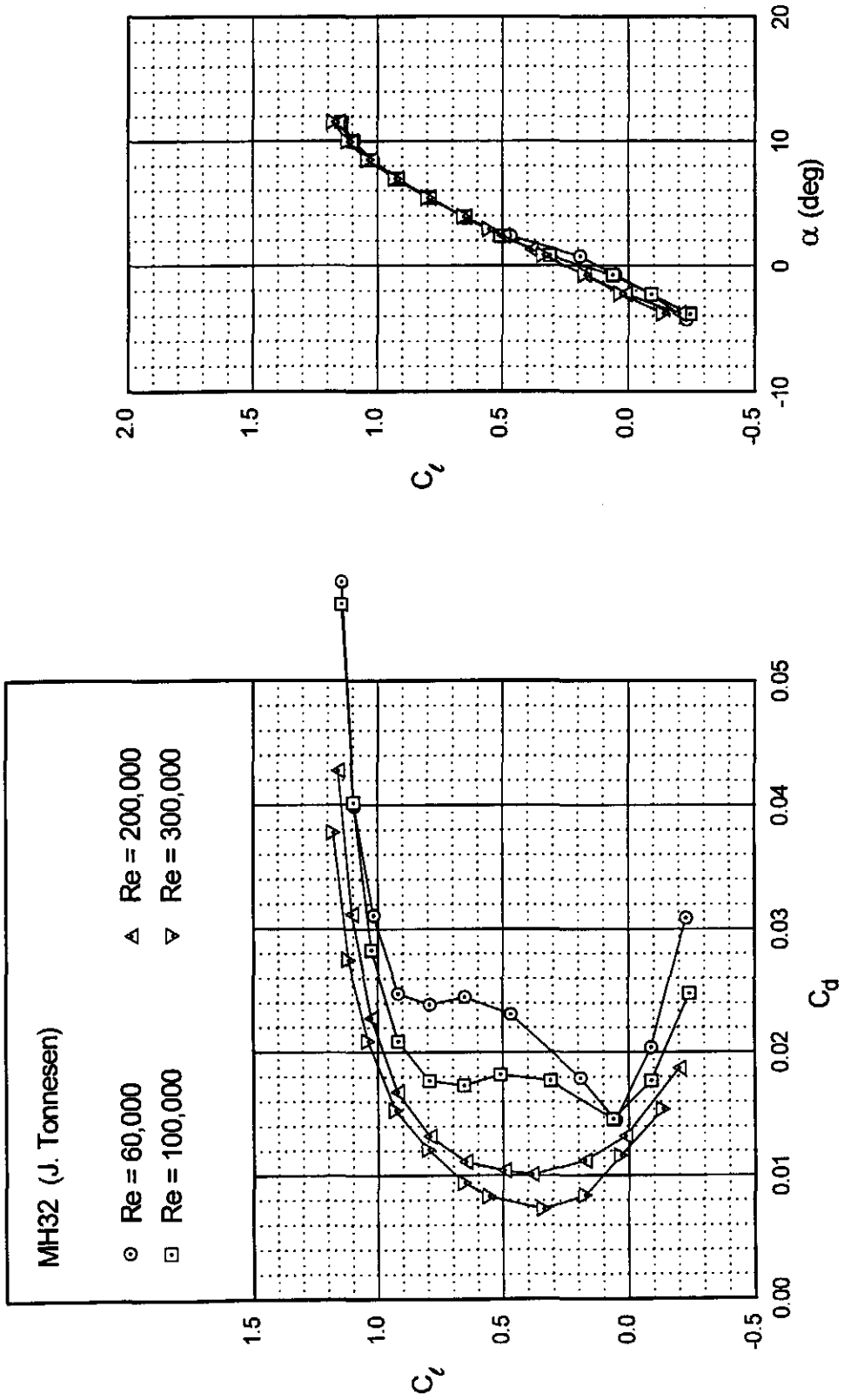
MH32 (J. Tonnesen)
Re = 60,000
Re = 100,000
Re = 200,000
Re = 300,000
C_l
C_d
α (deg)
2.0
1.5
1.0
0.5
0.0
-0.5
20
10
0
-10
0.05
0.04
0.03
0.02
0.01
0.00

Fig. 5.44

MH32

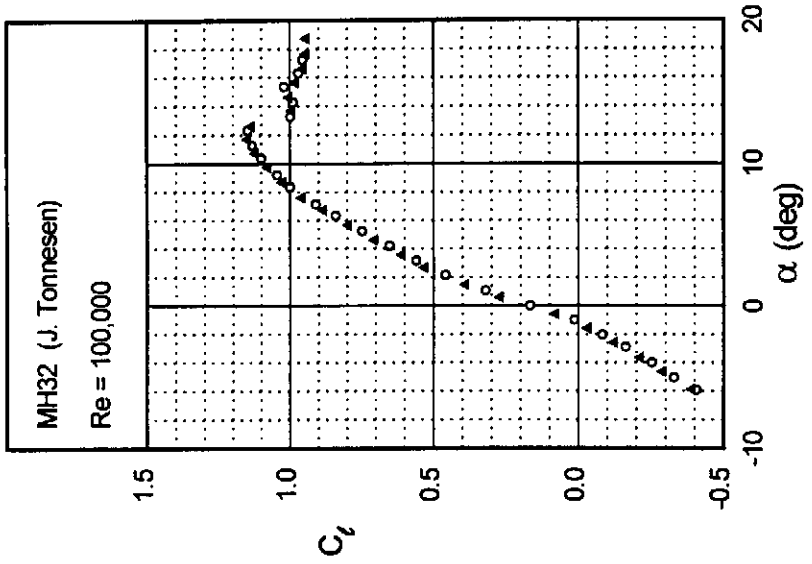
MH32 (J. Tonnesen)
Re = 100,000
1.5
1.0
0.5
0.0
-0.5
C_l
-10
0
10
20
α (deg)

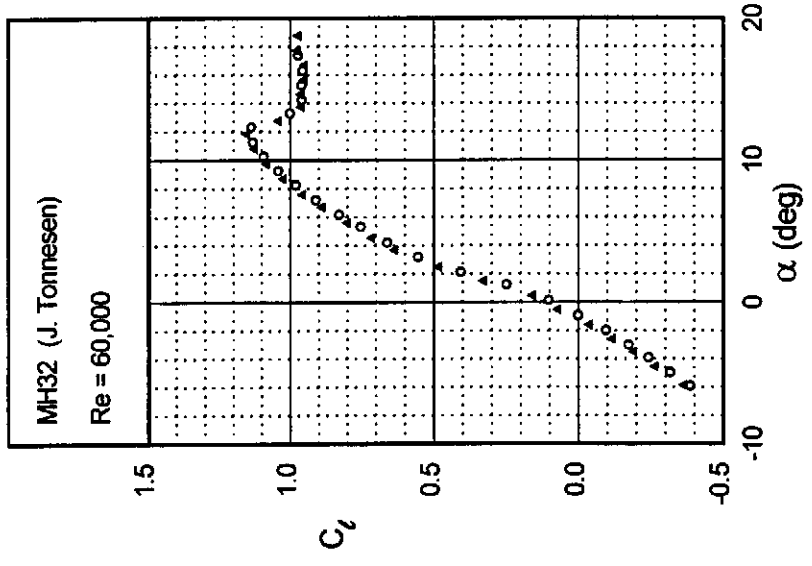
MH32 (J. Tonnesen)
Re = 60,000
1.5
1.0
0.5
0.0
-0.5
C_l
-10
0
10
20
α (deg)

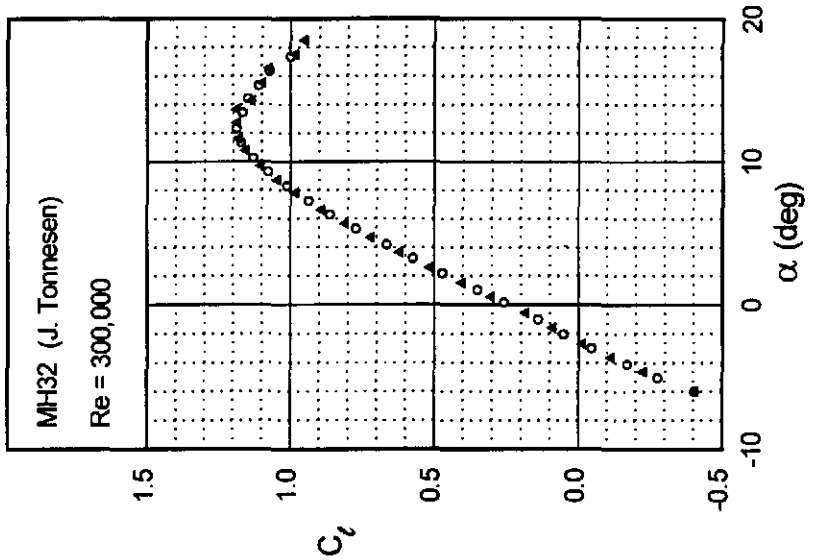
MH32 (J. Tonnesen)
Re = 300,000
1.5
1.0
0.5
0.0
-0.5
C_l
-10
0
10
20
α (deg)

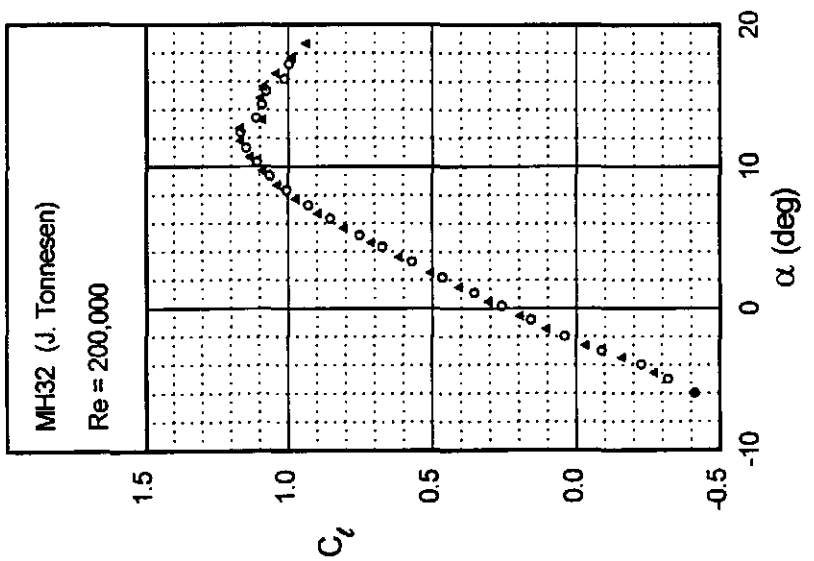
MH32 (J. Tonnesen)
Re = 200,000
1.5
1.0
0.5
0.0
-0.5
C_l
-10
0
10
20
α (deg)

NACA 2414

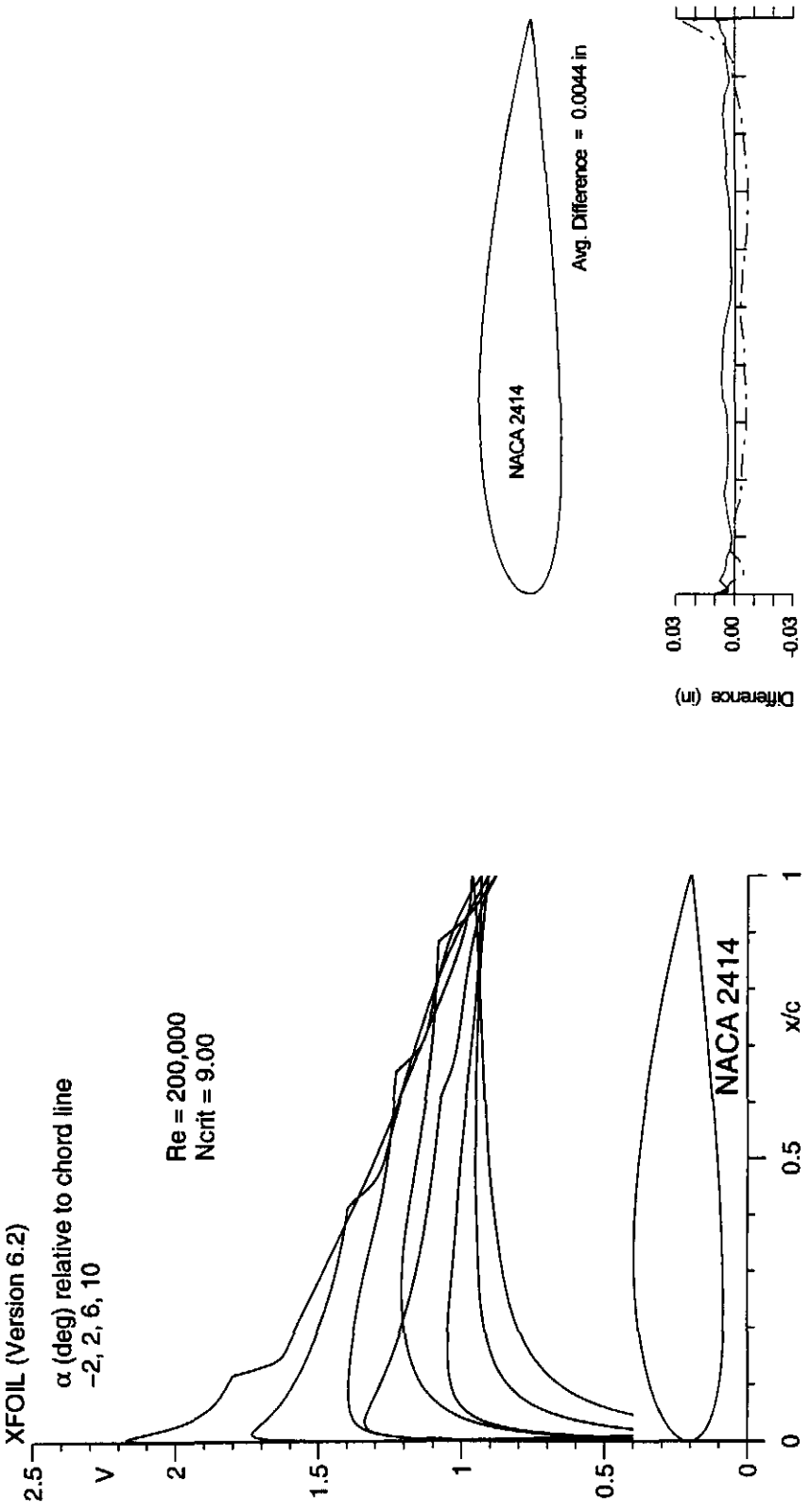
XFOIL (Version 6.2)
α (deg) relative to chord line
-2, 2, 6, 10
Re = 200,000
Ncrit = 9.00
V
2.5
2
1.5
1
0.5
0
NACA 2414
0
0.5
1
x/c
NACA 2414
Avg. Difference = 0.0044 in
0.03
0.00
-0.03
Difference (in)

NACA 2414

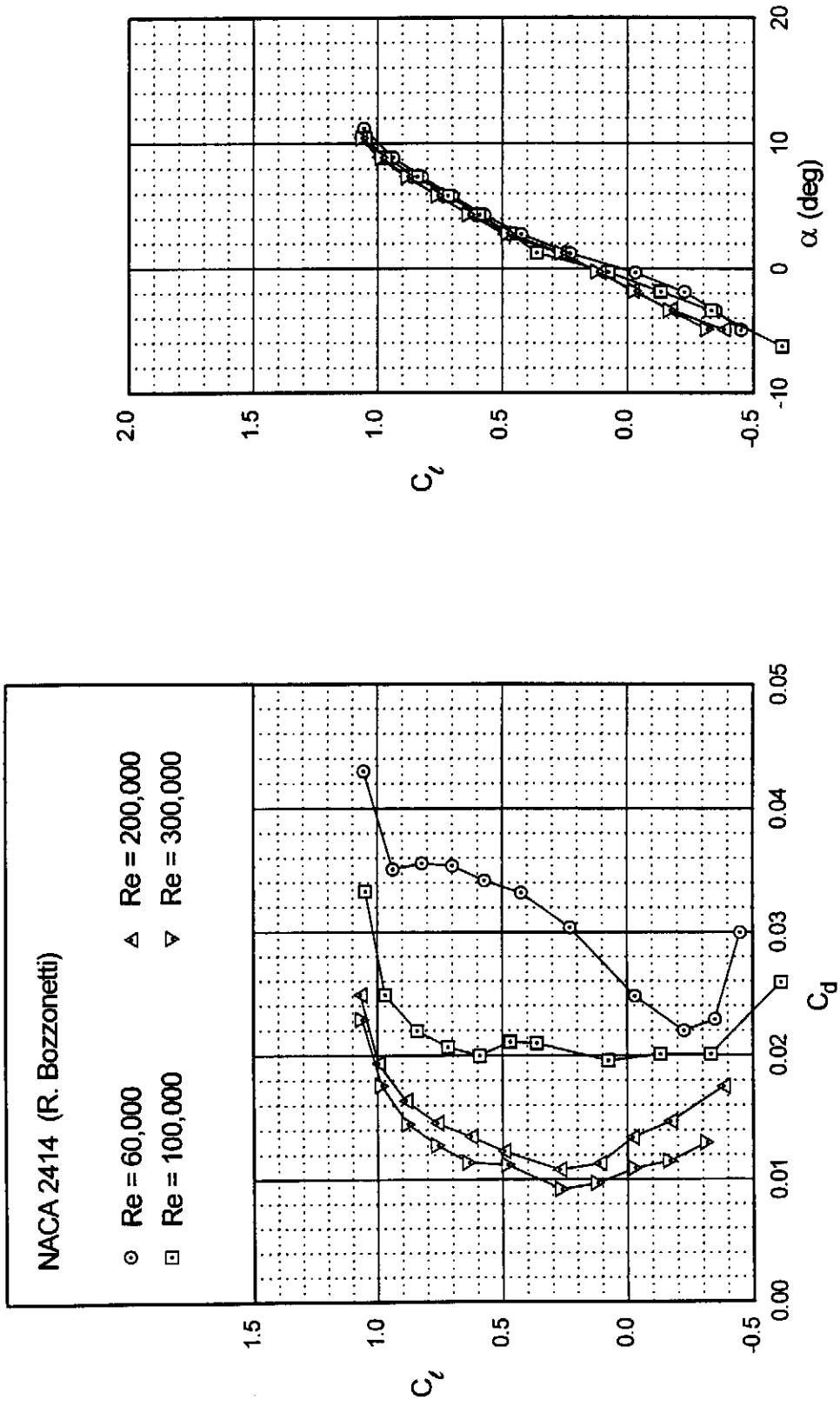
NACA 2414 (R. Bozzonetti)
Re = 60,000
Re = 100,000
Re = 200,000
Re = 300,000
C_l
C_d
α (deg)
2.0
1.5
1.0
0.5
0.0
-0.5
20
10
0
-10
0.05
0.04
0.03
0.02
0.01
0.00

Fig. 5.48

NACA 2414

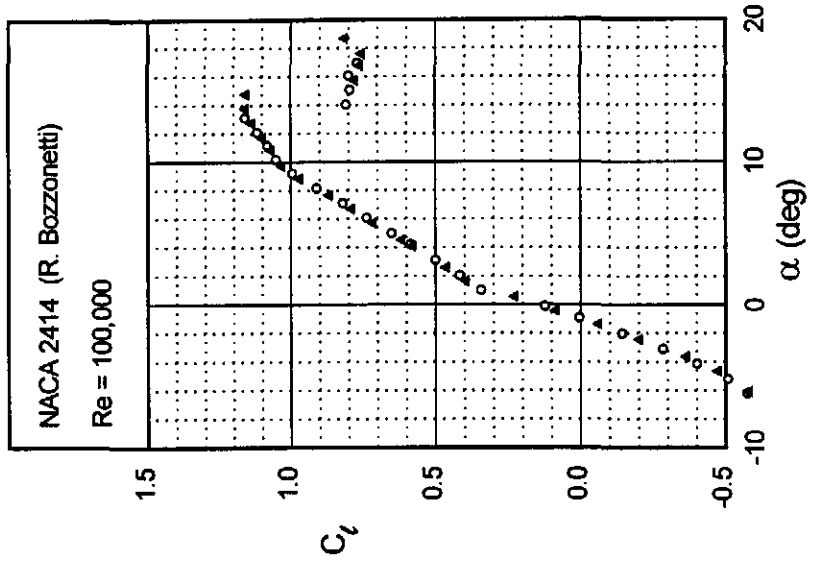

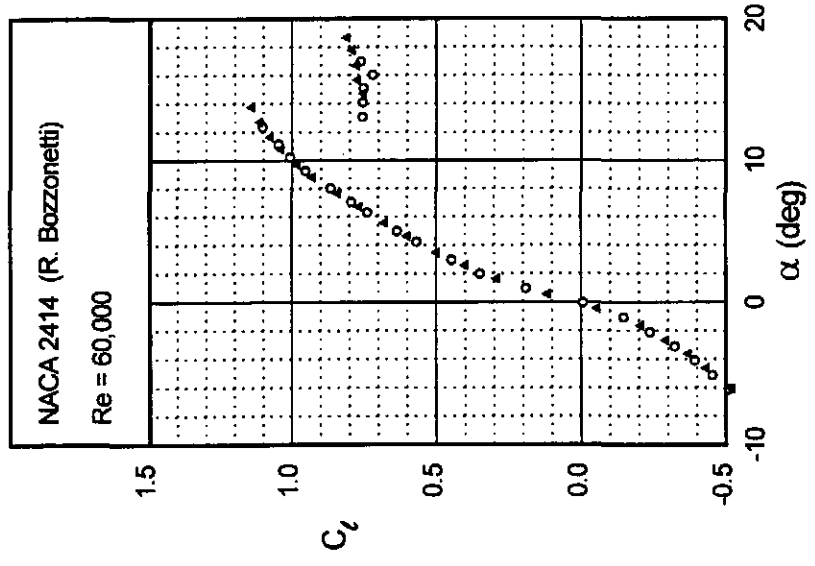

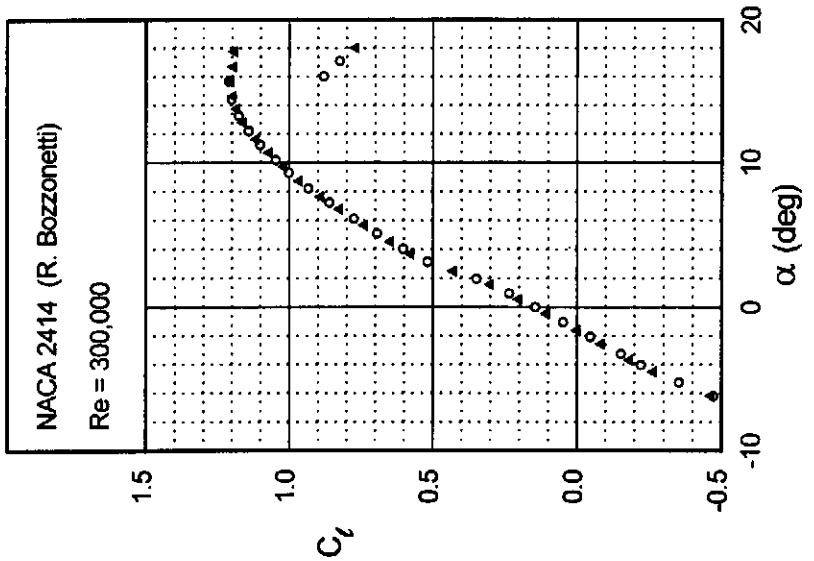
NACA 2414 (R. Bozzonetti)
Re = 300,000
1.5
1.0
0.5
0.0
-0.5
C_l
-10
0
10
20
α (deg)

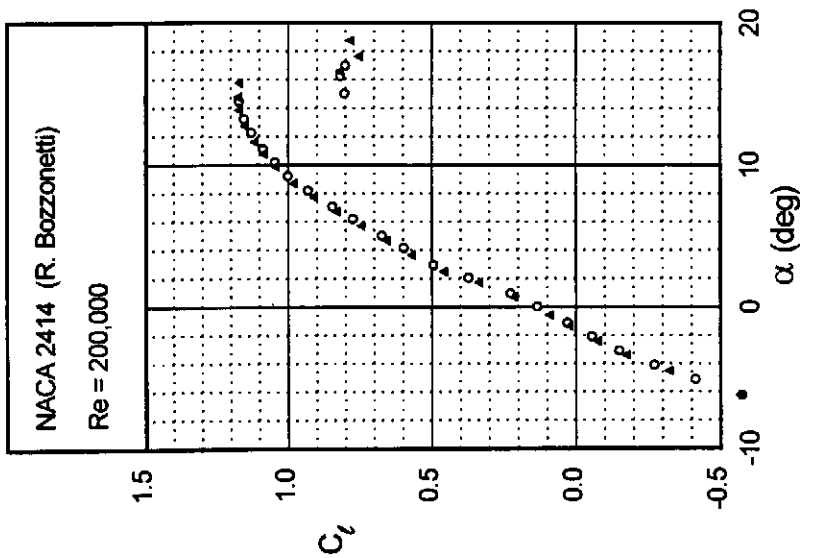
NACA 2414 (R. Bozzonetti)
Re = 200,000
1.5
1.0
0.5
0.0
-0.5
C_l
-10
0
10
20
α (deg)

NACA 2415

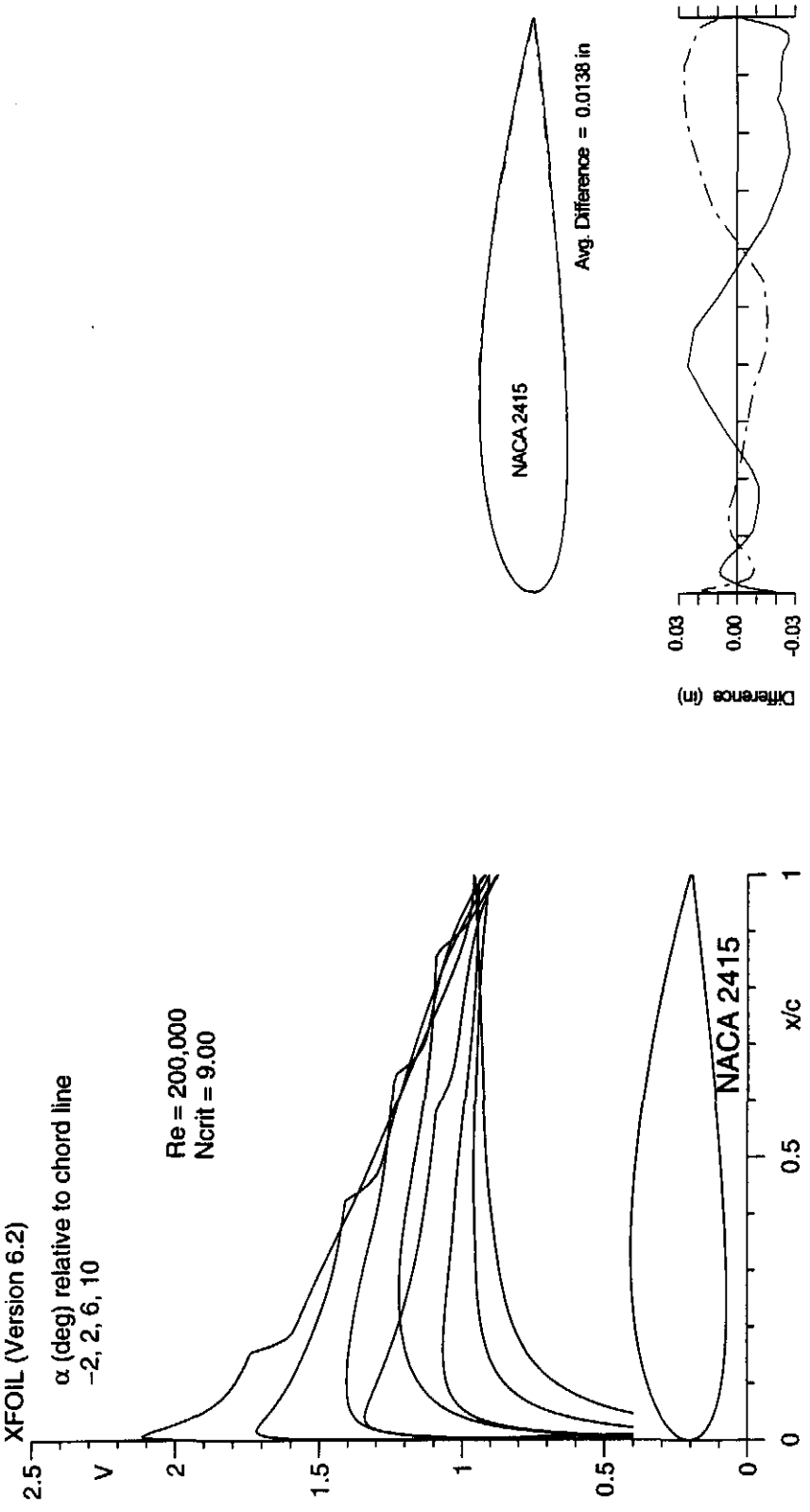
XFOIL (Version 6.2)
α (deg) relative to chord line
-2, 2, 6, 10
Re = 200,000
Ncrit = 9.00
V
2.5
2
1.5
1
0.5
0
NACA 2415
0
0.5
1
x/c
NACA 2415
Avg. Difference = 0.0138 in
0.03
0.00
-0.03
Difference (in)

NACA 2415

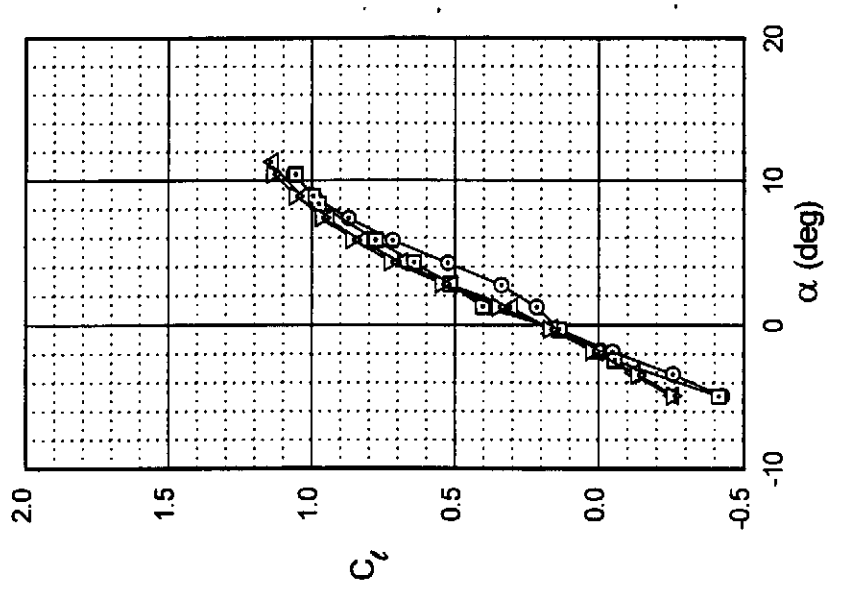
2.0
1.5
1.0
0.5
0.0
-0.5
C_l
20
10
0
-10
α (deg)

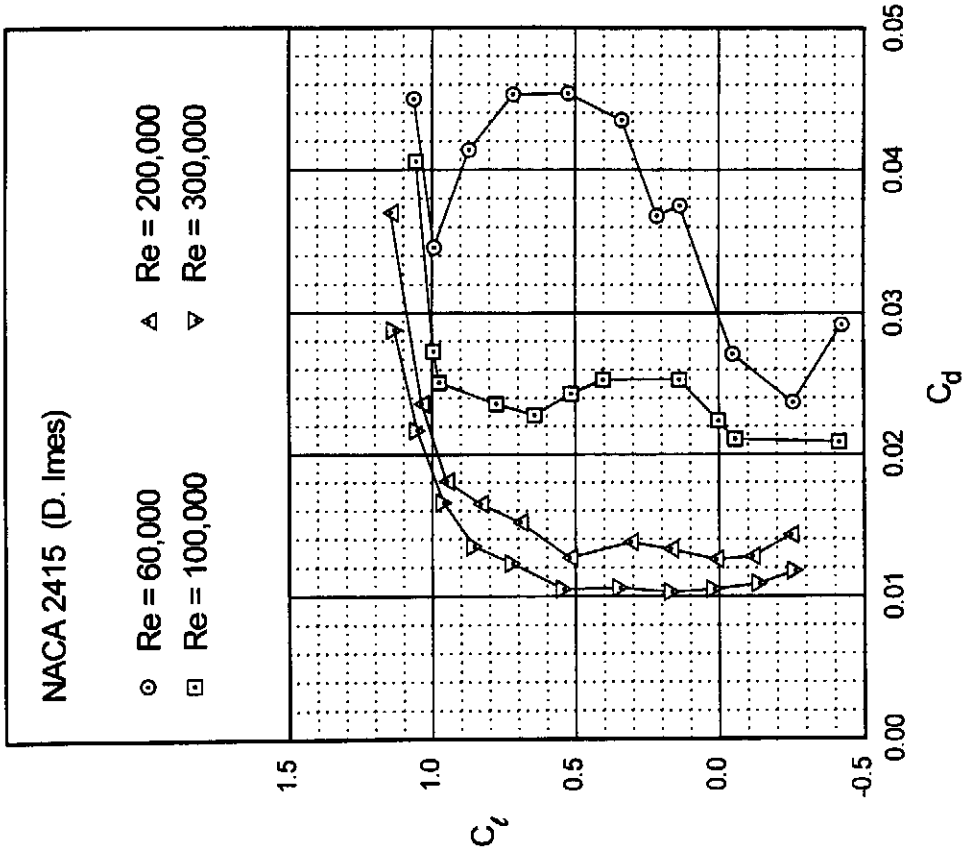
NACA 2415 (D. Imes)
Re = 60,000
Re = 100,000
Re = 200,000
Re = 300,000
1.5
1.0
0.5
0.0
-0.5
C_l
0.05
0.04
0.03
0.02
0.01
0.00
C_d

Fig. 5.52

NACA 2415

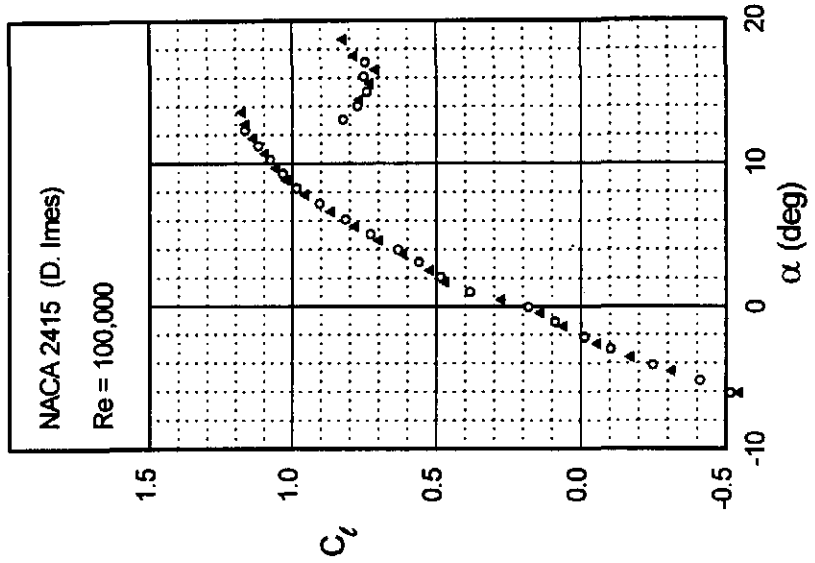

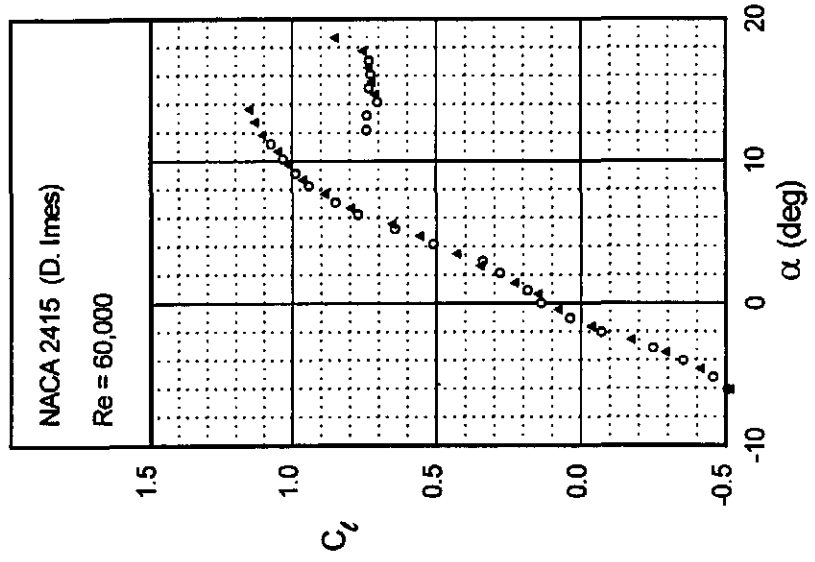

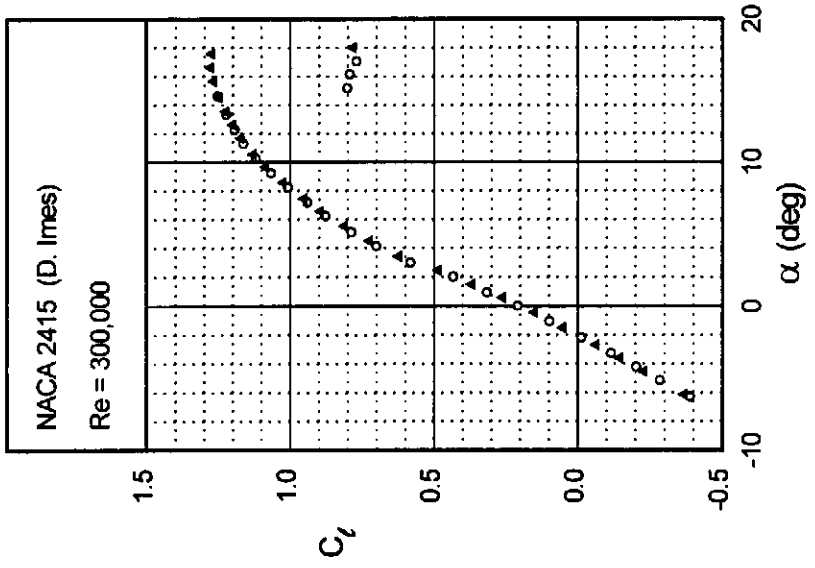
NACA 2415 (D. Imes)
Re = 300,000
1.5
1.0
0.5
0.0
-0.5
C_l
-10
0
10
20
α (deg)

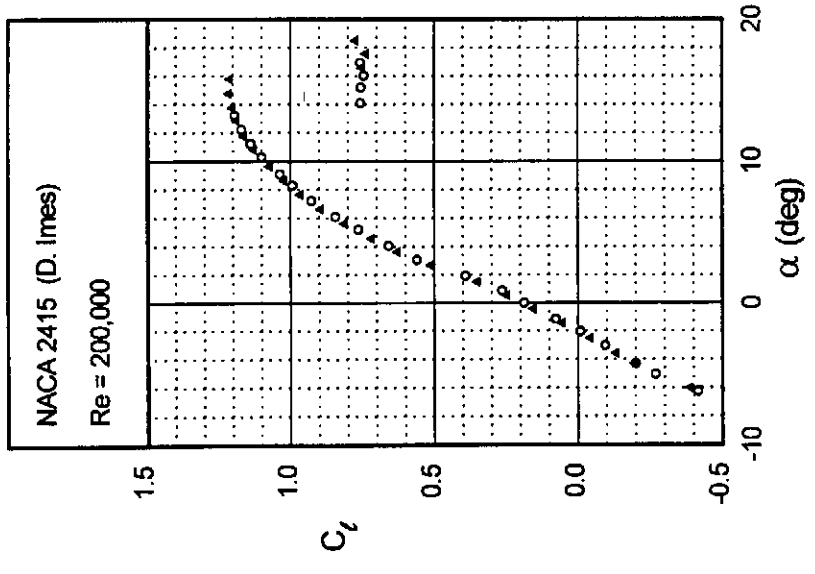
NACA 2415 (D. Imes)
Re = 200,000
1.5
1.0
0.5
0.0
-0.5
C_l
-10
0
10
20
α (deg)

RG15 (C)

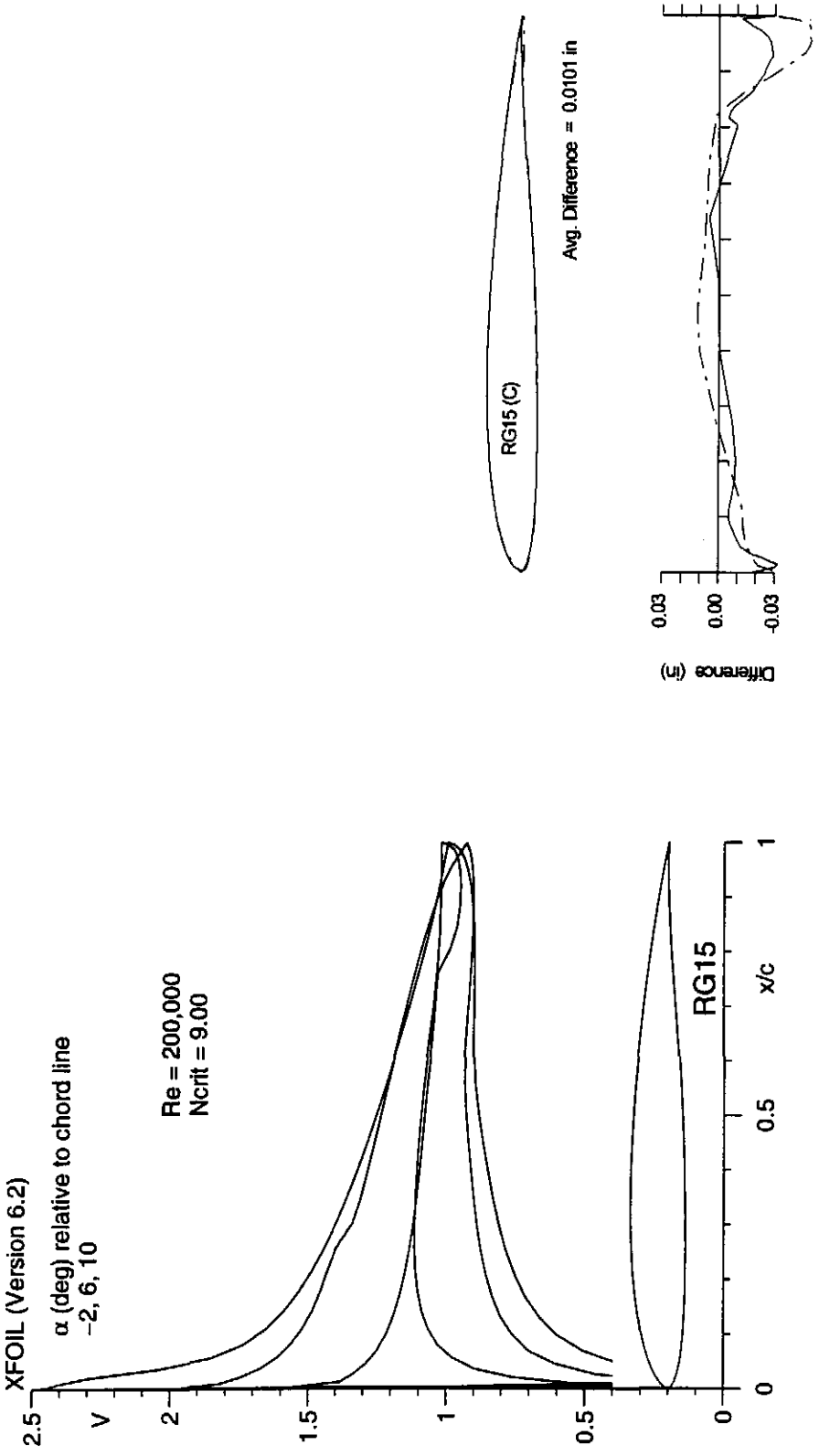
XFOIL (Version 6.2)
α (deg) relative to chord line
-2, 6, 10
Re = 200,000
Ncrit = 9.00
V
2.5
2
1.5
1
0.5
0
0.5
1
x/c
RG15
RG15 (C)
Avg. Difference = 0.0101 in
0.03
0.00
-0.03
Difference (in)

RG15 (C)

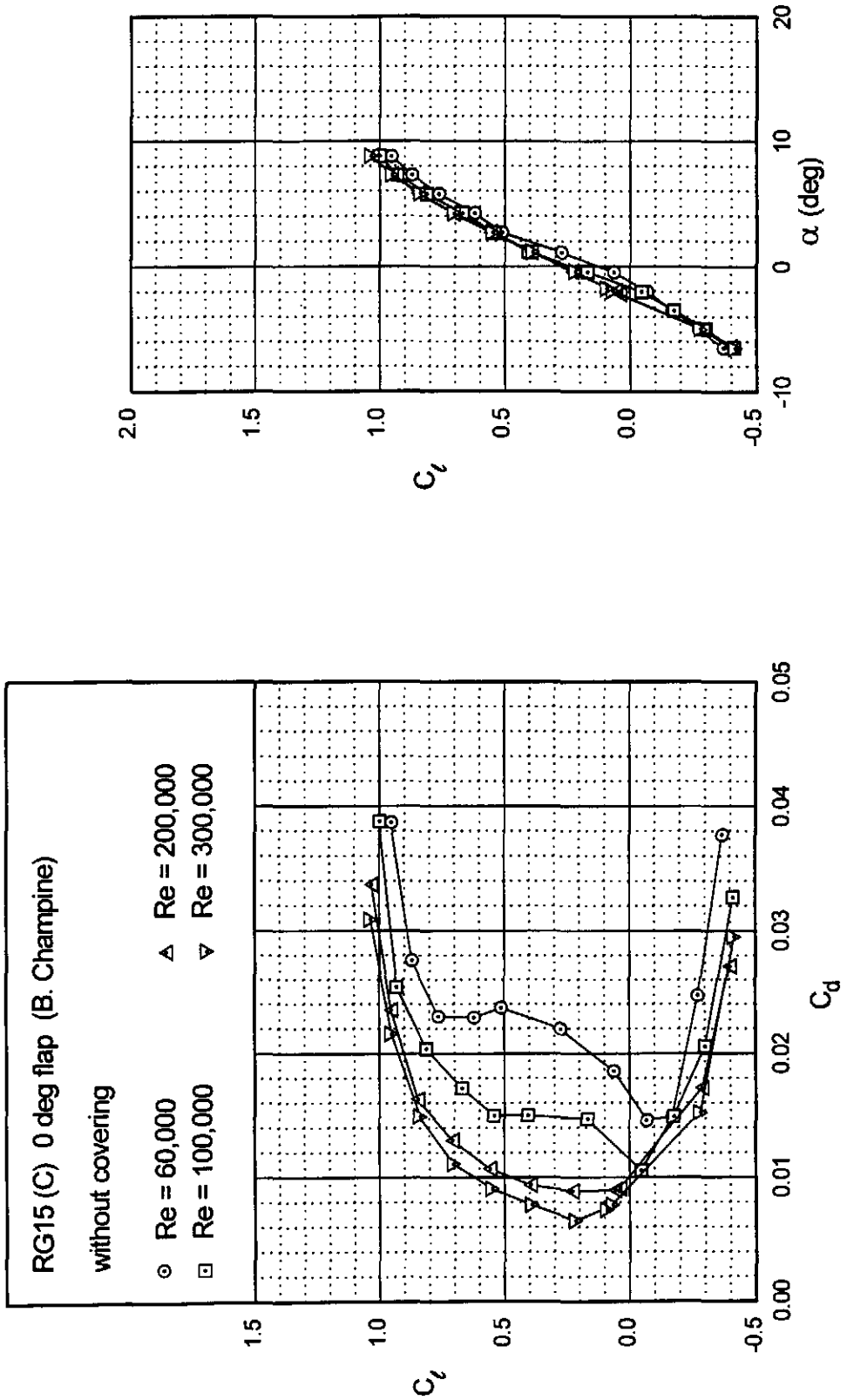
RG15 (C) 0 deg flap (B. Champine)
without covering
Re = 60,000
Re = 100,000
Re = 200,000
Re = 300,000
C_l
C_d
α (deg)

RG15 (C)

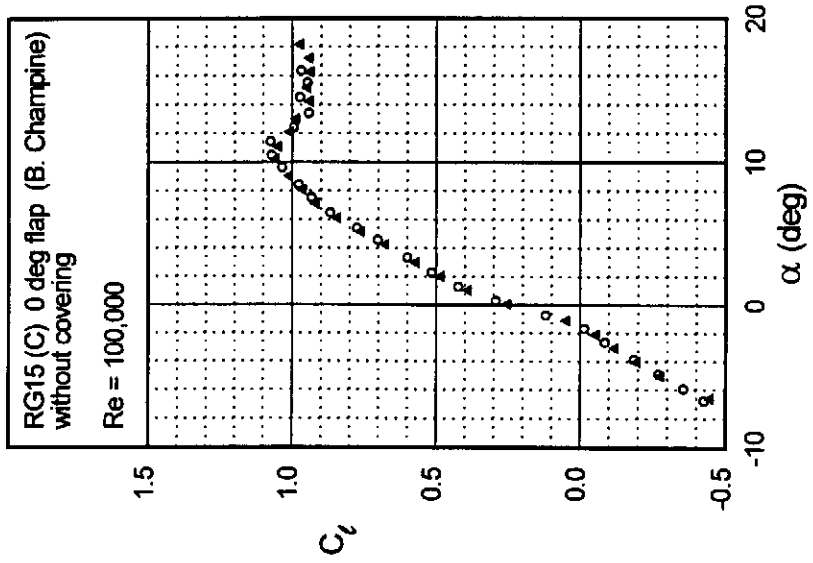
RG15 (C) 0 deg flap (B. Champine)
without covering
Re = 100,000
1.5
1.0
0.5
0.0
-0.5
C_l
-10
0
10
20
α (deg)

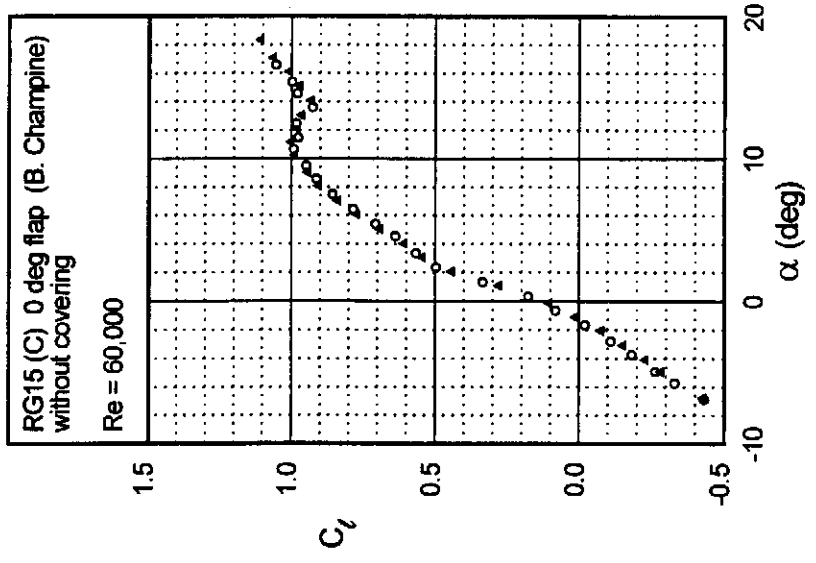
RG15 (C) 0 deg flap (B. Champine)
without covering
Re = 60,000
1.5
1.0
0.5
0.0
-0.5
C_l
-10
0
10
20
α (deg)

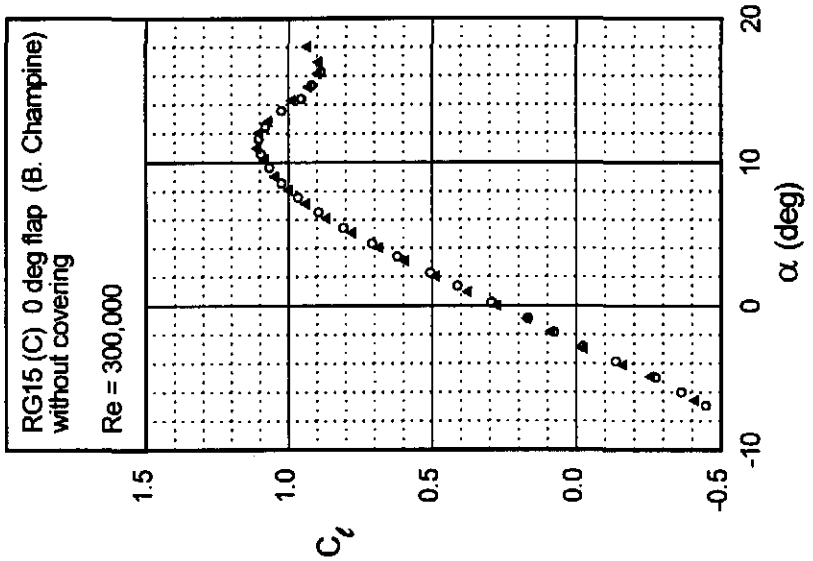
RG15 (C) 0 deg flap (B. Champine)
without covering
Re = 300,000
1.5
1.0
0.5
0.0
-0.5
C_l
-10
0
10
20
α (deg)

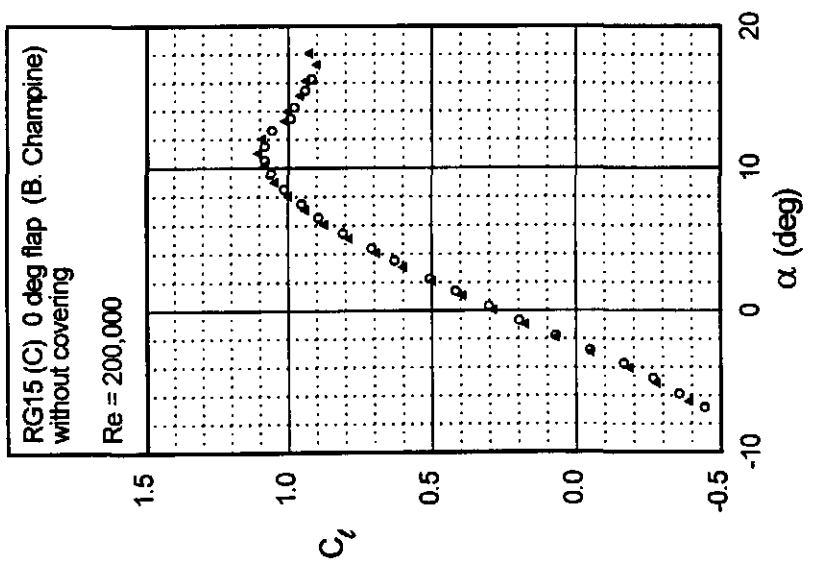
RG15 (C) 0 deg flap (B. Champine)
without covering
Re = 200,000
1.5
1.0
0.5
0.0
-0.5
C_l
-10
0
10
20
α (deg)

RG15 (C)

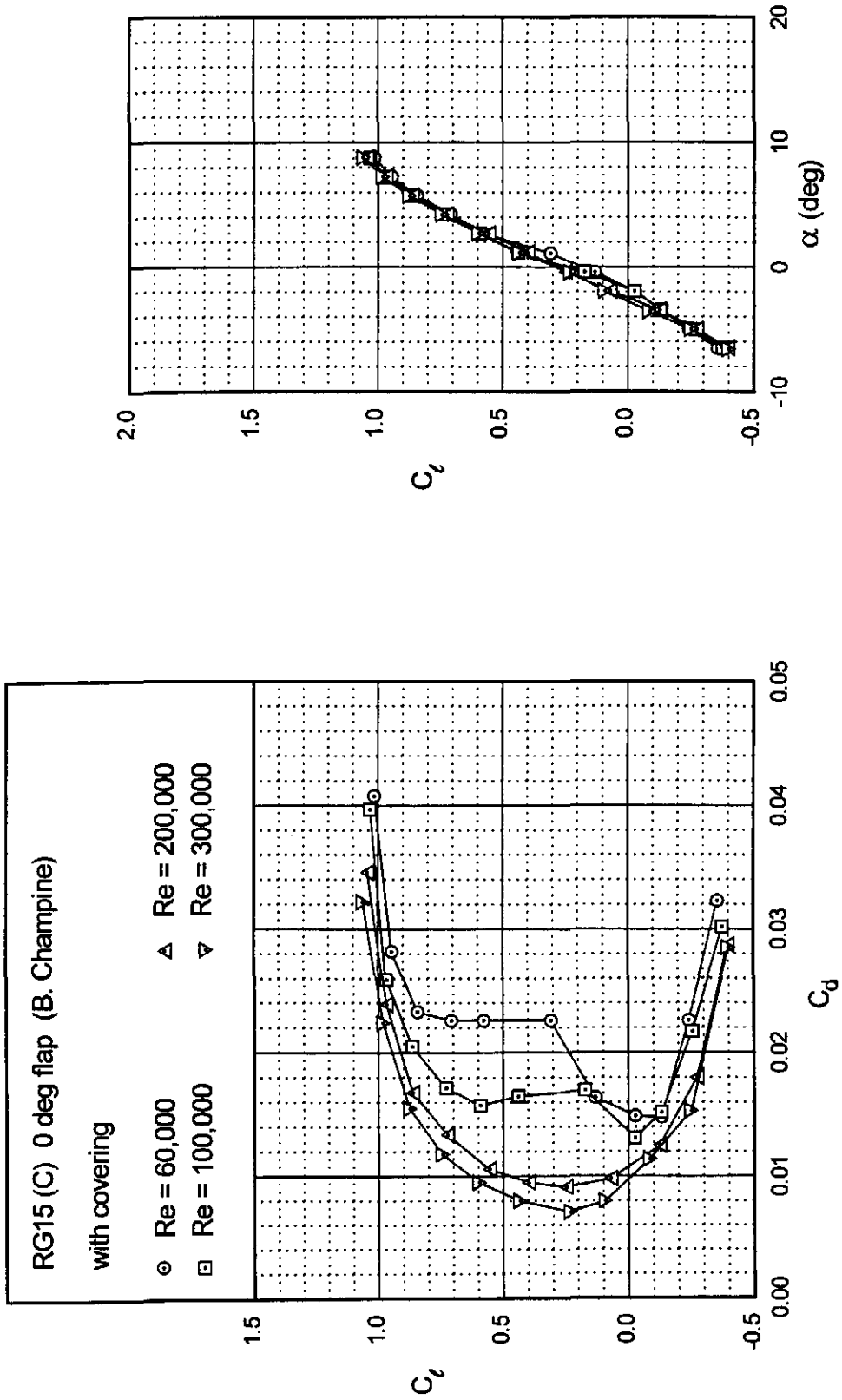
RG15 (C) 0 deg flap (B. Champine)
with covering
Re = 60,000
Re = 100,000
Re = 200,000
Re = 300,000
C_l
C_d
α (deg)
2.0
1.5
1.0
0.5
0.0
-0.5
20
10
0
-10
0.05
0.04
0.03
0.02
0.01
0.00

RG15 (C)

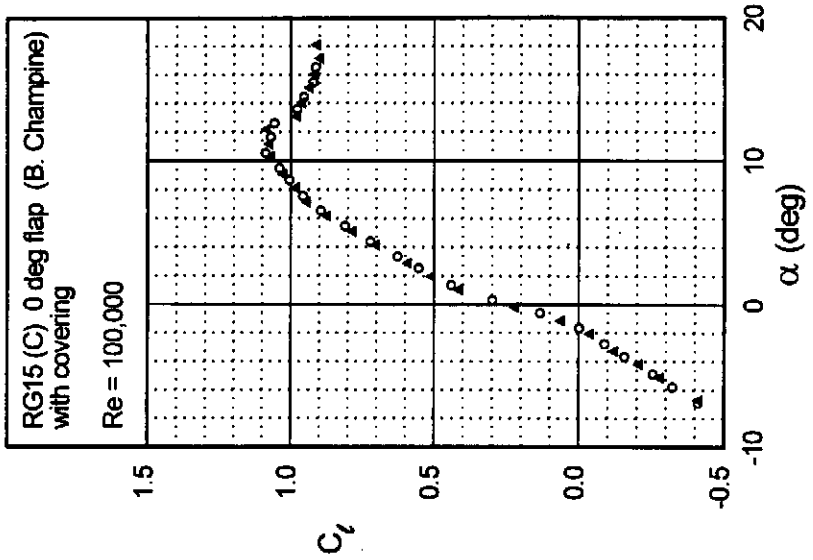
RG15 (C) 0 deg flap (B. Champine)
with covering
Re = 100,000
1.5
1.0
0.5
0.0
-0.5
C_l
-10
0
10
20
α (deg)

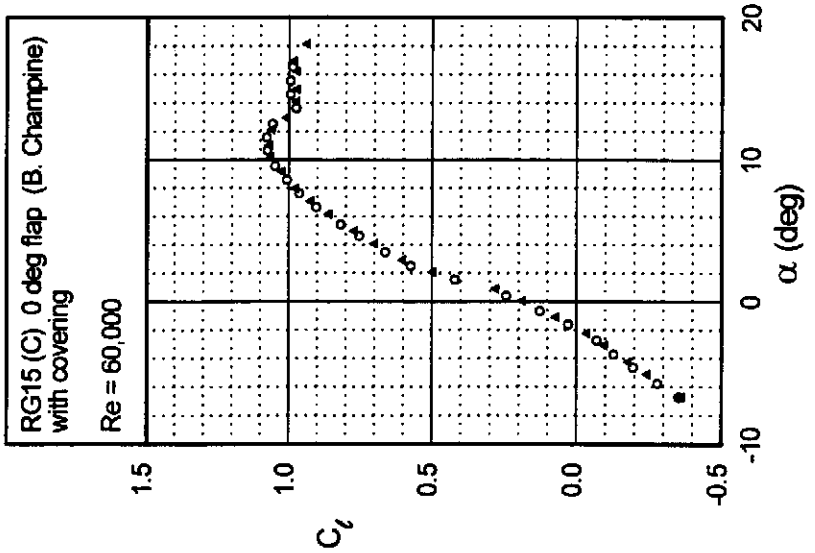
RG15 (C) 0 deg flap (B. Champine)
with covering
Re = 60,000
1.5
1.0
0.5
0.0
-0.5
C_l
-10
0
10
20
α (deg)

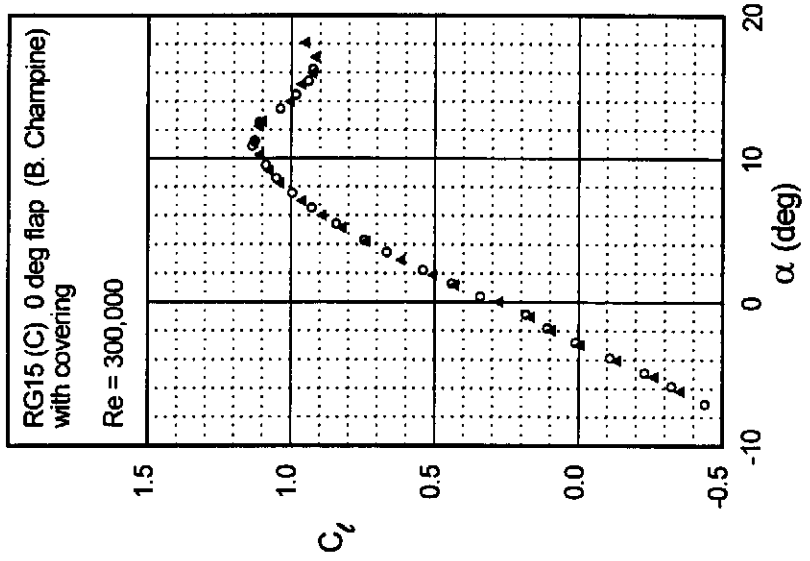
RG15 (C) 0 deg flap (B. Champine)
with covering
Re = 300,000
1.5
1.0
0.5
0.0
-0.5
C_l
-10
0
10
20
α (deg)

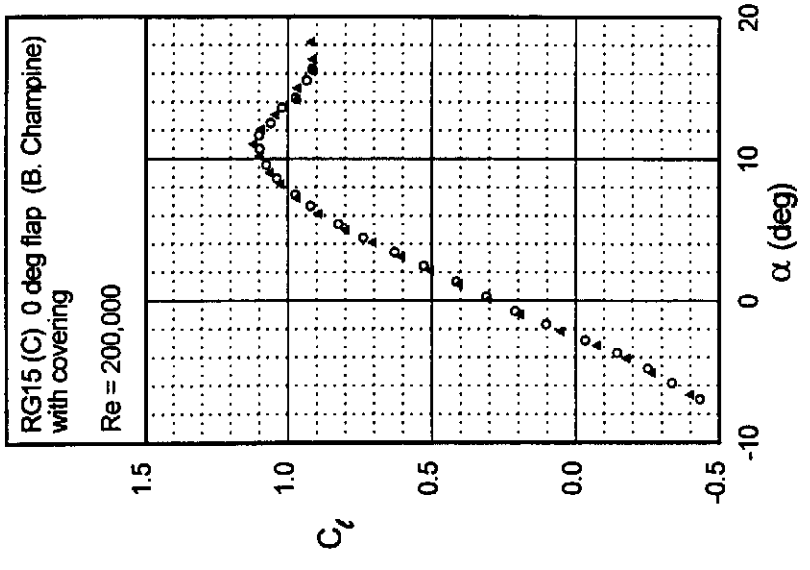
RG15 (C) 0 deg flap (B. Champine)
with covering
Re = 200,000
1.5
1.0
0.5
0.0
-0.5
C_l
-10
0
10
20
α (deg)

RG15 (C)

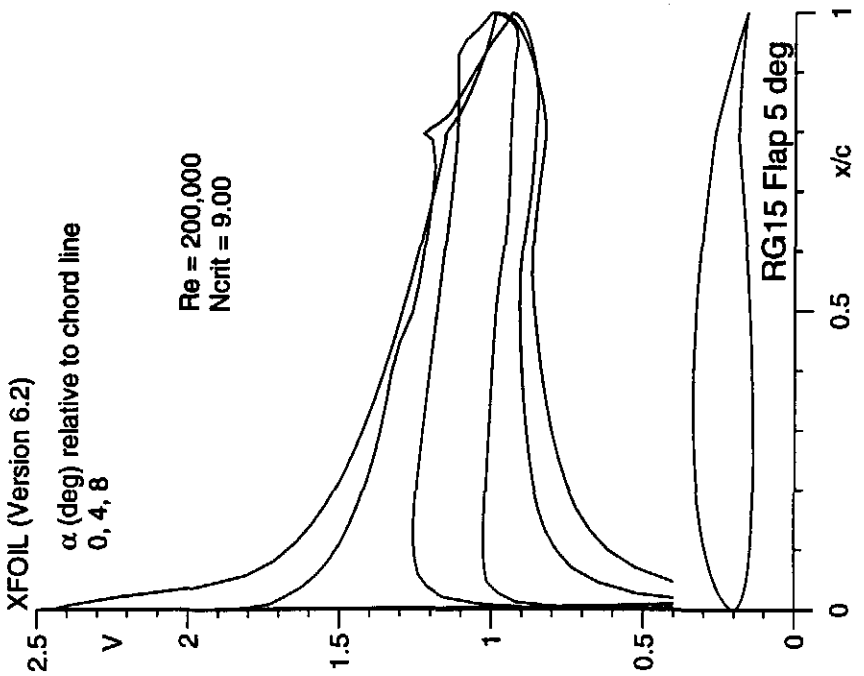
XFOIL (Version 6.2)
α (deg) relative to chord line
0, 4, 8
Re = 200,000
Ncrit = 9.00
RG15 Flap 5 deg
V
x/c
2.5
2
1.5
1
0.5
0
0
0.5
1

RG15 (C)

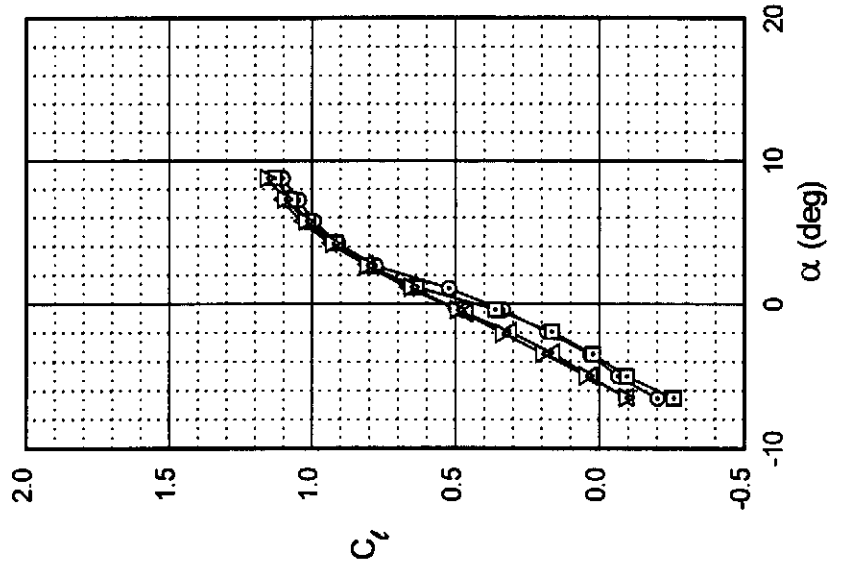
2.0
1.5
1.0
0.5
0.0
-0.5
C_l
20
10
0
-10
α (deg)

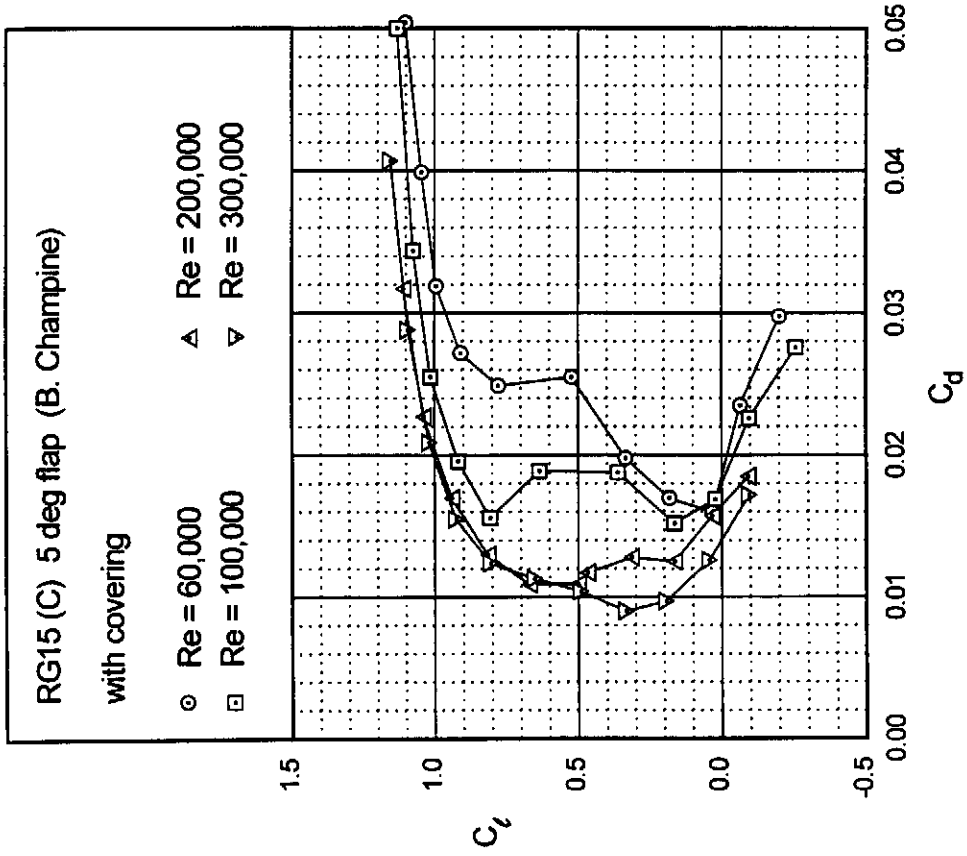
RG15 (C) 5 deg flap (B. Champine)
with covering
Re = 60,000
Re = 100,000
Re = 200,000
Re = 300,000
1.5
1.0
0.5
0.0
-0.5
C_l
0.05
0.04
0.03
0.02
0.01
0.00
C_d

RG15 (C)

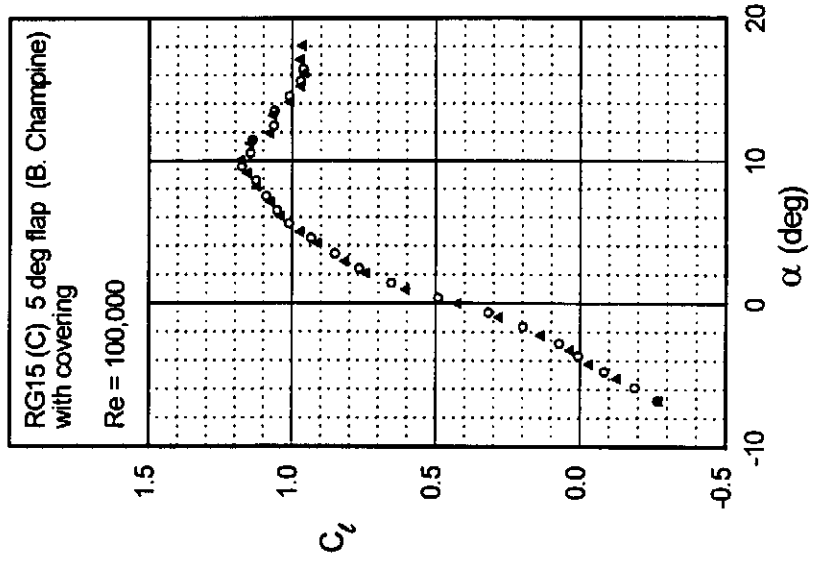
RG15 (C) 5 deg flap (B. Champine)
with covering
Re = 100,000
1.5
1.0
0.5
0.0
-0.5
C_l
-10
0
10
20
α (deg)

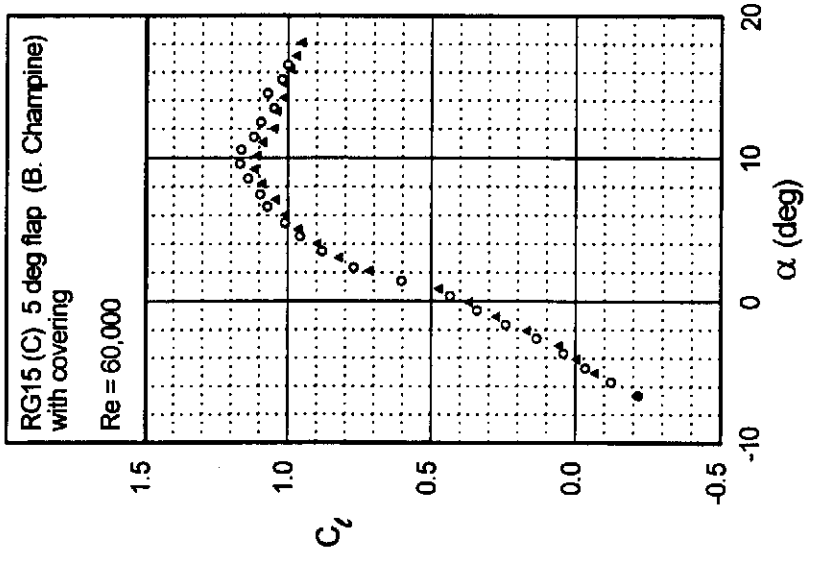
RG15 (C) 5 deg flap (B. Champine)
with covering
Re = 60,000
1.5
1.0
0.5
0.0
-0.5
C_l
-10
0
10
20
α (deg)

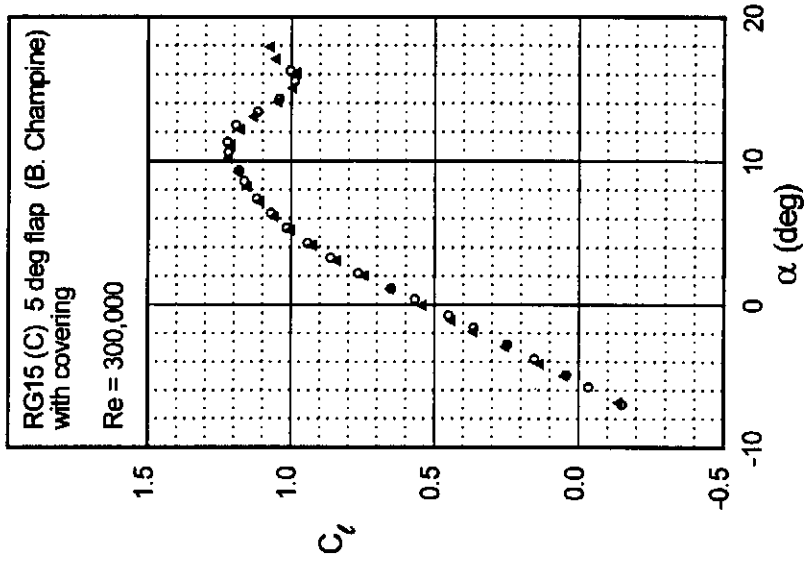
RG15 (C) 5 deg flap (B. Champine)
with covering
Re = 300,000
1.5
1.0
0.5
0.0
-0.5
C_l
-10
0
10
20
α (deg)

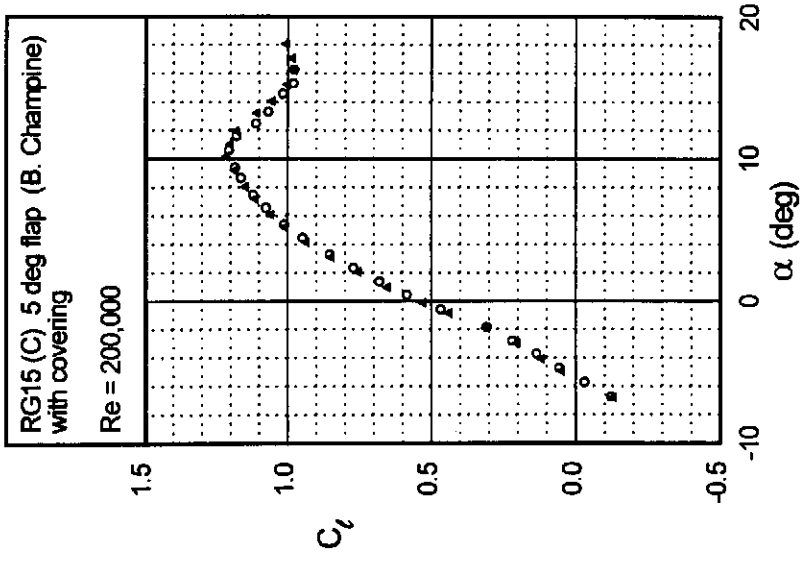
RG15 (C) 5 deg flap (B. Champine)
with covering
Re = 200,000
1.5
1.0
0.5
0.0
-0.5
C_l
-10
0
10
20
α (deg)

RG15 (C)

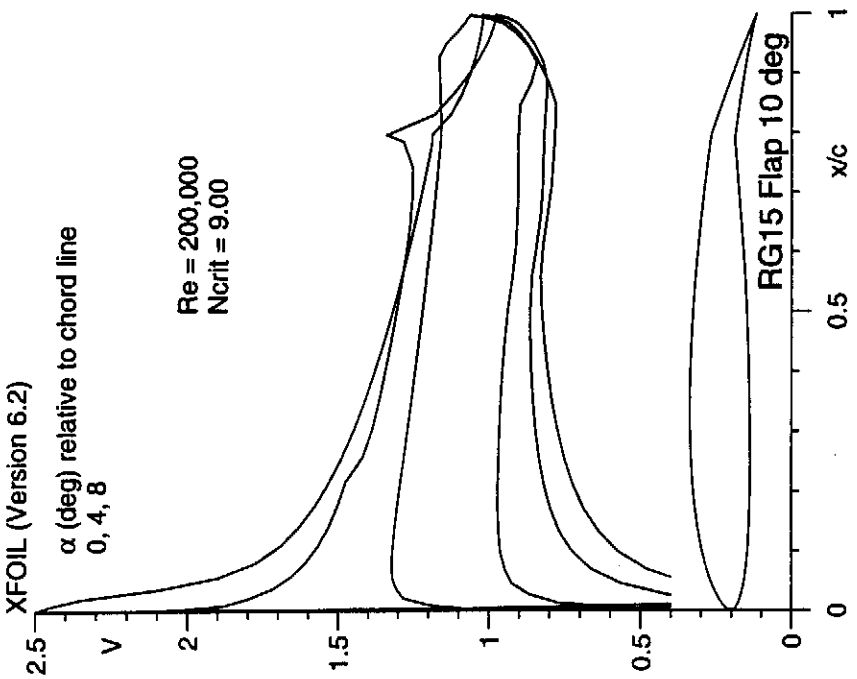
XFOIL (Version 6.2)
α (deg) relative to chord line
0, 4, 8
Re = 200,000
Ncrit = 9.00
V
2.5
2
1.5
1
0.5
0
RG15 Flap 10 deg
0
0.5
1
x/c

RG15 (C)

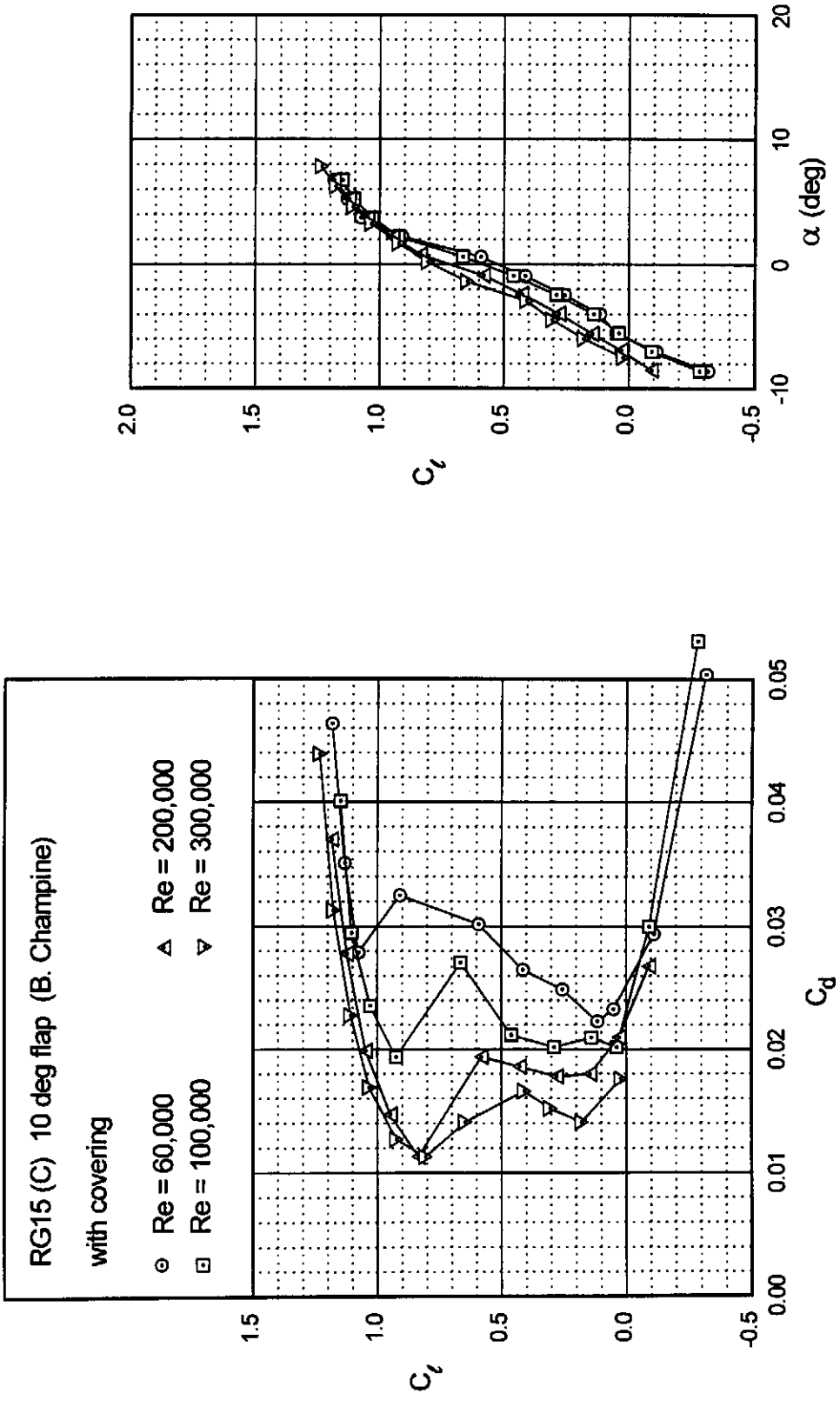
RG15 (C) 10 deg flap (B. Champine)
with covering
Re = 60,000
Re = 100,000
Re = 200,000
Re = 300,000
C_l
C_d
α (deg)

RG15 (C)

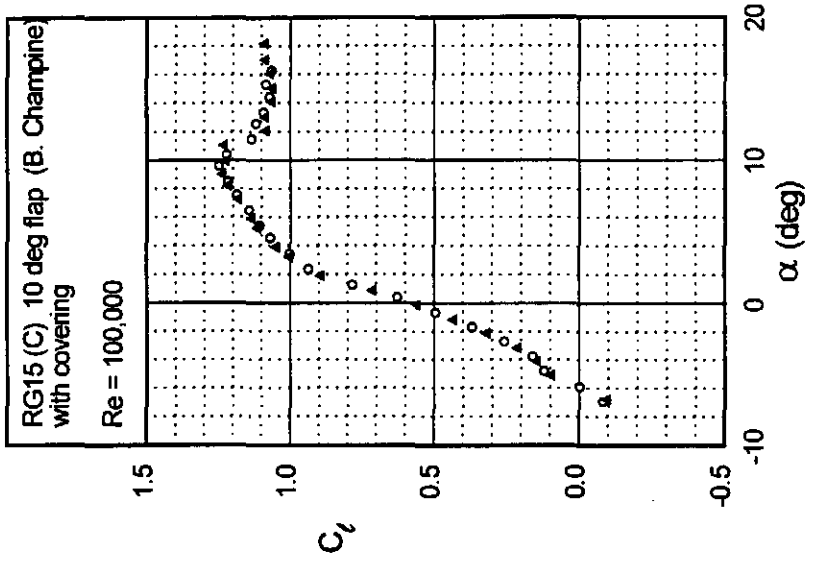
RG15 (C) 10 deg flap (B. Champine)
with covering
Re = 100,000
1.5
1.0
0.5
0.0
-0.5
C_l
-10
0
10
20
α (deg)

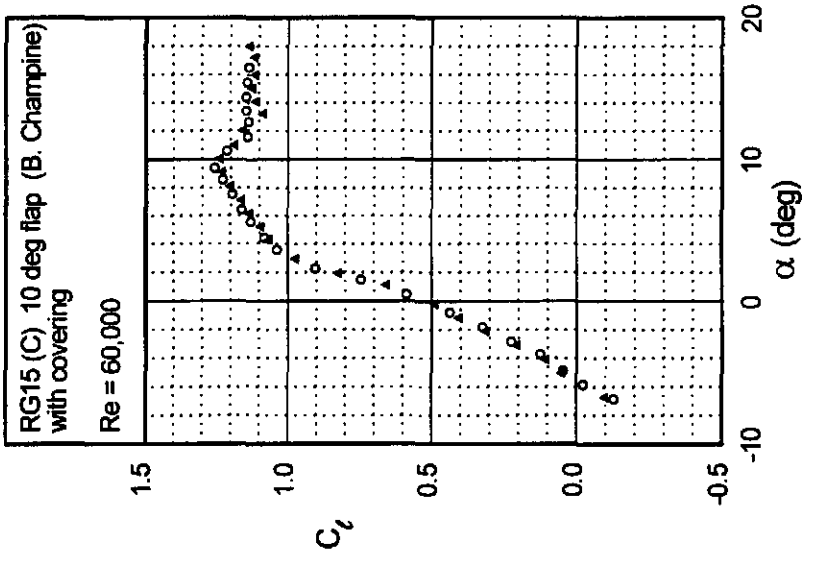
RG15 (C) 10 deg flap (B. Champine)
with covering
Re = 60,000
1.5
1.0
0.5
0.0
-0.5
C_l
-10
0
10
20
α (deg)

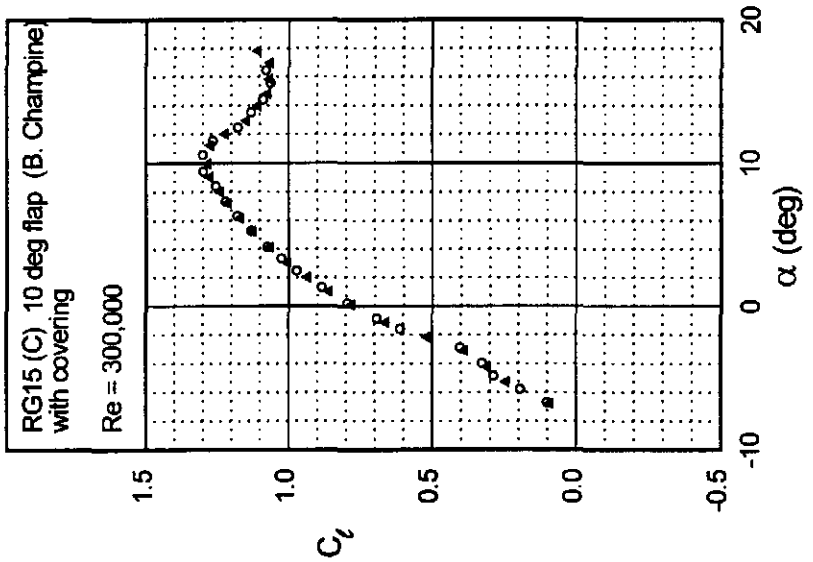
RG15 (C) 10 deg flap (B. Champine)
with covering
Re = 300,000
1.5
1.0
0.5
0.0
-0.5
C_l
-10
0
10
20
α (deg)

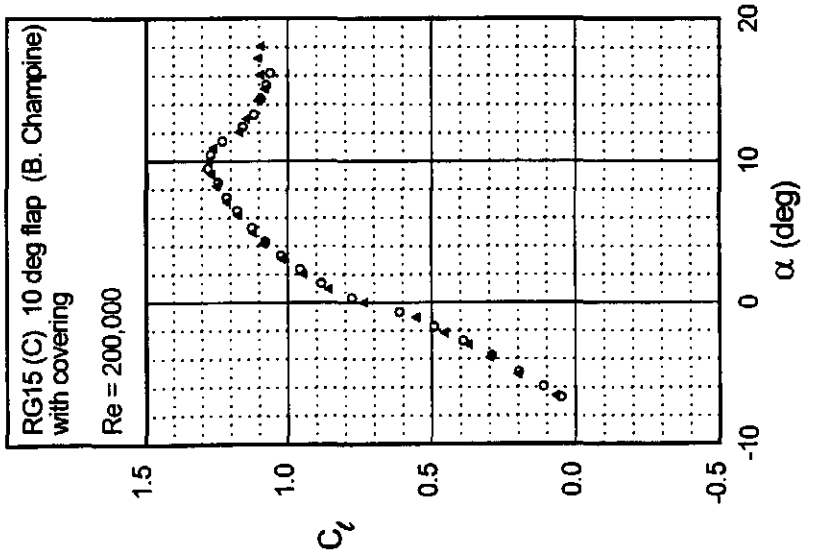
RG15 (C) 10 deg flap (B. Champine)
with covering
Re = 200,000
1.5
1.0
0.5
0.0
-0.5
C_l
-10
0
10
20
α (deg)

S822

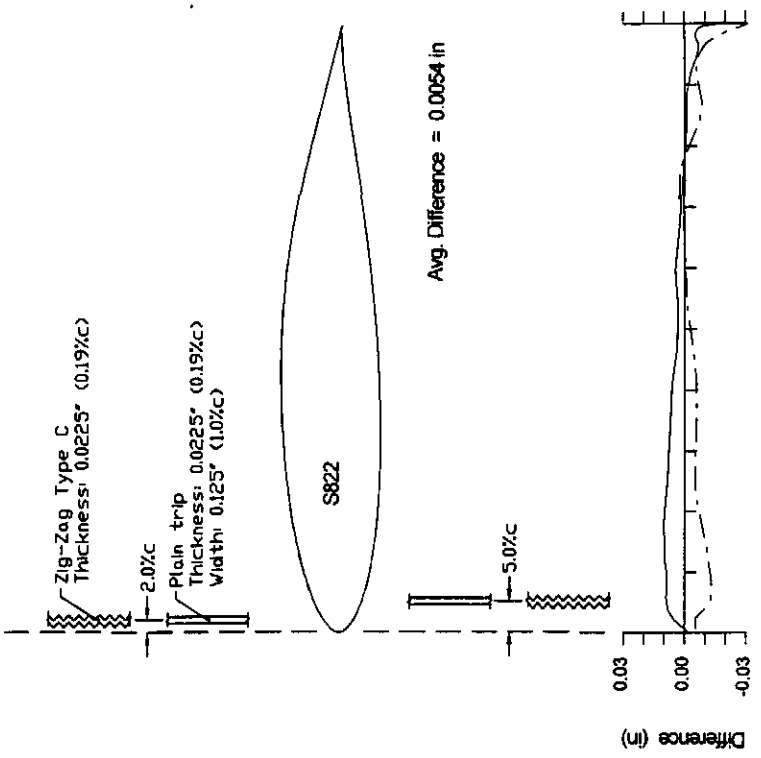
Zig-Zag Type C
Thickness: 0.0225" (0.19%c)
2.0%c
Plain trip
Thickness: 0.0225" (0.19%c)
Width: 0.125" (1.0%c)
S822
5.0%c
Avg. Difference = 0.0054 in
0.03
0.00
-0.03
Difference (in)

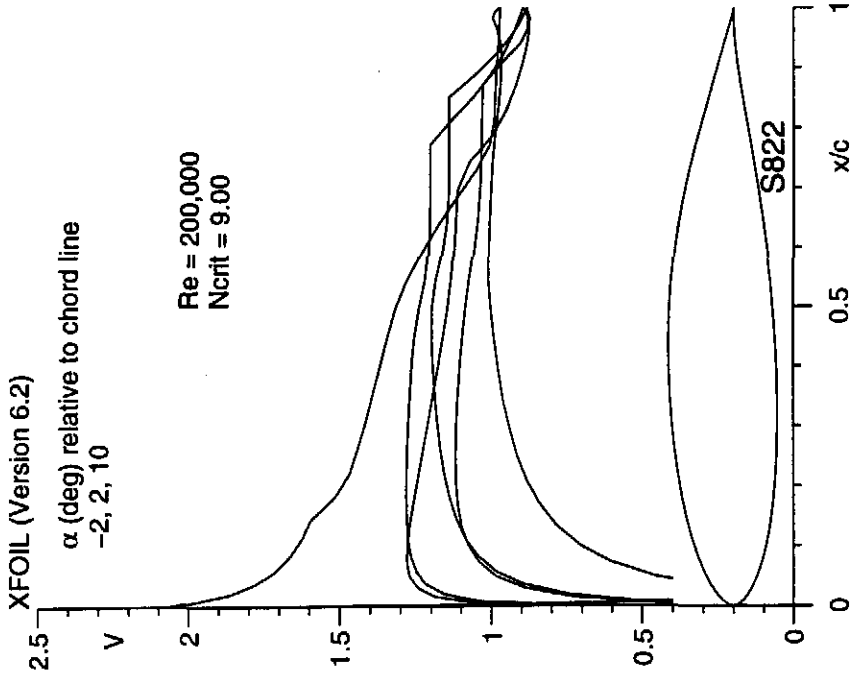
XFOIL (Version 6.2)
α (deg) relative to chord line
-2, 2, 10
Re = 200,000
Ncrit = 9.00
S822
2.5
2
1.5
1
0.5
0
Cl
0
0.5
1
x/c

S822

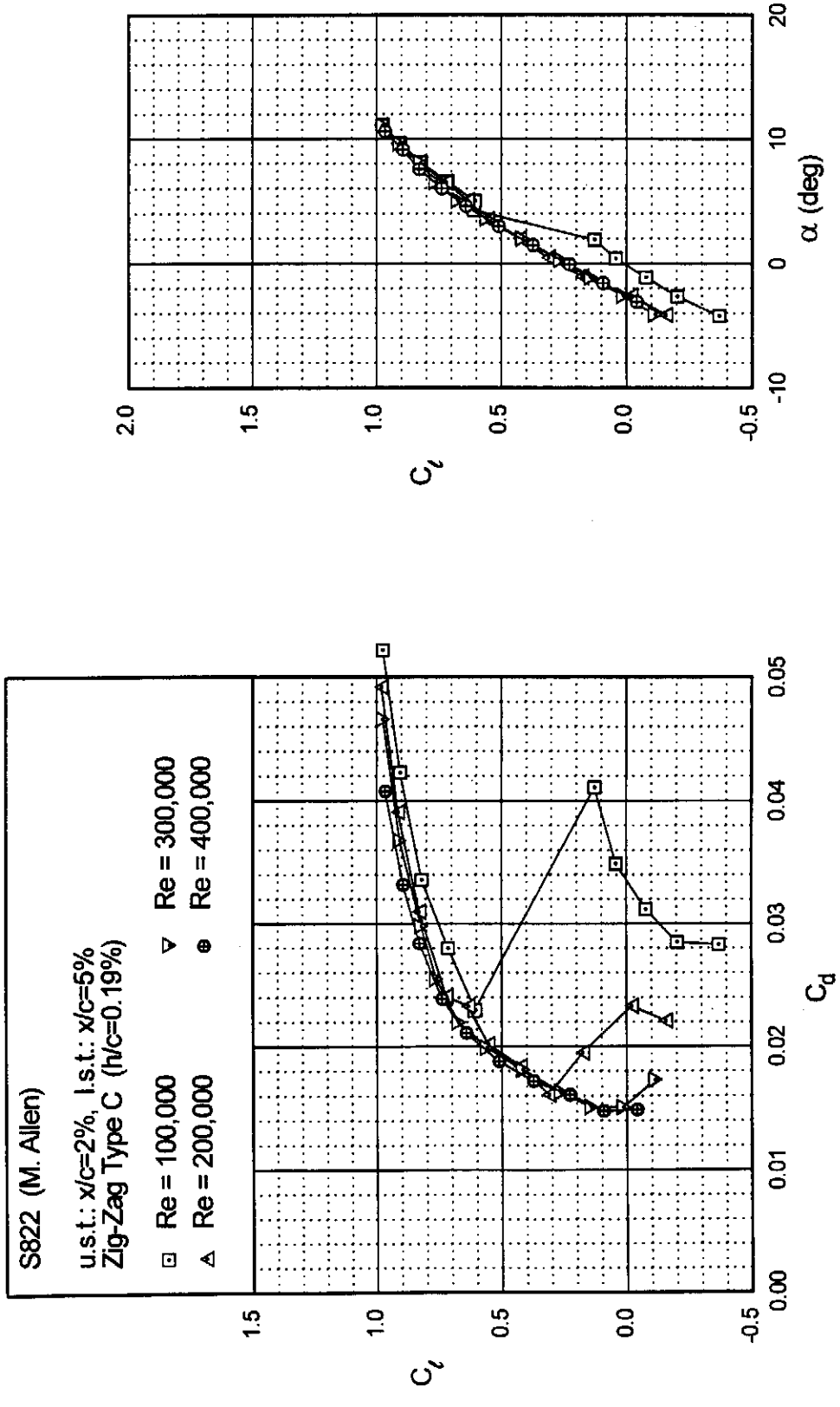
S822 (M. Allen)
u.s.t.: x/c=2%, l.s.t.: x/c=5%
Zig-Zag Type C (h/c=0.19%)
Re = 100,000
Re = 200,000
Re = 300,000
Re = 400,000
C_l
C_d
α (deg)

S822

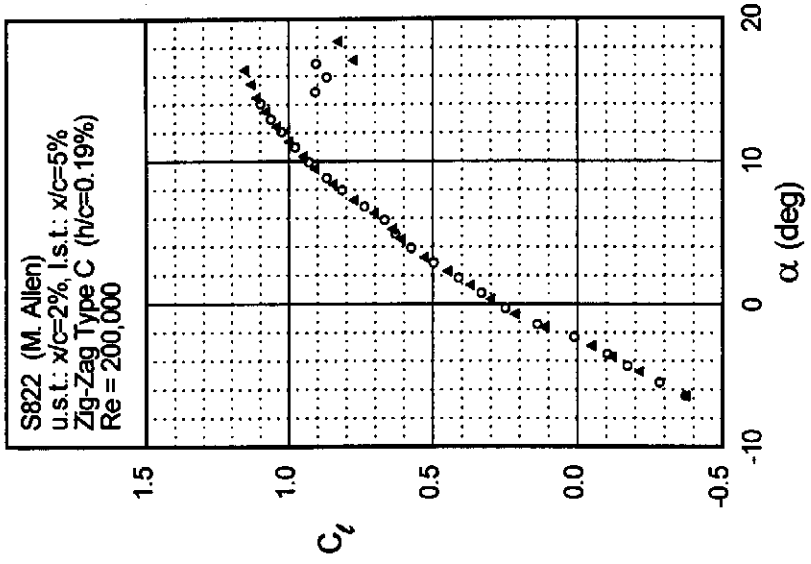
S822 (M. Allen)
u.s.t.: x/c=2%, l.s.t.: x/c=5%
Zig-Zag Type C (h/c=0.19%)
Re = 200,000
1.5
1.0
0.5
0.0
-0.5
C_l
-10
0
10
20
α (deg)

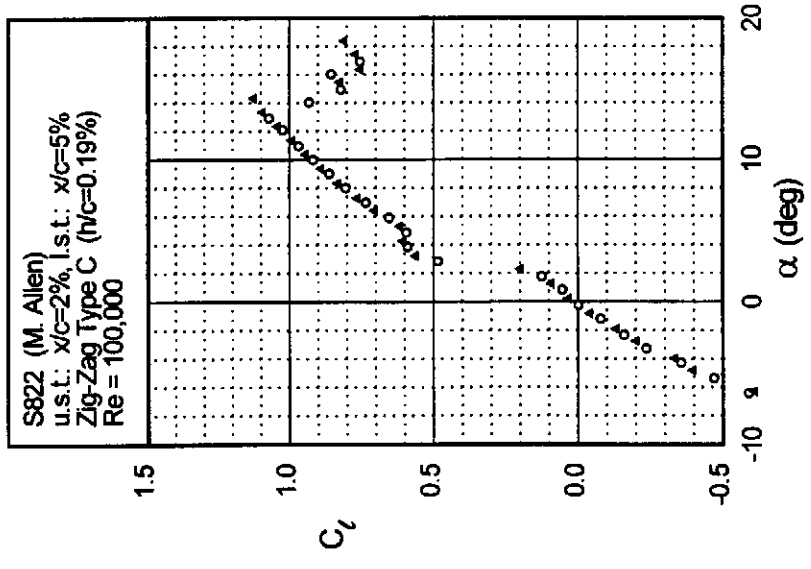
S822 (M. Allen)
u.s.t.: x/c=2%, l.s.t.: x/c=5%
Zig-Zag Type C (h/c=0.19%)
Re = 100,000
1.5
1.0
0.5
0.0
-0.5
C_l
-10
0
10
20
α (deg)

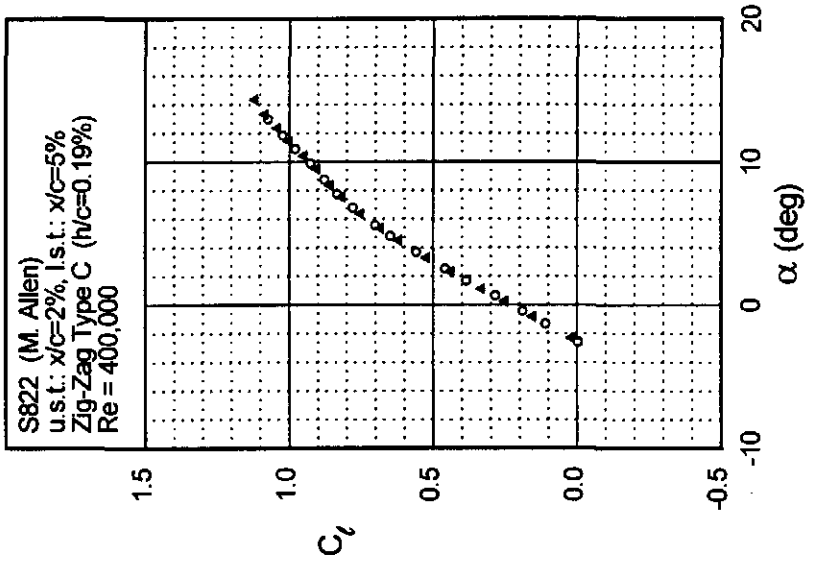
S822 (M. Allen)
u.s.t.: x/c=2%, l.s.t.: x/c=5%
Zig-Zag Type C (h/c=0.19%)
Re = 400,000
1.5
1.0
0.5
0.0
-0.5
C_l
-10
0
10
20
α (deg)

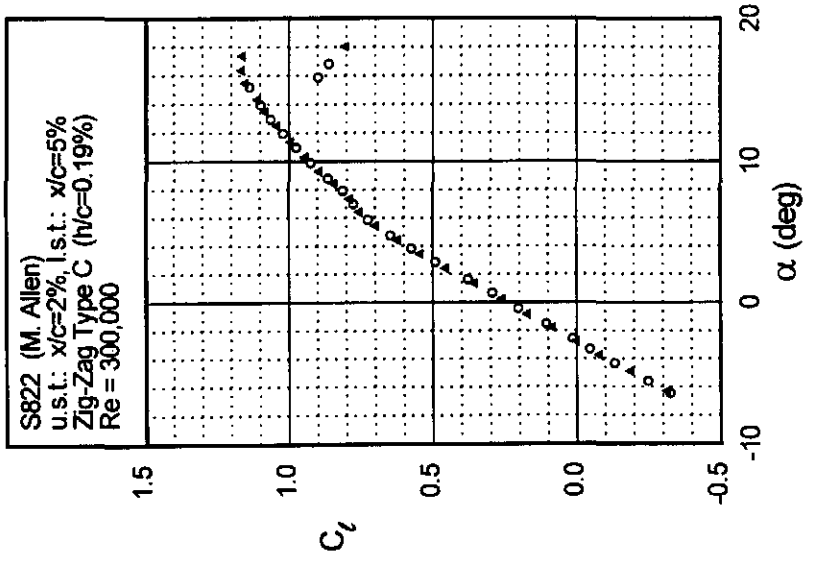
S822 (M. Allen)
u.s.t.: x/c=2%, l.s.t.: x/c=5%
Zig-Zag Type C (h/c=0.19%)
Re = 300,000
1.5
1.0
0.5
0.0
-0.5
C_l
-10
0
10
20
α (deg)

S822

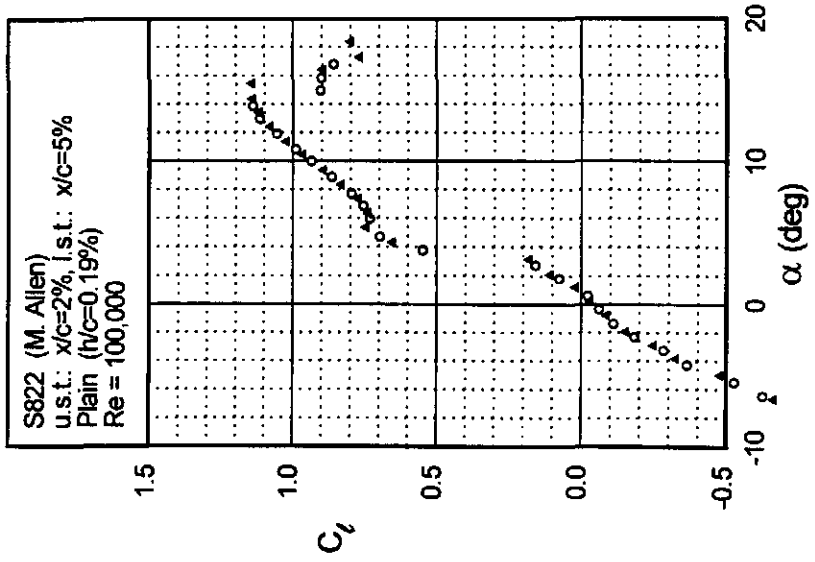
S822 (M. Allen)
u.s.t.: x/c=2%, l.s.t.: x/c=5%
Plain (h/c=0.19%)
Re = 100,000
1.5
1.0
0.5
0.0
-0.5
C_l
-10
0
10
20
α (deg)

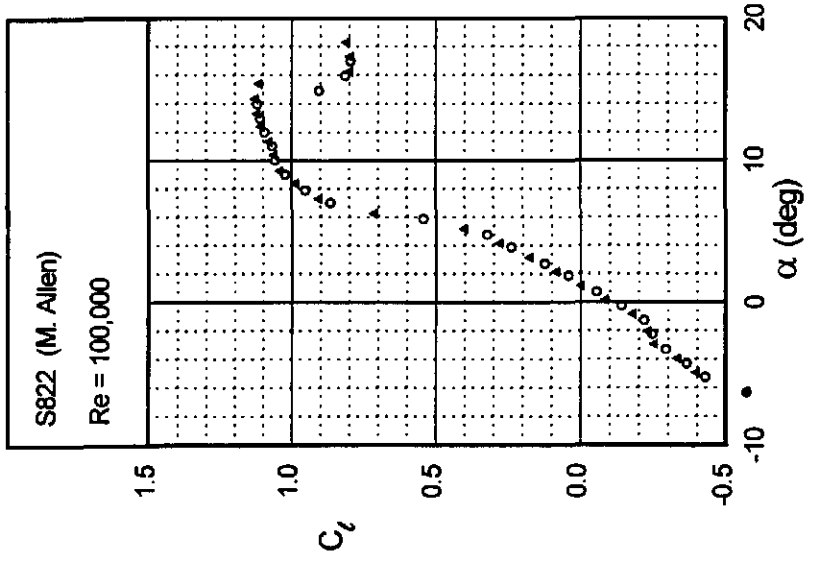
S822 (M. Allen)
Re = 100,000
1.5
1.0
0.5
0.0
-0.5
C_l
-10
0
10
20
α (deg)

S823

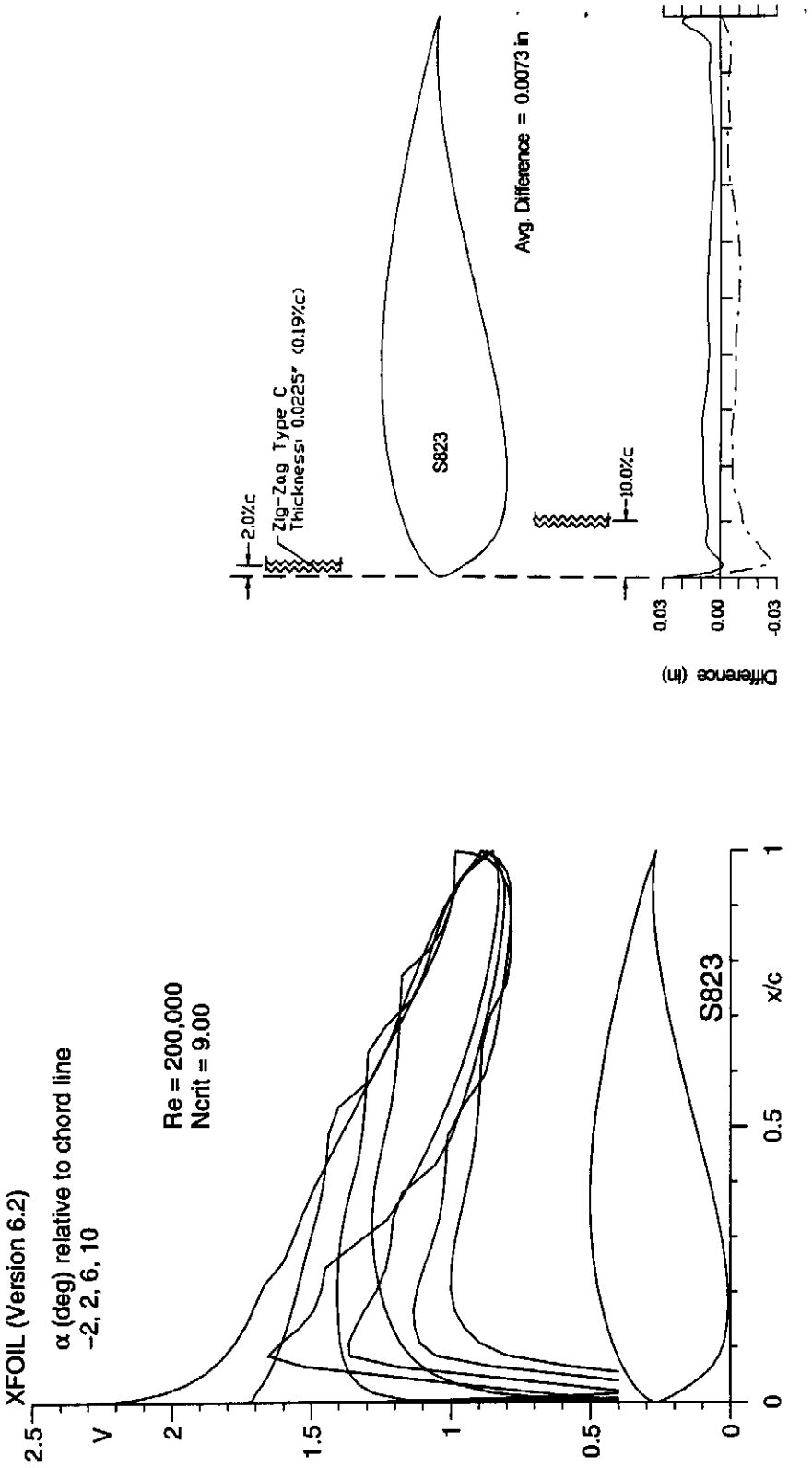
XFOIL (Version 6.2)
α (deg) relative to chord line
-2, 2, 6, 10
Re = 200,000
Ncrit = 9.00
2.5
2
1.5
1
0.5
0
V
S823
0
0.5
1
x/c
2.0%c
Zig-Zag Type C
Thickness: 0.0225" (0.19%c)
S823
10.0%c
Avg. Difference = 0.0073 in
0.03
0.00
-0.03
Difference (in)

S823

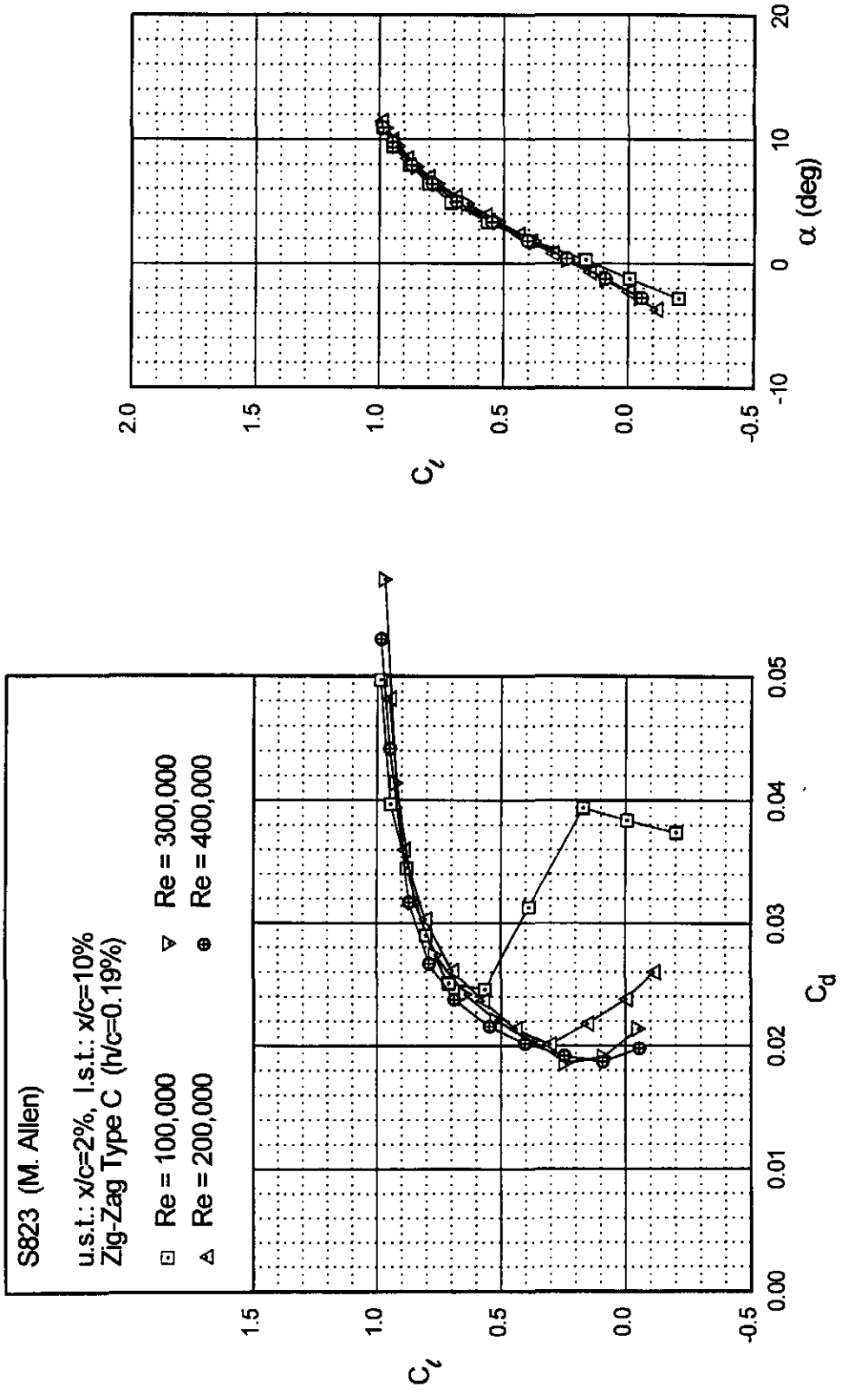
S823 (M. Allen)
u.s.t.: x/c=2%, l.s.t.: x/c=10%
Zig-Zag Type C (h/c=0.19%)
Re = 100,000
Re = 200,000
Re = 300,000
Re = 400,000
Cl
Cd
α (deg)
2.0
1.5
1.0
0.5
0.0
-0.5
-10
0
10
20
0.00
0.01
0.02
0.03
0.04
0.05

S823

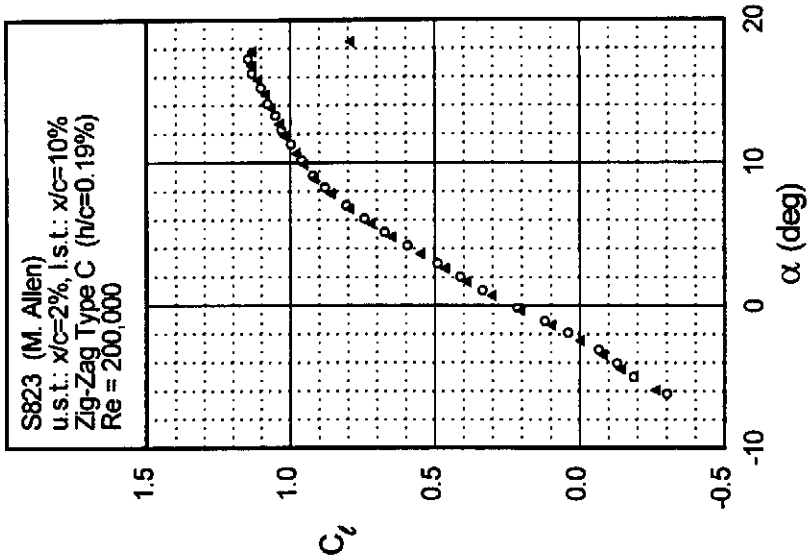
S823 (M. Allen)
u.s.t.: x/c=2%, l.s.t.: x/c=10%
Zig-Zag Type C (h/c=0.19%)
Re = 200,000
1.5
1.0
0.5
0.0
-0.5
C_l
-10
0
10
20
α (deg)

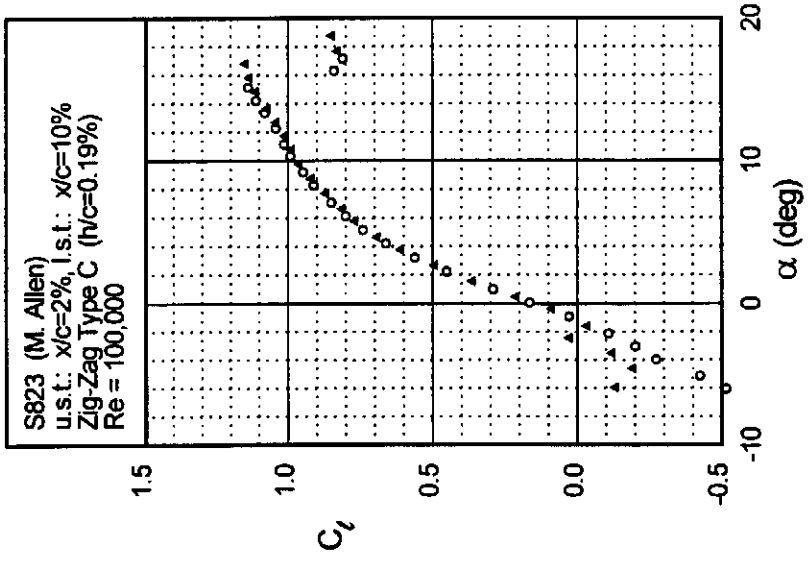
S823 (M. Allen)
u.s.t.: x/c=2%, l.s.t.: x/c=10%
Zig-Zag Type C (h/c=0.19%)
Re = 100,000
1.5
1.0
0.5
0.0
-0.5
C_l
-10
0
10
20
α (deg)

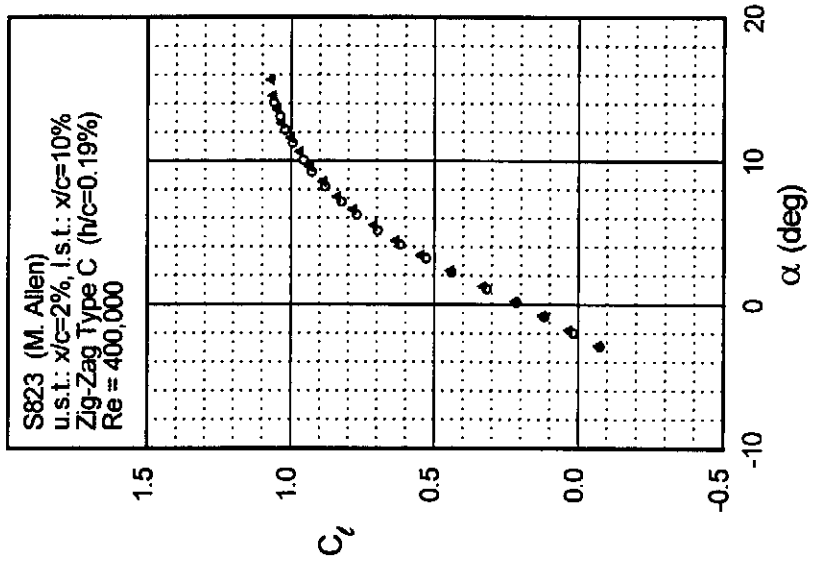
S823 (M. Allen)
u.s.t.: x/c=2%, l.s.t.: x/c=10%
Zig-Zag Type C (h/c=0.19%)
Re = 400,000
1.5
1.0
0.5
0.0
-0.5
C_ℓ
-10
0
10
20
α (deg)

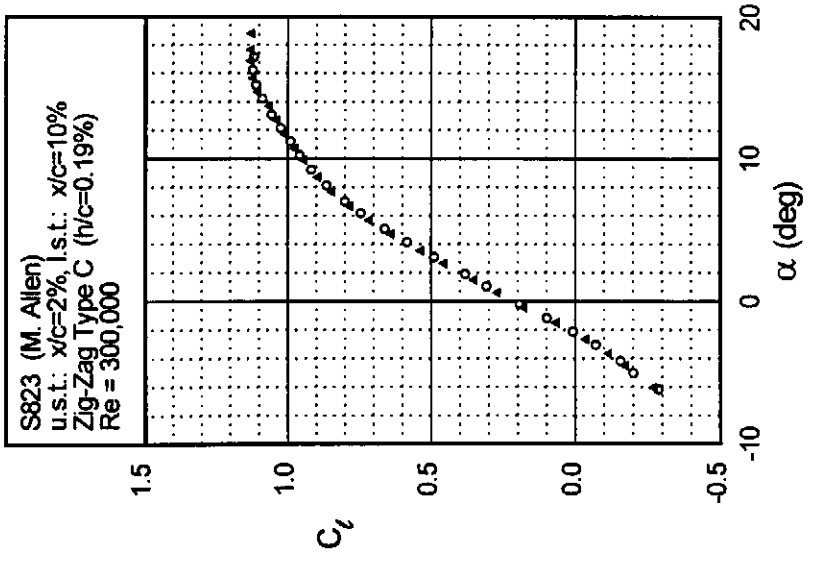
S823 (M. Allen)
u.s.t.: x/c=2%, l.s.t.: x/c=10%
Zig-Zag Type C (h/c=0.19%)
Re = 300,000
1.5
1.0
0.5
0.0
-0.5
C_ℓ
-10
0
10
20
α (deg)

S1223

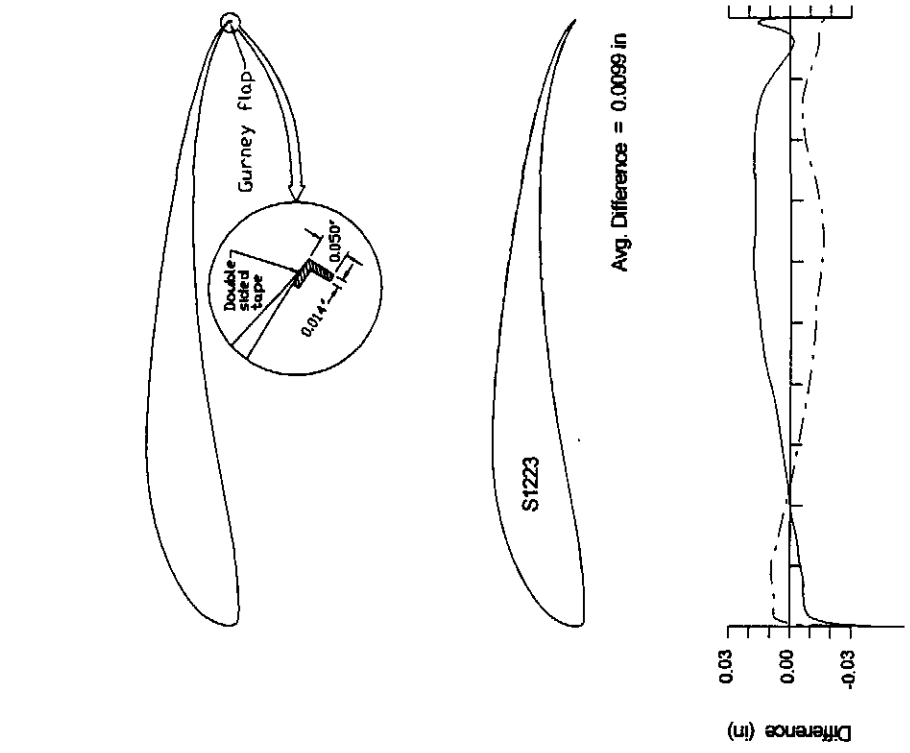
Gurney flop
Double sided tape
0.050"
0.014"
S1223
Avg. Difference = 0.0099 in
0.03
0.00
-0.03
Difference (in)

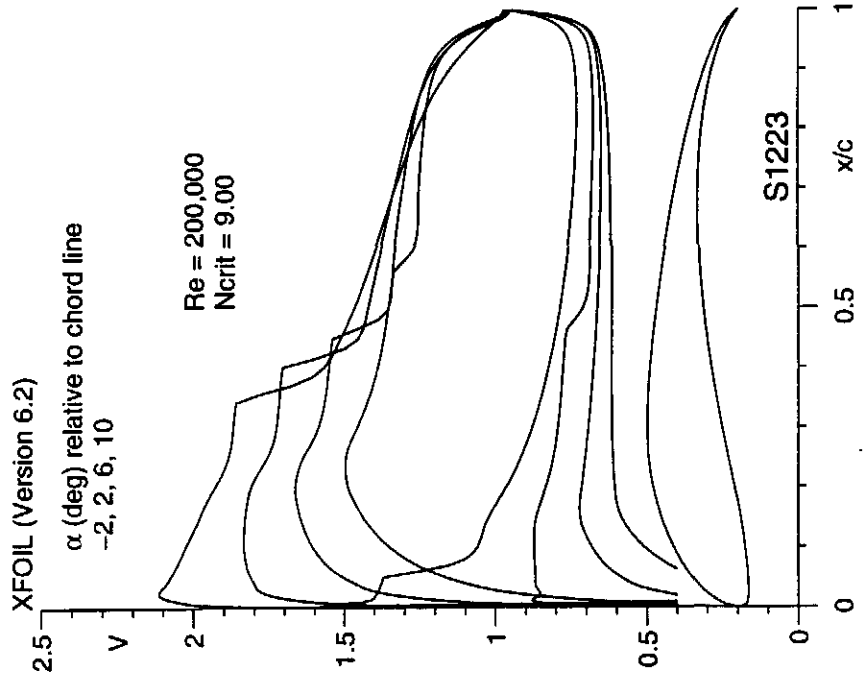
XFOIL (Version 6.2)
α (deg) relative to chord line
-2, 2, 6, 10
Re = 200,000
Ncrit = 9.00
S1223
x/c
V
2.5
2
1.5
1
0.5
0
0.5
1

S1223

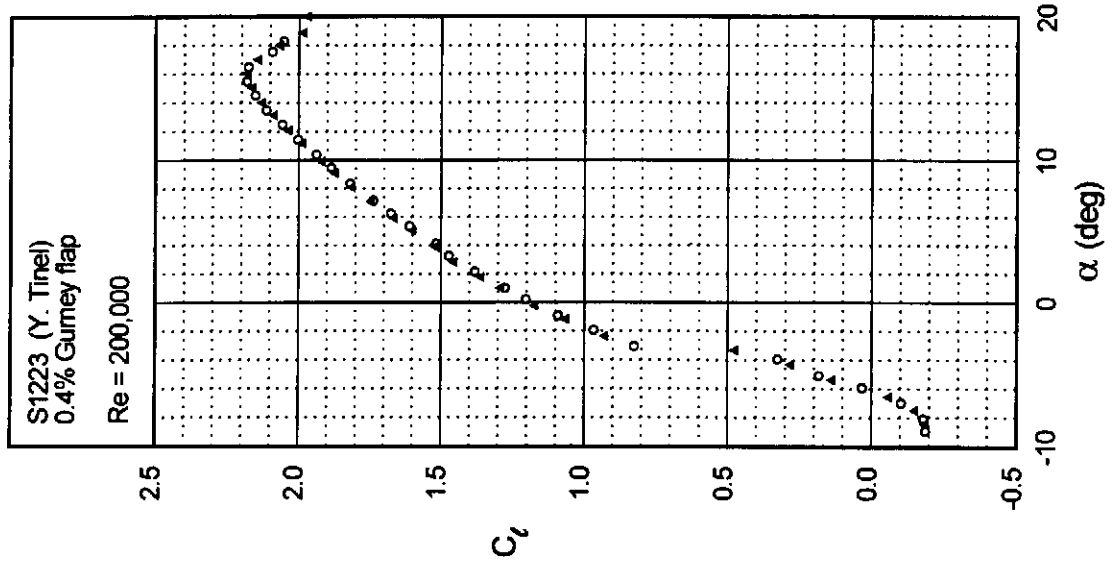
S1223 (Y. Tinel)
0.4% Gurney flap
Re = 200,000
2.5
2.0
1.5
1.0
0.5
0.0
-0.5
C_l
20
10
0
-10
α (deg)

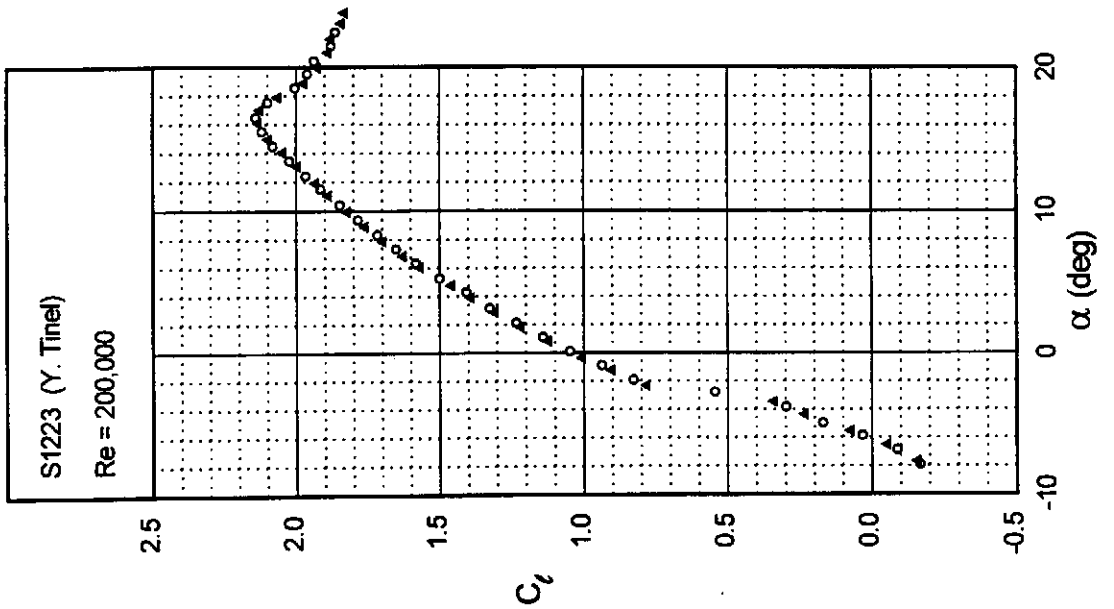
S1223 (Y. Tinel)
Re = 200,000
2.5
2.0
1.5
1.0
0.5
0.0
-0.5
C_l
20
10
0
-10
α (deg)

S1223 RTL

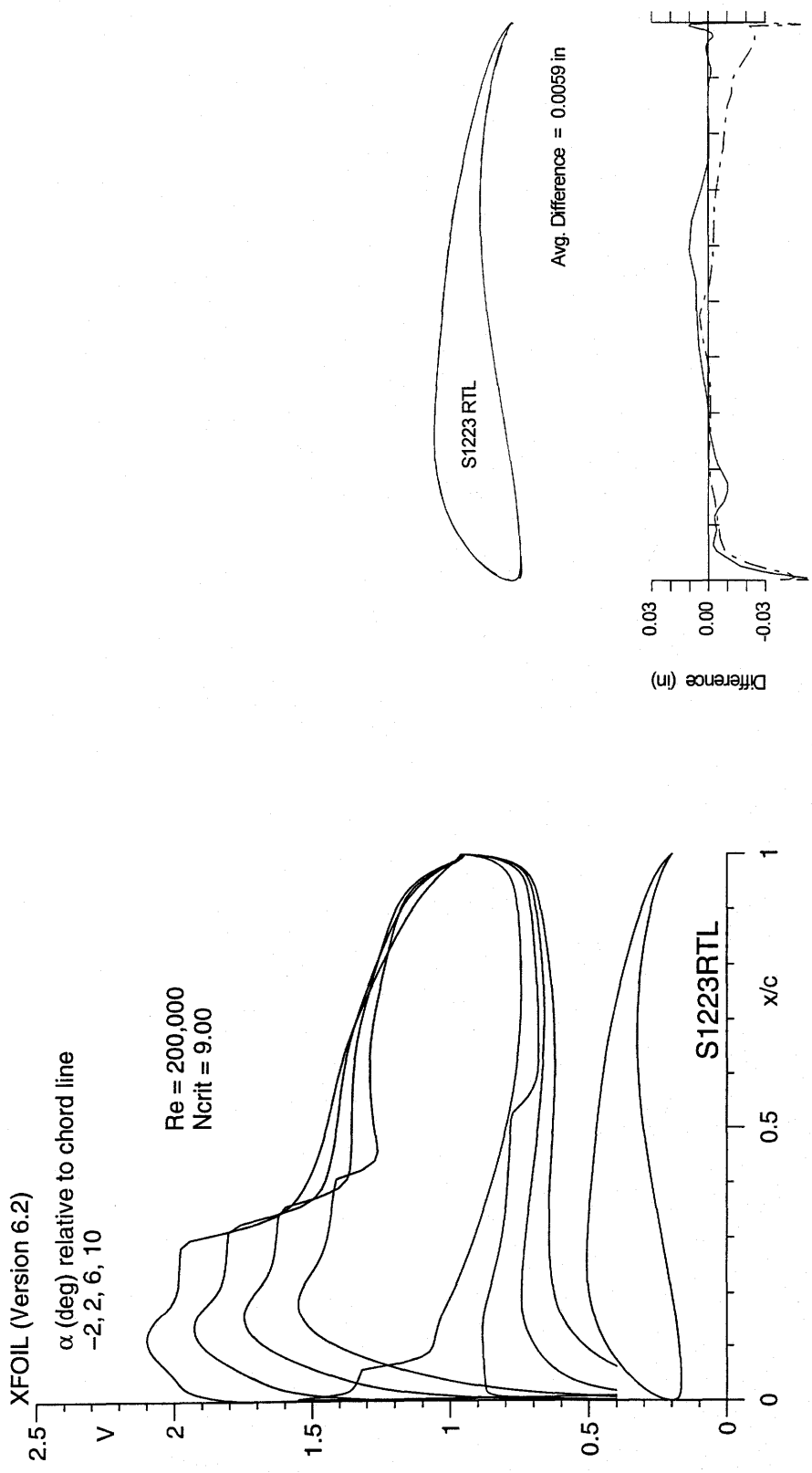
S1223 RTL
Avg. Difference = 0.0059 in
0.03
0.00
-0.03
Difference (in)
XFOIL (Version 6.2)
α (deg) relative to chord line
-2, 2, 6, 10
Re = 200,000
Ncrit = 9.00
2.5
2
1.5
1
0.5
0
V
S1223RTL
0
0.5
1
x/c

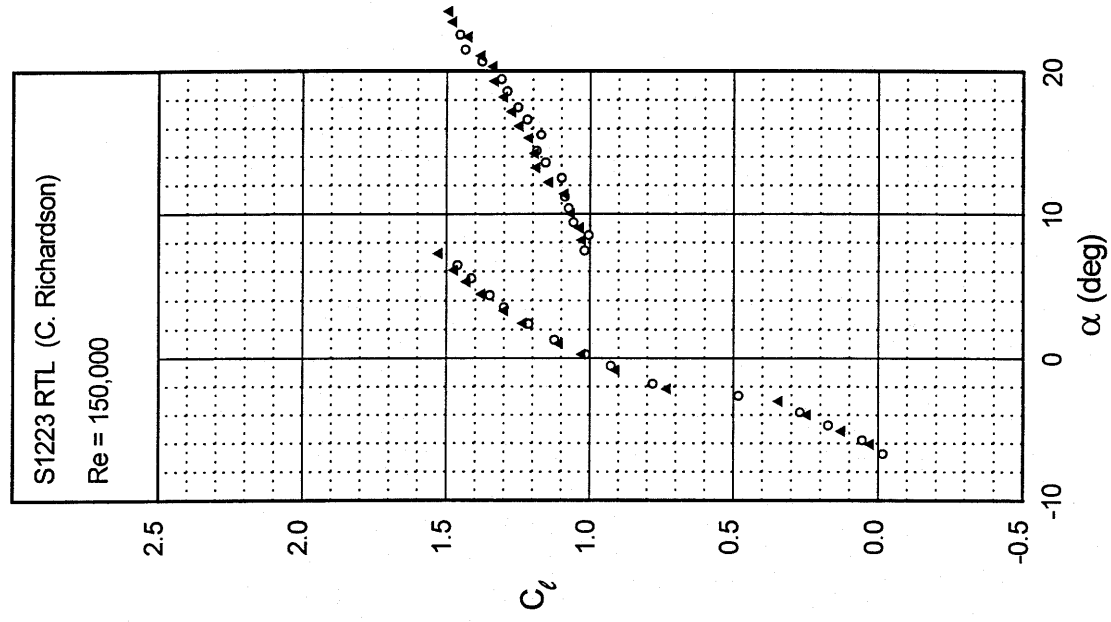
S1223 RTL (C. Richardson)
Re = 150,000
2.5
2.0
1.5
1.0
0.5
0.0
-0.5
C_l
-10
0
10
20
α (deg)

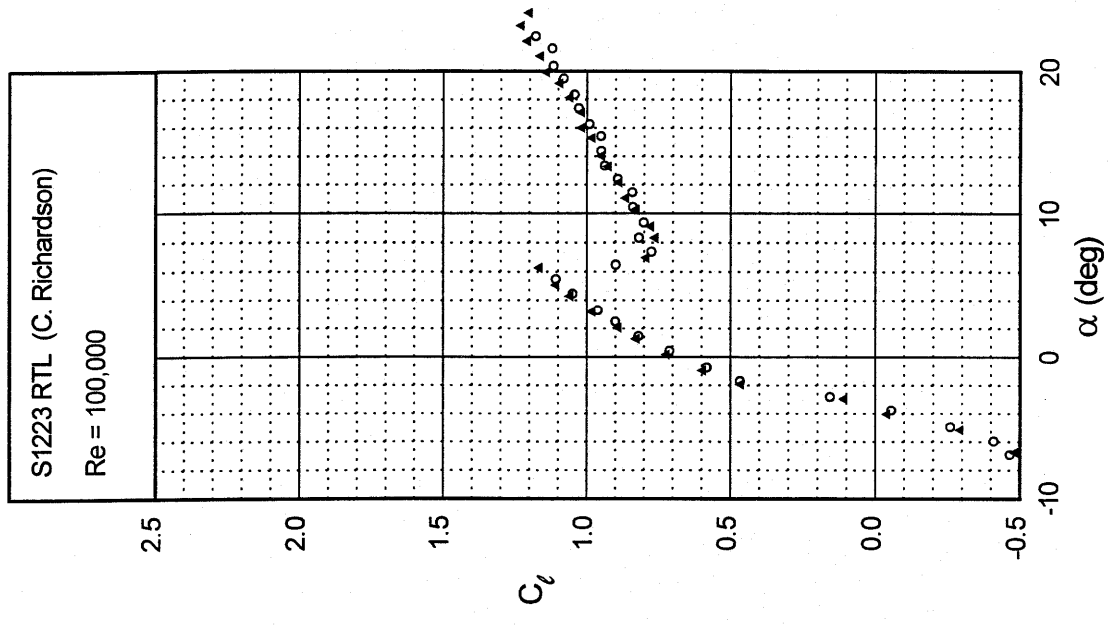
S1223 RTL (C. Richardson)
Re = 100,000
2.5
2.0
1.5
1.0
0.5
0.0
-0.5
C_l
-10
0
10
20
α (deg)

Fig. 5.81 (continued)

S1223 RTL

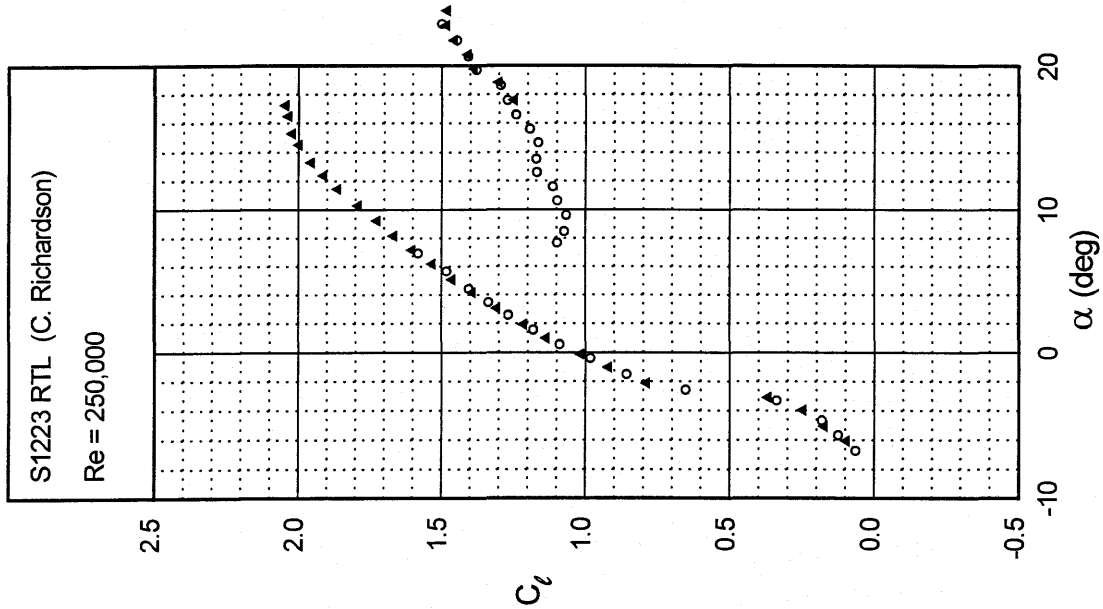

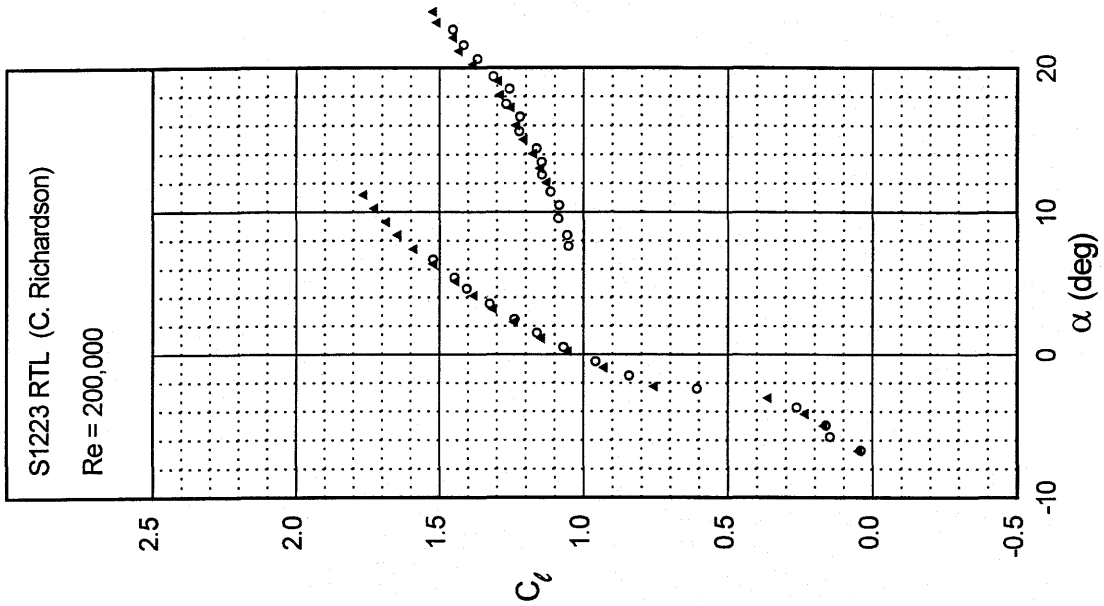

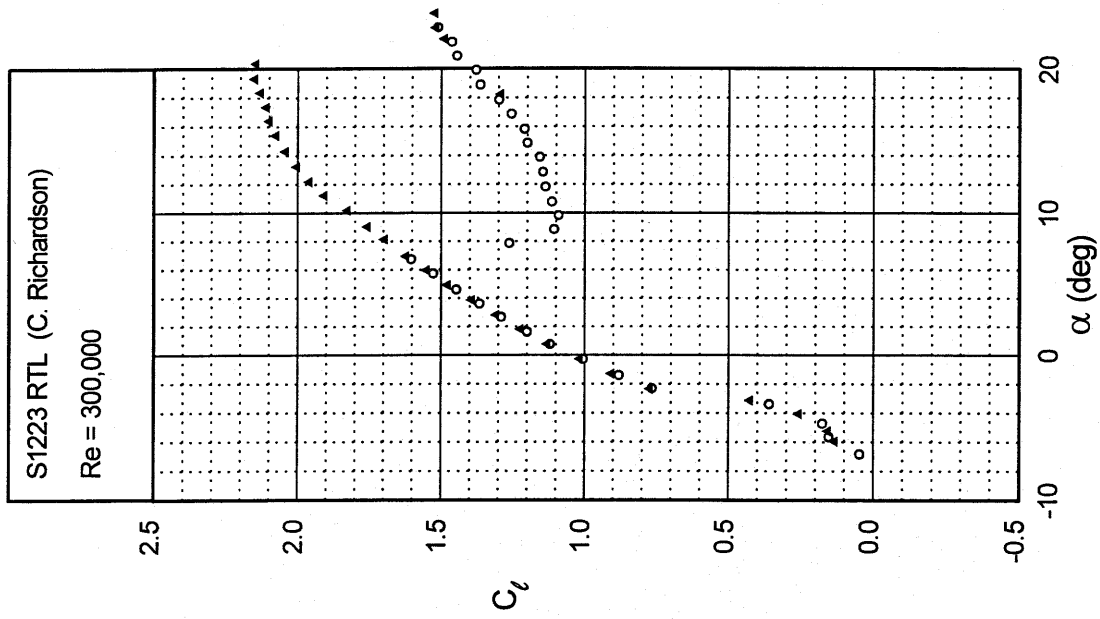
S1223 RTL (C. Richardson)
Re = 300,000
2.5
2.0
1.5
1.0
0.5
0.0
-0.5
C_l
-10
0
10
20
α (deg)

S4083 (A)

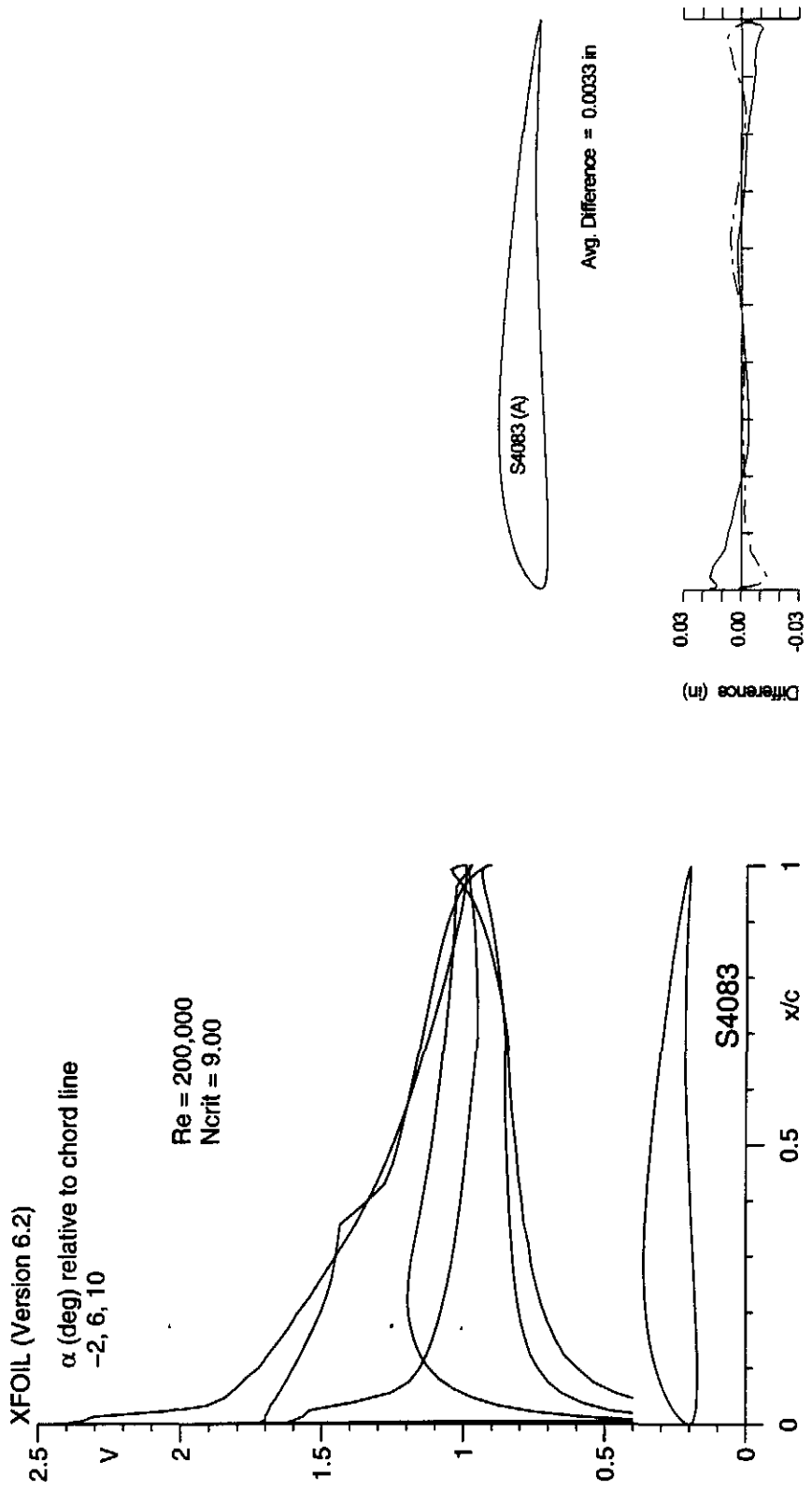
S4083 (A)
Avg. Difference = 0.0033 in
0.03
0.00
-0.03
Difference (in)
XFOIL (Version 6.2)
α (deg) relative to chord line
-2, 6, 10
Re = 200,000
Ncrit = 9.00
V
2.5
2
1.5
1
0.5
0
S4083
0
0.5
1
x/c

S4083 (A)

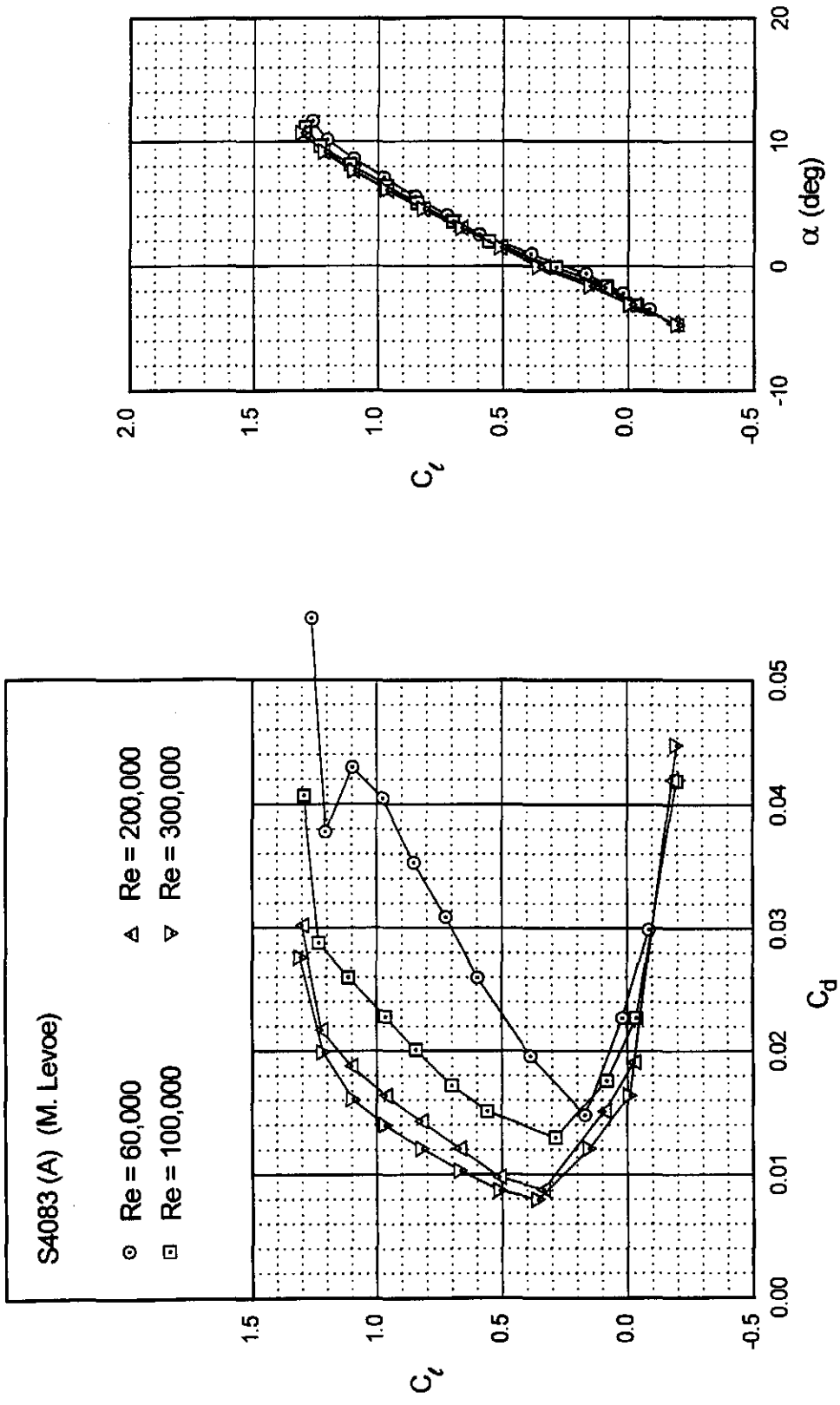
S4083 (A) (M. Levoe)
Re = 60,000
Re = 100,000
Re = 200,000
Re = 300,000
C_l
C_d
α (deg)
2.0
1.5
1.0
0.5
0.0
-0.5
20
10
0
-10
0.05
0.04
0.03
0.02
0.01
0.00

Fig. 5.85

S4083 (A)

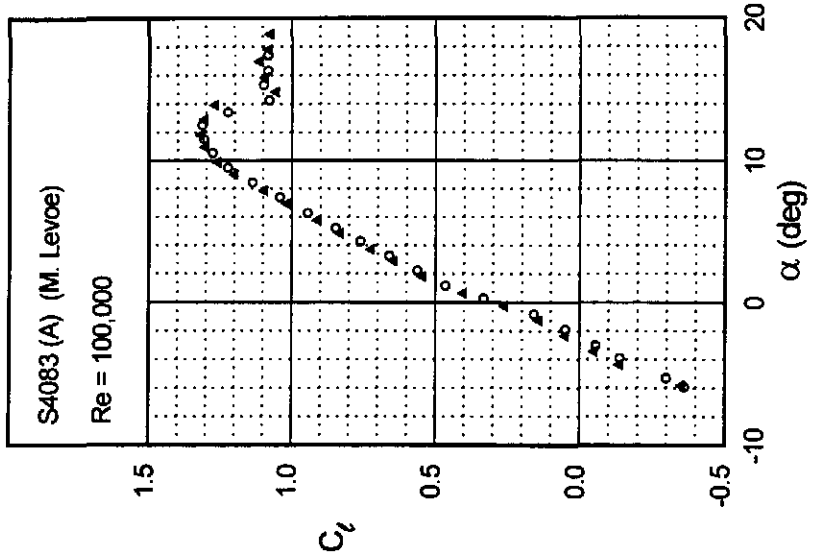

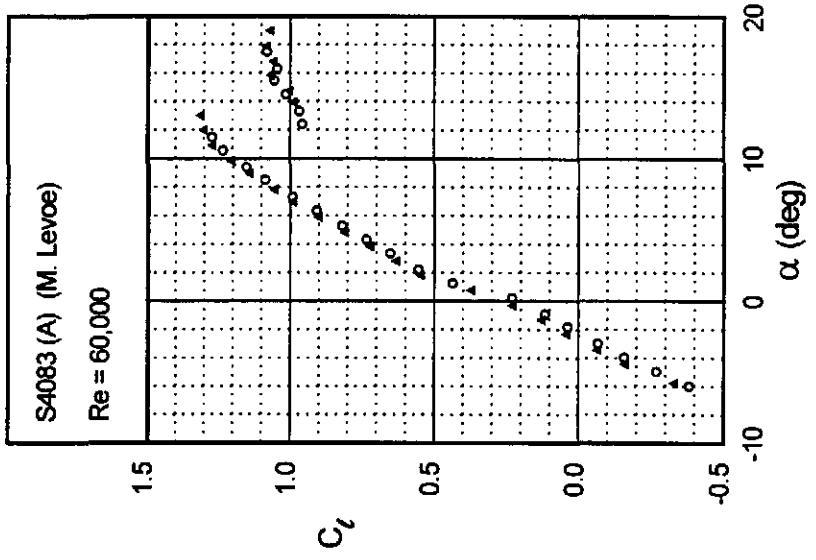

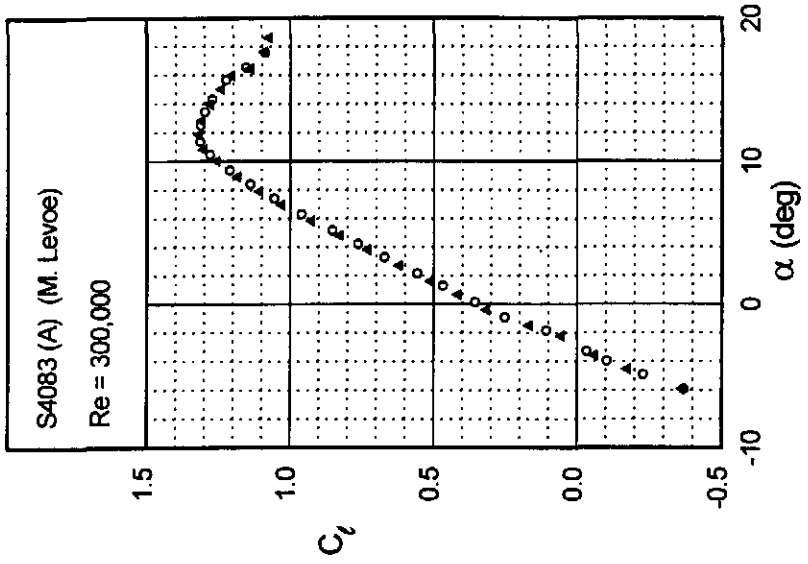
S4083 (A) (M. Levoe)
Re = 300,000
1.5
1.0
0.5
0.0
-0.5
C_l
-10
0
10
20
α (deg)

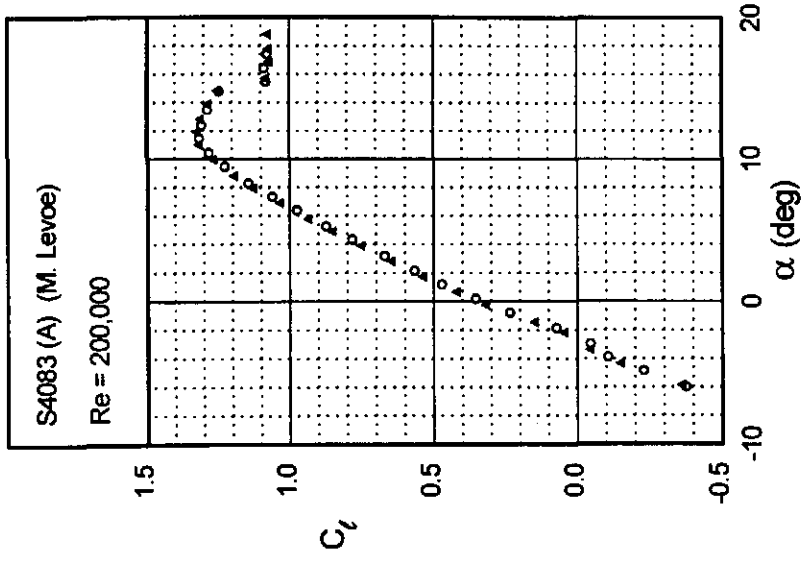
S4083 (A) (M. Levoe)
Re = 200,000
1.5
1.0
0.5
0.0
-0.5
C_l
-10
0
10
20
α (deg)

S4083 (B)

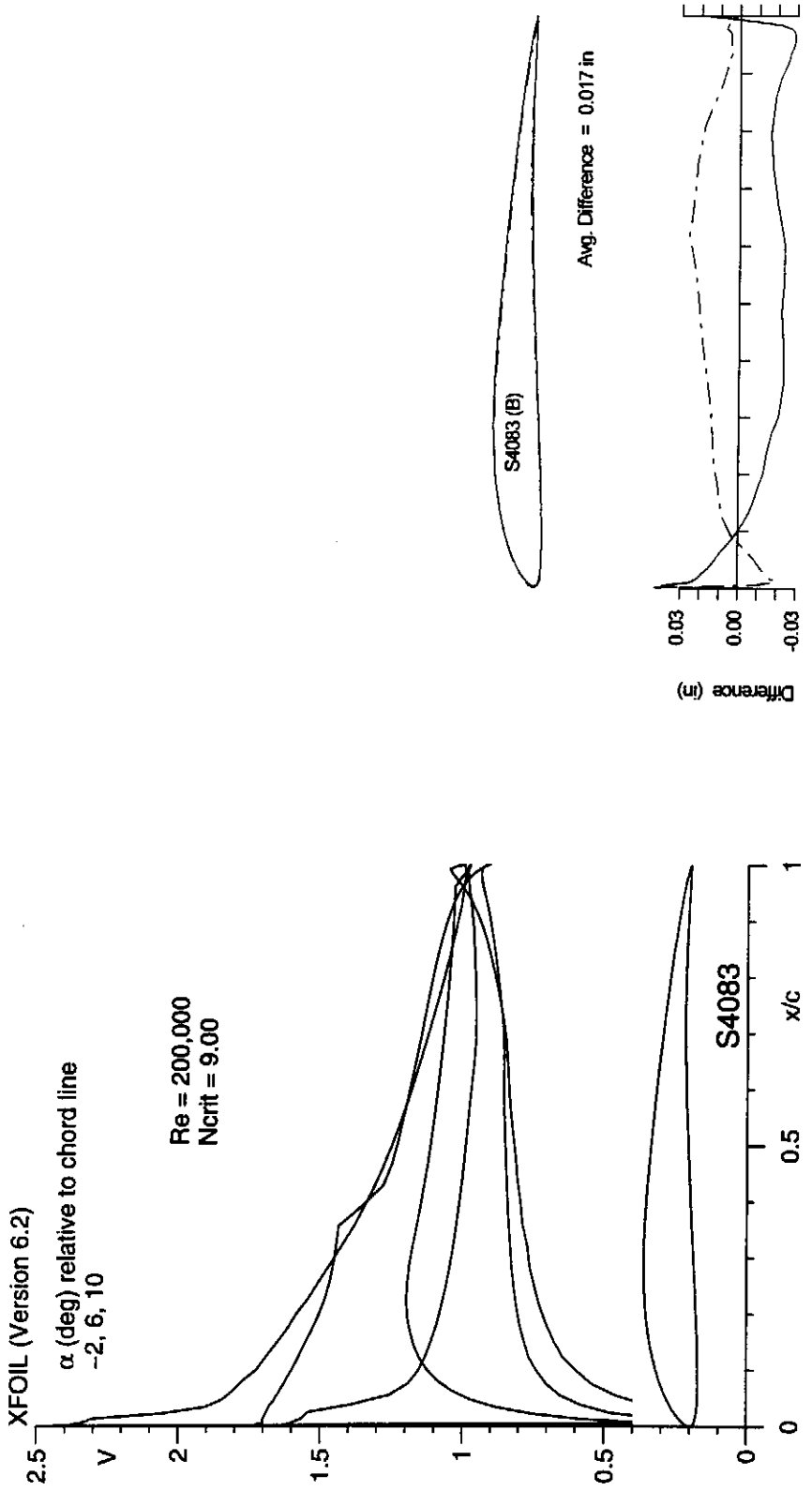
S4083 (B)
Avg. Difference = 0.017 in
0.03
0.00
-0.03
Difference (in)
XFOIL (Version 6.2)
α (deg) relative to chord line
-2, 6, 10
Re = 200,000
Ncrit = 9.00
2.5
2
1.5
1
0.5
V
0
0.5
1
x/c
S4083

S4083 (B)

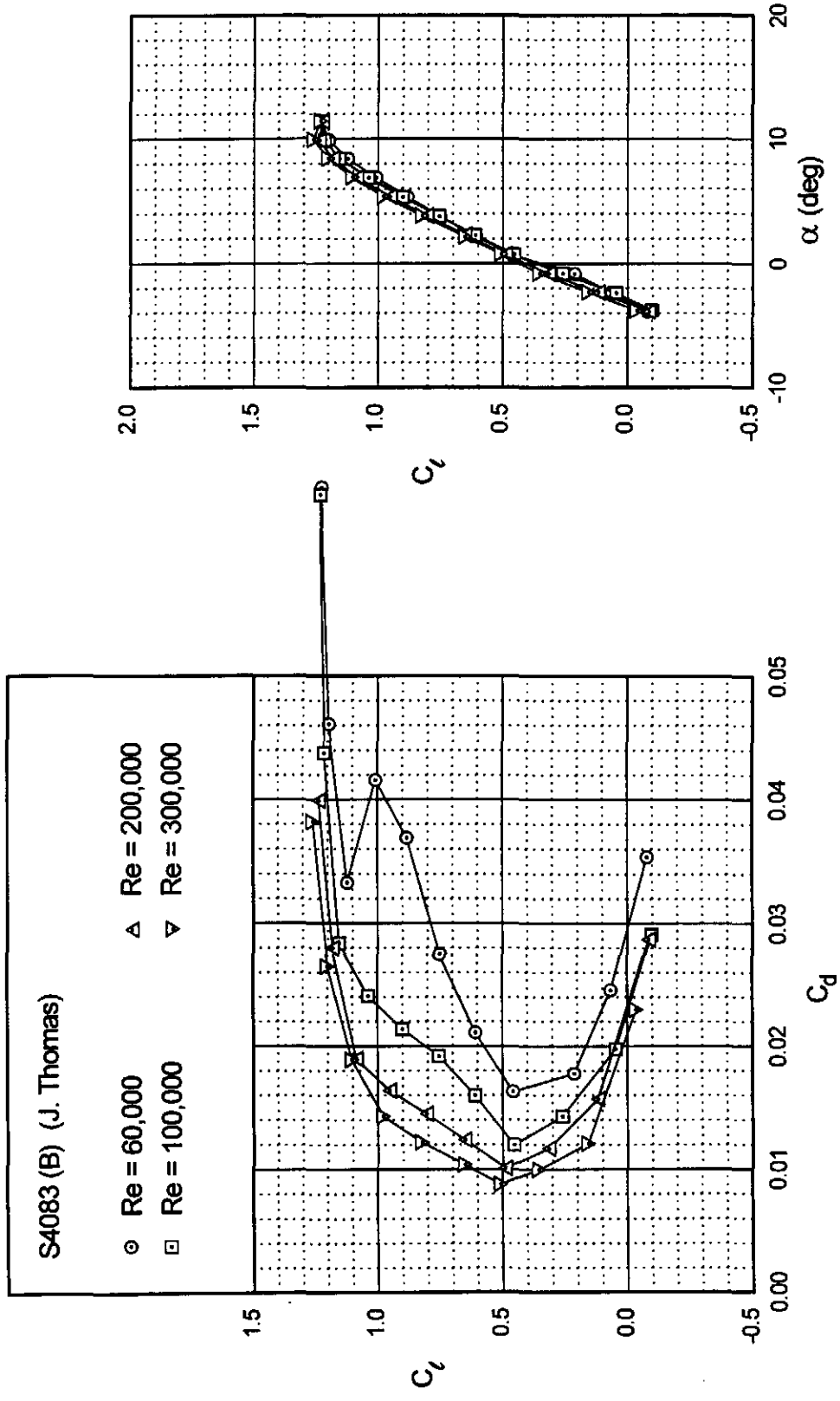
S4083 (B) (J. Thomas)
Re = 60,000
Re = 100,000
Re = 200,000
Re = 300,000
C_l
C_d
α (deg)
2.0
1.5
1.0
0.5
0.0
-0.5
-10
0
10
20
0.00
0.01
0.02
0.03
0.04
0.05

Fig. 5.89

S4083 (B)

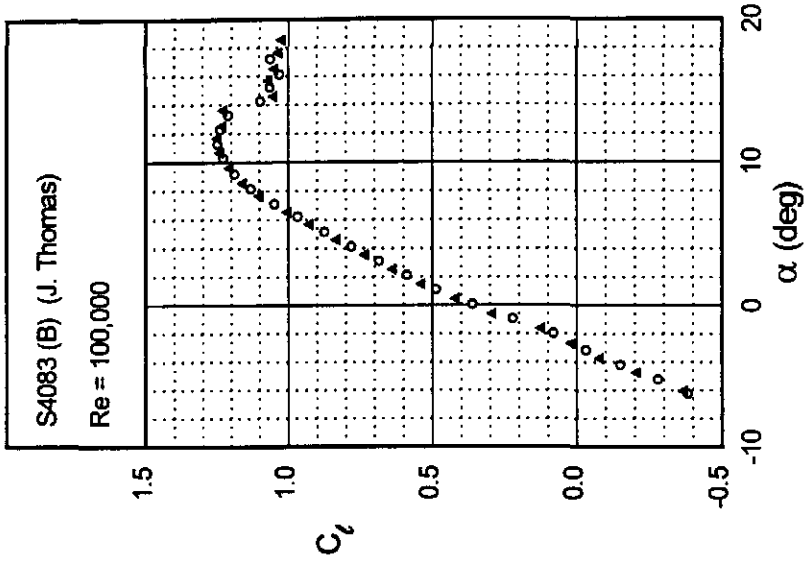

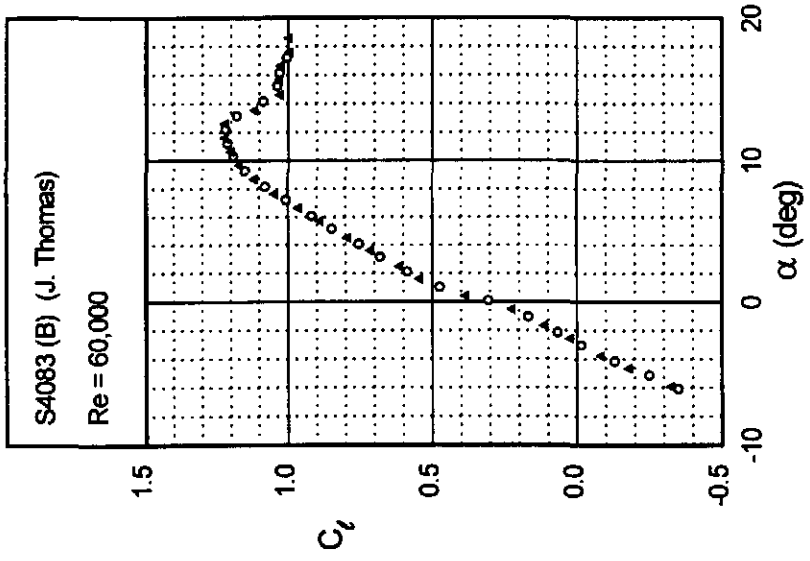

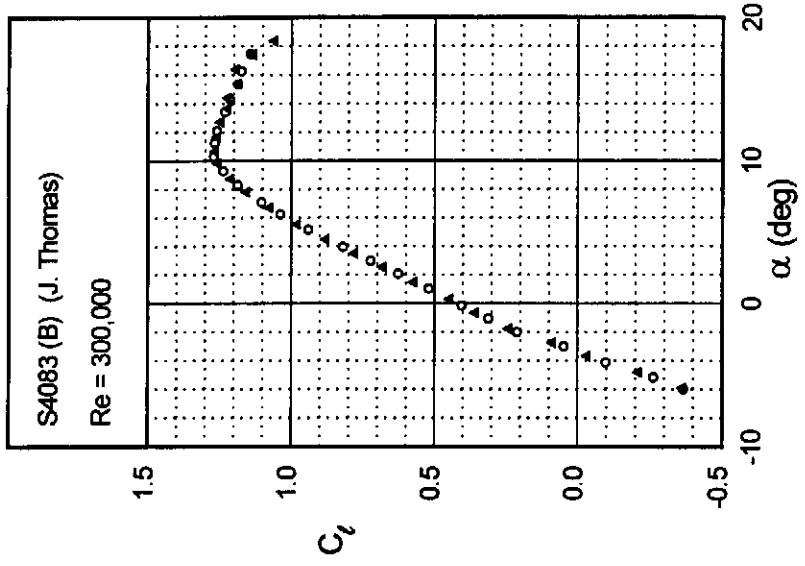
S4083 (B) (J. Thomas)
Re = 300,000
1.5
1.0
0.5
0.0
-0.5
C_l
-10
0
10
20
α (deg)

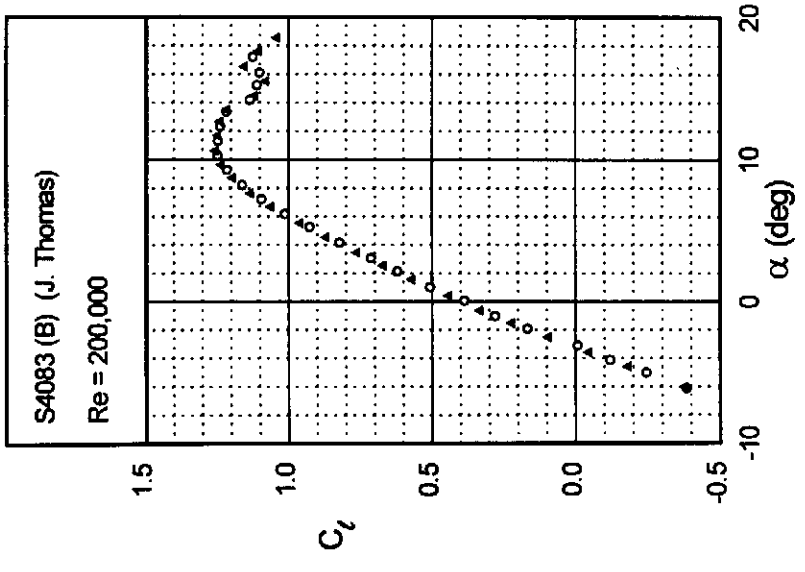
S4083 (B) (J. Thomas)
Re = 200,000
1.5
1.0
0.5
0.0
-0.5
C_l
-10
0
10
20
α (deg)

S5010

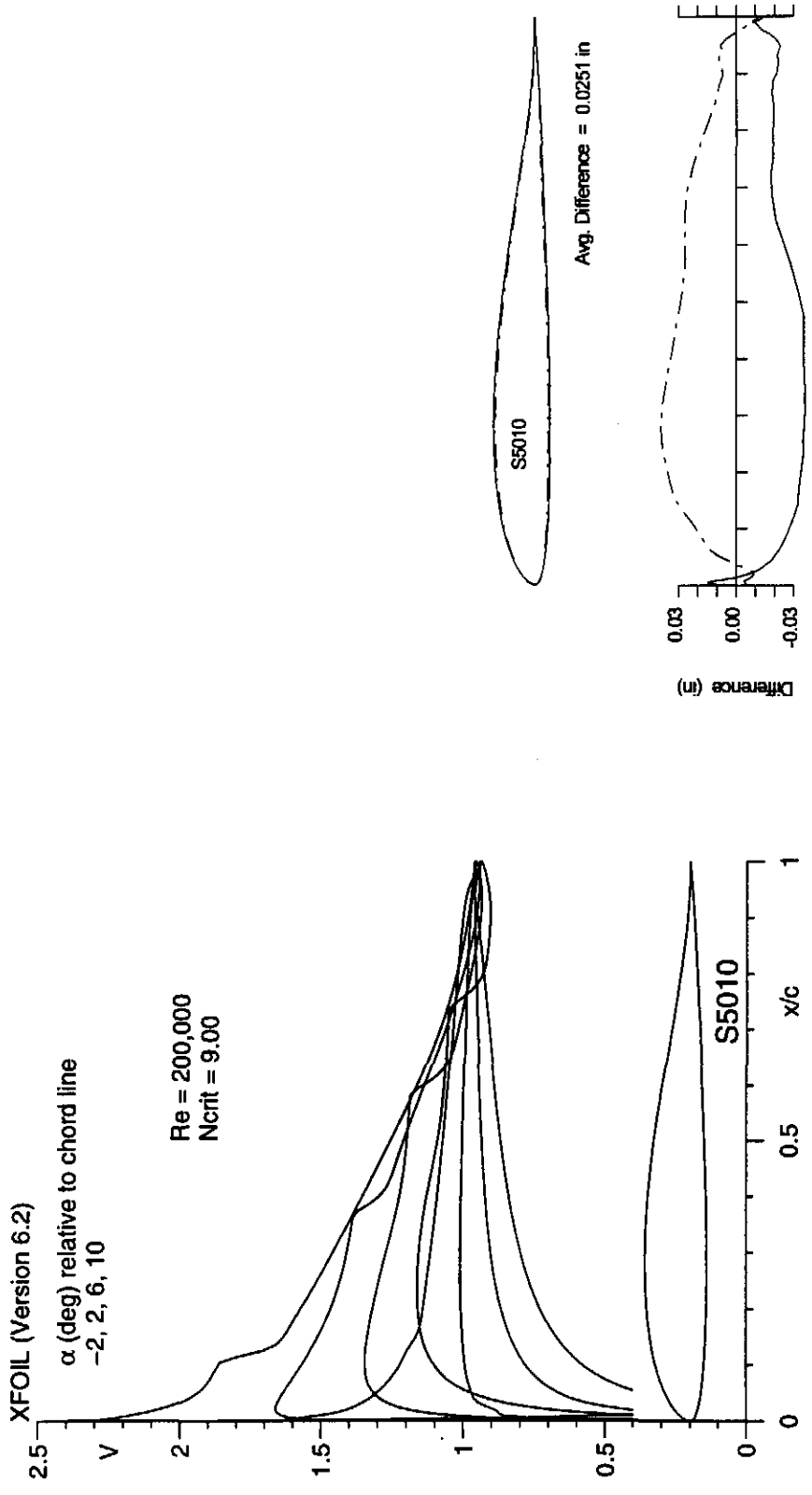
S5010
Avg. Difference = 0.0251 in
0.03
0.00
-0.03
Difference (in)
XFOIL (Version 6.2)
α (deg) relative to chord line
-2, 2, 6, 10
Re = 200,000
Ncrit = 9.00
2.5
2
1.5
1
0.5
0
V
S5010
0
0.5
1
x/c

S5010

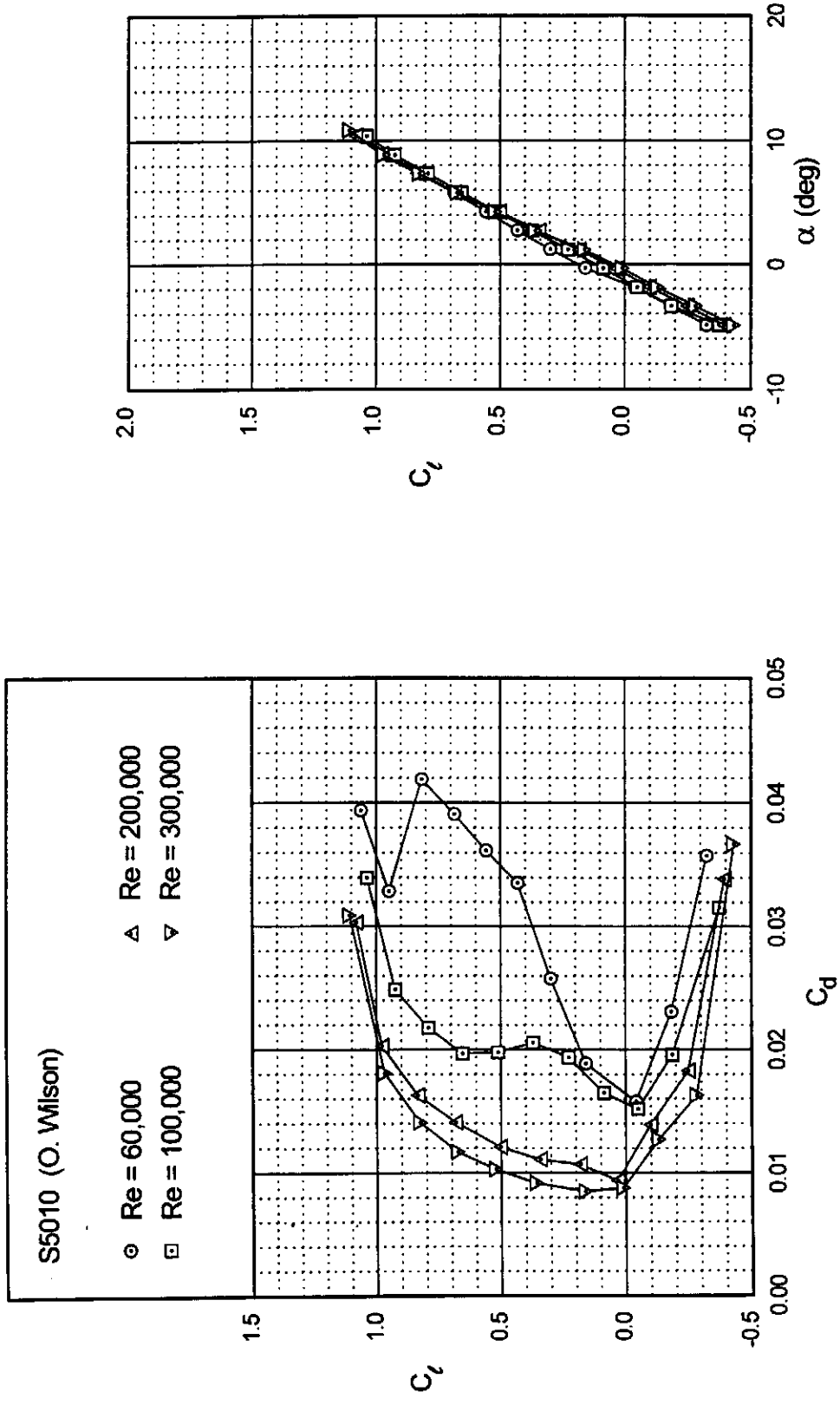
S5010 (O. Wilson)
Re = 60,000
Re = 100,000
Re = 200,000
Re = 300,000
C_l
C_d
α (deg)
2.0
1.5
1.0
0.5
0.0
-0.5
20
10
0
-10
0.05
0.04
0.03
0.02
0.01
0.00

Fig. 5.93

S5010

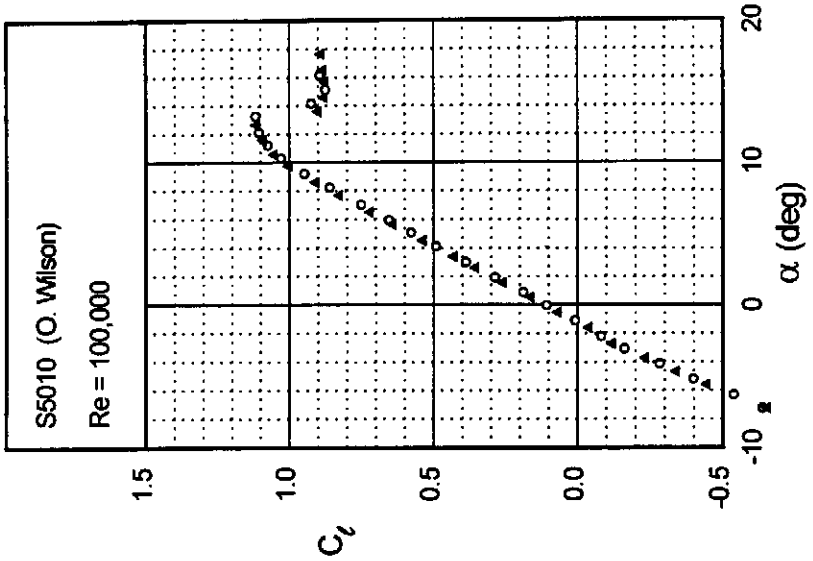

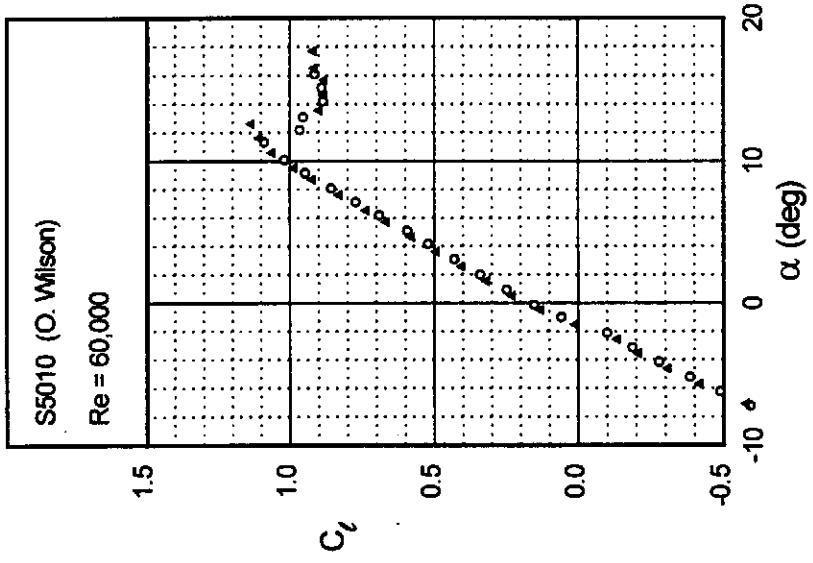

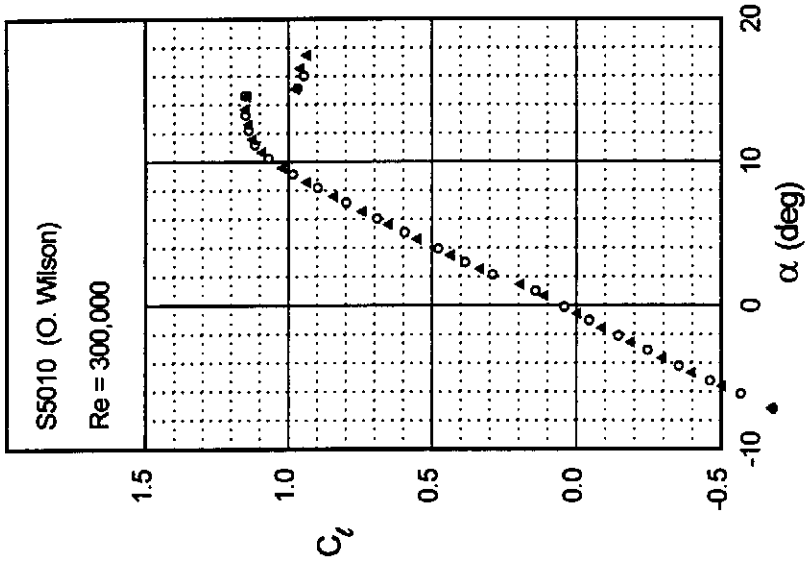
S5010 (O. Wilson)
Re = 300,000
1.5
1.0
0.5
0.0
-0.5
C_l
-10
0
10
20
α (deg)

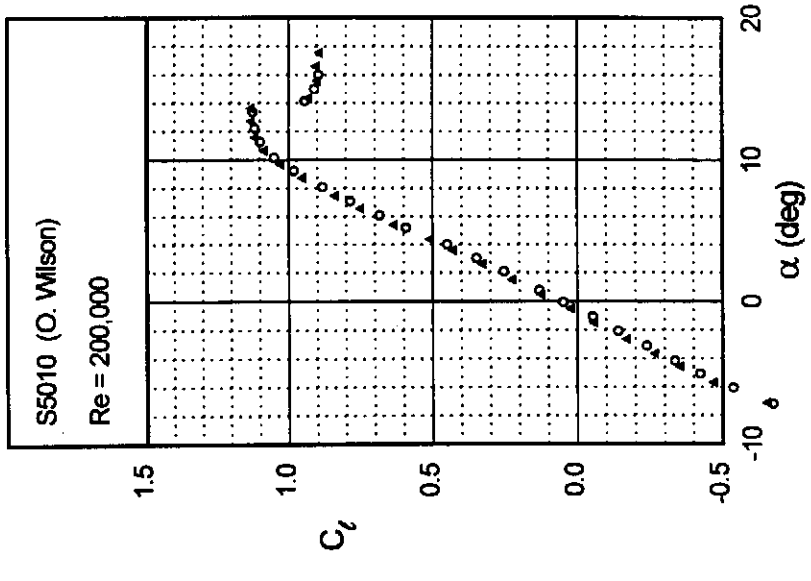
S5010 (O. Wilson)
Re = 200,000
1.5
1.0
0.5
0.0
-0.5
C_l
-10
0
10
20
α (deg)

S7012 (B)

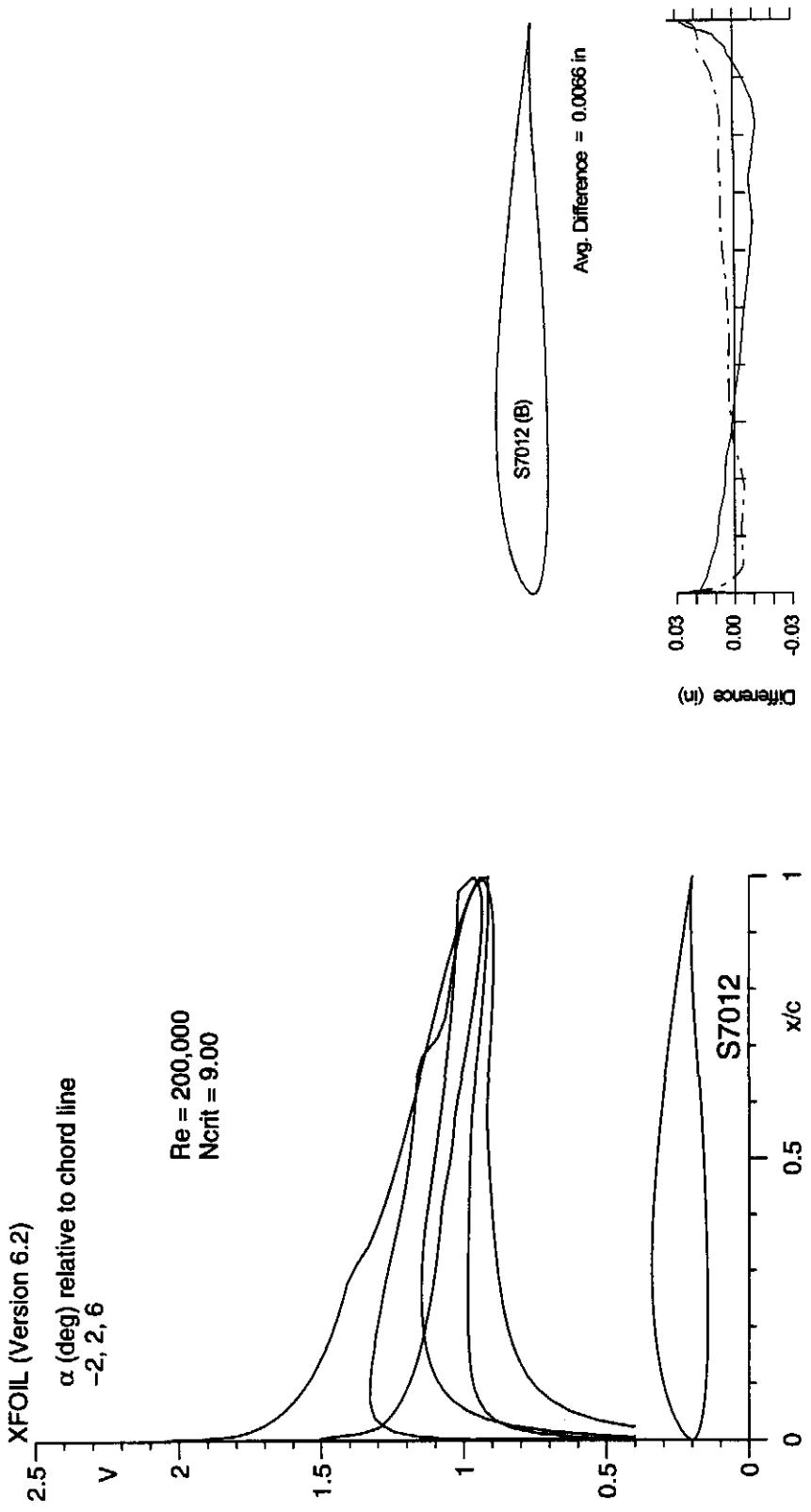
XFOIL (Version 6.2)
α (deg) relative to chord line
-2, 2, 6
Re = 200,000
Ncrit = 9.00
V
2.5
2
1.5
1
0.5
0
S7012
x/c
0
0.5
1
S7012 (B)
Avg. Difference = 0.0066 in
0.03
0.00
-0.03
Difference (in)

S7012 (B)

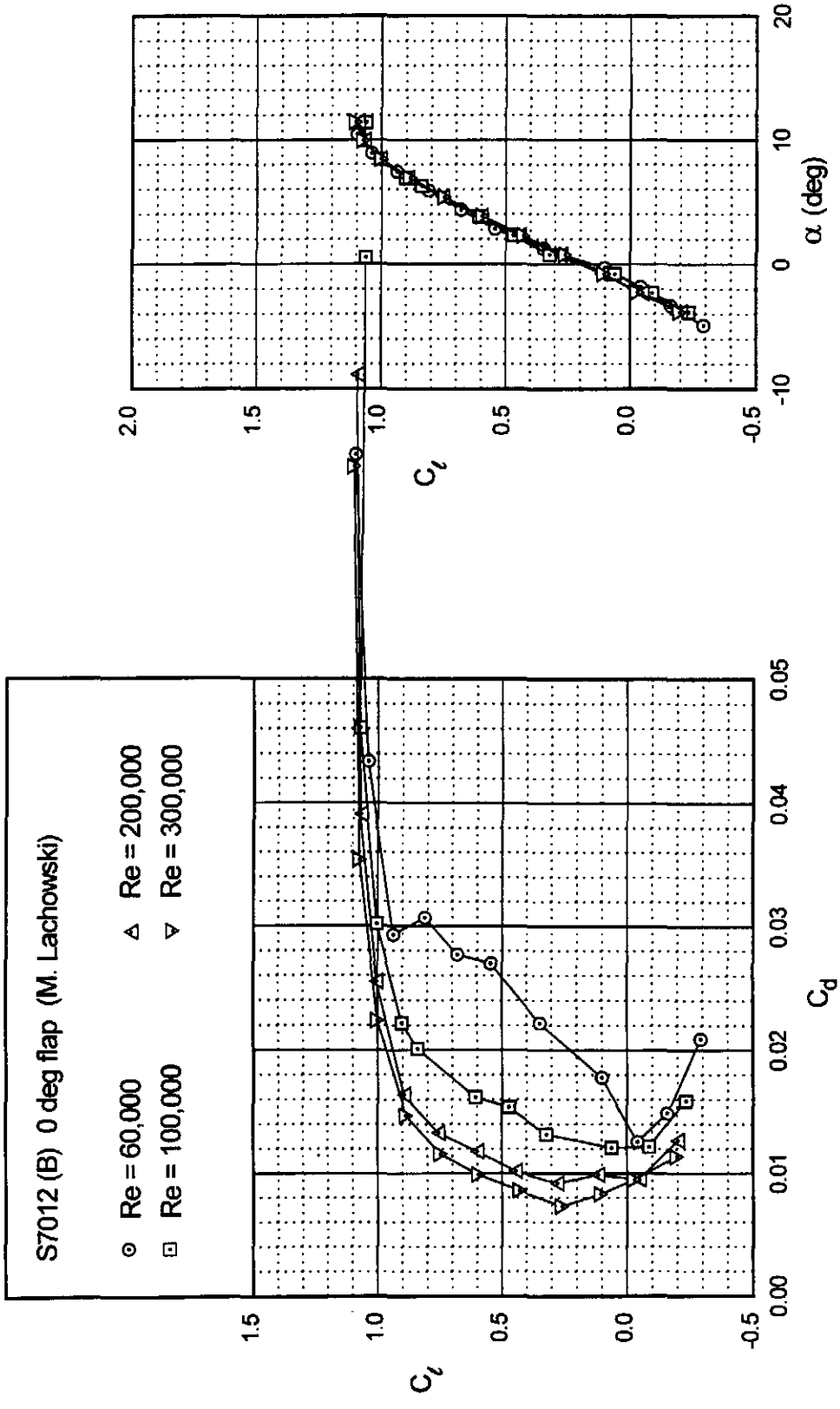
S7012 (B) 0 deg flap (M. Lachowski)
Re = 60,000
Re = 100,000
Re = 200,000
Re = 300,000
C_l
C_d
α (deg)

Fig. 5.97

S7012 (B)

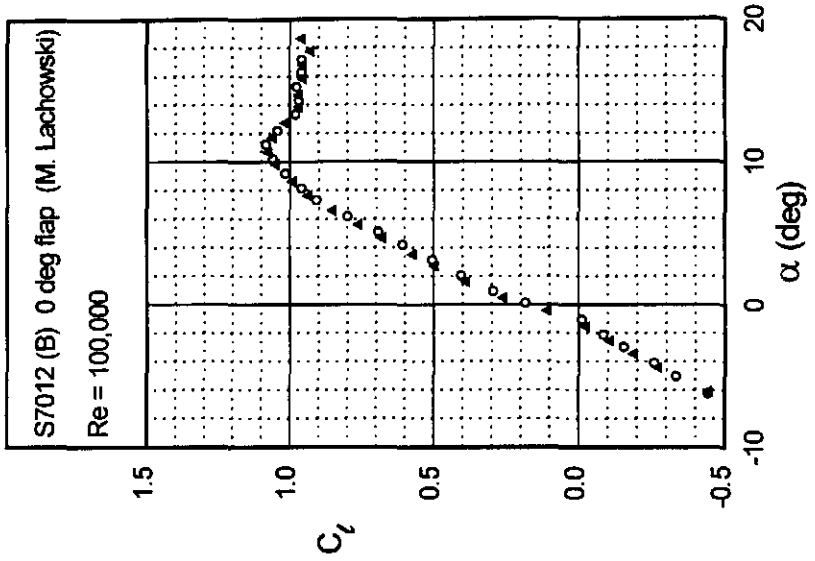

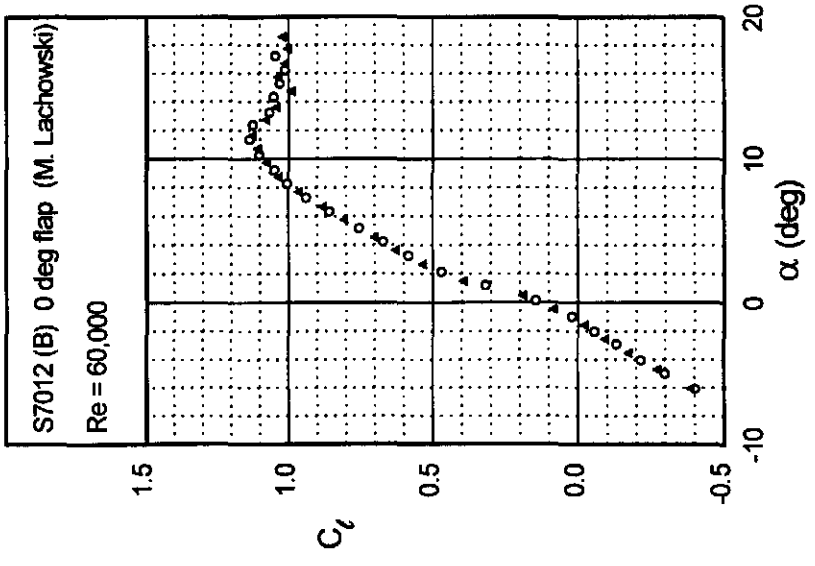

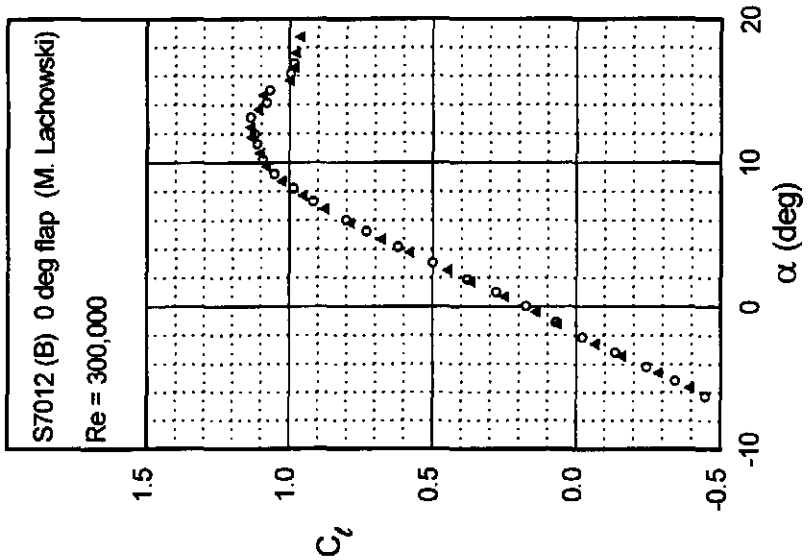
S7012 (B) 0 deg flap (M. Lachowski)
Re = 300,000
1.5
1.0
0.5
0.0
-0.5
C_l
-10
0
10
20
α (deg)

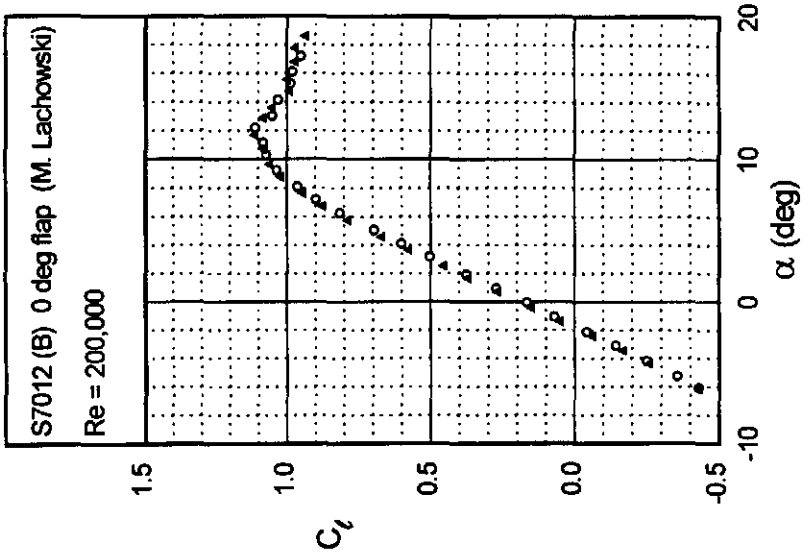
S7012 (B) 0 deg flap (M. Lachowski)
Re = 200,000
1.5
1.0
0.5
0.0
-0.5
C_l
-10
0
10
20
α (deg)

S7012 (B)

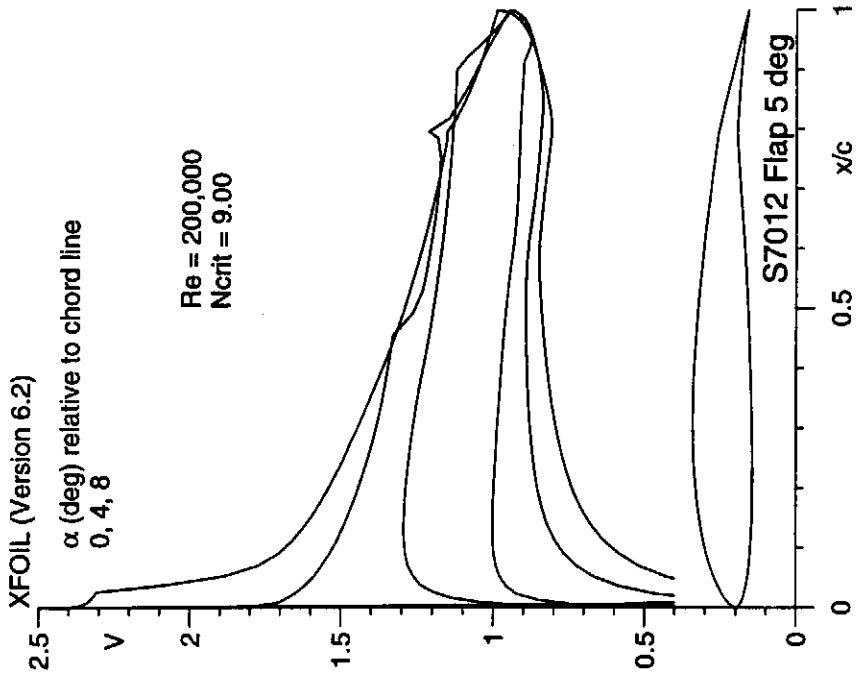
XFOIL (Version 6.2)
α (deg) relative to chord line
0, 4, 8
Re = 200,000
Ncrit = 9.00
S7012 Flap 5 deg
V
x/c
2.5
2
1.5
1
0.5
0
0.5
1

S7012 (B)

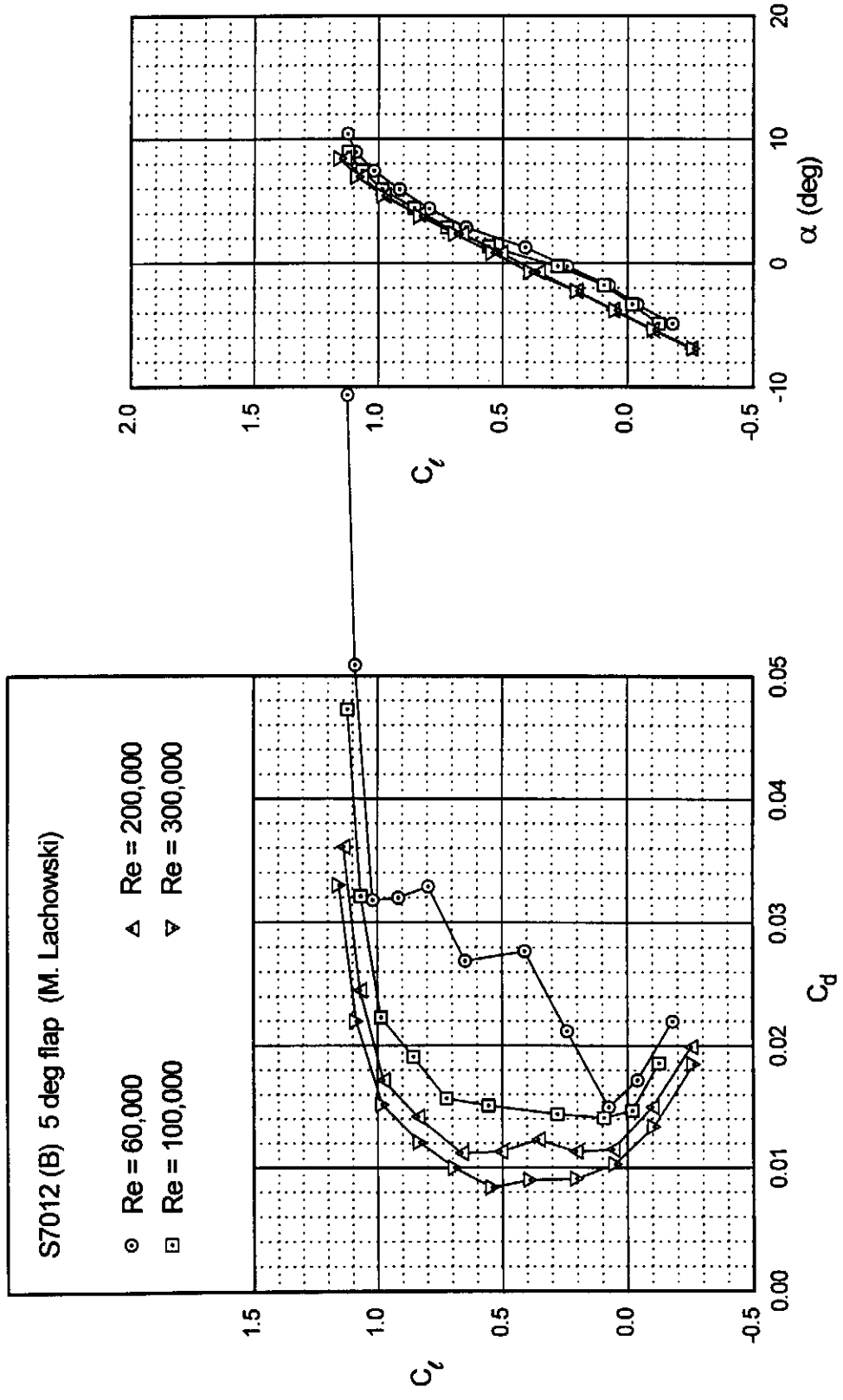
S7012 (B) 5 deg flap (M. Lachowski)
Re = 60,000
Re = 100,000
Re = 200,000
Re = 300,000
C_l
C_d
α (deg)
2.0
1.5
1.0
0.5
0.0
-0.5
0.00
0.01
0.02
0.03
0.04
0.05
-10
0
10
20

S7012 (B)

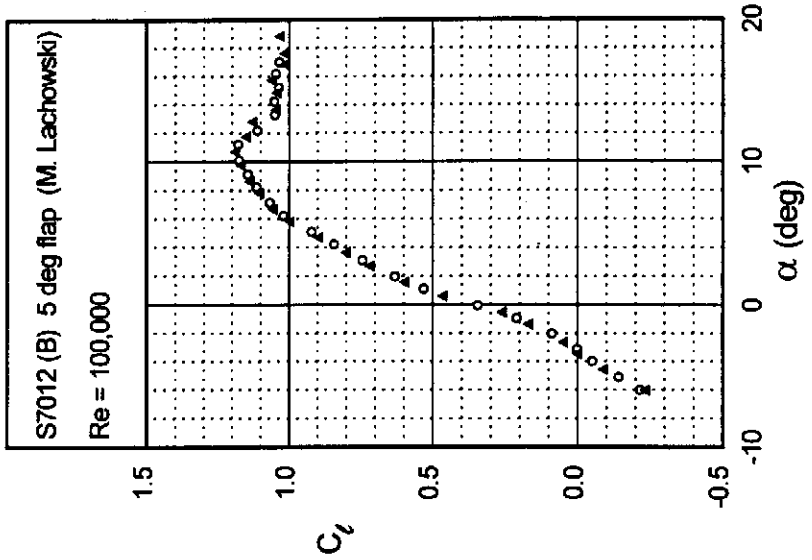
S7012 (B) 5 deg flap (M. Lachowski)
Re = 100,000
1.5
1.0
0.5
0.0
-0.5
C_l
-10
0
10
20
α (deg)

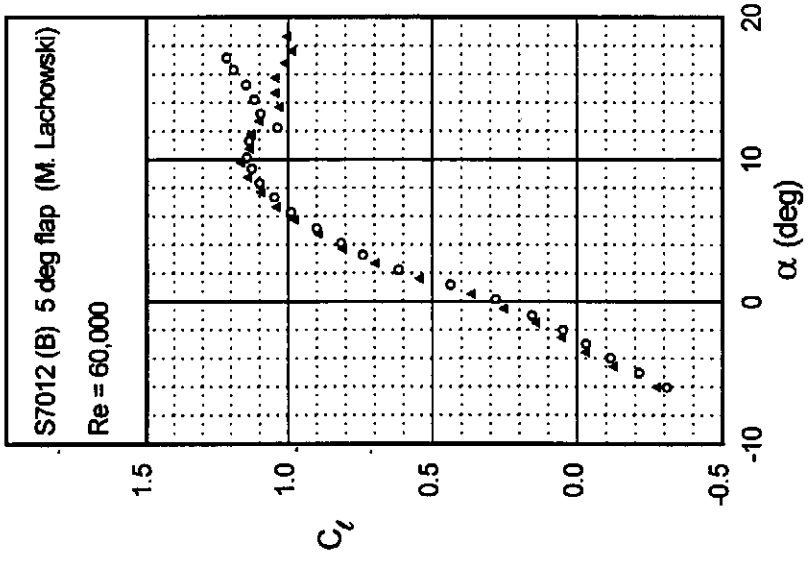
S7012 (B) 5 deg flap (M. Lachowski)
Re = 60,000
1.5
1.0
0.5
0.0
-0.5
C_l
-10
0
10
20
α (deg)

S7012 (B)

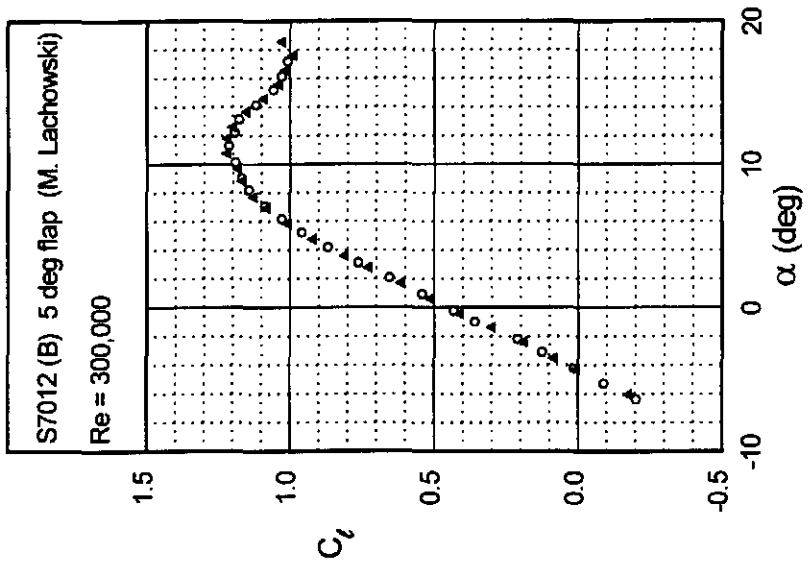
S7012 (B) 5 deg flap (M. Lachowski)
Re = 300,000
1.5
1.0
0.5
0.0
-0.5
C_l
-10
0
10
20
α (deg)

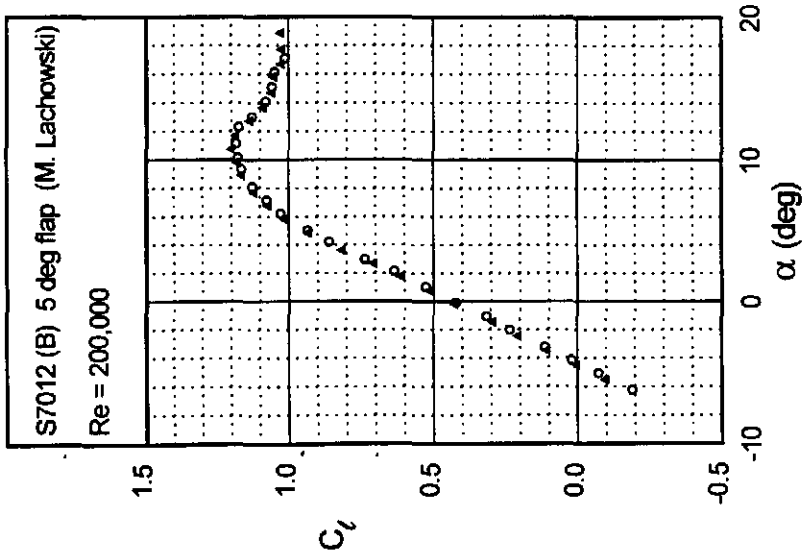
S7012 (B) 5 deg flap (M. Lachowski)
Re = 200,000
1.5
1.0
0.5
0.0
-0.5
C_l
-10
0
10
20
α (deg)

S7012 (B)

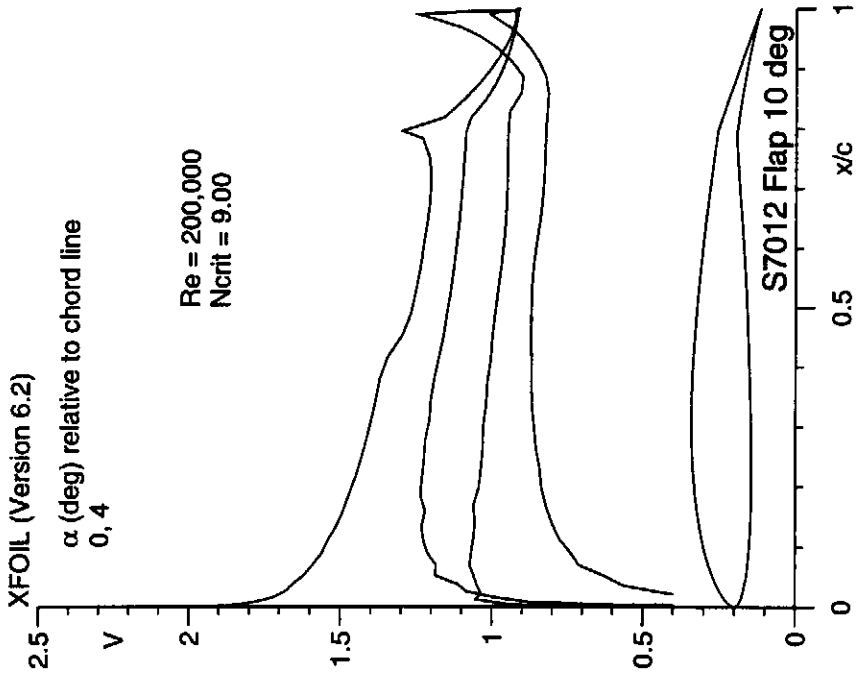
XFOIL (Version 6.2)
α (deg) relative to chord line
0, 4
Re = 200,000
Ncrit = 9.00
V
2.5
2
1.5
1
0.5
0
0
0.5
1
x/c
S7012 Flap 10 deg

S7012 (B)

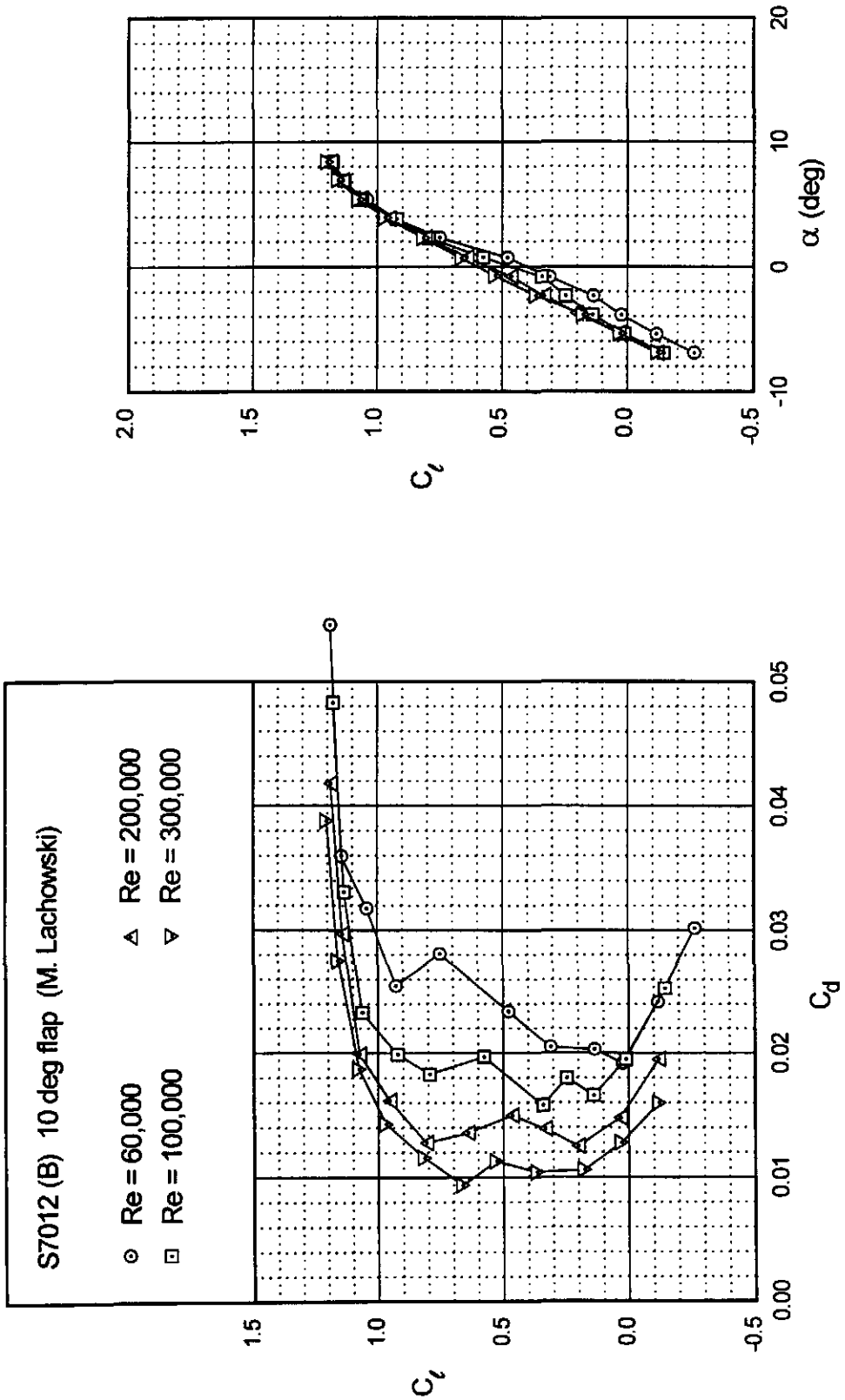
S7012 (B) 10 deg flap (M. Lachowski)
Re = 60,000
Re = 100,000
Re = 200,000
Re = 300,000
C_l
C_d
α (deg)
2.0
1.5
1.0
0.5
0.0
-0.5
20
10
0
-10
0.05
0.04
0.03
0.02
0.01
0.00

Fig. 5.103

S7012 (B)

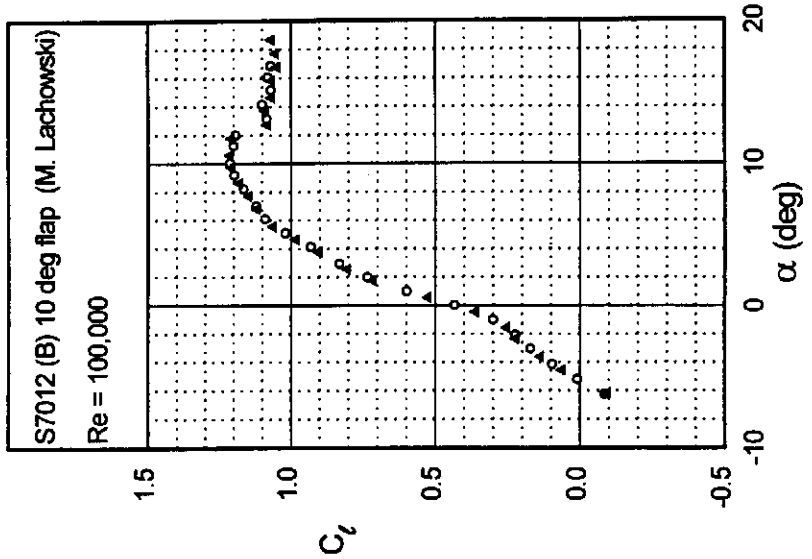

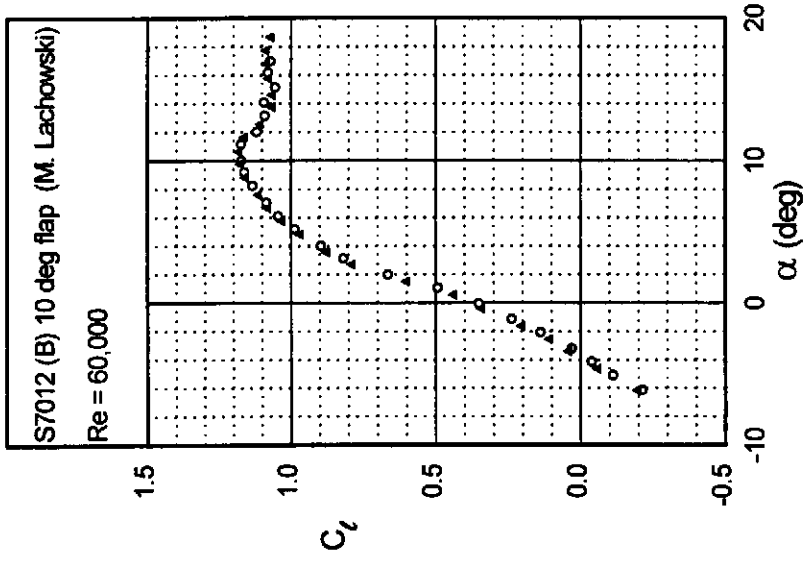

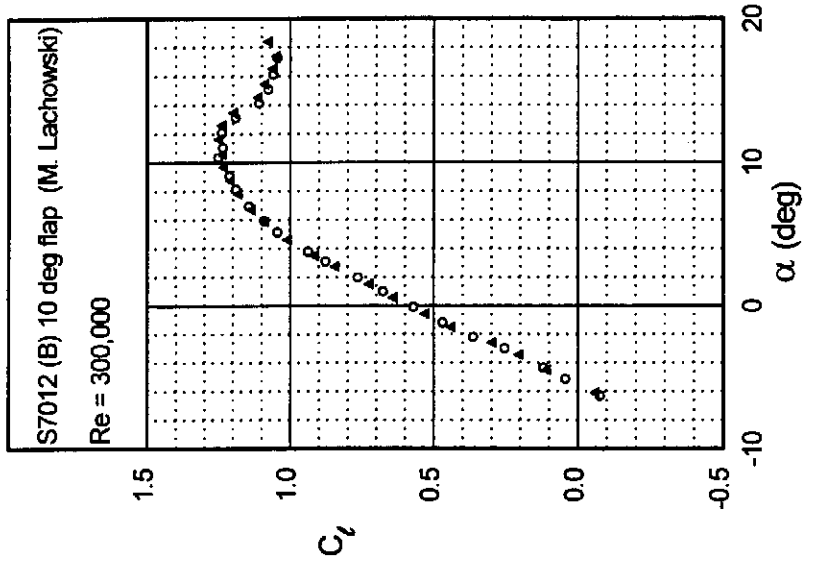
S7012 (B) 10 deg flap (M. Lachowski)
Re = 300,000
1.5
1.0
0.5
0.0
-0.5
C_l
-10
0
10
20
α (deg)

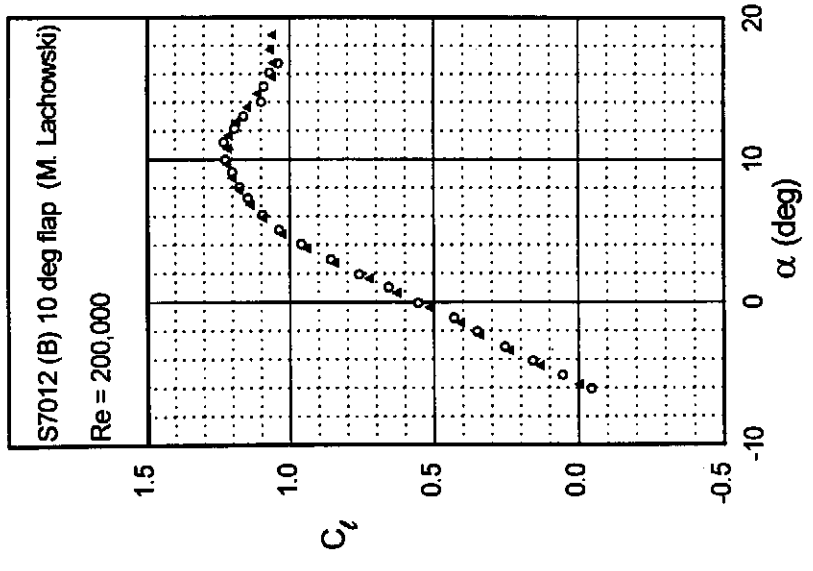
S7012 (B) 10 deg flap (M. Lachowski)
Re = 200,000
1.5
1.0
0.5
0.0
-0.5
C_l
-10
0
10
20
α (deg)

S7055

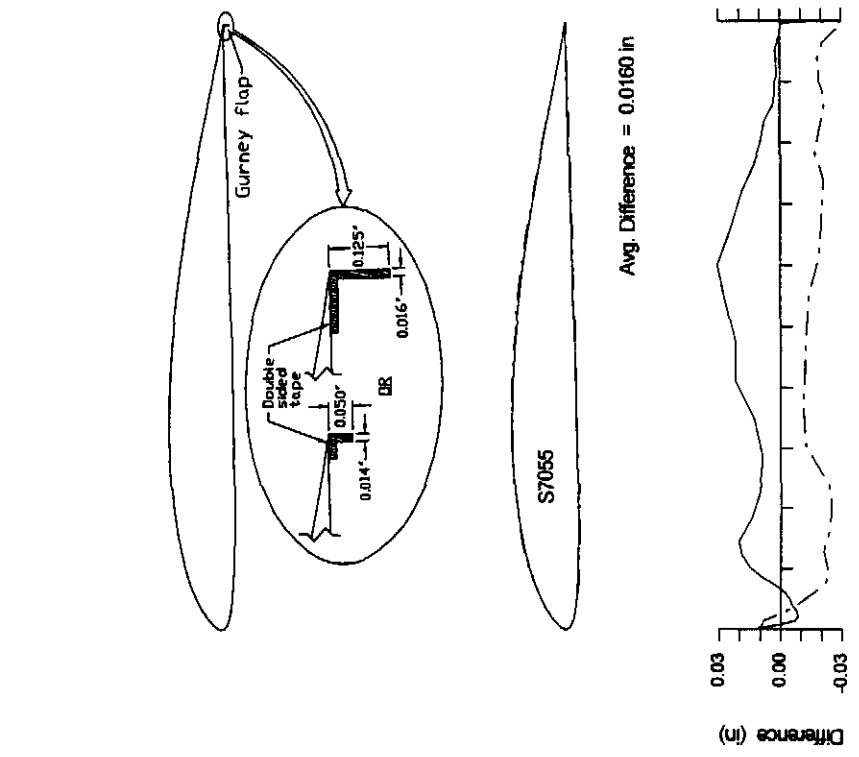
Gurney flap
Double sided tape
0.125"
0.016"
0.050"
0.014"
OR
S7055
Avg. Difference = 0.0160 in
0.03
0.00
-0.03
Difference (in)

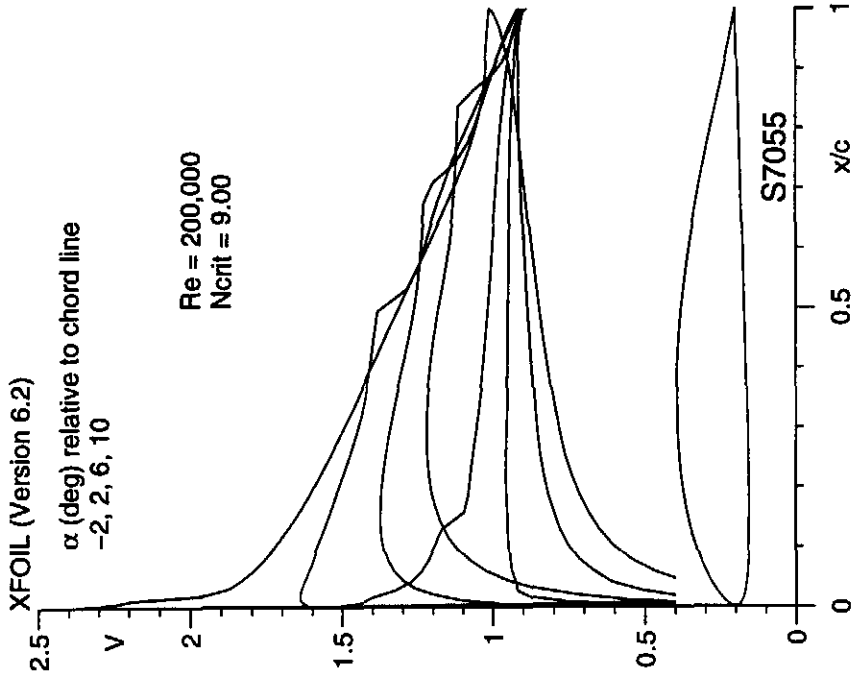
XFOIL (Version 6.2)
α (deg) relative to chord line
-2, 2, 6, 10
Re = 200,000
Ncrit = 9.00
V
2.5
2
1.5
1
0.5
0
S7055
0
0.5
1
x/c

S7055

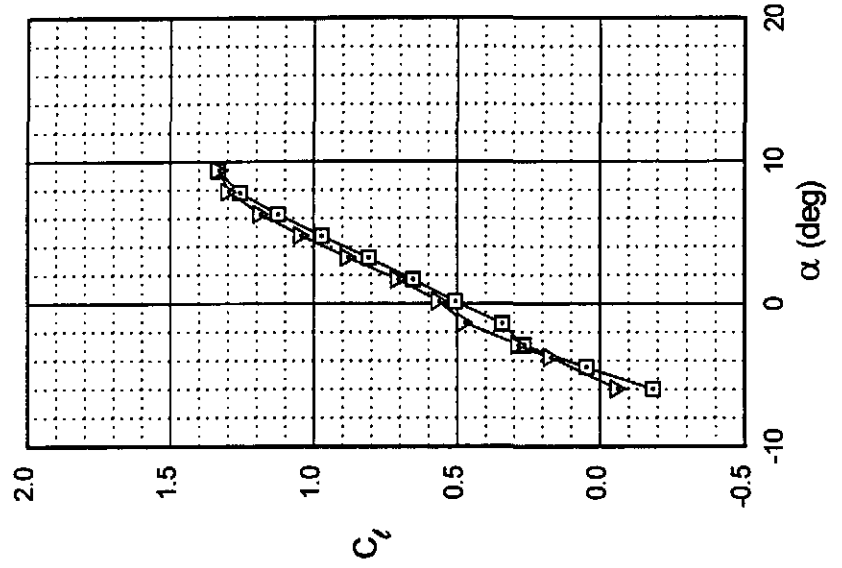
2.0
1.5
1.0
0.5
0.0
-0.5
C_l
20
10
0
-10
α (deg)

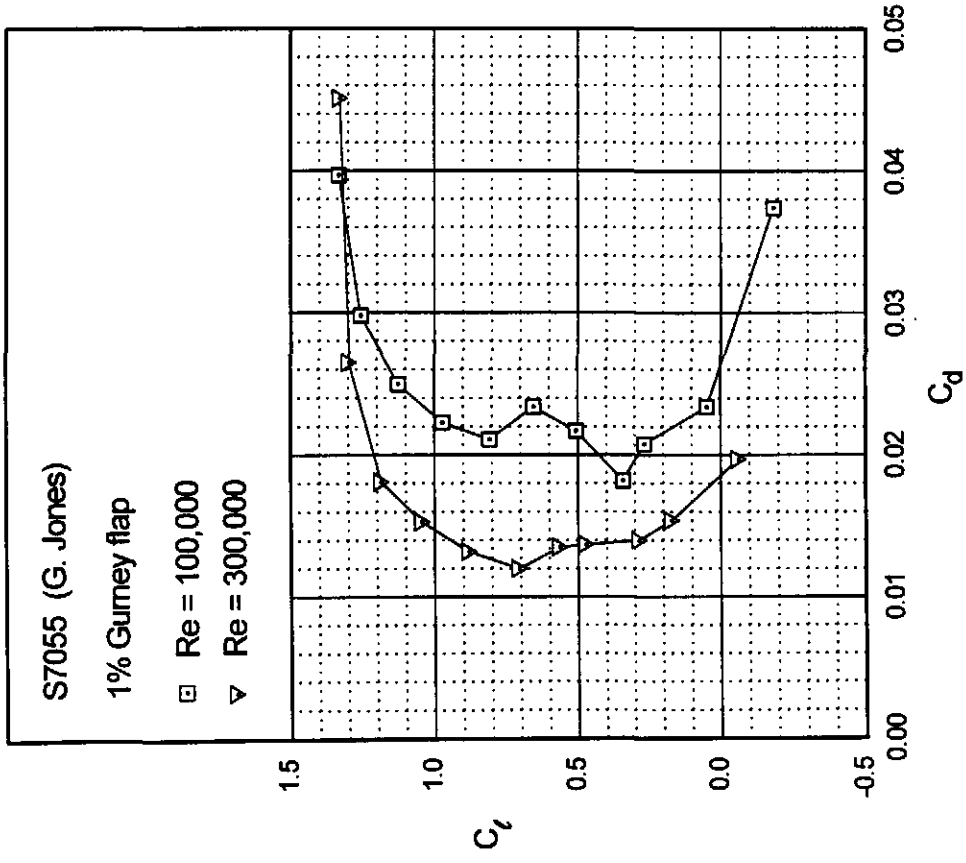
S7055 (G. Jones)
1% Gurney flap
Re = 100,000
Re = 300,000
1.5
1.0
0.5
0.0
-0.5
C_l
0.05
0.04
0.03
0.02
0.01
0.00
C_d

Fig. 5.107

S7055

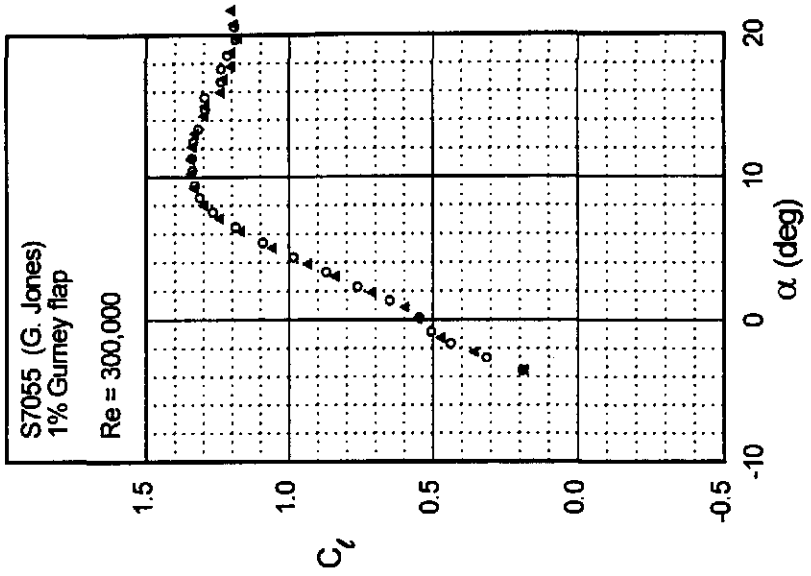

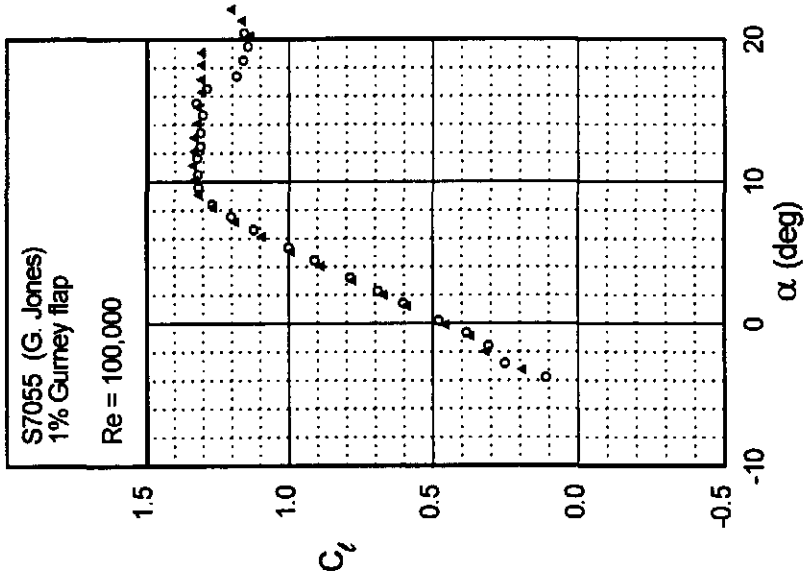

S7055

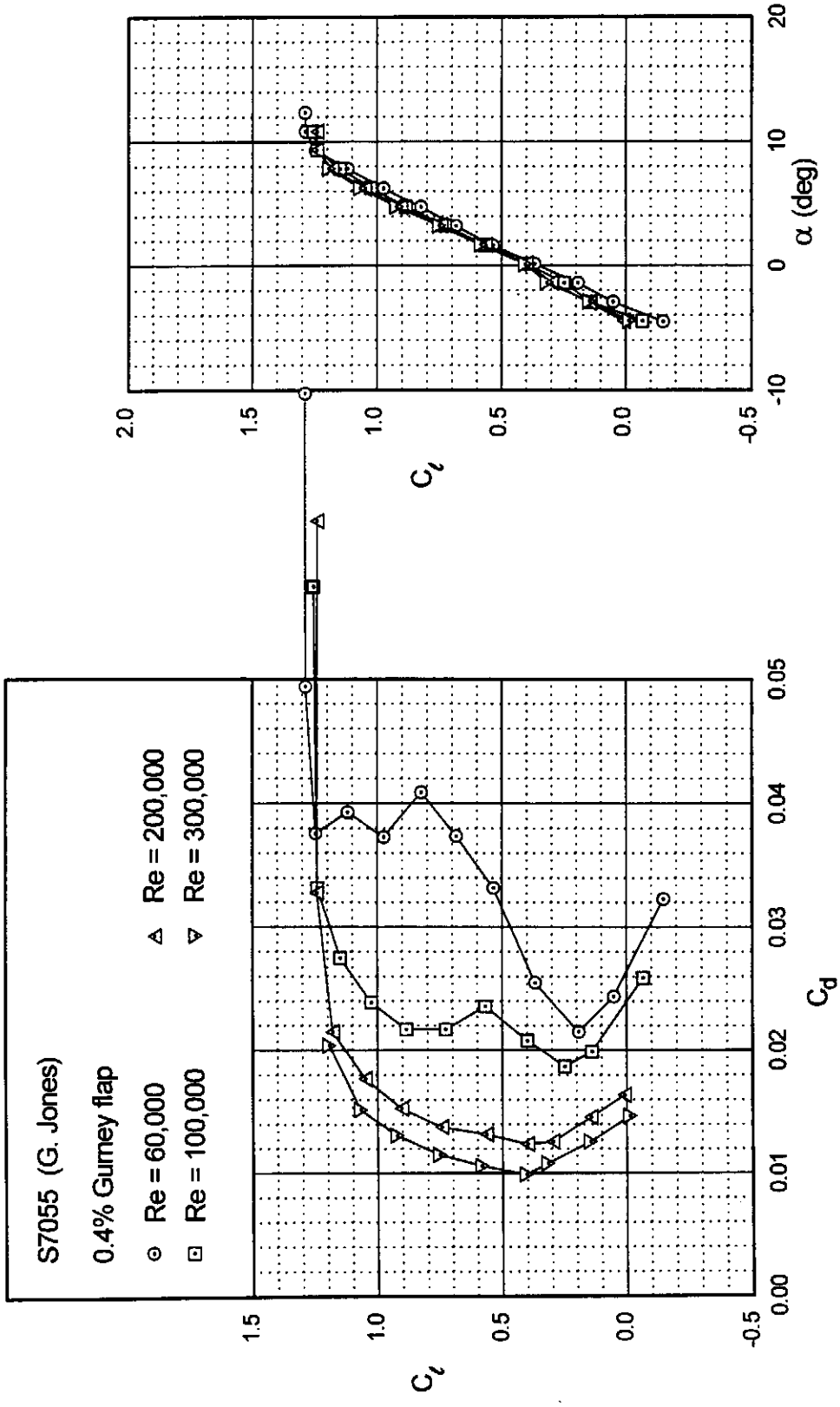
S7055 (G. Jones)
0.4% Gurney flap
Re = 60,000
Re = 100,000
Re = 200,000
Re = 300,000
C_l
C_d
α (deg)
2.0
1.5
1.0
0.5
0.0
-0.5
-10
0
10
20
0.00
0.01
0.02
0.03
0.04
0.05

Fig. 5.109

S7055

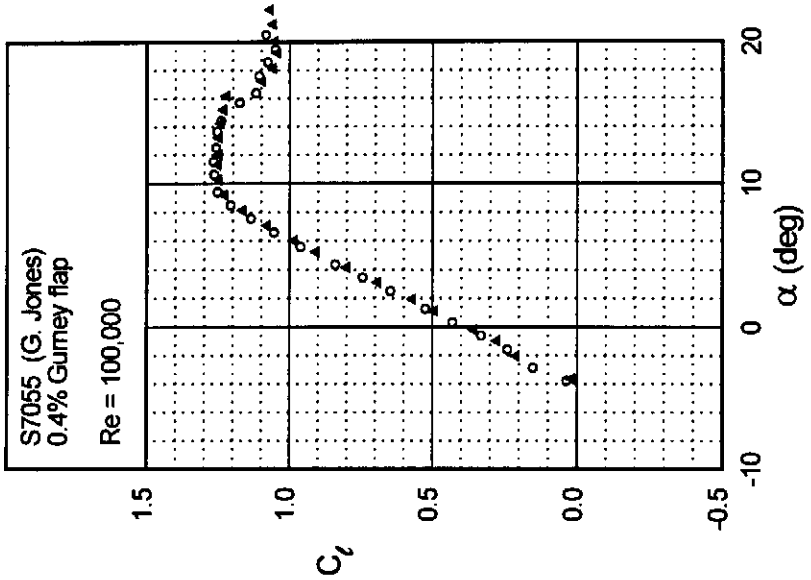

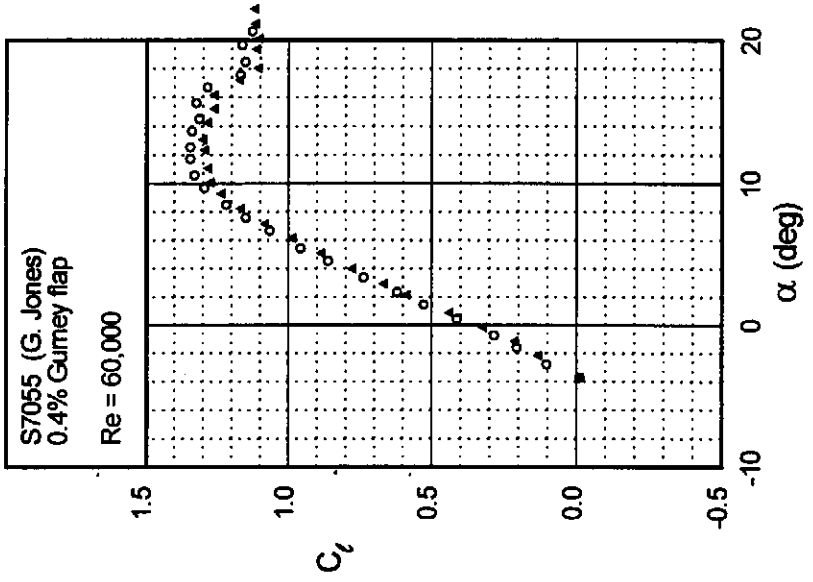

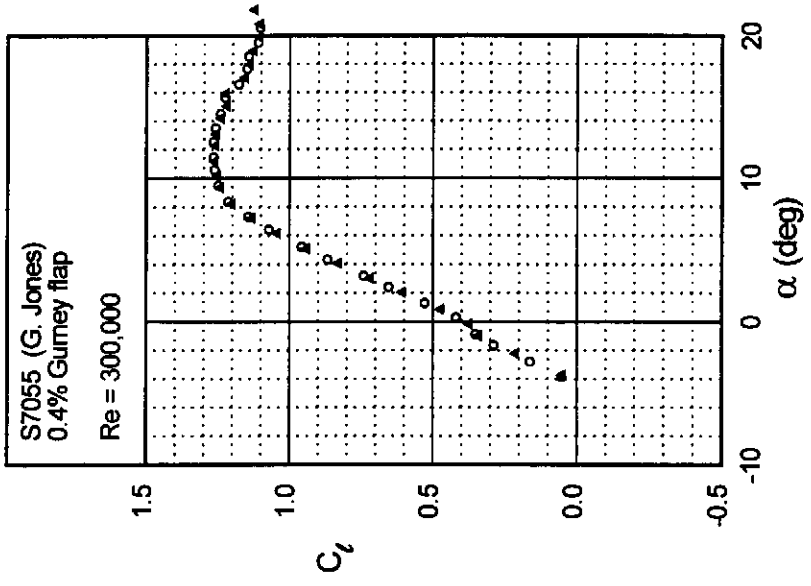
S7055 (G. Jones)
0.4% Gurney flap
Re = 300,000
1.5
1.0
0.5
0.0
-0.5
C_l
-10
0
10
20
α (deg)

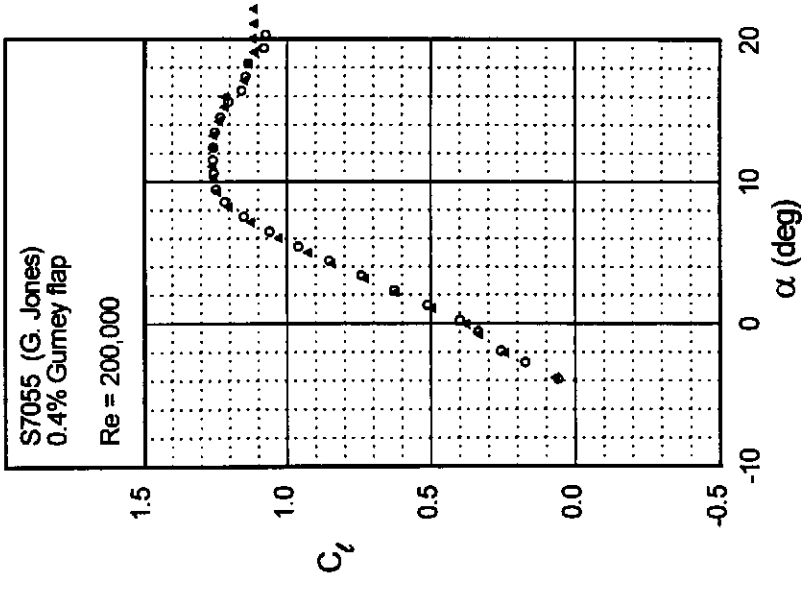
S7055 (G. Jones)
0.4% Gurney flap
Re = 200,000
1.5
1.0
0.5
0.0
-0.5
C_l
-10
0
10
20
α (deg)

S7075 (A)

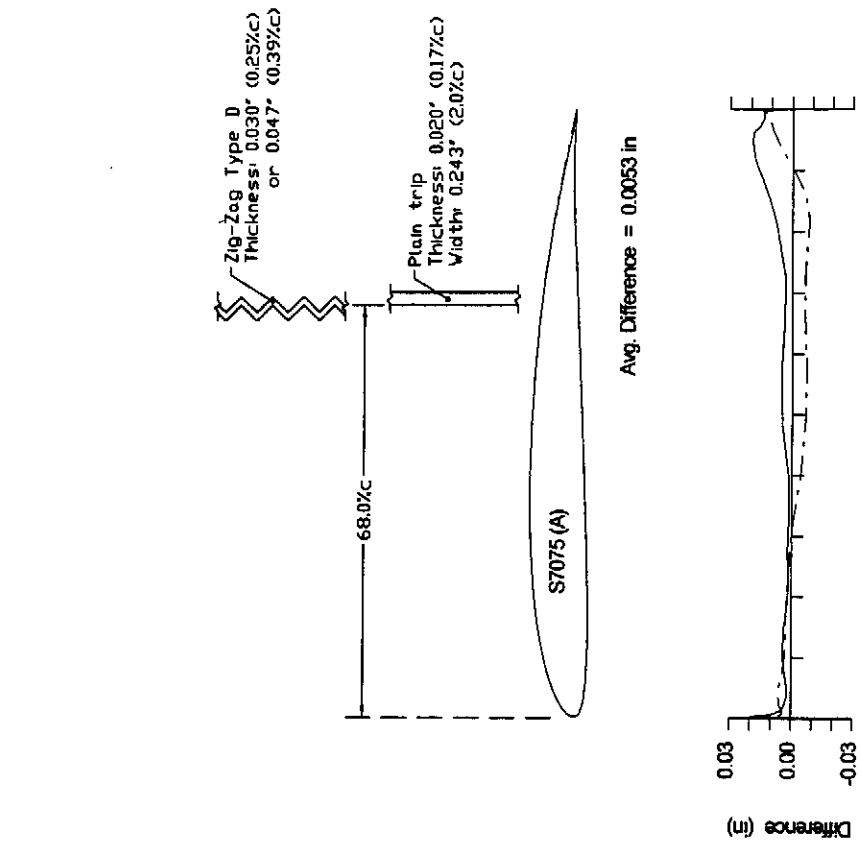
Zig-Zag Type D
Thickness: 0.030" (0.25%c)
or 0.047" (0.39%c)
Plain trip
Thickness: 0.020" (0.17%c)
Width: 0.243" (2.0%c)
68.0%c
S7075 (A)
Avg. Difference = 0.0053 in
0.03
0.00
-0.03
Difference (in)

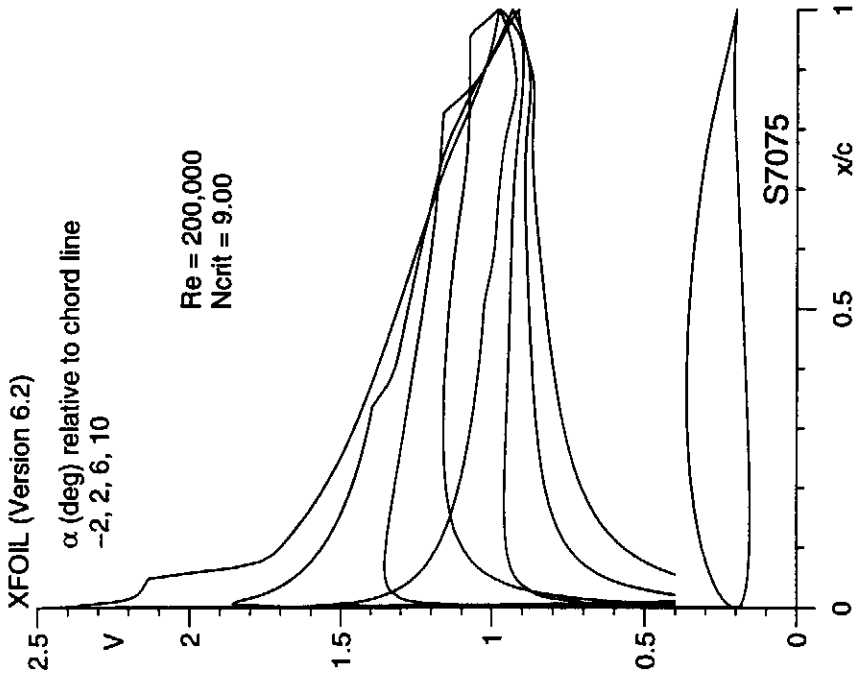
XFOIL (Version 6.2)
α (deg) relative to chord line
-2, 2, 6, 10
Re = 200,000
Ncrit = 9.00
2.5
2
1.5
1
0.5
0
V
S7075
0
0.5
1
x/c

S7075 (A)

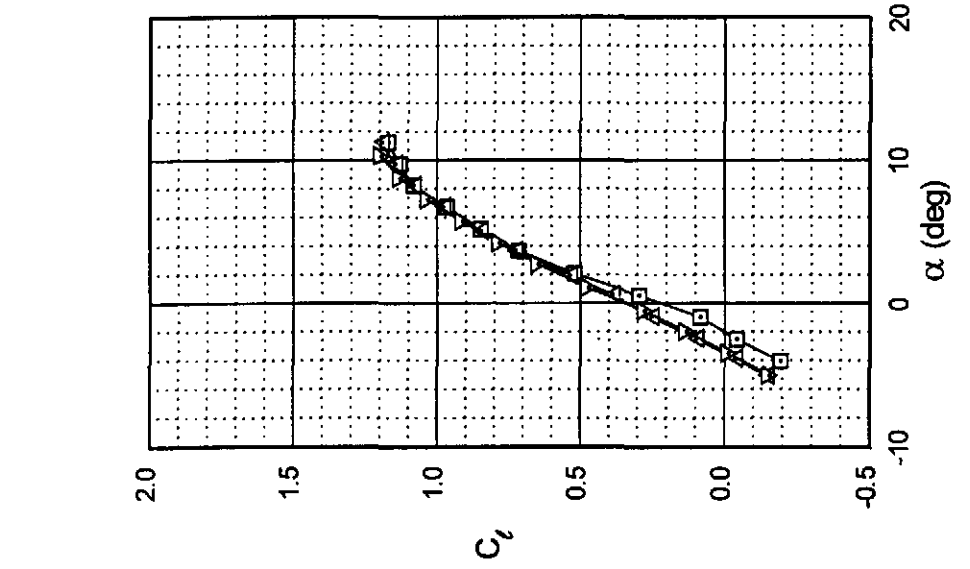
2.0
1.5
1.0
0.5
0.0
-0.5
C_l
20
10
0
-10
α (deg)

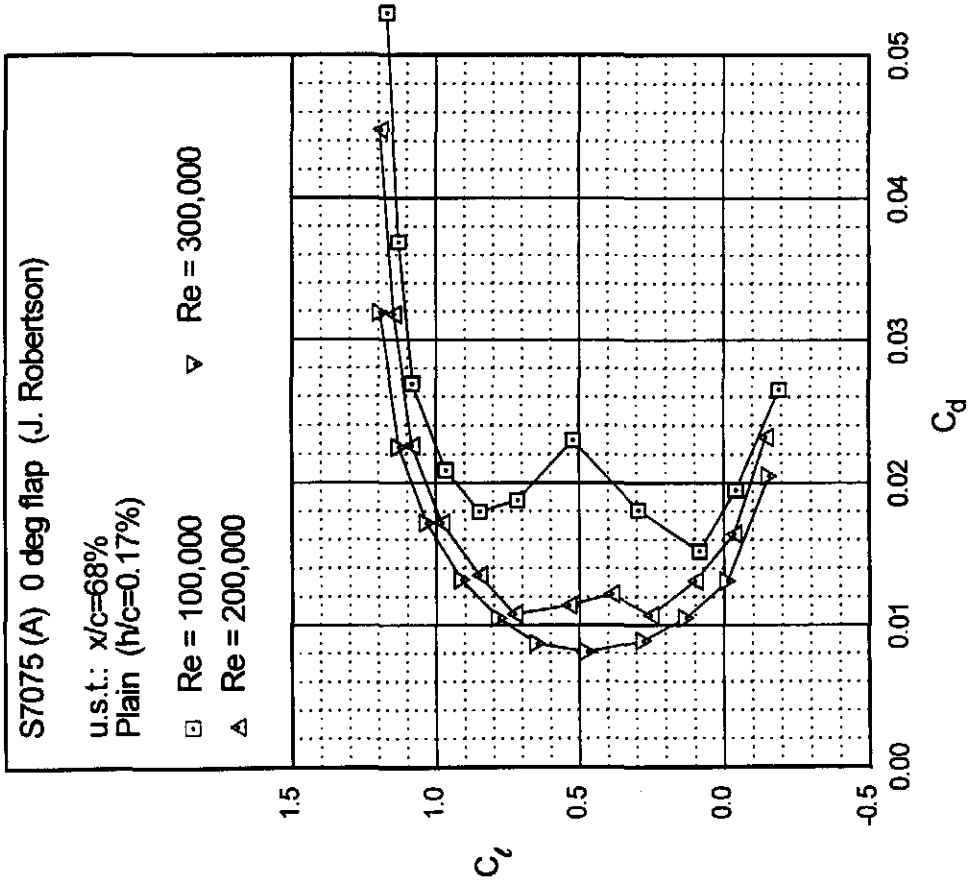
S7075 (A) 0 deg flap (J. Robertson)
u.s.t.: x/c=68%
Plain (h/c=0.17%)
Re = 100,000
Re = 200,000
Re = 300,000
1.5
1.0
0.5
0.0
-0.5
C_l
0.05
0.04
0.03
0.02
0.01
0.00
C_d

Fig. 5.113

S7075 (A)

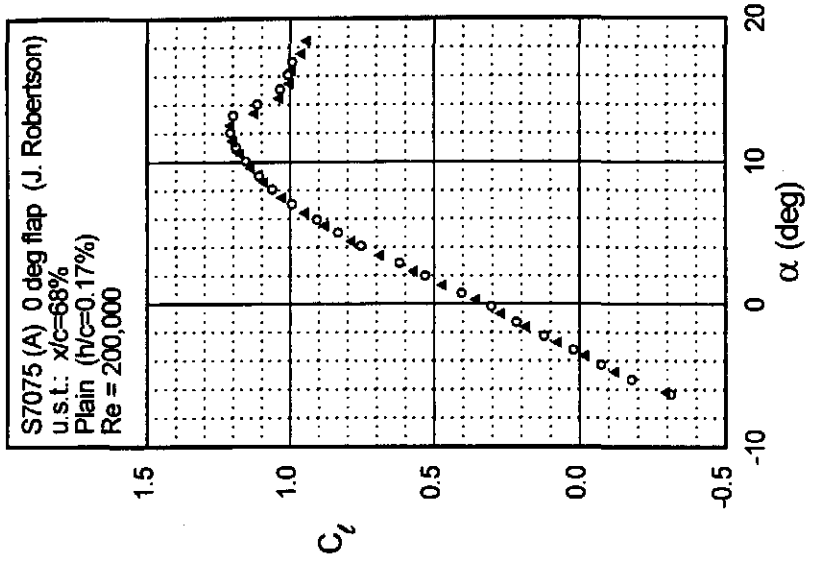

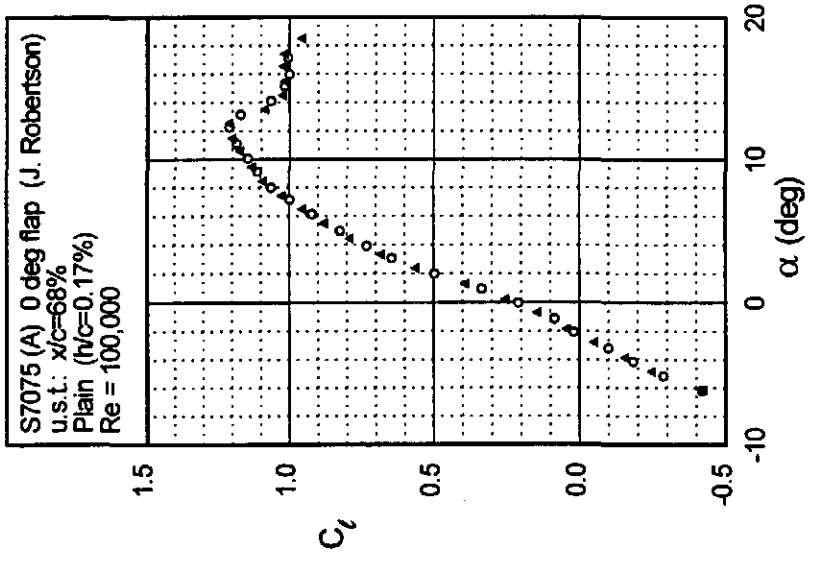

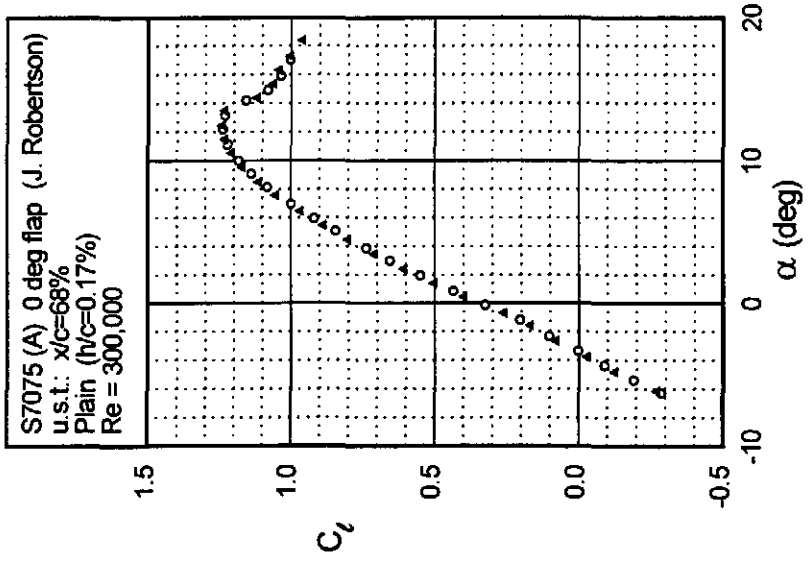
S7075 (A) 0 deg flap (J. Robertson)
u.s.t.: x/c=68%
Plain (h/c=0.17%)
Re = 300,000
1.5
1.0
0.5
0.0
-0.5
C_l
20
10
0
-10
α (deg)

S7075 (A)

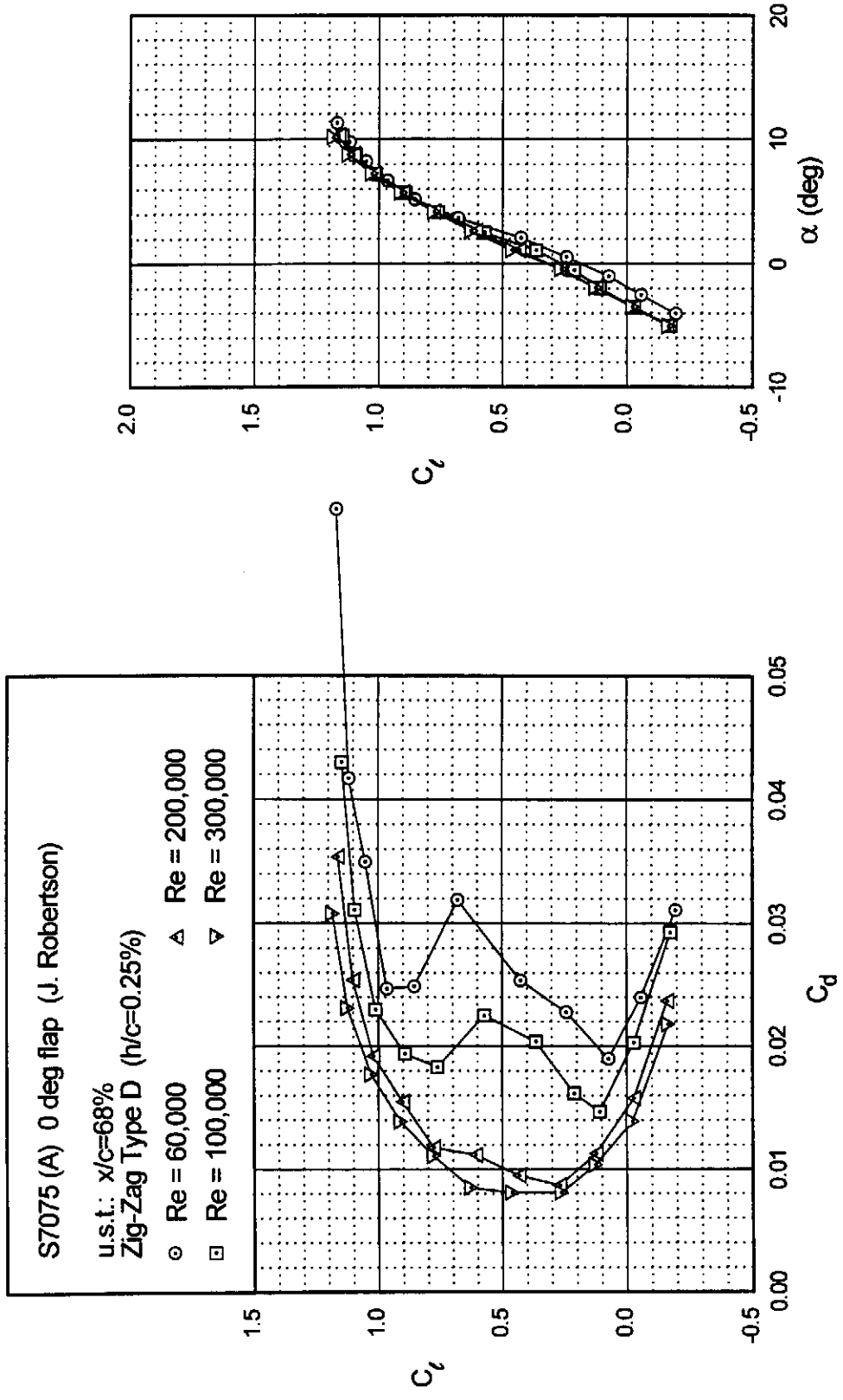
S7075 (A) 0 deg flap (J. Robertson)
u.s.t.: x/c=68%
Zig-Zag Type D (h/c=0.25%)
Re = 60,000
Re = 100,000
Re = 200,000
Re = 300,000
C_l
C_d
α (deg)
2.0
1.5
1.0
0.5
0.0
-0.5
20
10
0
-10
0.05
0.04
0.03
0.02
0.01
0.00

Fig. 5.115

S7075 (A)

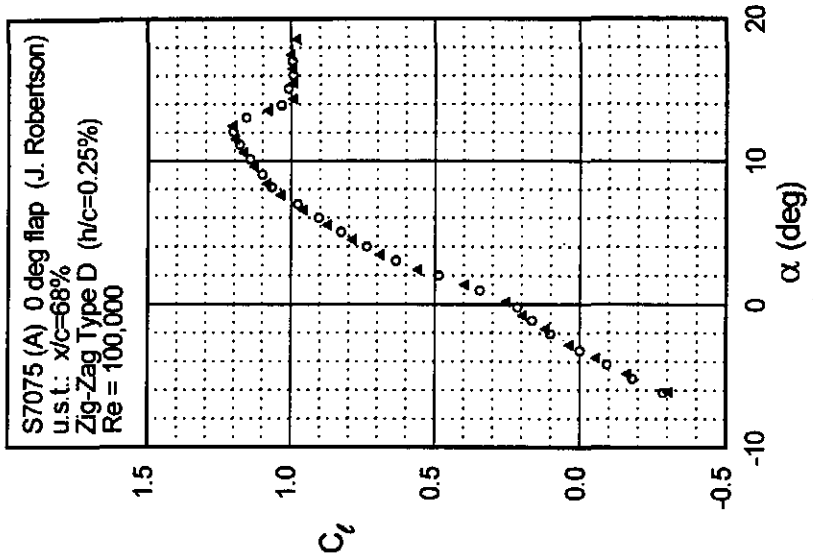

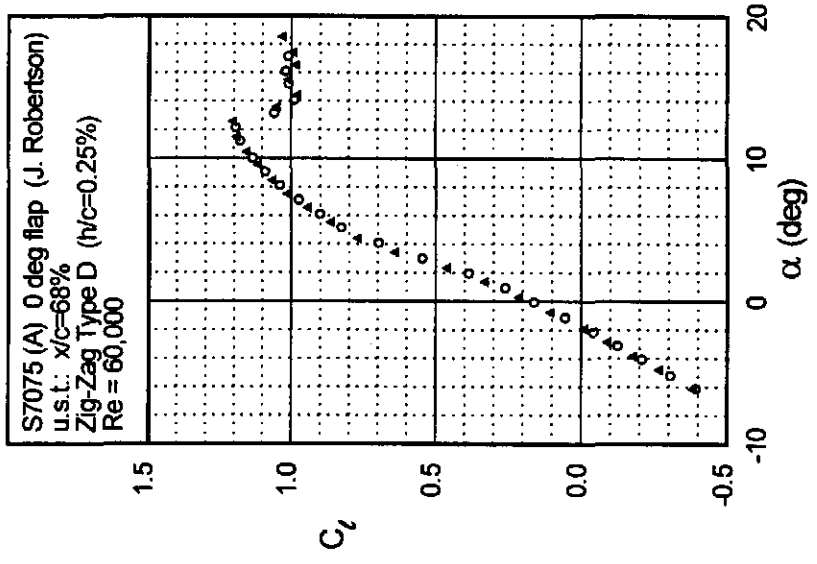

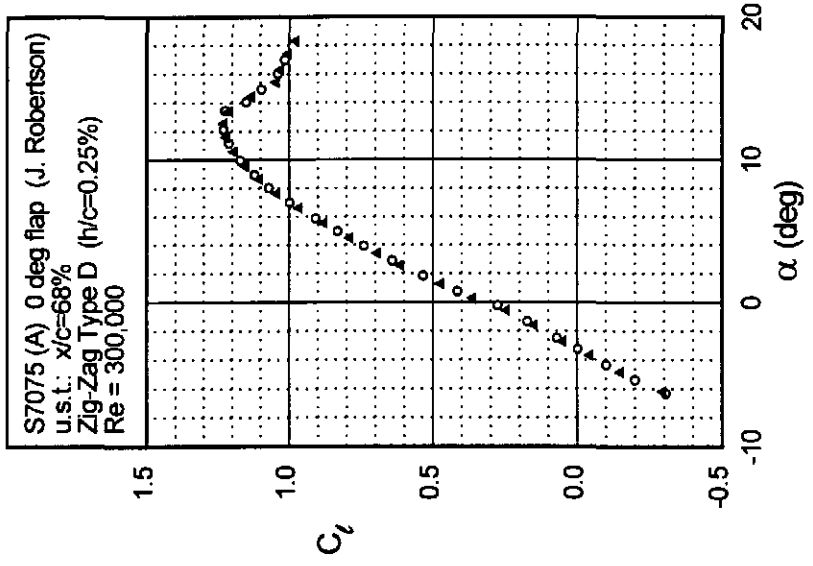
S7075 (A) 0 deg flap (J. Robertson)
u.s.t.: x/c=68%
Zig-Zag Type D (h/c=0.25%)
Re = 300,000
1.5
1.0
0.5
0.0
-0.5
C_l
-10
0
10
20
α (deg)

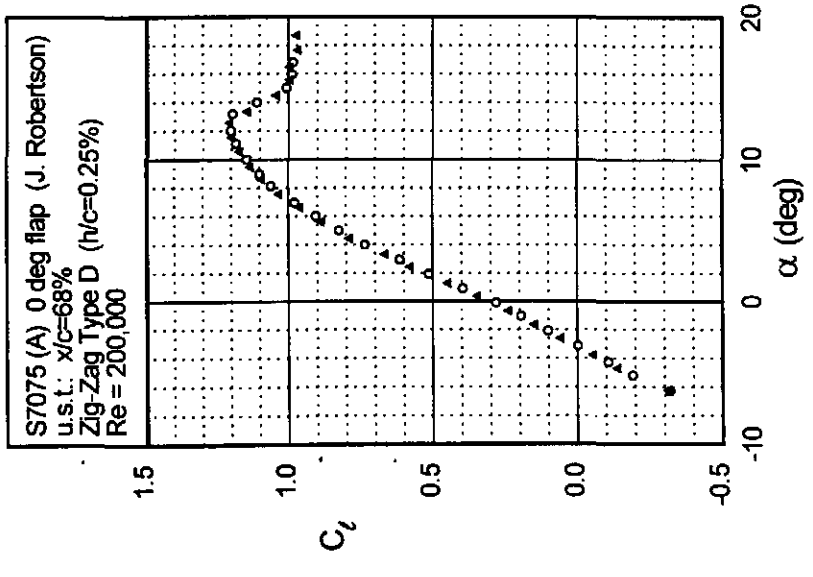
S7075 (A) 0 deg flap (J. Robertson)
u.s.t.: x/c=68%
Zig-Zag Type D (h/c=0.25%)
Re = 200,000
1.5
1.0
0.5
0.0
-0.5
C_l
-10
0
10
20
α (deg)

S7075 (A)

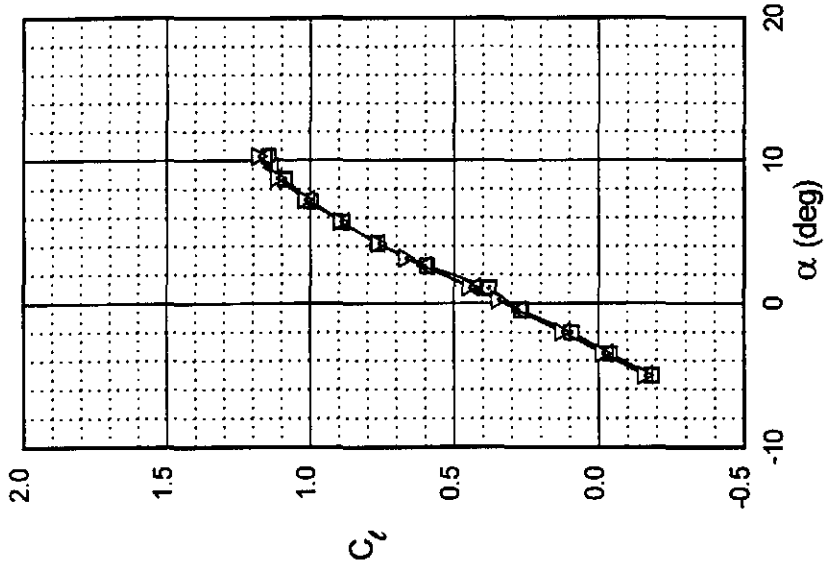
2.0
1.5
1.0
0.5
0.0
-0.5
C_l
20
10
0
-10
α (deg)

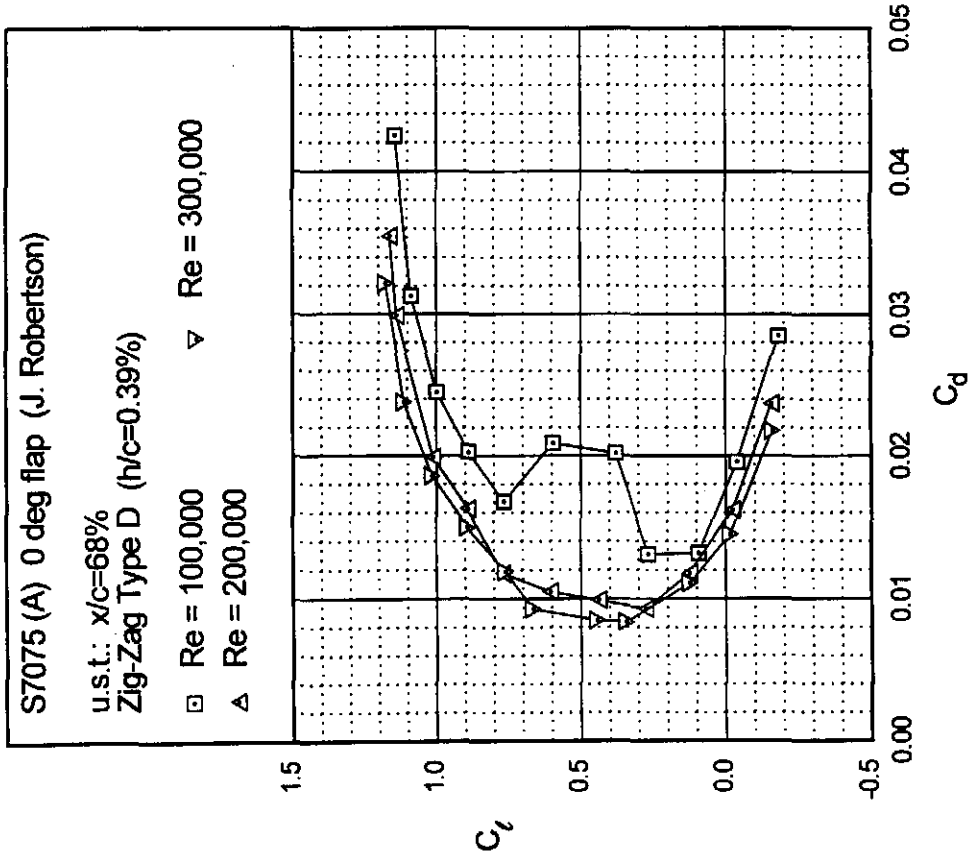
S7075 (A) 0 deg flap (J. Robertson)
u.s.t.: x/c=68%
Zig-Zag Type D (h/c=0.39%)
Re = 100,000
Re = 200,000
Re = 300,000
1.5
1.0
0.5
0.0
-0.5
C_l
0.05
0.04
0.03
0.02
0.01
0.00
C_d

S7075 (A)

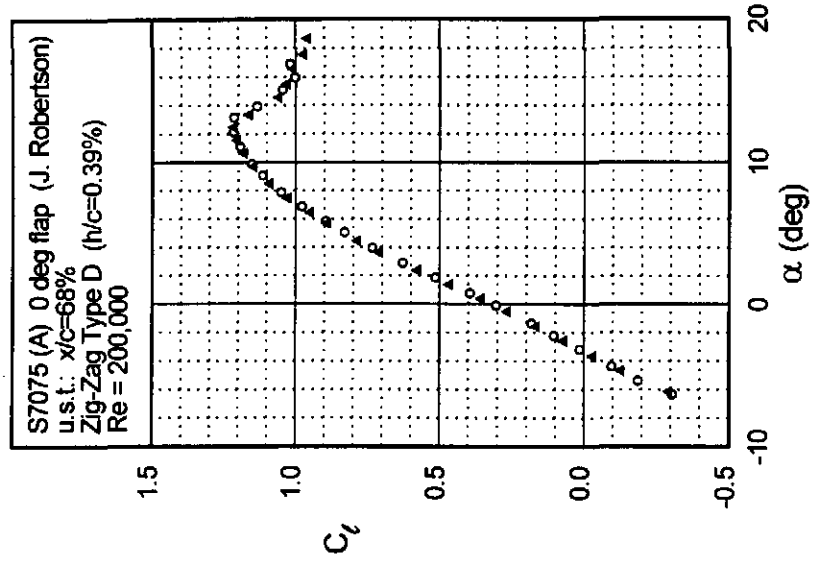
S7075 (A) 0 deg flap (J. Robertson)
u.s.t.: x/c=68%
Zig-Zag Type D (h/c=0.39%)
Re = 200,000
1.5
1.0
0.5
0.0
-0.5
C_ℓ
-10
0
10
20
α (deg)

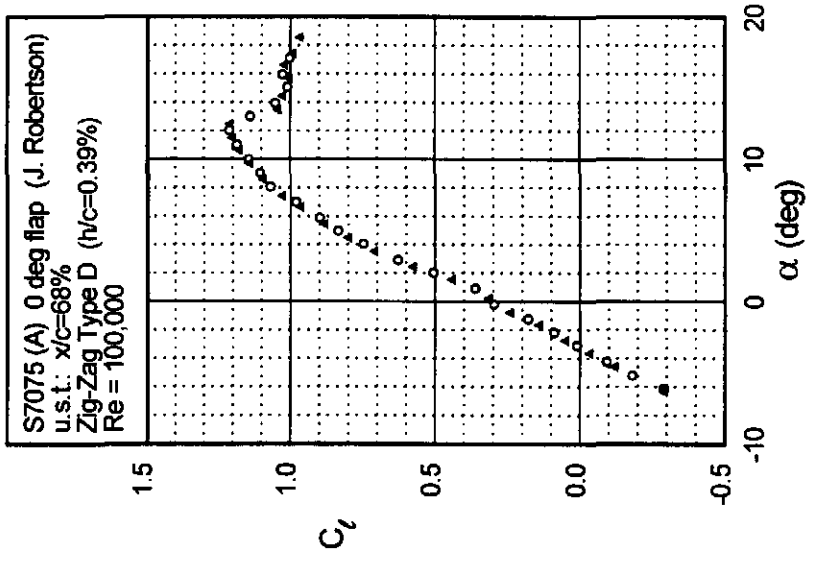
S7075 (A) 0 deg flap (J. Robertson)
u.s.t.: x/c=68%
Zig-Zag Type D (h/c=0.39%)
Re = 100,000
1.5
1.0
0.5
0.0
-0.5
C_ℓ
-10
0
10
20
α (deg)

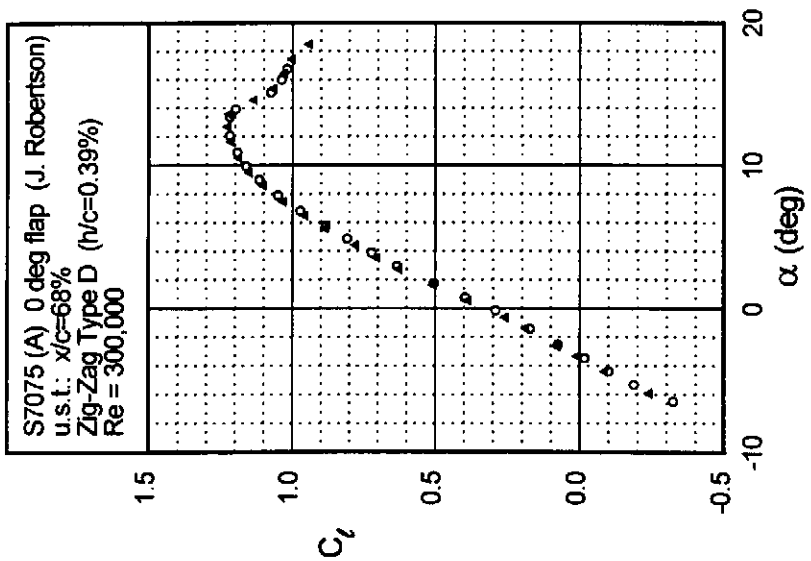
S7075 (A) 0 deg flap (J. Robertson)
u.s.t.: x/c=68%
Zig-Zag Type D (h/c=0.39%)
Re = 300,000
1.5
1.0
0.5
0.0
-0.5
C_ℓ
-10
0
10
20
α (deg)

S7075 (A)

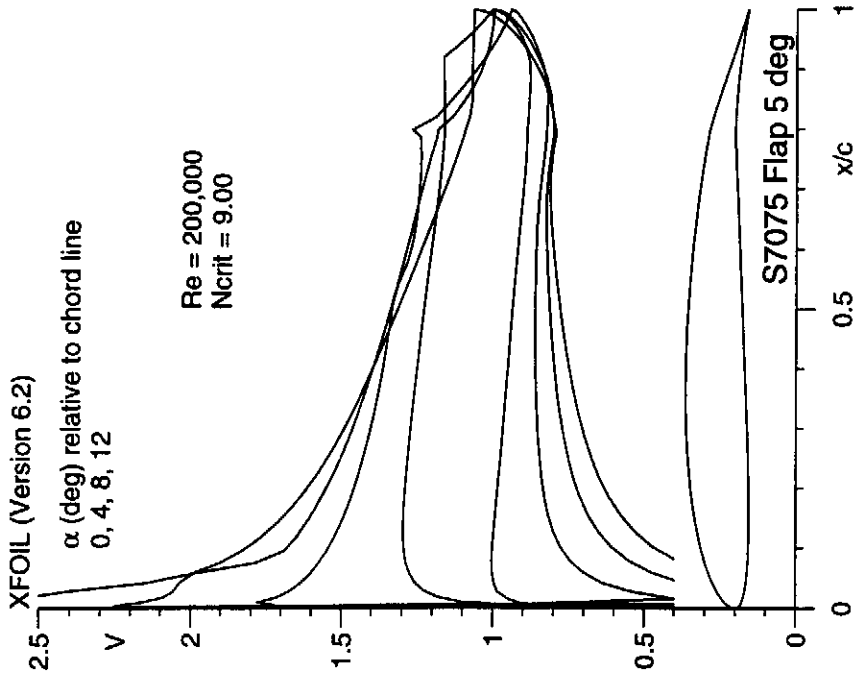
XFOIL (Version 6.2)
α (deg) relative to chord line
0, 4, 8, 12
Re = 200,000
Ncrit = 9.00
S7075 Flap 5 deg
V
x/c
2.5
2
1.5
1
0.5
0
0
0.5
1

S7075 (A)

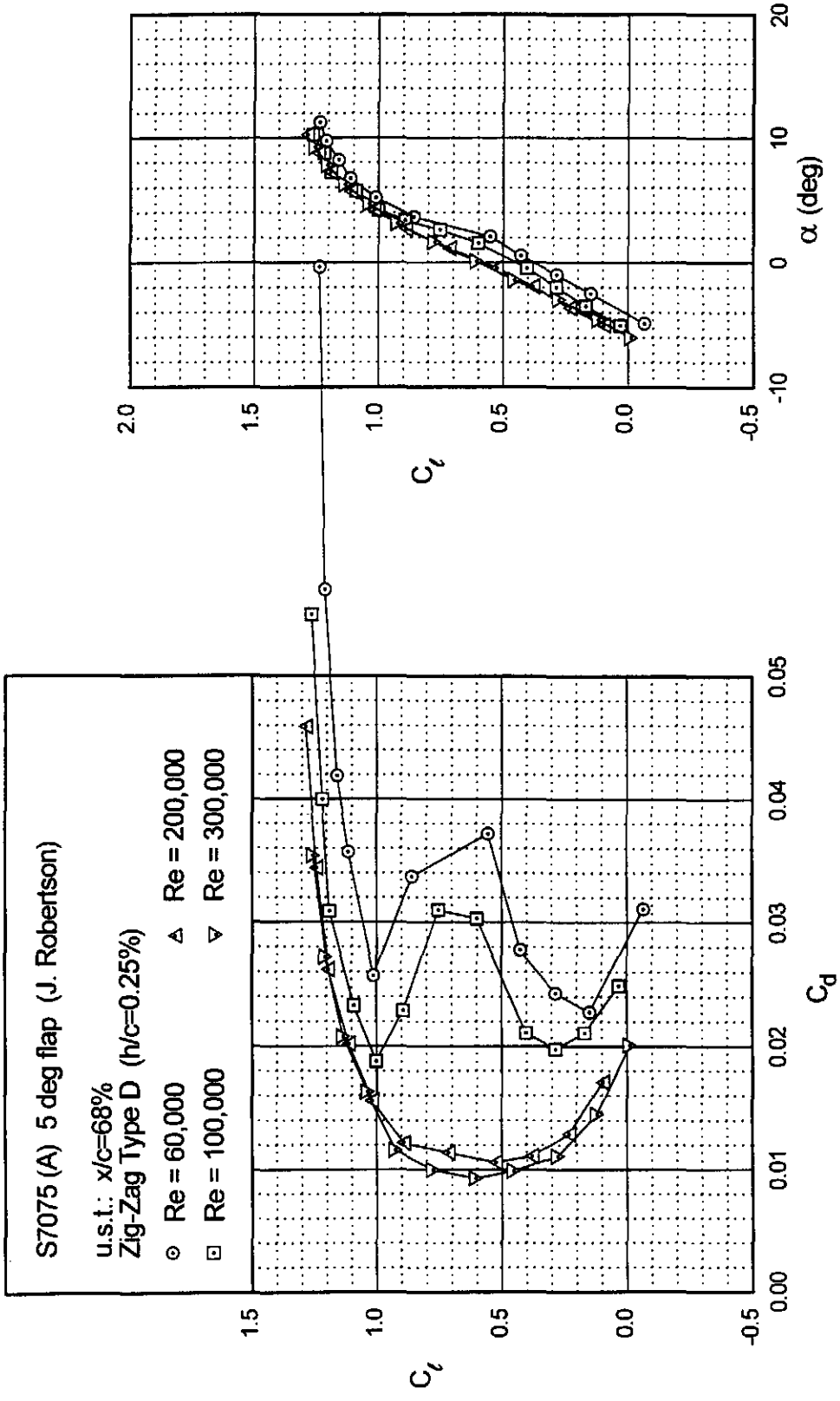
S7075 (A) 5 deg flap (J. Robertson)
u.s.t.: x/c=68%
Zig-Zag Type D (h/c=0.25%)
Re = 60,000
Re = 100,000
Re = 200,000
Re = 300,000
C_l
C_d
α (deg)

Fig. 5.120

S7075 (A)

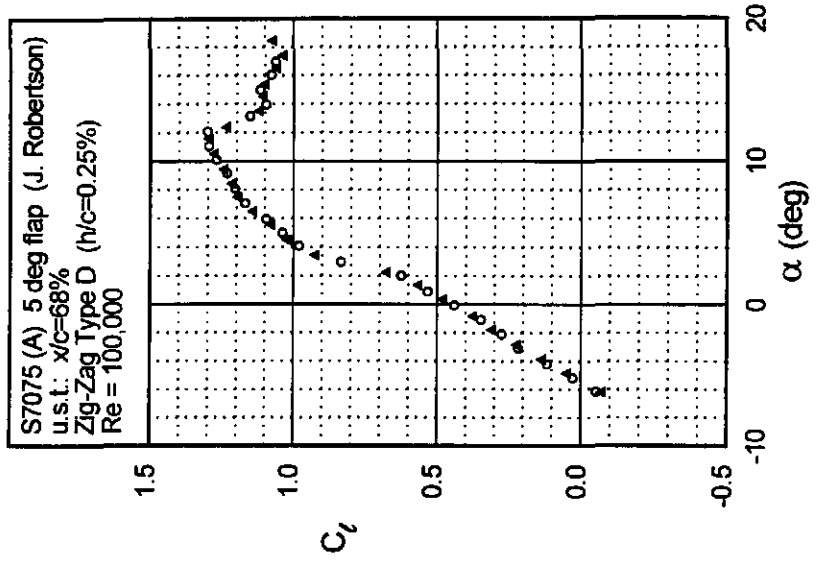

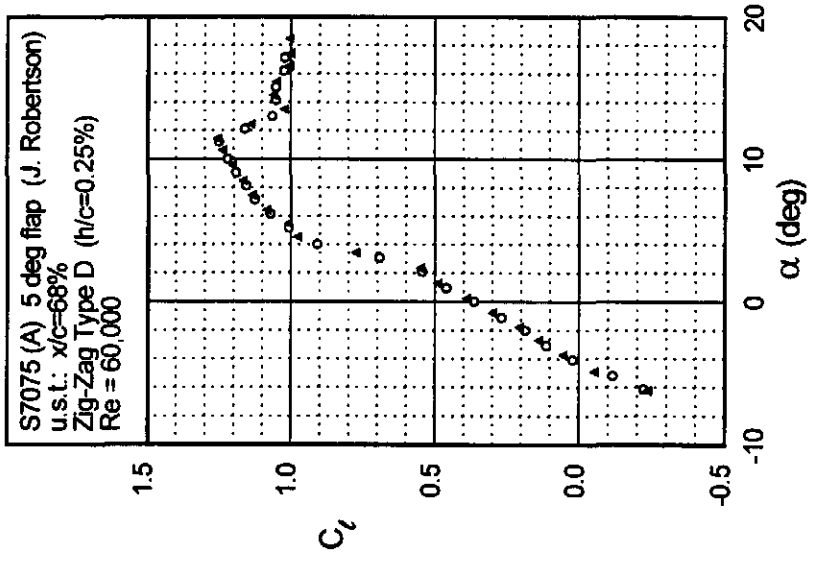

S7075 (A)

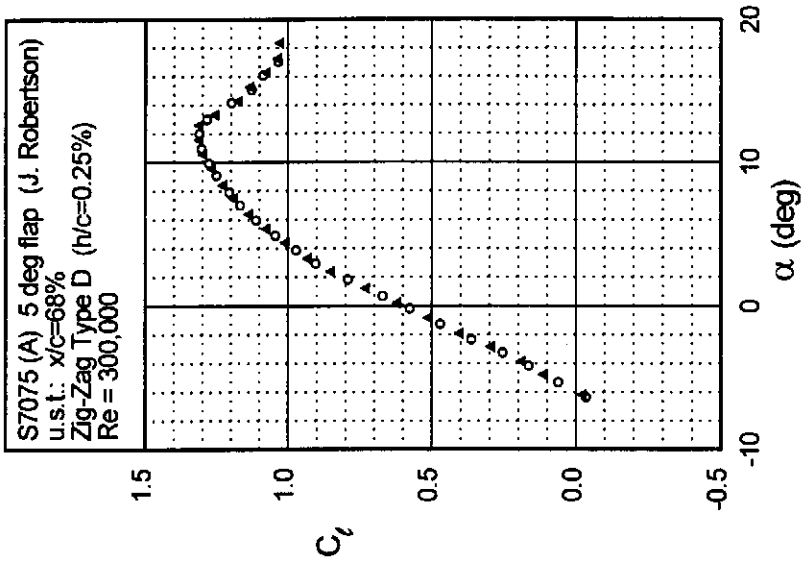
S7075 (A) 5 deg flap (J. Robertson)
u.s.t.: x/c=68%
Zig-Zag Type D (h/c=0.25%)
Re = 300,000
1.5
1.0
0.5
0.0
-0.5
C_l
-10
0
10
20
α (deg)

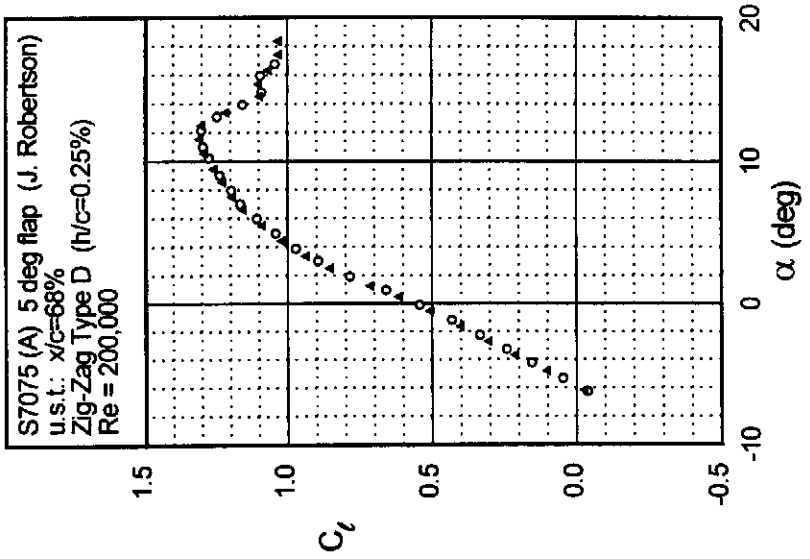
S7075 (A) 5 deg flap (J. Robertson)
u.s.t.: x/c=68%
Zig-Zag Type D (h/c=0.25%)
Re = 200,000
1.5
1.0
0.5
0.0
-0.5
C_l
-10
0
10
20
α (deg)

S7075 (A)

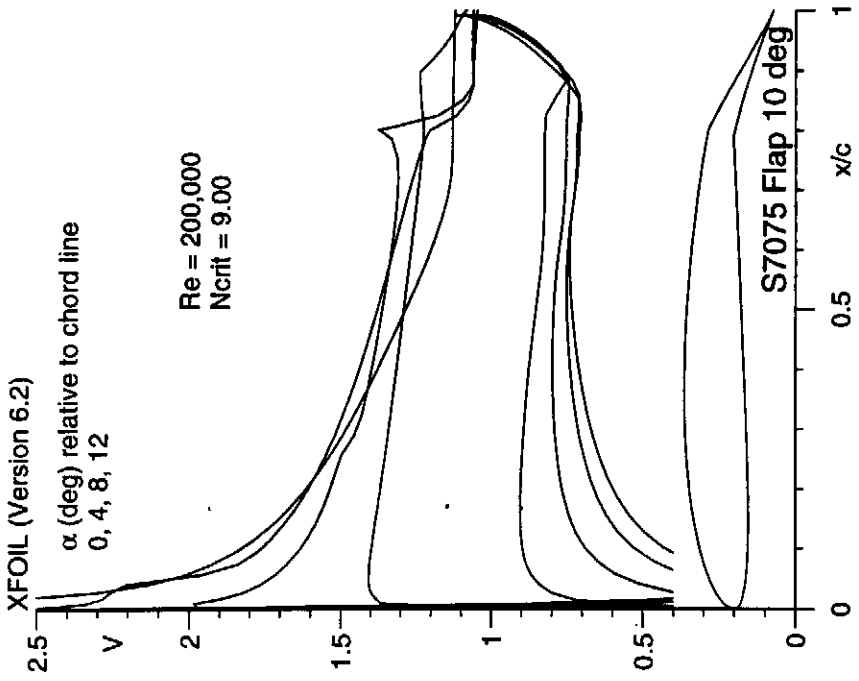
XFOIL (Version 6.2)
α (deg) relative to chord line
0, 4, 8, 12
Re = 200,000
Ncrit = 9.00
S7075 Flap 10 deg
V
x/c
2.5
2
1.5
1
0.5
0
0
0.5
1

S7075 (A)

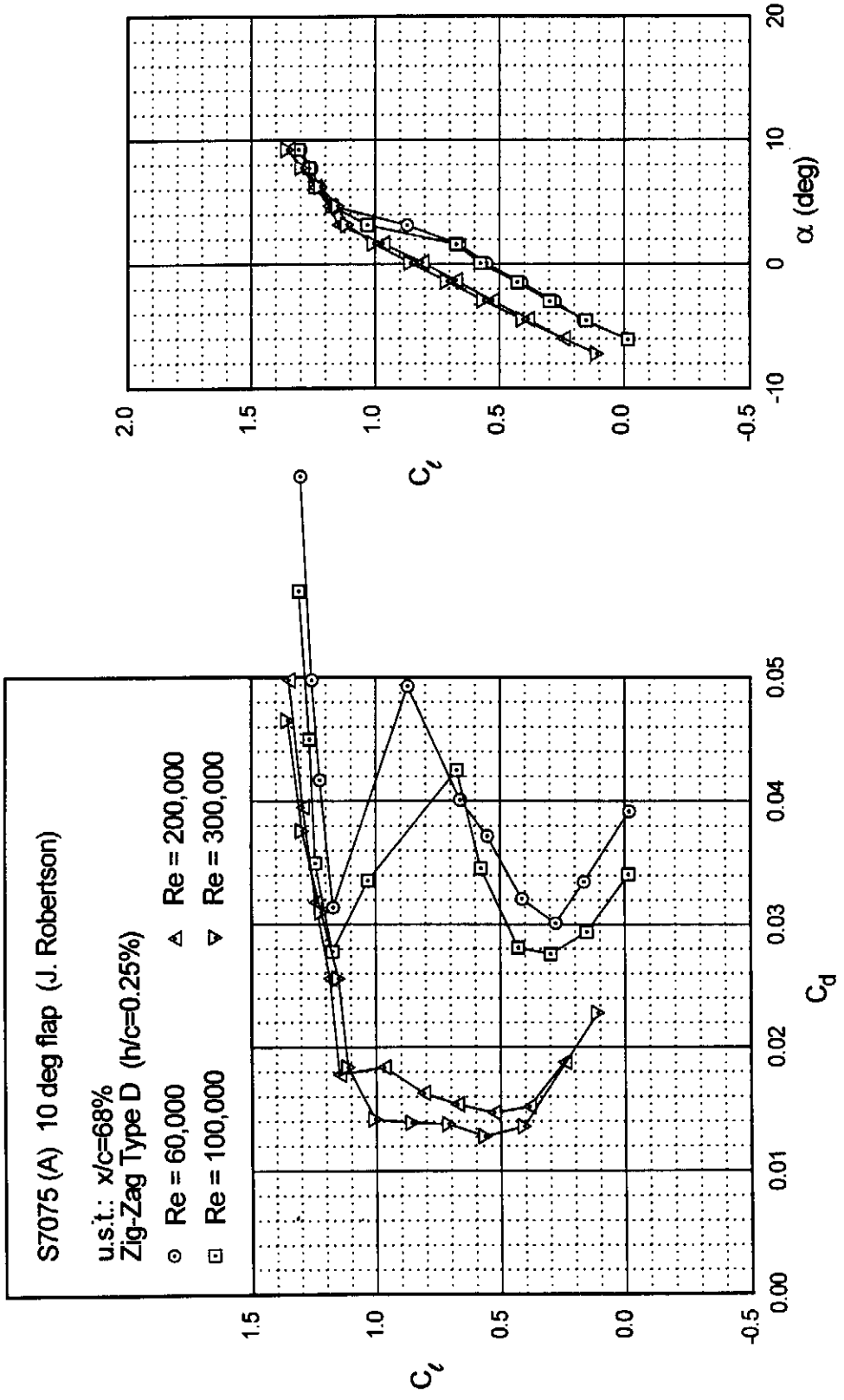
S7075 (A) 10 deg flap (J. Robertson)
u.s.t.: x/c=68%
Zig-Zag Type D (h/c=0.25%)
Re = 60,000
Re = 100,000
Re = 200,000
Re = 300,000
C_l
C_d
α (deg)

Fig. 5.123

S7075 (A)

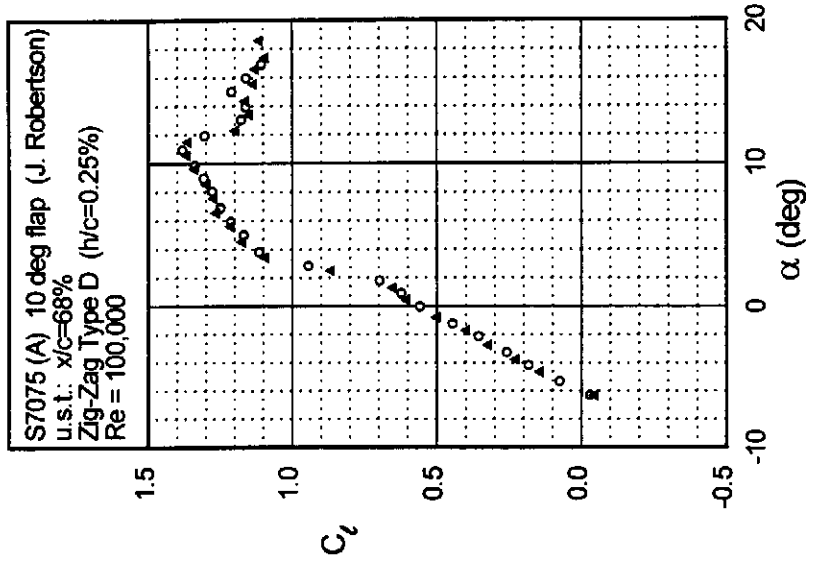

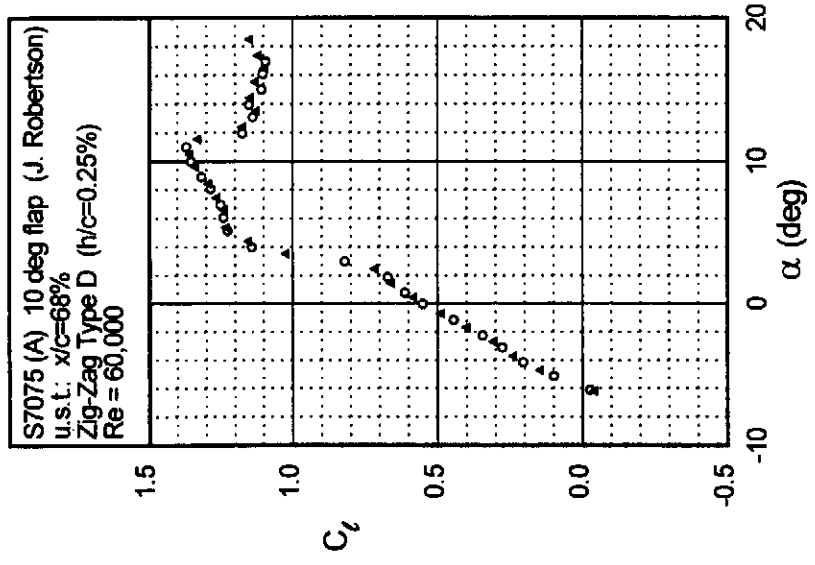

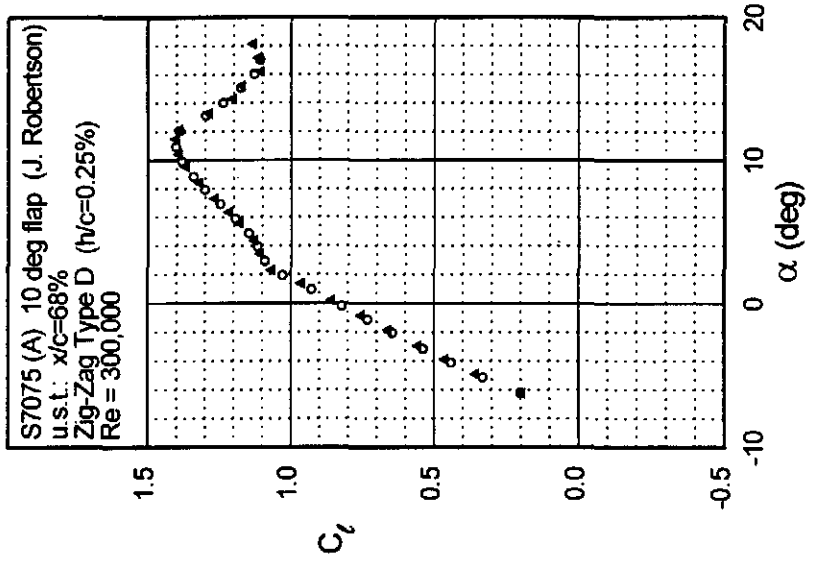
S7075 (A) 10 deg flap (J. Robertson)
u.s.t.: x/c=68%
Zig-Zag Type D (h/c=0.25%)
Re = 300,000
1.5
1.0
0.5
0.0
-0.5
C_l
-10
0
10
20
α (deg)

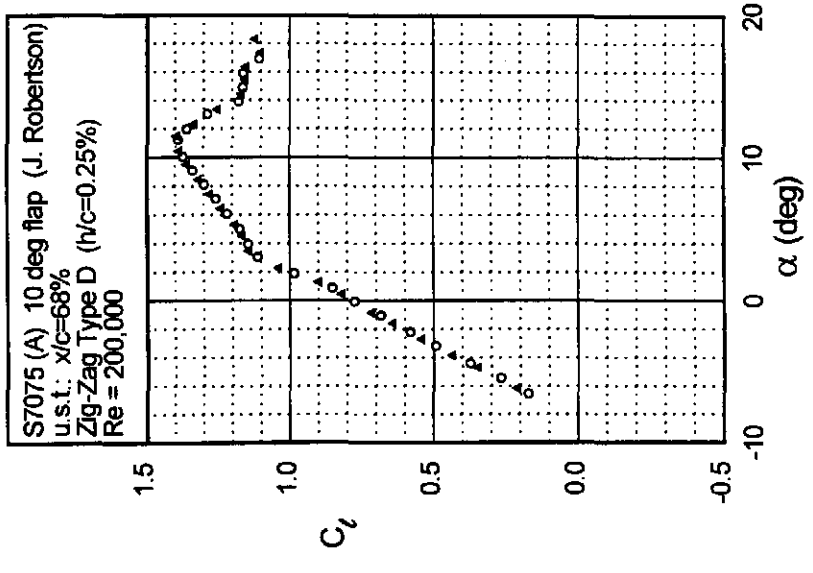
S7075 (A) 10 deg flap (J. Robertson)
u.s.t.: x/c=68%
Zig-Zag Type D (h/c=0.25%)
Re = 200,000
1.5
1.0
0.5
0.0
-0.5
C_l
-10
0
10
20
α (deg)

S7075 (B)

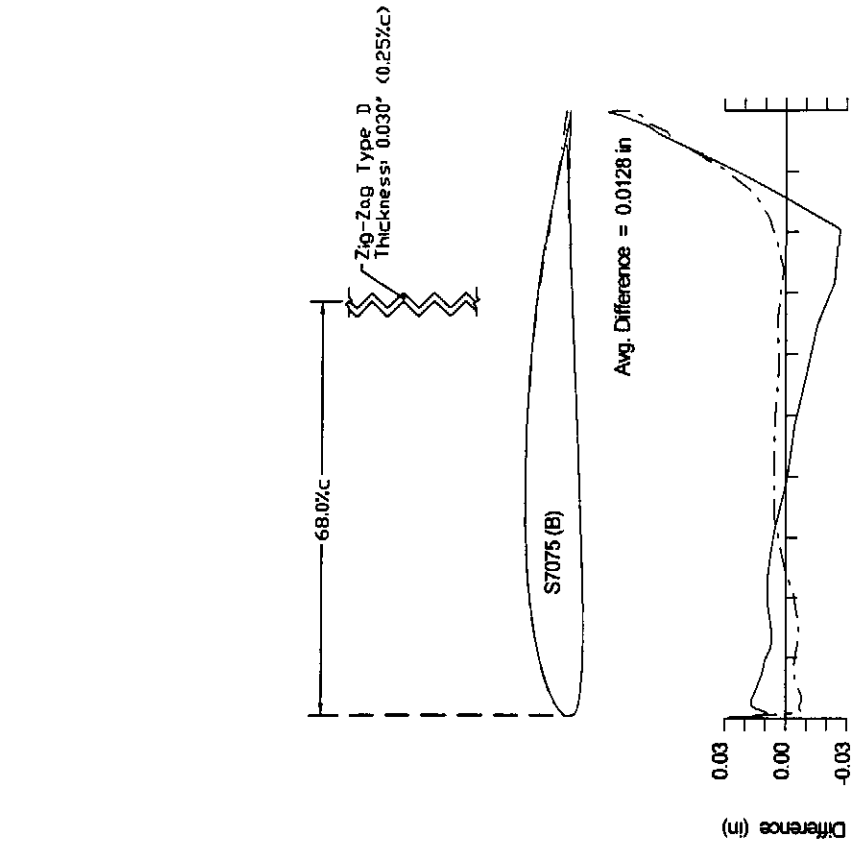
Zig-Zag Type D
Thickness 0.030" (0.25%c)
68.0%c
S7075 (B)
Avg. Difference = 0.0128 in
0.03
0.00
-0.03
Difference (in)

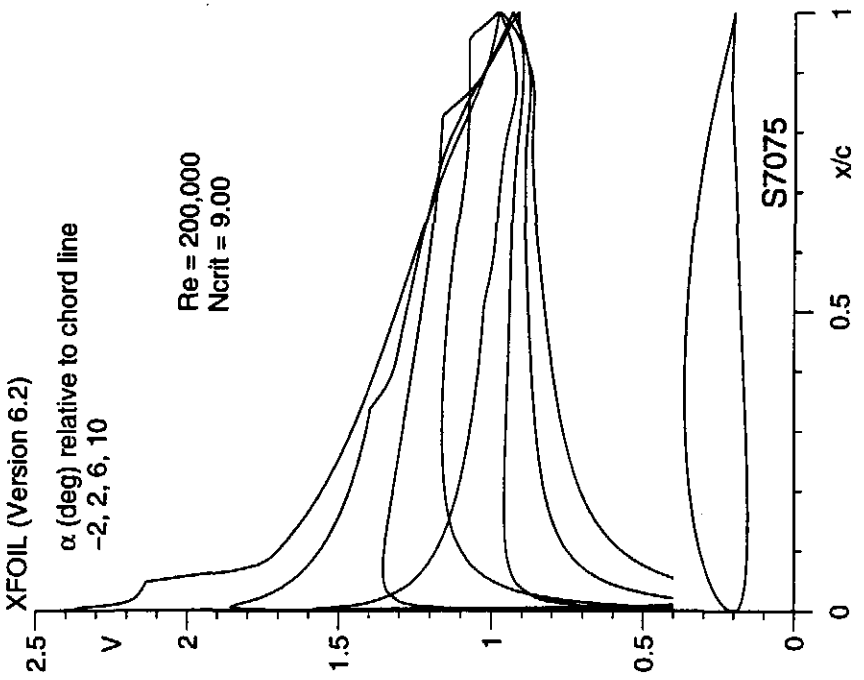
XFOIL (Version 6.2)
α (deg) relative to chord line
-2, 2, 6, 10
Re = 200,000
Ncrit = 9.00
S7075
V
x/c
2.5
2
1.5
1
0.5
0
0.5
1

S7075 (B)

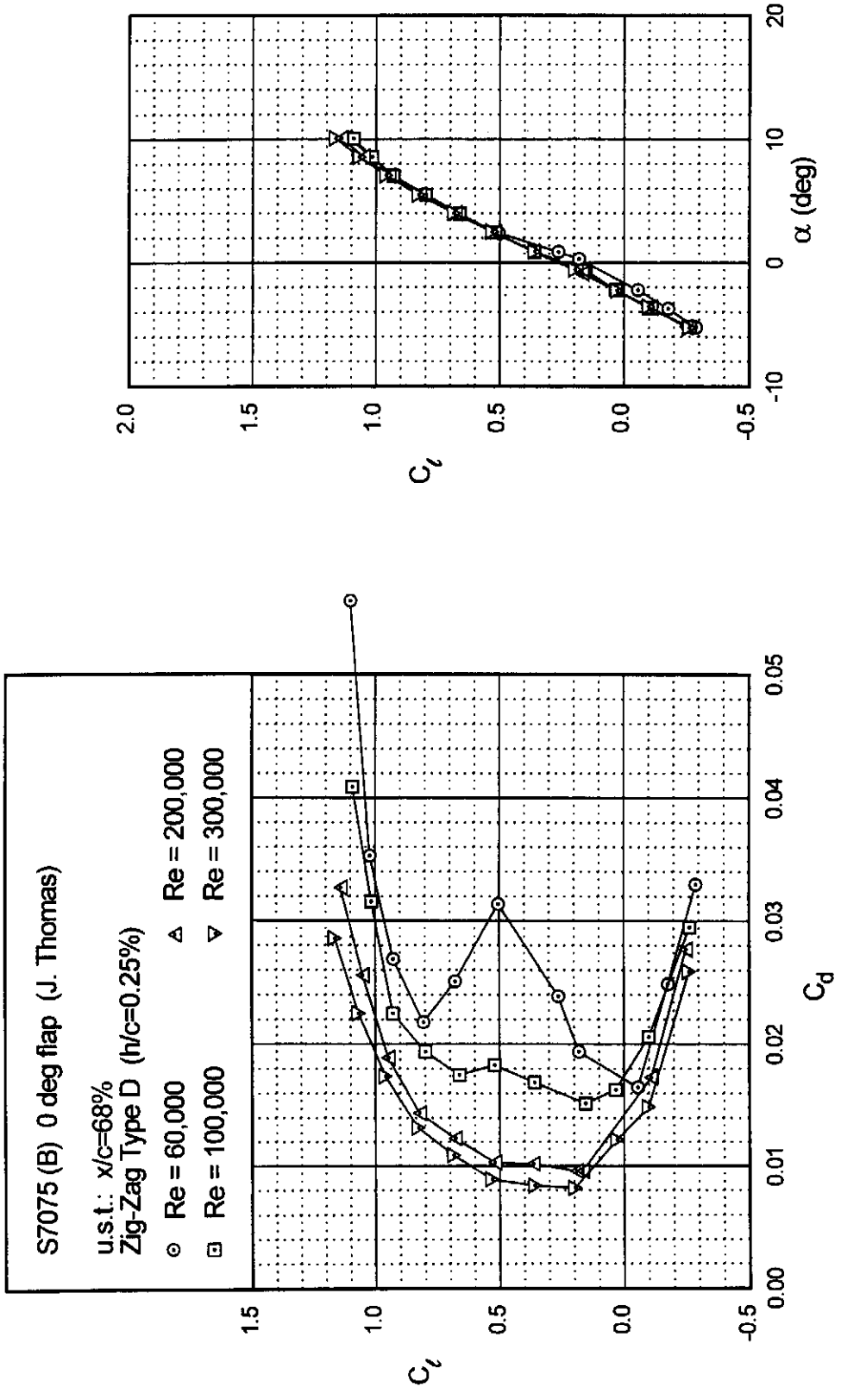
S7075 (B) 0 deg flap (J. Thomas)
u.s.t.: x/c=68%
Zig-Zag Type D (h/c=0.25%)
Re = 60,000
Re = 100,000
Re = 200,000
Re = 300,000
C_l
C_d
α (deg)

S7075 (B)

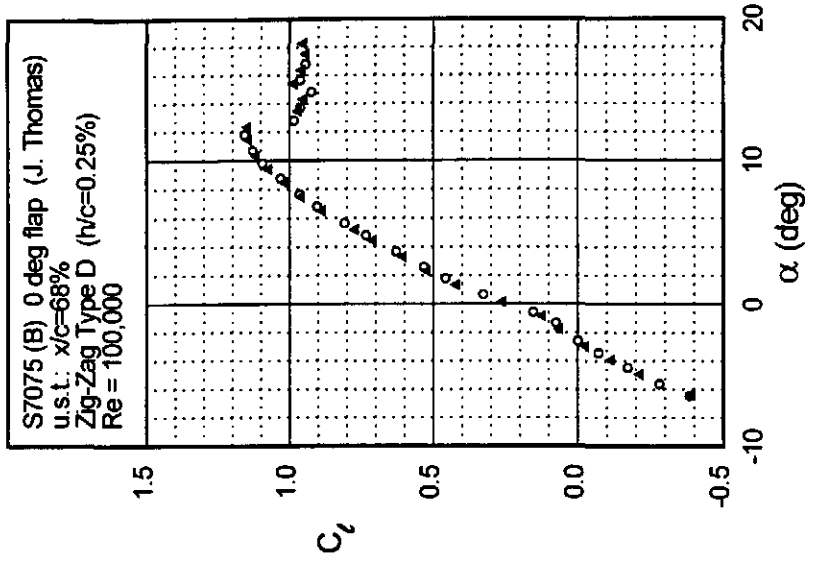
S7075 (B) 0 deg flap (J. Thomas)
u.s.t.: x/c=68%
Zig-Zag Type D (h/c=0.25%)
Re = 100,000
1.5
1.0
0.5
0.0
-0.5
C_l
-10
0
10
20
α (deg)

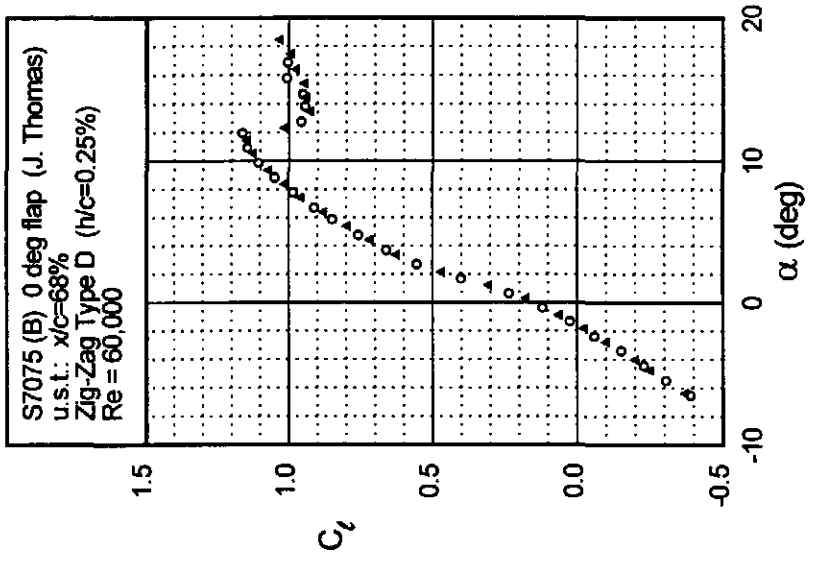
S7075 (B) 0 deg flap (J. Thomas)
u.s.t.: x/c=68%
Zig-Zag Type D (h/c=0.25%)
Re = 60,000
1.5
1.0
0.5
0.0
-0.5
C_l
-10
0
10
20
α (deg)

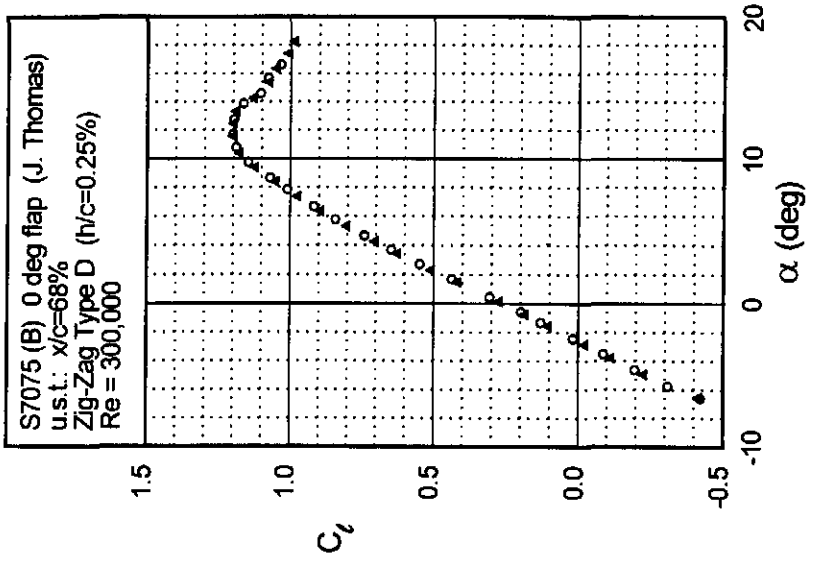
S7075 (B) 0 deg flap (J. Thomas)
u.s.t.: x/c=68%
Zig-Zag Type D (h/c=0.25%)
Re = 300,000
1.5
1.0
0.5
0.0
-0.5
C_l
-10
0
10
20
α (deg)

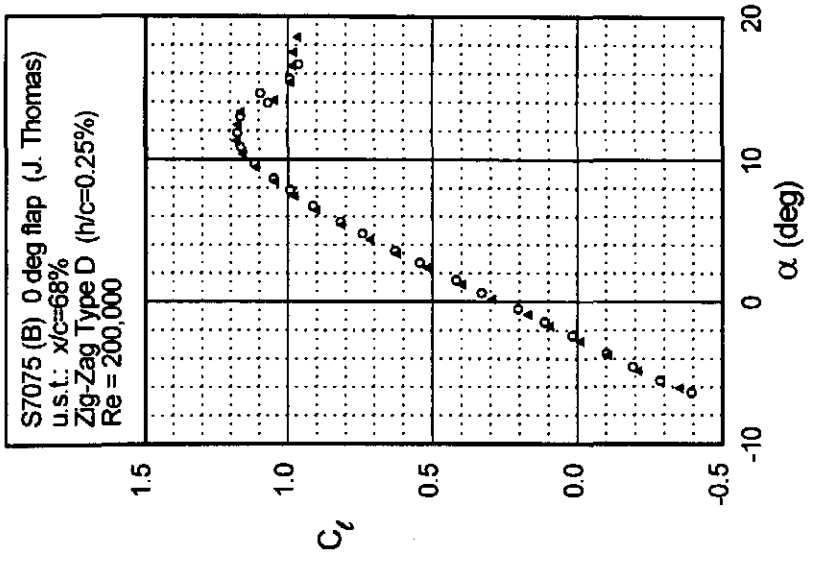
S7075 (B) 0 deg flap (J. Thomas)
u.s.t.: x/c=68%
Zig-Zag Type D (h/c=0.25%)
Re = 200,000
1.5
1.0
0.5
0.0
-0.5
C_l
-10
0
10
20
α (deg)

S8025

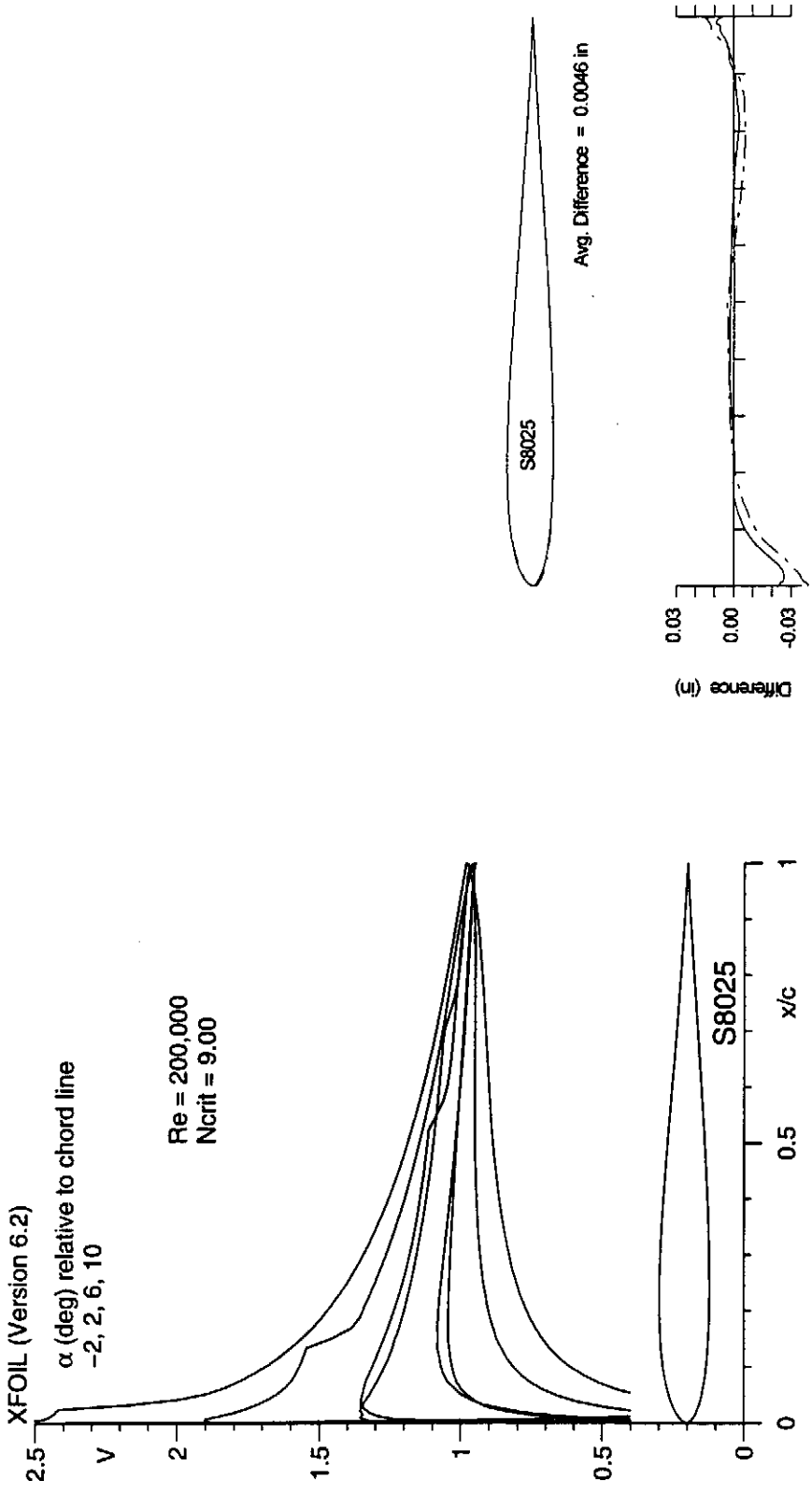
S8025
Avg. Difference = 0.0046 in
0.03
0.00
-0.03
Difference (in)
XFOIL (Version 6.2)
α (deg) relative to chord line
-2, 2, 6, 10
Re = 200,000
Ncrit = 9.00
2.5
2
1.5
1
0.5
0
V
S8025
0
0.5
1
x/c

S8025

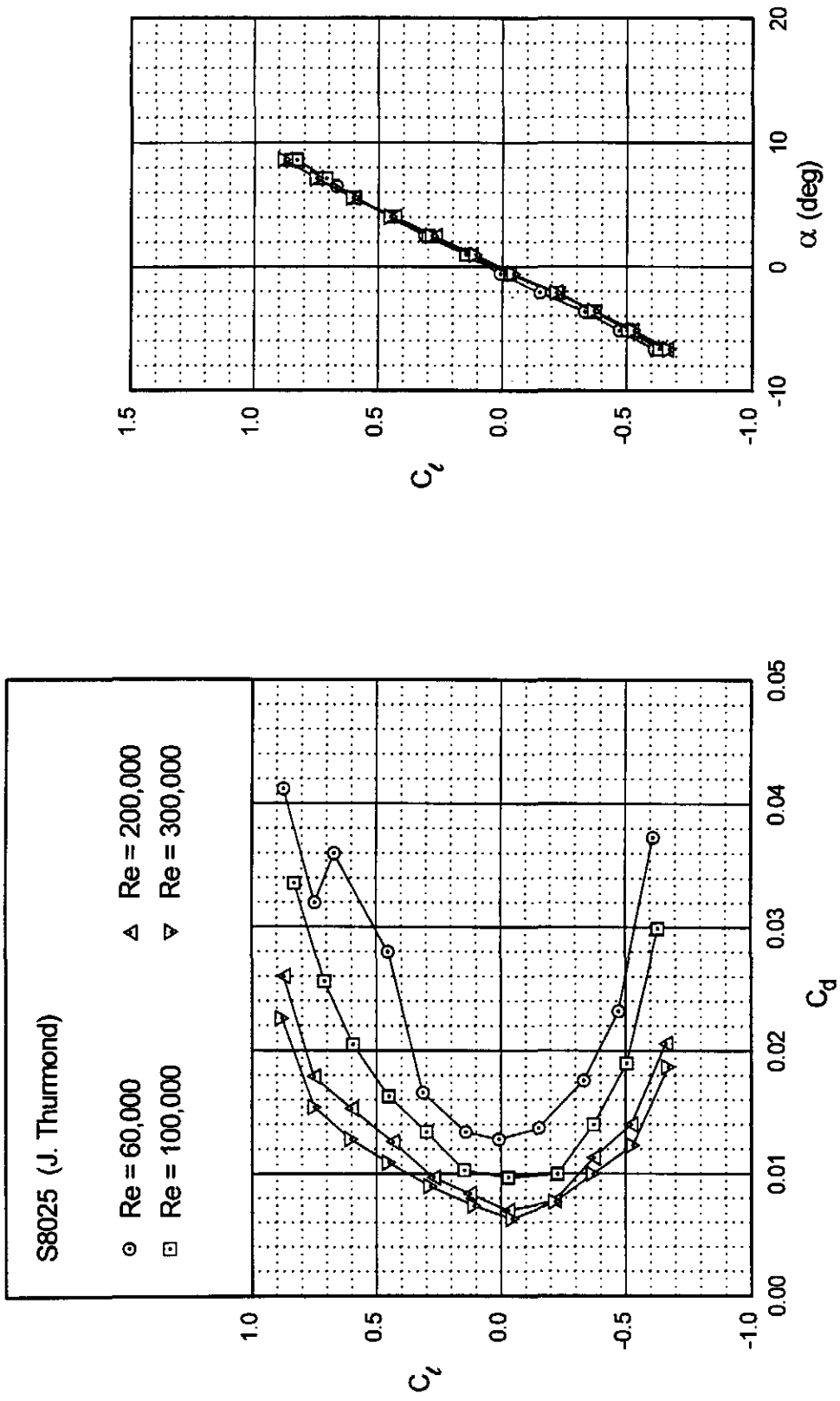
S8025 (J. Thurmond)
Re = 60,000
Re = 100,000
Re = 200,000
Re = 300,000
C_l
C_d
α (deg)
1.5
1.0
0.5
0.0
-0.5
-1.0
0.05
0.04
0.03
0.02
0.01
0.00
20
10
0
-10

Fig. 5.131

S8025

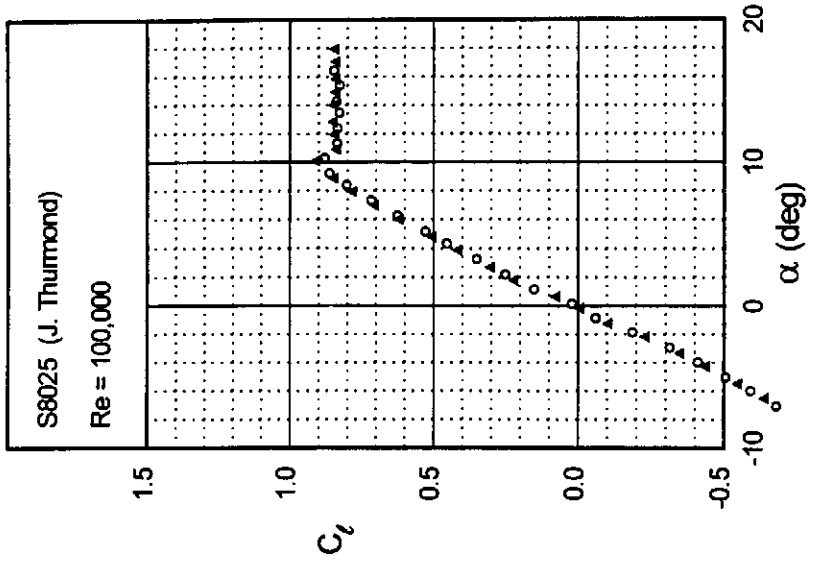

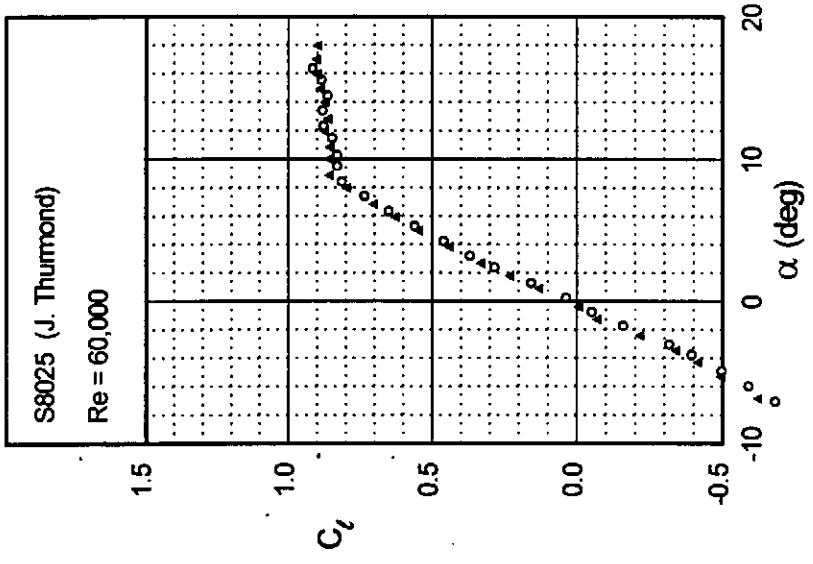

S8025

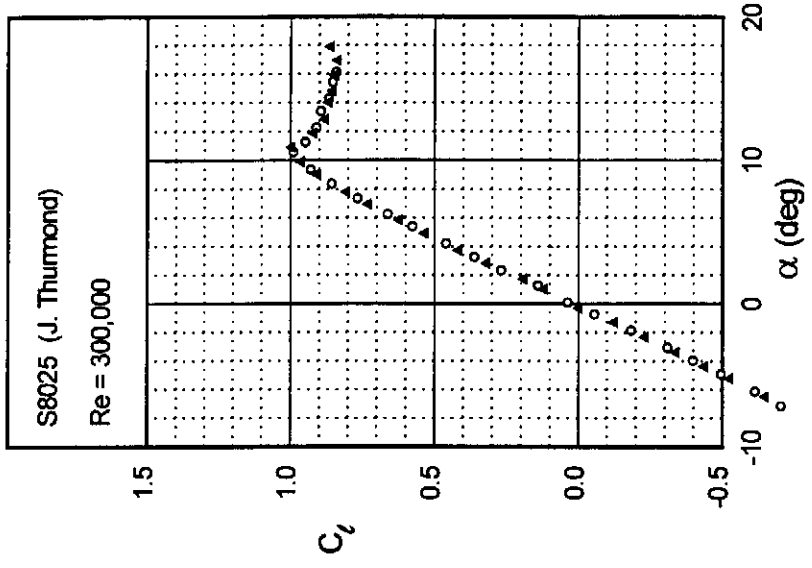
S8025 (J. Thurmond)
Re = 300,000
1.5
1.0
0.5
0.0
-0.5
C_l
-10
0
10
20
α (deg)

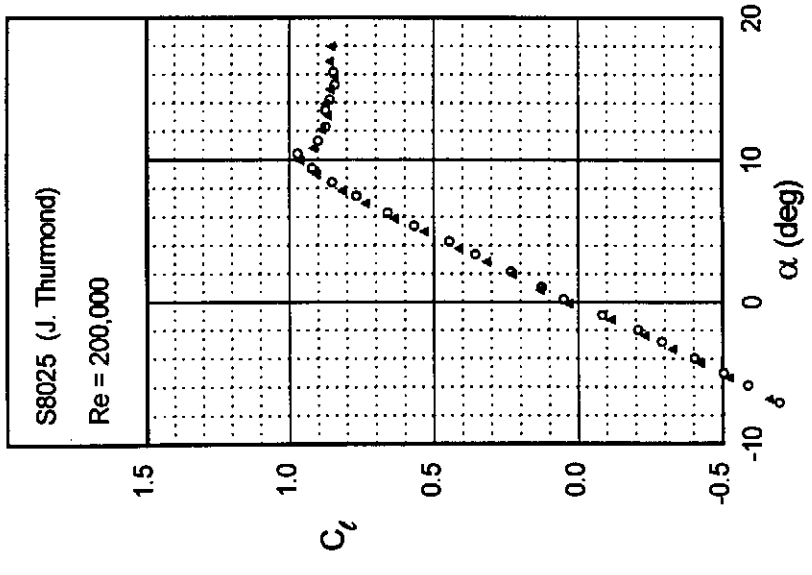
S8025 (J. Thurmond)
Re = 200,000
1.5
1.0
0.5
0.0
-0.5
C_l
-10
0
10
20
α (deg)

SD7037 (B)

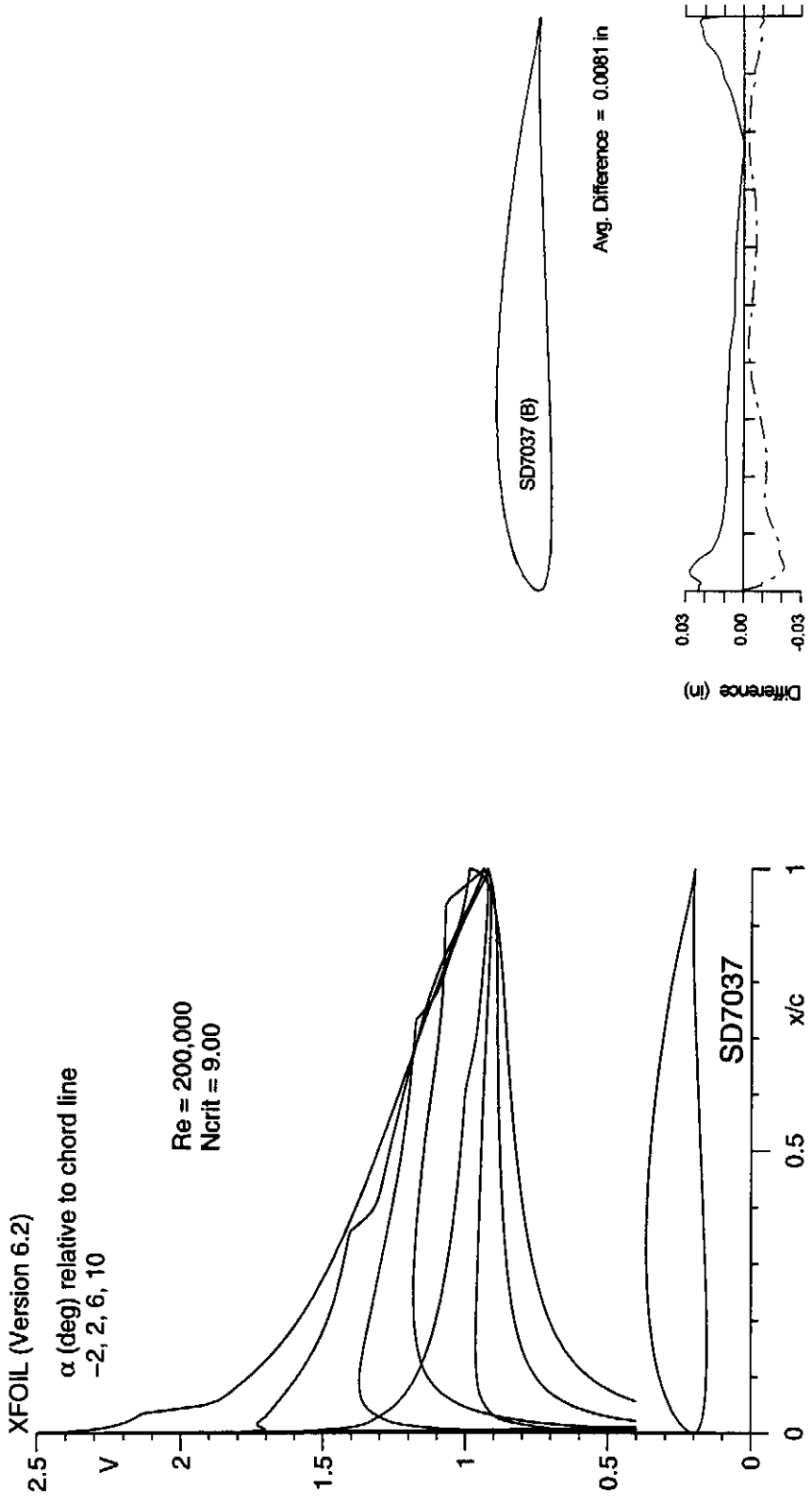
XFOIL (Version 6.2)
α (deg) relative to chord line
-2, 2, 6, 10
Re = 200,000
Ncrit = 9.00
V
2.5
2
1.5
1
0.5
0
SD7037
0
0.5
1
x/c
SD7037 (B)
Avg. Difference = 0.0081 in
0.03
0.00
-0.03
Difference (in)

SD7037 (B)

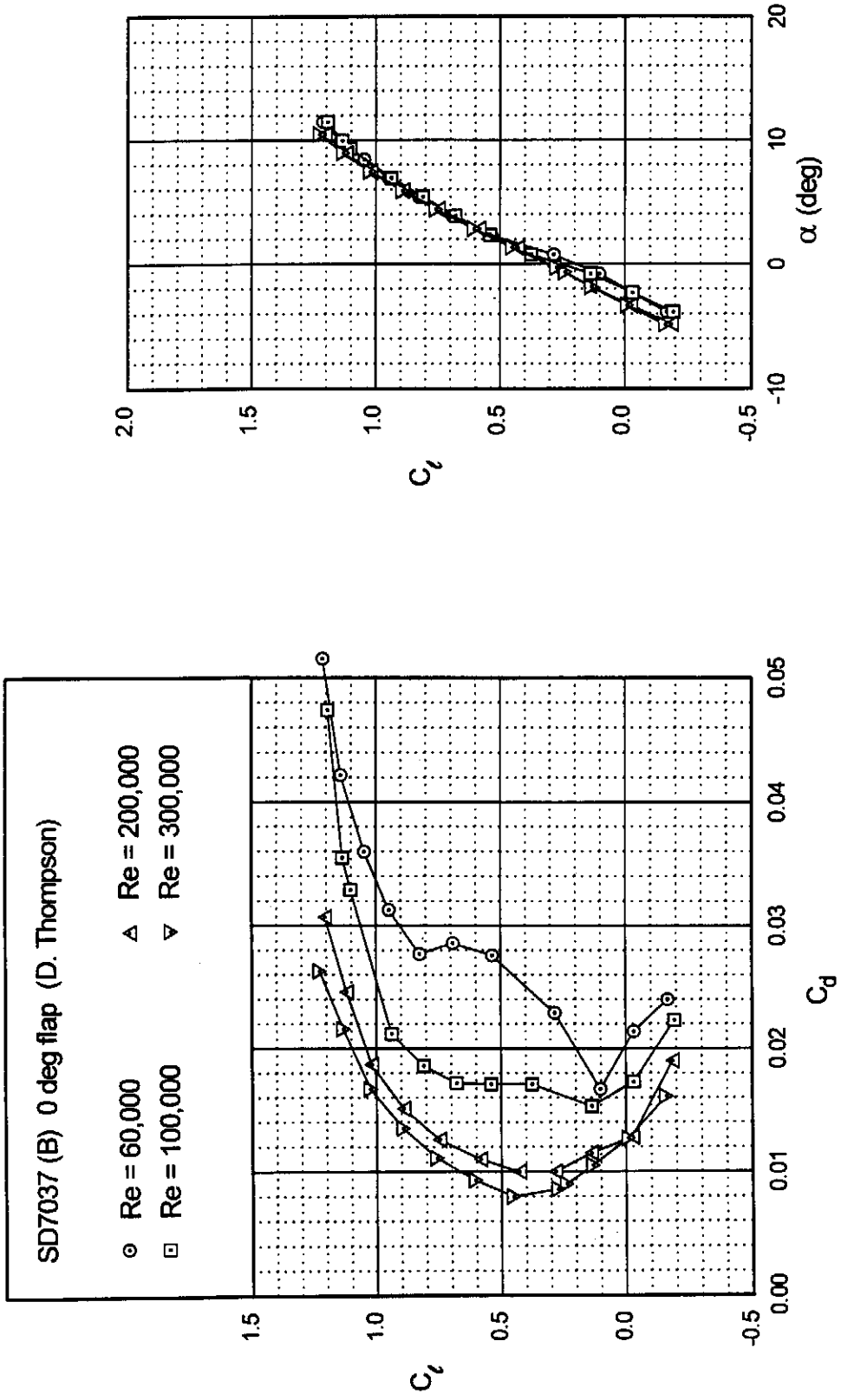
SD7037 (B) 0 deg flap (D. Thompson)
Re = 60,000
Re = 100,000
Re = 200,000
Re = 300,000
C_l
C_d
α (deg)
2.0
1.5
1.0
0.5
0.0
-0.5
20
10
0
-10
0.05
0.04
0.03
0.02
0.01
0.00

SD7037 (B)

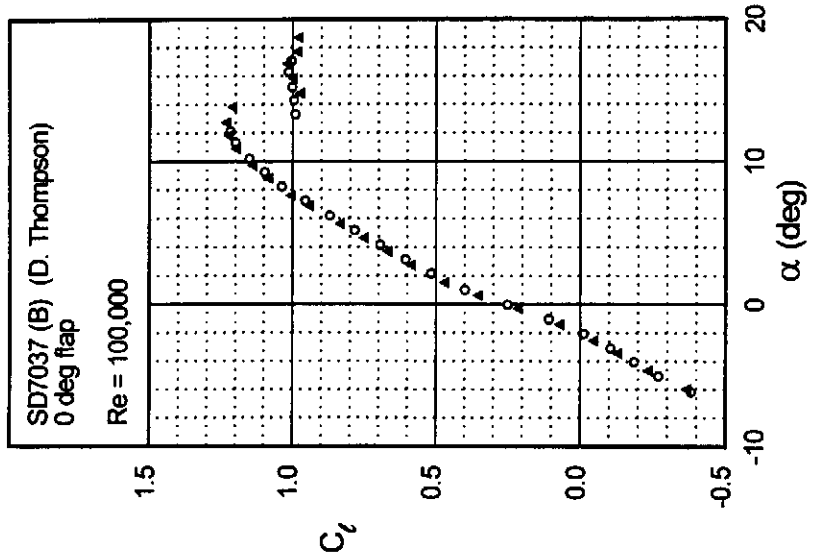
SD7037 (B) (D. Thompson)
0 deg flap
Re = 100,000
1.5
1.0
0.5
0.0
-0.5
C_l
-10
0
10
20
α (deg)

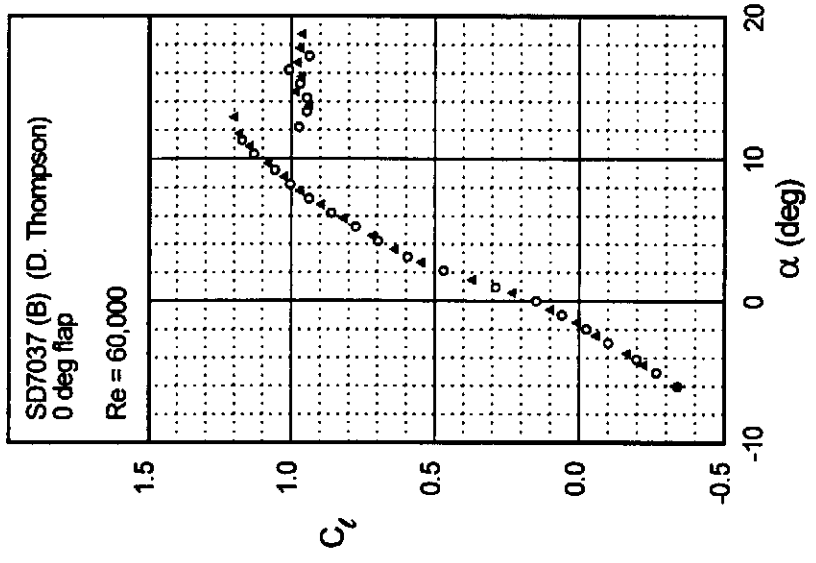
SD7037 (B) (D. Thompson)
0 deg flap
Re = 60,000
1.5
1.0
0.5
0.0
-0.5
C_l
-10
0
10
20
α (deg)

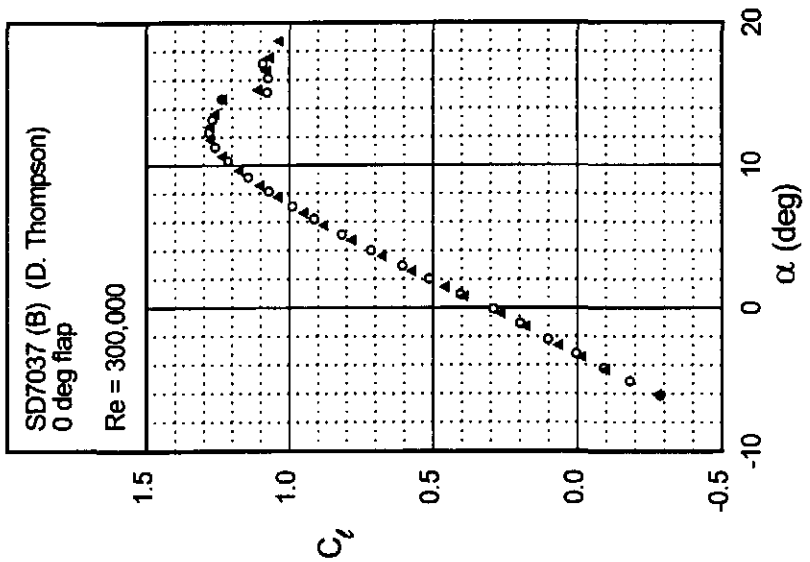
SD7037 (B) (D. Thompson)
0 deg flap
Re = 300,000
1.5
1.0
0.5
0.0
-0.5
C_l
-10
0
10
20
α (deg)

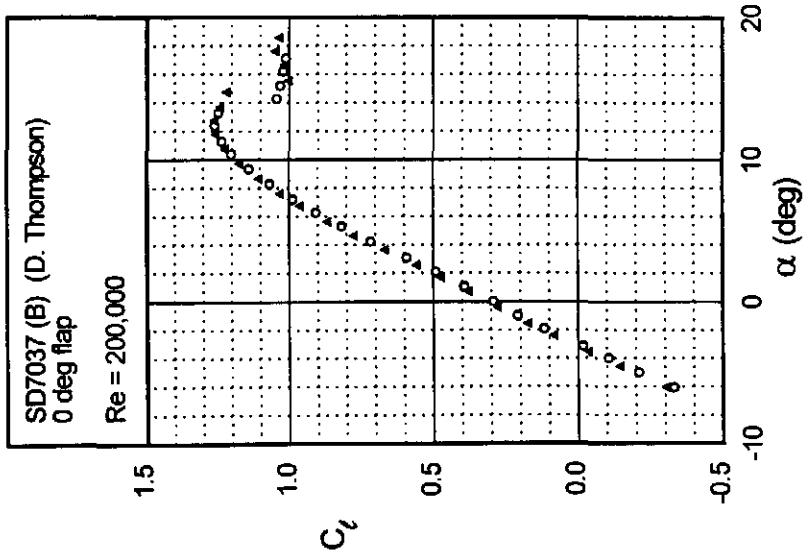
SD7037 (B) (D. Thompson)
0 deg flap
Re = 200,000
1.5
1.0
0.5
0.0
-0.5
C_l
-10
0
10
20
α (deg)

SD7037 (B)

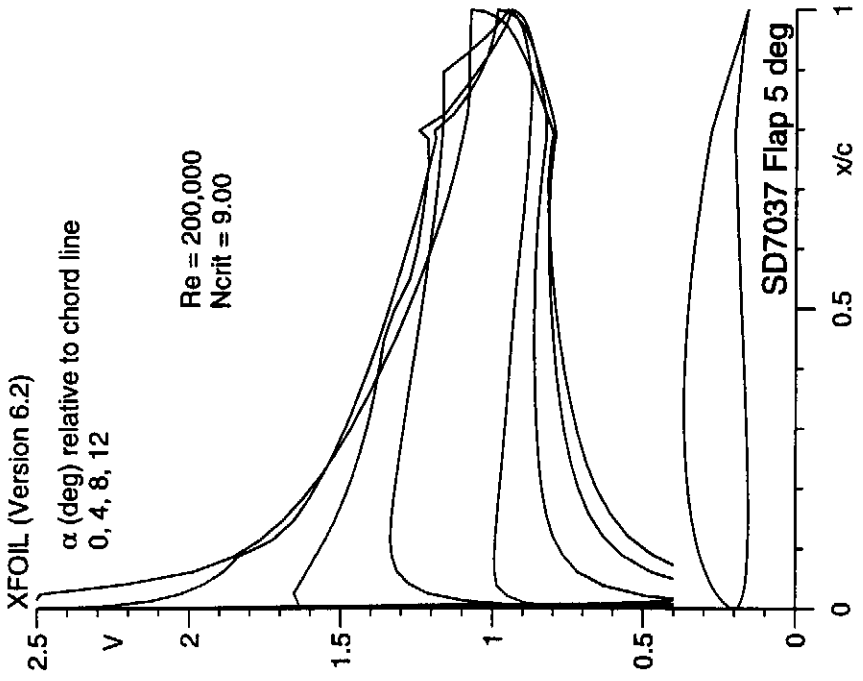
XFOIL (Version 6.2)
α (deg) relative to chord line
0, 4, 8, 12
Re = 200,000
Ncrit = 9.00
SD7037 Flap 5 deg
V
x/c
2.5
2
1.5
1
0.5
0
0
0.5
1

SD7037 (B)

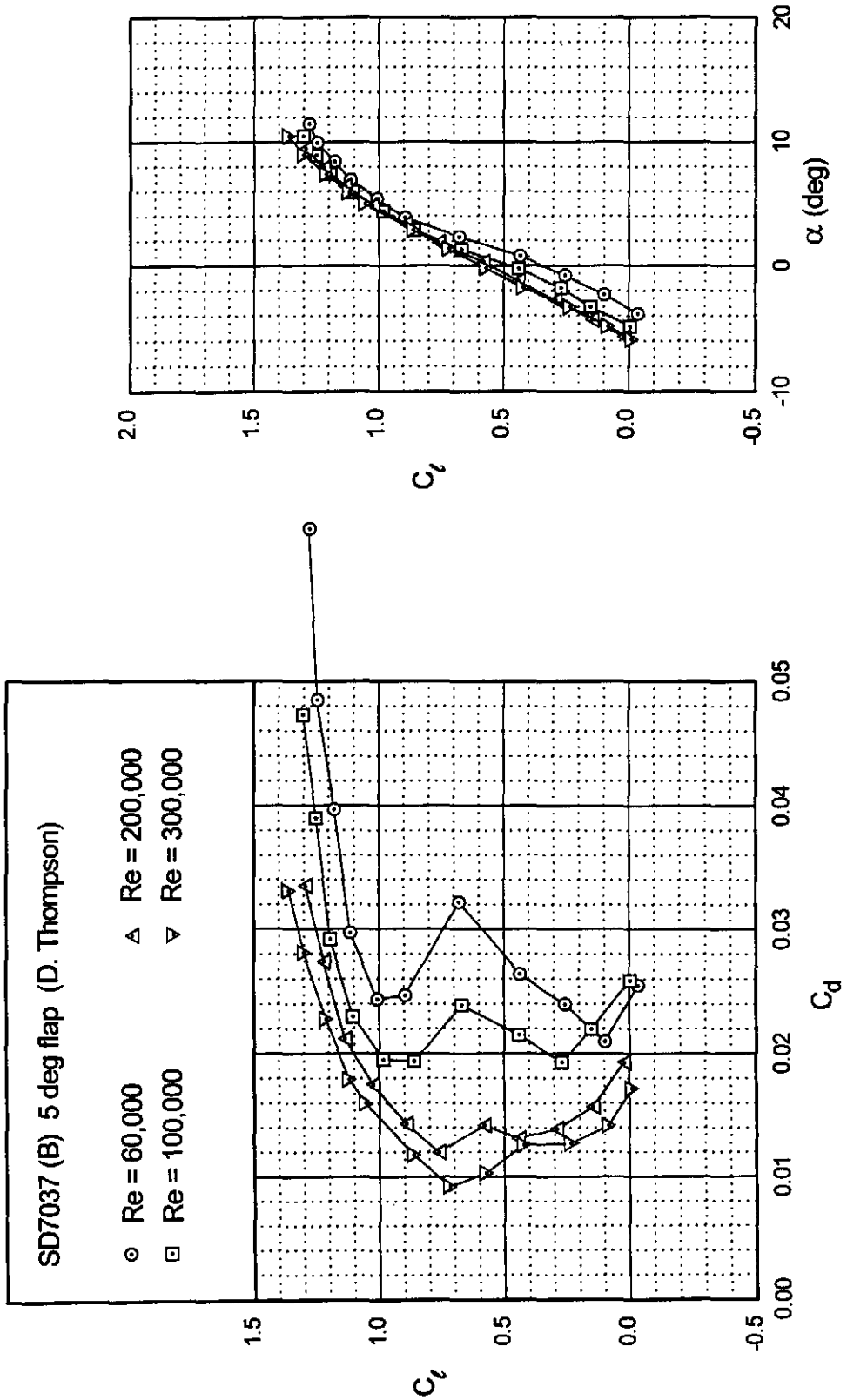
SD7037 (B) 5 deg flap (D. Thompson)
Re = 60,000
Re = 100,000
Re = 200,000
Re = 300,000
C_l
C_d
α (deg)
2.0
1.5
1.0
0.5
0.0
-0.5
-10
0
10
20
0.00
0.01
0.02
0.03
0.04
0.05

SD7037 (B)

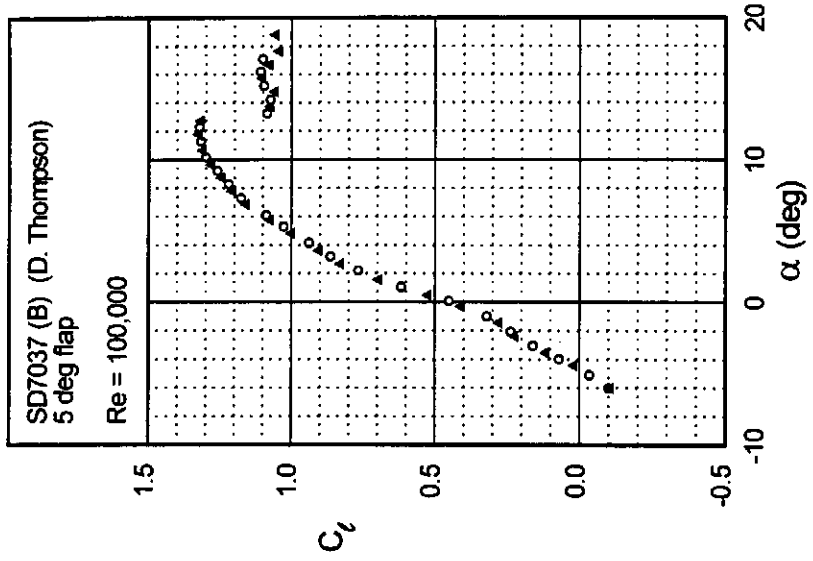
SD7037 (B) (D. Thompson)
5 deg flap
Re = 100,000
1.5
1.0
0.5
0.0
-0.5
C_l
-10
0
10
20
α (deg)

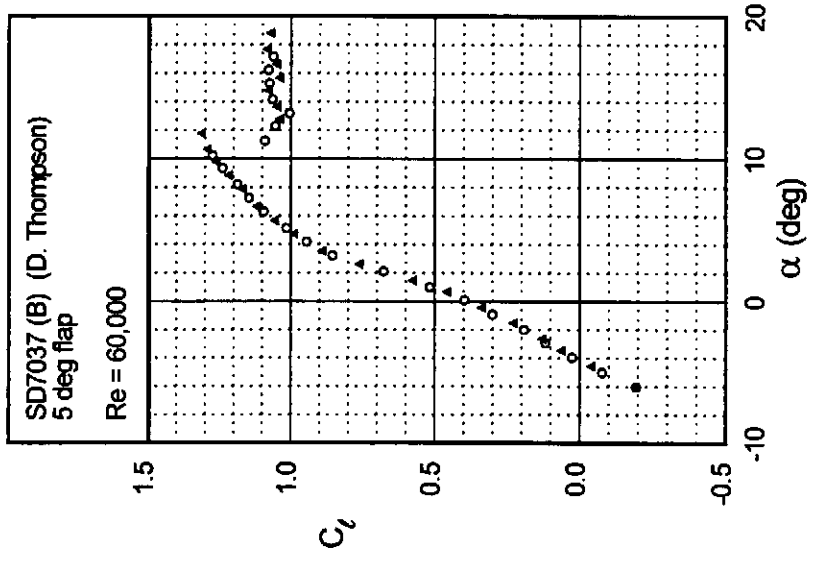
SD7037 (B) (D. Thompson)
5 deg flap
Re = 60,000
1.5
1.0
0.5
0.0
-0.5
C_l
-10
0
10
20
α (deg)

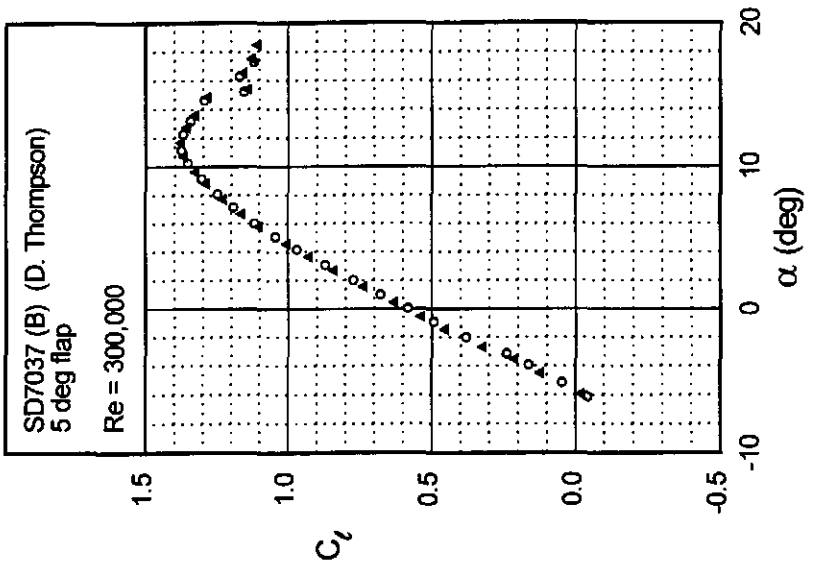
SD7037 (B) (D. Thompson)
5 deg flap
Re = 300,000
1.5
1.0
0.5
0.0
-0.5
C_l
-10
0
10
20
α (deg)

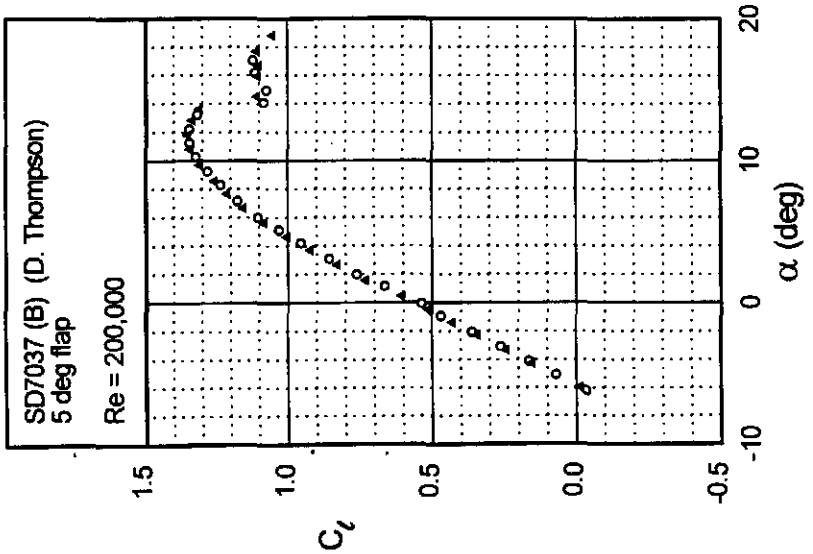
SD7037 (B) (D. Thompson)
5 deg flap
Re = 200,000
1.5
1.0
0.5
0.0
-0.5
C_l
-10
0
10
20
α (deg)

SD7037 (B)

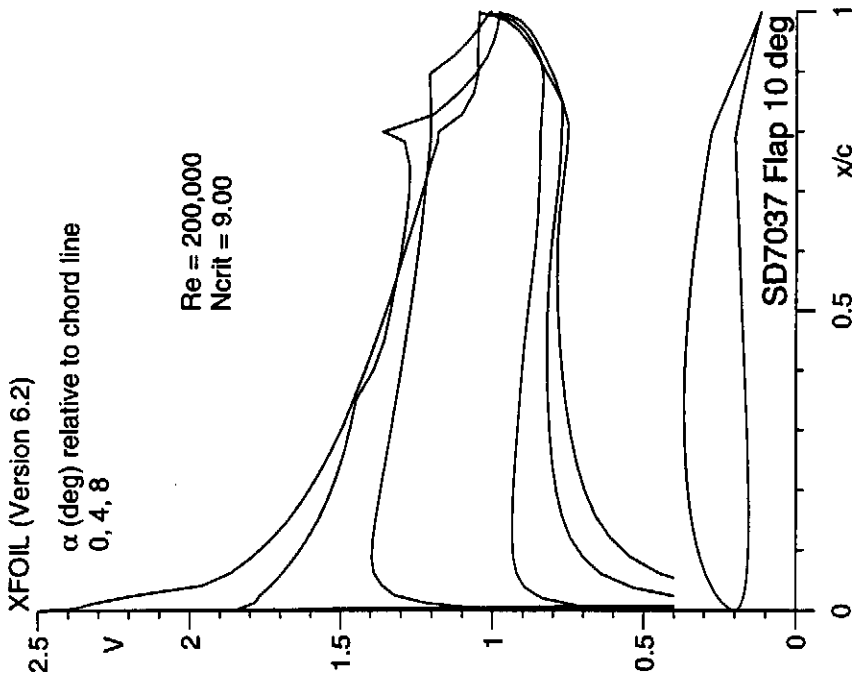
XFOIL (Version 6.2)
α (deg) relative to chord line
0, 4, 8
Re = 200,000
Ncrit = 9.00
SD7037 Flap 10 deg
V
x/c
2.5
2
1.5
1
0.5
0
0
0.5
1

SD7037 (B)

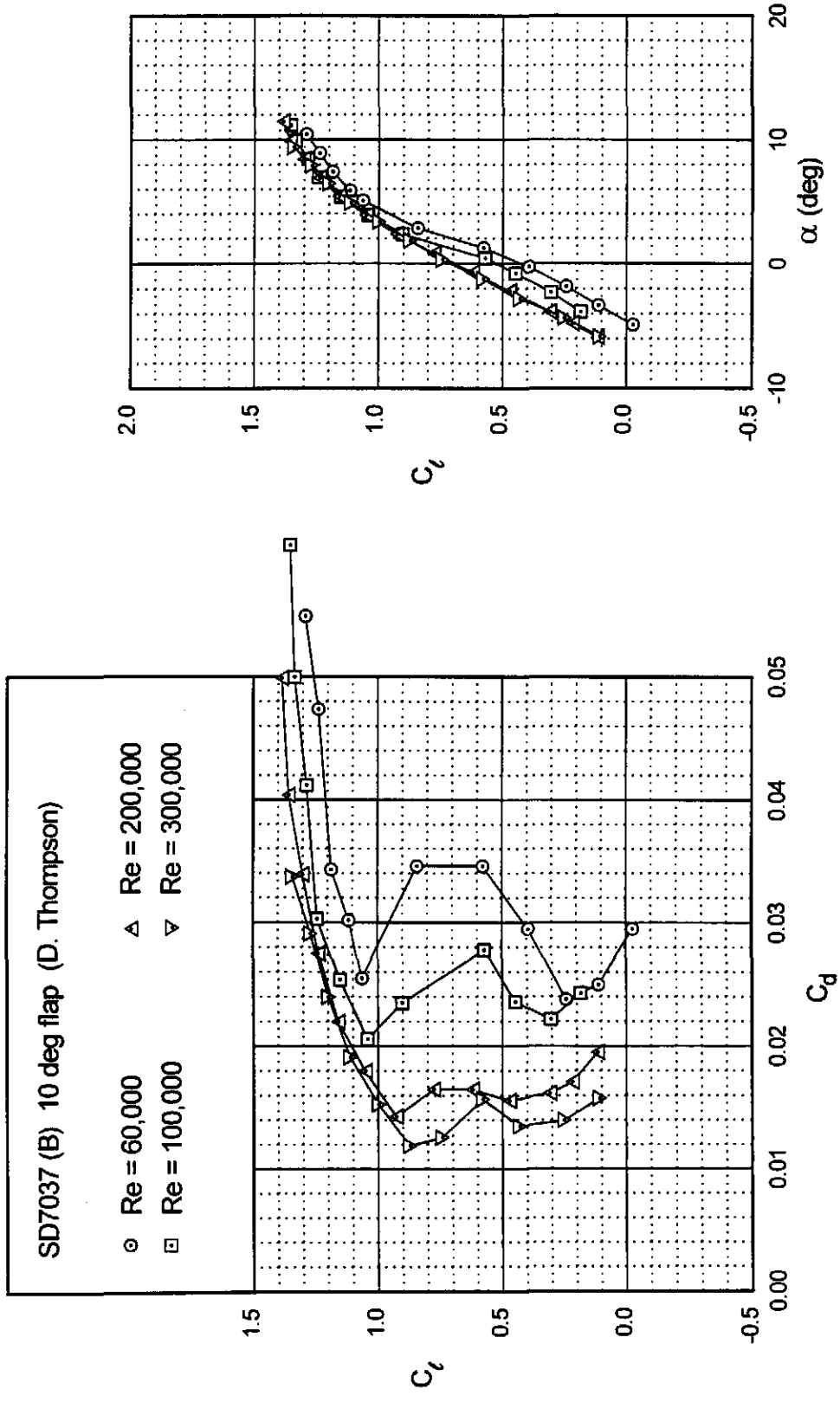
SD7037 (B) 10 deg flap (D. Thompson)
Re = 60,000
Re = 100,000
Re = 200,000
Re = 300,000
C_l
C_d
α (deg)

Fig. 5.141

SD7037 (B)

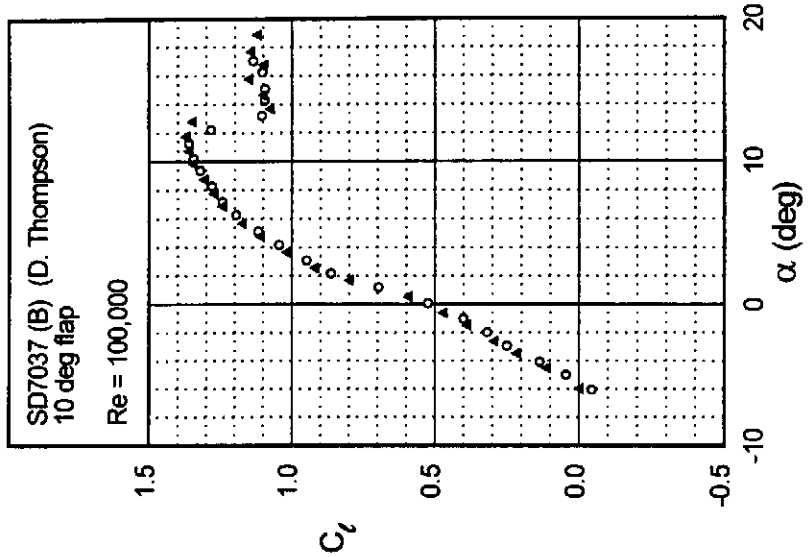

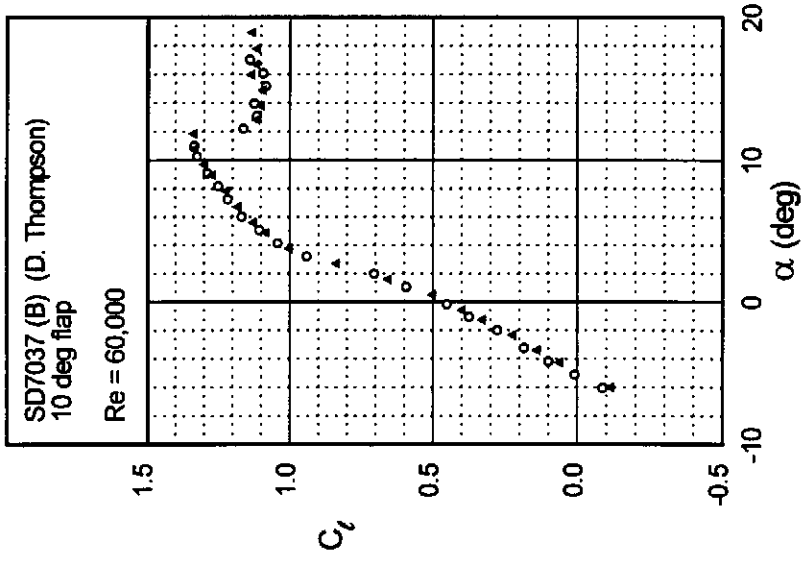

Fig. 5.141 (continued)

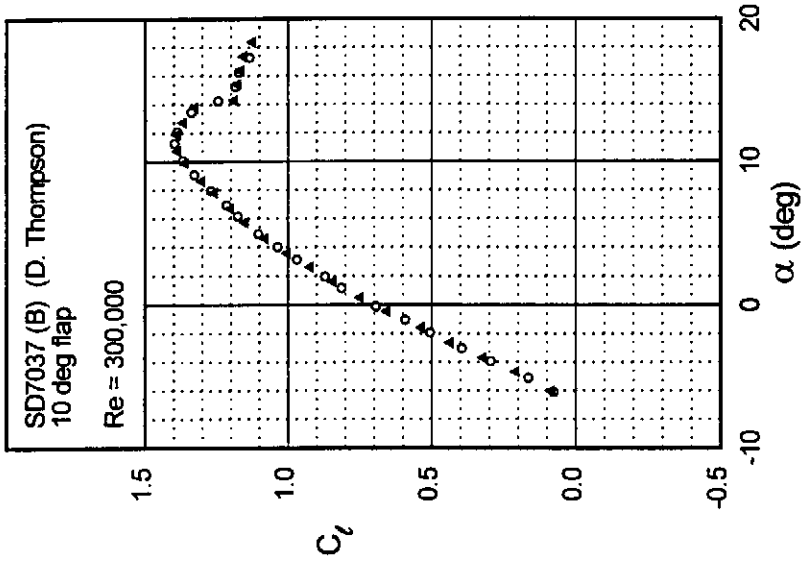

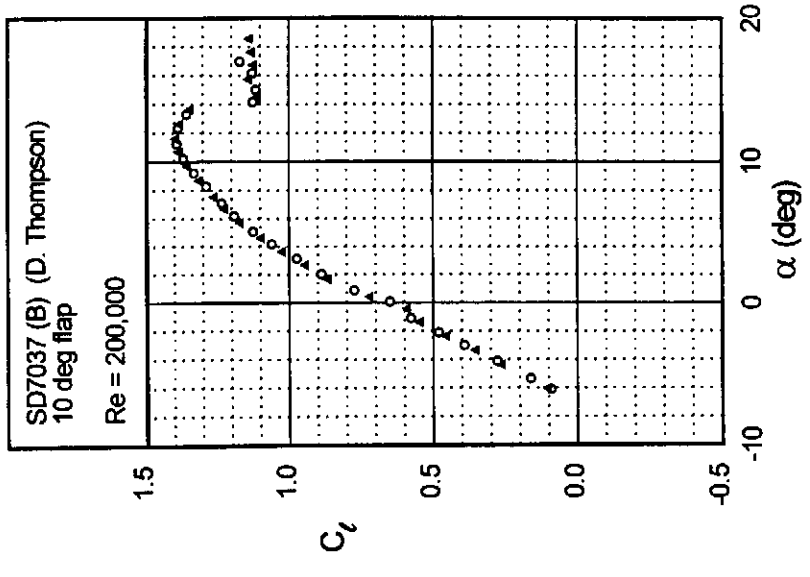

SD7037 (C)

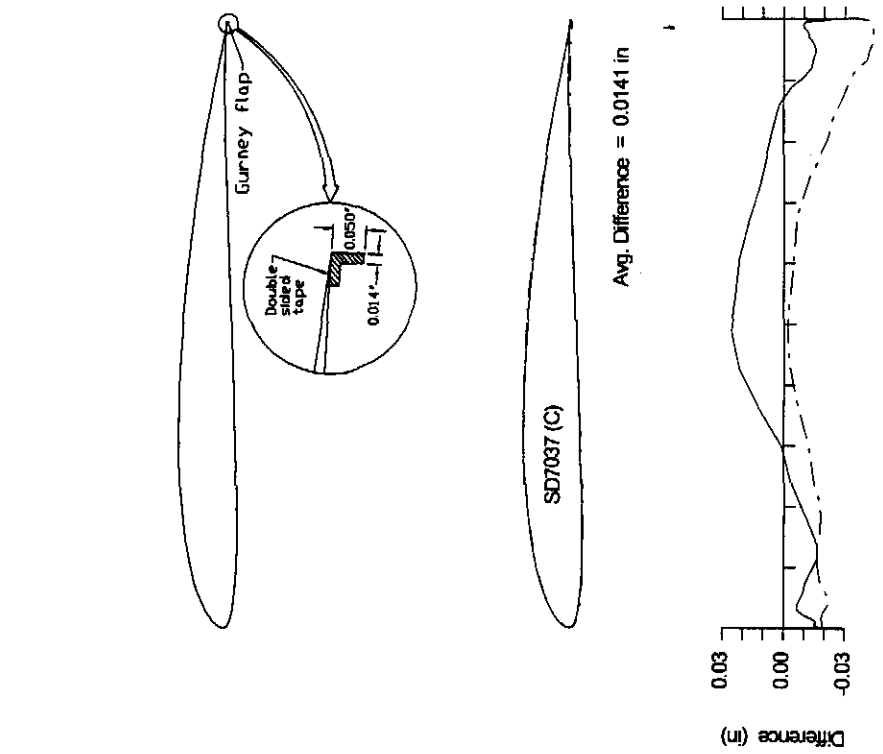
Gurney flap
Double sided tape
0.050"
0.014"
SD7037 (C)
Avg. Difference = 0.0141 in
0.03
0.00
-0.03
Difference (in)

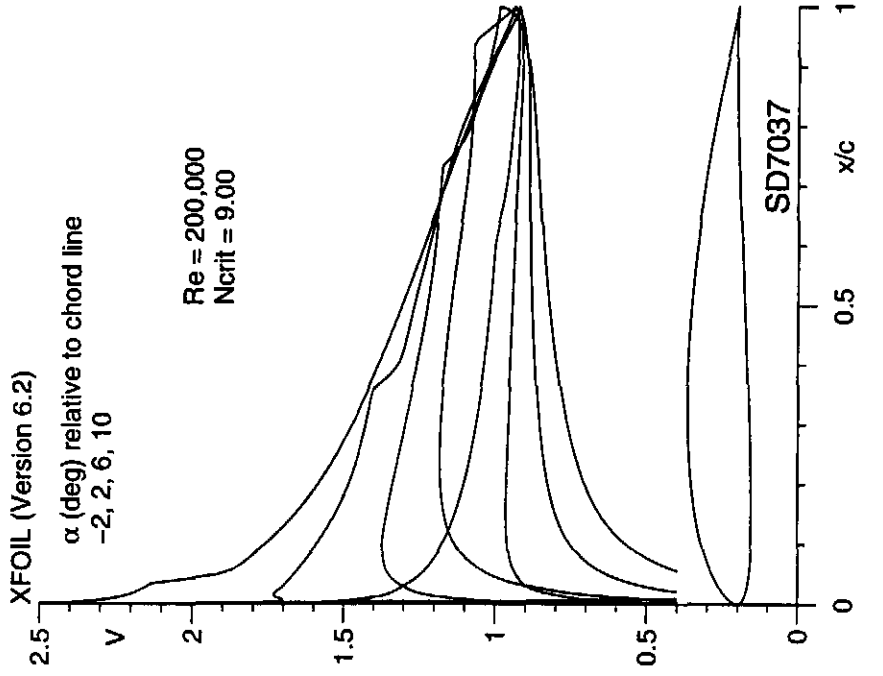
XFOIL (Version 6.2)
α (deg) relative to chord line
-2, 2, 6, 10
Re = 200,000
Ncrit = 9.00
SD7037
2.5
2
1.5
1
0.5
0
V
0
0.5
1
x/c

SD7037 (C)

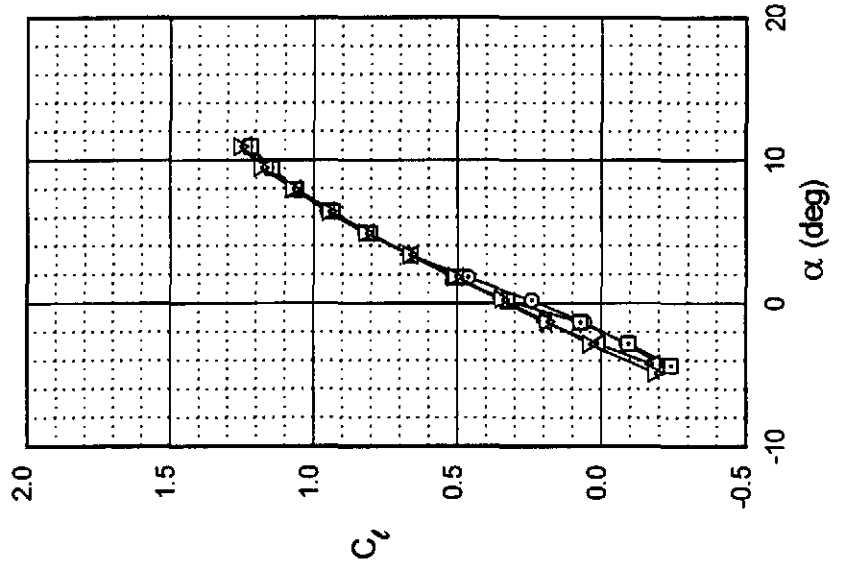
2.0
1.5
1.0
0.5
0.0
-0.5
C_l
20
10
0
-10
α (deg)

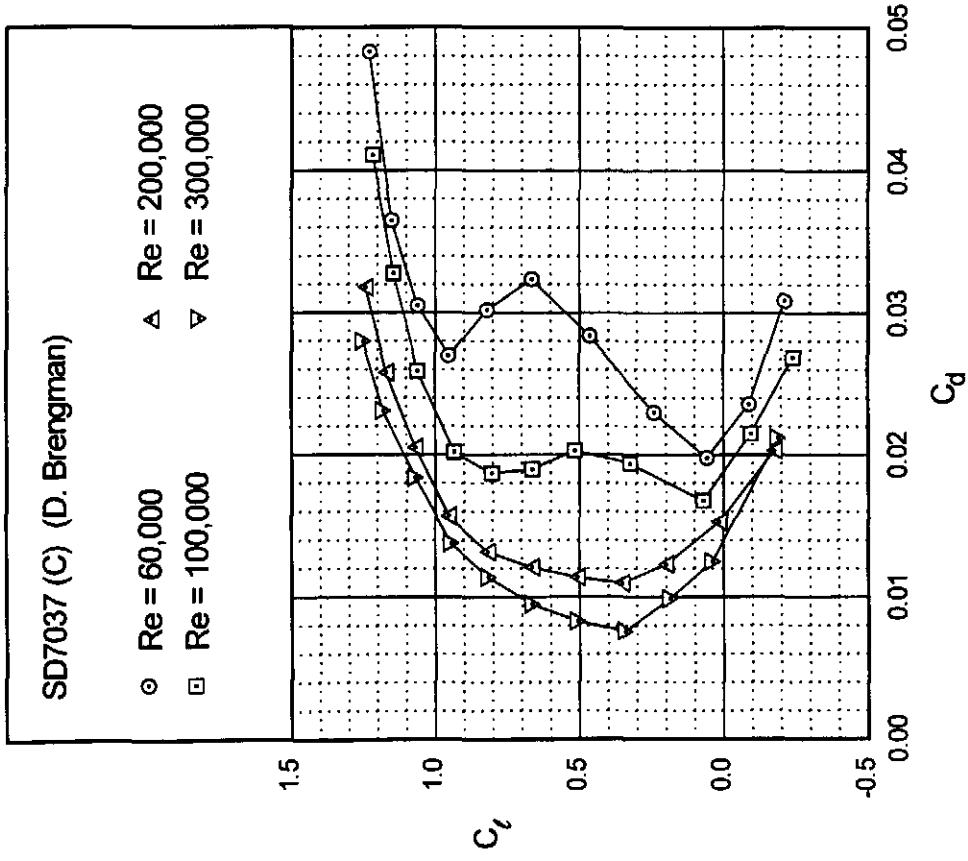
SD7037 (C) (D. Brengman)
Re = 60,000
Re = 100,000
Re = 200,000
Re = 300,000
1.5
1.0
0.5
0.0
-0.5
C_l
0.05
0.04
0.03
0.02
0.01
0.00
C_d

Fig. 5.145

SD7037 (C)

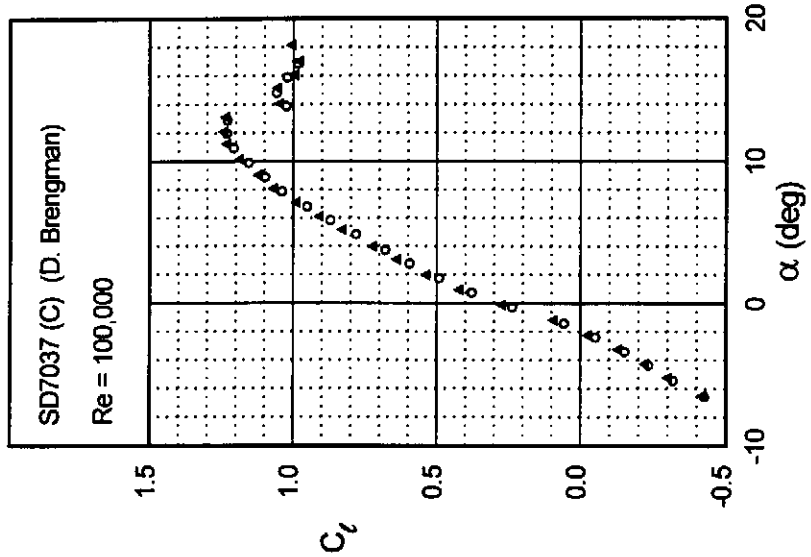

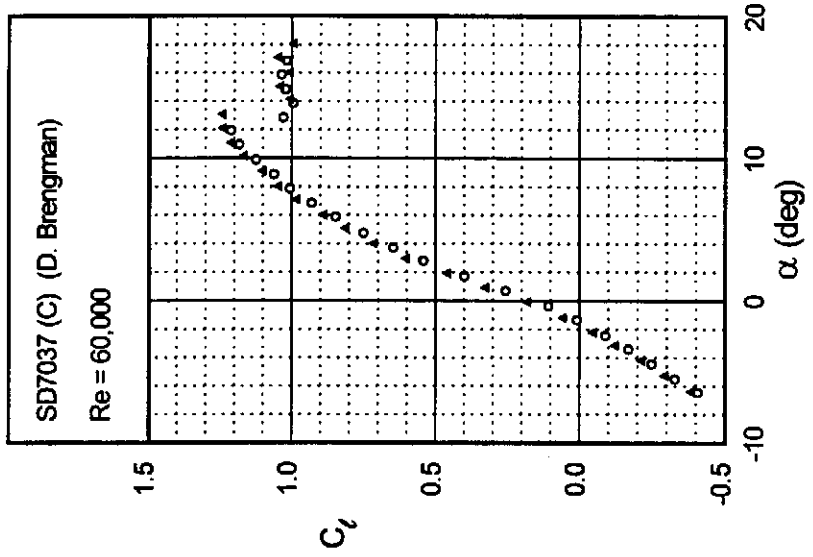

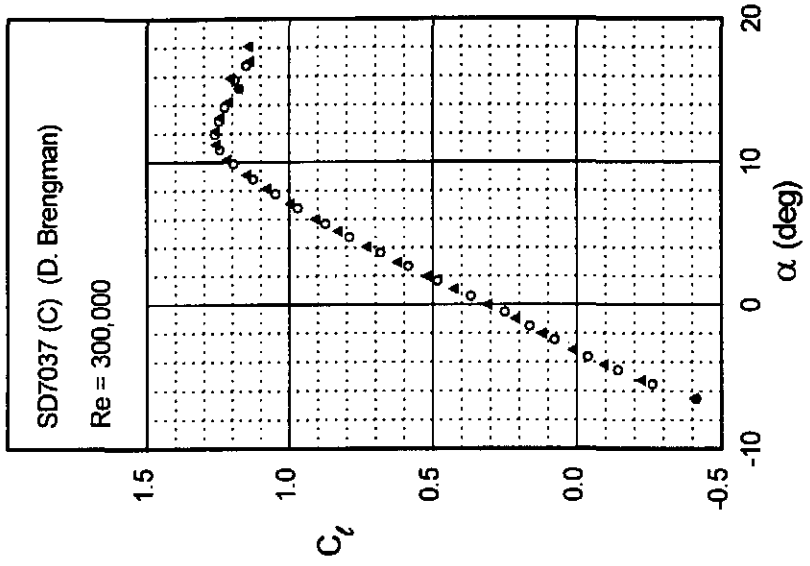
SD7037 (C) (D. Brengman)
Re = 300,000
1.5
1.0
0.5
0.0
-0.5
C_l
-10
0
10
20
α (deg)

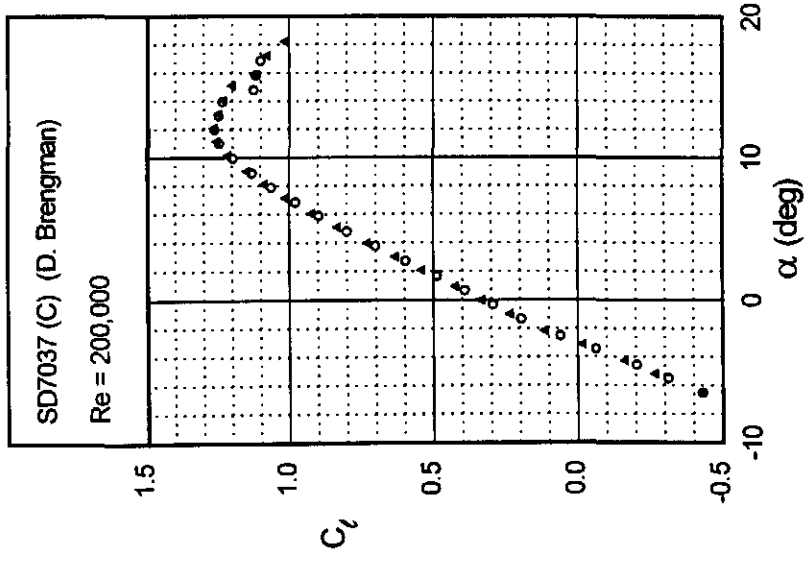
SD7037 (C) (D. Brengman)
Re = 200,000
1.5
1.0
0.5
0.0
-0.5
C_l
-10
0
10
20
α (deg)

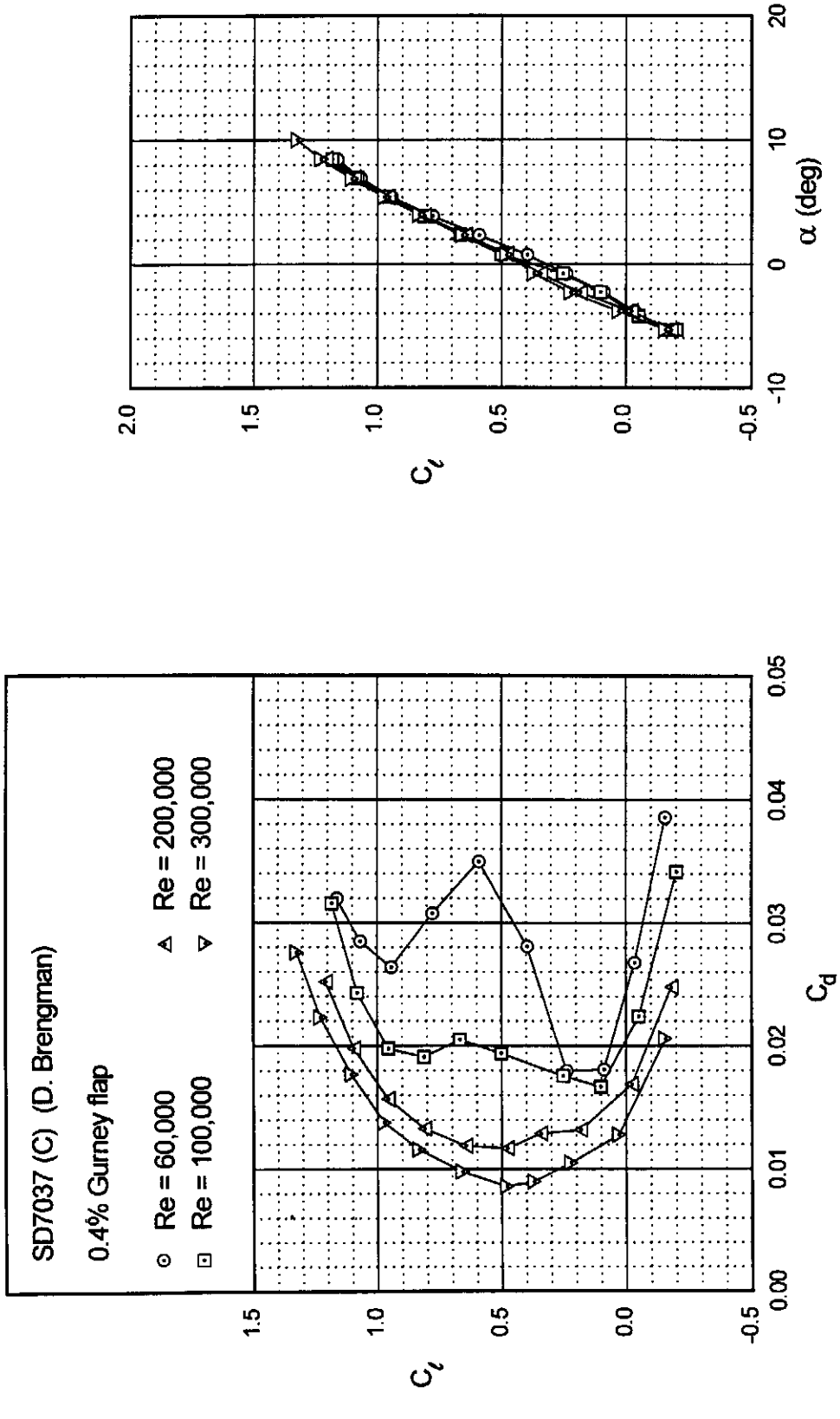
SD7037 (C) (D. Brengman)
0.4% Gurney flap
Re = 60,000
Re = 100,000
Re = 200,000
Re = 300,000
C_l
C_d
α (deg)
2.0
1.5
1.0
0.5
0.0
-0.5
20
10
0
-10
0.05
0.04
0.03
0.02
0.01
0.00

SD7037 (C)

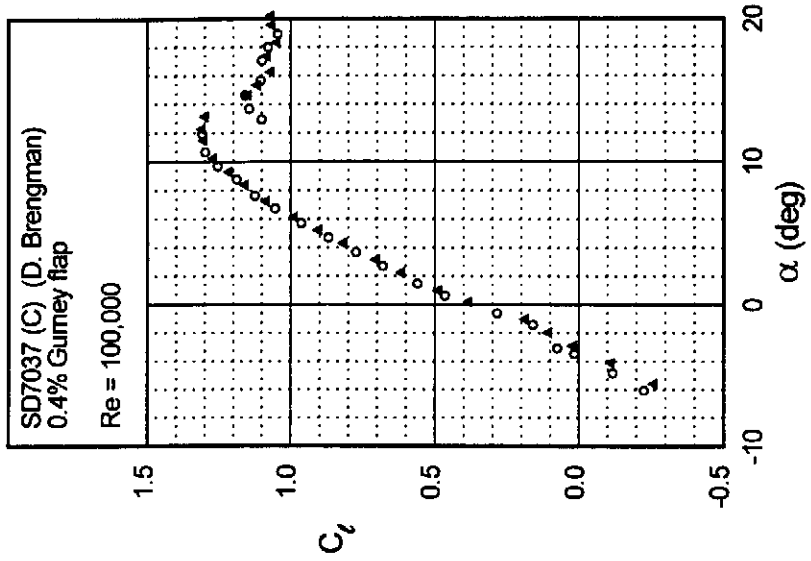
SD7037 (C) (D. Brengman)
0.4% Gurney flap
Re = 100,000
1.5
1.0
0.5
0.0
-0.5
C_l
-10
0
10
20
α (deg)

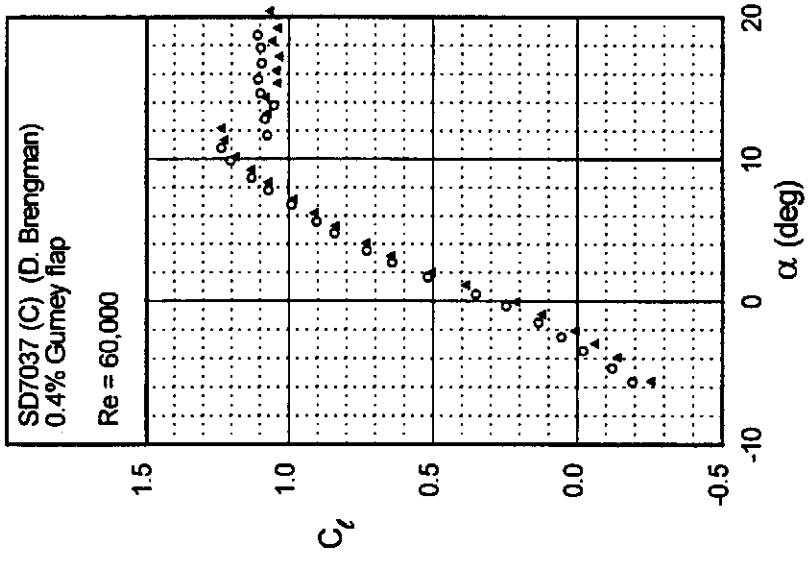
SD7037 (C) (D. Brengman)
0.4% Gurney flap
Re = 60,000
1.5
1.0
0.5
0.0
-0.5
C_l
-10
0
10
20
α (deg)

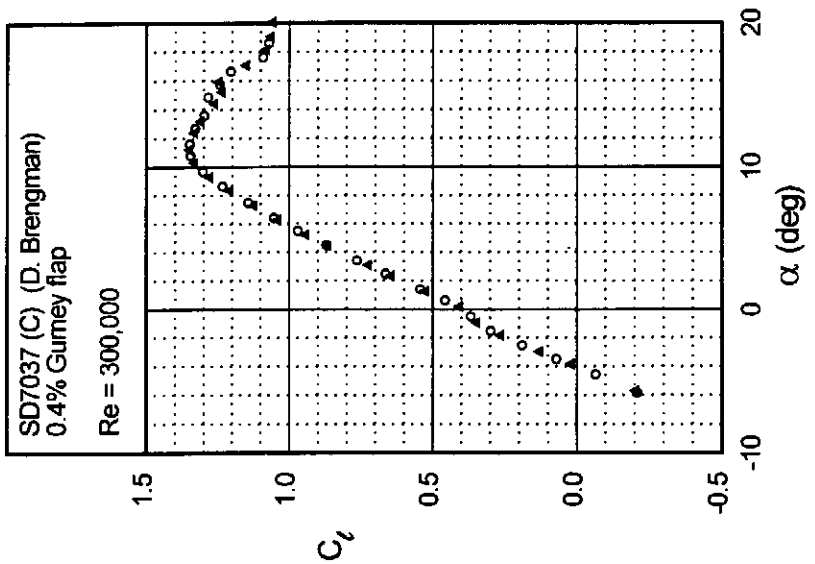
SD7037 (C) (D. Brengman)
0.4% Gurney flap
Re = 300,000
1.5
1.0
0.5
0.0
-0.5
C_l
-10
0
10
20
α (deg)

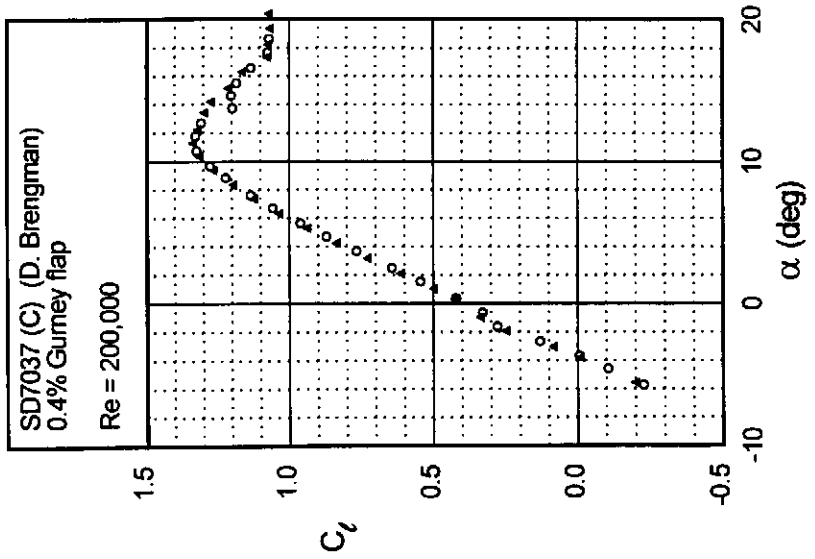
SD7037 (C) (D. Brengman)
0.4% Gurney flap
Re = 200,000
1.5
1.0
0.5
0.0
-0.5
C_l
-10
0
10
20
α (deg)

Extended Notes to the Text

n1. To extensively cover the topic of Gurney flaps would have required a chapter by itself. Instead, what is given here is a brief summary of the main points of this high-lift device. The reader will find a more detailed discussion of Gurney flaps in Ref. 23, which includes an extensive literature review, lift and drag data as well as pressure measurements on two low-speed airfoils, and a discussion of the physical mechanism associated with this kind of flap. Note that the effects of Gurney flaps on the aerodynamic characteristics of airfoils are well documented in the literature, while the physics of Gurney flaps are still not well understood.

A Gurney flap consists of a small flat plate positioned at the trailing-edge, perpendicular to the lower surface of the airfoil (e.g., Fig. 5.26). Named after former race car driver Dan S. Gurney, the Gurney flap has been and is still widely used on the wings of race cars to increase down force, improving lateral traction for increased cornering speeds.[24,25] It seems, however, that a fairly similar device has been used previously by free flight model enthusiasts in an effort to improve the glide characteristics of model airplanes.[26]

In short, a Gurney flap can provide a significant increase in lift at possibly little or no cost in drag when properly sized. The increase in lift, which provides an increase in pitching moment, is due to the increase in trailing-edge camber provided by a Gurney flap.[22] In some instances, the drag for a given lift coefficient can even be reduced. The lift-to-drag ratio and endurance parameter ($C_l^{3/2}/C_d$) can then be improved. The addition of a Gurney flap to a wing also increases the rigidity of the trailing-edge. The height of the Gurney flap is normally expressed in percentage of the airfoil chord. For example, a 1% Gurney flap means a Gurney flap with $h/c = 0.01$.

It has been proposed that to maximize the benefits of a Gurney flap when drag is a consideration, its height should be kept between 1% and 2% because beyond 2%, the drag increases noticeably.[24] A recent investigation of Gurney flaps has indicated that beneficial Gurney flaps seem to scale with boundary-layer thickness.[23] As discussed in Ref. 23, the most efficient Gurney flaps, in terms of increasing the lift-to-drag ratio, were found to have a height not greater than the boundary-layer thickness measured at the Gurney flap location on the unflapped airfoil. Optimum Gurney flap heights are then a function of the angle of attack/operating lift condition. The boundary-layer thickness on the pressure side of an airfoil decreases with increasing angle of attack, and thus optimum flap heights become smaller with an increase in the lift condition. Furthermore, the boundary-layer thickness increases in height with decreasing Reynolds number. The direct

consequence of this finding is that optimum Gurney flap heights, in term of the lift-to-drag ratio, are normally less than 1%. For fairly low operating chord Reynolds numbers, such as the ones experienced on some free flight models, longer flaps may then be found to yield optimum performance.

References

[1] Selig, M.S., Donovan, J.F. and Fraser, D.B., *Airfoils at Low Speeds*, Soartech 8, SoarTech Publications, 1504 N. Horseshoe Circle, Virginia Beach, VA, 23451, 1989.

[2] Selig, M.S., Guglielmo, J.J., Broeren, A.P. and Giguère, P., *Summary of Low-Speed Airfoil Data - Vol. 1*, SoarTech Publications, Virginia Beach, VA, 1995.

[3] Guglielmo, J.J. and Selig, M.S., "Large Spanwise Variations in Profile Drag for Airfoils at Low Reynolds Numbers," AIAA Paper 95-1783, June 1995. Accepted for publication in the *J. of Aircraft.*

[4] Guglielmo, J.J., "Spanwise Variations in Profile Drag for Airfoils at Low Reynolds Numbers," Master's Thesis, University of Illinois at Urbana-Champaign, Dept. of Aeronautical and Astronautical Engineering, 1996.

[5] Eppler, R. and Somers, D.M., "A Computer Program for the Design and Analysis of Low-Speed Airfoils, Including Transition," NASA TM 80210, August 1980.

[6] Eppler, R., *Airfoil Design and Data*, Springer-Verlag, New York, 1990.

[7] Drela, M. and Giles, M.B., "Two-Dimensional Transonic Aerodynamic Design Method," *AIAA Journal*, Vol. 25, No. 9, September 1987, pp. 1199–1206.

[8] Drela, M. and Giles, M.B., "ISES: A Two-Dimensional Viscous Aerodynamic Design and Analysis Code," AIAA Paper 87-0424, January 1987.

[9] Drela, M., "XFOIL: An Analysis and Design System for Low Reynolds Number Airfoils," *Lecture Notes in Engineering: Low Reynolds Number Aerodynamics*, T.J. Mueller (ed.), Vol. 54, Springer-Verlag, New York, June 1989.

[10] Selig, M.S. and Maughmer, M.D., "Multipoint Inverse Airfoil Design Method Based on Conformal Mapping," *AIAA J.*, Vol. 30, No. 5, May 1992, pp. 1162–1170.

[11] Selig, M.S. and Maughmer, M.D., "Generalized Multipoint Inverse Airfoil Design," *AIAA J.*, Vol. 30, No. 11, November 1992, pp. 2618–2625.

[12] Drela, M., "Low-Reynolds-Number Airfoil Design for the M.I.T. Daedalus Prototype: A Case Study," *J. of Aircraft*, Vol. 25, No. 8, Aug 1988, pp. 724–732.

[13] Evangelista, R., McGhee, R.J. and Walker, B.S., "Correlation of Theory to Wind-Tunnel Data at Reynolds Numbers Below 500,000," Lecture Notes in Engineering: Low Reynolds Number Aerodynamics, T.J. Mueller (ed.), Vol. 54, Springer-Verlag, New-York, June 1989.

[14] Evangelista, R. and Vemuru, C.S., Evaluation of an Analysis Method for Low-Speed Airfoils by Comparison with Wind Tunnel Results, AIAA 89-0266, 27th Aerospace Sciences Meeting, Reno, Nevada, January 1989.

[15] Morgan, H.L, Jr., "Computer Program for Smoothing and Scaling Airfoil Coordinates," NASA TM 84666, July 1983.

[16] Vincenti, W.G., *What Engineers Know and How They Know It, Analytical Studies from Aeronautical History*, The Johns Hopkins University Press, Baltimore, 1993.

[17] Cole, H., "HC17 Tiltwing, F1B," National Free Flight Society Twenty-Fifth Annual Report 1992.

[18] DeWitt, L, "Wakefield Model of the Year, Iconoclast," National Free Flight Society Symposium Report 1979.

[19] Boermans, L.M.M., Duyvis, F.J. Donker, Ingen, J.L. van and Timmer, W.A., "Experimental Aerodynamic Characteristics of the Airfoils LA 5055 and DU 86-084/18 at Low Reynolds Numbers," Lecture Notes in Engineering: Low Reynolds Number Aerodynamics, T.J. Mueller (ed.), Vol. 54, Springer-Verlag, New-York, June 1989.

[20] Tangler, J.L. and Somers, D.M., "NREL Airfoil Families for HAWTs," AWEA WINDPOWER Conference, Washington, DC, March 1995.

[21] Kerho, K. and Bragg, M., "Effect of Large Distributed Leading-Edge Roughness on Boundary Layer Development and Transition," AIAA Paper 95-1803, June 1995.

[22] Neuhart, D.H. and Pendergraft, O.C. Jr., "A Water Tunnel Study of Gurney Flaps," NASA TM 4071, November 1988.

[23] Giguère, P., Lemay, J. and Dumas, G., "Gurney flap Effects and Scaling for Low-Speed Airfoils," AIAA Paper 95-1881, June 1995.

[24] Liebeck, R.H., "Design of Subsonic Airfoils for High-Lift," Journal of Aircraft, Vol. 15, No. 9, September 1978, pp. 547-561.

[25] Katz, J., *Race Car Aerodynamics*, Robert Bentley Publishers, Cambridge, MA, 1995.

[26] Gieskieng, B. Jr., "Indoor H.L. Glider Section," Model Aeronautic Year Book, Frank Zaic (ed.), 1964–1965.

Appendix A

Airfoil Coordinates

This appendix lists the airfoil coordinates. For any given airfoil, the true airfoil coordinates, if provided, are listed first. If the original coordinates were not 'mathematically' smooth or if there were too few points defining the airfoil (especially in the vicinity of the leading and trailing edges), the airfoil coordinates were smoothed with the program AFSMO[15] developed at NASA Langley. For the Davis 3R and CR-001 airfoils, the smoothed coordinates were determined by smoothing the actual coordinates. As to be expected in these cases, the average difference between the smoothed airfoil and actual airfoil seen in the profile plots in Chapter 5 is quite small ($\sim$0.003 in) and is due to the model surface waviness and measurement error. Only the actual wind-tunnel model coordinates are listed for the LD-79 since no original coordinates were available and since the actual coordinates could not be smoothed because of the sharp leading edge. Following the true coordinates and (if generated) smoothed coordinates, the actual wind-tunnel model coordinates are given. Finally, coordinates for the NREL S822 and S823 airfoils designed by D.M. Somers (Airfoils, Inc.) can be acquired from NREL under a licensing agreement.

CR-001
smoothed model

x/c	y/c
1.00000	-0.00001
0.99754	0.00091
0.99070	0.00289
0.98037	0.00531
0.96698	0.00833
0.95044	0.01199
0.93064	0.01619
0.90775	0.02074
0.88202	0.02558
0.85370	0.03061
0.82309	0.03573
0.79048	0.04085
0.75616	0.04586
0.72043	0.05066
0.68359	0.05518
0.64594	0.05935
0.60778	0.06310
0.56937	0.06639
0.53099	0.06918
0.49265	0.07145
0.45435	0.07317
0.41638	0.07429
0.37887	0.07477
0.34204	0.07456
0.30609	0.07364
0.27120	0.07200
0.23760	0.06968
0.20549	0.06673
0.17504	0.06318
0.14648	0.05904
0.11999	0.05431
0.09576	0.04900
0.07395	0.04314
0.05468	0.03682
0.03811	0.03018
0.02433	0.02336
0.01338	0.01648
0.00548	0.00980
0.00098	0.00373
0.00000	-0.00008
0.00098	-0.00330
0.00548	-0.00651
0.01338	-0.00827
0.02433	-0.00929
0.03811	-0.00989
0.05468	-0.01015
0.07395	-0.01007
0.09576	-0.00965
0.11999	-0.00891
0.14648	-0.00788
0.17504	-0.00656
0.20549	-0.00499
0.23760	-0.00323
0.27120	-0.00133
0.30609	0.00064
0.34204	0.00261
0.37887	0.00453
0.41638	0.00635
0.45435	0.00800
0.49265	0.00948
0.53099	0.01074
0.56937	0.01176
0.60778	0.01250
0.64594	0.01295
0.68359	0.01311
0.72043	0.01296
0.75616	0.01249
0.79048	0.01172
0.82309	0.01068
0.85370	0.00941
0.88202	0.00797
0.90775	0.00643
0.93064	0.00490
0.95044	0.00348
0.96698	0.00226
0.98037	0.00129
0.99070	0.00058
0.99754	0.00014
1.00000	-0.00002

CR-001
actual model

x/c	y/c
1.00000	-0.00045
0.99795	0.00021
0.99318	0.00129
0.98754	0.00264
0.98253	0.00367
0.96322	0.00811
0.94764	0.01151
0.93598	0.01407
0.92205	0.01692
0.90964	0.01935
0.89318	0.02249
0.87388	0.02613
0.84711	0.03078
0.81581	0.03599
0.77400	0.04246
0.73316	0.04819
0.64636	0.05862
0.56527	0.06615
0.48040	0.07160
0.39679	0.07427
0.35843	0.07443
0.31573	0.07370
0.27069	0.07170
0.23403	0.06913
0.20613	0.06657
0.18216	0.06389
0.14478	0.05857
0.08585	0.04627
0.03258	0.02789
0.00134	0.00374
0.00031	-0.00179
0.00143	-0.00384
0.00280	-0.00506
0.00684	-0.00683
0.01144	-0.00779
0.01566	-0.00836
0.01813	-0.00858
0.03733	-0.00970
0.06680	-0.01024
0.17925	-0.00708
0.28778	-0.00077
0.40535	0.00614
0.57454	0.01231
0.73887	0.01292
0.86001	0.00925
0.90681	0.00662
0.96114	0.00236
0.99435	-0.00021
1.00000	-0.00045

Davis 3R
smoothed model

x/c	y/c
1.00000	0.00588
0.99754	0.00719
0.99070	0.01009
0.98037	0.01307
0.96698	0.01585
0.95044	0.01919
0.93064	0.02337
0.90775	0.02831
0.88202	0.03384
0.85370	0.03980
0.82309	0.04598
0.79048	0.05217
0.75616	0.05819
0.72043	0.06387
0.68359	0.06908
0.64594	0.07373
0.60778	0.07774
0.56937	0.08107
0.53099	0.08369
0.49265	0.08559
0.45435	0.08675
0.41638	0.08712
0.37887	0.08671
0.34204	0.08547
0.30609	0.08342
0.27120	0.08053
0.23760	0.07682
0.20549	0.07230
0.17504	0.06696
0.14648	0.06085
0.11999	0.05408
0.09576	0.04697
0.07395	0.04001
0.05468	0.03359
0.03811	0.02757
0.02433	0.02159
0.01338	0.01552
0.00548	0.00957
0.00098	0.00384
0.00000	-0.00003
0.00098	-0.00354
0.00548	-0.00727
0.01338	-0.00901
0.02433	-0.00845
0.03811	-0.00648
0.05468	-0.00385
0.07395	-0.00091
0.09576	0.00220
0.11999	0.00545
0.14648	0.00879
0.17504	0.01218
0.20549	0.01557
0.23760	0.01884
0.27120	0.02191
0.30609	0.02468
0.34204	0.02707
0.37887	0.02901
0.41638	0.03047
0.45435	0.03140
0.49265	0.03181
0.53099	0.03168
0.56937	0.03104
0.60778	0.02987
0.64594	0.02822
0.68359	0.02613
0.72043	0.02364
0.75616	0.02082
0.79048	0.01776
0.82309	0.01453
0.85370	0.01124
0.88202	0.00798
0.90775	0.00486
0.93064	0.00191
0.95044	-0.00086
0.96698	-0.00339
0.98037	-0.00530
0.99070	-0.00620
0.99754	-0.00612
1.00000	-0.00590

Davis 3R
actual model

x/c	y/c
1.00000	0.00579
0.99981	0.00678
0.99506	0.00863
0.99254	0.00910
0.98861	0.01022
0.98264	0.01145
0.97624	0.01291
0.97030	0.01447
0.96429	0.01580
0.95228	0.01846
0.94044	0.02083
0.92587	0.02399
0.89973	0.02977
0.85282	0.03945
0.82380	0.04520
0.79001	0.05156
0.72521	0.06272
0.65321	0.07253
0.60214	0.07785
0.53903	0.08264
0.47525	0.08580
0.41730	0.08680
0.35623	0.08585
0.31276	0.08345
0.26555	0.07968
0.23381	0.07599
0.19871	0.07103
0.17190	0.06626
0.14588	0.06063
0.12921	0.05638
0.11074	0.05116
0.09555	0.04659
0.08161	0.04219
0.06806	0.03772

0.05904	0.03472
0.04956	0.03149
0.03770	0.02717
0.02829	0.02326
0.02067	0.01956
0.01401	0.01573
0.00838	0.01070
0.00754	0.00974
0.00000	0.00000
0.00314	-0.00617
0.00552	-0.00818
0.00924	-0.00902
0.01467	-0.00932
0.01965	-0.00905
0.02494	-0.00852
0.03492	-0.00714
0.04629	-0.00534
0.06136	-0.00306
0.07726	-0.00068
0.08978	0.00103
0.10168	0.00267
0.13921	0.00770
0.16057	0.01027
0.18711	0.01319
0.21491	0.01607
0.24883	0.01935
0.31012	0.02484
0.37457	0.02887
0.43761	0.03115
0.49945	0.03170
0.56334	0.03123
0.62641	0.02906
0.68822	0.02562
0.74825	0.02137
0.81174	0.01557
0.84575	0.01202
0.87931	0.00823
0.91108	0.00437
0.92630	0.00221
0.93901	0.00083
0.95407	-0.00114
0.96752	-0.00297
0.97894	-0.00458
0.98533	-0.00533
0.99075	-0.00606
0.99525	-0.00673
0.99927	-0.00679
1.00000	-0.00574

DU 86-084/18

x/c	y/c
1.00000	0.00000
0.99882	0.00014
0.99537	0.00058
0.98990	0.00119
0.98235	0.00178
0.97260	0.00240
0.96064	0.00315
0.94653	0.00408
0.93035	0.00530
0.91222	0.00684
0.89230	0.00877
0.87068	0.01098
0.84721	0.01342
0.82178	0.01677
0.79567	0.02203
0.77033	0.02796
0.74534	0.03265
0.71959	0.03627
0.69280	0.03929
0.66515	0.04192
0.63676	0.04423
0.60777	0.04626
0.57829	0.04801
0.54846	0.04950
0.51838	0.05075
0.48819	0.05175
0.45800	0.05250
0.42794	0.05301
0.39813	0.05328
0.36869	0.05329
0.33973	0.05306
0.31136	0.05257
0.28370	0.05183
0.25684	0.05085
0.23089	0.04962
0.20596	0.04815
0.18213	0.04645
0.15951	0.04452
0.13818	0.04235
0.11822	0.03995
0.09968	0.03730
0.08261	0.03442
0.06707	0.03133
0.05308	0.02804
0.04069	0.02459
0.02993	0.02100
0.02081	0.01729
0.01335	0.01353
0.00755	0.00971
0.00334	0.00595
0.00075	0.00252
0.00003	-0.00047
0.00157	-0.00310
0.00525	-0.00577
0.01083	-0.00852
0.01833	-0.01117
0.02763	-0.01377
0.03871	-0.01624
0.05154	-0.01857
0.06607	-0.02073
0.08226	-0.02270
0.10006	-0.02447
0.11942	-0.02604
0.14028	-0.02740
0.16256	-0.02855
0.18619	-0.02950
0.21109	-0.03024
0.23716	-0.03080
0.26431	-0.03117
0.29244	-0.03138
0.32144	-0.03144
0.35118	-0.03136
0.38154	-0.03115
0.41241	-0.03082
0.44366	-0.03038
0.47514	-0.02986
0.50673	-0.02926
0.53829	-0.02860
0.56967	-0.02786
0.60072	-0.02706
0.63131	-0.02620
0.66131	-0.02526
0.69058	-0.02422
0.71897	-0.02309
0.74639	-0.02181
0.77270	-0.02039
0.79780	-0.01873
0.82155	-0.01672
0.84412	-0.01415
0.86587	-0.01104
0.88688	-0.00800
0.90687	-0.00539
0.92550	-0.00332
0.94247	-0.00179
0.95751	-0.00081
0.97041	-0.00029
0.98104	-0.00002
0.98934	0.00004
0.99528	0.00003
0.99879	0.00001
1.00000	0.00000

DU 86-084/18
actual model

x/c	y/c
1.00000	-0.00020
0.99977	0.00117
0.99717	0.00179
0.99325	0.00218
0.99055	0.00240
0.98560	0.00273
0.97505	0.00330
0.96270	0.00381
0.95062	0.00427
0.93135	0.00533
0.90899	0.00707
0.86853	0.01109
0.82684	0.01735
0.74294	0.03401
0.65841	0.04501
0.57683	0.05174
0.48759	0.05608
0.41036	0.05739
0.36819	0.05742
0.32470	0.05682
0.28482	0.05558
0.24594	0.05367
0.21946	0.05195
0.19869	0.05038
0.18003	0.04873
0.15893	0.04653
0.14690	0.04512
0.08957	0.03640
0.05499	0.02836
0.02442	0.01745
0.00208	0.00359
0.00117	-0.00267
0.00166	-0.00318
0.00288	-0.00510
0.00442	-0.00655
0.01167	-0.01039
0.01812	-0.01265
0.02452	-0.01430
0.03044	-0.01558
0.03748	-0.01691
0.04730	-0.01855
0.05664	-0.01992
0.06666	-0.02119
0.07606	-0.02220
0.09416	-0.02382
0.11975	-0.02561
0.15343	-0.02727
0.18629	-0.02826
0.22549	-0.02878
0.28654	-0.02882
0.36869	-0.02768
0.45525	-0.02571
0.54238	-0.02409
0.62163	-0.02272
0.70439	-0.02097
0.79055	-0.01753
0.83179	-0.01415
0.87295	-0.00917
0.91199	-0.00465
0.92399	-0.00355
0.93423	-0.00281
0.94623	-0.00213
0.95427	-0.00171
0.96544	-0.00151
0.97935	-0.00150
0.98803	-0.00155
0.99317	-0.00155
0.99565	-0.00149
0.99987	-0.00117
1.00000	-0.00020

E374

x/c	y/c
1.00000	0.00000
0.99640	0.00045
0.98610	0.00204
0.97000	0.00485
0.94864	0.00846
0.92214	0.01264
0.89078	0.01747
0.85508	0.02297
0.81560	0.02905
0.77293	0.03560
0.72769	0.04246
0.68053	0.04944
0.63210	0.05629
0.58309	0.06269
0.53398	0.06821
0.48511	0.07252
0.43682	0.07544
0.38939	0.07685
0.34312	0.07670
0.29824	0.07507
0.25510	0.07217
0.21415	0.06817
0.17583	0.06319
0.14053	0.05734
0.10860	0.05073
0.08036	0.04351
0.05605	0.03581
0.03589	0.02781

0.02004	0.01973
0.00862	0.01186
0.00178	0.00459
0.00014	-0.00121
0.00437	-0.00622
0.01427	-0.01130
0.02935	-0.01600
0.04949	-0.02015
0.07454	-0.02369
0.10428	-0.02660
0.13845	-0.02890
0.17669	-0.03060
0.21861	-0.03175
0.26374	-0.03238
0.31158	-0.03255
0.36159	-0.03228
0.41320	-0.03163
0.46580	-0.03064
0.51877	-0.02931
0.57150	-0.02767
0.62336	-0.02569
0.67382	-0.02333
0.72243	-0.02059
0.76873	-0.01760
0.81228	-0.01450
0.85254	-0.01153
0.88892	-0.00882
0.92085	-0.00643
0.94783	-0.00432
0.96958	-0.00241
0.98594	-0.00091
0.99637	-0.00016
1.00000	0.00000

E374 (B)
actual model

x/c	y/c
1.00000	-0.00002
0.99931	0.00133
0.99547	0.00193
0.99075	0.00259
0.98553	0.00323
0.97942	0.00403
0.97449	0.00478
0.96606	0.00620
0.95897	0.00737
0.95051	0.00873
0.94089	0.01035
0.92731	0.01261
0.91006	0.01542
0.88922	0.01879
0.87081	0.02175
0.84125	0.02638
0.80842	0.03160
0.76422	0.03834
0.72768	0.04383
0.66531	0.05294
0.60199	0.06157
0.54234	0.06862
0.41405	0.07751
0.34811	0.07769
0.28951	0.07547
0.22319	0.07015
0.17954	0.06464
0.14136	0.05815
0.11425	0.05246
0.09448	0.04762
0.08072	0.04382
0.06739	0.03970
0.05486	0.03534
0.04468	0.03137
0.03449	0.02693
0.02480	0.02219
0.01653	0.01759
0.00821	0.01213
0.00459	0.00912
0.00059	0.00354
0.00003	0.00062
0.00177	-0.00446
0.00544	-0.00769
0.00958	-0.01000
0.01319	-0.01157
0.02096	-0.01420
0.03009	-0.01668
0.03948	-0.01882
0.05464	-0.02171
0.06817	-0.02379
0.08950	-0.02626
0.10662	-0.02784
0.13833	-0.02995
0.16421	-0.03111
0.19316	-0.03200
0.23635	-0.03279
0.29760	-0.03315
0.35915	-0.03278
0.42077	-0.03187
0.48279	-0.03053
0.54271	-0.02895
0.60527	-0.02673
0.66857	-0.02379
0.73107	-0.02022
0.77240	-0.01746
0.81508	-0.01434
0.85142	-0.01141
0.87900	-0.00911
0.89676	-0.00765
0.91943	-0.00589
0.93686	-0.00452
0.95206	-0.00329
0.96402	-0.00250
0.97295	-0.00191
0.98200	-0.00151
0.99124	-0.00145
0.99865	-0.00133
1.00000	-0.00002

E423

x/c	y/c
1.00000	0.00000
0.99655	0.00159
0.98706	0.00650
0.97304	0.01434
0.95530	0.02381
0.93358	0.03376
0.90734	0.04400
0.87671	0.05481
0.84221	0.06620
0.80436	0.07803
0.76373	0.09010
0.72090	0.10215
0.67644	0.11391
0.63092	0.12506
0.58491	0.13524
0.53893	0.14410
0.49347	0.15116
0.44870	0.15593
0.40464	0.15828
0.36149	0.15824
0.31947	0.15590
0.27885	0.15138
0.23987	0.14485
0.20286	0.13657
0.16816	0.12676
0.13611	0.11562
0.10700	0.10337
0.08106	0.09023
0.05852	0.07646
0.03953	0.06232
0.02421	0.04812
0.01262	0.03419
0.00481	0.02093
0.00071	0.00879
0.00002	0.00088
0.00033	-0.00192
0.00071	-0.00362
0.00125	-0.00518
0.00157	-0.00590
0.00194	-0.00656
0.00237	-0.00717
0.00288	-0.00771
0.00348	-0.00823
0.00415	-0.00874
0.00571	-0.00969
0.00751	-0.01057
0.01065	-0.01177
0.01365	-0.01266
0.02892	-0.01485
0.04947	-0.01482
0.07533	-0.01236
0.10670	-0.00740
0.14385	-0.00002
0.18727	0.00922
0.23688	0.01913
0.29196	0.02865
0.35163	0.03687
0.41449	0.04283
0.47867	0.04626
0.54275	0.04760
0.60579	0.04715
0.66690	0.04501
0.72503	0.04126
0.77912	0.03625
0.82836	0.03050
0.87219	0.02444
0.91012	0.01844
0.94179	0.01286
0.96692	0.00794
0.98519	0.00390
0.99629	0.00106
1.00000	0.00000

E423
actual model

x/c	y/c
1.00000	-0.00043
0.99948	0.00041
0.99442	0.00451
0.98959	0.00803
0.98287	0.01250
0.97781	0.01547
0.97157	0.01883
0.96401	0.02263
0.94641	0.03039
0.92547	0.03889
0.90399	0.04678
0.88916	0.05193
0.86447	0.05998
0.84439	0.06633
0.82456	0.07250
0.80871	0.07729
0.79400	0.08157
0.76504	0.09000
0.74663	0.09515
0.72506	0.10099
0.70556	0.10600
0.66881	0.11493
0.61630	0.12652
0.58157	0.13360
0.54219	0.14066
0.48881	0.14881
0.44025	0.15356
0.39237	0.15517
0.34094	0.15439
0.29143	0.14968
0.23723	0.14057
0.19484	0.13085
0.16547	0.12223
0.15289	0.11809
0.14066	0.11360
0.12832	0.10873
0.11212	0.10159
0.09939	0.09542
0.08562	0.08815
0.07379	0.08138
0.05777	0.07108
0.04822	0.06423
0.03793	0.05599
0.02786	0.04694
0.01851	0.03749
0.00993	0.02674
0.00609	0.02048
0.00174	0.01020
0.00080	0.00639
0.00022	0.00334
0.00050	-0.00573
0.00113	-0.00780
0.00289	-0.01047
0.00951	-0.01510
0.02037	-0.01741
0.03284	-0.01838
0.04421	-0.01853
0.06718	-0.01736
0.08836	-0.01493
0.10945	-0.01187
0.13137	-0.00827

0.15498	-0.00390
0.18871	0.00272
0.22305	0.00949
0.25703	0.01598
0.29052	0.02148
0.31940	0.02611
0.34759	0.03032
0.38602	0.03499
0.42539	0.03798
0.46338	0.04061
0.51036	0.04248
0.55069	0.04262
0.59347	0.04281
0.63559	0.04228
0.68006	0.04051
0.71793	0.03823
0.74532	0.03638
0.77525	0.03377
0.82332	0.02855
0.84718	0.02514
0.86215	0.02325
0.87304	0.02177
0.88531	0.01978
0.89329	0.01821
0.90502	0.01608
0.91524	0.01424
0.92249	0.01293
0.93220	0.01115
0.94525	0.00881
0.95433	0.00723
0.96572	0.00532
0.97544	0.00369
0.98168	0.00259
0.99005	0.00095
0.99996	-0.00041
1.00000	-0.00043

LD-79

actual model

x/c	y/c
0.99999	-0.00179
0.99974	0.00596
0.99076	0.00752
0.98256	0.00831
0.97070	0.00921
0.95698	0.01059
0.93462	0.01176
0.91285	0.01294
0.89112	0.01491
0.85985	0.01728
0.82891	0.01934
0.79502	0.02123
0.73472	0.02936
0.67171	0.03593
0.61002	0.04234
0.54984	0.04817
0.48783	0.05407
0.42679	0.05922
0.36461	0.06325
0.30582	0.06613
0.24301	0.06726
0.20432	0.06609
0.17720	0.06401
0.15010	0.06082
0.13077	0.05777
0.11593	0.05498
0.09724	0.05059
0.08754	0.04773
0.07946	0.04499
0.07013	0.04130
0.06088	0.03684
0.05350	0.03234
0.05024	0.02761
0.04566	0.02419
0.03667	0.02030
0.02815	0.01652
0.01986	0.01268
0.01350	0.00967
0.00000	0.00000
0.00590	0.00008
0.01215	0.00255
0.02163	0.00622
0.02884	0.00902
0.03583	0.01176
0.04491	0.01520
0.05812	0.01881
0.07292	0.01864
0.08925	0.01829
0.10439	0.01804
0.12385	0.01767
0.14747	0.01718
0.17261	0.01660
0.19977	0.01597
0.22878	0.01526
0.26280	0.01452
0.32484	0.01280
0.39562	0.01108
0.45314	0.00959
0.58133	0.00641
0.64011	0.00488
0.70217	0.00337
0.74892	0.00206
0.77196	0.00184
0.80650	0.00143
0.83856	0.00087
0.87191	0.00016
0.88604	-0.00030
0.89884	-0.00056
0.91450	-0.00124
0.92919	-0.00150
0.94092	-0.00218
0.94979	-0.00271
0.95721	-0.00343
0.96431	-0.00395
0.97207	-0.00448
0.97831	-0.00498
0.98866	-0.00566
1.00026	-0.00596
0.99999	-0.00179

M06-13-128

x/c	y/c
1.00000	0.00000
0.99896	0.00015
0.99152	0.00088
0.97756	0.00198
0.95718	0.00370
0.93068	0.00631
0.89849	0.01002
0.86112	0.01499
0.81923	0.02139
0.77354	0.02930
0.72493	0.03878
0.67434	0.04980
0.62288	0.06225
0.57180	0.07584
0.52265	0.09002
0.47756	0.10309
0.43510	0.11094
0.39263	0.11489
0.35032	0.11617
0.30873	0.11531
0.26838	0.11256
0.22975	0.10814
0.19328	0.10220
0.15942	0.09487
0.12857	0.08605
0.10057	0.07583
0.07558	0.06460
0.05382	0.05305
0.03551	0.04122
0.02083	0.02960
0.00994	0.01862
0.00296	0.00878
0.00098	0.00452
0.00005	0.00087
0.00030	-0.00183
0.00233	-0.00372
0.01203	-0.00669
0.02803	-0.00901
0.04987	-0.01077
0.07718	-0.01203
0.10959	-0.01287
0.14667	-0.01333
0.18796	-0.01349
0.23296	-0.01339
0.28111	-0.01308
0.33185	-0.01260
0.38456	-0.01200
0.43862	-0.01129
0.49338	-0.01053
0.54820	-0.00972
0.60242	-0.00890
0.65541	-0.00809
0.70652	-0.00729
0.75516	-0.00652
0.80073	-0.00577
0.84269	-0.00506
0.88053	-0.00437
0.91379	-0.00370
0.94205	-0.00302
0.96496	-0.00228
0.98232	-0.00147
0.99393	-0.00073
0.99942	-0.00014
1.00000	0.00000

M06-13-128 (B)

actual model

x/c	y/c
1.00000	0.00013
0.99991	0.00090
0.99740	0.00124
0.99257	0.00149
0.98566	0.00162
0.97902	0.00196
0.96956	0.00242
0.96139	0.00305
0.95256	0.00383
0.94342	0.00472
0.93006	0.00616
0.91687	0.00765
0.90392	0.00925
0.88712	0.01146
0.86530	0.01451
0.84546	0.01744
0.81718	0.02197
0.78112	0.02819
0.74243	0.03529
0.69893	0.04428
0.64065	0.05777
0.58100	0.07280
0.51924	0.09047
0.46121	0.10537
0.39966	0.11277
0.32971	0.11417
0.26768	0.11073
0.20710	0.10258
0.17032	0.09508
0.14567	0.08875
0.12535	0.08252
0.10647	0.07575
0.08239	0.06552
0.06396	0.05623
0.05228	0.04960
0.03982	0.04178
0.03050	0.03527
0.02092	0.02762
0.01126	0.01820
0.00491	0.01044
0.00032	0.00263
0.00347	-0.00885
0.00859	-0.01029
0.01784	-0.01219
0.03226	-0.01399
0.05462	-0.01559
0.08276	-0.01664
0.11168	-0.01712
0.16316	-0.01750
0.22105	-0.01733
0.27285	-0.01695
0.33585	-0.01621
0.39924	-0.01526
0.46002	-0.01418
0.52606	-0.01287
0.58351	-0.01167
0.64698	-0.01036
0.70823	-0.00913
0.74706	-0.00844
0.78928	-0.00765
0.82743	-0.00701
0.85713	-0.00651
0.89265	-0.00579
0.91175	-0.00536
0.93322	-0.00478
0.94441	-0.00440
0.95421	-0.00399

0.96515	-0.00344
0.97685	-0.00279
0.98503	-0.00227
0.99239	-0.00166
0.99927	-0.00090
1.00000	0.00013

M6 (65%)

x/c	y/c
1.00000	0.00000
0.95000	0.00520
0.90000	0.01008
0.80000	0.01989
0.70000	0.02977
0.60000	0.03920
0.50000	0.04719
0.40000	0.05233
0.30000	0.05343
0.25000	0.05207
0.20000	0.04907
0.15000	0.04433
0.10000	0.03711
0.07500	0.03211
0.05000	0.02620
0.02500	0.01826
0.01250	0.01280
0.01000	0.01144
0.00600	0.00891
0.00400	0.00734
0.00200	0.00488
0.00000	0.00000
0.00250	-0.00618
0.00500	-0.00800
0.00750	-0.00962
0.01000	-0.01053
0.01250	-0.01144
0.02500	-0.01430
0.05000	-0.01774
0.07500	-0.01970
0.10000	-0.02106
0.15000	-0.02255
0.20000	-0.02353
0.25000	-0.02411
0.30000	-0.02464
0.40000	-0.02535
0.50000	-0.02561
0.60000	-0.02483
0.70000	-0.02262
0.80000	-0.01839
0.90000	-0.01151
0.95000	-0.00702
1.00000	0.00000

M6 (65%)
actual model

x/c	y/c
1.00000	0.00190
0.99982	0.00084
0.99663	0.00165
0.99280	0.00225
0.98855	0.00273
0.98212	0.00338
0.97715	0.00389
0.96878	0.00475
0.95545	0.00602
0.94611	0.00683
0.92632	0.00859
0.90365	0.01067
0.86154	0.01445
0.81998	0.01823
0.73830	0.02583
0.65316	0.03393
0.57053	0.04122
0.48781	0.04740
0.40306	0.05175
0.36193	0.05292
0.31648	0.05372
0.28351	0.05378
0.24081	0.05299
0.22427	0.05227
0.19739	0.05062
0.17812	0.04907
0.15751	0.04705
0.14499	0.04565
0.13012	0.04382
0.11502	0.04173
0.10258	0.03978
0.08682	0.03703
0.07209	0.03417
0.06038	0.03164
0.05047	0.02924
0.03747	0.02575
0.02979	0.02334
0.02607	0.02205
0.02072	0.01992
0.01704	0.01822
0.01218	0.01548
0.00904	0.01324
0.00592	0.01071
0.00323	0.00787
0.00061	0.00315
0.00019	0.00173
0.00204	-0.00580
0.00356	-0.00742
0.00627	-0.00953
0.01039	-0.01156
0.01554	-0.01328
0.02261	-0.01492
0.02686	-0.01562
0.03569	-0.01673
0.04431	-0.01760
0.05417	-0.01850
0.06689	-0.01956
0.08861	-0.02100
0.11819	-0.02261
0.14666	-0.02383
0.18032	-0.02449
0.22336	-0.02498
0.28579	-0.02577
0.36746	-0.02653
0.45273	-0.02692
0.53784	-0.02687
0.61883	-0.02629
0.70235	-0.02444
0.78815	-0.01996
0.82782	-0.01705
0.86969	-0.01349
0.91000	-0.00985
0.93243	-0.00778
0.94554	-0.00666
0.95307	-0.00595
0.96303	-0.00503
0.97365	-0.00402
0.98473	-0.00291
0.98937	-0.00237
0.99380	-0.00176
0.99911	-0.00084
1.00000	0.00190

M6 (85%)

x/c	y/c
1.00000	0.00000
0.95000	0.00680
0.90000	0.01318
0.80000	0.02601
0.70000	0.03893
0.60000	0.05125
0.50000	0.06171
0.40000	0.06842
0.30000	0.06987
0.25000	0.06808
0.20000	0.06418
0.15000	0.05797
0.10000	0.04853
0.07500	0.04199
0.05000	0.03426
0.02500	0.02388
0.01250	0.01674
0.01000	0.01496
0.00600	0.01165
0.00400	0.00960
0.00200	0.00638
0.00000	0.00000
0.00250	-0.00808
0.00500	-0.01046
0.00750	-0.01258
0.01000	-0.01377
0.01250	-0.01496
0.02500	-0.01870
0.05000	-0.02321
0.07500	-0.02576
0.10000	-0.02754
0.15000	-0.02950
0.20000	-0.03077
0.25000	-0.03154
0.30000	-0.03221
0.40000	-0.03315
0.50000	-0.03349
0.60000	-0.03247
0.70000	-0.02958
0.80000	-0.02405
0.90000	-0.01505
0.95000	-0.00918
1.00000	0.00000

M6 (85%)
actual model

x/c	y/c
1.00000	-0.00045
0.99923	0.00140
0.99626	0.00228
0.99207	0.00313
0.98790	0.00387
0.98266	0.00470
0.97479	0.00597
0.96549	0.00733
0.95520	0.00882
0.94271	0.01056
0.92118	0.01343
0.89147	0.01734
0.85430	0.02231
0.80978	0.02819
0.72542	0.03915
0.63946	0.04938
0.56050	0.05761
0.47313	0.06427
0.43131	0.06662
0.39307	0.06806
0.35171	0.06904
0.31025	0.06920
0.27068	0.06815
0.22773	0.06543
0.20285	0.06323
0.18625	0.06144
0.16665	0.05890
0.14726	0.05600
0.13516	0.05396
0.11861	0.05084
0.10592	0.04814
0.09350	0.04524
0.07709	0.04095
0.06263	0.03675
0.05304	0.03366
0.04428	0.03061
0.03776	0.02821
0.03184	0.02590
0.02637	0.02362
0.02157	0.02142
0.01674	0.01887
0.01135	0.01535
0.00777	0.01249
0.00504	0.00975
0.00306	0.00720
0.00150	0.00503
0.00221	-0.00623
0.00650	-0.00963
0.01187	-0.01206
0.01609	-0.01350
0.02424	-0.01563
0.02974	-0.01678
0.03615	-0.01790
0.05438	-0.02035
0.07492	-0.02229
0.10594	-0.02433
0.13480	-0.02563
0.16243	-0.02640
0.20124	-0.02709
0.24517	-0.02773
0.28730	-0.02833
0.32713	-0.02872
0.40816	-0.02924
0.49140	-0.02914
0.57774	-0.02818
0.66008	-0.02676
0.74329	-0.02382
0.82878	-0.01862

0.86929	-0.01549
0.90686	-0.01225
0.93314	-0.00970
0.95137	-0.00769
0.96141	-0.00659
0.97198	-0.00533
0.98345	-0.00393
0.98930	-0.00312
0.99394	-0.00239
0.99928	-0.00140
1.00000	-0.00045

MA409

x/c	y/c
1.00000	0.00070
0.95000	0.01246
0.90000	0.02308
0.80000	0.04015
0.70000	0.05236
0.65000	0.06154
0.55000	0.06543
0.50000	0.06945
0.45000	0.07186
0.40000	0.07391
0.35000	0.07434
0.30000	0.07398
0.25000	0.07302
0.20000	0.06925
0.15000	0.06421
0.10000	0.05673
0.07500	0.05132
0.05000	0.04479
0.02500	0.03500
0.01250	0.02831
0.00000	0.01749
0.01250	0.00878
0.02500	0.00437
0.05000	0.00082
0.07500	0.00022
0.10000	0.00000
0.15000	0.00122
0.20000	0.00280
0.25000	0.00514
0.30000	0.00789
0.35000	0.01031
0.40000	0.01229
0.45000	0.01424
0.50000	0.01499
0.55000	0.01525
0.60000	0.01536
0.70000	0.01384
0.80000	0.01107
0.90000	0.00704
0.95000	0.00355
1.00000	0.00000

MA409
smoothed

x/c	y/c
1.00000	0.00034
0.99754	0.00094
0.99070	0.00259
0.98037	0.00498
0.96698	0.00793
0.95044	0.01136
0.93064	0.01521
0.90775	0.01937
0.88202	0.02373
0.85370	0.02817
0.82309	0.03261
0.79048	0.03694
0.75616	0.04112
0.72043	0.04505
0.68359	0.04869
0.64594	0.05198
0.60778	0.05486
0.56937	0.05732
0.53099	0.05933
0.49265	0.06089
0.45435	0.06202
0.41638	0.06270
0.37887	0.06291
0.34204	0.06260
0.30609	0.06172
0.27120	0.06025
0.23760	0.05819
0.20549	0.05555
0.17504	0.05234
0.14648	0.04859
0.11999	0.04433
0.09576	0.03961
0.07395	0.03450
0.05468	0.02913
0.03811	0.02369
0.02433	0.01831
0.01338	0.01305
0.00548	0.00797
0.00098	0.00318
0.00000	-0.00004
0.00098	-0.00302
0.00548	-0.00664
0.01338	-0.00968
0.02433	-0.01213
0.03811	-0.01400
0.05468	-0.01527
0.07395	-0.01590
0.09576	-0.01589
0.11999	-0.01527
0.14648	-0.01416
0.17504	-0.01264
0.20549	-0.01081
0.23760	-0.00875
0.27120	-0.00653
0.30609	-0.00421
0.34204	-0.00186
0.37887	0.00039
0.41638	0.00245
0.45435	0.00422
0.49265	0.00565
0.53099	0.00674
0.56937	0.00754
0.60778	0.00808
0.64594	0.00837
0.68359	0.00844
0.72043	0.00830
0.75616	0.00798
0.79048	0.00749
0.82309	0.00687
0.85370	0.00613
0.88202	0.00529
0.90775	0.00439
0.93064	0.00347
0.95044	0.00256
0.96698	0.00170
0.98037	0.00093
0.99070	0.00028
0.99754	-0.00018
1.00000	-0.00036

MA409
actual model

x/c	y/c
1.00000	-0.00018
0.99720	0.00043
0.99175	0.00133
0.98504	0.00240
0.97808	0.00336
0.97095	0.00424
0.96274	0.00536
0.95052	0.00716
0.94205	0.00843
0.92669	0.01072
0.91083	0.01322
0.89909	0.01491
0.86881	0.01946
0.84319	0.02298
0.81288	0.02684
0.77221	0.03143
0.72759	0.03588
0.67018	0.04107
0.61345	0.04551
0.55514	0.04947
0.49831	0.05310
0.44066	0.05540
0.38248	0.05684
0.33651	0.05671
0.29551	0.05636
0.25040	0.05530
0.21036	0.05254
0.17822	0.04967
0.14297	0.04628
0.11363	0.04257
0.09503	0.03950
0.08197	0.03694
0.06768	0.03368
0.05445	0.03018
0.04538	0.02745
0.03432	0.02377
0.02440	0.01984
0.01444	0.01477
0.00787	0.01033
0.00213	0.00509
0.00043	0.00228
0.00055	-0.00262
0.00328	-0.00600
0.00830	-0.00907
0.01423	-0.01167
0.01996	-0.01369
0.02550	-0.01504
0.03360	-0.01635
0.04220	-0.01731
0.05421	-0.01795
0.06552	-0.01827
0.08973	-0.01834
0.10067	-0.01821
0.11201	-0.01798
0.13732	-0.01725
0.16378	-0.01619
0.19399	-0.01505
0.23873	-0.01281
0.28061	-0.01034
0.33952	-0.00702
0.39707	-0.00433
0.45727	-0.00184
0.51627	-0.00082
0.57355	-0.00006
0.62624	0.00021
0.67937	0.00048
0.72125	0.00013
0.76715	-0.00014
0.81282	-0.00015
0.84246	-0.00012
0.87766	-0.00015
0.91173	-0.00071
0.92537	-0.00084
0.94213	-0.00111
0.95522	-0.00122
0.96880	-0.00129
0.97824	-0.00111
0.98517	-0.00084
0.99321	-0.00043
1.00000	-0.00018

MH32

x/c	y/c
1.00000	0.00000
0.99672	0.00035
0.98706	0.00150
0.97145	0.00363
0.95035	0.00676
0.92423	0.01084
0.89361	0.01573
0.85898	0.02123
0.82086	0.02714
0.77973	0.03319
0.73604	0.03910
0.69017	0.04467
0.64252	0.04977
0.59354	0.05432
0.54374	0.05830
0.49372	0.06161
0.44401	0.06409
0.39503	0.06565
0.34730	0.06627
0.30128	0.06586
0.25734	0.06439
0.21589	0.06192
0.17735	0.05844
0.14203	0.05398
0.11019	0.04861
0.08208	0.04245
0.05792	0.03562
0.03783	0.02829
0.02193	0.02067
0.01026	0.01308
0.00289	0.00595

0.00100	0.00004
0.00000	0.00000
0.00281	-0.00462
0.01171	-0.00882
0.02583	-0.01270
0.04500	-0.01604
0.06906	-0.01873
0.09783	-0.02074
0.13106	-0.02206
0.16847	-0.02271
0.20969	-0.02274
0.25432	-0.02223
0.30188	-0.02126
0.35184	-0.01990
0.40366	-0.01824
0.45647	-0.01634
0.51048	-0.01429
0.56428	-0.01216
0.61750	-0.01003
0.66952	-0.00797
0.71971	-0.00605
0.76746	-0.00433
0.81218	-0.00286
0.85329	-0.00169
0.89023	-0.00082
0.92250	-0.00026
0.94964	0.00003
0.97125	0.00012
0.98701	0.00011
0.99670	0.00005
1.00000	0.00000

MH32

actual model

x/c	y/c
1.00000	0.00011
0.99716	0.00135
0.99360	0.00197
0.98925	0.00240
0.98422	0.00337
0.97748	0.00436
0.97029	0.00557
0.96004	0.00686
0.94810	0.00886
0.93330	0.01123
0.91865	0.01344
0.90491	0.01563
0.89057	0.01818
0.86047	0.02297
0.82757	0.02792
0.79333	0.03296
0.73256	0.04107
0.66972	0.04872
0.60516	0.05538
0.54499	0.06042
0.48153	0.06442
0.42104	0.06668
0.35884	0.06766
0.29801	0.06718
0.23628	0.06483
0.20108	0.06241
0.17311	0.05951
0.14700	0.05618
0.12877	0.05330
0.11036	0.04988
0.09563	0.04673
0.08366	0.04382
0.07188	0.04070
0.06030	0.03722
0.04991	0.03374
0.04127	0.03048
0.03575	0.02820
0.02756	0.02466
0.02023	0.02081
0.01484	0.01756
0.00846	0.01225
0.00469	0.00793
0.00312	0.00606
0.00134	-0.00392
0.00923	-0.01030
0.01645	-0.01236
0.02157	-0.01364
0.02774	-0.01492
0.03727	-0.01657
0.04594	-0.01778
0.05589	-0.01877
0.06731	-0.01990
0.07799	-0.02065
0.08840	-0.02131
0.10441	-0.02222
0.11872	-0.02288
0.13821	-0.02355
0.15760	-0.02402
0.18209	-0.02428
0.20966	-0.02418
0.24658	-0.02363
0.30406	-0.02211
0.36915	-0.02000
0.43295	-0.01722
0.49586	-0.01428
0.55946	-0.01106
0.61917	-0.00819
0.68439	-0.00587
0.74866	-0.00388
0.80949	-0.00253
0.84404	-0.00195
0.87525	-0.00140
0.90626	-0.00080
0.92180	-0.00084
0.93566	-0.00091
0.95166	-0.00083
0.96507	-0.00090
0.97838	-0.00077
0.98812	-0.00073
0.99246	-0.00076
0.99668	-0.00053
0.99853	-0.00049
1.00000	0.00011

NACA 2414

x/c	y/c
1.00000	0.00147
0.99739	0.00210
0.98929	0.00396
0.97587	0.00700
0.95729	0.01112
0.93372	0.01620
0.90542	0.02207
0.87267	0.02857
0.83582	0.03552
0.79527	0.04274
0.75143	0.05004
0.70480	0.05723
0.65586	0.06412
0.60515	0.07053
0.55324	0.07629
0.50069	0.08120
0.44808	0.08512
0.39598	0.08787
0.34454	0.08913
0.29482	0.08866
0.24740	0.08645
0.20285	0.08255
0.16169	0.07707
0.12440	0.07014
0.09141	0.06198
0.06310	0.05281
0.03977	0.04289
0.02165	0.03245
0.00892	0.02171
0.00169	0.01085
0.00000	0.00000
0.00379	-0.01031
0.01293	-0.01956
0.02730	-0.02770
0.04669	-0.03471
0.07087	-0.04054
0.09957	-0.04516
0.13246	-0.04858
0.16918	-0.05082
0.20937	-0.05195
0.25260	-0.05208
0.29844	-0.05133
0.34644	-0.04987
0.39611	-0.04787
0.44739	-0.04537
0.49931	-0.04232
0.55129	-0.03886
0.60276	-0.03516
0.65316	-0.03132
0.70194	-0.02745
0.74857	-0.02365
0.79252	-0.01998
0.83331	-0.01650
0.87048	-0.01328
0.90360	-0.01035
0.93230	-0.00776
0.95626	-0.00557
0.97518	-0.00381
0.98886	-0.00252
0.99713	-0.00173
1.00000	-0.00147

NACA 2414

actual model

x/c	y/c
1.00000	-0.00029
0.99870	0.00082
0.99660	0.00198
0.99143	0.00299
0.98353	0.00477
0.97624	0.00635
0.96513	0.00863
0.95400	0.01109
0.93480	0.01516
0.90790	0.02062
0.89046	0.02405
0.86818	0.02855
0.83451	0.03491
0.79833	0.04124
0.76286	0.04705
0.72515	0.05306
0.68285	0.05908
0.63218	0.06576
0.59351	0.07036
0.55366	0.07462
0.51118	0.07865
0.46116	0.08277
0.41046	0.08576
0.37393	0.08708
0.34478	0.08752
0.31403	0.08726
0.28063	0.08631
0.25517	0.08500
0.23005	0.08318
0.20154	0.08043
0.17484	0.07713
0.12426	0.06791
0.10782	0.06400
0.09433	0.06041
0.07743	0.05541
0.06512	0.05134
0.05171	0.04612
0.04013	0.04091
0.03066	0.03604
0.02266	0.03116
0.01796	0.02771
0.01097	0.02153
0.00728	0.01751
0.00444	0.01365
0.00390	0.01309
0.00050	-0.00455
0.00145	-0.00781
0.00318	-0.01135
0.00721	-0.01677
0.01151	-0.02087
0.01389	-0.02262
0.02116	-0.02722
0.02750	-0.03058
0.03334	-0.03322
0.03811	-0.03498
0.04661	-0.03758
0.06007	-0.04098
0.07596	-0.04385
0.09175	-0.04645
0.10667	-0.04858
0.12457	-0.05030
0.14495	-0.05199
0.16912	-0.05346
0.19412	-0.05428
0.22746	-0.05472
0.25683	-0.05466
0.28288	-0.05436
0.31149	-0.05362
0.35509	-0.05216
0.39326	-0.05044
0.43745	-0.04825

0.47803	-0.04578
0.51813	-0.04321
0.55788	-0.04051
0.60178	-0.03736
0.63835	-0.03464
0.72471	-0.02767
0.81056	-0.02018
0.83861	-0.01765
0.89998	-0.01182
0.92655	-0.00940
0.93771	-0.00819
0.95347	-0.00660
0.99500	-0.00082
1.00000	-0.00029

NACA 2415

x/c	y/c
1.00000	0.00157
0.99740	0.00223
0.98930	0.00419
0.97590	0.00739
0.95733	0.01172
0.93377	0.01705
0.90548	0.02323
0.87275	0.03006
0.83591	0.03738
0.79536	0.04498
0.75154	0.05267
0.70490	0.06025
0.65595	0.06753
0.60524	0.07431
0.55331	0.08040
0.50074	0.08562
0.44811	0.08978
0.39597	0.09272
0.34448	0.09409
0.29469	0.09366
0.24722	0.09140
0.20261	0.08736
0.16142	0.08163
0.12411	0.07438
0.09112	0.06580
0.06282	0.05615
0.03952	0.04566
0.02145	0.03460
0.00878	0.02319
0.00161	0.01161
0.00000	0.00000
0.00387	-0.01106
0.01308	-0.02103
0.02750	-0.02985
0.04694	-0.03748
0.07115	-0.04387
0.09986	-0.04899
0.13275	-0.05282
0.16945	-0.05539
0.20960	-0.05676
0.25278	-0.05703
0.29857	-0.05633
0.34651	-0.05483
0.39612	-0.05272
0.44737	-0.05003
0.49926	-0.04673
0.55122	-0.04298
0.60267	-0.03893
0.65306	-0.03472
0.70184	-0.03048
0.74846	-0.02628
0.79242	-0.02222
0.83322	-0.01836
0.87040	-0.01477
0.90354	-0.01151
0.93225	-0.00862
0.95622	-0.00616
0.97516	-0.00419
0.98885	-0.00275
0.99712	-0.00187
1.00000	-0.00157

NACA 2415
actual model

x/c	y/c
1.00000	-0.00026
0.99951	0.00115
0.99632	0.00182
0.99232	0.00232
0.98738	0.00299
0.98173	0.00388
0.97536	0.00510
0.96984	0.00623
0.96350	0.00772
0.95801	0.00894
0.94969	0.01093
0.94001	0.01324
0.91755	0.01826
0.90215	0.02152
0.88879	0.02434
0.87520	0.02714
0.85855	0.03060
0.83103	0.03565
0.79980	0.04132
0.76635	0.04713
0.70565	0.05736
0.64543	0.06672
0.58218	0.07577
0.51994	0.08333
0.46075	0.08936
0.39601	0.09335
0.33624	0.09385
0.28034	0.09192
0.24595	0.08938
0.21421	0.08611
0.18418	0.08221
0.15704	0.07802
0.12987	0.07283
0.10987	0.06822
0.09153	0.06346
0.07808	0.05952
0.06212	0.05413
0.04949	0.04899
0.03946	0.04418
0.03184	0.03993
0.02326	0.03410
0.01753	0.02950
0.01276	0.02504
0.00833	0.01981
0.00533	0.01530
0.00263	0.01008
0.00065	-0.00488
0.00239	-0.00939
0.00476	-0.01313
0.00723	-0.01647
0.01228	-0.02200
0.01797	-0.02681
0.02591	-0.03181
0.03149	-0.03457
0.03847	-0.03746
0.04570	-0.04002
0.05472	-0.04263
0.06698	-0.04552
0.08282	-0.04843
0.09942	-0.05079
0.11464	-0.05266
0.13069	-0.05430
0.14928	-0.05583
0.17721	-0.05758
0.20156	-0.05844
0.23767	-0.05906
0.29843	-0.05847
0.36019	-0.05659
0.42250	-0.05410
0.48179	-0.05054
0.54351	-0.04592
0.60419	-0.04005
0.66681	-0.03352
0.72978	-0.02728
0.79140	-0.02102
0.82656	-0.01745
0.85843	-0.01426
0.88788	-0.01132
0.90052	-0.01005
0.91767	-0.00833
0.93097	-0.00707
0.94410	-0.00581
0.95532	-0.00476
0.96528	-0.00380
0.97507	-0.00286
0.98200	-0.00222
0.99076	-0.00170
0.99472	-0.00155
0.99950	-0.00115
1.00000	-0.00026

RG15

x/c	y/c
1.00000	0.00000
0.99671	0.00054
0.98726	0.00229
0.97237	0.00514
0.95248	0.00865
0.92764	0.01254
0.89810	0.01685
0.86427	0.02152
0.82660	0.02644
0.78557	0.03149
0.74165	0.03654
0.69537	0.04146
0.64723	0.04612
0.59778	0.05039
0.54753	0.05414
0.49702	0.05727
0.44676	0.05966
0.39727	0.06123
0.34902	0.06190
0.30248	0.06162
0.25809	0.06036
0.21624	0.05810
0.17730	0.05486
0.14161	0.05068
0.10945	0.04564
0.08108	0.03985
0.05673	0.03343
0.03658	0.02654
0.02076	0.01935
0.00932	0.01214
0.00235	0.00526
0.00000	0.00000
0.00002	-0.00048
0.00336	-0.00534
0.01247	-0.01006
0.02670	-0.01436
0.04596	-0.01811
0.07010	-0.02123
0.09896	-0.02372
0.13224	-0.02559
0.16963	-0.02688
0.21073	-0.02762
0.25509	-0.02785
0.30221	-0.02762
0.35156	-0.02696
0.40257	-0.02590
0.45463	-0.02446
0.50713	-0.02262
0.55944	-0.02025
0.61128	-0.01717
0.66244	-0.01366
0.71237	-0.01015
0.76037	-0.00691
0.80575	-0.00413
0.84779	-0.00192
0.88583	-0.00034
0.91925	0.00062
0.94748	0.00101
0.97003	0.00097
0.98652	0.00064
0.99660	0.00021
1.00000	0.00000

RG15 (C)
actual model

x/c	y/c
1.00000	-0.00024
0.99647	0.00094
0.99433	0.00204
0.98701	0.00312
0.98064	0.00415
0.97295	0.00525
0.96264	0.00683
0.95233	0.00844
0.94060	0.01030
0.92945	0.01192
0.91047	0.01499
0.89599	0.01717
0.87631	0.02024
0.86324	0.02220
0.83897	0.02612

0.82833	0.02765
0.81670	0.02921
0.80412	0.03037
0.76364	0.03545
0.70294	0.04250
0.64030	0.04899
0.57900	0.05383
0.51810	0.05775
0.46034	0.06075
0.39616	0.06279
0.33166	0.06310
0.27013	0.06166
0.20295	0.05776
0.16678	0.05440
0.13880	0.05103
0.10659	0.04599
0.09000	0.04263
0.07935	0.04011
0.06859	0.03733
0.05791	0.03421
0.04626	0.03036
0.03259	0.02465
0.02689	0.02168
0.02093	0.01841
0.01508	0.01471
0.00921	0.01079
0.00007	-0.00094
0.00382	-0.00693
0.01256	-0.01065
0.02571	-0.01441
0.03395	-0.01618
0.04233	-0.01763
0.05243	-0.01904
0.06081	-0.02010
0.07531	-0.02161
0.09147	-0.02299
0.10610	-0.02398
0.12471	-0.02492
0.14900	-0.02572
0.17770	-0.02629
0.21123	-0.02657
0.27086	-0.02624
0.33679	-0.02518
0.39699	-0.02360
0.46204	-0.02161
0.52766	-0.01922
0.58622	-0.01632
0.65052	-0.01211
0.71310	-0.00773
0.77826	-0.00357
0.82242	-0.00114
0.83722	-0.00077
0.86207	-0.00038
0.88093	-0.00037
0.90115	-0.00046
0.91952	-0.00064
0.93417	-0.00087
0.94813	-0.00094
0.95746	-0.00095
0.96431	-0.00084
0.97202	-0.00097
0.97874	-0.00109
0.98505	-0.00119
0.99343	-0.00094
1.00000	-0.00024

S1223

x/c	y/c
1.00000	0.00000
0.99838	0.00126
0.99417	0.00494
0.98825	0.01037
0.98075	0.01646
0.97111	0.02250
0.95884	0.02853
0.94389	0.03476
0.92639	0.04116
0.90641	0.04768
0.88406	0.05427
0.85947	0.06089
0.83277	0.06749
0.80412	0.07402
0.77369	0.08044
0.74166	0.08671
0.70823	0.09277
0.67360	0.09859
0.63798	0.10412
0.60158	0.10935
0.56465	0.11425
0.52744	0.11881
0.49025	0.12303
0.45340	0.12683
0.41721	0.13011
0.38193	0.13271
0.34777	0.13447
0.31488	0.13526
0.28347	0.13505
0.25370	0.13346
0.22541	0.13037
0.19846	0.12594
0.17286	0.12026
0.14863	0.11355
0.12591	0.10598
0.10482	0.09770
0.08545	0.08879
0.06789	0.07940
0.05223	0.06965
0.03855	0.05968
0.02694	0.04966
0.01755	0.03961
0.01028	0.02954
0.00495	0.01969
0.00155	0.01033
0.00005	0.00178
0.00044	-0.00561
0.00264	-0.01120
0.00789	-0.01427
0.01718	-0.01550
0.03006	-0.01584
0.04627	-0.01532
0.06561	-0.01404
0.08787	-0.01202
0.11282	-0.00925
0.14020	-0.00563
0.17006	-0.00075
0.20278	0.00535
0.23840	0.01213
0.27673	0.01928
0.31750	0.02652
0.36044	0.03358
0.40519	0.04021
0.45139	0.04618
0.49860	0.05129
0.54639	0.05534
0.59428	0.05820
0.64176	0.05976
0.68832	0.05994
0.73344	0.05872
0.77660	0.05612
0.81729	0.05219
0.85500	0.04706
0.88928	0.04088
0.91966	0.03387
0.94573	0.02624
0.96693	0.01822
0.98255	0.01060
0.99268	0.00468
0.99825	0.00115
1.00000	0.00000

S1223
actual model

x/c	y/c
1.00000	0.00013
0.99720	0.00333
0.99187	0.00839
0.98689	0.01260
0.98075	0.01692
0.97339	0.02127
0.96293	0.02660
0.95370	0.03080
0.94176	0.03581
0.92548	0.04204
0.91053	0.04728
0.88969	0.05399
0.87178	0.05924
0.84496	0.06638
0.81744	0.07305
0.78334	0.08061
0.74802	0.08779
0.71868	0.09328
0.68153	0.09976
0.65038	0.10483
0.61072	0.11087
0.59071	0.11368
0.56407	0.11720
0.53542	0.12074
0.50578	0.12419
0.47863	0.12718
0.44641	0.13039
0.41610	0.13304
0.38752	0.13509
0.35962	0.13665
0.32854	0.13771
0.29648	0.13794
0.26356	0.13679
0.23263	0.13393
0.21283	0.13114
0.19561	0.12802
0.17473	0.12336
0.15733	0.11868
0.14032	0.11348
0.12497	0.10819
0.11009	0.10247
0.09550	0.09613
0.08018	0.08863
0.06800	0.08199
0.04897	0.07000
0.03568	0.05999
0.02846	0.05369
0.01989	0.04487
0.01503	0.03884
0.01082	0.03257
0.00706	0.02587
0.00482	0.02100
0.00221	0.01365
0.00080	0.00745
0.00019	0.00286
0.00005	-0.00138
0.00083	-0.00593
0.00139	-0.00690
0.00312	-0.00872
0.00790	-0.01068
0.01449	-0.01150
0.02138	-0.01185
0.03330	-0.01196
0.04627	-0.01153
0.06389	-0.01040
0.08117	-0.00888
0.10354	-0.00663
0.12948	-0.00369
0.16404	0.00134
0.20100	0.00781
0.25115	0.01690
0.29610	0.02479
0.33392	0.03100
0.38160	0.03816
0.43006	0.04455
0.47940	0.05004
0.52654	0.05432
0.57684	0.05747
0.63172	0.05939
0.67649	0.05980
0.71559	0.05921
0.73675	0.05844
0.76333	0.05703
0.78942	0.05506
0.80947	0.05310
0.83028	0.05062
0.86994	0.04446
0.89924	0.03838
0.92149	0.03274
0.94479	0.02561
0.95707	0.02117
0.97177	0.01493
0.98900	0.00570
0.99231	0.00363
0.99800	-0.00013
1.00000	-0.00178

S1223 RTL

x/c	y/c
1.00000	0.00000
0.99358	0.00517
0.98424	0.01272
0.97345	0.01996
0.96062	0.02672
0.94517	0.03343

0.92664	0.04043
0.90488	0.04774
0.88017	0.05525
0.85315	0.06278
0.82459	0.07017
0.79513	0.07728
0.76524	0.08403
0.73520	0.09033
0.70515	0.09613
0.67507	0.10141
0.64489	0.10617
0.61447	0.11043
0.58366	0.11424
0.55230	0.11767
0.52031	0.12081
0.48770	0.12375
0.45461	0.12656
0.42134	0.12929
0.38833	0.13190
0.35606	0.13430
0.32506	0.13634
0.29587	0.13785
0.26882	0.13861
0.24382	0.13842
0.22049	0.13717
0.19852	0.13482
0.17766	0.13135
0.15777	0.12677
0.13877	0.12109
0.12066	0.11436
0.10348	0.10665
0.08735	0.09811
0.07246	0.08897
0.05906	0.07960
0.04738	0.07040
0.03747	0.06170
0.02926	0.05366
0.02255	0.04628
0.01710	0.03951
0.01270	0.03328
0.00915	0.02754
0.00631	0.02224
0.00408	0.01732
0.00237	0.01273
0.00113	0.00843
0.00034	0.00440
-0.00001	0.00060
0.00014	-0.00301
0.00104	-0.00653
0.00309	-0.00959
0.00627	-0.01179
0.01020	-0.01321
0.01471	-0.01413
0.01984	-0.01474
0.02573	-0.01513
0.03260	-0.01534
0.04078	-0.01536
0.05075	-0.01516
0.06316	-0.01465
0.07889	-0.01373
0.09868	-0.01226
0.12242	-0.01013
0.14904	-0.00721
0.17761	-0.00342
0.20791	0.00114
0.23971	0.00625
0.27250	0.01166
0.30575	0.01721
0.33893	0.02270
0.37173	0.02803
0.40404	0.03309
0.43585	0.03780
0.46716	0.04209
0.49803	0.04590
0.52849	0.04918
0.55862	0.05190
0.58844	0.05401
0.61803	0.05550
0.64740	0.05634
0.67662	0.05652
0.70569	0.05602
0.73464	0.05484
0.76344	0.05298
0.79205	0.05043
0.82034	0.04722
0.84807	0.04337
0.87484	0.03895
0.90001	0.03406
0.92292	0.02886
0.94306	0.02346
0.96035	0.01795
0.97500	0.01237
0.98734	0.00680
1.00000	0.00000

S1223 RTL

actual model

x/c	y/c
1.00000	-0.00095
0.99750	0.00425
0.99427	0.00697
0.99055	0.00972
0.98589	0.01307
0.98042	0.01680
0.97421	0.02080
0.96703	0.02502
0.96019	0.02853
0.95354	0.03159
0.94543	0.03497
0.93478	0.03905
0.92739	0.04172
0.91607	0.04559
0.90470	0.04934
0.89290	0.05310
0.88087	0.05675
0.87155	0.05946
0.86033	0.06258
0.84152	0.06765
0.82152	0.07273
0.78855	0.08064
0.75717	0.08769
0.70252	0.09897
0.64637	0.10883
0.59277	0.11627
0.53566	0.12226
0.48160	0.12726
0.42089	0.13233
0.36790	0.13636
0.31670	0.13966
0.26730	0.14145
0.24203	0.14110
0.22451	0.14014
0.20946	0.13874
0.19220	0.13630
0.17387	0.13280
0.16017	0.12965
0.14198	0.12459
0.12745	0.11978
0.11445	0.11465
0.10176	0.10870
0.09017	0.10256
0.07732	0.09509
0.06304	0.08558
0.05279	0.07773
0.04242	0.06878
0.03436	0.06106
0.02535	0.05145
0.01654	0.03987
0.01112	0.03121
0.00614	0.02149
0.00334	0.01455
0.00111	0.00752
0.00089	0.00667
0.00048	0.00486
0.00002	-0.00101
0.00022	-0.00324
0.00096	-0.00647
0.00519	-0.01160
0.01318	-0.01398
0.01938	-0.01407
0.02959	-0.01375
0.04232	-0.01313
0.05479	-0.01242
0.07444	-0.01127
0.10075	-0.00932
0.14633	-0.00469
0.17649	-0.00063
0.22153	0.00626
0.26151	0.01263
0.29945	0.01888
0.33382	0.02452
0.38160	0.03223
0.43867	0.04104
0.47576	0.04608
0.53232	0.05187
0.57715	0.05537
0.62709	0.05776
0.66016	0.05836
0.69736	0.05795
0.73902	0.05608
0.77283	0.05347
0.81395	0.04910
0.85029	0.04396
0.87252	0.04005
0.89200	0.03635
0.90463	0.03359
0.91605	0.03081
0.93077	0.02691
0.94306	0.02329
0.95440	0.01963
0.96769	0.01479
0.97929	0.01002
0.98596	0.00697
0.99094	0.00456
0.99371	0.00315
0.99577	-0.00027
1.00000	-0.00095

S4083

x/c	y/c
1.00000	0.00000
0.99815	0.00055
0.99308	0.00220
0.98528	0.00445
0.97469	0.00689
0.96115	0.00948
0.94473	0.01230
0.92555	0.01533
0.90374	0.01855
0.87944	0.02193
0.85282	0.02544
0.82404	0.02907
0.79330	0.03277
0.76080	0.03653
0.72675	0.04031
0.69137	0.04410
0.65491	0.04787
0.61762	0.05157
0.57975	0.05519
0.54158	0.05867
0.50338	0.06196
0.46541	0.06498
0.42794	0.06768
0.39121	0.06995
0.35544	0.07169
0.32082	0.07282
0.28758	0.07322
0.25575	0.07277
0.22538	0.07150
0.19665	0.06938
0.16955	0.06640
0.14416	0.06271
0.12060	0.05835
0.09893	0.05339
0.07927	0.04795
0.06168	0.04208
0.04618	0.03591
0.03289	0.02953
0.02180	0.02306
0.01293	0.01669
0.00632	0.01057
0.00201	0.00493
0.00000	0.00016
0.00099	-0.00346
0.00541	-0.00618
0.01305	-0.00842
0.02383	-0.01019
0.03765	-0.01146
0.05447	-0.01227
0.07419	-0.01265
0.09672	-0.01261
0.12192	-0.01219
0.14968	-0.01143
0.17983	-0.01037
0.21221	-0.00907
0.24659	-0.00757
0.28279	-0.00593
0.32055	-0.00420

0.35964	-0.00243
0.39979	-0.00067
0.44075	0.00104
0.48221	0.00264
0.52390	0.00412
0.56552	0.00546
0.60684	0.00667
0.64768	0.00768
0.68776	0.00824
0.72657	0.00826
0.76358	0.00787
0.79860	0.00723
0.83138	0.00643
0.86173	0.00551
0.88946	0.00454
0.91437	0.00355
0.93632	0.00262
0.95515	0.00179
0.97082	0.00115
0.98328	0.00067
0.99239	0.00031
0.99805	0.00010
1.00000	0.00000

S4083 (A)
actual model

x/c	y/c
1.00000	-0.00032
0.99899	0.00022
0.99779	0.00067
0.99445	0.00155
0.98949	0.00257
0.98313	0.00412
0.97670	0.00574
0.96542	0.00804
0.95181	0.01054
0.93862	0.01273
0.92404	0.01500
0.90887	0.01719
0.89536	0.01915
0.86278	0.02361
0.83105	0.02775
0.79685	0.03196
0.73659	0.03880
0.67089	0.04585
0.61038	0.05204
0.54536	0.05798
0.48544	0.06284
0.42388	0.06716
0.36160	0.07043
0.30323	0.07200
0.27176	0.07192
0.23877	0.07101
0.20632	0.06918
0.18025	0.06682
0.15303	0.06338
0.13539	0.06051
0.11796	0.05718
0.10096	0.05339
0.08601	0.04948
0.07236	0.04537
0.06063	0.04145
0.05198	0.03828
0.04046	0.03340
0.02916	0.02763
0.02180	0.02323
0.01340	0.01706
0.00875	0.01293
0.00359	0.00728
0.00216	0.00536
0.00080	-0.00322
0.00292	-0.00616
0.00876	-0.00926
0.01415	-0.01078
0.02192	-0.01225
0.03300	-0.01330
0.04237	-0.01369
0.05615	-0.01405
0.06694	-0.01412
0.07710	-0.01417
0.08733	-0.01413
0.10593	-0.01383
0.12001	-0.01346
0.13794	-0.01294
0.15741	-0.01234
0.18217	-0.01141
0.20778	-0.01033
0.24781	-0.00848
0.30471	-0.00575
0.36968	-0.00283
0.43138	-0.00011
0.49352	0.00252
0.55772	0.00512
0.62074	0.00715
0.68371	0.00814
0.74509	0.00787
0.80830	0.00674
0.84327	0.00582
0.87584	0.00494
0.90677	0.00409
0.92060	0.00367
0.93566	0.00309
0.95025	0.00256
0.96574	0.00203
0.97600	0.00156
0.98445	0.00109
0.99028	0.00056
0.99498	0.00008
0.99699	-0.00022
1.00000	-0.00032

S4083 (B)
actual model

x/c	y/c
1.00000	-0.00036
0.99963	0.00062
0.99545	0.00100
0.98849	0.00178
0.98344	0.00220
0.97707	0.00322
0.97073	0.00439
0.96376	0.00565
0.94910	0.00821
0.93488	0.01065
0.92034	0.01293
0.90586	0.01517
0.89203	0.01725
0.86009	0.02167
0.83179	0.02529
0.79411	0.02987
0.73315	0.03653
0.67105	0.04275
0.60817	0.04856
0.54789	0.05399
0.48555	0.05924
0.42635	0.06336
0.36367	0.06671
0.30013	0.06858
0.27322	0.06873
0.23882	0.06791
0.20233	0.06566
0.17799	0.06335
0.15175	0.05997
0.13378	0.05708
0.11660	0.05387
0.09952	0.05012
0.08633	0.04680
0.07427	0.04339
0.06262	0.03965
0.05398	0.03652
0.04506	0.03291
0.03492	0.02826
0.02585	0.02349
0.01637	0.01747
0.00903	0.01175
0.00424	0.00771
0.00001	-0.00040
0.00043	-0.00246
0.00257	-0.00712
0.00584	-0.01090
0.01199	-0.01357
0.01858	-0.01447
0.02728	-0.01537
0.03544	-0.01590
0.04830	-0.01637
0.06622	-0.01643
0.09344	-0.01577
0.12227	-0.01490
0.14665	-0.01405
0.16761	-0.01321
0.18522	-0.01245
0.21253	-0.01111
0.24735	-0.00944
0.31156	-0.00624
0.37241	-0.00312
0.43314	-0.00015
0.49331	0.00246
0.55681	0.00497
0.61759	0.00717
0.68194	0.00838
0.74465	0.00835
0.80886	0.00710
0.84296	0.00597
0.87461	0.00468
0.90853	0.00323
0.92228	0.00262
0.93592	0.00193
0.95012	0.00139
0.96167	0.00094
0.96947	0.00066
0.97700	0.00057
0.98634	0.00013
0.99140	-0.00021
0.99799	-0.00062
1.00000	-0.00036

S5010

x/c	y/c
1.00000	0.00000
0.99676	0.00001
0.98707	0.00007
0.97101	0.00036
0.94870	0.00108
0.92041	0.00256
0.88667	0.00516
0.84828	0.00903
0.80608	0.01406
0.76076	0.02008
0.71307	0.02688
0.66377	0.03420
0.61355	0.04163
0.56296	0.04877
0.51247	0.05529
0.46251	0.06093
0.41346	0.06546
0.36576	0.06873
0.31969	0.07063
0.27560	0.07113
0.23383	0.07023
0.19473	0.06799
0.15860	0.06445
0.12573	0.05968
0.09637	0.05377
0.07071	0.04688
0.04889	0.03915
0.03102	0.03081
0.01718	0.02214
0.00739	0.01348
0.00167	0.00533
0.00015	-0.00140
0.00424	-0.00650
0.01456	-0.01084
0.03028	-0.01471
0.05123	-0.01804
0.07718	-0.02082
0.10785	-0.02306
0.14291	-0.02481
0.18194	-0.02609
0.22448	-0.02688
0.27008	-0.02715
0.31829	-0.02691
0.36864	-0.02623
0.42055	-0.02517
0.47345	-0.02381
0.52675	-0.02219
0.57983	-0.02039
0.63209	-0.01846
0.68292	-0.01645
0.73173	-0.01443
0.77792	-0.01243
0.82095	-0.01049
0.86030	-0.00865
0.89547	-0.00691
0.92603	-0.00527
0.95163	-0.00367
0.97211	-0.00212
0.98730	-0.00088

0.99678	-0.00019
1.00000	0.00000

S5010

actual model

x/c	y/c
1.00000	0.00000
0.99880	0.00017
0.99759	0.00013
0.99357	0.00030
0.99104	0.00042
0.98690	0.00026
0.98286	0.00021
0.97620	0.00018
0.96871	-0.00001
0.96024	-0.00002
0.94892	0.00015
0.93371	0.00097
0.91780	0.00186
0.90296	0.00294
0.88761	0.00438
0.86533	0.00652
0.84186	0.00894
0.80547	0.01329
0.78173	0.01635
0.75430	0.02000
0.72126	0.02478
0.68489	0.03002
0.64201	0.03617
0.59984	0.04191
0.55984	0.04709
0.51751	0.05222
0.47561	0.05678
0.43477	0.06078
0.39442	0.06401
0.35312	0.06636
0.31179	0.06771
0.26737	0.06795
0.22542	0.06670
0.18383	0.06398
0.16297	0.06188
0.14234	0.05923
0.12258	0.05617
0.10568	0.05303
0.09296	0.05023
0.07792	0.04645
0.06173	0.04157
0.04364	0.03485
0.02820	0.02766
0.02190	0.02415
0.01379	0.01897
0.00573	0.01222
0.00185	0.00618
0.00099	0.00406
0.00042	-0.00260
0.00149	-0.00494
0.00445	-0.00769
0.00733	-0.00929
0.01253	-0.01149
0.02026	-0.01393
0.02849	-0.01549
0.03999	-0.01684
0.05239	-0.01797
0.06099	-0.01870
0.07090	-0.01949
0.10929	-0.02171
0.12963	-0.02236
0.15341	-0.02290
0.18149	-0.02353
0.20838	-0.02390
0.23924	-0.02406
0.28010	-0.02401
0.32173	-0.02377
0.36479	-0.02329
0.40329	-0.02267
0.44275	-0.02185
0.48710	-0.02076
0.52716	-0.01961
0.57191	-0.01812
0.61247	-0.01659
0.65303	-0.01495
0.69354	-0.01334
0.73636	-0.01175
0.78018	-0.01009
0.82107	-0.00855
0.84788	-0.00750
0.87844	-0.00614
0.89666	-0.00535
0.91469	-0.00432
0.92683	-0.00349
0.93982	-0.00289
0.94969	-0.00210
0.96091	-0.00155
0.97746	-0.00085
0.98949	-0.00033
0.99538	-0.00030
0.99832	-0.00017
1.00000	0.00000

S7012

x/c	y/c
1.00000	0.00000
0.99819	0.00024
0.99294	0.00104
0.98451	0.00231
0.97296	0.00392
0.95833	0.00586
0.94077	0.00817
0.92044	0.01080
0.89749	0.01372
0.87210	0.01689
0.84445	0.02029
0.81474	0.02386
0.78318	0.02757
0.74999	0.03138
0.71540	0.03524
0.67965	0.03909
0.64298	0.04287
0.60563	0.04654
0.56785	0.05002
0.52988	0.05324
0.49193	0.05615
0.45426	0.05870
0.41710	0.06081
0.38070	0.06241
0.34520	0.06335
0.31071	0.06360
0.27741	0.06319
0.24543	0.06209
0.21486	0.06033
0.18590	0.05795
0.15865	0.05496
0.13326	0.05143
0.10983	0.04738
0.08846	0.04287
0.06926	0.03798
0.05229	0.03274
0.03759	0.02728
0.02525	0.02167
0.01528	0.01605
0.00773	0.01058
0.00266	0.00542
0.00007	0.00087
0.00069	-0.00278
0.00486	-0.00600
0.01208	-0.00918
0.02223	-0.01220
0.03523	-0.01495
0.05102	-0.01739
0.06952	-0.01950
0.09065	-0.02126
0.11428	-0.02265
0.14032	-0.02368
0.16861	-0.02436
0.19900	-0.02471
0.23131	-0.02474
0.26535	-0.02448
0.30091	-0.02396
0.33778	-0.02318
0.37572	-0.02220
0.41449	-0.02101
0.45383	-0.01965
0.49348	-0.01813
0.53316	-0.01644
0.57261	-0.01453
0.61171	-0.01227
0.65044	-0.00978
0.68859	-0.00732
0.72582	-0.00504
0.76182	-0.00300
0.79628	-0.00128
0.82889	0.00010
0.85936	0.00112
0.88743	0.00178
0.91283	0.00211
0.93533	0.00214
0.95473	0.00192
0.97084	0.00153
0.98352	0.00105
0.99266	0.00055
0.99816	0.00016
1.00000	0.00000

S7012 (B)

actual model

x/c	y/c
1.00000	0.00045
0.99960	0.00001
0.99669	0.00037
0.99294	0.00079
0.98842	0.00130
0.98375	0.00163
0.98021	0.00179
0.97454	0.00222
0.96582	0.00324
0.95379	0.00447
0.94289	0.00586
0.92317	0.00810
0.89969	0.01080
0.85933	0.01547
0.81885	0.02027
0.72430	0.03165
0.65062	0.03941
0.56792	0.04762
0.48218	0.05482
0.40016	0.05987
0.35677	0.06158
0.31806	0.06223
0.27607	0.06193
0.23573	0.06066
0.21576	0.05950
0.19547	0.05795
0.17212	0.05577
0.15611	0.05399
0.14086	0.05204
0.12842	0.05018
0.11345	0.04764
0.09970	0.04497
0.08488	0.04171
0.07186	0.03851
0.05937	0.03499
0.05303	0.03298
0.04160	0.02897
0.03516	0.02640
0.02900	0.02369
0.02277	0.02065
0.01803	0.01807
0.01372	0.01545
0.01036	0.01313
0.00691	0.01039
0.00395	0.00746
0.00111	0.00315
0.00065	0.00185
0.00031	0.00127
0.00204	-0.00328
0.00498	-0.00575
0.00772	-0.00748
0.01262	-0.00981
0.01756	-0.01160
0.02682	-0.01423
0.03026	-0.01506
0.03536	-0.01618
0.04633	-0.01816
0.06809	-0.02082
0.08995	-0.02263
0.12249	-0.02450
0.15033	-0.02555
0.18373	-0.02627
0.22489	-0.02629
0.26479	-0.02578
0.33064	-0.02459
0.38760	-0.02311
0.45196	-0.02111
0.54060	-0.01747
0.62609	-0.01264
0.70349	-0.00776
0.75671	-0.00464

0.82717	-0.00154
0.87128	-0.00003
0.91142	0.00083
0.95396	0.00123
0.96538	0.00084
0.97772	0.00051
0.98740	0.00016
0.99328	-0.00010
0.99939	-0.00001
1.00000	0.00045

S7055

x/c	y/c
1.00000	0.00000
0.99808	0.00023
0.99243	0.00104
0.98327	0.00251
0.97083	0.00464
0.95526	0.00738
0.93671	0.01073
0.91539	0.01470
0.89155	0.01924
0.86543	0.02431
0.83728	0.02981
0.80738	0.03565
0.77601	0.04169
0.74337	0.04770
0.70958	0.05354
0.67484	0.05920
0.63934	0.06454
0.60327	0.06949
0.56688	0.07399
0.53032	0.07791
0.49374	0.08125
0.45740	0.08391
0.42142	0.08584
0.38601	0.08706
0.35133	0.08749
0.31754	0.08713
0.28483	0.08599
0.25332	0.08404
0.22311	0.08132
0.19440	0.07787
0.16729	0.07370
0.14189	0.06891
0.11833	0.06352
0.09668	0.05760
0.07705	0.05125
0.05952	0.04455
0.04413	0.03761
0.03097	0.03054
0.02008	0.02346
0.01148	0.01655
0.00524	0.00998
0.00139	0.00398
0.00007	-0.00091
0.00214	-0.00493
0.00762	-0.00871
0.01587	-0.01193
0.02720	-0.01436
0.04175	-0.01620
0.05938	-0.01763
0.07995	-0.01870
0.10333	-0.01944
0.12935	-0.01989
0.15784	-0.02009
0.18857	-0.02006
0.22132	-0.01980
0.25590	-0.01927
0.29218	-0.01849
0.32993	-0.01757
0.36889	-0.01656
0.40878	-0.01551
0.44933	-0.01445
0.49021	-0.01338
0.53116	-0.01230
0.57188	-0.01123
0.61212	-0.01018
0.65160	-0.00914
0.69009	-0.00813
0.72734	-0.00716
0.76303	-0.00622
0.79681	-0.00533
0.82841	-0.00450
0.85793	-0.00373
0.88544	-0.00301
0.91063	-0.00235
0.93322	-0.00175
0.95293	-0.00124
0.96949	-0.00080
0.98266	-0.00046
0.99224	-0.00020
0.99805	-0.00005
1.00000	0.00000

S7055
actual model

x/c	y/c
1.00000	0.00040
0.99562	0.00203
0.99010	0.00284
0.98345	0.00397
0.97668	0.00506
0.96982	0.00632
0.96240	0.00763
0.95470	0.00905
0.94683	0.01044
0.93714	0.01212
0.92450	0.01445
0.91234	0.01666
0.90178	0.01871
0.88154	0.02256
0.86177	0.02643
0.83545	0.03185
0.79854	0.03912
0.76066	0.04651
0.72058	0.05398
0.66018	0.06405
0.60023	0.07286
0.53588	0.07980
0.47323	0.08473
0.41034	0.08802
0.34779	0.08827
0.28557	0.08628
0.22639	0.08189
0.18440	0.07689
0.14489	0.07040
0.12239	0.06522
0.10318	0.05983
0.08536	0.05384
0.07289	0.04896
0.06069	0.04381
0.04943	0.03870
0.03860	0.03320
0.02930	0.02774
0.02098	0.02225
0.01432	0.01724
0.00716	0.01110
0.00294	0.00641
0.00005	-0.00085
0.00025	-0.00185
0.00422	-0.00712
0.00819	-0.00946
0.01368	-0.01173
0.01940	-0.01365
0.02561	-0.01527
0.03578	-0.01721
0.04885	-0.01892
0.05964	-0.02005
0.07697	-0.02144
0.09621	-0.02215
0.12762	-0.02249
0.15810	-0.02285
0.19891	-0.02277
0.24187	-0.02203
0.30328	-0.01968
0.36843	-0.01772
0.43049	-0.01599
0.49304	-0.01422
0.55200	-0.01265
0.61392	-0.01127
0.67063	-0.00971
0.73894	-0.00781
0.78119	-0.00628
0.82139	-0.00528
0.85601	-0.00448
0.88476	-0.00359
0.90230	-0.00292
0.92436	-0.00225
0.93865	-0.00180
0.95219	-0.00156
0.96302	-0.00127
0.97314	-0.00124
0.98332	-0.00121
0.99112	-0.00125
0.99936	-0.00105
1.00000	0.00040

S7075

x/c	y/c
1.00000	0.00000
0.99811	0.00030
0.99262	0.00130
0.98384	0.00301
0.97189	0.00532
0.95689	0.00825
0.93906	0.01183
0.91865	0.01599
0.89590	0.02064
0.87105	0.02565
0.84435	0.03084
0.81590	0.03603
0.78585	0.04114
0.75438	0.04596
0.72152	0.05039
0.68736	0.05452
0.65213	0.05833
0.61605	0.06181
0.57936	0.06492
0.54228	0.06762
0.50502	0.06988
0.46782	0.07165
0.43086	0.07290
0.39436	0.07362
0.35853	0.07377
0.32355	0.07334
0.28961	0.07232
0.25690	0.07072
0.22556	0.06854
0.19578	0.06579
0.16769	0.06249
0.14143	0.05868
0.11714	0.05438
0.09490	0.04963
0.07485	0.04451
0.05704	0.03906
0.04155	0.03336
0.02846	0.02751
0.01783	0.02158
0.00974	0.01572
0.00426	0.00983
0.00112	0.00396
0.00012	-0.00127
0.00205	-0.00532
0.00740	-0.00861
0.01586	-0.01154
0.02736	-0.01403
0.04182	-0.01616
0.05915	-0.01785
0.07927	-0.01912
0.10208	-0.01997
0.12746	-0.02041
0.15527	-0.02049
0.18536	-0.02022
0.21756	-0.01965
0.25167	-0.01880
0.28749	-0.01774
0.32478	-0.01649
0.36331	-0.01510
0.40283	-0.01360
0.44306	-0.01205
0.48375	-0.01047
0.52460	-0.00889
0.56534	-0.00734
0.60568	-0.00584
0.64532	-0.00438
0.68397	-0.00291
0.72149	-0.00140
0.75769	0.00009
0.79235	0.00160
0.82543	0.00301
0.85679	0.00399
0.88582	0.00420
0.91190	0.00378
0.93478	0.00312
0.95435	0.00237
0.97053	0.00163

0.98322	0.00099
0.99243	0.00051
0.99808	0.00016
1.00000	0.00000

S7075 (A)
actual model

x/c	y/c
1.00000	-0.00094
0.99880	-0.00018
0.99573	0.00071
0.99003	0.00183
0.98361	0.00306
0.97892	0.00407
0.97211	0.00546
0.96259	0.00758
0.94762	0.01058
0.93380	0.01333
0.91794	0.01650
0.90252	0.01953
0.88967	0.02201
0.85223	0.02910
0.81262	0.03612
0.72316	0.04930
0.64651	0.05807
0.56353	0.06542
0.48020	0.07034
0.39574	0.07258
0.35700	0.07272
0.31528	0.07211
0.27103	0.07051
0.23201	0.06801
0.21012	0.06617
0.19375	0.06457
0.17123	0.06201
0.14505	0.05840
0.13058	0.05602
0.11998	0.05411
0.10489	0.05105
0.09076	0.04780
0.07660	0.04411
0.06308	0.04008
0.05197	0.03634
0.04408	0.03338
0.03647	0.03025
0.03025	0.02744
0.01964	0.02185
0.01273	0.01733
0.00542	0.01099
0.00146	0.00538
0.00021	0.00202
0.00074	-0.00388
0.00443	-0.00786
0.00722	-0.00938
0.01242	-0.01132
0.02049	-0.01338
0.02870	-0.01496
0.03540	-0.01596
0.04184	-0.01684
0.05288	-0.01802
0.06188	-0.01880
0.07265	-0.01956
0.08391	-0.02018
0.11360	-0.02115
0.14319	-0.02145
0.17676	-0.02128
0.21366	-0.02072
0.26263	-0.01957
0.31707	-0.01795
0.40010	-0.01521
0.48486	-0.01211
0.56908	-0.00895
0.65267	-0.00577
0.73469	-0.00254
0.82017	0.00097
0.86467	0.00249
0.90401	0.00282
0.93582	0.00241
0.96612	0.00152
0.97825	0.00100
0.99095	0.00046
0.99950	0.00018
1.00000	-0.00094

S7075 (B)
actual model

x/c	y/c
1.00000	0.00019
0.99824	0.00040
0.99737	0.00091
0.99129	0.00151
0.98450	0.00248
0.97371	0.00392
0.96111	0.00598
0.94657	0.00822
0.93151	0.01051
0.91847	0.01250
0.90383	0.01480
0.89029	0.01698
0.85440	0.02265
0.80416	0.02991
0.71546	0.04355
0.64805	0.05212
0.56423	0.06027
0.48340	0.06597
0.39636	0.06926
0.31389	0.06961
0.27336	0.06844
0.23433	0.06634
0.21456	0.06480
0.19055	0.06253
0.17320	0.06052
0.15512	0.05810
0.13958	0.05574
0.12759	0.05373
0.11461	0.05139
0.09668	0.04783
0.08151	0.04425
0.06785	0.04057
0.05766	0.03749
0.04516	0.03318
0.03759	0.03022
0.02896	0.02640
0.02160	0.02253
0.01709	0.01968
0.01206	0.01584
0.00874	0.01287
0.00365	0.00752
0.00174	0.00518
0.00473	-0.00869
0.00703	-0.01106
0.01091	-0.01338
0.01618	-0.01491
0.02114	-0.01613
0.02532	-0.01704
0.03219	-0.01829
0.04092	-0.01948
0.05730	-0.02100
0.07905	-0.02239
0.10531	-0.02354
0.13410	-0.02421
0.16315	-0.02427
0.20550	-0.02371
0.24315	-0.02266
0.32792	-0.01992
0.40932	-0.01721
0.49307	-0.01435
0.57704	-0.01165
0.65876	-0.00892
0.73955	-0.00629
0.82431	-0.00238
0.86455	-0.00079
0.90509	0.00013
0.93527	0.00053
0.94952	0.00061
0.96477	0.00015
0.97852	0.00016
0.99012	-0.00021
0.99842	-0.00040
1.00000	0.00019

S8025

x/c	y/c
1.00000	0.00000
0.99919	0.00002
0.99678	0.00012
0.99284	0.00034
0.98745	0.00066
0.98063	0.00104
0.97238	0.00147
0.96270	0.00196
0.95165	0.00253
0.93925	0.00318
0.92556	0.00391
0.91060	0.00473
0.89445	0.00563
0.87713	0.00662
0.85872	0.00769
0.83927	0.00885
0.81884	0.01009
0.79749	0.01141
0.77528	0.01281
0.75230	0.01429
0.72860	0.01585
0.70427	0.01749
0.67938	0.01921
0.65405	0.02100
0.62835	0.02284
0.60235	0.02471
0.57615	0.02658
0.54980	0.02845
0.52339	0.03031
0.49702	0.03212
0.47073	0.03387
0.44461	0.03555
0.41873	0.03714
0.39318	0.03862
0.36801	0.03997
0.34327	0.04118
0.31906	0.04223
0.29543	0.04311
0.27244	0.04379
0.25013	0.04426
0.22857	0.04452
0.20782	0.04454
0.18791	0.04428
0.16884	0.04377
0.15069	0.04301
0.13350	0.04199
0.11729	0.04067
0.10203	0.03908
0.08779	0.03725
0.07462	0.03516
0.06250	0.03280
0.05141	0.03021
0.04137	0.02743
0.03244	0.02448
0.02461	0.02134
0.01781	0.01806
0.01210	0.01472
0.00752	0.01136
0.00406	0.00796
0.00163	0.00458
0.00025	0.00141
0.00020	-0.00126
0.00177	-0.00376
0.00481	-0.00649
0.00907	-0.00932
0.01451	-0.01216
0.02109	-0.01496
0.02877	-0.01763
0.03761	-0.02012
0.04765	-0.02244
0.05882	-0.02462
0.07109	-0.02660
0.08447	-0.02836
0.09896	-0.02993
0.11451	-0.03130
0.13107	-0.03247
0.14862	-0.03343
0.16716	-0.03417
0.18662	-0.03474
0.20694	-0.03511
0.22809	-0.03530
0.25002	-0.03530
0.27267	-0.03515
0.29596	-0.03483
0.31986	-0.03436
0.34431	-0.03374
0.36923	-0.03299
0.39455	-0.03211
0.42021	-0.03112
0.44614	-0.03002
0.47227	-0.02883
0.49851	-0.02754
0.52481	-0.02615
0.55113	-0.02470

0.57738	-0.02320
0.60349	-0.02168
0.62936	-0.02015
0.65494	-0.01862
0.68013	-0.01712
0.70485	-0.01564
0.72904	-0.01420
0.75261	-0.01281
0.77549	-0.01147
0.79761	-0.01020
0.81890	-0.00899
0.83929	-0.00786
0.85871	-0.00681
0.87710	-0.00583
0.89441	-0.00494
0.91057	-0.00413
0.92552	-0.00340
0.93922	-0.00276
0.95163	-0.00219
0.96269	-0.00170
0.97237	-0.00127
0.98062	-0.00090
0.98745	-0.00057
0.99284	-0.00029
0.99677	-0.00010
0.99919	-0.00001

S8025

actual model

x/c	y/c
1.00000	-0.00026
0.99986	-0.00036
0.99402	0.00015
0.98846	0.00056
0.98424	0.00063
0.97665	0.00109
0.95839	0.00180
0.94238	0.00254
0.92402	0.00359
0.89924	0.00479
0.86398	0.00686
0.81653	0.00975
0.73427	0.01547
0.65368	0.02140
0.56642	0.02799
0.48461	0.03398
0.40262	0.03940
0.36281	0.04168
0.31945	0.04374
0.28407	0.04504
0.23556	0.04613
0.21646	0.04628
0.19674	0.04625
0.17931	0.04599
0.15547	0.04519
0.14147	0.04442
0.12642	0.04331
0.11139	0.04185
0.09802	0.04024
0.08546	0.03838
0.07223	0.03598
0.06102	0.03348
0.05152	0.03100
0.04368	0.02867
0.03502	0.02575
0.02687	0.02256
0.02004	0.01942
0.01311	0.01563
0.00854	0.01247
0.00410	0.00851
0.00031	0.00213
0.00002	-0.00052
0.00053	-0.00276
0.00287	-0.00569
0.00671	-0.00850
0.01291	-0.01192
0.01522	-0.01300
0.02082	-0.01532
0.02846	-0.01785
0.03723	-0.02016
0.04625	-0.02209
0.05700	-0.02396
0.06953	-0.02572
0.08288	-0.02722
0.10036	-0.02887
0.11859	-0.03024
0.13111	-0.03102
0.14564	-0.03172
0.15889	-0.03224
0.17631	-0.03278
0.20020	-0.03325
0.23962	-0.03358
0.28663	-0.03331
0.32294	-0.03270
0.40814	-0.03024
0.48975	-0.02684
0.57407	-0.02275
0.65798	-0.01837
0.73924	-0.01402
0.78416	-0.01160
0.81916	-0.00971
0.85814	-0.00769
0.90136	-0.00529
0.92776	-0.00381
0.94581	-0.00287
0.96014	-0.00195
0.97458	-0.00098
0.98700	-0.00040
0.99897	0.00036
1.00000	-0.00026

SD7037

x/c	y/c
1.00000	0.00000
0.99672	0.00042
0.98707	0.00180
0.97146	0.00436
0.95041	0.00811
0.92450	0.01295
0.89425	0.01865
0.86015	0.02490
0.82261	0.03141
0.78201	0.03788
0.73865	0.04413
0.69294	0.05011
0.64539	0.05572
0.59655	0.06085
0.54693	0.06538
0.49706	0.06917
0.44745	0.07211
0.39862	0.07410
0.35101	0.07504
0.30508	0.07488
0.26125	0.07358
0.21989	0.07113
0.18137	0.06754
0.14601	0.06286
0.11410	0.05715
0.08586	0.05049
0.06146	0.04300
0.04102	0.03486
0.02462	0.02632
0.01232	0.01770
0.00418	0.00936
0.00021	0.00185
0.00127	-0.00393
0.00806	-0.00839
0.02038	-0.01227
0.03800	-0.01541
0.06074	-0.01777
0.08844	-0.01934
0.12084	-0.02017
0.15765	-0.02032
0.19850	-0.01987
0.24296	-0.01891
0.29055	-0.01754
0.34071	-0.01586
0.39288	-0.01396
0.44643	-0.01190
0.50074	-0.00976
0.55519	-0.00760
0.60914	-0.00549
0.66197	-0.00349
0.71305	-0.00168
0.76178	-0.00014
0.80752	0.00104
0.84964	0.00182
0.88756	0.00220
0.92071	0.00218
0.94859	0.00185
0.97077	0.00132
0.98690	0.00071
0.99671	0.00021
1.00000	0.00000

SD7037 (B)

actual model

x/c	y/c
1.00000	0.00024
0.99970	0.00101
0.99598	0.00202
0.99205	0.00266
0.98502	0.00365
0.97716	0.00484
0.96931	0.00617
0.96189	0.00740
0.95176	0.00908
0.93747	0.01138
0.92491	0.01353
0.90813	0.01654
0.89082	0.01969
0.87337	0.02265
0.84839	0.02689
0.82124	0.03133
0.77629	0.03808
0.73714	0.04373
0.67533	0.05168
0.61304	0.05864
0.55026	0.06448
0.48609	0.06920
0.42380	0.07261
0.36212	0.07430
0.29770	0.07411
0.23632	0.07153
0.19389	0.06803
0.15198	0.06297
0.12033	0.05764
0.09461	0.05214
0.07954	0.04827
0.06942	0.04532
0.05672	0.04144
0.04558	0.03723
0.03513	0.03261
0.02605	0.02761
0.01987	0.02350
0.01370	0.01882
0.01022	0.01598
0.00719	0.01306
0.00167	0.00588
0.00022	0.00212
0.00211	-0.00668
0.00487	-0.00914
0.01007	-0.01186
0.01523	-0.01365
0.02322	-0.01605
0.02997	-0.01761
0.04075	-0.01936
0.05077	-0.02039
0.06403	-0.02134
0.07854	-0.02223
0.09895	-0.02280
0.13065	-0.02300
0.15845	-0.02281
0.20002	-0.02238
0.24292	-0.02137
0.30574	-0.01912
0.36946	-0.01644
0.43210	-0.01382
0.49408	-0.01144
0.55674	-0.00899
0.61627	-0.00666
0.68273	-0.00401
0.74376	-0.00163
0.78840	-0.00022
0.82871	0.00066
0.86231	0.00116
0.89094	0.00125
0.90746	0.00133
0.92920	0.00109
0.94526	0.00087
0.95938	0.00051
0.97400	0.00017
0.98276	-0.00013
0.99226	-0.00073
0.99963	-0.00101
1.00000	0.00024

SD7037 (C)
actual model

x/c	y/c
1.00000	-0.00018
0.99471	0.00188
0.98993	0.00265
0.98364	0.00354
0.97691	0.00447
0.97093	0.00549
0.96112	0.00700
0.94809	0.00924
0.93348	0.01206
0.91936	0.01479
0.90397	0.01800
0.88898	0.02128
0.86071	0.02691
0.82971	0.03249
0.79470	0.03836
0.73310	0.04760
0.66981	0.05602
0.60853	0.06307
0.54757	0.06884
0.48767	0.07341
0.42723	0.07627
0.36050	0.07727
0.29903	0.07610
0.27049	0.07507
0.23667	0.07314
0.20022	0.06990
0.17648	0.06711
0.15006	0.06330
0.13187	0.06019
0.11262	0.05652
0.09747	0.05328
0.08465	0.05015
0.07330	0.04697
0.05830	0.04203
0.04937	0.03870
0.04047	0.03498
0.03129	0.03049
0.02227	0.02503
0.01432	0.01904
0.00958	0.01485
0.00593	0.01123
0.00172	0.00535
0.00100	0.00385
0.00028	-0.00201
0.00233	-0.00583
0.00685	-0.00863
0.01315	-0.01103
0.01759	-0.01228
0.02481	-0.01395
0.03350	-0.01560
0.03951	-0.01652
0.04807	-0.01757
0.05944	-0.01842
0.07477	-0.01923
0.09128	-0.01987
0.10023	-0.02013
0.11760	-0.02046
0.13620	-0.02065
0.15474	-0.02072
0.18180	-0.02053
0.20703	-0.02003
0.24336	-0.01897
0.30521	-0.01681
0.36871	-0.01409
0.42979	-0.01139
0.49173	-0.00877
0.55317	-0.00642
0.61206	-0.00418
0.67850	-0.00173
0.73952	-0.00007
0.80408	0.00100
0.83774	0.00152
0.86997	0.00161
0.90165	0.00148
0.91780	0.00121
0.93104	0.00069
0.94705	0.00041
0.96182	-0.00005
0.98081	-0.00064
0.99007	-0.00093
0.99521	-0.00112
0.99832	-0.00099
1.00000	-0.00018

Appendix B

Airfoil Polar Data

All of the polar data shown in Chapter 5 is listed in this appendix and identified by airfoil name, figure number, and run number. This same data in addition to the four spanwise C_d values used to obtain the average C_d are included with the data distribution disk. Also included on the disk but not listed here is the lift data plotted in the C_l-α curves shown in Chapter 5.

CR-001
Fig. 5.3

Run: 658
$Re = 59800$

α	C_l	C_d
-4.23	-0.109	0.0445
-2.70	0.063	0.0279
-1.16	0.221	0.0216
0.38	0.386	0.0227
1.81	0.566	0.0261
3.47	0.786	0.0321
4.99	0.969	0.0285
6.53	1.089	0.0292
8.05	1.187	0.0327
9.57	1.246	0.0432
11.07	1.283	0.0642

Run: 660
$Re = 100000$

α	C_l	C_d
-4.25	-0.178	0.0487
-2.67	0.052	0.0243
-1.18	0.214	0.0201
0.38	0.433	0.0191
1.93	0.651	0.0225
3.48	0.827	0.0203
5.01	0.958	0.0190
6.54	1.079	0.0206
7.96	1.174	0.0279
9.57	1.243	0.0371
11.07	1.268	0.0556

Run: 662
$Re = 200700$

α	C_l	C_d
-5.27	-0.309	0.0746
-3.75	-0.051	0.0348
-2.17	0.176	0.0171
-0.62	0.410	0.0126
0.90	0.581	0.0106
2.48	0.738	0.0110
3.99	0.883	0.0121
5.51	1.016	0.0143
7.05	1.131	0.0187
8.57	1.215	0.0262
10.08	1.270	0.0360

Run: 664
$Re = 301500$

α	C_l	C_d
-5.30	-0.251	0.0694
-3.70	0.041	0.0266
-2.29	0.246	0.0132
-0.62	0.438	0.0088
0.94	0.595	0.0078
2.46	0.752	0.0086
4.02	0.900	0.0103
5.53	1.031	0.0129
7.07	1.145	0.0174
8.60	1.236	0.0236
10.10	1.292	0.0330

Davis 3R
Fig. 5.7

Run: 752
$Re = 40600$

α	C_l	C_d
-1.99	0.132	0.0493
-0.46	0.342	0.0396
1.07	0.523	0.0370
2.62	0.695	0.0371
4.16	0.848	0.0470
5.66	0.981	0.0467
7.21	1.141	0.0351
8.73	1.196	0.0397
10.23	1.237	0.0554
11.75	1.294	0.0702
13.24	1.288	0.1081

Run: 754
$Re = 60400$

α	C_l	C_d
-1.97	0.275	0.0473
-0.43	0.477	0.0340
1.11	0.655	0.0283
2.65	0.817	0.0269
4.18	0.959	0.0296
5.71	1.099	0.0291
7.24	1.186	0.0323
8.74	1.232	0.0430
10.25	1.293	0.0567
11.78	1.342	0.0714
13.25	1.330	0.1092

Run: 756
$Re = 100600$

α	C_l	C_d
-1.94	0.324	0.0344
-0.41	0.518	0.0244
1.11	0.672	0.0198
2.65	0.823	0.0187
4.16	0.962	0.0203
5.71	1.086	0.0224
7.23	1.152	0.0333
8.73	1.215	0.0441
10.25	1.276	0.0565
11.75	1.315	0.0762
13.21	1.304	0.1129

Run: 872
$Re = 200700$

α	C_l	C_d
-2.95	0.039	0.0547
-1.47	0.261	0.0357
0.13	0.613	0.0175
1.66	0.779	0.0154
3.02	0.916	0.0166
4.66	1.057	0.0220
6.08	1.132	0.0304
7.73	1.214	0.0401
9.24	1.271	0.0531

Run: 874
$Re = 301100$

α	C_l	C_d
-3.12	0.025	0.0599
-1.42	0.478	0.0239
0.09	0.654	0.0177
1.64	0.819	0.0164
3.18	0.976	0.0180
4.68	1.083	0.0241
6.25	1.172	0.0322
7.77	1.243	0.0414

DU 86-084/18
Fig. 5.11

Run: 790
$Re = 59800$

α	C_l	C_d
-5.76	-0.417	0.0308
-4.23	-0.332	0.0230
-2.74	-0.228	0.0152
-1.19	-0.110	0.0160
0.32	0.025	0.0163
1.88	0.181	0.0216
3.43	0.419	0.0287
4.95	0.584	0.0244
6.50	0.689	0.0236
8.02	0.774	0.0368
9.54	0.854	0.0567

Run: 792
$Re = 100300$

α	C_l	C_d
-5.73	-0.470	0.0294
-4.21	-0.355	0.0210
-2.71	-0.225	0.0153
-1.18	-0.107	0.0130
0.38	0.072	0.0158
1.92	0.273	0.0186
3.46	0.482	0.0201
5.00	0.601	0.0167
6.50	0.716	0.0206
8.03	0.814	0.0331
9.56	0.894	0.0538

Run: 794
$Re = 201400$

α	C_l	C_d
-5.70	-0.411	0.0227
-4.21	-0.263	0.0155
-2.70	-0.119	0.0122
-0.13	0.124	0.0118
0.39	0.206	0.0125
1.92	0.337	0.0129
3.46	0.455	0.0120
5.00	0.601	0.0114
6.55	0.732	0.0184
8.05	0.841	0.0277
9.58	0.924	0.0472

Run: 796
$Re = 301700$

α	C_l	C_d
-5.69	-0.426	0.0231
-4.30	-0.299	0.0158
-2.59	-0.131	0.0112
0.08	0.085	0.0102
0.40	0.141	0.0102
1.91	0.306	0.0101
3.47	0.452	0.0091
4.98	0.591	0.0106
6.51	0.725	0.0167
8.03	0.840	0.0248
9.58	0.940	0.0463

E374 (B)
Fig. 5.15

Run: 616
$Re = 60400$

α	C_l	C_d
-6.44	-0.366	0.0339
-5.44	-0.320	0.0277
-4.41	-0.270	0.0229
-3.40	-0.209	0.0186
-2.36	-0.099	0.0188
-1.33	0.006	0.0233
-0.32	0.154	0.0266
0.69	0.261	0.0308
1.73	0.338	0.0328
2.73	0.402	0.0387
4.00	0.519	0.0439
4.82	0.681	0.0409
5.84	0.792	0.0384
6.86	0.890	0.0330
7.88	0.972	0.0270
8.87	0.983	0.0386
10.07	1.013	0.0512

Run: 618
$Re = 100900$

α	C_l	C_d
-6.45	-0.452	0.0297
-5.46	-0.406	0.0241
-4.42	-0.311	0.0198
-3.39	-0.165	0.0166
-2.34	-0.004	0.0180
-1.32	0.141	0.0199
-0.02	0.268	0.0219
0.71	0.326	0.0241
1.75	0.411	0.0275
2.78	0.501	0.0307
3.80	0.601	0.0310
4.82	0.707	0.0264
5.84	0.803	0.0218
6.87	0.892	0.0211
7.88	0.947	0.0265
8.86	0.970	0.0353
9.88	1.006	0.0436

Run: 620
$Re = 201500$

α	C_l	C_d
-6.43	-0.451	0.0231
-5.39	-0.315	0.0172
-4.38	-0.186	0.0134
-3.36	-0.101	0.0113
-2.34	-0.031	0.0097
-1.32	0.062	0.0115
-0.30	0.195	0.0117
0.73	0.329	0.0122
1.76	0.421	0.0129
2.77	0.519	0.0135
3.81	0.623	0.0139
4.78	0.718	0.0137
5.85	0.821	0.0142
6.87	0.897	0.0168

7.88	0.935	0.0245
8.89	0.974	0.0305
9.90	1.006	0.0386

Run: 622
$Re = 302200$

α	C_l	C_d
-6.43	-0.407	0.0197
-5.38	-0.284	0.0146
-3.99	-0.165	0.0119
-3.42	-0.121	0.0110
-2.34	-0.031	0.0091
-1.32	0.057	0.0088
-0.30	0.159	0.0094
0.74	0.328	0.0105
1.71	0.422	0.0101
2.78	0.525	0.0103
3.82	0.627	0.0107
4.83	0.726	0.0110
5.86	0.821	0.0117
6.87	0.886	0.0168
7.85	0.928	0.0228
8.88	0.972	0.0281
9.89	1.007	0.0361

E423

Fig. 5.19

Run: 844
$Re = 60600$

α	C_l	C_d
-4.55	-0.200	0.1032
-3.03	-0.251	0.1068
-1.48	-0.054	0.1034
0.08	0.270	0.1011
1.63	0.478	0.1109
3.13	0.586	0.1213
4.65	0.673	0.1354
6.18	0.747	0.1562
7.70	0.810	0.1660
9.20	0.847	0.1790
10.72	0.891	0.2098

Run: 846
$Re = 100800$

α	C_l	C_d
-4.43	0.217	0.0646
-2.91	0.357	0.0549
-1.30	0.694	0.0326
0.20	0.852	0.0364
1.74	0.964	0.0442
3.26	1.097	0.0455
4.82	1.239	0.0450
6.19	0.901	0.1364
7.68	0.924	0.1496
9.22	0.925	0.2004
10.66	0.981	0.1992

Run: 848
$Re = 201600$

α	C_l	C_d
-4.44	0.250	0.0612
-2.89	0.431	0.0484
-1.30	0.793	0.0208
0.18	0.939	0.0223
1.73	1.084	0.0239
3.29	1.224	0.0245
4.82	1.350	0.0251
7.18	1.538	0.0293
7.86	1.587	0.0307
9.28	1.688	0.0326
10.95	1.806	0.0346

Run: 850
$Re = 302300$

α	C_l	C_d
-2.32	0.724	0.0180
-0.78	0.877	0.0172
0.74	1.023	0.0184
2.28	1.169	0.0193
3.80	1.304	0.0199
5.33	1.431	0.0201
6.86	1.556	0.0219
8.40	1.668	0.0237
9.89	1.769	0.0259
11.42	1.870	0.0279
12.96	1.944	0.0319

Run: 851
$Re = 302300$

α	C_l	C_d
-4.48	0.275	0.0623
-3.38	0.414	0.0518

LD-79

Fig. 5.23

Run: 945
$Re = 59900$

α	C_l	C_d
-5.59	-0.364	0.0863
-4.06	-0.190	0.0488
-2.52	0.022	0.0340
-1.01	0.200	0.0271
0.57	0.455	0.0234
2.15	0.622	0.0207
3.64	0.764	0.0252
5.15	0.896	0.0299
6.70	1.029	0.0272
8.24	1.115	0.0401
9.74	1.164	0.0606

Run: 947
$Re = 100300$

α	C_l	C_d
-4.57	-0.272	0.0576
-3.09	-0.036	0.0395
-1.48	0.179	0.0267
0.04	0.388	0.0212
1.61	0.540	0.0208
3.14	0.696	0.0192
4.66	0.844	0.0212
6.15	0.967	0.0268
7.71	1.073	0.0357
9.24	1.159	0.0490

Run: 951
$Re = 150400$

α	C_l	C_d
-4.55	-0.255	0.0564
-2.97	-0.029	0.0352
-1.51	0.172	0.0246
0.12	0.379	0.0199
1.59	0.532	0.0184
3.15	0.729	0.0173
4.61	0.863	0.0195
6.21	0.988	0.0289
7.73	1.092	0.0379

Run: 949
$Re = 200700$

α	C_l	C_d
-4.58	-0.267	0.0567
-3.33	-0.073	0.0372
-1.39	0.189	0.0230
0.08	0.396	0.0182
1.58	0.558	0.0168
3.14	0.718	0.0154
6.04	0.971	0.0270
6.20	0.979	0.0277
7.75	1.083	0.0374
9.22	1.152	0.0502

M06-13-128 (B)

Fig. 5.27

Run: 918
$Re = 302500$

α	C_l	C_d
-4.45	0.012	0.0437
-2.88	0.188	0.0298
-1.33	0.401	0.0292
0.19	0.510	0.0316
1.76	0.659	0.0382
3.28	0.822	0.0377
4.90	0.994	0.0345
6.33	1.140	0.0309
7.90	1.308	0.0272
9.39	1.459	0.0230
10.91	1.594	0.0245

M6 (65%)

Fig. 5.31

Run: 758
$Re = 60800$

α	C_l	C_d
-5.52	-0.476	0.0434
-3.44	-0.326	0.0245
-2.47	-0.233	0.0205
-0.94	-0.037	0.0152
0.59	0.029	0.0142
2.12	0.228	0.0204
3.67	0.421	0.0200
5.18	0.527	0.0210
6.74	0.656	0.0247
8.25	0.747	0.0344
9.77	0.836	0.0522

Run: 760
$Re = 100300$

α	C_l	C_d
-5.54	-0.509	0.0483
-4.01	-0.361	0.0269
-2.47	-0.233	0.0187
-0.92	-0.018	0.0119
0.59	0.052	0.0133
2.16	0.321	0.0136
3.67	0.446	0.0154
5.19	0.565	0.0161
6.74	0.678	0.0204
8.25	0.783	0.0306
9.78	0.869	0.0465

Run: 762
$Re = 201500$

α	C_l	C_d
-5.53	-0.530	0.0510
-4.00	-0.380	0.0246
-2.47	-0.245	0.0157
-0.95	-0.101	0.0111
0.58	0.124	0.0087
2.14	0.285	0.0097
3.67	0.425	0.0106
5.86	0.618	0.0140
6.74	0.691	0.0184
8.26	0.801	0.0258
9.79	0.887	0.0428

Run: 764
$Re = 301400$

α	C_l	C_d
-5.54	-0.542	0.0523
-4.02	-0.403	0.0240
-2.48	-0.263	0.0137
-0.96	-0.091	0.0109
0.59	0.077	0.0087
2.23	0.293	0.0084
3.68	0.443	0.0091
5.22	0.577	0.0116
6.73	0.695	0.0162
8.27	0.811	0.0223
9.78	0.908	0.0391

M6 (85%)

Fig. 5.35

Run: 666
$Re = 60200$

α	C_l	C_d
-5.48	-0.430	0.0417
-4.02	-0.334	0.0289
-2.45	-0.237	0.0215
-0.91	-0.057	0.0163
0.64	0.118	0.0212
2.20	0.367	0.0237
3.73	0.512	0.0312
5.25	0.631	0.0329
6.77	0.748	0.0294
8.30	0.869	0.0276
9.82	0.914	0.0391

Run: 715
$Re = 100900$

α	C_l	C_d
-4.30	-0.363	0.0262
-2.95	-0.287	0.0203
-1.43	-0.098	0.0137
0.14	0.196	0.0136
1.68	0.366	0.0153
3.23	0.485	0.0179
4.74	0.608	0.0187
6.28	0.738	0.0190
7.80	0.858	0.0222

9.32	0.921	0.0324
10.83	0.991	0.0454

Run: 723
$Re = 201500$

α	C_l	C_d
-4.79	-0.427	0.0283
-2.32	-0.155	0.0123
-1.40	-0.056	0.0095
0.73	0.232	0.0103
1.68	0.319	0.0108
3.84	0.521	0.0118
4.74	0.601	0.0124
7.00	0.807	0.0145
7.36	0.821	0.0167
9.32	0.919	0.0271
10.84	0.984	0.0382

Run: 725
$Re = 301900$

α	C_l	C_d
-4.47	-0.411	0.0231
-2.90	-0.212	0.0122
-2.17	-0.130	0.0117
0.14	0.091	0.0097
1.67	0.329	0.0090
4.07	0.565	0.0101
5.59	0.701	0.0116
7.11	0.810	0.0150
7.79	0.841	0.0184
9.32	0.928	0.0243
11.50	1.012	0.0414

MA409
Fig. 5.39

Run: 921
$Re = 60000$

α	C_l	C_d
-4.95	-0.243	0.0299
-3.47	-0.131	0.0244
-1.99	0.019	0.0172
-0.42	0.170	0.0159
1.11	0.339	0.0161
2.65	0.512	0.0199
4.24	0.668	0.0221
5.74	0.808	0.0255
7.25	0.901	0.0365
8.78	0.995	0.0515
10.30	1.029	0.0957

Run: 923
$Re = 100200$

α	C_l	C_d
-5.98	-0.393	0.0605
-4.49	-0.195	0.0249
-3.00	-0.058	0.0189
-1.43	0.071	0.0138
0.11	0.217	0.0133
1.64	0.431	0.0143
3.15	0.616	0.0153
4.73	0.766	0.0163
6.29	0.880	0.0228
7.77	0.969	0.0330
9.26	1.048	0.0532

Run: 925
$Re = 200900$

α	C_l	C_d
-6.03	-0.352	0.0530
-4.41	-0.167	0.0163
-2.87	-0.008	0.0137
-1.37	0.148	0.0108
0.07	0.302	0.0087
2.83	0.598	0.0102
3.13	0.627	0.0106
4.71	0.777	0.0137
6.23	0.914	0.0192
7.77	1.017	0.0279
9.31	1.092	0.0468

Run: 927
$Re = 301100$

α	C_l	C_d
-5.99	-0.304	0.0196
-4.54	-0.155	0.0137
-2.95	0.010	0.0121
-1.46	0.173	0.0096
0.09	0.328	0.0075
1.64	0.480	0.0080
3.26	0.648	0.0099
6.07	0.910	0.0165
6.35	0.933	0.0176
7.78	1.030	0.0254
9.21	1.100	0.0389

MH32
Fig. 5.43

Run: 632
$Re = 59900$

α	C_l	C_d
-4.26	-0.228	0.0309
-2.25	-0.089	0.0204
-0.71	0.052	0.0145
0.75	0.190	0.0179
2.38	0.468	0.0231
3.82	0.652	0.0245
5.44	0.792	0.0239
6.98	0.918	0.0248
8.51	1.017	0.0311
10.00	1.094	0.0399
11.54	1.143	0.0580

Run: 634
$Re = 100100$

α	C_l	C_d
-3.81	-0.242	0.0248
-2.26	-0.090	0.0177
-0.72	0.062	0.0146
0.83	0.310	0.0177
2.38	0.509	0.0182
3.92	0.655	0.0173
5.46	0.794	0.0177
6.98	0.917	0.0209
8.50	1.026	0.0283
10.02	1.097	0.0402
11.53	1.145	0.0562

Run: 636
$Re = 200700$

α	C_l	C_d
-3.77	-0.202	0.0187
-2.23	0.013	0.0132
-0.69	0.174	0.0112
1.28	0.386	0.0101
2.38	0.495	0.0104
3.93	0.650	0.0111
5.45	0.791	0.0132
6.99	0.921	0.0168
8.52	1.026	0.0228
10.00	1.104	0.0312
11.54	1.158	0.0428

Run: 638
$Re = 301200$

α	C_l	C_d
-3.76	-0.137	0.0154
-2.22	0.032	0.0116
-0.69	0.172	0.0084
0.85	0.337	0.0073
2.92	0.554	0.0083
3.94	0.656	0.0094
5.46	0.799	0.0121
7.00	0.929	0.0153
8.53	1.039	0.0209
9.98	1.118	0.0275
11.56	1.177	0.0378

NACA 2414
Fig. 5.47

Run: 774
$Re = 60400$

α	C_l	C_d
-4.91	-0.450	0.0300
-3.37	-0.349	0.0229
-1.85	-0.225	0.0220
-0.31	-0.032	0.0248
1.25	0.228	0.0304
2.80	0.423	0.0332
4.32	0.572	0.0342
5.85	0.700	0.0354
7.40	0.821	0.0356
8.93	0.937	0.0351
11.23	1.055	0.0430

Run: 776
$Re = 100800$

α	C_l	C_d
-6.23	-0.612	0.0259
-3.35	-0.332	0.0201
-1.84	-0.133	0.0201
-0.26	0.076	0.0196
1.31	0.362	0.0210
2.82	0.469	0.0211
4.34	0.592	0.0200
5.87	0.718	0.0207
7.41	0.841	0.0220
8.93	0.969	0.0249
10.45	1.049	0.0333

Run: 778
$Re = 201600$

α	C_l	C_d
-4.88	-0.382	0.0175
-3.28	-0.171	0.0147
-1.77	-0.020	0.0134
-0.28	0.112	0.0113
1.28	0.271	0.0108
2.80	0.494	0.0123
4.33	0.628	0.0135
5.88	0.762	0.0146
7.42	0.887	0.0164
8.94	0.996	0.0194
10.45	1.069	0.0249

Run: 780
$Re = 302700$

α	C_l	C_d
-4.87	-0.316	0.0130
-3.35	-0.169	0.0115
-1.80	-0.030	0.0109
-0.23	0.119	0.0097
1.27	0.263	0.0092
2.86	0.479	0.0112
4.36	0.634	0.0114
5.88	0.759	0.0128
7.41	0.878	0.0145
8.93	0.983	0.0176
10.45	1.062	0.0229

NACA 2415
Fig. 5.51

Run: 782
$Re = 60000$

α	C_l	C_d
-4.89	-0.426	0.0292
-3.38	-0.255	0.0237
-1.82	-0.048	0.0271
-0.30	0.135	0.0375
1.25	0.215	0.0368
2.76	0.338	0.0435
4.30	0.525	0.0454
5.85	0.717	0.0453
7.39	0.871	0.0414
8.91	0.993	0.0346
10.44	1.065	0.0450

Run: 784
$Re = 101300$

α	C_l	C_d
-4.91	-0.415	0.0209
-2.42	-0.056	0.0211
-1.81	0.002	0.0224
-0.28	0.138	0.0253
1.29	0.403	0.0253
2.81	0.516	0.0243
4.33	0.643	0.0228
5.87	0.776	0.0236
8.40	0.975	0.0251
8.92	0.996	0.0273
10.43	1.056	0.0406

Run: 786
$Re = 201900$

α	C_l	C_d
-4.87	-0.248	0.0143
-3.29	-0.114	0.0128
-1.80	0.011	0.0126
-0.22	0.169	0.0133
1.25	0.309	0.0138
2.80	0.520	0.0127
4.34	0.693	0.0152
5.84	0.831	0.0165
7.40	0.950	0.0181
8.93	1.037	0.0236
11.33	1.144	0.0370

Run: 788
$Re = 303100$

α	C_l	C_d
-4.87	-0.263	0.0118
-3.43	-0.139	0.0109
-1.79	0.017	0.0105
-0.29	0.165	0.0103
1.25	0.344	0.0106
2.82	0.541	0.0105
4.35	0.720	0.0123
5.87	0.853	0.0135
7.41	0.960	0.0166
8.92	1.051	0.0217
10.44	1.130	0.0288

RG15 (C)
Fig. 5.55

Run: 884
$Re = 60000$

α	C_l	C_d
-6.48	-0.370	0.0377
-4.98	-0.273	0.0247
-3.46	-0.169	0.0149
-1.96	-0.070	0.0146
-0.40	0.063	0.0186
1.14	0.273	0.0220
2.70	0.512	0.0237
4.24	0.621	0.0229
5.76	0.764	0.0230
7.28	0.871	0.0276
8.80	0.953	0.0387

Run: 886
$Re = 100600$

α	C_l	C_d
-6.48	-0.412	0.0327
-4.98	-0.300	0.0206
-3.47	-0.176	0.0149
-1.97	-0.047	0.0106
-0.40	0.167	0.0147
1.17	0.406	0.0150
2.70	0.543	0.0150
4.22	0.670	0.0172
5.77	0.813	0.0204
7.30	0.930	0.0254
8.83	1.000	0.0388

Run: 888
$Re = 201400$

α	C_l	C_d
-6.39	-0.397	0.0271
-4.99	-0.288	0.0172
-2.15	0.040	0.0091
-1.92	0.057	0.0090
-0.38	0.229	0.0089
1.15	0.395	0.0094
2.70	0.558	0.0107
4.23	0.708	0.0130
5.77	0.847	0.0163
7.30	0.952	0.0235
8.82	1.030	0.0337

Run: 890
$Re = 301700$

α	C_l	C_d
-6.53	-0.415	0.0295
-4.99	-0.280	0.0152
-1.73	0.091	0.0074
-1.92	0.067	0.0078
-0.38	0.215	0.0065
1.15	0.389	0.0078
2.69	0.549	0.0091
4.23	0.703	0.0111
5.77	0.839	0.0149
7.30	0.951	0.0216
8.81	1.035	0.0309

RG15 (C)
Fig. 5.57

Run: 929
$Re = 60100$

α	C_l	C_d
-6.49	-0.356	0.0323
-4.96	-0.242	0.0226
-3.43	-0.133	0.0148
-1.93	-0.027	0.0149
-0.39	0.132	0.0164
1.15	0.309	0.0226
2.71	0.577	0.0226
4.25	0.707	0.0226
5.79	0.844	0.0233
7.30	0.945	0.0282
8.82	1.015	0.0408

Run: 931
$Re = 100600$

α	C_l	C_d
-6.47	-0.376	0.0302
-4.96	-0.256	0.0217
-3.45	-0.132	0.0152
-1.93	-0.026	0.0131
-0.37	0.173	0.0170
1.18	0.439	0.0165
2.71	0.590	0.0158
4.25	0.729	0.0172
5.78	0.864	0.0205
7.30	0.969	0.0259
8.81	1.032	0.0397

Run: 933
$Re = 201000$

α	C_l	C_d
-6.49	-0.397	0.0287
-4.98	-0.273	0.0180
-3.45	-0.126	0.0125
-1.90	0.070	0.0098
-0.37	0.248	0.0091
1.18	0.398	0.0095
2.71	0.555	0.0106
4.25	0.723	0.0134
5.78	0.862	0.0168
7.32	0.968	0.0239
8.84	1.043	0.0346

Run: 935
$Re = 301600$

α	C_l	C_d
-6.56	-0.400	0.0285
-4.98	-0.252	0.0153
-3.56	-0.086	0.0114
-1.91	0.092	0.0080
-0.37	0.230	0.0071
1.18	0.432	0.0080
2.74	0.596	0.0095
4.25	0.743	0.0118
5.77	0.874	0.0155
7.29	0.980	0.0224
8.83	1.061	0.0322

RG15 (C)
Fig. 5.60

Run: 954
$Re = 60700$

α	C_l	C_d
-6.51	-0.202	0.0298
-4.97	-0.065	0.0235
-3.45	0.033	0.0160
-1.91	0.183	0.0170
-0.40	0.336	0.0198
1.13	0.523	0.0255
2.70	0.778	0.0249
4.23	0.908	0.0272
5.76	0.994	0.0319
7.26	1.047	0.0399
8.79	1.103	0.0504

Run: 956
$Re = 100500$

α	C_l	C_d
-6.47	-0.258	0.0276
-4.96	-0.096	0.0226
-3.45	0.023	0.0169
-1.92	0.164	0.0152
-0.36	0.362	0.0188
1.20	0.635	0.0189
2.73	0.807	0.0156
4.26	0.917	0.0196
5.78	1.014	0.0255
7.29	1.075	0.0344
8.80	1.132	0.0500

Run: 958
$Re = 200900$

α	C_l	C_d
-6.43	-0.093	0.0185
-4.95	0.034	0.0157
-3.36	0.164	0.0125
-0.60	0.467	0.0117
-0.33	0.501	0.0109
1.19	0.671	0.0109
2.75	0.816	0.0130
4.25	0.939	0.0170
5.79	1.039	0.0227
7.30	1.110	0.0317

Run: 959
$Re = 201900$

α	C_l	C_d
-1.88	0.314	0.0128

Run: 961
$Re = 301500$

α	C_l	C_d
-6.46	-0.096	0.0172
-4.95	0.043	0.0126
-3.41	0.193	0.0097
-2.03	0.333	0.0090
-0.39	0.492	0.0104
1.20	0.653	0.0113
2.68	0.805	0.0124
4.23	0.925	0.0155
5.76	1.018	0.0209
7.32	1.093	0.0288
8.80	1.155	0.0407

RG15 (C)
Fig. 5.63

Run: 965
$Re = 60500$

α	C_l	C_d
-8.57	-0.316	0.0504
-7.02	-0.112	0.0294
-5.47	0.051	0.0233
-3.98	0.116	0.0223
-2.43	0.255	0.0249
-0.91	0.414	0.0265
0.64	0.592	0.0302
2.21	0.910	0.0325
3.75	1.076	0.0279
5.26	1.132	0.0351
6.76	1.184	0.0464

Run: 967
$Re = 100300$

α	C_l	C_d
-8.56	-0.283	0.0531
-7.00	-0.092	0.0300
-5.49	0.038	0.0202
-3.97	0.140	0.0210
-2.42	0.289	0.0202
-0.89	0.461	0.0212
0.64	0.664	0.0271
2.22	0.925	0.0194
3.75	1.029	0.0236
5.26	1.103	0.0295
6.75	1.150	0.0401

Run: 969
$Re = 200800$

α	C_l	C_d
-8.51	-0.091	0.0268
-6.90	0.029	0.0210
-5.55	0.145	0.0180
-3.92	0.279	0.0178
-2.34	0.428	0.0186
-0.86	0.581	0.0194
0.78	0.835	0.0113
2.20	0.948	0.0147
3.70	1.047	0.0199
5.25	1.123	0.0278
6.77	1.184	0.0370

Run: 963
$Re = 301500$

α	C_l	C_d
-7.49	0.022	0.0176
-5.95	0.179	0.0141
-4.43	0.304	0.0152
-2.91	0.409	0.0166
-1.36	0.646	0.0141
0.20	0.807	0.0113
1.68	0.923	0.0127
3.27	1.033	0.0169
4.64	1.107	0.0228
6.25	1.177	0.0313
7.85	1.234	0.0439

S822
Fig. 5.67

Run: 827
$Re = 100900$

α	C_l	C_d
-4.17	-0.369	0.0283
-2.62	-0.203	0.0285
-1.09	-0.078	0.0312
0.44	0.042	0.0349
1.94	0.127	0.0411
4.28	0.610	0.0229
5.05	0.605	0.0230
6.57	0.714	0.0280
8.11	0.820	0.0336
9.62	0.906	0.0423
11.15	0.976	0.0522

Run: 829
$Re = 202300$

α	C_l	C_d
-4.10	-0.157	0.0221
-2.56	-0.021	0.0233
-1.03	0.177	0.0195
0.50	0.311	0.0161
2.02	0.426	0.0184
3.55	0.553	0.0202
5.07	0.634	0.0233
6.56	0.722	0.0241
8.09	0.830	0.0310
9.63	0.914	0.0391
11.14	0.981	0.0492

Run: 831
$Re = 303400$

α	C_l	C_d
-4.09	-0.114	0.0173
-2.56	0.013	0.0151
-1.10	0.142	0.0151
0.33	0.263	0.0163
2.01	0.416	0.0181
3.62	0.559	0.0199
5.08	0.673	0.0220
6.57	0.762	0.0255
8.10	0.822	0.0298
9.63	0.907	0.0368
11.13	0.976	0.0466

Run: 854
$Re = 404700$

α	C_l	C_d
-3.05	-0.041	0.0149
-1.55	0.093	0.0148
-0.05	0.228	0.0161
1.50	0.373	0.0172
3.03	0.510	0.0188
4.64	0.642	0.0211
6.06	0.739	0.0239
7.60	0.828	0.0284
9.14	0.894	0.0332
10.63	0.966	0.0408

S823
Fig. 5.73

Run: 730
$Re = 101400$

α	C_l	C_d
-2.79	-0.201	0.0374
-1.22	-0.006	0.0384
0.30	0.170	0.0394
1.83	0.387	0.0313
3.38	0.565	0.0246
4.91	0.712	0.0251
6.42	0.801	0.0290
7.95	0.879	0.0345
9.46	0.945	0.0397
10.97	0.986	0.0497

Run: 834
$Re = 202700$

α	C_l	C_d
-3.69	-0.113	0.0260
-2.25	0.001	0.0238
-0.72	0.155	0.0218
0.80	0.305	0.0201
2.35	0.442	0.0214
3.90	0.574	0.0237
5.40	0.696	0.0261
6.94	0.804	0.0303
8.45	0.893	0.0360
9.95	0.951	0.0482
11.47	0.991	0.0703

Run: 836
$Re = 304100$

α	C_l	C_d
-2.74	-0.053	0.0214
-1.23	0.087	0.0191
0.30	0.240	0.0186
1.80	0.373	0.0204
3.36	0.519	0.0221
4.83	0.644	0.0242
6.41	0.762	0.0274
7.79	0.847	0.0317
9.44	0.923	0.0414
10.91	0.970	0.0578

Run: 733
$Re = 405800$

α	C_l	C_d
-2.75	-0.055	0.0198
-1.22	0.092	0.0187
0.40	0.246	0.0192
1.85	0.404	0.0202
3.36	0.548	0.0216
4.99	0.690	0.0238
6.42	0.787	0.0267
7.93	0.870	0.0317
9.77	0.949	0.0442
10.99	0.986	0.0530

S4083 (A)
Fig. 5.84

Run: 648
$Re = 60500$

α	C_l	C_d
-3.46	-0.085	0.0299
-2.17	0.019	0.0227
-0.59	0.168	0.0148
0.98	0.386	0.0196
2.51	0.596	0.0260
4.05	0.726	0.0309
5.57	0.850	0.0353
7.09	0.977	0.0405
8.63	1.098	0.0430
10.16	1.205	0.0378
11.67	1.264	0.0550

Run: 650
$Re = 100900$

α	C_l	C_d
-4.67	-0.196	0.0419
-3.12	-0.036	0.0227
-1.61	0.083	0.0176
2.00	0.557	0.0151
3.55	0.702	0.0172
5.06	0.843	0.0201
6.44	0.965	0.0228
8.14	1.111	0.0260
9.65	1.234	0.0288
11.16	1.293	0.0407

Run: 651
$Re = 101000$

α	C_l	C_d
-0.07	0.286	0.0130

Run: 653
$Re = 200700$

α	C_l	C_d
-4.56	-0.178	0.0420
-3.12	-0.026	0.0191
-1.75	0.090	0.0151
-0.05	0.335	0.0088
1.49	0.510	0.0098
3.05	0.669	0.0121
4.57	0.821	0.0143
6.10	0.966	0.0164
7.63	1.103	0.0188
9.15	1.222	0.0217
10.68	1.300	0.0302

Run: 656
$Re = 301400$

α	C_l	C_d
-4.69	-0.197	0.0448
-3.09	-0.009	0.0164
-1.60	0.149	0.0121
-0.05	0.355	0.0080
1.50	0.507	0.0087
3.03	0.665	0.0103
4.56	0.817	0.0121
6.11	0.963	0.0140
7.63	1.096	0.0161
9.17	1.215	0.0199
10.71	1.306	0.0276

S4083 (B)
Fig. 5.88

Run: 640
$Re = 60300$

α	C_l	C_d
-3.85	-0.079	0.0354
-2.32	0.067	0.0246
-0.79	0.213	0.0178
0.76	0.459	0.0163
2.17	0.609	0.0211
3.82	0.753	0.0275
5.35	0.883	0.0369
6.89	1.008	0.0416
8.42	1.122	0.0333
9.91	1.197	0.0461
11.45	1.228	0.0653

Run: 642
$Re = 100100$

α	C_l	C_d
-3.74	-0.097	0.0291
-2.34	0.047	0.0198
-0.78	0.260	0.0143
0.76	0.454	0.0120
2.29	0.611	0.0160
3.80	0.756	0.0192
5.36	0.900	0.0214
6.89	1.037	0.0241
8.43	1.155	0.0284
9.94	1.214	0.0438
11.44	1.232	0.0647

Run: 644
$Re = 200700$

α	C_l	C_d
-3.85	-0.085	0.0287
-2.31	0.118	0.0157
-0.76	0.315	0.0117
0.77	0.489	0.0101
2.32	0.652	0.0124
3.84	0.805	0.0145
5.38	0.952	0.0164

6.91	1.085	0.0190
8.44	1.182	0.0280
9.88	1.236	0.0399
11.44	1.224	0.0837

Run: 646
$Re = 301300$

α	C_l	C_d
-3.77	-0.036	0.0230
-2.29	0.157	0.0121
-0.75	0.353	0.0100
0.78	0.506	0.0088
2.18	0.652	0.0104
3.86	0.823	0.0122
5.40	0.978	0.0143
6.94	1.103	0.0189
8.45	1.201	0.0265
9.96	1.260	0.0382
11.48	1.231	0.1014

S5010
Fig. 5.92

Run: 766
$Re = 60200$

α	C_l	C_d
-4.89	-0.325	0.0358
-3.38	-0.183	0.0231
-1.84	-0.041	0.0158
-0.29	0.159	0.0189
1.25	0.299	0.0258
2.78	0.431	0.0336
4.33	0.557	0.0362
5.84	0.685	0.0391
7.36	0.816	0.0419
8.91	0.949	0.0329
10.42	1.062	0.0394

Run: 768
$Re = 100200$

α	C_l	C_d
-4.88	-0.375	0.0316
-3.35	-0.186	0.0196
-1.83	-0.049	0.0152
-0.31	0.087	0.0165
1.24	0.228	0.0194
2.77	0.369	0.0206
4.29	0.511	0.0198
5.82	0.654	0.0197
7.37	0.790	0.0218
8.87	0.924	0.0249
10.42	1.037	0.0340

Run: 770
$Re = 201300$

α	C_l	C_d
-4.91	-0.395	0.0339
-3.38	-0.249	0.0183
-1.82	-0.099	0.0139
-0.34	0.032	0.0094
1.19	0.182	0.0107
2.75	0.341	0.0111
4.29	0.502	0.0121
5.84	0.682	0.0141
7.38	0.834	0.0163
8.92	0.977	0.0203
10.44	1.081	0.0303

Run: 772
$Re = 301900$

α	C_l	C_d
-4.92	-0.432	0.0367
-3.38	-0.283	0.0163
-1.86	-0.131	0.0127
-0.32	0.010	0.0088
1.21	0.162	0.0085
2.75	0.358	0.0092
4.29	0.521	0.0103
5.82	0.673	0.0117
7.37	0.826	0.0141
8.89	0.968	0.0181
10.87	1.107	0.0309

S7012 (B)
Fig. 5.96

Run: 825
$Re = 60400$

α	C_l	C_d
-4.88	-0.292	0.0209
-3.31	-0.160	0.0149
-1.80	-0.042	0.0126
-0.28	0.100	0.0178
1.28	0.346	0.0222
2.82	0.545	0.0270
4.36	0.682	0.0277
5.89	0.812	0.0307
7.43	0.938	0.0293
8.95	1.039	0.0434
10.45	1.097	0.0681

Run: 838
$Re = 100600$

α	C_l	C_d
-3.81	-0.233	0.0159
-2.29	-0.088	0.0122
-0.78	0.061	0.0121
0.78	0.320	0.0132
2.34	0.470	0.0154
3.86	0.609	0.0162
6.28	0.840	0.0201
6.94	0.903	0.0222
8.45	1.004	0.0302
9.97	1.072	0.0461
11.43	1.061	0.0839

Run: 840
$Re = 200800$

α	C_l	C_d
-3.80	-0.201	0.0127
-2.28	-0.049	0.0095
-0.75	0.116	0.0099
0.78	0.278	0.0092
2.33	0.444	0.0102
3.83	0.600	0.0118
5.38	0.755	0.0133
6.91	0.896	0.0164
8.44	1.004	0.0255
9.97	1.070	0.0391
11.45	1.093	0.0745

Run: 842
$Re = 301900$

α	C_l	C_d
-3.82	-0.198	0.0114
-2.24	-0.029	0.0095
-0.77	0.104	0.0083
0.78	0.259	0.0073
2.31	0.429	0.0086
3.85	0.595	0.0099
5.39	0.748	0.0116
6.91	0.885	0.0147
8.44	1.000	0.0224
9.96	1.073	0.0354
11.46	1.103	0.0671

S7012 (B)
Fig. 5.99

Run: 856
$Re = 60700$

α	C_l	C_d
-4.81	-0.179	0.0220
-3.29	-0.040	0.0172
-1.78	0.075	0.0150
-0.23	0.241	0.0212
1.29	0.408	0.0277
2.87	0.648	0.0269
4.39	0.796	0.0329
5.94	0.915	0.0320
7.45	1.018	0.0318
8.98	1.092	0.0509
10.46	1.124	0.0727

Run: 858
$Re = 100600$

α	C_l	C_d
-4.82	-0.125	0.0186
-3.29	-0.019	0.0147
-1.76	0.095	0.0141
-0.22	0.279	0.0144
1.35	0.555	0.0151
2.88	0.723	0.0157
4.41	0.856	0.0191
5.94	0.986	0.0223
7.47	1.066	0.0321
8.98	1.122	0.0473

Run: 860
$Re = 201100$

α	C_l	C_d
-6.83	-0.252	0.0199
-5.31	-0.100	0.0150
-3.74	0.058	0.0115
-2.23	0.205	0.0113
-0.69	0.354	0.0123
0.83	0.507	0.0113
2.36	0.663	0.0112
3.92	0.837	0.0142
5.43	0.977	0.0172
6.95	1.070	0.0245
8.48	1.136	0.0361

Run: 862
$Re = 301900$

α	C_l	C_d
-6.84	-0.263	0.0185
-5.30	-0.106	0.0134
-3.78	0.048	0.0103
-2.24	0.202	0.0091
-0.70	0.387	0.0090
0.87	0.541	0.0084
2.36	0.690	0.0100
3.76	0.831	0.0121
5.43	0.981	0.0152
6.97	1.085	0.0220
8.46	1.153	0.0330

S7012 (B)
Fig. 5.102

Run: 864
$Re = 59900$

α	C_l	C_d
-6.86	-0.266	0.0302
-5.37	-0.117	0.0242
-3.84	0.024	0.0192
-2.32	0.136	0.0203
-0.80	0.310	0.0205
0.75	0.478	0.0234
2.34	0.751	0.0281
3.85	0.929	0.0255
5.39	1.042	0.0318
6.90	1.144	0.0360
8.42	1.191	0.0546

Run: 866
$Re = 100400$

α	C_l	C_d
-6.87	-0.145	0.0253
-5.33	0.011	0.0195
-3.83	0.139	0.0166
-2.30	0.246	0.0180
-0.79	0.340	0.0158
0.78	0.576	0.0197
2.32	0.794	0.0183
3.84	0.922	0.0199
5.39	1.063	0.0233
6.92	1.133	0.0331
8.42	1.179	0.0483

Run: 868
$Re = 201200$

α	C_l	C_d
-6.89	-0.120	0.0195
-5.32	0.033	0.0148
-3.71	0.201	0.0125
-2.30	0.332	0.0139
-0.76	0.464	0.0150
0.80	0.640	0.0136
2.33	0.807	0.0128
3.87	0.953	0.0162
5.38	1.073	0.0199
6.90	1.140	0.0297
8.42	1.188	0.0418

Run: 870
$Re = 302000$

α	C_l	C_d
-6.85	-0.121	0.0160
-5.33	0.029	0.0128
-3.83	0.175	0.0106
-2.27	0.365	0.0104

-0.72	0.527	0.0113
0.70	0.663	0.0094
2.33	0.815	0.0116
3.91	0.968	0.0143
5.39	1.075	0.0187
6.95	1.158	0.0275
8.41	1.203	0.0388

S7055

Fig. 5.106

Run: 909
$Re = 100600$

α	C_l	C_d
-5.93	-0.184	0.0374
-4.41	0.047	0.0234
-2.86	0.266	0.0208
-1.37	0.342	0.0182
0.17	0.506	0.0217
1.73	0.654	0.0234
3.25	0.809	0.0211
4.79	0.971	0.0223
6.33	1.125	0.0250
7.84	1.257	0.0298
9.38	1.333	0.0397
10.86	1.327	0.0672

Run: 911
$Re = 301900$

α	C_l	C_d
-5.94	-0.063	0.0197
-3.72	0.170	0.0154
-2.88	0.285	0.0140
-1.33	0.472	0.0137
0.18	0.563	0.0135
1.72	0.705	0.0120
3.26	0.880	0.0132
4.81	1.043	0.0153
6.33	1.185	0.0181
7.89	1.296	0.0265
9.41	1.329	0.0451
10.91	1.319	0.0845

S7055

Fig. 5.108

Run: 892
$Re = 60800$

α	C_l	C_d
-4.47	-0.149	0.0323
-2.90	0.051	0.0244
-1.38	0.192	0.0215
0.16	0.368	0.0255
1.66	0.534	0.0332
3.22	0.684	0.0374
4.76	0.824	0.0409
6.26	0.974	0.0373
7.83	1.119	0.0393
9.36	1.247	0.0376
10.88	1.288	0.0494
12.38	1.288	0.0731

Run: 894
$Re = 100500$

α	C_l	C_d
-4.45	-0.067	0.0259
-2.92	0.139	0.0199
-1.37	0.247	0.0187
0.14	0.398	0.0208
1.68	0.567	0.0236
3.25	0.728	0.0217
4.77	0.884	0.0217
6.29	1.024	0.0239
7.82	1.148	0.0275
9.35	1.241	0.0332
10.85	1.255	0.0575

Run: 895
$Re = 100300$

α	C_l	C_d
12.35	1.233	0.0944

Run: 897
$Re = 201200$

α	C_l	C_d
-4.45	0.008	0.0164
-2.99	0.143	0.0146
-1.35	0.298	0.0126
0.20	0.400	0.0124
1.70	0.564	0.0132
3.30	0.744	0.0138
4.76	0.904	0.0153
6.22	1.049	0.0177
7.83	1.179	0.0215
9.35	1.242	0.0328
10.84	1.241	0.0628

Run: 899
$Re = 302000$

α	C_l	C_d
-4.41	-0.014	0.0147
-2.88	0.146	0.0126
-1.35	0.318	0.0108
0.14	0.405	0.0099
1.71	0.583	0.0106
3.24	0.753	0.0115
4.79	0.922	0.0131
6.28	1.067	0.0152
7.85	1.193	0.0204

S7075 (A)

Fig. 5.112

Run: 700
$Re = 100600$

α	C_l	C_d
-4.02	-0.192	0.0265
-2.51	-0.041	0.0195
-0.96	0.084	0.0152
0.60	0.294	0.0181
2.13	0.521	0.0230
3.69	0.715	0.0188
5.21	0.849	0.0180
6.74	0.965	0.0209
8.26	1.080	0.0269
9.77	1.129	0.0369
11.29	1.171	0.0529

Run: 702
$Re = 200800$

α	C_l	C_d
-3.82	-0.034	0.0164
-2.44	0.100	0.0131
-0.91	0.253	0.0107
0.62	0.388	0.0122
1.99	0.537	0.0114
3.70	0.727	0.0108
5.10	0.849	0.0135
6.75	0.980	0.0172
8.28	1.081	0.0226
9.79	1.147	0.0318
11.30	1.193	0.0448

Run: 703
$Re = 202500$

α	C_l	C_d
-5.00	-0.146	0.0232

Run: 705
$Re = 302300$

α	C_l	C_d
-5.01	-0.157	0.0205
-3.47	-0.013	0.0131
-1.94	0.132	0.0105
-0.51	0.275	0.0089
1.12	0.471	0.0081
2.77	0.645	0.0087
4.22	0.782	0.0105
5.74	0.911	0.0132
7.26	1.032	0.0172
8.79	1.127	0.0225
10.32	1.194	0.0319

S7075 (A)

Fig. 5.114

Run: 707
$Re = 60600$

α	C_l	C_d
-4.01	-0.194	0.0311
-2.50	-0.057	0.0240
-0.99	0.073	0.0190
0.56	0.242	0.0228
2.12	0.426	0.0254
3.69	0.680	0.0319
5.21	0.855	0.0249
6.70	0.966	0.0247
8.25	1.052	0.0350
9.78	1.119	0.0417
11.29	1.169	0.0636

Run: 709
$Re = 100900$

α	C_l	C_d
-5.01	-0.175	0.0293
-3.48	-0.028	0.0203
-1.96	0.109	0.0147
-0.51	0.211	0.0162
1.11	0.364	0.0204
2.53	0.572	0.0225
4.18	0.762	0.0183
5.73	0.893	0.0194
7.25	1.011	0.0230
8.77	1.094	0.0311
10.28	1.146	0.0430

Run: 711
$Re = 201100$

α	C_l	C_d
-4.99	-0.161	0.0237
-3.48	-0.028	0.0158
-1.95	0.123	0.0113
-0.42	0.269	0.0087
1.12	0.433	0.0095
2.66	0.607	0.0112
4.21	0.778	0.0118
5.74	0.902	0.0155
7.25	1.019	0.0192
8.77	1.103	0.0254
10.30	1.162	0.0354

Run: 713
$Re = 302000$

α	C_l	C_d
-5.01	-0.166	0.0218
-3.46	-0.023	0.0139
-1.91	0.126	0.0104
-0.42	0.262	0.0081
1.13	0.461	0.0081
2.65	0.627	0.0085
4.21	0.778	0.0111
5.74	0.911	0.0139
7.27	1.029	0.0177
8.80	1.123	0.0231
10.17	1.183	0.0308

S7075 (A)

Fig. 5.116

Run: 717
$Re = 100600$

α	C_l	C_d
-5.01	-0.182	0.0285
-3.49	-0.039	0.0196
-1.96	0.093	0.0132
-0.41	0.266	0.0131
1.09	0.379	0.0202
2.65	0.596	0.0209
4.21	0.766	0.0168
5.71	0.888	0.0203
7.16	0.998	0.0245
8.72	1.088	0.0313
10.28	1.144	0.0425

Run: 719
$Re = 200900$

α	C_l	C_d
-5.00	-0.159	0.0237
-3.48	-0.023	0.0162
-1.97	0.123	0.0118
-0.42	0.275	0.0093
1.13	0.438	0.0099
2.65	0.605	0.0105
4.22	0.769	0.0118
5.74	0.892	0.0163
7.26	1.012	0.0199
9.54	1.138	0.0299
10.29	1.161	0.0355

Run: 721
$Re = 301300$

α	C_l	C_d
-5.02	-0.161	0.0218
-3.47	-0.017	0.0145
-1.97	0.123	0.0111
0.22	0.343	0.0084
1.11	0.445	0.0085
3.15	0.666	0.0093
4.21	0.760	0.0119
5.73	0.892	0.0150
7.26	1.016	0.0186
8.79	1.112	0.0238
10.30	1.176	0.0322

S7075 (A)
Fig. 5.119

Run: 736
$Re = 59900$

α	C_l	C_d
-4.85	-0.064	0.0311
-2.46	0.149	0.0228
-0.94	0.284	0.0243
0.60	0.427	0.0278
2.11	0.554	0.0372
3.67	0.859	0.0337
5.22	1.012	0.0257
6.75	1.113	0.0357
8.23	1.160	0.0419
9.78	1.210	0.0570
11.28	1.235	0.0830

Run: 738
$Re = 100400$

α	C_l	C_d
-5.00	0.033	0.0249
-3.46	0.169	0.0211
-1.95	0.286	0.0198
-0.42	0.403	0.0211
1.59	0.601	0.0303
2.65	0.754	0.0310
4.21	1.002	0.0188
5.75	1.091	0.0233
7.25	1.190	0.0309
8.78	1.219	0.0400
10.29	1.263	0.0550

Run: 976
$Re = 100000$

α	C_l	C_d
3.38	0.893	0.0229

Run: 740
$Re = 201000$

α	C_l	C_d
-4.98	0.097	0.0171
-3.59	0.230	0.0129
-1.92	0.379	0.0111
-0.41	0.524	0.0106
1.15	0.714	0.0114
2.73	0.891	0.0122
4.23	1.018	0.0156
5.73	1.112	0.0202
7.26	1.193	0.0262
8.78	1.241	0.0344
10.28	1.285	0.0459

Run: 742
$Re = 301900$

α	C_l	C_d
-6.00	-0.011	0.0201
-4.54	0.119	0.0145
-2.96	0.276	0.0111
-1.40	0.453	0.0099
0.12	0.606	0.0093
1.67	0.775	0.0100
3.15	0.923	0.0116
4.73	1.037	0.0163
6.27	1.134	0.0208
7.82	1.204	0.0272
9.27	1.254	0.0354

S7075 (A)
Fig. 5.122

Run: 744
$Re = 60900$

α	C_l	C_d
-6.03	-0.018	0.0392
-4.48	0.164	0.0335
-2.98	0.277	0.0301
-1.46	0.412	0.0321
0.08	0.552	0.0372
1.61	0.660	0.0401
3.15	0.870	0.0493
4.73	1.171	0.0314
6.24	1.224	0.0417
7.74	1.257	0.0498
9.25	1.301	0.0663

Run: 746
$Re = 100600$

α	C_l	C_d
-6.04	-0.014	0.0341
-4.51	0.153	0.0294
-2.97	0.298	0.0276
-1.45	0.428	0.0281
0.09	0.578	0.0346
1.62	0.675	0.0425
3.18	1.031	0.0336
4.72	1.174	0.0278
6.25	1.242	0.0350
7.75	1.266	0.0450
9.26	1.308	0.0570

Run: 748
$Re = 200900$

α	C_l	C_d
-5.96	0.243	0.0188
-4.40	0.386	0.0152
-2.93	0.527	0.0147
-1.31	0.675	0.0154
0.15	0.809	0.0163
1.67	0.967	0.0184
3.20	1.146	0.0178
4.69	1.184	0.0256
6.24	1.241	0.0318
7.74	1.293	0.0395
9.27	1.349	0.0498

Run: 750
$Re = 301400$

α	C_l	C_d
-7.20	0.109	0.0228
-4.43	0.406	0.0136
-2.91	0.564	0.0128
-1.39	0.709	0.0138
0.13	0.856	0.0139
1.67	1.004	0.0142
3.20	1.112	0.0184
4.70	1.149	0.0256
6.25	1.219	0.0310
7.79	1.295	0.0376
9.26	1.354	0.0465

S7075 (B)
Fig. 5.126

Run: 937
$Re = 60200$

α	C_l	C_d
-5.22	-0.289	0.0330
-3.70	-0.177	0.0249
-2.20	-0.056	0.0165
0.31	0.181	0.0194
0.90	0.263	0.0239
2.44	0.504	0.0314
3.99	0.679	0.0251
5.53	0.807	0.0218
7.05	0.928	0.0269
8.58	1.023	0.0353
10.07	1.102	0.0560

Run: 939
$Re = 100700$

α	C_l	C_d
-5.17	-0.264	0.0295
-3.66	-0.099	0.0206
-2.18	0.033	0.0163
-0.62	0.154	0.0152
0.91	0.359	0.0169
2.46	0.520	0.0183
4.00	0.662	0.0175
5.53	0.798	0.0194
7.06	0.928	0.0225
8.58	1.015	0.0316
10.08	1.092	0.0409

Run: 941
$Re = 201100$

α	C_l	C_d
-5.19	-0.250	0.0277
-3.65	-0.109	0.0173
-0.87	0.166	0.0096
-0.62	0.191	0.0096
0.93	0.365	0.0102
2.45	0.520	0.0103
4.01	0.679	0.0123
5.54	0.822	0.0144
7.07	0.948	0.0189
8.60	1.050	0.0256
10.11	1.140	0.0327

Run: 943
$Re = 302100$

α	C_l	C_d
-5.24	-0.262	0.0259
-3.54	-0.099	0.0149
-2.23	0.027	0.0122
-0.56	0.197	0.0082
0.93	0.358	0.0084
2.51	0.531	0.0089
4.02	0.686	0.0109
5.53	0.828	0.0132
7.10	0.958	0.0174
8.59	1.067	0.0225
10.10	1.163	0.0286

S8025
Fig. 5.130

Run: 876
$Re = 60100$

α	C_l	C_d
-6.67	-0.611	0.0373
-5.15	-0.471	0.0232
-3.63	-0.332	0.0176
-2.09	-0.153	0.0137
-0.54	0.009	0.0128
0.98	0.142	0.0134
2.53	0.315	0.0166
4.06	0.453	0.0280
6.51	0.670	0.0360
7.14	0.747	0.0320
8.63	0.875	0.0412

Run: 878
$Re = 100500$

α	C_l	C_d
-6.63	-0.631	0.0299
-5.13	-0.505	0.0190
-3.63	-0.372	0.0140
-2.10	-0.228	0.0100
-0.56	-0.030	0.0097
1.00	0.147	0.0103
2.52	0.300	0.0134
4.07	0.450	0.0163
5.61	0.594	0.0205
7.14	0.711	0.0256
8.65	0.830	0.0336

Run: 880
$Re = 201000$

α	C_l	C_d
-6.67	-0.661	0.0206
-5.17	-0.523	0.0140
-3.66	-0.373	0.0113
-2.08	-0.217	0.0078
-0.55	-0.030	0.0070
0.96	0.124	0.0084
2.50	0.271	0.0097
4.07	0.434	0.0126
5.57	0.600	0.0153
7.14	0.752	0.0179
8.66	0.874	0.0260

Run: 882
$Re = 301600$

α	C_l	C_d
-6.68	-0.671	0.0187
-5.14	-0.530	0.0123
-3.58	-0.370	0.0100
-2.10	-0.219	0.0077
-0.56	-0.046	0.0063
0.98	0.107	0.0074
2.51	0.284	0.0090
4.06	0.450	0.0109
5.60	0.603	0.0128
7.14	0.750	0.0154
8.66	0.881	0.0226

SD7037 (B)

Fig. 5.134

Run: 977
$Re = 60000$

α	C_l	C_d
-3.82	-0.166	0.0240
-2.28	-0.032	0.0214
-0.76	0.102	0.0167
0.78	0.283	0.0229
2.34	0.535	0.0276
3.88	0.692	0.0286
5.41	0.825	0.0277
6.95	0.947	0.0313
8.45	1.047	0.0360
9.98	1.143	0.0422
11.51	1.214	0.0516

Run: 800
$Re = 100300$

α	C_l	C_d
-3.82	-0.193	0.0223
-2.29	-0.032	0.0173
-0.75	0.137	0.0153
0.81	0.374	0.0171
2.35	0.539	0.0171
3.88	0.678	0.0172
5.42	0.809	0.0186
6.94	0.937	0.0212
9.33	1.102	0.0329
9.99	1.136	0.0355
11.50	1.194	0.0474

Run: 802
$Re = 201600$

α	C_l	C_d
-4.79	-0.185	0.0190
-3.30	-0.026	0.0128
-1.75	0.139	0.0115
-0.22	0.281	0.0100
1.32	0.428	0.0100
2.86	0.583	0.0110
4.40	0.748	0.0126
5.93	0.890	0.0151
7.47	1.019	0.0187
8.97	1.118	0.0246
10.49	1.206	0.0307

Run: 804
$Re = 301700$

α	C_l	C_d
-4.85	-0.160	0.0161
-3.28	-0.010	0.0127
-0.65	0.237	0.0090
-0.27	0.272	0.0086
1.36	0.450	0.0080
2.86	0.604	0.0093
4.41	0.757	0.0111
5.89	0.892	0.0135
7.46	1.023	0.0167
8.97	1.132	0.0216
10.49	1.226	0.0263

Run: 975
$Re = 300900$

α	C_l	C_d
-1.82	0.132	0.0105

SD7037 (B)

Fig. 5.137

Run: 806
$Re = 60500$

α	C_l	C_d
-3.80	-0.036	0.0255
-2.27	0.099	0.0210
-0.74	0.256	0.0240
0.80	0.435	0.0264
2.35	0.678	0.0322
3.90	0.895	0.0247
5.43	1.008	0.0244
6.96	1.115	0.0297
8.45	1.177	0.0397
9.97	1.247	0.0485
11.49	1.279	0.0623

Run: 808
$Re = 100900$

α	C_l	C_d
-4.82	-0.005	0.0259
-3.27	0.153	0.0220
-1.74	0.268	0.0193
-0.21	0.441	0.0215
1.33	0.670	0.0239
2.88	0.859	0.0194
4.42	0.982	0.0195
5.95	1.106	0.0230
7.46	1.195	0.0292
8.96	1.250	0.0390
10.49	1.303	0.0473

Run: 810
$Re = 200900$

α	C_l	C_d
-5.66	0.020	0.0193
-4.27	0.146	0.0157
-2.73	0.291	0.0139
-1.19	0.443	0.0131
0.32	0.582	0.0142
1.85	0.761	0.0120
3.37	0.893	0.0143
4.92	1.025	0.0175
6.45	1.137	0.0212
7.94	1.221	0.0274
9.49	1.293	0.0335

Run: 812
$Re = 301800$

α	C_l	C_d
-4.80	0.083	0.0142
-3.27	0.233	0.0127
-1.72	0.421	0.0126
-0.18	0.573	0.0103
1.34	0.720	0.0092
2.89	0.861	0.0118
5.04	1.054	0.0160
5.94	1.120	0.0179
7.41	1.212	0.0228
9.01	1.301	0.0281
10.50	1.360	0.0331

Run: 813
$Re = 301800$

α	C_l	C_d
-5.83	-0.010	0.0172

SD7037 (B)

Fig. 5.140

Run: 815
$Re = 60000$

α	C_l	C_d
-4.85	-0.027	0.0295
-3.31	0.113	0.0250
-1.79	0.243	0.0238
-0.25	0.394	0.0295
1.27	0.578	0.0346
2.85	0.842	0.0346
5.08	1.064	0.0255
5.92	1.116	0.0302
7.44	1.185	0.0343
8.93	1.237	0.0474
10.44	1.292	0.0549

Run: 817
$Re = 100600$

α	C_l	C_d
-3.81	0.183	0.0243
-2.26	0.304	0.0222
-0.74	0.447	0.0236
0.45	0.571	0.0278
2.36	0.903	0.0235
3.91	1.043	0.0206
5.41	1.152	0.0254
6.95	1.242	0.0303
8.45	1.286	0.0412
9.97	1.335	0.0500
11.20	1.355	0.0606

Run: 819
$Re = 201000$

α	C_l	C_d
-3.80	0.308	0.0162
-2.17	0.471	0.0156
-0.69	0.620	0.0165
0.83	0.776	0.0165
2.37	0.926	0.0143
3.90	1.051	0.0180
5.42	1.158	0.0220
6.92	1.237	0.0275
8.45	1.301	0.0339
9.93	1.358	0.0404
11.48	1.386	0.0499

Run: 820
$Re = 201300$

α	C_l	C_d
-5.86	0.116	0.0195
-4.74	0.217	0.0171

Run: 822
$Re = 302000$

α	C_l	C_d
-5.82	0.108	0.0158
-4.30	0.250	0.0140
-2.76	0.429	0.0135
-1.22	0.579	0.0157
0.33	0.742	0.0126
1.84	0.871	0.0119
3.37	0.997	0.0153
4.90	1.110	0.0191
6.47	1.198	0.0240
7.93	1.269	0.0291
9.44	1.343	0.0337

Run: 823
$Re = 301200$

α	C_l	C_d
-7.87	-0.144	0.0646
-6.83	0.010	0.0203

SD7037 (C)

Fig. 5.144

Run: 624
$Re = 60800$

α	C_l	C_d
-4.31	-0.212	0.0309
-2.85	-0.089	0.0236
-1.29	0.058	0.0198
0.26	0.241	0.0230
1.82	0.465	0.0284
3.36	0.665	0.0324
4.92	0.820	0.0302
6.43	0.953	0.0270
7.93	1.062	0.0305
9.49	1.151	0.0365
11.00	1.228	0.0483

Run: 626
$Re = 100900$

α	C_l	C_d
-4.32	-0.242	0.0269
-2.80	-0.094	0.0215
-1.27	0.071	0.0168
0.24	0.324	0.0194
1.82	0.516	0.0203
3.36	0.664	0.0190
4.90	0.805	0.0187
6.42	0.934	0.0202
7.97	1.061	0.0259
9.47	1.143	0.0328
10.99	1.217	0.0411

Run: 628
$Re = 200800$

α	C_l	C_d
-4.23	-0.176	0.0203

-2.76	0.014	0.0153
-1.23	0.200	0.0123
0.30	0.352	0.0110
1.83	0.508	0.0114
3.37	0.665	0.0121
4.91	0.818	0.0132
6.43	0.954	0.0157
7.96	1.070	0.0205
9.49	1.169	0.0258
11.02	1.242	0.0318

Run: 630
$Re = 301300$

α	C_l	C_d
-4.89	-0.189	0.0212
-2.84	0.037	0.0125
-1.23	0.186	0.0099
0.30	0.343	0.0076
1.85	0.506	0.0083
3.38	0.665	0.0095
4.91	0.815	0.0114
6.39	0.945	0.0138
7.97	1.069	0.0184
9.50	1.180	0.0231
10.97	1.251	0.0280

SD7037 (C)
Fig. 5.146

Run: 901
$Re = 60500$

α	C_l	C_d
-5.31	-0.156	0.0386
-3.77	-0.034	0.0268
-2.25	0.089	0.0181
-0.74	0.239	0.0180
0.80	0.395	0.0281
2.37	0.590	0.0350
3.90	0.777	0.0308
5.43	0.943	0.0264
6.97	1.068	0.0285
8.47	1.162	0.0320

Run: 903
$Re = 100700$

α	C_l	C_d
-5.28	-0.202	0.0342
-4.18	-0.051	0.0224
-2.22	0.101	0.0167
-0.70	0.252	0.0176
0.83	0.502	0.0194
2.38	0.667	0.0205
3.91	0.811	0.0191
5.44	0.955	0.0198
6.98	1.081	0.0243
8.49	1.183	0.0316

Run: 905
$Re = 201200$

α	C_l	C_d
-5.31	-0.181	0.0248
-3.78	-0.023	0.0169
-2.26	0.183	0.0132
-0.72	0.341	0.0129
0.85	0.477	0.0117
2.37	0.646	0.0119
3.92	0.809	0.0133
5.43	0.956	0.0157
6.98	1.094	0.0198
8.51	1.208	0.0252

Run: 907
$Re = 301800$

α	C_l	C_d
-5.29	-0.157	0.0206
-3.76	0.029	0.0128
-2.25	0.220	0.0105
-0.70	0.368	0.0090
0.78	0.480	0.0086
2.37	0.658	0.0098
4.00	0.832	0.0116
5.43	0.971	0.0138
6.93	1.104	0.0177
8.49	1.229	0.0223
10.02	1.324	0.0276

Appendix C

UIUC Low-Speed Airfoil Tests Manifesto

The UIUC Low-Speed Airfoil Tests Manifesto which appears below is a modified version of the initial announcement of the wind-tunnel test program written in December 1993. At the risk of being redundant with respect to what was included in the Preface, most of the original content of the announcement is retained. For recent information on the UIUC LSATs, please see the latest bulletin available from either the coordinator at the address given or from `http://www.uiuc.edu/ph/www/m-selig` *on the World Wide Web.*

We are searching for a group of experienced modelers to build a variety of airfoil wind-tunnel models for tests at the University of Illinois at Urbana-Champaign (UIUC). A low-speed, low-turbulence wind tunnel has been instrumented to take lift and drag measurements on airfoils at low speeds over the Reynolds number range from 40,000 to 500,000 (40k to 500k). The scope of the airfoil wind-tunnel tests will be limited only by the number of wind-tunnel models provided and the amount of funding received. Hopefully, the proposed modeler-supported airfoil test program will become self-sustaining. Your support and help of any kind will be acknowledged in reports on the project to be published through SoarTech Publications (Herk Stokely). We plan to publish the results through SoarTech frequently—possibly twice per year.

A similar undertaking (with substantial support from modelers) was started by Michael Selig, John Donovan and the late David Fraser in 1987 at Princeton University. In a two year period, over 60 various low-speed airfoils were wind-tunnel tested, involving over 1200 hours of wind-tunnel test time. The results were published in SoarTech 8 in 1989, and many of the new airfoil designs produced and tested during the program are now widely used on R/C sailplanes. As of November 1993, over 2200 copies of SoarTech 8 are in circulation worldwide. SoarTech 8 is available from

SoarTech Publications
c/o H.A. Stokely
1504 N. Horseshoe Circle
Virginia Beach, VA 23451
e-mail: herkstok@aol.com

At the present time, there is a need for new airfoils for R/C sailplanes. For example, R/C hand launch soaring is booming, but few good airfoils (e.g., E387 and SD7037) presently exist for such sailplanes. Sailplanes for the new F3J competition are just beginning to evolve, and new airfoils will probably be required. What will they look like? In the past, only a few airfoils (e.g., HQ 1.5/8.5, RG15 and SD7003) have been favored for F3B competition. In shape, handling and performance the SD7003 is quite different from the other airfoils mentioned. These significant differences suggest that it may be possible to design new airfoils that have better overall characteristics for F3B competition. In addition to the design and wind-tunnel testing of new airfoils, several existing airfoils should be tested. The SD7037 and RG15 are quite popular and often used with flaps. The flap effectiveness of these airfoils should be quantified through wind-tunnel tests, and the results should be used in the design of new airfoils.

There is also a need for new airfoils for R/C sport, aerobatic, and electric planes, as well as R/C helicopters. Often, NACA airfoils are used for these applications, but as compared with airfoils that could be designed today, many of the NACA airfoils (which were designed decades ago mostly by trial and error) are inferior. At the time the NACA airfoils were designed, little was known about the complex aerodynamics of airfoils operating at low Reynolds numbers. (Airfoils with small chords at low speeds, such as those on model aircraft, are said to operate in the low Reynolds number flight regime). In recent years, much has been learned about low Reynolds number aerodynamics, and this knowledge has successfully been applied to the design of new airfoils for R/C sailplanes, ushering in a new era in R/C soaring. Overall, R/C sailplane performance has improved dramatically. Older airfoils are no longer used. R/C power aircraft performance could likewise be dramatically improved through the use of newly designed, specially tailored airfoils.

Unique airfoil design requirements also exist for other categories of model aircraft. For example, FAI free flight aircraft (which incorporate both a powered launch segment and gliding flight) operate over a wide range of speeds. In the past, many airfoils with good performance characteristics have been designed for FAI free flight. These airfoils should be wind-tunnel tested to quantify their performance. The results gleaned from the tests could then be applied in the design process in an effort to develop new airfoils with improved performance. Also, the Society of Automotive Engineers (SAE) sponsors an annual model airplane design competition in which university student teams design, build and fly an R/C cargo aircraft. The record cargo weight that has been carried now stands at 24 3/4 lb for a model with a 60-size engine and 1200 in^2 total projected area. Conceivably, this record could be broken by an aircraft with an airfoil (or airfoils) specifically designed for the competition. Clearly, the need for new airfoils and data on existing airfoils is not limited just to R/C sailplanes, but applies to any type of model aircraft where better handling qualities and overall performance are desired.

Other topics of interest include the effects of turbulators and contour accuracy. Are boundary layer trips simply "repairs" to otherwise bad airfoils, or can trips be integrated with the airfoil and result in improvements over, say, the SD7037? The Princeton tests began to address this issue, but many questions still remain. For example, what is the best trip height for a given airfoil? Also, what is the best trip geometry, where should the trip be located for best performance, and what type of airfoils respond best to trips? The Princeton tests also shed some light on how accurate airfoils must be in order to achieve expected performance, but a more systematic effort should be made to test the best airfoils for sensitivity to contour accuracy. Also, we are interested in designing and testing families of airfoils for use in, say, "transitioning" from one airfoil at the root to a different airfoil at the tip. It is unlikely that the best performance can be obtained from a single airfoil used along the entire wing span. This is especially true for flying wings. Companion airfoils for blending should be designed for use with the most popular existing airfoils, e.g., SD7037 and RG15. It is expected that the practice of blending airfoils along the span will become much more popular than it is today. In an effort to maximize low Reynolds number airfoil performance for model aircraft, all of these topics should be addressed.

Overall, the UIUC test objectives will be to design and wind-tunnel test new airfoils for each category of aircraft listed above and also to examine the effects of flaps, turbulators and contour accuracy. We are especially interested in testing existing airfoils that are known to have superior performance. Wind-tunnel data on such airfoils will be used during the design of new and better airfoils. If you believe that we have overlooked an important area, we would be interested in your input and may consider expanding the scope of the project. The number of airfoil models to be tested has not been predefined; rather, it will be depend on the level of interest and support from the modeling community.

The wind-tunnel models should have a 33 5/8 in span with a 12 in chord and can either be built-up or foam core. To insure a uniform contour, the built-up models need to be fully sheeted. For the foam core models, we may be able to supply two 12 inch chord wing templates. The surface finish can either be fiberglass or monokote; however, we are interested in the effects of surface finish and will consider testing models with non-smooth surfaces. The models will be attached to the wind-tunnel balance by standard model wing rods. Standard model construction techniques should provide the necessary strength (supporting 15–20 lb of lift when pinned at both ends). The brass tubing and collars for the models will be supplied along with full-scale plots and/or coordinates of the airfoil, if requested. (Please contact us before starting any construction on a wind-tunnel model.)

The airfoils will be tested in the UIUC open-circuit 3×4 ft subsonic wind tunnel. The turbulence intensity level is minimal and more than sufficient to ensure good flow integrity at low Reynolds numbers. The experimental apparatus

used at Princeton will be modified for the UIUC tests. Lift and drag measurements for each airfoil will be taken at Reynolds numbers of 60k, 100k, 200k and 300k. In some instances, it may be possible to take limited data over an expanded range (40k–500k). The lift characteristics will be determined through force-balance measurements, while the drag will be evaluated by the momentum method through the use of pitot-static probes traversed through the airfoil wake at several spanwise locations. We are also interested in airfoil pitching moment measurements, but the current apparatus does not have such a capability. However, a pitching moment balance has been recently designed and should provide pitching moment data in the near future.

If you are interested in building wind-tunnel models for the tests or wish to request information, please write, fax or send e-mail to the coordinator

UIUC LSATs Coordinator
c/o Prof. Michael Selig
Dept. of Aeronautical and Astronautical Eng.
University of Illinois at Urbana-Champaign
306 Talbot Laboratory, 104 S. Wright St.
Urbana, IL 61801-2935
e-mail: uiuclsats@opus.aae.uiuc.edu
fax: (217) 244-0720

The program will be self-sustaining so long as funds are made available for equipment maintenance/upgrades and graduate student stipend support and tuition and fees (approximately $16,000/yr per student). The initial goal is to raise enough money to support at least two graduate students for a three year period. It is envisioned that a small level of support from a large number of modeling enthusiasts could sustain the airfoil design wind-tunnel test program indefinitely. The impact on model aviation could be tremendous. Donations can be mailed to

Prof. Michael Selig
Dept. of Aeronautical and Astronautical Eng.
University of Illinois at Urbana-Champaign
306 Talbot Laboratory, 104 S. Wright St.
Urbana, IL 61801-2935
e-mail: m-selig@uiuc.edu

Please make checks payable to "University of Illinois, AAE Dept." Also, please write on the check "Selig — Wind Tunnel Testing/AAE Unrestricted Funds," and provide a letter stating that your contribution is to be used by Prof. Selig and his group of students (both undergraduate and graduate) in support of the airfoil wind-tunnel tests. Finally, for a suggested donation of $18 in US, Canada, and Mexico (or $22 in other countries) you can receive a UIUC LSATs white short-sleeve shirt. All proceeds will go toward the continuation of the project.

Errata

Equations (2.4) and (2.11) in *Volume 1* were incorrect; the correct Eqs. are

$$d = 2\int_{-\infty}^{\infty} \left\{ \sqrt{P_{0,1} - P_s}\sqrt{P_{0,\infty} - P_s} - (P_{0,1} - P_s) \right\} dy \tag{2.4}$$

$$\varepsilon_{sb} = \frac{K_1 M_v}{A_{ts}^{3/2}} \tag{2.11}$$

SoarTech Publications

ISBN 0-9646747-2-6